



---

seit 1558

Friedrich-Schiller-Universität Jena

---

Chemisch-Geowissenschaftliche Fakultät

# **Synthesis of D-fructose conjugated metal complexes and polymers for breast cancer targeting**

Dissertation

(kumulativ)

zur Erlangung des akademischen Grades

doctor rerum naturalium (Dr. rer. nat.)

vorgelegt dem Rat der Chemisch-Geowissenschaftlichen Fakultät

der Friedrich-Schiller-Universität Jena

von Michael Pröhl

geboren am 06.12.1988 in Köthen (Anhalt)

*Dedicated to*  
*Helmut Johannes Pröhl*  
*(1937-2014)*

Gutachter:

1. Prof. Dr. Ulrich S. Schubert, FSU Jena
2. Prof. Dr. Wolfgang Weigand, FSU Jena

Tag der öffentlichen Verteidigung: 11.04.2018

## **Table of contents**

<b>Documentation of authorship</b>	<b>1</b>
<b>1 Introduction</b>	<b>5</b>
<b>2 Sugar conjugated metal complexes</b>	<b>12</b>
2.1 Curcumin metal complexes	13
2.2 Synthesis of D-fructose conjugated curcumin and its corresponding ruthenium complex	17
2.3 Sucrose as precursor for D-fructose derivatives functionalized at the C6 position	24
<b>3 Carbohydrate conjugated polymers</b>	<b>31</b>
3.1 D-Fructose conjugated linear poly(ethylenimine)	31
3.2 Carbohydrate conjugated polyacrylates	41
<b>4 Summary and outlook</b>	<b>51</b>
<b>5 Zusammenfassung</b>	<b>55</b>
<b>References</b>	<b>59</b>
<b>List of abbreviations</b>	<b>64</b>
<b>Publication list</b>	<b>67</b>
<b>Acknowledgement / Danksagung</b>	<b>69</b>
<b>Declaration of authorship / Selbstständigkeitserklärung</b>	<b>71</b>
<b>Publications P1 to P6</b>	<b>72</b>



## Documentation of authorship

This section contains a list of the individual contribution of the authors to the publications reprinted in the present thesis.

<b>P1</b> M. Pröhl, <sup>1</sup> U. S. Schubert, <sup>2</sup> W. Weigand, <sup>3</sup> M. Gottschaldt, <sup>4</sup> "Metal complexes of curcumin and curcumin derivatives for molecular imaging and anticancer therapy", <i>Coord. Chem. Rev.</i> <b>2016</b> , 307, 32-41.				
<b>Author</b>	<b>1</b>	<b>2</b>	<b>3</b>	<b>4</b>
Development of concept	x			x
Preparation of the manuscript	x			
Correction of the manuscript		x	x	x
Supervision of M. Pröhl				x
Proposed publication equivalent	0.5			

<b>P2</b> M. Pröhl, <sup>1</sup> T. Bus, <sup>2</sup> J. A. Czaplewski, <sup>3</sup> A. Traeger, <sup>4</sup> M. Deicke, <sup>5</sup> H. Weiss, <sup>6</sup> W. Weigand, <sup>7</sup> U. S. Schubert, <sup>8</sup> M. Gottschaldt, <sup>9</sup> "Synthesis and <i>in vitro</i> toxicity of D-glucose and D-fructose conjugated curcumin–ruthenium complexes", <i>Eur. J. Inorg. Chem.</i> <b>2016</b> , 5197-5204.									
<b>Author</b>	<b>1</b>	<b>2</b>	<b>3</b>	<b>4</b>	<b>5</b>	<b>6</b>	<b>7</b>	<b>8</b>	<b>9</b>
Chemical synthesis	x		x			x			
Structural characterization	x				x				
Biological evaluation		x		x					
Development of concept	x						x		x
Preparation of the manuscript	x								
Correction of the manuscript		x	x	x		x	x	x	x
Supervision of M. Pröhl									x
Proposed publication equivalent	1.0								

**P3** C. Englert,<sup>1,†</sup> M. Pröhl,<sup>2,†</sup> J. A. Czaplewska,<sup>3</sup> C. Fritzsche,<sup>4</sup> E. Preußger,<sup>5</sup> U. S. Schubert,<sup>6</sup> A. Traeger,<sup>7</sup> M. Gottschaldt,<sup>8</sup> "D-Fructose-decorated poly(ethylene imine) for human breast cancer cell targeting", *Macromol. Biosci.* **2017**, *17*, 1600502.  
<sup>†</sup> Authors contributed equally.

Author	1	2	3	4	5	6	7	8
Development of concept	x	x						x
Sugar synthesis		x	x					
Sugar characterization		x						
Polymer synthesis	x							
Polymer characterization	x							
Biological investigations				x	x		x	
Preparation of the manuscript	x	x						
Correction of the manuscript			x			x	x	x
Supervision of M. Pröhl								x
Proposed publication equivalent		0.5						

**P4** M. Pröhl,<sup>1</sup> P. D. Moser,<sup>2</sup> J. A. Czaplewska,<sup>3</sup> P. Hoffmann,<sup>4</sup> T. Bus,<sup>5</sup> A. Traeger,<sup>6</sup> H. Görls,<sup>7</sup> U. S. Schubert,<sup>8</sup> M. Gottschaldt,<sup>9</sup> "Synthesis of D-fructose conjugated ligands via C6 and C1 and their corresponding [Ru(bpy)<sub>2</sub>(L)]Cl<sub>2</sub> complexes", *Carbohydr. Res.* **2017**, *446–447*, 19-27.

Author	1	2	3	4	5	6	7	8	9
Development of concept	x								x
Chemical synthesis	x	x	x	x					
Structural characterization	x	x		x			x		
Biological evaluation					x	x			
Preparation of the manuscript	x								
Correction of the manuscript			x	x	x	x		x	x
Supervision of M. Pröhl									x
Proposed publication equivalent	1.0								

<b>P5</b> M. Pröhl, <sup>1</sup> C. Englert, <sup>2</sup> M. Gottschaldt, <sup>3</sup> U. S. Schubert, <sup>4</sup> J. C. Brendel, <sup>5</sup> "RAFT polymerization and thio-bromo substitution: an efficient way towards well-defined, large glycopolymers", <i>J. Polym. Sci., Part A: Polym. Chem.</i> <b>2017</b> , 55, 3617-3626.					
Author	1	2	3	4	5
Development of concept	x				x
Chemical synthesis	x	x			x
Structural characterization	x	x			x
Lectin interaction	x				
Preparation of the manuscript	x				
Correction of the manuscript		x	x	x	x
Supervision of M. Pröhl			x		x
Proposed publication equivalent	1.0				

<b>P6</b> H. Weiss, <sup>1</sup> J. Reichel, <sup>2</sup> H. Görls, <sup>3</sup> K. R. A. Schneider, <sup>4</sup> M. Micheel, <sup>5</sup> M. Pröhl, <sup>6</sup> M. Gottschaldt, <sup>7</sup> B. Dietzek, <sup>8</sup> W. Weigand, <sup>9</sup> "Curcuminoid-BF <sub>2</sub> -complexes: Synthesis, fluorescence and optimization of BF <sub>2</sub> group cleavage", <i>Beilstein J. Org. Chem.</i> <b>2017</b> , 13, 2264-2272.									
Author	1	2	3	4	5	6	7	8	9
Development of concept	x						x		x
Chemical synthesis	x	x				x			
Structural characterization	x		x		x	x			
Preparation of the manuscript	x								
Correction of the manuscript			x	x	x	x	x	x	x
Supervision of M. Pröhl							x		
Proposed publication equivalent						0.25			

**Erklärung zu den Eigenanteilen des Promovenden sowie der weiteren Doktoranden/Doktorandinnen als Koautoren an Publikationen und Zweitpublikationsrechten bei einer kumulativen Dissertation**

**Für alle in dieser kumulativen Dissertation verwendeten Manuskripte liegen die notwendigen Genehmigungen der Verlage („Reprint permissions“) für die Zweitpublikation vor.**

**Die Co-Autoren der in dieser kumulativen Dissertation verwendeten Manuskripte sind sowohl über die Nutzung als auch über die oben angegebenen Eigenanteile informiert und stimmen dem zu.**

**Die Anteile der Co-Autoren an den Publikationen sind in den vorausgehenden Tabellen aufgeführt.**

**Ich bin mit der Abfassung der Dissertation als publikationsbasiert, d.h. kumulativ, einverstanden und bestätige die vorstehenden Angaben. Eine entsprechend begründete Befürwortung mit Angabe des wissenschaftlichen Anteils des Doktoranden an den verwendeten Publikationen werde ich parallel an den Rat der Fakultät der Chemisch-Geowissenschaftlichen Fakultät richten.**

**Prof. Dr. Ulrich S. Schubert**

**Jena, der\_\_\_\_\_**

**Michael Pröhl**

**Jena, der\_\_\_\_\_**

## 1 Introduction

Around 200 billion tons of carbohydrates are accumulated by photosynthesis every year, which makes them the most abundant group of natural products.<sup>[1]</sup> Carbohydrates possess multiple functional groups, including one carbonyl and several hydroxyl groups per saccharide unit and various stereocenters.<sup>[2]</sup> One or more of these groups can participate in oligomerization or polymerization reactions, which result in linear as well as in branched structures.<sup>[3]</sup> The large structural diversity of (poly)carbohydrates covalently bound to non-sugar natural products results in a tremendous pool of functions in living organisms. Even though they do not carry information within the meaning of a biological code as in oligonucleotides, they are able to store biological information due to their three-dimensional structure.<sup>[2]</sup> This is of great importance in recognition processes on the molecular level, such as cell-cell adhesion or cell-cell communication.<sup>[4]</sup> Glycosylated proteins and lipids are major constituents of mammalian cells. The carbohydrates decorate the outer surface of cells as a kind of a carbohydrate coat, which is distinctive for a particular species, the type of cell and its status of development.<sup>[2, 5]</sup> Additionally, they can mediate the interaction between multiple organisms, for instance between a host and a symbiont or a parasite. The glycan *N*-acetylneuraminic acid on the outer cell surface mediates the attachment of human influenza virus by interaction with the hemagglutinin trimers on the surface of the virus.<sup>[6]</sup> The human ABO and Lewis blood group system is based on the presence or the lack of fucose, *N*-acetylgalactosamine and galactose residues as glycoconjugate oligosaccharides.<sup>[7]</sup> However, there are more biomolecules which interact non-covalently with carbohydrate residues. These include carbohydrate-specific enzymes, antibodies, lectins and transport proteins. Lectins are highly selective for specific carbohydrate structures and can interact with multiple glycoconjugates at the same time. The concept of multivalency in nature is predominantly used to transmit signals and to trigger various biological events.<sup>[5, 8]</sup>

Most of the eukaryotic cells need a continuous supply with various carbohydrates, which are used to produce adenosine-5'-triphosphate (ATP). The transport of carbohydrates into cells ensues either by Na<sup>+</sup> coupled carrier systems (SGLTs) or by glucose transporters, so-called GLUTs.<sup>[9]</sup> The GLUTs are encoded by the SLC2 genes and facilitate the energy-independent transport through the lipid bilayers of cells along the concentration gradient.<sup>[10]</sup> Up to now, 14 members of the GLUT

family are identified and basically, one or more of different GLUTs are embedded in every cell of the human body.<sup>[11]</sup> The different membrane proteins can be divided into three classes according to characteristics such as specific sequences of amino acids.<sup>[9]</sup> Eleven of the 14 members are capable for the transport of D-glucose, which can be explained by the predominant use of D-glucose as energy source in comparison to all other sugars and the need of multiple transporter systems.<sup>[11]</sup> Whereas most of GLUTs accept multiple sugars (for instance GLUT1 is tolerating glucose, galactose, mannose and glucosamine), GLUT5 reveals exclusive binding for D-fructose and is expressed in the membranes of cells of the small intestine, testis and kidney. Since the selectivity of GLUT5 for D-fructose was clearly shown in 1992,<sup>[12]</sup> many studies were performed on this topic. The structure of the GLUT5 transporter was confirmed recently<sup>[13]</sup> and studies showed the interaction of GLUT5 with other molecules than D-fructose, such as 2,5-anhydro-D-mannitol.<sup>[14]</sup> However, the GLUT5 membrane transporter is also investigated regarding its connection to various pathological structures.<sup>[15-16]</sup> Patients suffering from diabetes type II exhibit significantly increased level of GLUT5 in tissues of the skeletal muscle<sup>[17]</sup> and small intestine.<sup>[18]</sup> Additionally, linkages between other diseases, such as cardiomyopathy<sup>[19]</sup> and obesity,<sup>[20]</sup> are proposed, but need to be further investigated. The connection between cancer and D-fructose intake, GLUT5 expression and D-fructose levels in the blood is well investigated and showed direct correlations with various types of cancers.<sup>[21-22]</sup>

An overexpression of the GLUT5 transporter in breast cancer cells is heavily discussed by the scientific community. Whereas one group claimed that there is no overexpression of GLUT5 in breast cancer tissues,<sup>[23]</sup> the results of various other groups supported the overexpression. When incubated with D-fructose, breast cancer cells revealed altered glycan structures on the cell membrane and enhanced proliferative activity.<sup>[24]</sup> GLUT5 was also shown to be overexpressed in breast carcinoma cell lines MDA-468 and MCF-7 and poorly expressed in mammary epithelial cells.<sup>[25]</sup> A large study about the existence of GLUTs in various types of cancer further revealed the overexpression of GLUT5 in about 21% of all tested cell lines and in more than 85% of 33 tested breast cancer cell lines.<sup>[22]</sup> Furthermore, the knockdown of the GLUT5 transporter by anti-sense oligonucleotides resulted in inhibited cell proliferation of breast cancer cell lines MDA-MB-231 and MCF-7.<sup>[26]</sup> Recent investigations might point to a correlation between cells of acute myeloid leukemia (AML) and overexpressed levels of GLUT5.<sup>[27]</sup>

In the light of these findings, the GLUT5 transporter represents a potential target for the treatment of the mentioned diseases, including various types of cancers with a focus on breast cancer. As a consequence, the conjugation with D-fructose could result in novel pharmaceuticals with increased GLUT5 affinity. In general, the considered compounds should be crudely divided into low molar mass (A) and macromolecular ones (B). The underlying mechanisms for the uptake of these classes into breast cancer cells are completely different (Figure 1.1).

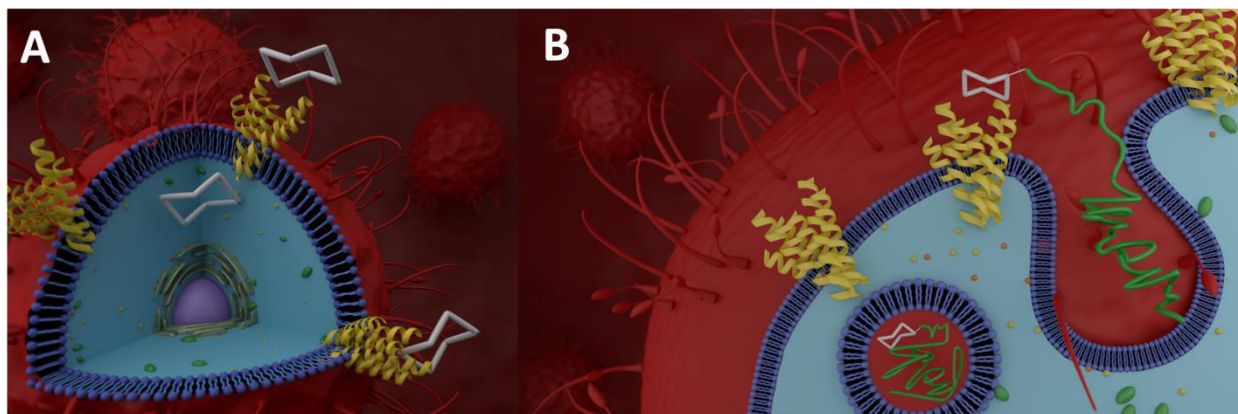


**Figure 1.1.** Uptake mechanisms of D-fructose conjugated compounds. A. Low molar mass molecules with D-fructose residue(s) are taken up by the GLUT5 transporter. B. Macromolecular assemblies bearing D-fructose unit(s) are accumulated outside of the cell due to binding to the GLUT5 and are internalized by endocytosis.

Small molecules, conjugated with D-fructose, are recognized by the GLUT5 transporter due to their targeting moiety and are taken up energy-independently through the lipid bilayer. Literature reports prove the GLUT5 targeting ability of low molar mass compounds functionalized with D-fructose in comparison to their sugar-free analogues. Labeling of D-fructose with  $e^+$  emitting  $^{18}\text{F}$  at various positions resulted in radiotracers, which could be easily detected by positron emission tomography (PET) and which revealed selectivity for GLUT5 overexpressing cells *in vitro*.<sup>[28-29]</sup> 7-Nitro-1,2,3-benzadiazole as fluorescent dye was used to label D-fructose and the resulting substances show the selective accumulation in breast cancer tissue quantified by flow cytometry.<sup>[30]</sup> Due to the unique properties of metal ions, a strong effort in the synthesis of D-fructose conjugated metal complexes was undertaken. A phosphorescent Re(I) complex bearing D-fructose exhibited selective accumulation in breast carcinoma cells MCF-7 and MDA-MB-231.<sup>[31]</sup> An Ir(III) complex functionalized with D-fructose displayed a 3.7 times increased uptake in MCF-7 cells compared to

non-cancerous cells, whereas the non-functionalized complex did not show any selective accumulation.<sup>[32]</sup> It is further mentionable that except for very few examples, D-fructose was connected *via* the C1 position of the sugar. A systematic study revealed the synthesis of various mono-allylated derivatives of D-fructose present in various ring forms, which allow to formulate some major tendencies about the position of choice in terms of chemical modification and the tolerance by the GLUT5 transporter.<sup>[33]</sup> The configuration of the C2, C3, C4 and C5 position are of crucial importance for the recognition and, therefore, epimers of D-fructose have low affinity for GLUT5. Also the 5-thio derivative of D-fructose showed poor binding affinity, indicating the involvement of the ring oxygen in the recognition by the GLUT5 protein.<sup>[34]</sup> All mono-allylated compounds exhibited poor tolerance except for the C6 derivative. In particular, the high  $K_i$  value for the C1 derivative indicated a reduced interaction with the GLUT5 transporter and, therefore, the need of substitution at other positions. In contrast to these findings, another study showed the substitution of the C1-OH by an allylamine group.<sup>[35]</sup> This derivative revealed a moderate  $K_i$  value, indicating a good affinity to GLUT5 even with substitution at the C1 position. Therefore, binding modes as depicted in Figure 1.2 are likely to occur. The red marked positions are not included in the interaction with the GLUT5 protein, whereas the C3, C4 and C5 positions always occupy binding sites of the receptor. As a consequence, C6 as well as C1 can be chemically modified and based on these structures also bulky substituents might be tolerated by the GLUT5 protein.



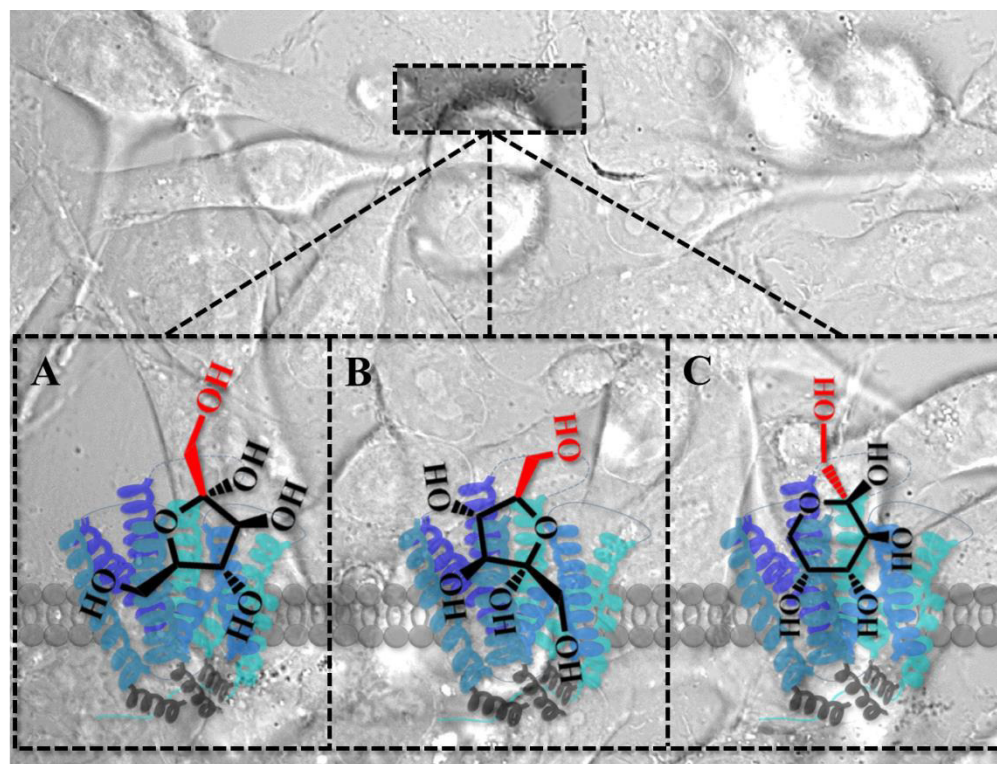


**Figure 1.2:** Schematic representation of various forms of D-fructose and the proposed orientation to the GLUT5 receptor in breast cancer cells.  $\beta$ -D-Fructofuranose occupies binding sites of the receptor with anomeric center trailing (A) or leading (B).  $\beta$ -D-Fructopyranose is limited with trailing of the anomeric center by occupation of the GLUT5 binding sites (C).

However, some central aspects for the design of D-fructose conjugated low molar mass compounds are not clarified yet. 1. With the aforementioned knowledge about the different positions of D-fructose at hand, the link between size of the substituents at varying positions and the recognition of the D-fructose unit by the GLUT5 transporter is still missing, even if C3, C4 and C5 could be excluded from this question. 2. What is the critical size of the substituents, which is tolerated by the transport protein? 3. How does the chosen linker affect the uptake of the D-fructose conjugated compound into breast cancer cells? Is there a beneficial functionality for the recognition? 4. Does D-fructose keep the targeting properties for GLUT5 even when a large biomolecule is attached to it? The present thesis tries to address these questions. For this purpose, the second chapter focuses on the synthesis of sugar bearing metal complexes. This includes a short overview about metal complexes of the bifunctional chelator curcumin (Chapter 2.1), the attachment of D-fructose to a derivative of curcumin by using “click” chemistry and the formation of the corresponding

[Ru(bpy)<sub>2</sub>(L)]Cl complex (Chapter 2.2). A strategy to address the C6 position of D-fructose selectively without tedious protection steps is also presented (Chapter 2.3).

However, due to their size, macromolecular assemblies are not capable of passing the lipid bilayer by a GLUT5 mediated transport. This fact changes the role of D-fructose to a mere targeting functionality, which causes the accumulation of the particles outside of the cells of interest by binding to GLUT5 in a multivalent fashion. The main process of particle internalization represents three different forms of endocytosis, in particular phagocytosis, fluid phase pinocytosis or receptor-mediated endocytosis.<sup>[36]</sup> The uptake mechanisms are highly complex events, which are dependent of plenty of variables, such as the concentration of the particles in- and outside of the cell, competition processes like exocytosis, the time after the first uptake and more. The underlying mechanisms could not be completely clarified up to now, but recent examples of polymer-D-fructose conjugates proofed their favorable properties in terms of selective uptake into breast cancer cells. D-Fructose conjugated methacrylate block copolymers were self-assembled to micelles in water. The micelles showed selective uptake into breast cancer cells, but only a very low uptake into macrophages.<sup>[37]</sup> The same group also investigated the influence of the attached sugar residues. Methacrylate-based block copolymers with different attached carbohydrates, in particular D-glucose, D-galactose and twice D-fructose *via* different positions were conjugated to a platinum-based anticancer agent and formulated micelles in water. The tested breast cancer cells showed a high preference for the D-fructose coated nanoparticles.<sup>[38]</sup> D-Fructose based nanoparticles revealed an increased uptake into breast carcinoma cells MDA-MB-231 in comparison to the polymers conjugated with other sugars in this study.<sup>[39]</sup> When the hydrophilic block of poly( $\epsilon$ -caprolactone)-*b*-poly(ethylene glycol) (PCL-PEG) was linked to D-fructose, the resulting mixed micelles exhibited breast cancer selectivity *in vitro* as well as *in vivo* in MCF-7 tumor bearing mice xenografts.<sup>[40]</sup>

In the last decade, many excellent studies on the uptake of D-fructose conjugated macromolecules into breast cancer cells were performed. But there are still important questions, which need to be addressed. 1. What are suitable sizes of the polymers? 2. Which polymeric backbone has the best properties, in terms of hydrophobicity, potential charges, flexibility and other parameters? 3. How many D-fructose units are required to target GLUT5 overexpressing cells and which distance between the D-fructose residues is favorable? 4. Does the implied multivalency affect the uptake of D-fructose conjugated polymers? These questions are discussed in the third chapter. The

functionalization of linear poly(ethyleneimine) (L-PEI) with D-fructose and the extensive biological evaluation of the glycopolymers is subject of Chapter 3.1. The last Chapter 3.2 discusses the attachment of various aldoses (D-glucose, D-galactose, D-mannose) to an acrylate backbone by  $S_N2$  reaction, which could be transferred to D-fructose. As a model for multivalent binding, the affinity of these polymers to the binding protein concanavalin A (Con A) is also investigated.

## 2 Sugar conjugated metal complexes

The attachment of sugar molecules to metal ions to form metal complexes can be achieved with two different approaches. First, the carbohydrate is attached directly to the metal ion after the introduction of suitable donor atoms or chelating units.<sup>[41]</sup> The second approach aims to attach the sugar molecule *via* a linking unit to a bifunctional molecule that is able to chelate the metal ion (Figure 2.1).

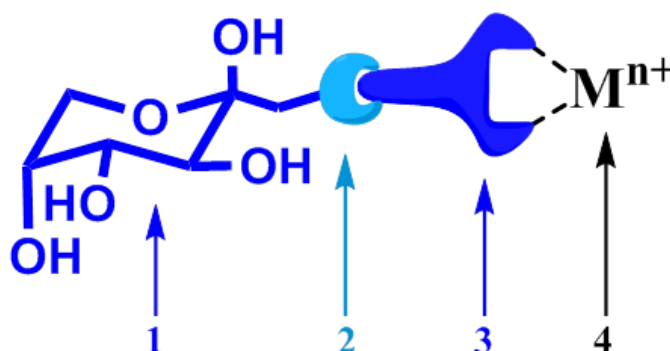


**Figure 2.1:** Schematic representation of the structure of a molecule following the bifunctional chelator concept containing a targeting unit (1), a linker unit (2), a bifunctional chelator (3) and the metal ion (4).

Due to the wide range of properties, various metal ions have gained increased attention in medical inorganic chemistry. Next to Pt-based agents, which are utilized for the treatment of solid tumors (*e.g.* colorectal and non-small cell lung cancers),<sup>[42]</sup> other metal complexes for different applications are used in hospital routines. Complexes of emitting metal ions, such as  $^{99\text{m}}\text{Tc}$  ( $\gamma$ ) and  $^{64}\text{Cu}$  ( $e^+$ ), were used for imaging. Metal complexes with different modes of actions to these of Pt-based drugs are investigated for their potential in the treatment of various diseases. To diminish side effects of the applied metal-based pharmaceuticals, an increase in selectivity is a key challenge in recent approaches.<sup>[43]</sup>

This can be achieved by suitable targeting moieties, such as monoclonal antibodies, small peptides or carbohydrates, which carry the metal complex to the tissue with an increased concentration of the corresponding receptor.<sup>[44]</sup> As mentioned before, D-fructose represents a suitable biomolecule for targeting the GLUT5 protein. But also other sugars are of interest. For instance, D-galactose

can be used to target asialoglycoprotein receptors associated with various diseases of the liver<sup>[45]</sup> or D-glucose, which interacts with the GLUT1 transporter that was shown to be overexpressed in various types of cancer.<sup>[46-47]</sup>

The carbohydrates have to be coupled to the bifunctional chelator (BFC) *via* a linker unit. There are multiple linkers available, such as cationic, anionic or neutral ones, and all of them result in altered pharmacokinetic properties. For instance, the use of an alkyl chain will enhance the lipophilicity, whereas a peptide sequence will increase the hydrophilicity.<sup>[44]</sup>

For the design of BFCs, some major requirements should be considered. The BFC should form thermodynamically and kinetically stable complexes with the metal ion of interest in an efficient and rapid synthesis suitable for biomolecules. The skeleton of the BFC can be cyclic, such as in 1,4,7,10-tetraazacyclododecane-1,4,7,10-tetraacetic acid (DOTA), or acyclic, like in diethylenetriaminepentaacetic acid (DTPA).<sup>[48]</sup> But also molecules besides the classical structures are under investigation by the scientific community. Amino acids were modified manifold to attach a biomolecule at the one and to chelate a metal ion on the other site.<sup>[49-50]</sup> Another highly active molecule is curcumin, which derives from the root of turmeric (*Curcuma longa*) and which can complex metal ions due to its  $\beta$ -diketone functionality.<sup>[51]</sup>

The first sub-chapter will address the variety of the metal complexes of curcumin. The second sub-chapter will focus on the synthesis of carbohydrate conjugated curcumin ligands and their corresponding ruthenium complexes. The third sub-chapter will emphasize sucrose as a starting molecule for the synthesis of D-fructose compounds conjugated *via* the C6 position of D-fructose.

## 2.1 Curcumin metal complexes

Parts of this chapter have been published in: **P1)** M. Pröhl, U. S. Schubert, W. Weigand, M. Gottschaldt, *Coord. Chem. Rev.* **2016**, 307, Part 1, 32-41.

Among a large variety of naturally occurring polyphenols curcumin (1,7-bis(4-hydroxy-3-methoxyphenyl)-1,6-heptadiene 3,5-dione) has been identified as a highly biologically active compound. Curcumin interacts with a large number of molecular targets by various mechanisms linked to the most prevalently diseases of modern societies. It shows not only anti-cancer, anti-inflammatory, anti-oxidant, anti-diabetic and anti-arthritis properties and protective effects against various cardiovascular diseases, but also against neurodegenerative afflictions such as Alzheimer

disease (AD), multiple sclerosis and others.<sup>[52]</sup> Curcumin is non-toxic in high doses up to 12 g·d<sup>-1</sup>, when administered orally.<sup>[53]</sup> However, curcuminoids in general show some major limitations in contrast to their miraculous biological activities. Curcumin is sensitive to light, the presence of solvents and oxygen.<sup>[54]</sup> Additionally, it is poorly stable in aqueous media with pH≤5.0 and it degrades rapidly (after 10 min at pH 7.4, only 10% of the initial amount of curcumin are left).<sup>[55]</sup> In the last decades, many attempts have been performed to overcome these limitations to improve the bioavailability of curcumin and its derivatives. Adjuvant molecules, such as piperine,<sup>[56]</sup> as well as delivery-systems based on liposomes,<sup>[57]</sup> micelles,<sup>[58]</sup> or nanoparticles<sup>[59]</sup> were studied. From a chemical point of view, curcumin is a bis- $\alpha,\beta$ -unsaturated  $\beta$ -diketone, where two oxy-substituted aryl groups are connected by a seven carbon chain.<sup>[60]</sup> Modification of this curcumin-skeleton is one strategy to improve the pharmacological properties. For instance, the stability in cultured cells was increased after the phenol groups were substituted with methoxy groups.<sup>[55, 61]</sup> Also the introduction of biomolecules can result in enhanced properties of the resulting compound in comparison to curcumin itself.<sup>[62]</sup> However, complexation reactions of curcumin and its derivatives with various metal ions yield not only in increased stability of the formed complexes, but also offering the synthesis of metal complexes with distinct properties. The potential applications of the novel formed metal complexes are strongly dependent on the structure of the curcumin skeleton, the complexed metal ion, ancillary ligand(s), the counterion and other parameters. From a perspective of medical applications of curcumin-based metal complexes, they can be crudely divided into 1. metal complexes for molecular imaging and 2. for the use as anti-cancer agents (Figure 2.2).

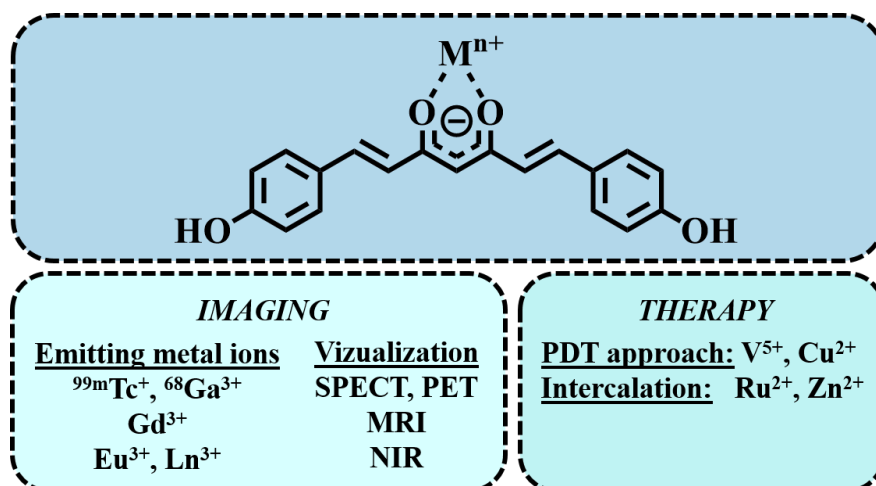


**Figure 2.2:** Schematic representation of the structure of the curcuminoid skeleton bound to a metal ion (top, anions, ancillary ligands and positions of modifications were omitted for clarity). The use of selected metal ions as potential imaging agents (left, including the visualization method) and anti-cancer therapy agents (right) is presented.

The coordination of curcumin and its derivatives to emitting metal ions led to a variety of novel complexes suitable for imaging of several diseases. Complexes of the general formula  $[^{68}Ga(L)_2]^+$  provided a high affinity for amyloid- $\beta$ ,<sup>[63]</sup> a peptide that can be correlated to AD.<sup>[64]</sup> Due to the positron emission of  $^{68}Ga$ , the formed complexes are suitable for PET imaging and additionally, when incubated with A549 lung cancer cells, the localization of them inside the cells differ from the parent ligands mediated by the hydrophobicity differences (Figure 2.3 A).

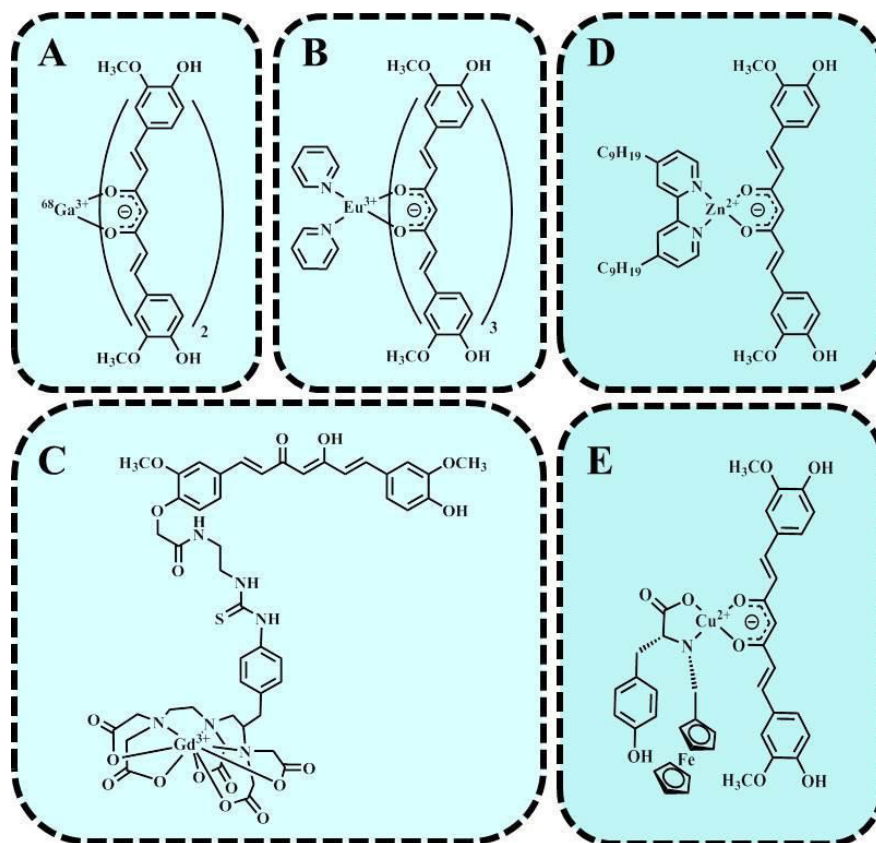


**Figure 2.3:** Schematic representation of selected curcumin conjugated metal complexes (anions are omitted for clarity).

An non-toxic  $\text{Eu}^{3+}$  based complex of the formula  $[\text{Eu}(\text{py})_2(\text{L})_3]$  ( $\text{py}$  = pyridine) revealed luminescence in the near infrared (NIR) region, which is mediated by the ancillary  $\text{py}$ -ligands and, therefore, by the extension of the  $\pi$ -conjugated system (Figure 2.3 B).<sup>[65]</sup> Curcumin was also linked to the known contrast agent  $\text{Gd}^{3+}$ -DTPA (Figure 2.3 C).<sup>[66]</sup> The novel formed complex possesses binding to amyloid- $\beta$  and an about four times higher longitudinal relaxivity than  $\text{Gd}^{3+}$ -DTPA, which represents a strong benefit for MRI imaging.

Planar molecules or compounds with planar elements can directly interact with the deoxyribonucleic acid (DNA) in multiple ways. For instance, two connected base pairs form a binding pocket for an intercalating molecule, which causes damage of the DNA by single strand breaks.<sup>[67-68]</sup> A curcumin conjugated  $\text{Zn}^{2+}$  complex revealed the strongest growth inhibition in all tested cell lines and a lower half maximal inhibitory concentration ( $\text{IC}_{50}$ ) in LAN-5 neuroblastoma cells than curcumin alone, caused by an intercalative binding mode (Figure 2.3 D).<sup>[69]</sup> Another class of curcumin conjugated  $\text{Cu}^{2+}$  complexes showed the use of ferrocenyl bearing amino acids as



ancillary ligands (Figure 2.3 D).<sup>[70]</sup> After irradiation at  $\lambda = 454$  nm the complexes revealed a complete cleavage of the DNA mediated by a radical pathway. The complexes were taken up and localized in the cytosol after incubation and showed an enhanced cytotoxicity in comparison to curcumin alone or the corresponding pentane-2,4-dione (acac) complex.

Curcumin is a highly biological active molecule that suffers from some major drawbacks, such as poor aqueous solubility and bioavailability. To overcome these limitations, the complexation with a wide variety of metals results in novel compounds with improved properties in comparison to curcumin alone. The reaction with emitting metal ions, such as  $^{99m}\text{Tc}^+$  or  $^{68}\text{Ga}^{3+}$ , yields curcumin conjugated metal complexes, which can be used for imaging of multiple diseases. But also  $\text{Cu}^{2+}$  or  $\text{Zn}^{2+}$  as metal ions can be used to synthesize novel complexes suitable for the treatment of cancer by various mechanism, including intercalation and photodynamic approach.

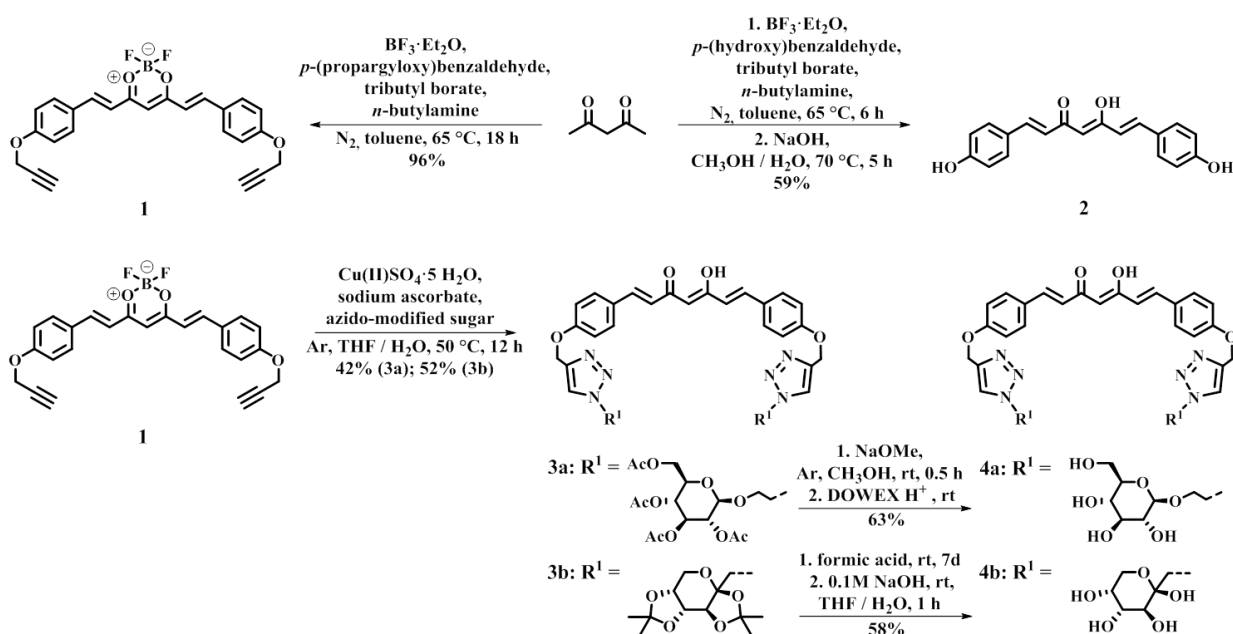
## 2.2 Synthesis of D-fructose conjugated curcumin and its corresponding ruthenium complex

Parts of this chapter have been published in: **P2)** M. Pröhl, T. Bus, J. A. Czaplewska, A. Traeger, M. Deicke, H. Weiss, W. Weigand, U. S. Schubert, M. Gottschaldt, *Eur. J. Inorg. Chem.* **2016**, 5197-5204. **P6)** H. Weiss, J. Reichel, H. Görls, K. R. A. Schneider, M. Micheel, M. Pröhl, M. Gottschaldt, B. Dietzek, W. Weigand, *Beilstein J. Org. Chem.* **2017**, 13, 2264-2272.

It was shown that the complexation of curcumin can result in novel complexes with advanced properties regarding their use as medical agents. The use of sugar molecules to modify curcumin is rarely described. Solely, the attachment of D-galactose by Cu(I) catalyzed Huisgen 1,3-dipolar cycloaddition (CuAAC), so called “click” reaction, between propargyl-modified curcumin and azide bearing D-galactose with subsequent deprotection of the sugar moiety resulted in a water soluble, non-toxic curcumin derivative with increased inhibition properties of amyloid- $\beta$  and  $\tau$ -peptide aggregation.<sup>[62]</sup> To the best of our knowledge the combination of the modification of curcumin with carbohydrates and the subsequent complexation with a suitable metal ion was demonstrated only once. A curcumin ligand bearing D-glucose and its corresponding oxovanadium complex revealed an increased solubility in water and enhanced uptake in the nucleus and cytoplasm of HaCaT (human adult low calcium high temperature keratinocytes) and HeLa (cervical

cancer cell line, which derived from Henrietta Lacks) cells in contrast to sugar-free complexes.<sup>[71]</sup> Vanadium was selected because it represents a biocompatible metal<sup>[72]</sup> and oxovanadium(IV) complexes are reported to be suitable for PDT (photodynamic therapy) due to their low energy d-d absorption band.<sup>[73]</sup> Ru<sup>2+</sup> represents another alternative metal ion. Ru-based complexes could overcome resistance problems, which are often linked to the application of Pt-containing drugs.<sup>[74]</sup> Additionally, Ru complexes reveal the interaction with *N*- or *O*-donor ligands comparable to that of Pt-based agents, the oxidation states +2 and +3 are easily available and they can be incorporated by transferrin into tumor cells.<sup>[75]</sup>

Our study aimed to combine the potential of D-fructose and its derivatives to interact with GLUT5 overexpressing cells, the biological activity of curcumin and its derivatives and metal complexes based on Ru<sup>2+</sup>. For this purpose, the synthesis of sugar conjugated bisdemethoxycurcumin ligands was carried out as depicted in Scheme 2.1.



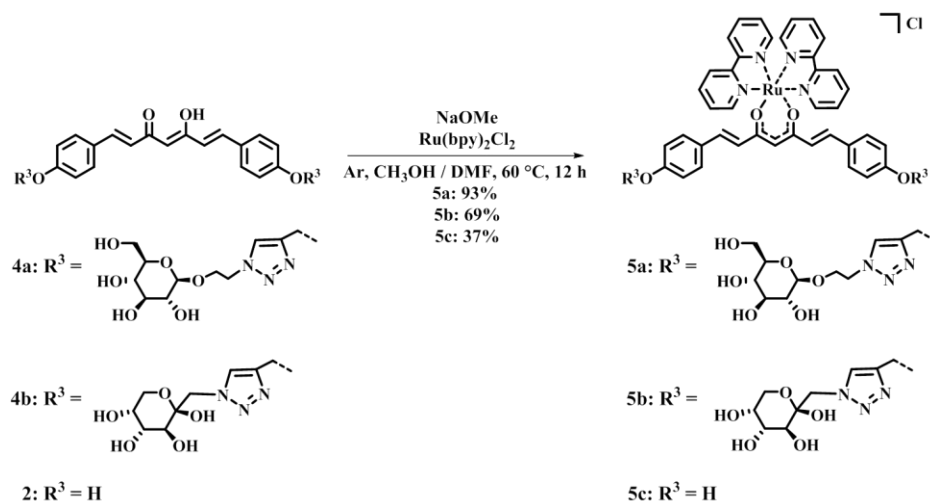
**Scheme 2.1:** Schematic representation of the syntheses of the ligands.

The synthesis of propargyl bearing bisdemethoxycurcumin derivative was conducted according a modified literature procedure.<sup>[76]</sup> Propargyl-modified bisdemethoxycurcumin **1** was obtained in a one-pot synthesis by double-times aldol condensation between  $\text{BF}_2$ -protected acetylacetone and *p*-(propargyloxy)-benzaldehyde in excellent yield (96%). The sugar-free ligand **2** was used for

comparison and was obtained in a similar reaction to that of ligand **1**. The BF<sub>2</sub>-group was cleaved under basic conditions with NaOH. Cu(I) catalyzed cycloaddition between azido-modified sugars and ligand **1** with CuSO<sub>4</sub>·5H<sub>2</sub>O and sodium ascorbate as catalyst forming pair yielded the sugar conjugated ligands (**3a** and **3b**) in moderate yields. During the “click” reaction, the BF<sub>2</sub> group of the curcumin skeleton was cleaved. In this context, the cleavage of the BF<sub>2</sub> group was reached by heating a mixture of THF (or another organic solvent) and water (or a base), whereas heating only in dry THF did not result in the formation of the free ligand. The proposed mechanism includes the formation of a difluoroboric acid ester, a hydroxydifluoro borate after nucleophilic attack and hydrolysis to create boric acid, HF and the corresponding curcumin in the anionic form. Copper complexes of curcumin and its derivatives were shown to be more stable than curcumin itself.<sup>[77]</sup> Competing ligands, such as ethylenediaminetetraacetic acid (EDTA) or NH<sub>3</sub>, could not be applied successfully to remove all Cu<sup>2+</sup> ions completely, which were bound in a stable fashion to the curcumin ligands, what also explains the relatively low yields. Additionally, due to their structural similarities curcuminoids are challenging to purify *via* chromatographic techniques.<sup>[78]</sup>

To use the ligands in aqueous media, the protection groups of the carbohydrates have to be cleaved off. Acetyl-groups of **3a** were cleaved off under basic conditions using sodium methoxide. When analyzing **4a** with nuclear magnetic resonance (NMR) spectroscopy, the signals remain sharp and well separated. Due to the glycosidic linkage at the C1 position of D-glucose, the sugar units are not able to undergo ring-opening reactions and, therefore, no stereoisomers are detectable. Isopropylidene-groups, which were used to protect the D-fructose units of **3b**, are usually cleaved in aqueous, acidic solvents. Due to the lability of curcumin towards acids,<sup>[55]</sup> neither standard deprotection conditions nor acidic exchange resins could be applied successfully. Stirring in 85% formic acid resulted in the replacement of the isopropylidene groups by formic acid esters, which were easily cleaved under basic conditions afterwards.<sup>[79]</sup> Cleavage of the protection groups resulted in an equilibrium between open-chained, furanose und pyranose forms of D-fructoses. This was clearly observable by the existence of more than one signal for the triazole group of the different forms of the ligand in the aromatic region in <sup>1</sup>H as well as in <sup>13</sup>C NMR. All of these forms result and in a single signal of the [M+Na]<sup>+</sup> ion in the ESI-MS spectrum.

To form the corresponding complexes, the β-diketone moieties of the ligands **2**, **4a** and **4b** were deprotonated with sodium methoxide and reacted with Ru(bpy)<sub>2</sub>Cl<sub>2</sub> (Scheme 2.2).



**Scheme 2.2:** Schematic representation of the syntheses of the complexes.

Due to the lack of carbohydrates in the structure of complex **5c**, the hydrophilicity of this compound was decreased and, therefore, dialysis *vs.* H<sub>2</sub>O could not be successfully applied for purification. A size exclusion column (Sephadex<sup>®</sup> LH-20) was used instead to isolate the Ru complex in high purity. The structure of **5b** was challenging to validate due to instability during mass spectrometry measurements. LC-MS-Measurements with an orbitrap mass analyzer and gentle measurement conditions identified the desired complex additionally to a set of fragments, which derived from the parent [M-Cl]<sup>+</sup> ion (Figure 2.4). For instance, tandem MS experiments revealed fragments with cleaved sugar unit(s) (**F1** and **F3**) or triazole unit(s) (**F4** and **F6**).

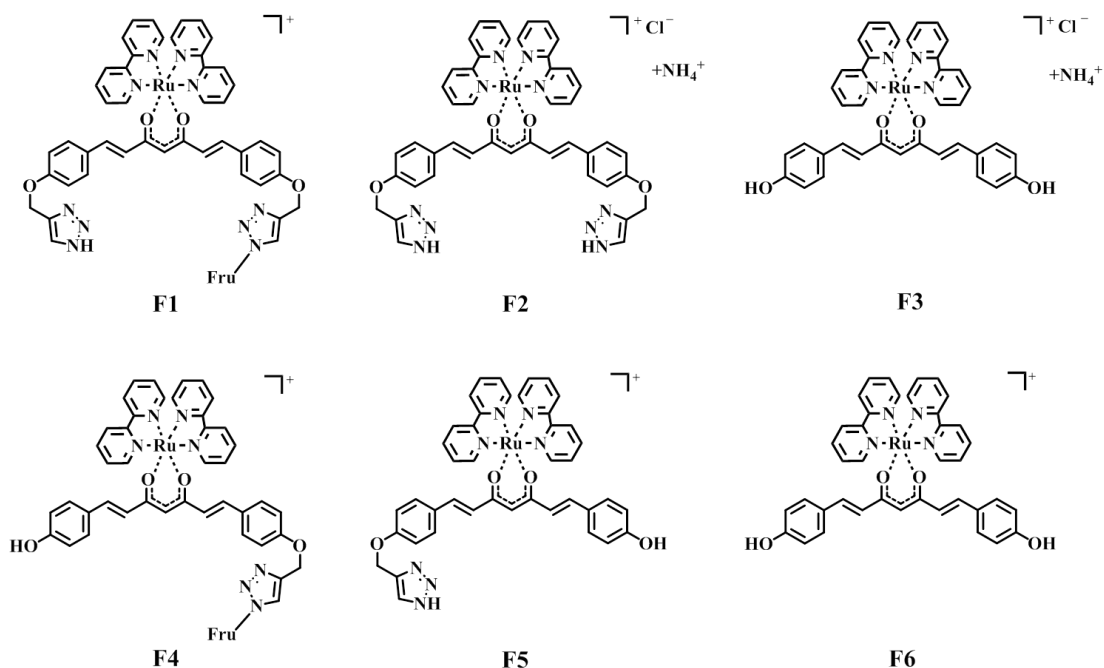


**Figure 2.4:** Schematic representation of fragments **F1** to **F6** resulting from the parent ion  $[M-Cl]^+$  obtained by ESI-Orbitrap-MS investigations of **5b**.

The ligands **2**, **4a** and **4b** as well as the complexes **5a** to **5c** were investigated for their cytotoxicity against various cell lines. Due to fluorescence quenching of  $[Ru(bpy)_2(L)]Cl_2$  complexes in aqueous solvents,<sup>[80]</sup> no uptake could be detected by standard methods, such as flow cytometry or confocal laser scanning microscopy (CLSM). However, inhibition of cellular metabolic activity in non-cancerous L929 cells, in liver cancer HepG2 cells and in breast cancer cells MDA-MB-231 was investigated, using a resazurin-based assay (alamarBlue). Since there is no significant concentration-dependent cytotoxicity, only one concentration for all compounds (100  $\mu$ M) in each cell line is depicted in Figure 2.5.

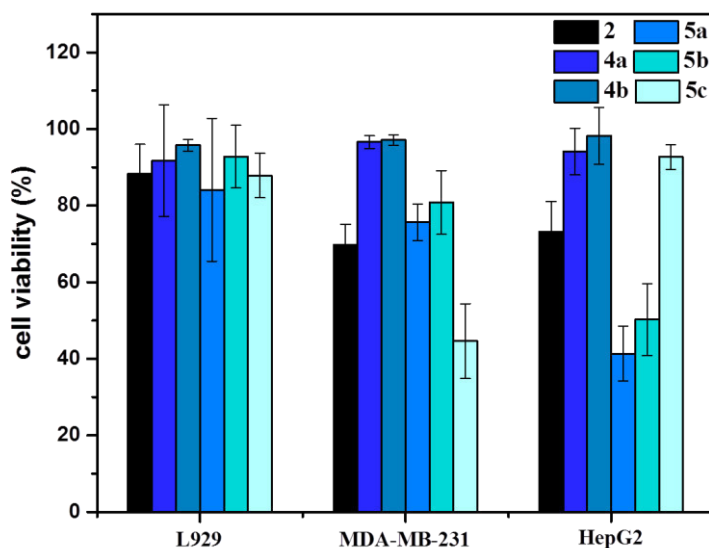


**Figure 2.5:** Relative viability of L929, MDA-MB-231 and HepG2 cells after 24 h incubation with the compounds **2** and **4a** to **5c** at 100  $\mu$ M. Values represent the mean  $\pm$  S.D. (n=3).

None of the tested compounds caused a reduction of the cell viability in non-cancerous cell line L929. Sugar-complexes **5a** and **5b** showed a slight inhibition effect of cellular metabolic activity in breast cancer MDA-MB-231 cells in comparison to their ligands. This might be induced by the 2,2'-bipyridine (bpy) groups of the complexes, which increase the lipophilicity and, therefore, facilitate the diffusion through the cell membrane contrary to the more polar ligands **4a** and **4b**. D-Fructose conjugated complex **5b** did not show cytotoxicity for MDA-MB-231 cells. The sugar-free compounds **2** and **5c** induced an inhibitory effect on cellular metabolic activity of relative viability of 70% for **2** and of 45% for **5c**. This might be attributed by the enhanced hydrophobicity of these compounds due to the missing sugar moieties. Liver cancer HepG2 cells did not reveal sensitivity against sugar-free complex **5c** and only a slight decrease of cell viability of 73% for ligand **2** was encountered. Sugar conjugated ligands **4a** and **4b** did not reveal any inhibitory effect as well. In contrast to that, HepG2 cells were strongly affected by sugar conjugated complexes **5a** (41%) and **5b** (50%). It has been reported that D-galactose inhibits the growth of HepG2 cells and that drug-induced mitochondrial toxicity is increased for HepG2 cells grown in D-galactose containing media instead of D-glucose.<sup>[81-82]</sup> HepG2 cells revealed also a significant decrease in cell viability after exposition to high D-glucose levels, which might be caused by an apoptotic mode.<sup>[83]</sup> Therefore, the decrease of cell viability of HepG2 cells, when incubated with sugar conjugated complexes **5a** and **5b** could be attributed to the interaction with the attached sugar units.

Additionally, another D-glucose conjugated  $[\text{Ru}(\text{L})_3]\text{Cl}_2$  complex showed an enhanced uptake into HepG2 cells in comparison to the D-galactosyl- respectively D-mannosylated complexes<sup>[84]</sup> and curcumin itself is reported to inhibit the cellular metabolic activity of HepG2 cells.<sup>[85-86]</sup>

The performed investigations show the synthesis and characterization of a D-fructose conjugated curcumin derivative as well as the corresponding Ru complex. To obtain this complex, multistep syntheses of a sensitive biomolecule were required, including challenging protection group chemistry and the purification from multiple side-products. In the light of these findings, some changes in the synthesis regarding linking structures and the use of other curcumin derivatives would elevate the synthesis of D-fructose conjugated curcumin metal complexes. A novel curcumin derivative, which is modified with carboxylic acid functionalities at the benzyl rings, was reported recently.<sup>[87]</sup> Amino-functionalized D-fructose can be readily synthesized, starting from D-glucose, which undergoes an Amadori rearrangement when reacted with *N,N*-dibenzylamine.<sup>[88]</sup> The formed 1-amino-dibenzyl D-fructose derivative can be hydrogenated to obtain amino-functionalized D-fructose, which could react in a very efficient manner with the activated carboxylic acid of the curcumin derivative to form a carboxamide linker. Using this approach, no protection groups of the D-fructose would be required and, therefore, introduction of formic acid esters instead of isopropylidene groups with subsequent basic deprotection procedures could be avoided. It was also shown that D-fructose bound to a Re complex *via* a carboxamide linker revealed an increased uptake into MCF-7 cells mediated by GLUT5 in comparison to the D-fructose free compounds tested in this study.<sup>[31]</sup> However, the step with the lowest yield was the “click” reaction between the sugar-azides and the propargyl-modified curcumin derivative **1** with mono-functionalized product and Cu-curcumin complexes as side-products. Removal of the excessive Cu ions with EDTA or ammonia solution was not satisfying. Copper-free reactions between azides and alkynes are of strong interest for the conjugation of biomolecules and could also offer an alternative approach to the Cu(I) catalyzed reaction.<sup>[89-90]</sup> The biological evaluation of the novel compounds revealed sensitivity of the liver cancer cell line HepG2 against sugar-conjugated  $[\text{Ru}(\text{bpy})_2(\text{L})]\text{Cl}_2$  complexes. Quenched fluorescence of these compounds in aqueous media hampered uptake studies by fluorescence-based methods. Further investigations by other methods, such as ICP-MS (inductively coupled plasma mass spectrometry), could provide new insights in the uptake of sugar conjugated curcumin Ru complexes.

### 2.3 Sucrose as precursor for D-fructose derivatives functionalized at the C6 position

Parts of this chapter have been published in: **P4)** M. Pröhl, P. D. Moser, J. A. Czaplewska, P. Hoffmann, T. Bus, A. Traeger, H. Görls, U. S. Schubert, M. Gottschaldt, *Carbohydr. Res.* **2017**, 446–447, 19–27.

As described above, the GLUT5 transporter might be a target in the design of novel pharmaceuticals for GLUT5 overexpressing cells related to various diseases such as different types of breast cancer and AML. As a consequence, the interest in derivatives of D-fructose is continuously increasing. Derivatives include modification and / or substitutions of hydroxyl groups to form ethers, carboxylic acids, epoxides and halides, but also *N*-derivatives, such as amines and *S*-derivatives, such as thiols or thioethers. However, almost all of the up to now synthesized compounds are derivatized only at the C1 or C3 position of D-fructose due to commercially available starting materials with suitable protective groups (1,2;4,5-di-*O*-isopropylidene- $\beta$ -D-fructopyranose and 2,3;4,5-di-*O*-isopropylidene- $\beta$ -D-fructo-pyranose). But also other positions of D-fructose are of interest for the design of novel derivatives, *e.g.* for complexation reactions. As aforementioned, C6 as well as C1 can be chemically modified without losing the affinity for the GLUT5 protein. The synthesis of C6-modified D-fructose derivatives is challenging. Starting from D-fructose, the equilibrium between the furanose and pyranose forms result in three primary hydroxyl groups (C1 in pyranose and C1 and C6 in furanose form), which impedes the selective protection of the C6 position. Hence, the synthesis of C6 derivatives usually includes the glycosidic linkage of the anomeric C2 position. Although, the C6 position of D-fructose might be interesting for the synthesis of GLUT5 targeting molecules, the increased number of steps for the synthesis plus the lack of commercially available starting materials effectively diminishes the available derivatives. As a starting point for the synthesis of C6 derivatives of D-fructose, sucrose is a suitable candidate (Figure 2.6). Sucrose contains one unit D-glucopyranose  $\alpha$ -(1 $\rightarrow$ 2)-glycosidically linked to one unit of D-fructofuranose, which prevents ring-opening reactions until this bond is cleaved under acidic conditions.



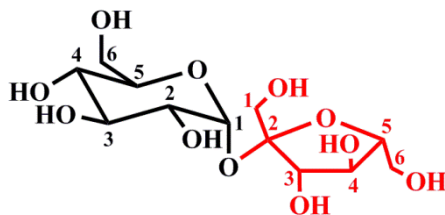
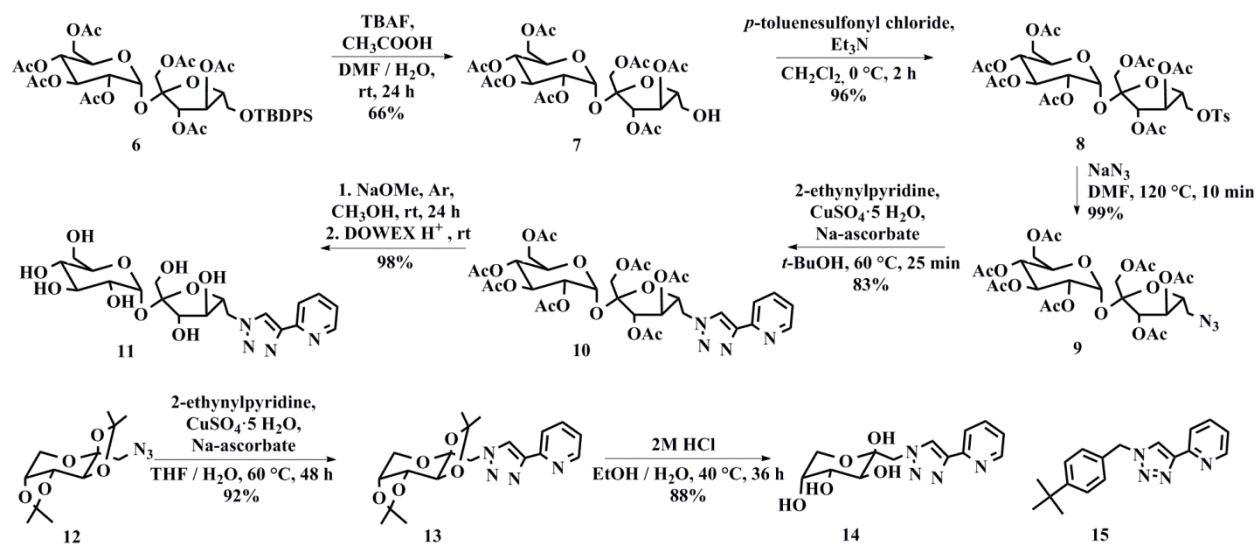


**Figure 2.6:** Schematic representation of the structure of sucrose with one unit of D-glucose (black) and one unit of D-fructose (red).

Our study aimed to modify the C6 position of D-fructose selectively. In a seven-step synthesis, pyridyl triazole group (pyta) as a two-dentate ligand was introduced to the C6 position of D-fructose in the sucrose molecule. Additionally, this group was also attached to the C1 position of D-fructose (Scheme 2.3).



**Scheme 2.3:** Schematic representation of the synthesis of the ligands.

Compound **6** was synthesized according to literature procedures. Starting from commercially available sucrose, the C6 position of the D-fructose unit was blocked with TBDPSCl and separated by column chromatography from di- and trisilylated derivatives. The purified product was acetylated with acetic acid anhydride in pyridine to obtain compound **6**.<sup>[91-92]</sup> Literature procedure for the deprotection of compound **6** includes the use of pyridinium fluoride as fluoride source for the cleavage of the silylether.<sup>[91]</sup> To avoid the formation of highly toxic HF, TBAF was used instead to cleave off the silyl group at the C6 position of the D-fructose unit. Due to the basic character of

TBAF in aqueous solutions, one equivalent acetic acid was added to prevent migration of acetyl groups within the molecule. To introduce the azide functionality, a suitable leaving group for  $S_N2$  conditions had to be installed at the C6 position before. A literature procedure reported the synthesis of mesylated sucrose, which was subsequently substituted using  $\text{NaN}_3$ .<sup>[91]</sup> This procedure could not be reproduced. The formation of compound **9** was hampered, which might be attributed to the stability of mesylated sucrose. Increasing the temperature did not result in a higher yield for compound **9**, but rather led to a cleavage of acetyl groups. Therefore, tosyl chloride was used to prepare tosylated sucrose **8** in high yield (96%). Crystallographic data for compounds **7** and **8** revealed the structure and the purity of these compounds (Figure 2.7).

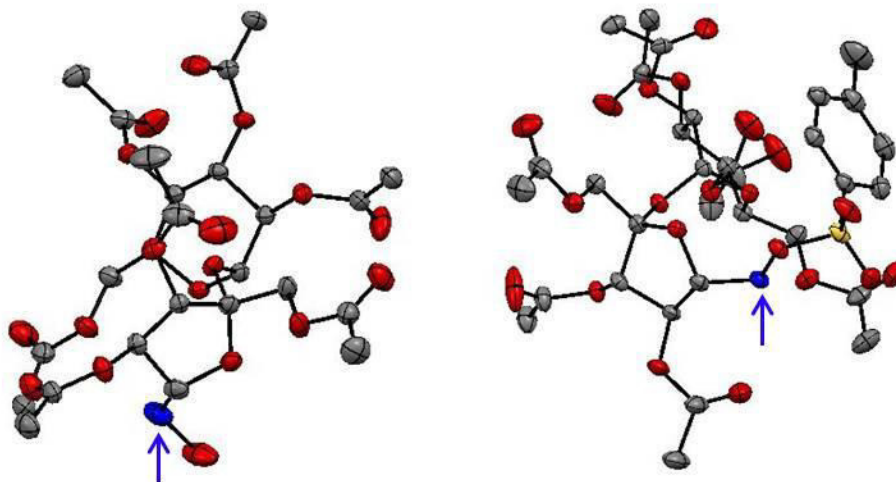


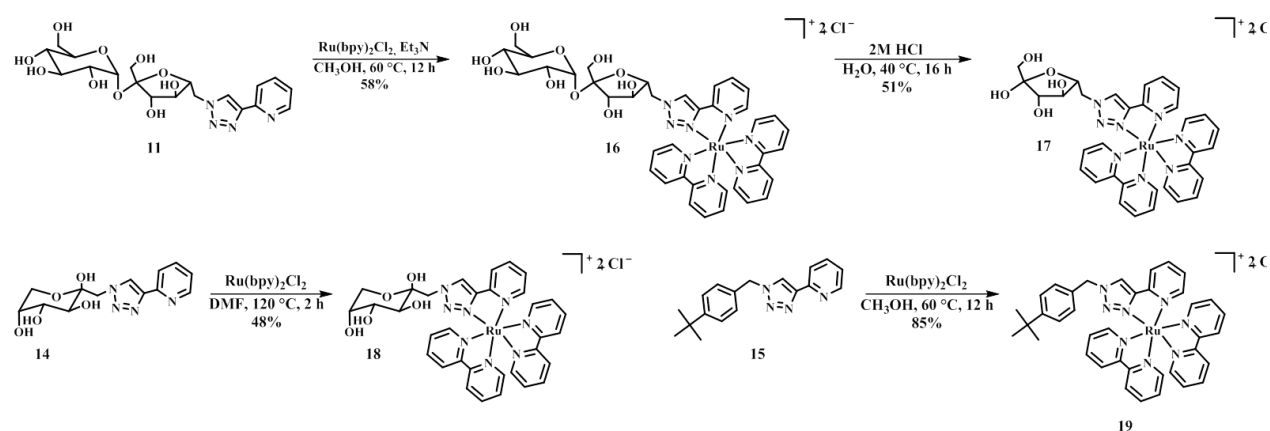
**Figure 2.7:** Schematic representation of the molecular structure of compounds **8** (left) and **9** (right). Crystals were obtained by diffusion of *n*-hexane into a solution of **8**, respectively **9** in  $\text{CHCl}_3$ . Thermal ellipsoids are drawn at 50% probability and hydrogen atoms and atom labels are omitted for clarity. Blue-colored carbons represent the oxygen at the C6' positions of the sucrose derivatives.

Azido-modified sucrose derivative **9** was obtained in quantitative yield after stirring tosylated sucrose **8** at 120 °C in DMF in the presence of  $\text{NaN}_3$  in the microwave. Microwave irradiation of **9** dissolved in a mixture of *t*-BuOH and  $\text{H}_2\text{O}$  with  $\text{CuSO}_4 \cdot 5\text{H}_2\text{O}$  and sodium ascorbate as catalyst forming pair as well as 2-ethynyl-pyridine resulted in the pyta-modified derivative **10** in high yield (83%).<sup>[91]</sup> Zemplén transesterification conditions using NaOMe in dry  $\text{CH}_3\text{OH}$  resulted in water-soluble sucrose derivative **11** bearing the pyta-group at the C6 of D-fructose unit in excellent yield (98%). Pyta-bearing D-fructose itself was not possible to synthesize by using 2 M HCl. ESI-MS investigations as well as thin layer chromatography (TLC) with RP18 coated on glass slides

revealed the formation of multiple side-products. Therefore, **11** was used as ligand for complexation to ruthenium and the D-glucose unit was cleaved off after the complexation reaction.

For comparison, the pyta-functionality was also introduced to the C1 position of D-fructose. Isopropylidene-protected azido-fructose derivative **12** was used and reacted in a Cu(I) catalyzed cycloaddition with 2-ethynyl-pyridine to obtain pyta-modified D-fructose derivative **13** in high yield. Acidic cleavage of acetal groups could be successfully applied by stirring in 2M HCl in H<sub>2</sub>O at 40 °C to yield water-soluble D-fructose derivative **14**. Also for comparison, ligand **15** was synthesized according to a literature procedure.<sup>[93]</sup>

Subsequently, the ligands were reacted with Ru(bpy)<sub>2</sub>Cl<sub>2</sub> to form complexes of the general formula [Ru(bpy)<sub>2</sub>(L)]Cl<sub>2</sub> (Scheme 2.4).



**Scheme 2.4:** Schematic representation of the syntheses of the complexes **16** to **19**.

The complexation reaction of compound **11** was carried out in the presence of Et<sub>3</sub>N to avoid the partial cleavage of the D-glucose unit of sucrose. Cleavage of the glycosidic linkage to form complex **17** was conducted with 2 M HCl in H<sub>2</sub>O. The reaction time was relatively long (> 1 week) and side-products were formed, when ligand **14** was stirred at 60 °C in methanol with the Ru(bpy)<sub>2</sub>Cl<sub>2</sub> precursor. Therefore, the synthesis was performed using a microwave for 2 h at higher temperatures (120 °C). Since the Re(I) tricarbonyl complex of compound **15** revealed high cytotoxicity in HepG2 cells,<sup>[93]</sup> the corresponding ruthenium complex was synthesized in a similar manner to that of ligand **11** and was used for comparison. All complexes were purified by size exclusion chromatography using Sephadex LH-20® in H<sub>2</sub>O (for **16** to **18**) or CH<sub>3</sub>OH (for **19**). <sup>1</sup>H NMR spectra of complex **18** revealed a set of signals (δ = 9.3 to 9.8 ppm) attributed to the triazole

proton of various stereoisomers of compound **18**, when dissolved in deuterated DMSO (Figure 2.8).

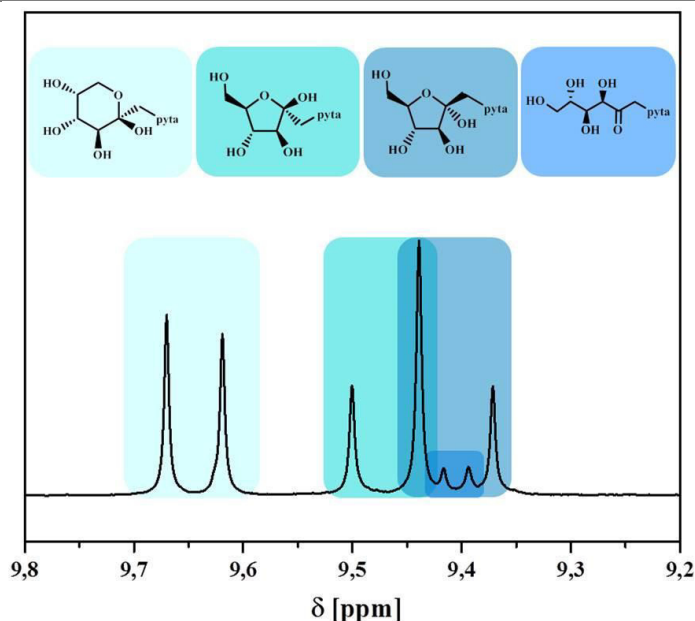


**Figure 2.8:** Zoom into the  $^1\text{H}$  NMR spectrum of **18** dissolved in deuterated DMSO and assignment of different forms of D-fructose to the signals.

An approximate amount of 37.5% of  $\beta$ -D-fructopyranose, 27% of  $\beta$ -D-fructofuranose, 27% of  $\alpha$ -D-fructopyranose and 8.5% of the open-chained form was detected by  $^1\text{H}$  NMR measurement. The ratio of the isomers in solution is strongly dependent from various factors such as pH value, temperature, solvent and others.<sup>[94-96]</sup> Additionally, each signal for the different stereoisomers of the complexes appeared twice and, therefore, indicates the existence of  $\lambda$ - and  $\Delta$ -diastereoisomers at the octahedral coordination spheres of the central Ru complexes. This double set of signals in  $^1\text{H}$  as well as in  $^{13}\text{C}$  NMR spectra was also observable for the other complexes, except for sugar-free complex **19**. Due to three two-dentate ligands in an octahedral coordination sphere, enantiomers should exist for this complex as well. However, the mixture shows a specific rotation of complex **19** ( $[\alpha]^{20}_{\text{D}} = -7.2^\circ$ ;  $c = 0.1 \text{ mg}\cdot\text{mL}^{-1}$ ;  $\text{CH}_3\text{OH}$ ), which indicates the dominance of one enantiomer and the lack of a racemic mixture. Absorption and emission spectra of all compounds were measured in aerated  $\text{CH}_3\text{OH}$ . The absorption bands of the ligands at  $\lambda_{\text{max}} = 280 \text{ nm}$  were associated with  $\pi \rightarrow \pi^*$  transitions. An additional band at  $\lambda_{\text{max}} = 440 \text{ nm}$  for the metal complexes derives from metal to ligand charge transfer (MLCT) transition. Excitation by about  $\lambda_{\text{ex}} = 440 \text{ nm}$  resulted in fluorescence in the visible region at around  $\lambda_{\text{max}} = 600 \text{ nm}$  for all complexes.

To evaluate the complexes regarding their biological properties, cytotoxicity and uptake studies with non-cancerous cell line L929 and breast cancer cell lines MDA-MB-231 and MCF-7 were conducted. As expected, none of the compounds revealed significant inhibition of the metabolic activity of the tested cell lines. Also for this complexes (like observed for the complexes in chapter 2.1), the fluorescence is quenched when measured in aqueous media and, therefore, the uptake studies by fluorescence-based methods are hampered.<sup>[80]</sup> Instead, ICP-MS studies with the Ru complexes were conducted (**Figure 2.9**).

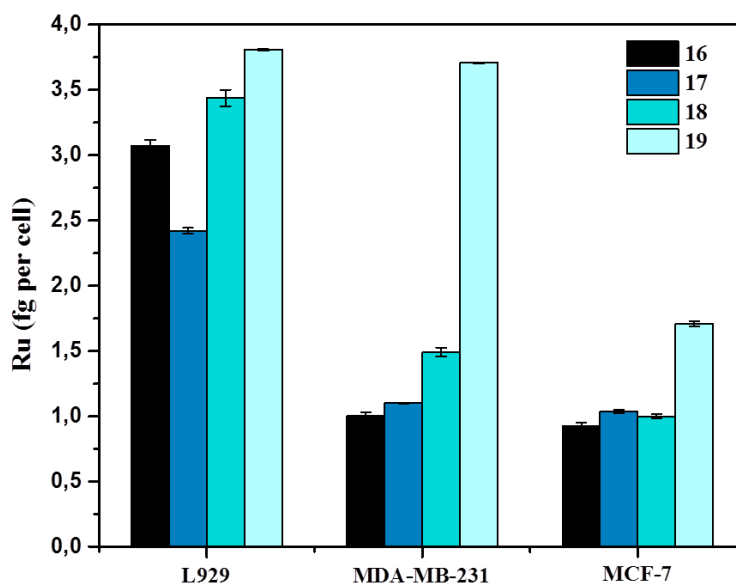


**Figure 2.9:** Uptake of complexes **16** to **19** (Ru in fg per cell). L929, MDA-MB-231 and MCF-7 cells were incubated at 50  $\mu$ M for 1 h. As a control, more cells were not incubated with Ru complexes and no Ru content was determined (Ru < 0.03 fg / cell) by applying the same measurements.

In contrast to the “soft” MS techniques, such as ESI- and MALDI-MS, elemental MS uses high temperature plasma (up to 7000 K) to form completely fragmented metal ions, which can be quantified out of solid, liquid or gaseous samples.<sup>[97]</sup> High sensitivity, accuracy and precision of the analytical data obtained by this method enlarges its application in the life science field.<sup>[98]</sup> Using ICP-MS, the data shows that the sugar-free complex **19** revealed an enhanced, unspecific uptake into all tested cell lines in comparison to the other compounds. This might be attributed to its increased hydrophobicity due to the missing sugar-units, which elevates the diffusion through the non-polar cell membrane. D-Fructose conjugated complexes **17** and **18** did not show any selectivity

for breast cancer cell lines. The results indicate that for this kind of metal complexes no enhanced uptake, independently of the substitution position of D-fructose, is observable.

In summary, in the performed study two D-fructose conjugated Ru complexes of the general formula  $[\text{Ru}(\text{bpy})_2(\text{L})]\text{Cl}_2$  could be synthesized and characterized. Sucrose was used as starting material since D-glucopyranose is  $\alpha$ -(1 $\rightarrow$ 2)-glycosidically linked to D-fructofuranose and, therefore, the anomeric centers are blocked, holding both carbohydrates in a full-acetal form. Using this approach, C6-derivatives of D-fructose are accessible in high yields, which might enlarge the availability of various D-fructose conjugated metal complexes in future investigations.

### 3 Carbohydrate conjugated polymers

Due to their important role in numerous biological events, saccharides gained also interest of polymer chemists. This chapter will focus on the synthesis of different glycopolymers by post-polymerization functionalization procedures. In detail, the first sub-chapter emphasizes the synthesis of D-fructose conjugated linear poly(ethylenimine) and its selectivity for MDA-MB-231 breast cancer cells. The synthesis of saccharide conjugated poly(acrylates) with varying the saccharides and block lengths as well as their lectin-binding ability is subject of the second sub-chapter.

#### 3.1 D-Fructose conjugated linear poly(ethylenimine)

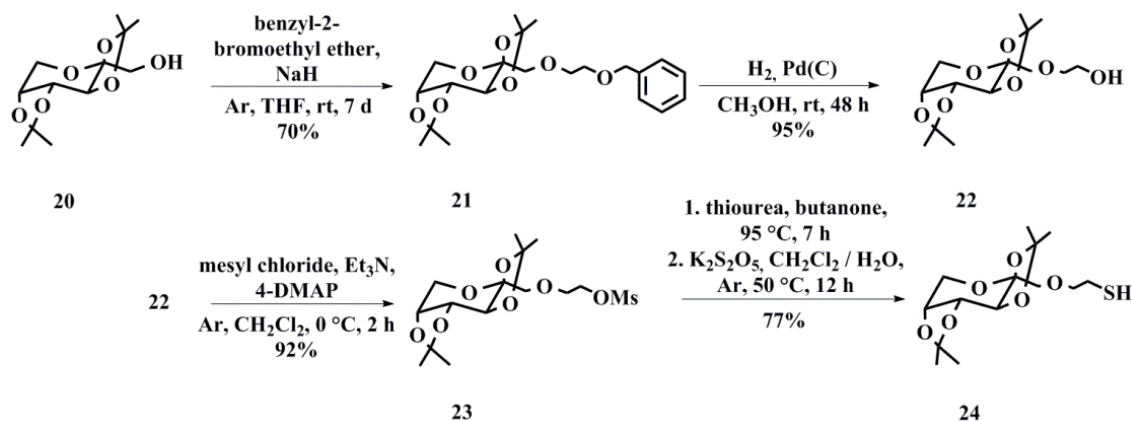
Parts of this chapter have been published in: **P3)** C. Englert, M. Pröhl, J. A. Czaplewska, C. Fritzsche, E. Preußger, U. S. Schubert, A. Traeger, M. Gottschaldt, *Macromol. Biosci.* **2017**, *17*, 1600502.

Since the fundamental importance of the DNA in the control of cellular processes was recognized and the first clinical trial of gene therapy was authorized in the USA in 1990, remarkable progress over the last almost three decades was reached. Various kinds of genetic material, such as DNA, anti-sense oligodeoxynucleotides or small interfering ribonucleic acid (siRNA), were delivered into cells to treat hereditary as well as acquired diseases.<sup>[99]</sup> However, genetic materials have to struggle with some major barriers *in vivo*, which limit their use in clinical applications. Due to their high density of negative charges, the strong hydrophilic genetic materials are not capable to pass the lipophilic cell membrane by diffusion. When administrated systematically, they have to detract macrophages, renal filtration and endogenous nucleases. Once they passed the cell membrane by the endocytic pathway, their efficiency is further restricted by endosomal entrapment, lysosomal degradation and cytosolic viscosity.<sup>[99-102]</sup> Therefore, the stability and efficiency of “naked” genetic material has to be increased by specific gene delivery vectors. Viral vectors offer beneficial

properties, such as intrinsic mechanisms for endosomal escape and high transduction efficiency. They are derived from adeno-, retro- and herpes simplex virus and are the most widely used systems. Unfortunately, their use is restricted by the size of the carried gene and by strong immune responses.<sup>[99]</sup> As an alternative, non-viral vectors are extensively investigated to deliver genes of interest into cells. Those naturally occurring or synthetic materials should be relatively easy to synthesize in large amounts and can be functionalized to enhance their specificity. Many systems, such as cell penetrating peptides,<sup>[103]</sup> antibodies<sup>[104]</sup> and lipid-based carriers<sup>[105]</sup> are used. But also cationic polymers represent a class of candidates forming polyplexes with genetic material due to the positive charges of the polymers. Among the cationic polymers, PEI is used as the gold standard because of its high buffering ability facilitating the endosomal escape of the attached genetic material by the known “proton sponge effect”.<sup>[106]</sup> However, its use is also restricted by various factors. PEI is non-degradable, its polyplexes aggregate during blood circulation *in vivo* and its cytotoxicity depends on the molar mass, structure and concentration of the polymer.<sup>[107]</sup> To overcome these limits the PEI backbone and / or the side-chains can be modified. For instance, PEGylation (poly(ethylene glycol)) is used to form PEI-PEG-copolymers, but non-degradable bonds between PEI and PEG, such as urea and thiourea, require the additional use of a biodegradable linker.<sup>[108]</sup> Also targeting moieties were successfully attached to PEI. Folates,<sup>[109]</sup> RGD peptides<sup>[110]</sup> and antibodies<sup>[111]</sup> were used to target various structures. Another approach represents the attachment of carbohydrates to the PEI backbone to form glycopolymers by post-polymerization functionalization procedures. For instance, D-mannose conjugated PEI was used to deliver DNA into dendritic cells and D-galactose was attached to target hepatocytes.<sup>[112]</sup>

We synthesized a D-fructose conjugated high molar mass linear poly(ethyleneimine) (L-PEI) by a post-polymerization modification procedure using the versatile thiol-ene photo-addition. Furthermore, its biological properties in terms of polyplex formation, breast cancer selectivity and toxicity were evaluated. For this purpose, a thiol-modified D-fructose derivative was synthesized and tested for reaction with double-bond modified L-PEI. First attempts showed a low reactivity between 1-deoxy-1-mercapto- $\beta$ -D-fructopyranose and the double-bond bearing copolymer, which might be attributed to sterical hindrance. Therefore, the introduction of a spacer unit between the sugar-ring and the thiol functionality was necessary (Scheme 3.1).

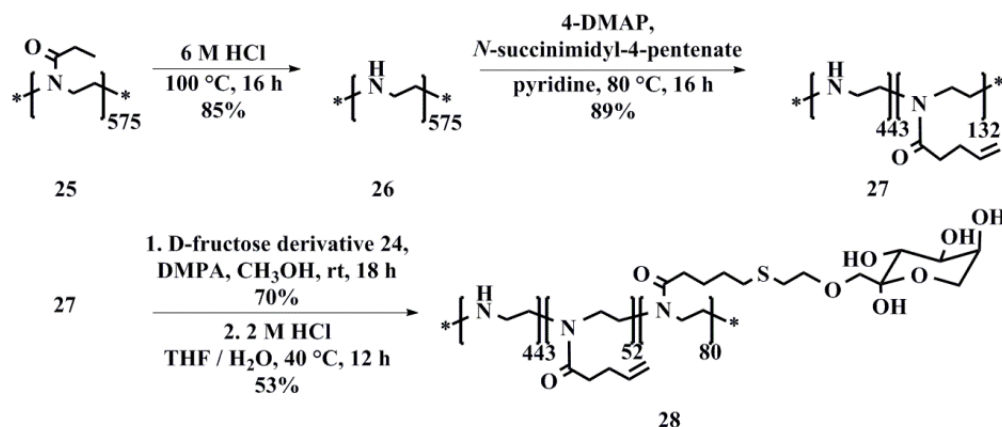




**Scheme 3.1:** Schematic representation of the synthesis of thiol-bearing D-fructose derivative **24**.

Commercially available, protected D-fructose derivative **20** was reacted in a Williamson ether synthesis with benzyl-2-bromoethyl ether to form (2-benzyloxy)-ethyl derivative **21** after purification by column chromatography. The benzyl group was cleaved under reductive conditions with hydrogen and Pd on activated charcoal to obtain 1-(2-hydroxy)-ethyl modified D-fructose **22** in high yield (95%). The novel hydroxyl group was transformed into a leaving group by reaction with mesyl chloride in  $\text{CH}_2\text{Cl}_2$  under an Ar atmosphere and with 4-DMAP as nucleophilic catalyst in accordance to literature procedures.<sup>[113]</sup>  $\text{S}_{\text{N}}2$  reaction with thiourea resulted in the formation of an isothioronium salt, which was hydrolyzed in the presence of  $\text{K}_2\text{S}_2\text{O}_5$  to avoid oxidation of the formed thiol group.

Subsequently, D-fructose conjugated L-PEI was synthesized as depicted in Scheme 3.2.



**Scheme 3.2:** Schematic representation of the synthesis of the D-fructose conjugated L-PEI **28**.

Poly(2-ethyl-2-oxazoline) (PEtOx, **25**) was synthesized by microwave supported cationic ring-opening polymerization according to literature procedures.<sup>[114]</sup> The tosylate signals in the  $^1\text{H}$  NMR were used to calculate the degree of polymerization (DP) of the homopolymer **25**. To obtain L-PEI **26** the amides were hydrolyzed by refluxing with aqueous 6 M HCl for 16 h. The amidation reaction of **26** with the activated acid *N*-succinimidyl-4-pentenat resulted in copolymer **27** with 23% of all ethylenimin units functionalized with terminal ene-group *via* amide linkage.<sup>[115]</sup> The previously synthesized thiol-bearing D-fructose derivative **24** was attached by thiol-ene photo-addition using 2,2-dimethoxy-1,2-diphenylethan-1-one (DMPA) as photo-catalyst. To verify the composition of the copolymer, the integral of the signals of the remained double bonds ( $\delta = 5.9$  ppm) was compared to the integral of the signal of the PEI backbone ( $\delta = 2.5$  to  $2.9$  ppm). Roughly 60% of all double bonds respectively 14% of all repeating units were functionalized with D-fructose. This is also in accordance to the amount of sulfur determined by elemental analysis of the polymers **27** (S: 0%) and **28** (4.66%). A higher degree of functionalization (DF) was not reachable, also not by increasing the irradiation time, amount of catalyst or thiol. This is mainly attributed to the sterical hindrance of the bulky side-chains and by the protection groups of the D-fructose units.<sup>[79]</sup> But a higher content of saccharides attached to PEI does not result inevitably in improved properties. As shown for a library of D-galactose conjugated PEIs with varying DFs, the increase of D-galactose units resulted in a lower transfection efficiency in mouse fibroblasts.<sup>[116]</sup> However, acidic cleavage of isopropylidene groups resulted in copolymer **28**, which represents the first literature-known D-fructose conjugated, cationic polymer. The success of the deprotection was shown by various NMR techniques. The disappearance of signals attributed to isopropylidene

groups and the appearance of signals of various forms of D-fructose in the  $^1\text{H}$  as well as in the  $^{13}\text{C}$  NMR spectra as a result of the formation of hemiketal structures proves the cleavage of the protection groups. Furthermore, diffusion-ordered NMR (DOSY NMR) showed a decrease in the hydrodynamic radius of polymer **28** in comparison to the polymer bearing the protected D-fructose units.

The polymers **26** to **28** were extensively studied in terms of cytotoxicity, hemocompatibility, polyplex formation, cell-type dependent uptake and transfection efficiency.

Cytotoxicity of non-viral vectors represents a major drawback for potential applications. Hence, the polymers were investigated regarding their inhibition effect of the cellular metabolic activities of L929, MDA-MB-231 and a primary human endothelial cells (HUVEC) using the AlamarBlue assay (Figure 3.1).

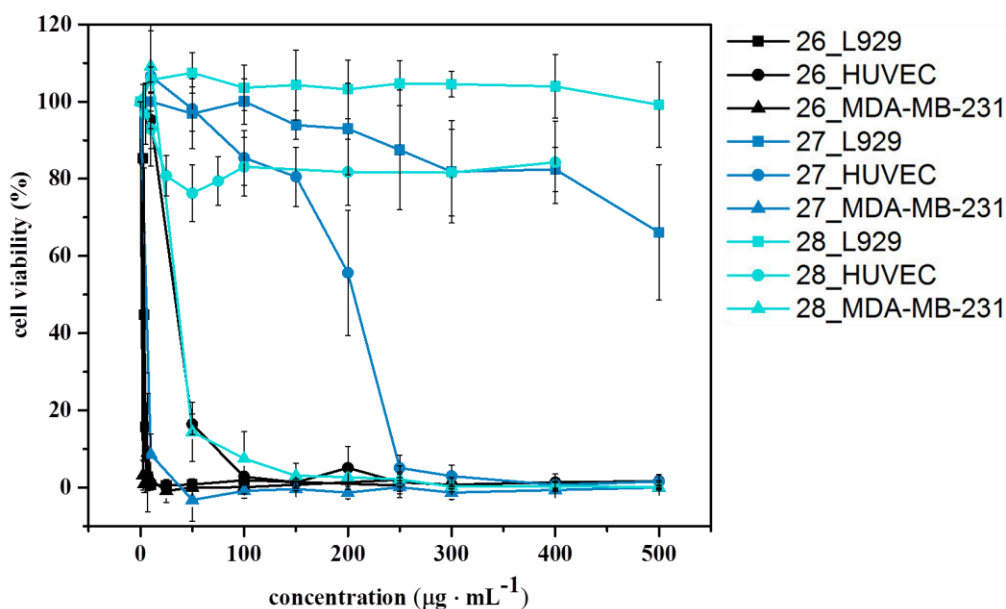


**Figure 3.1:** Relative viability of L929, HUVEC and MDA-MB-231 cells after 24 h incubation with the polymers **26** to **28** at varying concentrations. Values represent the mean  $\pm$  S.D. (n=3).

The cell viability of all tested cell lines was reduced to below 3% for L-PEI **26** at  $100 \mu\text{g} \cdot \text{mL}^{-1}$ , which is in accordance to literature results.<sup>[117]</sup> Compound **27** showed moderate biocompatibility for L929 ( $c \leq 400 \mu\text{g} \cdot \text{mL}^{-1}$ ; viability  $\geq 80\%$ ) and HUVEC cells ( $c \leq 150 \mu\text{g} \cdot \text{mL}^{-1}$ ;

viability  $\geq 80\%$ ). In contrast to that, it inhibited the metabolic activity of MDA-MB-231 cells entirely at  $50 \mu\text{g}\cdot\text{mL}^{-1}$ . D-Fructose bearing polymer **28** revealed a significant reduction of the cell viability of MDA-MB-231 cells to 3% at  $150 \mu\text{g}\cdot\text{mL}^{-1}$  with no significant cytotoxicity over the full concentration range in L929 ( $\sim 100\%$ ) and HUVEC cells ( $\sim 80\%$ ).

Cationic polymers interact with various components of the blood. Due to the formation of bridges between the membranes of red blood cells and the polymer, irreversible erythrocyte aggregation can occur. As a result of this interaction, the viscosity of the blood is increased, which can be harmful for vital organs.<sup>[118]</sup> Furthermore, cationic polymers disrupt the membranes of erythrocytes. This hemolytic effect can be measured by the detection of hemoglobin with spectroscopic methods. Therefore, polymers **26** to **28** were investigated for their erythrocyte aggregation and hemolytic potential (Figure 3.2).

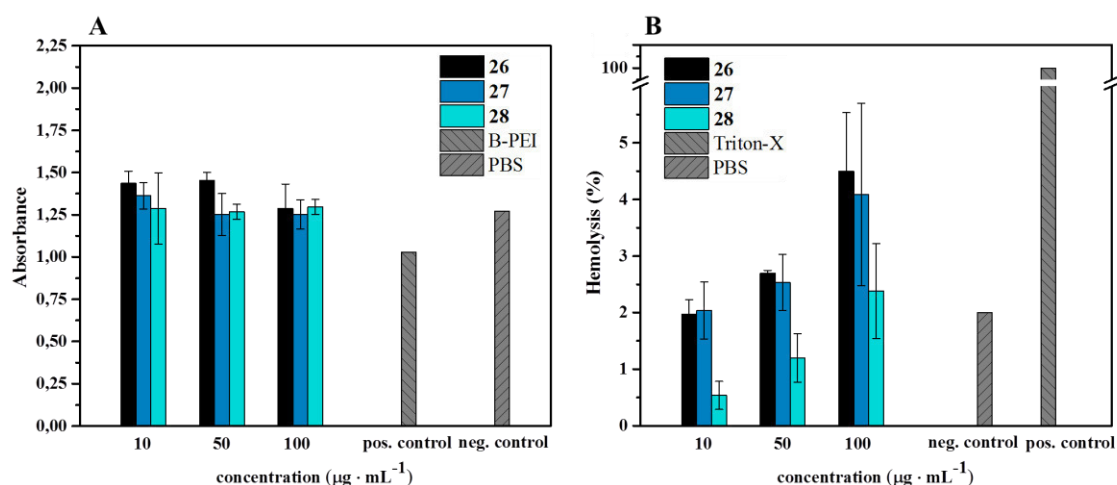


**Figure 3.2:** Investigations of the hemocompatibility. **A.** Erythrocyte aggregation assay of polymers at indicated concentrations. Branched PEI served as positive control and PBS as negative control; **B.** Hemolysis assay of erythrocytes after incubation with polymers at indicated concentrations. Triton X-100 served as positive control (100% hemolysis) and PBS as negative control (1.99%). A value less than 2% hemolysis rate is classified as non-hemolytic, 2 to 5% as slightly hemolytic and  $>5\%$  as hemolytic. Values represent the mean  $\pm$  SD ( $n = 3$ ).

None of the tested polymers (**26** to **28**) showed erythrocyte aggregation up to  $100 \mu\text{g mL}^{-1}$ . Compounds **26** and **27** were slightly hemolytic over the full concentration range, whereas the D-fructose conjugated polymer **28** is non-hemolytic until  $50 \mu\text{g mL}^{-1}$  and only revealed very low hemolytic activity at  $100 \mu\text{g mL}^{-1}$ .

Plasmid deoxyribonucleic acid (pDNA) was used to investigate the binding properties of the polymers with genetic material by using the ethidium bromide assay (EBA). Therefore, the pDNA was pre-incubated with the intercalator ethidium bromide, which results in a fluorescent adduct. When adding a competitor for the negative binding sites of the pDNA, a decrease of the fluorescence is caused due to the displacement of the ethidium bromide by the cationic polymer. Various ratios of polymer (N from nitrogen of the PEI backbone) to DNA (P from phosphate of the DNA backbone) were investigated (Figure 3.3A).

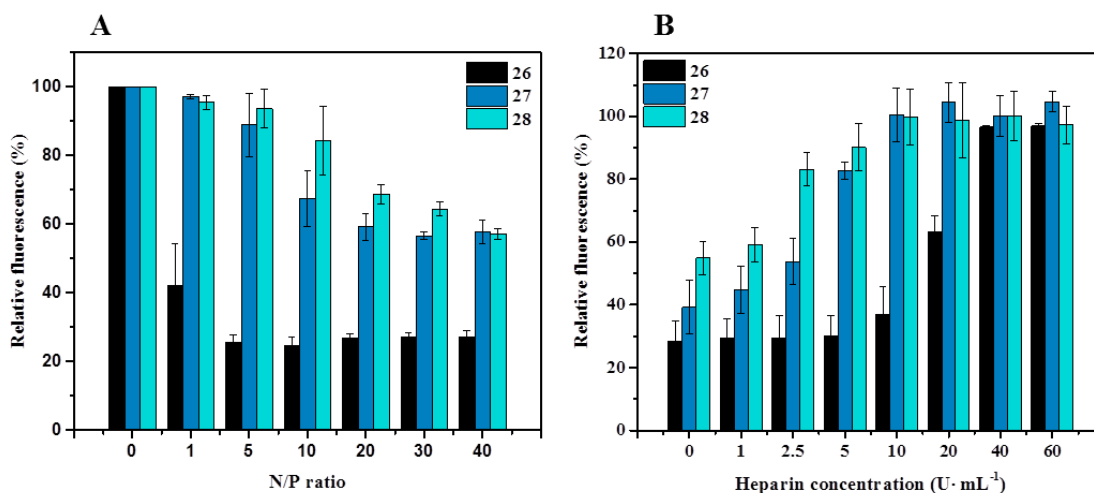


**Figure 3.3:** Investigation of the polyplex formation and stability with plasmid DNA. **A.** Decrease in relative fluorescence (RFU) at indicated N/P ratios; **B.** Dissociation assay of polyplexes formed at N/P 20 using heparin (0-60 U mL<sup>-1</sup>). Values represent the mean  $\pm$  SD ( $n = 3$ ).

Polymer **26** showed a formation of stable polyplexes for N/P ratios between 10 and 40 (~25% RFU). Compounds **27** and **28** showed a fairly constant RFU of around 60% from N/P 20 to 40 for various reasons. The amidation of **26** resulted in the decrease of 23% of available nitrogen atoms for the polyplex formation for compound **27** and **28**. Additionally, sterically demanding side-chains and the attached D-fructose units lower effectively the binding of the polymers to pDNA and, therefore, increasing the RFU. The obtained data is in accordance to comparable polymers.<sup>[119]</sup>

For the evaluation of the stability of the polyplexes and the release of the genetic material, the heparin assay was used. Heparin is a highly negatively charged glycosaminoglycan, which competes with the pDNA in the polyplex.<sup>[120]</sup> If added together with ethidium bromide, the increasing RFU is proportional to the displacement of the nucleic acid out of the polyplex and the

subsequent formation of the fluorescent DNA adduct (Figure 3.3B). The pDNA of polyplexes of **27** and **28** was rapidly released ( $\sim 100\%$ ) after adding only  $10 \text{ U} \cdot \text{mL}^{-1}$  heparin, whereas the full pDNA release of the polyplexes of L-PEI (**26**) required higher amounts of heparin ( $40 \text{ U} \cdot \text{mL}^{-1}$ ).

Also the size of the polyplexes is of great importance for their properties, since the size of nanocarriers is recommended to be below 200 nm for an effective uptake into cells.<sup>[121]</sup> All polyplexes of the polymers with pDNA revealed favorable sizes, when their dispersions in HBG buffer were analyzed by DLS (Table 3.1).

**Table 3.1:** Size and zeta potential of pDNA polyplexes of **26** to **28** at N/P = 20 in HBG buffer, measured by dynamic and electrophoretic light scattering.

Abbrev.	z-Average ( $\text{d} \cdot \text{nm}^{-1}$ )	PDI	Number-weighted size ( $\text{d} \cdot \text{nm}^{-1}$ )	Zeta potential (mV)
<b>26</b>	$217 \pm 8$	0.47	$71 \pm 13$	$24.0 \pm 0.4$
<b>27</b>	$264 \pm 11$	0.35	$109 \pm 33$	$24.3 \pm 1.1$
<b>28</b>	$165 \pm 1$	0.26	$83 \pm 29$	$17.6 \pm 0.4$

Another crucial parameter for the design of non-viral gene delivery vectors represents the effective uptake of the functionalized polyplexes into cells. Non-functionalized polyplexes are shown to be internalized by an endocytic pathway with subsequent release of the pDNA in the cytosol into many cells in an unspecific fashion.<sup>[122]</sup> The functionalization with D-fructose was aimed to target the GLUT5 transporter. As a consequence, GLUT5 overexpressing cell lines, such as MDA-MB-231, should reveal a higher uptake of the polyplexes of **28** relative to these of **26** and **27**. This was investigated using flow cytometry and CLSM. Therefore, the used pDNA was pre-incubated with YOYO-1, a DNA specific dye with a high fluorescence intensity once intercalated and with no displacement during the polyplex formation.

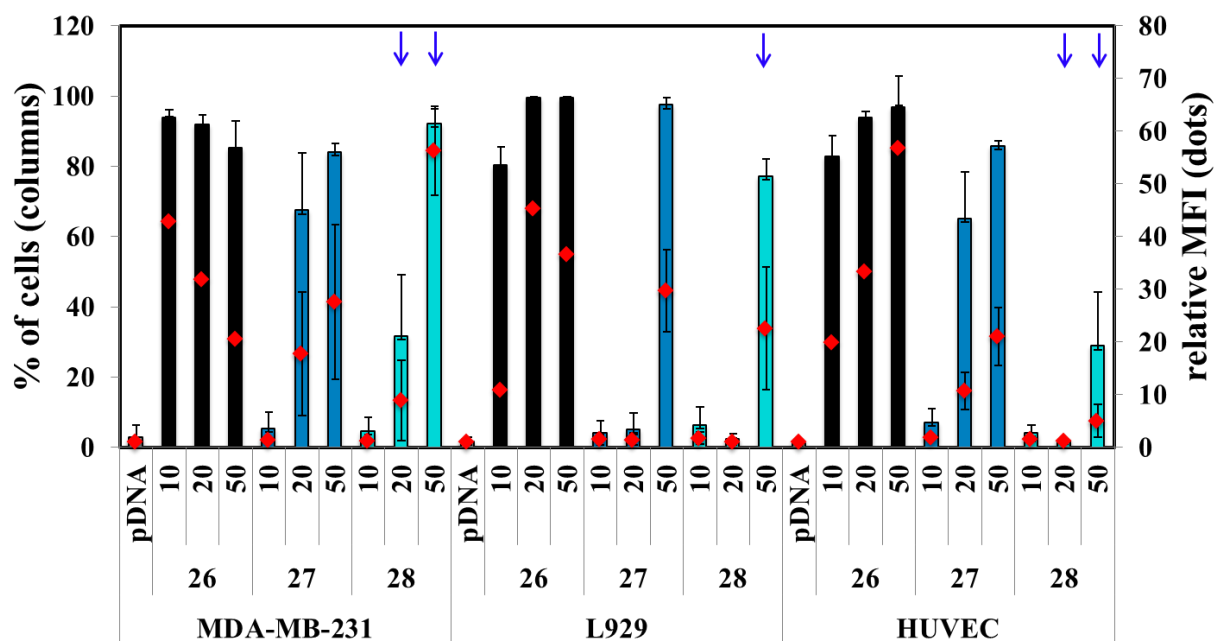


**Figure 3.4:** Polyplexes of **26** to **28** with YOYO-1 labeled pDNA were incubated with L929, HUVEC, and MDA-MB-231 cells for 1 h at indicated N/P ratios. The percentages of cells (columns), which have taken up pDNA polyplexes as well as the mean fluorescence intensity (MFI) of all viable cells compared to pDNA control without polymers were depicted. Values represent the mean  $\pm$  SD ( $n \geq 3$ ).

As expected, the non-functionalized polymer **26** showed an unspecific, strong uptake into all cell lines for all N/P ratios. Polyplexes of **27** revealed no uptake in any cell line for N/P = 10, a slight uptake into HUVEC and MDA-MB-231 cells for N/P = 20 and an enhanced unspecific uptake into all cell lines for N/P = 50. In contrast to that, polyplexes of D-fructose bearing polymer **28** were exclusively incorporated by breast-cancer MDA-MB-231 cells at N/P = 20. At N/P = 50 polyplexes of **28** were taken up more into MDA-MB-231 cells and to a lower extent into all other cell lines relative to the polyplexes of **26** and **27**, emphasizing the selectivity of **28** towards GLUT5 overexpressing cells. To further investigate the uptake mechanism and to rule out distortive effects, such as sticking of the polyplexes at the cell membranes, CLSM studies of labeled polyplexes were performed. Before the polymers were stirred in an appropriate solvent and adding the reactive derivative cyanine-5-NHS-ester for **26** or rhodamin B isothiocyanate for **27** and **28**. Free dyes were removed by precipitating the labeled polymers, re-dissolving the precipitated solid and dialysis against  $H_2O$ . Under consideration of the distinct labeling efficiencies, the labeled polymers were mixed with different amounts of their unlabeled counterparts and were incubated with MDA-MB-

231, L929 and HUVEC cells. The CLSM data is in accordance with the results obtained by flow cytometry and revealed the uptake of the polyplexes into the cells with location in the cytosol.

After formation of the polyplexes and uptake into the cells of interest, the ultimate aim of non-viral vectors is the release of the cargo into the cell. This can, *e.g.*, be monitored by the expression of the enhanced green fluorescent protein (EGFP), which is coded on a pDNA applying a standard procedure. For the polymers **26** to **28** the genetic material was released up to 30% from the polyplexes for **26** and up to 40% for **27**, whereas **28** revealed only transfection efficiencies lower than 1% for all investigated N/P ratios. This is most probably attributed to the complex interaction between polyplexes and cell components. Usually, polyplexes release their cargo after the endosomal escape mediated by the proton sponge effect. The accumulation of weak basic groups inside the endosome increases its osmolarity and, as a consequence, the endosomes swell and release their content into the cytosol.<sup>[123]</sup> Due to the modification of the PEI backbone by amidation reaction, only 77% of all amines are available for protonation, which effectively reduces the swelling behavior.

In summary, a D-fructose conjugated L-PEI could be synthesized and evaluated for its biological properties. A novel, thiolated D-fructose derivative was reacted with modified L-PEI *via* photocatalyzed thiol-ene addition in high yield. The deprotected polymer **28** showed a pool of beneficial properties in terms of its use as non-viral vector. Surprisingly, just the polymer **28** revealed already a cell-specific toxicity in breast cancer cell line MDA-MB-231 without affecting the viability of the other cell lines on a significant level in comparison to polymers **26** and **27**. Furthermore, it shows an enhanced hemocompatibility relative to the other tested materials. Polymer **28** forms with pDNA stable polyplexes of advantageous size regarding efficient delivery for N/P ratios above 20 and it requires only small amounts of the competitor molecule heparin to release the pDNA. The uptake of the dye-labeled polyplexes was quantified by flow cytometry and CLSM. The polyplexes containing D-fructose bearing polymer **28** exhibited specific uptake into MDA-MB-231 cells at N/P = 20 in comparison to the other polyplexes. Unfortunately, the transfection efficiency was strongly decreased even when compared to the already low transfection efficiencies of compounds **26** and **27**. This might be attributed to the decreased amount of secondary amines in the backbone and, therefore, to the reduced proton sponge effect. Increased transfection efficiencies, in particular for the use of around 250 times smaller and more rigid siRNA, might be reachable by using B-PEI instead of L-PEI.<sup>[124]</sup> But also the molar mass of the polymers matters. The properties of polyplexes



containing siRNA and B-PEI of different molar masses were shown to be strongly dependent of the molar mass of the polymer: The polyplexes of high molar mass B-PEI showed an enhanced stability and uptake.<sup>[125]</sup> Also, the decrease of the sugar-content might result in higher transfection efficiencies due to the higher amounts of secondary amines available for protonation. However, by changing parameters to reach higher transfection efficiencies, it should be also noted that this might influences other properties, such as polyplex formation, toxicity and stability. Therefore, further systematic studies are required.

### 3.2 Carbohydrate conjugated polyacrylates

Parts of this chapter have been published in: **P5)** M. Pröhl, C. Englert, M. Gottschaldt, U. S. Schubert, J. C. Brendel, *J. Polym. Sci., Part A: Polym. Chem.* **2017**, 55, 3617-3626.

The interactions between saccharides and proteins play central roles on a cellular level in cell adhesion and differentiation, viral replication, inflammation, parasitic infection as well as other processes.<sup>[3, 126]</sup> Lectins represent a group of important proteins, responsible for selective binding of carbohydrates with high stereo-specificity. Whereas a single saccharide reveals only low binding affinity to its natural ligand, multivalency, caused by the interaction between multiple carbohydrates with one lectin molecule and / or the formation of higher-order clusters of multiple lectins, is of fundamental importance in nature.<sup>[5, 8]</sup> In light of this, the so-called “cluster effect”<sup>[127]</sup> strongly emphasizes the need of well-defined polymers bearing carbohydrate residues (glycopolymers) to address the multivalency in cell-cell communications by artificial entities bearing multiple sugar residues.

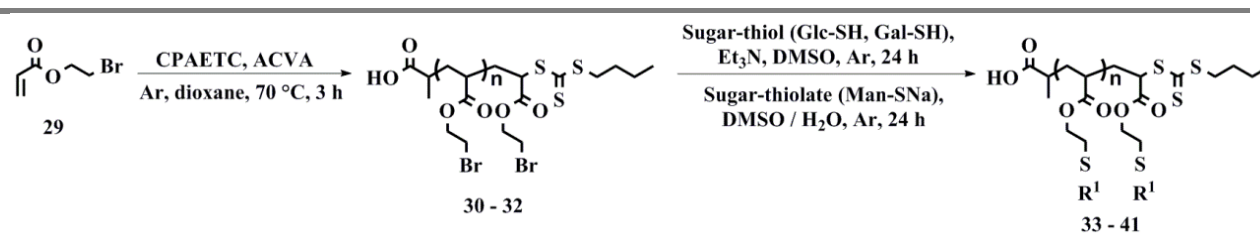
Glycopolymer architectures can be obtained in two different ways: Polymerization of carbohydrates functionalized with polymerizable groups (glycomonomers) or the functionalization with carbohydrates after polymerization of reactive monomers (post-polymerization functionalization). Glycopolymers were obtained by polymerizing various glycomonomers using free radical,<sup>[128]</sup> controlled radical,<sup>[129-130]</sup> anionic,<sup>[131]</sup> cationic,<sup>[132]</sup> ring-opening<sup>[133]</sup> and other polymerization techniques.<sup>[134]</sup> However, the use of glycomonomers also reveals disadvantages,

such as multi-step synthesis of the glycomonomers, incompatibility of unprotected carbohydrates with various polymerization techniques and challenging synthesis of polymers with high molar masses as well as narrow distributions.<sup>[135]</sup> Alternative post-polymerization functionalization procedures include the uses of various reactive groups, such as *para*-fluoro-phenyl,<sup>[136]</sup> alkynyl-,<sup>[137]</sup> alkenyl-groups<sup>[138]</sup> and others.<sup>[135]</sup>

The S<sub>N</sub>2 substitution of halide-containing polymers with suitable nucleophiles represents a relatively unexplored reaction in the design of glycopolymers. This might be attributed to the sensitivity of halides against abstraction by radicals and, therefore, to the limited use of reversible deactivation radical polymerization (RDRP) techniques. However, alkyl halides offer great reactivity in terms of post-modification by substitution reactions with suitable nucleophiles. Poly(epichlorhydrin) (PECH) was reacted with a SH-bearing derivative of D-glucose to form bristle-like polymers.<sup>[4]</sup> Stenzel and coworkers showed the synthesis of poly(vinyl benzylchlorid) (PVBC) *via* reversible addition-fragmentation chain transfer polymerization (RAFT). Equimolar amounts of the sodium salt of 1-SH-D-glucose were used to substitute the chloride in the polymer and to form glycopolymers with moderate dispersities.<sup>[139]</sup> Furthermore, the Perrier group showed the synthesis of poly(bromoethyl acrylate) (PBEA) and the post-substitution with various nucleophiles, including *P*- (*e.g.* trimethylphosphine), *N*- (*e.g.* sodium azide) and *S*-nucleophiles (*e.g.* thiophenol) emphasizing the versatility of this polymer scaffold.<sup>[140]</sup>

The study aimed to synthesize glyco-homopolymers by controlled radical polymerization techniques with low dispersities and DPs exceeding 100 units. The DP of the obtained polymers ranges from 45 to 115 and various saccharides were attached, in detail D-glucose, D-galactose as well as D-mannose, by post-polymerization functionalization. Additionally, the affinity of the synthesized polymers for the lectin concanavalin A (Con A) was investigated using turbidimetry experiments.

The polymers were synthesized as depicted in Scheme 3.3.



**Scheme 3.3:** Schematic representation of the polymer syntheses.

Monomer **29** was obtained in higher purity than in reported procedures<sup>[140]</sup> due to the removal of side-products by stirring with 0.1 M NaOH<sub>(aq)</sub> with subsequent vacuum distillation. Therefore, it could be used to form PBEA *via* RAFT without loss of control with (4-cyanopentanoic acid)ylethyl trithiocarbonate (CPAETC) as chain transfer agent (CTA) and AIBN (azobisisobutyronitrile) as radical initiator. By varying the ratio [monomer]·[CTA]<sup>-1</sup>, various DPs were obtained with good conversions (>55%), low dispersities ( $\bar{D} \leq 1.2$ ) and narrow distributions (Table 3.2).

**Table 3.2:** List of polymers obtained by polymerization of BEA.

Abbrev.	[M] <sub>0</sub> /CTA	[CTA]/I <sub>0</sub>	conv. <sup>a)</sup> (%)	M <sub>n,th</sub> <sup>b)</sup>	M <sub>n,NMR</sub> <sup>c)</sup>	M <sub>n,SEC</sub> <sup>d)</sup>	Đ
				g·mol <sup>-1</sup>			
<b>30</b>	60	10	75	7,600	8,300	8,800	1.10
<b>31</b>	100	10	78	15,700	14,200	11,200	1.21
<b>32</b>	200	10	58	22,700	20,800	18,000	1.11

<sup>a)</sup> Determined from <sup>1</sup>H NMR of the polymerization mixture before precipitation. <sup>b)</sup> Calculated from monomer conversion. <sup>c)</sup> Determined from <sup>1</sup>H NMR end-group analysis (calculated from signal intensity of the proton of the tertiary C-atom next to trithiocarbonate (δ = 4.93 ppm) in comparison to the proton signal of the C1 atom of the acryl ester (δ = 4.43 ppm) before post-polymerization modification). <sup>d)</sup> SEC: DMAc + 0.21 wt.% LiCl, polystyrene calibration.

Post-polymerization functionalization was carried out using thiol(ate) modified carbohydrates D-glucose, D-galactose and D-mannose (Table 3.3).

**Table 3.3:** List of glycopolymers synthesized in this study.

Abbrev.	DP <sup>a)</sup>	Attached sugar (R <sup>1</sup> )	M <sub>n,th</sub> <sup>b)</sup>	M <sub>n,SEC</sub> <sup>c)</sup>	Đ
				g·mol <sup>-1</sup>	
<b>33</b>	45	Glc	13,500	10,000	1.19
<b>34</b>	45	Gal	13,500	9,900	1.22
<b>35</b>	45	Man	13,500	3,300	1.44
<b>36</b>	78	Glc	23,200	17,400	1.25
<b>37</b>	78	Gal	23,200	16,400	1.28
<b>38</b>	78	Man	23,200	9,400	1.34
<b>39</b>	115	Glc	34,100	23,300	1.26
<b>40</b>	115	Gal	34,100	23,300	1.28
<b>41</b>	115	Man	34,100	15,900	1.33

<sup>a)</sup> DP was assumed from precursor polymers **30** to **32**. <sup>b)</sup> The theoretical Mn was calculated assuming 100% substitution of the Br. <sup>c)</sup> SEC: H<sub>2</sub>O, 0.1 M NaNO<sub>3</sub>, 0.05% NaN<sub>3</sub>, Pullulan calibration.

D-Glucose and D-galactose were attached using 1.1 equivalents of their deprotected 1-SH-derivatives by stirring them together with the respective polymer in DMSO in the presence of Et<sub>3</sub>N for 24 h. D-Mannose was conjugated using 1.1 equiv. of 1-deoxy-1-mercaptothiolate- $\alpha$ -D-mannopyranose in a DMSO-H<sub>2</sub>O mixture without any base. All low molar mass impurities were separated by dialysis vs. H<sub>2</sub>O (molecular weight cut-off [MWCO] 3.5 kDa). The polymers were analyzed by various techniques, including <sup>1</sup>H and DOSY NMR as well as by elemental analysis (Table 3.4) and SEC (Figure 3.5).

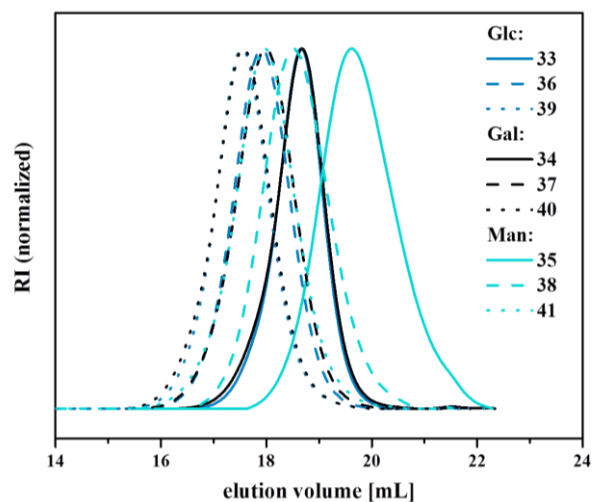


**Figure 3.5:** SEC traces of polymers **33** to **41** (H<sub>2</sub>O, 0.1 M NaNO<sub>3</sub>, 0.05% NaN<sub>3</sub>, Pullulan standard).

The attachment of sugar residues resulted in the increase of the hydrodynamic volume relative to the polymers **30** to **32** and the SEC traces appeared mono-modal with narrow dispersities ( $\mathcal{D} \leq 1.50$ ). Using only a slight excess of the sugar resulted in the lack of side-reactions, such as cleavage of the CTA with subsequent disulfide formation, in comparison to previous studies.<sup>[140]</sup> The increased dispersities are caused by the use of different SEC systems for polymers **30** to **32** and for **33** to **41**. The interaction of the glycopolymers with the column material was also responsible for the decreased  $M_n$  of the D-mannolysated polymers relative to all other glycopolymers, although the hydrodynamic radius should be comparable. One difference between the attached aldoses represents the axial alignment of the OH group at the C2 atom in D-mannose, whereas the other aldoses possess equatorial orientation at this position. Therefore, as the reason for the later elution the interaction between the hydroxyl group at the C2 of D-mannose and the column material and / or the polymeric backbone is proposed.

The DF was calculated to further evaluate the substitution reactions and some tendencies are mentionable (Table 3.4).

**Table 3.4:** Elemental compositions of polymers **30** to **41**.

Abbrev.	DP	Saccharide	Elemental composition <sup>a)</sup> (%)				DF <sup>b)</sup> (%)
			C	H	S	Br	
<b>30</b>	45	-	<b>33.74</b>	<b>4.00</b>	<b>1.16</b>	<b>43.35</b>	-
<b>33</b>	45	Glc	43.87	6.17	10.81	0.89	97.9
<b>34</b>	45	Gal	41.88	6.13	11.99	1.99	95.4
<b>35</b>	45	Man	43.76	6.27	10.36	0	100
<b>31</b>	78	-	<b>33.66</b>	<b>3.97</b>	<b>0.68</b>	<b>43.89</b>	-
<b>36</b>	78	Glc	44.15	6.18	9.48	2.14	95.1
<b>37</b>	78	Gal	43.28	6.18	9.31	3.09	93
<b>38</b>	78	Man	43.80	6.14	10.45	0	100
<b>32</b>	115	-	<b>33.63</b>	<b>3.96</b>	<b>0.46</b>	<b>44.12</b>	-
<b>39</b>	115	Glc	43.53	6.20	10.20	1.54	96.5
<b>40</b>	115	Gal	41.73	6.05	10.58	2.52	94.3
<b>41</b>	115	Man	43.83	6.16	10.42	0.36	99.2

<sup>a)</sup> Elemental composition of starting polymers **30** to **32** was calculated assuming one polymer species with the depicted DP. <sup>b)</sup> Calculated DFs are based on theoretical Br content of polymers **30** to **32**.

The DFs range from 93 to 100%, indicating high efficiency. The D-mannosylated polymers **35**, **38** and **41** showed a remaining Br content between 0% and 0.36%, which represents also the lower detection limit of the determination of the elemental composition. This effect might be attributed to the use of sodium thiolate instead of the thiol and a suitable base.

An important variable for potential applications represents the ability to bind to lectins, which are specific for the respective sugars. Con A is a binding protein which is specific for  $\alpha$ -D-mannose and  $\alpha$ -D-glucose. It consists of aggregates of 25 kDa units and is predominantly existing as tetramers above pH = 7.<sup>[141]</sup> By adding glycopolymers with suitable carbohydrate residues to a solution of Con A, various aggregates are precipitating time-dependently.<sup>[142]</sup> The change in the turbidity can be monitored in real-time by measuring the absorbance at  $\lambda = 420$  nm over the time

immediately after mixing the solutions. The slope of the steepest portion of the initial curve was determined and represents the clustering rate  $k_c$  expressed in arbitrary units per second (a.u. · s<sup>-1</sup>).<sup>[143]</sup> The initial increase of the turbidity is caused by isolated Con A polymer clusters, whereas the formation of cross-linked clusters of higher order is attributed to later points.<sup>[144]</sup> The results are summarized in Figure 3.6.

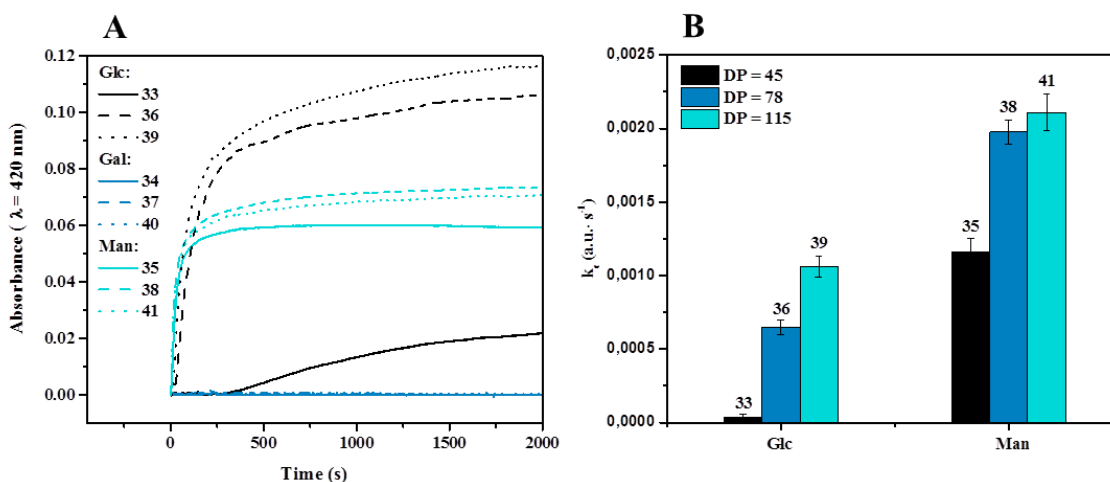


**Figure 3.6:** Results of the turbidimetry assays. **A.** Absorbance ( $\lambda = 420$  nm) curves after adding 1 mL solutions of polymers **33** to **41** (50  $\mu$ M per sugar unit) to 1  $\mu$ M solutions of Con A in HBS buffer; **B.** Calculated rates of clustering between Con A tetramers and D-glucosyl- or D-mannosylated polymers obtained by a linear fit of the steepest portions of the curves,  $k_c$  values represent the average of three replicates.

As previously reported,<sup>[136]</sup> D-galactosylated polymers did not form measurable amounts of Con A clusters, whereas D-glucosylated and D-mannosylated polymers aggregated in the presence of Con A with varying clustering rates  $k_c$ . Due to the higher binding affinity of Con A towards  $\alpha$ -D-mannose in comparison to  $\alpha$ -D-glucose and the use of  $\beta$ -D-glucose in polymers **33**, **36** and **39**, the  $k_c$  values for the polymers grafted with D-mannose are higher than for the corresponding D-glucosylated compounds. The high clustering rates, obtained for **35**, **38** and **41**, indicate the rapid precipitation of most of the Con A tetramers, whereas D-glucose bearing polymers revealed a slower, but continuous increase in turbidity, which indicates to secondary interactions, such as the formation of higher-order clusters. Also the comparison of polymers with the same sugar residues, but with different DP values, revealed general tendencies. The clustering rates increase with increasing DP for both kinds of saccharide bearing polymers, which is also in accordance with literature reports.<sup>[144-145]</sup> The clustering rates of the investigated D-mannosylated polymers seem to

approximate to a constant level with higher DPs. Therefore, no large increase for  $k_c$  is expected for D-mannosylated polymers of this structure with DPs higher than 115.

To investigate the strength of the previously formed clusters, competition experiments were conducted. Hence, the precipitate was allowed to rest for additional 2 h to ensure that all secondary interactions are past and a large excess of  $\alpha$ -D-methyl-mannopyranose ( $\alpha$ MeMan) was added.  $\alpha$ MeMan represents a competitor for the binding sites of the Con A and as a result, the clusters were dissolved again and the change in the turbidity is monitored by the absorbance at  $\lambda = 420$  nm over the time immediately after adding the competitor (Figure 3.7).

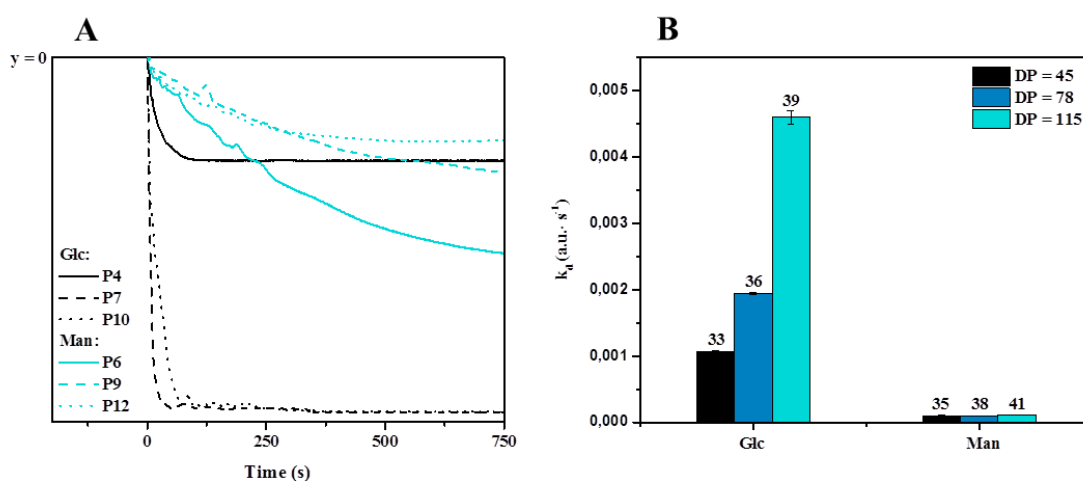


**Figure 3.7:** Results of the competition assays. **A.** Absorbance ( $\lambda = 420$  nm) curves after adding 0.2 mL solution of  $\alpha$ MeMan (54 mM) to the polymer solutions (50  $\mu\text{M}$  per sugar unit) in HBS buffer. **B.** Calculated rates of the reverse interaction between Con A aggregates and the competitor  $\alpha$ MeMan obtained by a linear fit of the steepest portions of the curves.

The dissolution rates  $k_d$  of the polymers grafted with D-glucose are strongly enhanced in comparison to the D-mannosylated polymers, indicating a rather weak interaction between Con A and the D-glucosylated polymers. Additionally, the turbidity caused by clusters of D-glucosylated polymers was decreasing faster to a constant level with increasing DP. In contrast to that, aggregates of polymers bearing D-mannose revealed very slow  $k_d$  values. The decrease of the turbidity was slow, but continuous to a constant level, which indicates the formation of stable clusters and which might hint to an incomplete dissolution of the precipitated aggregates. This can be shown by comparing the difference between the highest and lowest absorption after adding Con A to the polymer solutions with the difference obtained after adding  $\alpha$ MeMan (Figure 3.8).



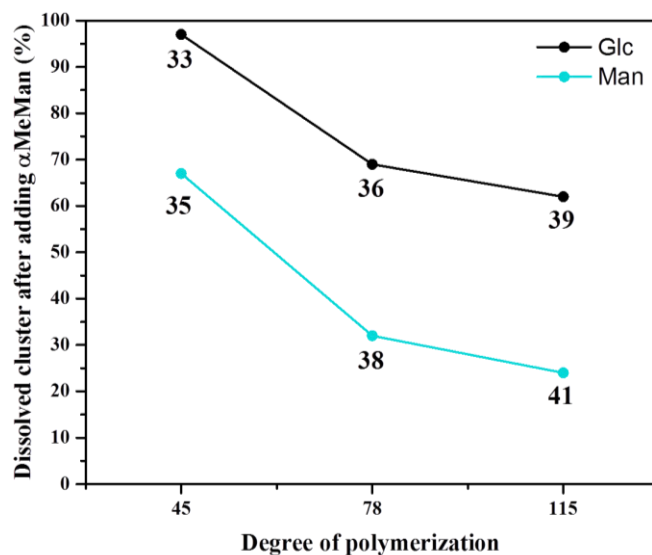


**Figure 3.8:** Ratio of the dissolved Con A polymer clusters after adding  $\alpha$ MeMan relative to the DP. The values were calculated by the ratio of the moduli of the difference between the highest and lowest absorbance after adding  $\alpha$ MeMan or Con A to the polymer solutions, respectively.

Previously reported examples commonly showed the full dissolution of clusters of D-glucosylated polymers and Con A.<sup>[143]</sup> In contrast to that, the presented D-glucosylated polymers **36** and **39** (69% or 62% re-dissolved clusters, respectively) revealed an incomplete dissolution despite the addition of the competitor  $\alpha$ MeMan in around 1000 fold excess. For the D-mannosylated polymers **35**, **38** and **41** an even higher stability of the clusters was observable, which is attributed to the flexibility of the polymeric backbone and therefore, to the increased interaction with the Con A tetramers.

In summary, a library of new glycopolymers was synthesized by RAFT polymerization of BEA monomer with subsequent  $S_N2$  reaction using various thiol(ate) aldoses, in detail D-glucose, D-galactose and D-mannose. Precursor polymers **30** to **32** were obtained with good conversions and different DPs. A DP of up to 115 could be achieved by changing the ratio  $[\text{monomer}] \cdot [\text{CTA}]^{-1}$ . In contrast to literature examples, this approach can be used to synthesize linear and reactive homopolymers with large DPs ( $> 100$ ) and high control during the polymerization. The DF of the  $S_N2$  reactions ranges from 93 to 100% and showed the efficiency of this approach. The carbohydrates were attached using only slight excesses of the deprotected thiol(ate) derivatives. Only non-toxic side-products were produced, which could be easily removed by dialysis in water. By the use of protected carbohydrates to functionalize the polymers, the backbones of the different blocks should not contain functionalities which have the same lability than the protection groups

of the sugar residues. This thought is obsolete by using the presented approach for the synthesis of co-polymeric architectures containing base- or acid-labile groups. The turbidity measurements of the synthesized polymers with Con A revealed an incomplete dissolution of the Con A cluster of the D-mannosylated polymers, which was not reported yet. It could be also possible to address higher DP values and to synthesize larger polymers, to vary the epitope density of one or more residues of different saccharides. Also the use as hydrophilic block in various block copolymers and their assemblies in water are worth to investigate. The attachment of D-fructose by using the sodium salt of the thiol derivative and the precursor polymer(s) would represent an interesting strategy for the synthesis of D-fructosylated (co-)polymers. All structural modifications could also be investigated regarding their affinity to suitable binding proteins to gain deeper insights into the multivalency as a central concept in nature.

## 4 Summary and outlook

The present thesis describes the synthesis, characterization and biological evaluation of D-fructose conjugated molecules. The work focused on two different classes of compounds: On one hand low molar mass metal complexes and on the other hand polymers with complete different types of interaction with GLUT5 transporters (Figure 4.1).

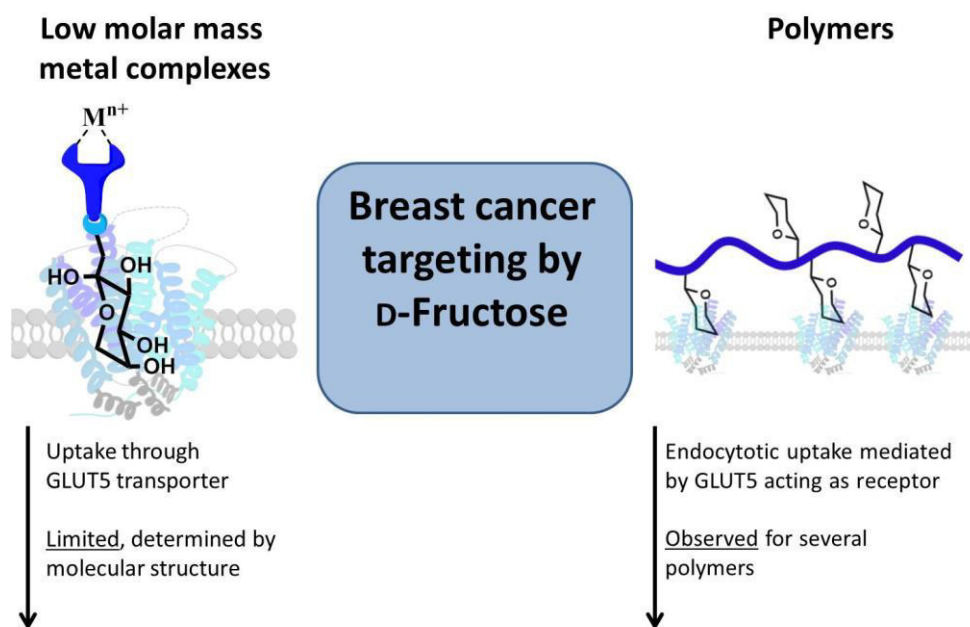


**Figure 4.1:** Schematic representation of the uptake of D-fructose conjugated molecules. Left: D-Fructose conjugated low molar mass metal complexes were taken up through the GLUT5 transporter, which is strongly dependent on the molecular structure. Right: D-Fructose conjugated polymers were taken up by an endocytotic pathway, which is mediated by the GLUT5 protein acting as receptor and which is observed for multiple polymer classes.

Before this work, only two literature examples about D-fructose conjugated metal complexes were available. They revealed an increased uptake of the D-fructose conjugated metal complexes into breast cancer cells mediated by the facilitative glucose transporter 5 (GLUT5) when compared to the D-fructose free analogues, which showed no selective accumulation. To further evaluate this hypothesis, a derivative of the highly biological active molecule curcumin was used and conjugated to two units of D-fructose by using the Cu(I) catalyzed alkyne azide cycladdition (CuAAC). The  $\beta$ -diketo moiety of the curcumin derivative was used afterwards to form ruthenium complexes of the

general formula  $[\text{Ru}(\text{bpy})_2(\text{L})]\text{Cl}$ . Due to the quenching of their fluorescence in aqueous media, the uptake of these complexes into breast cancer cells could not be evaluated. The mentioned studies were limited to D-fructose derivatives bound to the ligand scaffold *via* the C1 of the D-fructose molecule. One major questions of the present thesis represented the influence of the substitution position in the D-fructose molecule. For this purpose, two novel D-fructose conjugated ruthenium complexes starting from sucrose or a commercially available D-fructose derivative, respectively, were synthesized. The D-fructose units were attached *via* the C1 and C6 position by maintaining the rest of the molecules without chemical modifications. Inductively coupled plasma mass spectrometry measurements (ICP-MS) were conducted to investigate the influence of the substitution position on the cellular uptake after the complexes were incubated with breast cancer cells. Unfortunately, ruthenium complexes of the general formula  $[\text{Ru}(\text{bpy})_2(\text{L})]\text{Cl}_2$  with pyridyl triazole functionalized D-fructose as ancillary ligand did not show selective accumulation in breast cancer cells, independently from the position of modification. This is not transferable to other metal complexes with D-fructose conjugated ligands and has to be evaluated for every new complex again in detail.

Literature examples for D-fructose conjugated macromolecules and their use for the selective uptake into breast cancer cells were rare as well, when the present thesis was started. But in the last four years, numerous studies were published and show the possibility to target GLUT5 by D-fructose conjugated macromolecules. In this work, results for the first literature-known, cationic polymer with covalently attached D-fructose molecules could be contributed to this field. A D-fructose conjugated high-molar mass linear poly(ethylenimine) (L-PEI) was synthesized and showed an excellent biocompatibility paired with selective toxicity. The hemolytic potential was clearly decreased in comparison to the parent polymers while the ability to form stable polyplexes with plasmid deoxyribonucleic acid (pDNA) was maintained. The formed polyplexes of this polymer were shown to be taken up exclusively in significant levels into breast cancer cells. It can be stated that high-molar mass L-PEI with a degree of functionalization (DF) of 14% with D-fructose offers a large pool of beneficial biological properties, but the influence of many other parameters, such as DF, length of the polymer or degree of branching, have to be studied in future investigations.

Besides the interaction of D-fructose with GLUT5, the interaction of sugar molecules with receptors and other binding proteins is of major interest for the synthesis of potential D-fructose bearing

polymers. The binding affinity of these receptors is strongly dependent from multiple variables including the epitope density and the polymer flexibility. The last chapter of the present thesis focused on these interactions. Therefore, bromide bearing acrylates with large degree of polymerization values (DP) obtained by RAFT polymerization were post-functionalized with various aldoses with high DF values and without tedious protection steps. The glycopolymers were tested for their affinity to the binding protein concanavalin A (Con A) using turbidity measurements. A length- and sugar-dependent behavior for the clustering as well as for the dissolution constants was shown. The clusters of the most of the glycopolymers and Con A were not fully dissolved despite a 1000-fold excess of the competitor  $\alpha$ -D-methyl-mannopyranose ( $\alpha$ MeMan). This indicates a high affinity of these polymers towards Con A, which is attributed to the flexibility of the acrylate backbone and therefore, to the increased interaction with the Con A tetramers. The precursor polymer can be used to readily attach D-fructose and to investigate its affinity for the transport protein GLUT5.

Several changes can be performed to further clarify the uptake mechanisms of the two classes of D-fructose conjugated molecules. The uptake of the curcumin metal complexes can be investigated with ICP-MS to gain deeper insights into the interaction of these compounds with GLUT5 overexpressing cells. All presented ligand can be applied to other metal ions with compatible coordination spheres, such as  $\text{Pt}^{2+}$  or  $\text{Ir}^{3+}$ . The presented strategy to address the C6 position of D-fructose by using sucrose offers the possibility to readily install functionalities, such as SH-,  $\text{N}_3$ - or  $\text{NH}_2$ -, at the C6 position and to create an entire set of novel D-fructose derivatives. The transfection efficiency of the D-fructose conjugated L-PEI was very low, which is mainly attributed to the decreased proton sponge effect mediated by the conjugated D-fructose units. Future studies have to systematically evaluate how much the DF can be lowered to increase the transfection efficiency while maintaining the beneficial properties at the same time. The size of the used cationic polymer can also be varied to find the intersection of optimal DF and best size for polyplex formation. Branched poly(ethylenimine)s (B-PEIs) of different sizes are of interest as well due to their advanced complexation abilities for genetic material and other labeling strategies for D-fructose, *e.g.* by using new C6 derivatives, can be evaluated as well. The presented poly(bromoethyl acrylate)s (PBEAs) can be readily functionalized by using the thiolate *via* C1 and C6 of D-fructose to form novel polyacrylates in an effective approach and to evaluate their affinity for the GLUT5 transporter.

In summary, the conjugation of metal complexes and polymers with D-fructose represents a strategy to address the GLUT5 transporter, which is overexpressed in most of the breast cancer cells. But not in all cases selectivity can be achieved. In particular, for the low molar mass metal complexes the selectivity seems to be very much depending on the molecular structure and the resulting properties, such as hydrophobicity and stability. There are different positions in the D-fructose molecule available and it should be considered, that the affinity of GLUT5 for derivatives of D-fructose is strongly dependent on the conformation of all positions, the sterical demand of the substituents and on the non-functionalized groups in terms of recognition. In the case of polymeric D-fructose conjugates other parameters have to be considered. The length of the used polymer, the flexibility of the backbone, the size of the macromolecular assemblies, the uptake mechanism by endocytosis and others have a major influence on the effective targeting of the GLUT5 protein and the selective uptake into GLUT5 overexpressing cells.

## 5 Zusammenfassung

Die vorliegende Arbeit fokussierte die Synthese, Charakterisierung und biologische Bewertung von verschiedenen D-Fructose-konjugierten Molekülen. Die Verbindungen können grob in zwei Klassen unterschieden werden: Niedermolekulare Metallkomplexe und Polymere (Figure 4.1).

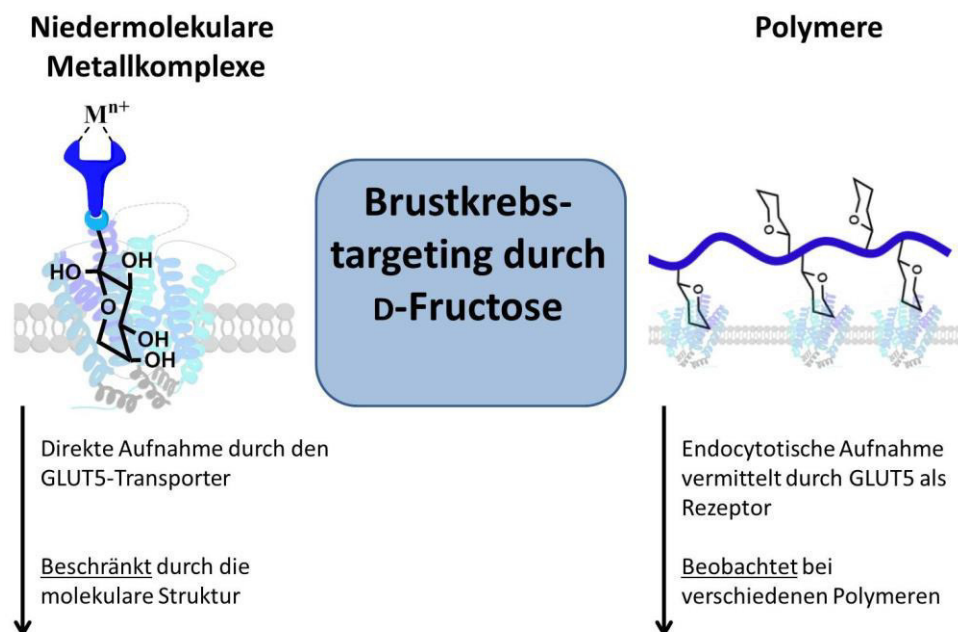


**Figure 5.1:** Schematische Darstellung der Aufnahme von D-Fructose konjugierten Verbindungen. Links: D-Fructose konjugierte niedermolekulare Metallkomplexe werden direkt vom GLUT5-Transporter aufgenommen, was jedoch stark von der molekularen Struktur beschränkt wird. Rechts: D-Fructose konjugierte Polymere werden, vermittelt durch das GLUT5-Protein als Rezeptor, endozytotisch aufgenommen. Das konnte bereits bei mehreren Polymeren gezeigt werden.

Als die vorliegende Dissertation begonnen wurde, waren nur zwei Beispiele über D-Fructose-konjugierte Metallkomplexe in der wissenschaftlichen Literatur verfügbar. Im Gegensatz zu den D-Fructose-freien Verbindungen konnte bei den betreffenden D-Fructose-konjugierten Metallkomplexen eine erhöhte Aufnahme in Brustkrebszellen durch einen Glucosetransporter 5 (GLUT5) abhängigen Weg gezeigt werden. Um diese Hypothese zu evaluieren, wurden zwei Einheiten D-Fructose mittels Cu(I) katalysierter Azid-Alkin-Cycloaddition (CuAAC) an das stark biologisch aktive Molekül Curcumin geklickt. Das  $\beta$ -Diketonat des Curcumin-Derivats wurde

anschließend zur Komplexbildung von Ruthenium genutzt, um Komplexe der allgemeinen Formel  $[\text{Ru}(\text{bpy})_2(\text{L})]\text{Cl}$  herzustellen. Durch Fluoreszenzauslöschung dieser Komplexe in wässrigen Medien konnte die Zellaufnahme in Brustkrebszellen durch spektroskopische Methoden nicht näher untersucht werden. Die anfangs erwähnten Studien nutzten ausschließlich Liganden, die über die C1-Position der D-Fructose verknüpft waren. Ein zentraler Schwerpunkt der vorliegenden Arbeit beschäftigte sich daher mit dem Einfluss der Substitutionsposition im D-Fructose-Molekül. Dafür wurden zwei neuartige D-Fructose-konjugierte Ruthenium-Komplexe hergestellt, deren Synthesen auf Saccharose bzw. einem kommerziell erwerblichen D-Fructose-Derivat als Startmaterial basieren. Die D-Fructose-Einheiten wurden über die C1- bzw. C6-Position verknüpft, während der Rest des Moleküls identisch war. Nachdem die Komplexe mit Brustkrebszellen inkubiert wurden, wurde Massenspektrometrie mit induktiv gekoppeltem Plasma (ICP-MS) durchgeführt, um den Einfluss der Substitutionsposition auf die Zellaufnahme zu untersuchen. Leider zeigten die hergestellten Komplexe mit der allgemeinen Formel  $[\text{Ru}(\text{bpy})_2(\text{L})]\text{Cl}$ , die über einen Pyridyltriazol-Linker mit den D-Fructose-Einheiten verknüpft sind, unabhängig von der gewählten Position keine selektive Akkumulation in Brustkrebszellen. Diese Erkenntnisse sind allerdings nicht übertragbar auf andere D-Fructose-konjugierte Metallkomplexe und müssen für jede Verbindung neu evaluiert werden.

Die Literatur über D-Fructose-konjugierte Polymere war zum Beginn der vorliegenden Arbeit ebenso rar, allerdings konnten in den letzten vier Jahren mehrere Studien die Möglichkeit zeigen, den GLUT5-Rezeptor durch D-Fructose-konjugierte Makromoleküle anzusteuern. Die vorliegende Arbeit konnte zu diesem Feld das erste kationische Polymer beitragen, welches kovalent gebundene D-Fructose-Einheiten trägt. Das hergestellte D-Fructose-konjugierte lineare Polyethylenimin (L-PEI) zeigt hervorragende Biokompatibilität gepaart mit selektiver Toxizität. Die hämolytische Verträglichkeit im Vergleich zu den anderen getesteten Polymeren war deutlich erhöht, während weiterhin stabile Polyplexe mit Plasmid-Desoxyribonucleinsäure (pDNA) gebildet werden konnten. Die Polyplexe des Polymers wurden in signifikant höheren Mengen und exklusiv in Brustkrebszellen aufgenommen. Mit diesen Erkenntnissen eröffnet ein Funktionalisierungsgrad des L-PEIs von 14% mit D-Fructose eine Vielzahl von positiven biologischen Eigenschaften, während in zukünftigen Studien der systematische Einfluss von anderen Parametern, wie z.B. Länge des Polymers, Verzweigungsgrad etc., untersucht werden muss.



Für die potentielle Synthese von D-Fructose-konjugierten Polymeren spielt die Interaktion von Zuckermolekülen mit Rezeptoren und Bindungsproteinen eine wesentliche Rolle. Die Affinität dieser Rezeptoren ist von mehreren Parametern, wie z.B. der Menge der angebrachten Zucker und der Flexibilität des Polymer-Rückgrats, abhängig. Das letzte Kapitel der vorliegenden Arbeit beschäftigte sich daher mit diesen Wechselwirkungen. Durch kontrollierte Radikalik hergestellte bromierte Polyacrylate mit hohem Polymerisationsgrad wurden mit verschiedenen Aldosen und ohne aufwändige Schutzgruppen-Chemie post-funktionalisiert. Durchgeführte Affinitätsstudien der Glycopolymere mit dem Bindungsprotein Concanavalin A (Con A) zeigten längen- und zuckerabhängige Clusterbildungs bzw. -auflösungsraten. Trotz eines tausendfachen Überschusses des Bindungskonkurrenten  $\alpha$ -D-Methylmannopyranose ( $\alpha$ MeMan), haben sich die meisten gebildeten Glycopolymer-Con A-Cluster nicht aufgelöst, was auf die erhöhte Interaktion der flexiblen Acrylate mit den Con A-Tetrameren zurückzuführen sein könnte.

Sowohl für die nieder- als auch für die makromolekularen Verbindungen sind Veränderungen denkbar. Die Aufnahme der Curcumin-Metall-Komplexe kann beispielsweise ebenso mit ICP-MS-Messungen untersucht werden um die Wechselwirkung dieser Verbindungen mit GLUT5-überexprimierenden Zellen besser verstehen zu können. Metallionen mit kompatiblen Koordinationssphären, wie z.B.  $\text{Pt}^{2+}$  oder  $\text{Ir}^{3+}$ , können mit den gezeigten Liganden komplexiert werden. Die präsentierte Strategie zur Synthese von D-Fructose-Derivaten an der C6-Position ausgehend von Saccharose kann ebenso genutzt werden, um verschiedenste Funktionalitäten, wie z.B. SH-,  $\text{N}_3$ - oder  $\text{NH}_2$ -, einzuführen und somit eine Vielzahl neuartiger Derivate herzustellen. Die verringerte Transfektionseffizienz des gezeigten D-Fructose-konjugierten L-PEIs kann durch eine Veränderung des Funktionalisierungsgrads behoben werden. Dabei muss allerdings systematisch untersucht werden, wie stark der Funktionalisierungsgrad verringert werden kann, ohne die anderen positiven Eigenschaften zu beeinflussen. Weiterhin kann die Größe des kationischen Polymers variiert werden, um die beste Größe für die Bildung von Polyplexen herauszukristallisieren. Durch die verbesserte Komplexierung von genetischem Material sind verzweigte Polyethylenimine (B-PEIs) ebenso von großem Interesse wie verbesserte Markierungsstrategien für D-Fructose an Polymere. Die verwendeten Vorläufer-Polymere auf Polybromoethylacrylat-Basis (PBEA) können außerdem für das einfache Anhängen von D-Fructose-Einheiten genutzt werden, um deren Affinität zum GLUT5-Transporter zu untersuchen

Zusammenfassend kann gesagt werden, dass die Konjugation von D-Fructose an Metallkomplexe und Polymere eine geeignete Strategie darstellt, um den in den meisten Brustkrebszellen überexprimierten GLUT5-Rezeptor anzusteuern. Das Anhängen von D-Fructose führt allerdings nicht zwangsläufig zu Selektivität. Besonders die Selektivität niedermolekularer Metallkomplexe ist nicht nur abhängig von der Molekülstruktur, sondern auch von den daraus resultierenden Eigenschaften, wie z.B. der Hydrophobizität und der Stabilität. Da verschiedene Positionen im D-Fructose-Molekül verfügbar sind, sollte insbesondere bedacht werden, dass die Affinität des GLUT5-Rezeptors für D-Fructose-Derivate stark abhängig von der Konformation **aller** Positionen, dem sterischen Bedarf der Substituenten und den nicht-funktionalisierten Positionen ist. Für D-Fructose-konjugierte Makromoleküle müssen weitere Parameter bedacht werden. Hier spielen u.a. die Länge des verwendeten Polymers, die Flexibilität des Rückgrats, die Größe der makromolekularen Anordnung in Wasser und der Zellaufnahmemechanismus durch Endozytose eine wesentliche Rolle, um ein maximales Ansteuern des GLUT5-Transporters und eine selektiven Aufnahme in GLUT5-überexprimierende Zellen zu erreichen.

## References

- [1] T. K. Lindhorst, *Chem. unserer Zeit* **2000**, *34*, 38-52.
- [2] T. K. Lindhorst, *Essentials of Carbohydrate Chemistry and Biochemistry*, Wiley, **2000**.
- [3] R. A. Dwek, *Chem. Rev.* **1996**, *96*, 683-720.
- [4] J. C. Kim, Y. Rho, G. Kim, M. Kim, H. Kim, I. J. Kim, J. R. Kim, M. Ree, *Polym. Chem.* **2013**, *4*, 2260-2271.
- [5] A. Ghadban, L. Albertin, *Polymers* **2013**, *5*, 431-526.
- [6] W. Weis, J. H. Brown, S. Cusack, J. C. Paulson, J. J. Skehel, D. C. Wiley, *Nature* **1988**, *333*, 426-431.
- [7] W. M. Watkins, P. Greenwell, A. D. Yates, P. H. Johnson, *Biochimie* **1988**, *70*, 1597-1611.
- [8] R. J. Pieters, *Org. Biomol. Chem.* **2009**, *7*, 2013-2025.
- [9] A. Scheepers, H. Joost, A. Schurmann, *J. Parenter. Enteral Nutr.* **2004**, *28*, 364-371.
- [10] M. L. Macheda, S. Rogers, J. D. Best, *J. Cell. Physiol.* **2005**, *202*, 654-662.
- [11] M. Mueckler, B. Thorens, *Mol. Asp. Med.* **2013**, *34*, 121-138.
- [12] C. F. Burant, J. Takeda, E. Brot-Laroche, G. I. Bell, N. O. Davidson, *J. Biol. Chem.* **1992**, *267*, 14523-14526.
- [13] N. Nomura, G. Verdon, H. J. Kang, T. Shimamura, Y. Nomura, Y. Sonoda, S. A. Hussien, A. A. Qureshi, M. Coincon, Y. Sato, H. Abe, Y. Nakada-Nakura, T. Hino, T. Arakawa, O. Kusano-Arai, H. Iwanari, T. Murata, T. Kobayashi, T. Hamakubo, M. Kasahara, S. Iwata, D. Drew, *Nature* **2015**, *526*, 397-401.
- [14] B. Niu, X. Wen, Z. Jia, X. Wu, W. Guo, H. Sun, *Chin. J. Chem.* **2013**, *31*, 1159-1163.
- [15] V. Douard, R. P. Ferraris, *Am. J. Physiol. Endocrinol. Metab.* **2008**, *295*, E227-E237.
- [16] V. Douard, R. P. Ferraris, *J. Physiol.* **2013**, *591*, 401-414.
- [17] C. A. Stuart, M. E. A. Howell, D. Yin, *Diabetes Care* **2007**, *30*, 925-931.
- [18] J. Dyer, I. S. Wood, A. Palejwala, A. Ellis, S. P. Shirazi-Beechey, *Am. J. Physiol. Gastrointest. Liver Physiol.* **2002**, *282*, G241-G248.
- [19] K. M. Mellor, J. R. Bell, I. R. Wendt, A. J. Davidoff, R. H. Ritchie, L. M. D. Delbridge, *PLoS One* **2011**, *6*, e25204.
- [20] I. Stuart Wood, B. Wang, S. Lorente-Cebrián, P. Trayhurn, *Biochem. Biophys. Res. Commun.* **2007**, *361*, 468-473.
- [21] H. Liu, A. P. Heaney, *Expert Opin. Ther. Targets* **2011**, *15*, 1049-1059.
- [22] A. Godoy, V. Ulloa, F. Rodríguez, K. Reinicke, A. J. Yañez, M. d. I. A. García, R. A. Medina, M. Carrasco, S. Barberis, T. Castro, F. Martínez, X. Koch, J. C. Vera, M. T. Poblete, C. D. Figueroa, B. Peruzzo, F. Pérez, F. Nualart, *J. Cell. Physiol.* **2006**, *207*, 614-627.
- [23] G. Gowrishankar, S. Zitzmann-Kolbe, A. Junutula, R. Reeves, J. Levi, A. Srinivasan, K. Bruus-Jensen, J. Cyr, L. Dinkelborg, S. S. Gambhir, *PLoS One* **2011**, *6*, e26902.
- [24] B. Monzavi-Karbassi, R. J. Hine, J. S. Stanley, V. P. Ramani, J. Carcel-Trullols, T. L. Whitehead, T. Kelly, E. R. Siegel, C. Artaud, S. Shaaf, R. Saha, F. Jousheghany, R. Henry-Tillman, T. Kieber-Emmons, *Int. J. Oncol.* **2010**, *37*, 615-622.
- [25] S. P. Zamora-León, D. W. Golde, I. I. Concha, C. I. Rivas, F. Delgado-López, J. Baselga, F. Nualart, J. C. Vera, *Proc. Natl. Acad. Sci. U. S. A.* **1996**, *93*, 1847-1852.
- [26] K. K. Chan, J. Y. W. Chan, K. K. W. Chung, K.-P. Fung, *J. Cell. Biochem.* **2004**, *93*, 1134-1142.

- [27] W.-L. Chen, Y.-Y. Wang, A. Zhao, L. Xia, G. Xie, M. Su, L. Zhao, J. Liu, C. Qu, R. Wei, C. Rajani, Y. Ni, Z. Cheng, Z. Chen, S.-J. Chen, W. Jia, *Cancer Cell* **2016**, *30*, 779-791.
- [28] O.-M. Soueidan, B. J. Trayner, T. N. Grant, J. R. Henderson, F. Wuest, F. G. West, C. I. Cheeseman, *Org. Biomol. Chem.* **2015**, *13*, 6511-6521.
- [29] M. Wuest, B. J. Trayner, T. N. Grant, H.-S. Jans, J. R. Mercer, D. Murray, F. G. West, A. J. B. McEwan, F. Wuest, C. I. Cheeseman, *Nucl. Med. Biol.* **2011**, *38*, 461-475.
- [30] J. Levi, Z. Cheng, O. Gheysens, M. Patel, C. T. Chan, Y. Wang, M. Namavari, S. S. Gambhir, *Bioconjugate Chem.* **2007**, *18*, 628-634.
- [31] K. Yin Zhang, K. Ka-Shun Tso, M.-W. Louie, H.-W. Liu, K. K.-W. Lo, *Organometallics* **2013**, *32*, 5098-5102.
- [32] K. K.-W. Lo, W. H.-T. Law, J. C.-Y. Chan, H.-W. Liu, K. Y. Zhang, *Metallomics* **2013**, *5*, 808-812.
- [33] A. Tatibouët, J. Yang, C. Morin, G. D. Holman, *Bioorg. Med. Chem.* **2000**, *8*, 1825-1833.
- [34] A. Tatibouët, M. Lefoix, J. Nadolny, O. R. Martin, P. Rollin, J. Yang, G. D. Holman, *Carbohydr. Res.* **2001**, *333*, 327-334.
- [35] J. Yang, J. Dowden, A. Tatibouët, Y. Hatanaka, G. D. Holman, *Biochem. J.* **2002**, *367*, 533-539.
- [36] J. Panyam, V. Labhasetwar, *Adv. Drug Deliv. Rev.* **2003**, *55*, 329-347.
- [37] J. Zhao, K. Babiuch, H. Lu, A. Dag, M. Gottschaldt, M. H. Stenzel, *Chem. Commun.* **2014**, *50*, 15928-15931.
- [38] A. Dag, M. Callari, H. Lu, M. H. Stenzel, *Polym. Chem.* **2016**, *7*, 1031-1036.
- [39] C. von der Ehe, A. Rinkenauer, C. Weber, D. Szamosvari, M. Gottschaldt, U. S. Schubert, *Macromol. Biosci.* **2016**, *16*, 508-521.
- [40] X. Zhou, X. Qin, T. Gong, Z.-R. Zhang, Y. Fu, *Macromol. Biosci.* **2017**, 1600529.
- [41] M. Gottschaldt, U. S. Schubert, *Chem. Eur. J.* **2009**, *15*, 1548-1557.
- [42] X. Wang, Z. Guo, *Chem. Soc. Rev.* **2013**, *42*, 202-224.
- [43] C. F. Ramogida, C. Orvig, *Chem. Commun.* **2013**, *49*, 4720-4739.
- [44] S. Liu, *Adv. Drug Deliv. Rev.* **2008**, *60*, 1347-1370.
- [45] M. Ahmed, R. Narain, *Nanomedicine* **2015**, *10*, 2263-2288.
- [46] A. Lidgren, A. Bergh, K. Grankvist, T. Rasmuson, B. Ljungberg, *BJU Int.* **2008**, *101*, 480-484.
- [47] M. Younes, R. W. Brown, M. Stephenson, M. Gondo, P. T. Cagle, *Cancer* **1997**, *80*, 1046-1051.
- [48] M. D. Bartholomä, *Inorg. Chim. Acta* **2012**, *389*, 36-51.
- [49] E. García Garayoa, D. Rüegg, P. Bläuenstein, M. Zwimpfer, I. U. Khan, V. Maes, A. Blanc, A. G. Beck-Sickinger, D. A. Tourwé, P. A. Schubiger, *Nucl. Med. Biol.* **2007**, *34*, 17-28.
- [50] Y.-S. Yang, X. Zhang, Z. Xiong, X. Chen, *Nucl. Med. Biol.* **2006**, *33*, 371-380.
- [51] K. Mahmood, K. M. Zia, M. Zuber, M. Salman, M. N. Anjum, *Int. J. Biol. Macromol.* **2015**, *81*, 877-890.
- [52] S. Prasad, S. C. Gupta, A. K. Tyagi, B. B. Aggarwal, *Biotechnol. Adv.* **2014**, *32*, 1053-1064.
- [53] C. D. Lao, M. T. Ruffin, D. Normolle, D. D. Heath, S. I. Murray, J. M. Bailey, M. E. Boggs, J. Crowell, C. L. Rock, D. E. Brenner, *BMC Complement. Altern. Med.* **2006**, *6*, 10.
- [54] A. Siviero, E. Gallo, V. Maggini, L. Gori, A. Mugelli, F. Firenzuoli, A. Vannacci, *J. Herb. Med.* **2015**, *5*, 57-70.
- [55] Y.-J. Wang, M.-H. Pan, A.-L. Cheng, L.-I. Lin, Y.-S. Ho, C.-Y. Hsieh, J.-K. Lin, *J. Pharm. Biomed. Anal.* **1997**, *15*, 1867-1876.
- [56] G. Shoba, D. Joy, T. Joseph, M. Majeed, R. Rajendran, P. S. S. R. Srinivas, *Planta Med.* **1998**, *64*, 353-356.

- [57] L. Li, F. S. Braiteh, R. Kurzrock, *Cancer* **2005**, *104*, 1322-1331.
- [58] Z. Ma, A. Shayeganpour, D. R. Brocks, A. Lavasanifar, J. Samuel, *Biomed. Chromatogr.* **2007**, *21*, 546-552.
- [59] W.-H. Lee, C.-Y. Loo, P. M. Young, D. Traini, R. S. Mason, R. Rohanizadeh, *Expert Opin. Drug Deliv.* **2014**, *11*, 1183-1201.
- [60] G. Kumar, S. Mittal, K. Sak, H. S. Tuli, *Life Sci.* **2016**, *148*, 313-328.
- [61] C. Tamvakopoulos, K. Dimas, Z. D. Sofianos, S. Hatziantoniou, Z. Han, Z.-L. Liu, J. H. Wyche, P. Pantazis, *Clin. Cancer Res.* **2007**, *13*, 1269-1277.
- [62] S. Dolai, W. Shi, C. Corbo, C. Sun, S. Averick, D. Obeysekera, M. Farid, A. Alonso, P. Banerjee, K. Raja, *ACS Chem. Neurosci.* **2011**, *2*, 694-699.
- [63] M. Asti, E. Ferrari, S. Croci, G. Atti, S. Rubagotti, M. Iori, P. C. Capponi, A. Zerbini, M. Saladini, A. Versari, *Inorg. Chem.* **2014**, *53*, 4922-4933.
- [64] M. Rak, M. R. Del Bigio, S. Mai, D. Westaway, K. Gough, *Biopolymers* **2007**, *87*, 207-217.
- [65] S.-S. Zhou, X. Xue, J.-F. Wang, Y. Dong, B. Jiang, D. Wei, M.-L. Wan, Y. Jia, *J. Mater. Chem.* **2012**, *22*, 22774-22780.
- [66] S. M. Vithanarachchi, M. J. Allen, *Chem. Commun.* **2013**, *49*, 4148-4150.
- [67] B. A. Armitage, in *DNA Binders and Related Subjects*, Vol. 253 (Eds.: M. Waring, J. Chaires), Springer Berlin Heidelberg, **2005**, pp. 55-76.
- [68] A. Mukherjee, W. D. Sasikala, in *Advances in Protein Chemistry and Structural Biology*, Vol. 92 (Ed.: K.-C. Tatyana), Academic Press, **2013**, pp. 1-62.
- [69] D. Pucci, T. Bellini, A. Crispini, I. D'Agnano, P. F. Liguori, P. Garcia-Orduna, S. Pirillo, A. Valentini, G. Zanchetta, *Med. Chem. Comm.* **2012**, *3*, 462-468.
- [70] T. K. Goswami, S. Gadadhar, B. Gole, A. A. Karande, A. R. Chakravarty, *Eur. J. Med. Chem.* **2013**, *63*, 800-810.
- [71] S. Banerjee, P. Prasad, I. Khan, A. Hussain, P. Kondaiah, A. R. Chakravarty, *Z. Anorg. Allg. Chem.* **2014**, *640*, 1195-1204.
- [72] D. C. Crans, A. S. Tracey, in *Vanadium Compounds*, Vol. 711, American Chemical Society, **1998**, pp. 2-29.
- [73] S. Banerjee, A. Hussain, P. Prasad, I. Khan, B. Banik, P. Kondaiah, A. R. Chakravarty, *Eur. J. Inorg. Chem.* **2012**, 3899-3908.
- [74] E. S. Antonarakis, A. Emadi, *Cancer Chemother. Pharmacol.* **2010**, *66*, 1-9.
- [75] A. Bergamo, C. Gaiddon, J. H. M. Schellens, J. H. Beijnen, G. Sava, *J. Inorg. Biochem.* **2012**, *106*, 90-99.
- [76] N. V. Sokolova, V. G. Nenajdenko, *RSC Adv.* **2013**, *3*, 16212-16242.
- [77] B. Zebib, Z. Mouloungui, V. Noirot, *Bioinorg. Chem. Appl.* **2010**, 292760.
- [78] W. Song, X. Qiao, W.-F. Liang, S. Ji, L. Yang, Y. Wang, Y.-W. Xu, Y. Yang, D.-A. Guo, M. Ye, *J. Sep. Sci.* **2015**, *38*, 3450-3453.
- [79] C. Weber, J. A. Czaplewska, A. Baumgaertel, E. Altuntas, M. Gottschaldt, R. Hoogenboom, U. S. Schubert, *Macromolecules* **2012**, *45*, 46-55.
- [80] G. Sprintschnik, H. W. Sprintschnik, P. P. Kirsch, D. G. Whitten, *J. Am. Chem. Soc.* **1976**, *98*, 2337-2338.
- [81] L. D. Marroquin, J. Hynes, J. A. Dykens, J. D. Jamieson, Y. Will, *Toxicol. Sci.* **2007**, *97*, 539-547.
- [82] A. Davit-Spraul, M. L. Pourci, T. Soni, A. Lemonnier, *Metabolism* **1994**, *43*, 945-952.
- [83] K. Chandrasekaran, K. Swaminathan, S. Chatterjee, A. Dey, *Toxicol. in Vitro* **2010**, *24*, 387-396.

- [84] M. Gottschaldt, U. S. Schubert, S. Rau, S. Yano, J. G. Vos, T. Kroll, J. Clement, I. Hilger, *ChemBioChem* **2010**, *11*, 649-652.
- [85] I. Ali, K. Saleem, D. Wesselinova, A. Haque, *Med. Chem. Res.* **2013**, *22*, 1386-1398.
- [86] C. Syng-Ai, A. L. Kumari, A. Khar, *Mol. Cancer Ther.* **2004**, *3*, 1101-1108.
- [87] K. Wada, J.-Y. Lee, H.-Y. Hung, Q. Shi, L. Lin, Y. Zhao, M. Goto, P.-C. Yang, S.-C. Kuo, H.-W. Chen, K.-H. Lee, *Bioorg. Med. Chem.* **2015**, *23*, 1507-1514.
- [88] Y. Hou, X. Wu, W. Xie, P. G. Braunschweiger, P. G. Wang, *Tetrahedron Lett.* **2001**, *42*, 825-829.
- [89] C. R. Becer, R. Hoogenboom, U. S. Schubert, *Angew. Chem. Int. Ed.* **2009**, *48*, 4900-4908.
- [90] J. C. Jewett, C. R. Bertozzi, *Chem. Soc. Rev.* **2010**, *39*, 1272-1279.
- [91] T. M. Potewar, K. T. Petrova, M. T. Barros, *Carbohydr. Res.* **2013**, *379*, 60-67.
- [92] M. T. Barros, K. T. Petrova, A. M. Ramos, *J. Org. Chem.* **2004**, *69*, 7772-7775.
- [93] J. A. Czaplewski, F. Theil, E. Altuntas, T. Niksch, M. Freesmeyer, B. Happ, D. Pretzel, H. Schäfer, M. Obata, S. Yano, U. S. Schubert, M. Gottschaldt, *Eur. J. Inorg. Chem.* **2014**, *2014*, 6290-6297.
- [94] M. Cockman, D. G. Kubler, A. S. Oswald, L. Wilson, *J. Carbohydr. Chem.* **1987**, *6*, 181-201.
- [95] F. Franks, *Pure Appl. Chem.* **1987**, *59*, 1189-1202.
- [96] W. J. Goux, *J. Am. Chem. Soc.* **1985**, *107*, 4320-4327.
- [97] D. Pröfrock, A. Prange, *Appl. Spectrosc.* **2012**, *66*, 843-868.
- [98] J. S. Becker, M. Zoriy, A. Matusch, B. Wu, D. Salber, C. Palm, J. S. Becker, *Mass Spectrom. Rev.* **2010**, *29*, 156-175.
- [99] T. Wang, J. R. Upponi, V. P. Torchilin, *Int. J. Pharm.* **2012**, *427*, 3-20.
- [100] A. M. Miller, D. A. Dean, *Adv. Drug Deliv. Rev.* **2009**, *61*, 603-613.
- [101] K. A. Whitehead, R. Langer, D. G. Anderson, *Nat. Rev. Drug Discov.* **2009**, *8*, 129-138.
- [102] J. Wang, Z. Lu, M. G. Wientjes, J. L.-S. Au, *AAPS J.* **2010**, *12*, 492-503.
- [103] N. Unnamalai, B. G. Kang, W. S. Lee, *FEBS Lett.* **2004**, *566*, 307-310.
- [104] E. Song, P. Zhu, S.-K. Lee, D. Chowdhury, S. Kussman, D. M. Dykxhoorn, Y. Feng, D. Palliser, D. B. Weiner, P. Shankar, W. A. Marasco, J. Lieberman, *Nat. Biotechnol.* **2005**, *23*, 709-717.
- [105] J. Halder, A. A. Kamat, C. N. Landen, L. Y. Han, S. K. Lutgendorf, Y. G. Lin, W. M. Merritt, N. B. Jennings, A. Chavez-Reyes, R. L. Coleman, D. M. Gershenson, R. Schmandt, S. W. Cole, G. Lopez-Berestein, A. K. Sood, *Clin. Cancer Res.* **2006**, *12*, 4916-4924.
- [106] O. Boussif, F. Lezoualc'h, M. A. Zanta, M. D. Mergny, D. Scherman, B. Demeneix, J. P. Behr, *Proc. Natl. Acad. Sci. U. S. A.* **1995**, *92*, 7297-7301.
- [107] M. A. Islam, T. E. Park, B. Singh, S. Maharjan, J. Firdous, M.-H. Cho, S.-K. Kang, C.-H. Yun, Y. J. Choi, C.-S. Cho, *J. Control. Release* **2014**, *193*, 74-89.
- [108] M. Neu, D. Fischer, T. Kissel, *J. Gene Med.* **2005**, *7*, 992-1009.
- [109] J. M. Bennis, R. I. Mahato, S. W. Kim, *J. Control. Release* **2002**, *79*, 255-269.
- [110] D. Pezzoli, P. Tarsini, L. Melone, G. Candiani, *J. Drug Deliv. Sci. Technol.* **2017**, *37*, 115-122.
- [111] J. Bae, M. Mie, E. Kobatake, *Appl. Biochem. Biotechnol.* **2012**, *168*, 2184-2190.
- [112] K. Sagara, S. W. Kim, *J. Control. Release* **2002**, *79*, 271-281.
- [113] G. Adiwidjaja, J.-S. Brunck, K. Polchow, J. Voss, *Carbohydr. Res.* **2000**, *325*, 237-244.
- [114] M. Bauer, C. Lautenschlaeger, K. Kempe, L. Tauhardt, U. S. Schubert, D. Fischer, *Macromol. Biosci.* **2012**, *12*, 986-998.
- [115] C. Englert, L. Tauhardt, M. Hartlieb, K. Kempe, M. Gottschaldt, U. S. Schubert, *Biomacromolecules* **2014**, *15*, 1124-1131.

- [116] K. Kunath, A. von Harpe, D. Fischer, T. Kissel, *J. Control. Release* **2003**, *88*, 159-172.
- [117] T. Bus, C. Englert, M. Reifarth, P. Borchers, M. Hartlieb, A. Vollrath, S. Hoeppener, A. Traeger, U. S. Schubert, *J. Mater. Chem. B* **2017**, *5*, 1258-1274.
- [118] M. Jawanda, B. F. L. Lai, J. N. Kizhakkedathu, K. Ishihara, R. Narain, *Polym. Chem.* **2013**, *4*, 3140-3146.
- [119] A. C. Rinkenauer, L. Tauhardt, F. Wendler, K. Kempe, M. Gottschaldt, A. Traeger, U. S. Schubert, *Macromol. Biosci.* **2015**, *15*, 414-425.
- [120] P. Xu, G. K. Quick, Y. Yeo, *Biomaterials* **2009**, *30*, 5834-5843.
- [121] J. Rejman, V. Oberle, I. S. Zuhorn, D. Hoekstra, *Biochem. J.* **2004**, *377*, 159-169.
- [122] A. C. Rinkenauer, S. Schubert, A. Traeger, U. S. Schubert, *J. Mater. Chem. B* **2015**, *3*, 7477-7493.
- [123] P. Midoux, C. Pichon, J.-J. Yaouanc, P.-A. Jaffrès, *Br. J. Pharmacol.* **2009**, *157*, 166-178.
- [124] A. Kwok, S. L. Hart, *Nanomedicine* **2011**, *7*, 210-219.
- [125] M. Wagner, A. C. Rinkenauer, A. Schallon, U. S. Schubert, *RSC Adv.* **2013**, *3*, 12774-12785.
- [126] Y. Miura, *Polym. J.* **2012**, *44*, 679-689.
- [127] J. J. Lundquist, E. J. Toone, *Chem. Rev.* **2002**, *102*, 555-578.
- [128] R. Roy, F. D. Tropper, A. Romanowska, *Bioconjugate Chem.* **1992**, *3*, 256-261.
- [129] D. M. Haddleton, R. Edmonds, A. M. Heming, E. J. Kelly, D. Kukulj, *New J. Chem.* **1999**, *23*, 477-479.
- [130] K. Ohno, Y. Tsujii, T. Fukuda, *J. Polym. Sci., Part A: Polym. Chem.* **1998**, *36*, 2473-2481.
- [131] S. Loykulnant, A. Hirao, *Macromolecules* **2000**, *33*, 4757-4764.
- [132] M.-P. Labeau, H. Cramail, A. Deffieux, *Macromol. Chem. Phys.* **1998**, *199*, 335-342.
- [133] K. Aoi, K. Tsutsumiuchi, M. Okada, *Macromolecules* **1994**, *27*, 875-877.
- [134] V. Ladmiral, E. Melia, D. M. Haddleton, *Eur. Polym. J.* **2004**, *40*, 431-449.
- [135] J. A. Burns, M. I. Gibson, C. R. Becer, in *Functional Polymers by Post-Polymerization Modification*, Wiley-VCH, **2012**, pp. 237-265.
- [136] C. R. Becer, K. Babiuch, D. Pilz, S. Hornig, T. Heinze, M. Gottschaldt, U. S. Schubert, *Macromolecules* **2009**, *42*, 2387-2394.
- [137] V. Ladmiral, G. Mantovani, G. J. Clarkson, S. Cauet, J. L. Irwin, D. M. Haddleton, *J. Am. Chem. Soc.* **2006**, *128*, 4823-4830.
- [138] G. Chen, S. Amajjahe, M. H. Stenzel, *Chem. Commun.* **2009**, 1198-1200.
- [139] Y. Chen, G. Chen, M. H. Stenzel, *Macromolecules* **2010**, *43*, 8109-8114.
- [140] T. R. Barlow, J. C. Brendel, S. Perrier, *Macromolecules* **2016**, *49*, 6203-6212.
- [141] S. M. Dimick, S. C. Powell, S. A. McMahon, D. N. Moothoo, J. H. Naismith, E. J. Toone, *J. Am. Chem. Soc.* **1999**, *121*, 10286-10296.
- [142] A. M. Puertas, F. J. d. I. Nieves, *J. Phys.: Condens. Matter* **1997**, *9*, 3313-3120.
- [143] Y. Gou, J. Geng, S.-J. Richards, J. Burns, C. Remzi Becer, D. M. Haddleton, *J. Polym. Sci., Part A: Polym. Chem.* **2013**, *51*, 2588-2597.
- [144] C. W. Cairo, J. E. Gestwicki, M. Kanai, L. L. Kiessling, *J. Am. Chem. Soc.* **2002**, *124*, 1615-1619.
- [145] C. Xiao, C. Zhao, P. He, Z. Tang, X. Chen, X. Jing, *Macromol. Rapid Commun.* **2010**, *31*, 991-997.

**List of abbreviations**

$\alpha$ MeMan	$\alpha$ -D-methyl-mannopyranose
4-DMAP	<i>N,N</i> -dimethylpyridine-4-amine
acac	pentane-2,4-dione, acetylacetone
AD	Alzheimer disease
AIBN	azobisisobutyronitrile
AML	acute myeloid leukemia
ATP	adenosine-5'-triphosphate
BDC	bisdemethoxycurcumin
bpy	2,2'-bipyridine
CLSM	confocal laser scanning microscopy
CPAETC	(4-cyanopentanoic acid)ylethyl trithiocarbonate
Con A	concanavalin A
CTA	chain transfer agent
CuAAC	Cu(I) catalyzed alkine azide cycladdition
DF	degree of functionalization
DP	degree of polymerization
DLS	dynamic light scattering
DMF	<i>N,N</i> -dimethylformamide
DMPA	2,2-dimethoxy-1,2-diphenylethan-1-one
DNA	deoxyribonucleic acid
DOSY	diffusion-ordered nuclear magnetic resonance spectroscopy
DOTA	1,4,7,10-tetraazacyclododecane-1,4,7,10-tetraacetic acid
DP	degree of polymerization
DTPA	diethylenetriaminepentaacetic acid
EBA	ethidium bromide assay
EDTA	Ethylenediaminetetraacetic acid
EGFP	enhanced green fluorescent protein
ESI	electron spray ionization
Et <sub>2</sub> O	diethylether



Et <sub>3</sub> N	triethylamine
EtOH	ethanol
GLUT	facilitative glucose transporter
HaCaT	human adult low calcium high temperature keratinocytes
HeLa	cervical cancer cell line, which derived from Henrietta Lacks
HUVEC	human umbilical vein endothelial cells
IC <sub>50</sub>	half maximal inhibitory concentration
ICP	inductively coupled plasma
MALDI	matrix assisted laser desorption ionization
MFI	mean fluorescence intensity
MLCT	metal to ligand charge transfer
MS	mass spectrometry
MWCO	molecular weight cut-off
NaOMe	sodium methanolate
NIR	near infrared
NMR	nuclear magnetic resonance
PBEA	poly(bromoethyl acrylate)
PCL	poly( $\epsilon$ -caprolactone)
pDNA	plasmid deoxyribonucleic acid
PDT	photodynamic therapy
PECH	poly(epichlorhydrin)
PEG	poly(ethylene glycol)
PEI	poly(ethylenimine)
PET	positron emission tomography
PEtOx	poly(2-ethyl-2-oxazoline)
PVBC	poly(vinyl benzylchlorid)
py	pyridine
pyta	pyridyl triazole
RDRP	reversible deactivation radical polymerization
RFU	relative fluorescence intensity
SGLT	sodium dependent glucose transporter
siRNA	small interfering ribonucleic acid

## List of abbreviations

---

TBAF	tetra- <i>n</i> -butylammonium fluoride
TBDPSCI	<i>tert</i> -butyldiphenyl-silylchloride
t-BuOH	<i>tert</i> -butanol
THF	tetrahydrofuran
TLC	thin layer chromatography

## Publication list

### Peer-reviewed publications:

M. Pröhl, U. S. Schubert, W. Weigand, M. Gottschaldt, "Metal complexes of curcumin and curcumin derivatives for molecular imaging and anticancer therapy", *Coord. Chem. Rev.* **2016**, *307*, 32-41.

M. Pröhl, T. Bus, J. A. Czaplewska, A. Traeger, M. Deicke, H. Weiss, W. Weigand, U. S. Schubert, M. Gottschaldt, "Synthesis and *in vitro* toxicity of D-glucose and D-fructose conjugated curcumin–ruthenium complexes", *Eur. J. Inorg. Chem.* **2016**, 5197-5204.

C. Englert, M. Pröhl, J. A. Czaplewska, C. Fritzsche, E. Preußger, U. S. Schubert, A. Traeger, M. Gottschaldt, "D-Fructose-decorated poly(ethylene imine) for human breast cancer cell targeting", *Macromol. Biosci.* **2017**, *17*, 1600502.

M. Pröhl, P. D. Moser, J. A. Czaplewska, P. Hoffmann, T. Bus, A. Traeger, H. Görls, U. S. Schubert, M. Gottschaldt, "Synthesis of D-fructose conjugated ligands *via* C6 and C1 and their corresponding [Ru(bpy)<sub>2</sub>(L)]Cl<sub>2</sub> complexes", *Carbohydr. Res.* **2017**, *446-447*, 19-27.

M. Pröhl, C. Englert, M. Gottschaldt, U. S. Schubert, J. C. Brendel, "RAFT polymerization and thio-bromo substitution: an efficient way towards well-defined, large glycopolymers", *J. Polym. Sci., Part A: Polym. Chem.* **2017**, *55*, 3617-3626.

H. Weiss, J. Reichel, H. Görls, K. R. A. Schneider, M. Micheel, M. Pröhl, M. Gottschaldt, B. Dietzek, W. Weigand, "Curcuminoid-BF<sub>2</sub>-complexes: Synthesis, fluorescence and optimization of BF<sub>2</sub> group cleavage", *Beilstein J. Org. Chem.* **2017**, *13*, 2264-2272.

C. Englert, C. Bader, P. Borchers, J. Alex, M. Pröhl, M. Hentschel, M. Hartlieb, A. Träger, G. Pohnert, M. Gottschaldt, U. S. Schubert, "Chemicals on demand: Light-induced opening of microparticle containers", *Angew. Chem. Int. Ed.* **2017**, submitted.

## Patents

M. Gottschaldt, M. Pröhl, C. Englert, U. S. Schubert, “Kationische Polymere mit D-Fructose-Substituenten”, Germ. Pat. Appl. Ref. No. 102017003004.9, 2017.

## Manuscripts in preparation

M. Pröhl, S. Seupel, P. Sungur, S. Höppener, M. Gottschaldt, J. C. Brendel, U. S. Schubert, “The influence of the grafting density of glycopolymers on the lectin binding affinity of block copolymer micelles”, *Polymer* **2017**, submitted.

## Acknowledgement / Danksagung

This thesis was not possible without the help of a lot of people I would like to thank here.

At first, I want to thank my scientific supervisor **Dr. Michael Gottschaldt**. I always found a sympathetic ear, when I had problems I struggled with. Your knowledge of carbohydrate chemistry strongly supported me over the years and I learned a lot. Additionally, I want to thank you for the opportunity I got at the beginning and for the trust.

I would also like to thank **Prof. Dr. Ulrich S. Schubert** for giving me the opportunity to work in his group and to prepare this thesis. I enjoyed working in an international and incredible well-equipped group like this.

Almost everything I did in the lab I learned from my practical supervisor and friend **Dr. Justyna Czaplewska**. I remain in deep gratitude for your practical skills you shared with me and I am sustainable impressed from the delicacy and taste of your food, you prepared plenty of times for the sugar sub-group.

I want to acknowledge **Dr. Johannes C. Brendel** for the perfect teamwork in the last year and for the great supervision.

I am grateful to **Prof. Dr. Wolfgang Weigand** for carefully reading this thesis and for the great collaboration.

Furthermore, I would like to thank all co-authors I worked with over the years for their contribution to the publications, in particular **Tanja Buś, Dr. Anja Träger, Michael Deicke, Henning E. A. H. Weiss, Christoph Englert, Carolin Kellner, Pascal D. Moser, Patrick Hoffmann** and **Dr. Helmar Görls**.

I also want to thank my former students **Fritz Schömberg** and **Pascal D. Moser** for the time they spent in the lab.

I would further like to thank **Meike N. Leiske** for the countless lunch-times in the spacebox. I always enjoyed this thirty minutes break together with you and I know that you are still impressed from the variety of my food over the last three years.

An incredible important part for the motivation and success represents the working atmosphere initiated by the coworkers. I would like to thank my valued colleagues, who had to sit in the office and work in the laboratory with me: **Dr. Justyna Czaplewska, Dr. Matthias Hartlieb, Dr. David Pretzel, Tobias Majdanski, Christoph Englert, Meike Leiske, Dr. Turgay Yildirim, Susanne Seupel** and **Patrick Hoffmann**. Also the people, I spent time with by various activities are acknowledged: **Dr. Pier F. Caponi** (a.k.a. Scimmietta) and **Renzo Paulus**

I would also like to thank some more group members, who contributed different things to my work: **Carolin Kellner** for performing plenty of bio assays fast and effectively, **Dr. Anja Träger** and **Tanja Buś** for flow cytometry and CLSM measurements, **Dr. Peter Bellstedt** and **Gabriele Sentis** for NMR measurements, mostly immediately after I asked, **Beate Lentvogt** and **Sandra Köhn** for elemental analysis, **Dr. Stephanie Höppener** for the support with IR measurements and **Dr. Helmar Görls** for X-Ray measurements of my compounds and of accidentally given glass and NaCl. Extraordinary acknowledged is also **Nicole Fritz** for her continuous support, when the ESI-MS did not do, what I wanted it to do. **Uwe** and **Sandra Köhn** are thanked for ordering and ensuring, that all shelves are filled with the necessary consumables. In terms of administrative work, I would also like to thank **Simone Burchardt, Sylvia Braunsdorf** and **Franca Frister** for organizing this huge group. Highly acknowledged is **Renzo Paulus** for his continuous support with all IT issues.

Also, people outside of the work deserved to be acknowledged here for their endorsement on another level. I want to thank my parents **Thomas** and **Heike Pröhl** for supporting me in any decision I ever made, my sister **Anja Zwicker**, my brother-in-law **Heiko Zwicker**, for being able of arranging and fixing everything in my apartment, my beautiful niece **Mia-Sophie Zwicker**, my grandmother **Wilma Pröhl** for basically supplying me with tons of food and my grandfather **Helmut Johannes Pröhl**, who was an example of kindheartedness and who in particular influenced me sustainably.

Dear **Thesi**, I would like to thank you for accepting me with all my whims and for your steady believe in my person. There is no woman out there, which fits better to me than you.

## **Declaration of authorship / Selbstständigkeitserklärung**

Ich erkläre, dass ich die vorliegende Arbeit selbständig und unter Verwendung der angegebenen Hilfsmittel, persönlichen Mitteilungen und Quellen angefertigt habe.

I certify that the work presented here is, to the best of my knowledge and belief, original and the result of my own investigations, except as acknowledged, and has not been submitted, either in part or whole, for a degree at this or any other university.

Jena, der

---

Michael Pröhl

## **Publications P1 to P6**

**P1:** Reprinted by permission of Elsevier.

**P2:** Reprinted by permission of Wiley VCH.

**P3:** Reprinted by permission of Wiley VCH.

**P4:** Reprinted by permission of Elsevier.

**P5:** Reprinted by permission of Wiley VCH.

**P6:** Reprinted by permission of Beilstein.

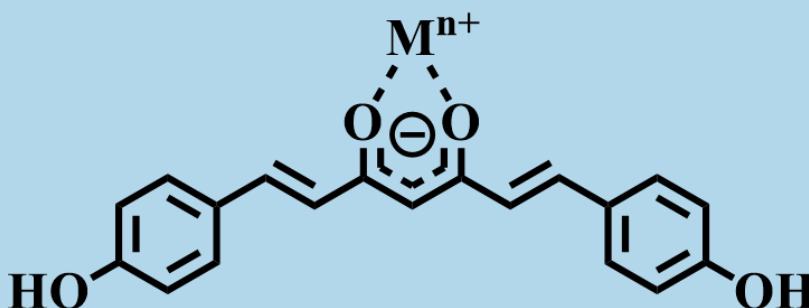


## Publication 1

### Metal complexes of curcumin and curcumin derivatives for molecular imaging and anticancer therapy

M. Pröhl, U. S. Schubert, W. Weigand, M. Gottschaldt

*Coord. Chem. Rev.* **2016**, 307, 32-41



#### *IMAGING*

##### Emitting metal ions

$^{99m}\text{Tc}^+$ ,  $^{68}\text{Ga}^{3+}$

$\text{Gd}^{3+}$

$\text{Eu}^{3+}$ ,  $\text{Ln}^{3+}$

##### Vizualization

SPECT, PET

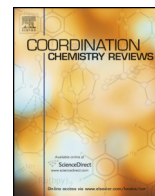
MRI

NIR

#### *THERAPY*

PDT approach:  $\text{V}^{5+}$ ,  $\text{Cu}^{2+}$

Intercalation:  $\text{Ru}^{2+}$ ,  $\text{Zn}^{2+}$



## Review

# Metal complexes of curcumin and curcumin derivatives for molecular imaging and anticancer therapy



Michael Pröhl<sup>a,b</sup>, Ulrich S. Schubert<sup>a,b</sup>, Wolfgang Weigand<sup>b,c</sup>, Michael Gottschaldt<sup>a,b,\*</sup>

<sup>a</sup> Laboratory of Organic and Macromolecular Chemistry (IOMC), Friedrich Schiller University Jena, Humboldtstraße 10, 07743 Jena, Germany

<sup>b</sup> Jena Center for Soft Matter (JCSM), Friedrich Schiller University Jena, Philosophenweg 7, 07743 Jena, Germany

<sup>c</sup> Institut für Anorganische und Analytische Chemie, Friedrich Schiller University Jena, Humboldtstraße 8, 07743 Jena, Germany

## Contents

1. Introduction.....	33
2. Complexes for molecular imaging.....	33
2.1. Radionuclides and MRI-tracer.....	33
2.2. Fluorescent probes.....	34
3. Potential anticancer agents.....	35
3.1. PDT-agents.....	35
3.2. DNA intercalating or binding agents.....	37
3.3. Complexes with other modes of action.....	39
4. Conclusions.....	40
Acknowledgements.....	40
References.....	40

## ARTICLE INFO

## Article history:

Received 20 May 2015

Accepted 2 September 2015

Available online 9 September 2015

## Keywords:

Anticancer

Imaging

PDT

Curcumin

Metal complexes

## ABSTRACT

Curcuminoids are highly bioactive, polyphenolic compounds derived from the roots of *Curcuma longa*. Among them, curcumin is the best known and shows potential against various diseases, such as cancer, neurodegenerative, autoimmune and infectious diseases combined with nontoxicity up to high dosages and fluorescent properties. Unfortunately, it has some disadvantages, e.g., a poor solubility in water or a rapid clearance, which prevent this natural compound from reaching its potential. There are many strategies to overcome these drawbacks, most notably the application of nanoparticulate, micellar or liposomal carriers. Various metals also have advantageous properties that can be used to mitigate the inherent disadvantages of curcumin, such as higher stability under physiological conditions and ease of detection *in vivo*. Metal complexes of curcumin and its derivatives broaden the potential applications in

**Abbreviations:** 2PM, two-photon microscopy; 9Accm, 1,7-(di-9-anthracene-1,6-heptadiene-3,5-dione); A2780, human ovarian carcinoma cell line; A549, human lung adenocarcinoma epithelial cell line; Aβ, beta-amyloid; acac, acetylacetone pentan-2,4-dione; acdppz, 1-(9-acridinyl)dipyrido[3,2-a:2',3'-c]phenazine; AchE, acetylcholine; AD, Alzheimer disease; B16, mouse melanoma cell line; BBB, blood–brain barrier; bDHC, bis(dehydroxy)curcumin, (1E,6E)-1,7-Bis(3-methoxyphenyl)-1,6-heptadiene-3,5-dione; bpy, 2,2'-bipyridyl; Cisplatin, cis-diamminedichloroplatinum(II); CRANAD-1 and -2, compounds 2 and 3 synthesized by Ran for Alzheimer disease; CUR, curcumin, (1E,6E)-1,7-Bis(4-hydroxy-3-methoxyphenyl)-1,6-heptadiene-3,5-dione; DAD, donor–acceptor–donor structure; DIP, 4,7-diphenyl-1,10-phenanthroline; dppz, dipyrido[3,2-a:2',3'-c]phenazine; DTPA, pentetic acid, 2-[Bis(2-[bis(carboxymethyl)amino]ethyl)amino]acetic acid; DAC, diacetylcurcumin, (1E,6E)-1,7-Bis(4-acetoxy-3-methoxyphenyl)-1,6-heptadiene-3,5-dione; EGFR, epidermal growth factor receptor; ESI-MS, electron spray ionization mass spectrometry; FDA, Food and Drug Administration; ferrocenyl, Fe, bis(η<sup>5</sup>-cyclopentadienyl)iron; HCT116, human colon-rectal tumor cell line; HeLa, human epithelial carcinoma cell line; HEK293, nontumorous human embryonic kidney cell line; HSA, human serum albumin; IC<sub>50</sub>, half maximal inhibitory concentration; ICT, intramolecular charge transfer; imi, imidazole; isc, isocyanocyclohexane; JNK, c-Jun N-terminal kinases; LAN-5, human neuroblastoma cell line; L-Met, L-methionine; log K<sub>ow</sub>, logarithm of partition coefficient in a octanol–water–system; L-Trp, L-tryptophan; L-Tyr, L-tyrosine; Ln, lanthanoid; MCF-7, human breast adenocarcinoma cell line; MRI, magnet resonance imaging; mRNA, messenger RNA; NIR, near infrared; p53, tumor protein p53; PBS, phosphate buffered saline; PDT, photodynamic therapy; PET, positron emission tomography; Ph, phenyl; phen, 1,10-phenanthroline; PI, propidium iodide; PTA, 1,3,5-triaza-7-phosphaadamantane; py, pyridine; RAPTA-C, [(η<sup>6</sup>-p-ymene)Ru(II)(PTA)Cl<sub>2</sub>]; RNS, radical nitrogen species; ROS, radical oxygen species; SPECT, single photon emission computed tomography; tpy, 2,2',6',2''-terpyridine; TPA, two photon absorption; tpp, triphenylphosphine; TPPBr, p-triphenylphosphoniummethylbromide; U-87, human glioblastoma cell line.

\* Corresponding author at: Laboratory of Organic and Macromolecular Chemistry (IOMC), Friedrich Schiller University Jena, Humboldtstraße 10, 07743 Jena, Germany. Tel.: +49 3641 9485 65; fax: +49 3641 9482 02.

E-mail address: [michael.gottschaldt@uni-jena.de](mailto:michael.gottschaldt@uni-jena.de) (M. Gottschaldt).

comparison to the parent ligand in modern imaging and anticancer strategies. A number of promising derivatives have been published so far. This review focuses on metal complexes of curcumin and its derivatives for imaging and anticancer application.

© 2015 Elsevier B.V. All rights reserved.

## 1. Introduction

Curcumin, also called diferuloylmethane, is an active, polyphenolic compound derived from the root of turmeric (*Curcuma longa*) [1]. It was first isolated in 1815 and synthesized for the first time in 1910 [2]. Many studies were published about curcumin, its analogs, and their biological activity. Curcumin seems to be toxic to cancerous cells and cytoprotective to healthy cells [1]. Furthermore, it interacts with a wide range of molecular targets related to different neurodegenerative, infectious, autoimmune, and other diseases [3]. Additionally, it is nontoxic up to high dosages [4]. However, phase I and II clinical trials involving several types of cancer revealed the major limitations of curcumin [1]. Its poor bioavailability caused by low serum levels, restricted tissue distribution, rapid metabolism, and poor solubility prevent the effective clinical application of curcumin [5]. Recently, many research groups have sought to overcome these disadvantages and improve the bioavailability of curcumin using a number of different strategies; notable among them are adjuvants such as piperine [6] as well as delivery systems based on nanoparticles [7], liposomes [8], or micelles [9]. Another strategy to increase the compound's biological activity is the modification of the curcumin skeleton as shown in Fig. 1. For instance, the introduction of various groups instead of phenolic hydroxyl-groups could avoid the abstraction of protons and the subsequent degradation of curcumin under basic conditions [10]. The diketo-moiety is part of the degradation process [11]. In the last few decades a considerable number of compounds with an altered curcumin structure were synthesized in order to evaluate the resulting changes in biological activity. Many advantageous structures were found and number of quality articles have been published covering the subject [4,12–15].

A variety of metal ions can be complexed by the  $\beta$ -diketo-moiety of curcumin. The metal complexes so formed often possess a higher stability than the easily degraded curcumin itself. The first complexes of curcumin with medically valuable transition metals, such as Pd, Pt, Rh, and In, were published in 1997 [16]. In most cases the resulting complexes exhibited favorable biological activity compared with the parent ligands for a number of molecular targets.

Already published review articles focused Cu- and Zn-complexes of curcumin [17,18], this article instead discusses complexes of curcumin and its derivatives with various metals including not only Cu- and Zn-complexes. Another excellent article was published recently [19]. It provides a more general overview about chemical properties of curcumin, the synthesis and characterization of various corresponding metal complexes and their non-medical and medical applications. The present work gives a complementary but more detailed view on metal complexes of curcumin and its derivatives strongly focusing on compounds for molecular imaging and anticancer therapy. The first part deals with complexes for imaging applications with an emphasis on

fluorescent probes and radionuclide complexes. The second part has a focus on complexes with potential anti-cancer activity via various mechanisms of action, such as photodynamic therapy or intercalative DNA binding.

## 2. Complexes for molecular imaging

Modern imaging is based primarily on the measurement of various signals with subsequent conversion to obtain interpretable data. Common strategies include the detection of positrons (PET, positron emission tomography), gamma rays (SPECT, single photon emission computed tomography), and other emitted radiation of different wavelengths (fluorescence, X-rays) as well as changes in electron environments (MRI). This section will focus on curcumin bearing complexes that can be detected using one of the aforementioned techniques.

The interaction of curcumin with a high number of biological targets [3] means that complexes of curcumin and its derivatives can be used to visualize various pathological structures linked to different diseases. Besides the Parkinson's disease, amyotrophic lateral sclerosis (ALS), and Alzheimer's disease (AD) are widespread neurodegenerative afflictions of modern societies. In the case of AD, its progression is multifactorial. One cause is the imbalance between pro-oxidant homeostasis supported by radical oxygen (ROS) and nitrogen species (RNS) and the anti-oxidant counterparts such as superoxide dismutase and glutathione. Furthermore, the aggregation of beta-amyloid (A $\beta$ ) and the inhibition of acetylcholine (AChE) can be correlated to AD. There are two kinds of A $\beta$  plaques associated with AD: dense core plaques are fibrillar and diffuse core ones are amorphous deposits.[20] Epidemiological studies exhibited that there is a significantly smaller AD rate in India, which could be linked to the elevated consumption of turmeric relative to other regions [13]. The hydrophobic part of the contained curcumin allows them to cross the blood–brain barrier (BBB), while the polar elements are responsible for protein binding. In addition, both the deprotonation of the phenolic groups and the stabilization of the resulting charge in the  $\pi$ -conjugated system seem to be important [21]. Metal complexes of curcumin and its derivatives might share these properties of the parent ligands and are therefore interesting candidates for imaging of A $\beta$  plaques. In addition, curcumin and its derivatives bind due to their miraculous bioactivities to many receptors, resulting in a higher selectivity for certain cancer cells, which means that they have significant potential for use in the imaging of cancer-related pathological structures [1,12,22].

### 2.1. Radionuclides and MRI-tracer

PET-based imaging exploits the emission of positrons by radionuclides, such as  $^{18}\text{F}$  or  $^{123}\text{I}$ , during their decay. A positron travels a short distance through the tissue before it is annihilated due to collision with an electron. The subsequent emission of two  $\gamma$ -rays is analyzed by the surrounding detectors [23]. Since the development of PET in 1975, interest in potentially useful nuclides has grown steadily. Currently, non-metallic positron emitters, such as  $^{18}\text{F}$  or  $^{123}\text{I}$ , are applied most frequently, but a number of metal-based compounds are either in the early or later clinical stages, such

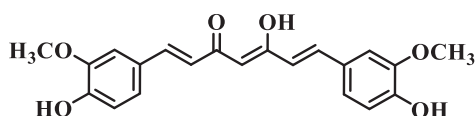


Fig. 1. Schematic representation of curcumin.

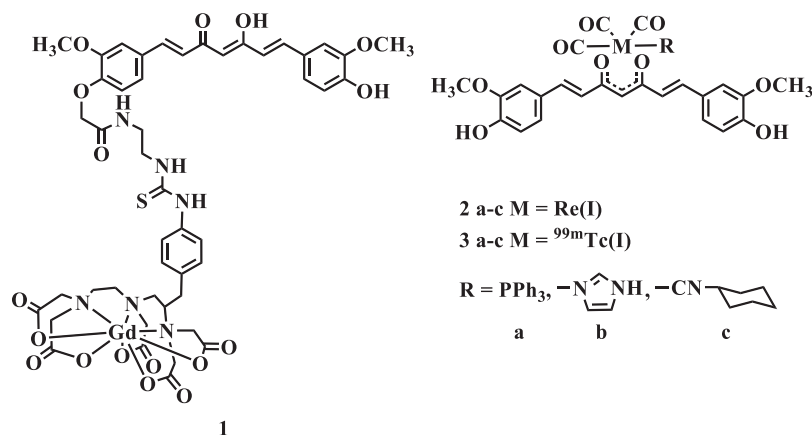


Fig. 2. Schematic representation of the complexes **1** [26], **2a–c** and **3a–c** [27,28] aimed to image A $\beta$  aggregates with different techniques.

as  ${}^{64}\text{Cu}$ -,  ${}^{111}\text{In}$ -, and  ${}^{90}\text{Y}$ -labeled radiopharmaceuticals [24]. SPECT devices make use directly  $\gamma$ -particle emitters. The use of collimators and a gamma camera widens the efficiency of this technique compared with common X-ray examinations [23]. Of preeminent importance for SPECT imaging is  ${}^{99\text{m}}\text{Tc}^+$ , a  $\gamma$ -emitter with nearly ideal properties, which is used in 70–80% of all radiodiagnostic examinations that utilize SPECT imaging [24]. Both SPECT and PET are non-invasive techniques and offer high sensitivity using only nanograms of molecular probes, but they are restricted by their poor spatial resolution. A much higher resolution is achieved with magnet resonance imaging (MRI). It can detect various endogenous and exogenous nuclei like  ${}^1\text{H}$  and  ${}^{19}\text{F}$  which are sensitive to their microenvironment. MRI offers the possibility to receive metabolic and spectroscopic information, but is limited because higher amounts of the molecular probe are required due to the technique's lower sensitivity compared with SPECT or PET [25]. Multimodal SPECT-MRI and PET-MRI devices combine the advantages of multiple systems and have sparked an intense interest in the development of multifunctional probes.

The complexes discussed in this part reflect the potential to image neurodegenerative and cancer related structures with the help of curcumin by using various modern techniques such as PET, SPECT and MRI. A Gd-curcumin complex **1** combines the advantages of fluorescence microscopy with those of MRI for multimodal detection [26]. One phenyl group of the curcumin was modified with an amine linker and the resulting structure was attached to the known contrast agent Gadopentetic acid ( $\text{Gd}^{3+}$ -DTPA), as shown in Fig. 2.

This compound is the first curcumin derivative with an amine linker on the phenyl ring, which might result in an enhanced resistance against hydrolysis, while also providing the option to perform further modifications. Changes in compound's optical properties (fluorescence wavelength and intensity) when placed in solution with A $\beta$  aggregates demonstrate the binding properties of the novel contrast agent. The longitudinal relaxivity  $r_1$  is one important parameter for MRI measurements. Contrast agents with higher relaxivities can be administered at lower doses while still providing the same image quality and the higher the relaxivity of a contrast agent the lower are the doses required of the agent [29]. The  $r_1$ -value of the amine-modified curcumin is four times higher than for  $\text{Gd}^{3+}$ -DTPA, a major advantage for MRI detection [26]. The complexation of curcumin with  ${}^{99\text{m}}\text{Tc}$  and Re was also described and does not influence the binding behavior with A $\beta$ -aggregates [27,28]. Further benefits are the emission of  $\gamma$ -particles by  ${}^{99\text{m}}\text{Tc}$  and the resulting ability to use advanced imaging techniques like SPECT. With respect to its properties, rhenium is an interesting metal for applications in radiotherapy [24], but most progressive is

the use of the  $[\text{M}(\text{CO})_3(\text{H}_2\text{O})_3]^+$  core (**2**  $M = \text{Re}$ , **3**  $M = {}^{99\text{m}}\text{Tc}$ ). The corresponding complexes can be varied by exchanging the relatively labile water ligand for different monodentate ligands such as triphenylphosphine, imidazole, or isocyanocyclohexane (Fig. 2). These “2+1”-complexes may have significant advantages over other complexes by changing properties like solubility, receptor specificity, and more. Other suitable complexes considered for multimodal applications were obtained by labeling curcumin (CUR), diacetylcurcumin (DAC) and bis(dehydroxy)curcumin (bDHC) successfully with the positron emitter  ${}^{68}\text{Ga}$  [30]. Complexes of the general structure  $[\text{GaL}_2]^+$  were prepared in high radiochemical yield and purity, extensively characterized, and revealed to possess high stability with regard to transmetalation and transchelation. In particular  $[\text{Ga}(\text{CUR})_2]^+$  and  $[\text{Ga}(\text{DAC})_2]^+$  demonstrated a high affinity for A $\beta$ -aggregates, and thus they represent potentially suitable reagents for the early diagnosis of AD with PET. Incubation of A549 lung cancer cells with the mentioned Ga-complexes revealed fluorescence intensity at least comparable to the parent ligands. Additionally, the localization of the complexes within the cells is different from conventional curcumin due to hydrophobicity differences and hydrogen bridge bonds. They also show very high stability when exposed to DTPA or  $\text{Fe}^{3+}$ ,  $\text{Cu}^{2+}$  and  $\text{Zn}^{2+}$  solutions. Therefore, they might be interesting candidates for multimodal diagnosis of lung cancer [30].

## 2.2. Fluorescent probes

In the case of curcumin and its derivatives, the emitted fluorescence is a result of the delocalized  $\pi$ -conjugated electronic system and is strongly influenced by solvents, tautomerism, and structural modifications [13].

Complex **4** has two *N,N'*-dimethyl groups in the *p*-positions of the aromatic rings of curcumin and a boron difluoride moiety at the enol–keto-group (Fig. 3) [31].

These modifications cause a strong red shift of the fluorescence, opening up the compound's application as a tracer in near-infrared (NIR) microscopy, a non-invasive, inexpensive technique with relatively high penetration depth [33]. In solution with A $\beta$ -aggregates the quantum yield was increased and the complex shows a blue shift of the fluorescence from  $\lambda = 805\text{ nm}$  to  $\lambda = 715\text{ nm}$ , which is attributed to its incorporation into the hydrophobic environment of the aggregates. With  $\log K_{\text{ow}} = 3$ , the complex is relatively hydrophobic and can pass the BBB. This was demonstrated by wild-type mice experiments. The injected complex concentration was measured at different time points postmortem and exhibited a fast clearance from the blood but a significantly slower clearance from the brain. *Ex vivo* histology further supported this observation

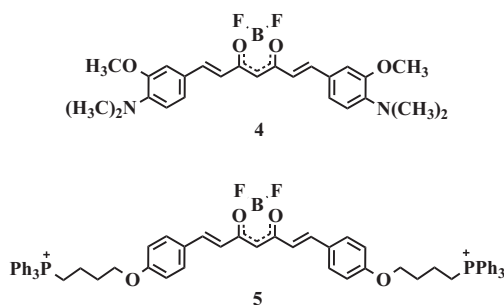


**Fig. 3.** Schematic representation of the complexes **4** [31] and **5** [32] showed beneficial fluorescent properties for NIR microscopy or enhanced cell uptake (anions omitted).

[31]. Another study sought to systematically alter the curcumin ligands in such  $\text{BF}_2$ -complexes [34]. For instance, the introduction of a *meso*-phenyl ring did not essentially change the photophysical properties. The interesting feature of this modification was the possibility to introduce further groups at the ring to modulate solubility and  $\pi$ - $\pi$ -stacking interactions without changes of the fluorescence properties. Moreover, some  $\text{BF}_2$ -complexes of curcumin and its derivatives have been recently synthesized [32]. The aromatic rings were modified with a variety of electron donors, resulting in the fine-tuning of the optical properties. All complexes show fairly high photostabilities and quantum yields. The conversion to an intermediate triphenylphosphane introduced charges which might support the absorption of complex **5** in the cell plasma (Fig. 3). Fluorescence measurements of this complex incorporated into gastric cancer cells revealed a strong green fluorescence without significant cell toxicity. However, due to aggregation effects, all  $\text{BF}_2$ -complexes show a strong decrease of fluorescence in phosphate-buffered saline (PBS) solution.

Some alterations of the curcumin ligand have been demonstrated to shift to the intended fluorescence wavelength. The introduction of two ethyl functionalities to the phenyl rings leads to a bipolar donor-acceptor-donor structure (D-A-D), that is favorable for two-photon microscopy (2PM) [35]. Complexation with copper (II) ions results in a square-planar complex. Due to intramolecular charge transfer (ICT), an approximately 3-times larger two photon absorption (TPA)-cross section ( $\sigma$ ) compared with the free ligand is observed. *In vitro* assays with MCF-7 breast cancer cells revealed that the complex is nontoxic and relatively stable under light exposure. *In vivo* studies in mice indicated an increased fluorescence in tumor tissues traced back by the authors to the overexpression of epidermal growth factor receptor (EGFR). Comparable results were obtained with the  $[\text{M}(\text{DAC})_2]$  complexes ( $\text{M} = \text{Zn}^{2+}, \text{Ni}^{2+}$ ) [36]. In terms of diagnostic advantages, the complex displayed moderate  $\sigma$ -values, optimal laser excitation wavelength of  $\lambda = 760 \text{ nm}$ , a low cellular toxicity even at longer incubation times or higher concentrations, and a cellular uptake in the cytosol or nucleus of MCF-7 cells. Two lanthanide (Ln) complexes  $[\text{M}(\text{py})_2(\text{CUR})_3]$  (**6**, **7**) with two additional pyridine ligands were synthesized by the same group (Fig. 4) [37].

The planar structure ensures an extension of the  $\pi$ -conjugated system. Therefore, increased fluorescence compared with the complexes with rare earth metals without the pyridine ligands, could be observed. Additionally, the Eu-complex shows luminescence in the NIR region, which is enabled by the pyridine ligands. Remarkably, both Ln-complexes are nontoxic and possess high  $\sigma$ -values and, therefore, seem to be suitable for single or two-photon fluorescence imaging. Further tests with propidium iodide (PI) demonstrated the increased hydrophobicity compared with the Zn- and Ni-complexes by enhanced localization on the cell membrane. Introduction of butyl groups creates bipolar D-A-D ligand like mentioned before and the resulting  $\text{Cu}_2$ -complex **8**

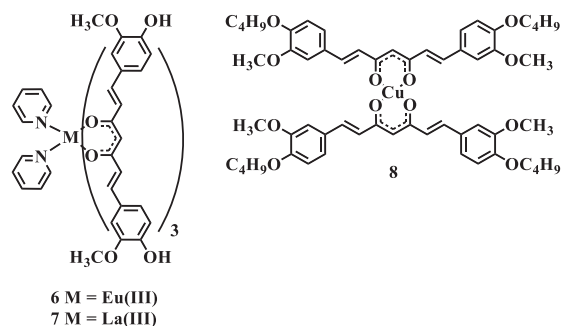


**Fig. 4.** Schematic representation of the curcumin complexes **6**, **7** [37] and **8** [38] used for cancer cell imaging.

exhibited the ability to distinguish between normal and cancerous lung tissue *in vivo*, being nontoxic up to high concentrations at the same time [38]. One reason could be the better matching of complex **8** and the monoclonal anti-EGFR antibody. These studies may provide important insights for the future development of novel imaging probes. The last few examples clearly revealed how the complexation of curcumin and its derivatives can result in improved  $\sigma$ -values. Such improvements are critical for applications in 2PM, which is advantageous for its large penetration depth and low tissue autofluorescence and self-absorption [36].

In conclusion, curcumin and its derivatives are suitable ligands for metal complexes. Re,  $^{99\text{m}}\text{Tc}$ ,  $^{68}\text{Ga}$ , and Gd complexes were successfully synthesized and tested toward application in PET, SPECT and MRI. Furthermore, the introduction of the  $\text{BF}_2$ -moiety, complexation with metals like  $\text{Cu}^{2+}$  or  $\text{Zn}^{2+}$  as well as the modification of the ligand itself can change its fluorescence excitation wavelength in either direction, resulting in the ability to utilize a wide range of different fluorescence techniques, such as NIR microscopy or 2PM. Finally, the highly bioactive curcumin skeleton binds to cancer-related or neurodegeneration related pathological structures and the coordinated metals allow metal complexes of curcumin and its derivatives to generate useful images of these structures.

### 3. Potential anticancer agents

Cancer is the leading cause of death in developed countries and the second-largest cause of death in developing countries after cardiovascular diseases [22]. More than 200 types of cancers are known in humans, depending on tissue and cell type [22]. The most clinically established cancer treatment strategies are surgery, radiotherapy, and chemotherapy. The chemotherapeutic approach uses a combination of drugs with various mechanisms of action to enhance the therapeutic efficiency. Roughly 80% of all FDA-approved drugs arise from natural products, targeting a huge number of molecular structures [39]. Among the large number of known phytochemicals, structures of curcumin and its derivatives offer high potential for the treatment of cancer. Curcumin itself inhibits tumor proliferation, growth, metastasis, invasion and angiogenesis and causes damage even in apoptosis resistant cells [12]. This section discusses potentially anticancerous metal complexes of curcumin and its derivatives with various mechanisms of action.

#### 3.1. PDT-agents

Photodynamic therapy (PDT) is a minimally invasive technique for the treatment of various diseases. It can be used to induce cancer death via apoptosis or necrosis, harm the tumor's critical vascular system or cause inflammatory reactions. PDT has many benefits compared with chemotherapy, radiotherapy, or surgery.



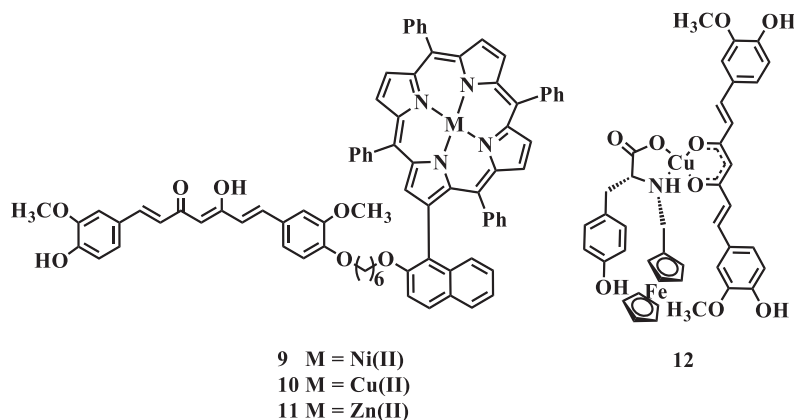


**Fig. 5.** Schematic representation of porphyrin linked curcumin complexes **9–11** [43] and curcumin copper complex with ferrocenyl conjugated reduced Schiff-base of L-tyrosin as ancillary ligand **12** [44].

Only a few of them will be discussed here, including reduced long-term morbidity, no resistance development due to the absence of  $^1\text{O}_2$ -eliminating mechanisms, and no negative consequences of repeated treatments. The three basic components of any photodynamic approach are light, oxygen, and the photosensitizer [40]. The most widely used photosensitizer in current clinical use is Photofrin®, a tetrapyrrole-containing compound. However, this compound has several disadvantages, e.g., long-lasting skin photosensitivity and low absorbance at  $\lambda = 630 \text{ nm}$  [41]. Hence there is great interest in alternatives which offer advantages over Photofrin®, including absorption between  $\lambda = 600 \text{ nm}$  and  $800 \text{ nm}$ , rapid clearance from non-pathological tissue, and low toxicity in the absence of an optical trigger is still high [40]. Curcumin displays strong antioxidant properties, which have been widely investigated for the treatment of and protection against neurodegenerative diseases [13]. However, it was proved multiple times that curcumin also have pro-oxidant properties, which means it is capable of both performing oxidation processes and protecting against them at the same time. Consequently, the underlying mechanism of radical generation by curcumin has been investigated. Laser flash photolysis ( $\lambda = 355 \text{ nm}$ ) of curcumin reveals its ability to generate  $^1\text{O}_2$  and  $\cdot\text{OH}$  radicals, potentially causing biological damage in the presence of oxygen and light [42]. Hence, curcumin and its derivatives are not simply ligands for increasing the bioavailability or selectivity of compounds used in PDT. They offer the potential to perform photodynamic therapy at different excitation wavelengths, a worthwhile approach for superficial diseases.

Bridging the curcumin moiety *via* 1,6-dibromohexane and a hydroxynaphthyl-group to a porphyrin molecule yielded in an interesting modification of the curcumin skeleton [43]. The ligand, as well as the resulting metal complexes **9–11**, show strong binding interactions with DNA and light-triggered cleavage activity (Fig. 5).

Those compounds combine the benefits of curcumin with the thoroughly investigated ones of porphyrin complexes, such as generating  $^1\text{O}_2$  and  $\text{OH}$  radicals, fine tuning of properties and others. A novel class of Cu-complexes (Fig. 5) contains the curcumin ligand on one site and biologically relevant L-amino acids such as, L-Tyr, L-Trp and L-Met bound to a ferrocenyl (Fc) moiety on the other [44]. They reveal complete cleavage of DNA after excitation at  $\lambda = 454 \text{ nm}$  and are nontoxic in the absence of an optical trigger. This effect was not observed under an Ar-atmosphere, which emphasizes the necessity of oxygen. Different inhibition tests identified the hydroxyl radical as the cleaving species. The curcumin-conjugated Cu-complexes showed a higher cytotoxicity after irradiation than the free ligand and the acetylacetonate-conjugated (acac) complexes. Curcumin is not just a fluorophore here, but rather the key structure for causing apoptotic cell death by the photodynamic

approach. All complexes which connect curcumin by a Cu-center with the Fc-appended reduced Schiff-bases of amino acids demonstrated a cytosolic localization just like current porphyrin-based PDT-agents. Other data was published that showed undesirable properties of the complexes compared with the parent compound [45]. The authors synthesized a set of curcumin-metal(II) hydroxo complexes ( $\text{M} = \text{Cu}^{2+}$ ,  $\text{Zn}^{2+}$ ,  $\text{Cd}^{2+}$ ) by using nitrate metal salts. The complexation inhibits the cytotoxicity of curcumin itself. Possible reasons could be the pre-exhaustion of curcumin due to the reaction with the nitrates or the geometry and symmetry of the resulting complexes. Similarly, the size of the cations might influence the cytotoxicity, since the Cd-complex shows higher  $\text{IC}_{50}$  values than the Cu- and Zn-ones in all tested cancer cell lines.

Since the curcumin-conjugated vanadyl complex with  $\text{VO}^{2+}$ -core showed complementary inhibition effects on mouse lymphoma cell proliferation like curcumin alone or vanadyl sulfate [46], it received significant attention from the scientific community. Banerjee et al. investigated for the first time the phototoxicity of curcumin complexes containing the  $\text{VO}^{2+}$ -core in HeLa cells [47]. The authors synthesized a complex **13** with comparable phototoxicity to that of Photofrin®. The complexation of curcumin increases the solubility, introduces metal-based NIR absorption, and supports the photocytotoxicity due to the dipyrrophenazine (dppz) ligand (Fig. 6).

Once taken up into HeLa cells, the complex mainly localizes in the cytoplasm with slight nuclear uptake and triggers cell death by apoptosis after photoirradiation. A conversion of supercoiled to nicked circular DNA of almost 90% at  $\lambda = 785 \text{ nm}$  indicates the excellent DNA cleavage activity of this compound. Moreover, a set of novel bioorganometallic oxovanadium complexes **14a–c** were tested in a photodynamic approach (Fig. 6) [48,49]. They contain several structures of curcumin and its derivatives combined with a terpyridine group to introduce different moieties. The complexation of curcumin and its derivatives can enhance the relevant properties. The Fc-methyl-bis-(2-pyridylmethylamine), bis-(2-pyridylmethyl)benzylamine and curcumin moieties did not show remarkable photo-induced cleavage activity of DNA. Additionally, the complexation overcomes the hydrolytic instability of curcumin in cell media. The resulting complexes bind to the DNA by surface aggregation and/or groove binding without significant changes of the specific viscosity of the DNA. They show toxicity following exposure to visible light by the formation of  $\text{OH}$  radicals *via* a redox pathway and low toxicity in the dark. The complexes with acac instead of curcumin exhibit much higher  $\text{IC}_{50}$  values, accentuating the major role of curcumin in phototoxicity. The attachment of Fc enhanced the phototoxicity and the cellular uptake with localization in the cytoplasm and nucleus

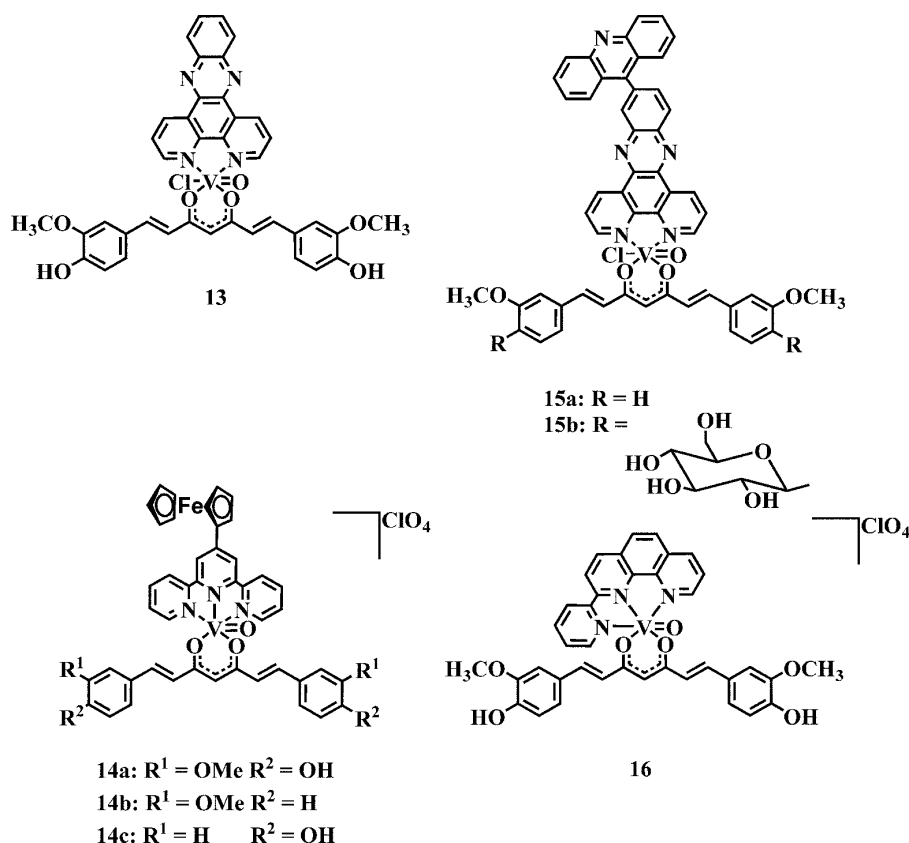


Fig. 6. Schematic representation of a set of selected oxovanadyl curcumin complexes **13** [47], **14a–c** [48,49], **15a**, **15b** [50] and **16** [51].

[48,49]. This could represent a novel approach for the design of curcumin-bearing complexes. Recently, more promising oxovanadium curcumin complexes were prepared by altering the tpy-ligand with a p-triphenylphosphonium methyl phenyl bromide (TPPBr-Ph) [52]. The resulting complex is highly toxic under light exposure in HeLa and MCF-7 cells by producing OH radicals. However, due to the TPPBr-moiety, they are also significantly toxic in the absence of light. The cationic TPPBr-group is responsible for mitochondrial targeting inside the cells. A nearly hundred percent uptake and such specific intracellular localization results in a higher phototoxicity of this curcumin complex compared with the acac-based one. Another oxovanadium complex with curcumin completed by a (modified) naphthalimide moiety was highly active [53]. An intercalative DNA binding mode of this complex is responsible for the cytotoxicity, resulting in low  $\text{IC}_{50}$  values comparable to Photofrin®. Other potential PDT agents that revealed excellent properties were prepared by the Banerjee group [50]. The oxovanadium complexes **15a** and **15b** bear (diglycosylated) curcumin as well as a 1-(9-acridinyl)dipyrido[3,2-a:2',3'-c]phenazine (acdppz)-moiety (Fig. 6). The glucose units increase the water solubility of the curcumin and enhance the cellular uptake in cancer cells. The planarity of the acdppz-group augments the photocytotoxicity and facilitates fluorescence measurements due to the strong green emission. Both complexes show phototoxicity in nanomolar concentrations, which is more efficient than Photofrin®, combined with low toxicity in the absence of light. NIR DNA cleavage by the  $^1\text{O}_2$  pathway, cellular damage by apoptosis, and intercalative DNA binding combined with advantageous imaging properties might lead to a new generation of PDT agents based on curcumin complexes. The novel complex **16** offers high photocytotoxicity and is less toxic in healthy cells compared with cancerous cells with or without an optical trigger, which highlights the potential advantages of curcumin complexes with the  $\text{VO}^{2+}$ -core [51].

In another study, curcumin was attached to a  $\text{Co}^{3+}$ -chaperone-system, which was used to deliver curcumin in hypoxic tumor regions by reduction to  $\text{Co}^{2+}$  [54]. Yet another study used bioessential cobalt to form novel heteroligand  $\text{Co}^{3+}$ -complexes of curcumin with various phenanthroline bases as ancillary ligands [55]. The photocytotoxicity of these complexes increased with the planarity of the phenanthroline base. The complex  $[\text{Co}(\text{dppz})_2(\text{CUR})](\text{ClO}_4)_2$  revealed photocytotoxicity comparable to Photofrin® and strong binding efficiency to human serum albumin (HSA). Thus, it has significant potential for photochemotherapeutic applications and opens up the possibility of utilizing bioessential cobalt for curcumin complexation.

Recently, comparable Ln-complexes were synthesized as well [56]. The library of La- and Gd-complexes contains curcumin and its glycosylated analogs with Ph-tpy or pyrenyl-tpy as the second ligand. The novel complexes with  $\text{LnO}_6\text{N}_3$  cores reveal DNA plasmid cleavage under visible light irradiation by the  $^1\text{O}_2$  and OH pathways. The metal complexes of curcumin show beneficial properties compared with curcumin alone and result in the first published lanthanide curcumin complex with photoactivated anticancer activity comparable to Photofrin®.

### 3.2. DNA intercalating or binding agents

Besides the photodynamic approach, there are more possibilities to cause damage in cancer cells. A widely used and strongly investigated one is the direct interaction of different compounds with DNA. Under physiological conditions, many interaction modes exist with various parts of the DNA, both covalently and non-covalently. A possible interaction for cationic molecules is available due to the negatively charged phosphodiester groups along the double helix backbone. Interactions with the major groove of the DNA occur more readily for macromolecules such as proteins than

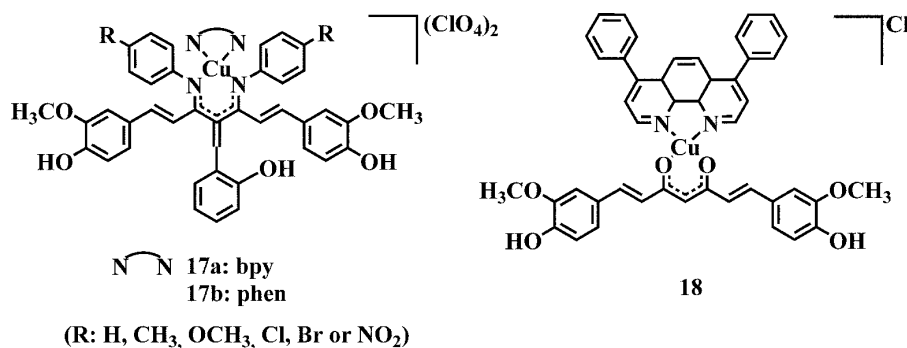


**Fig. 7.** Schematic representation of Cu-complexes with Knoevenagel condensates of curcumin and bpy **17a** or phen as second ligands **17b** [59] and DIP **18** [60] as ancillary ligands.

for small compounds. The typical minor groove binder requires the flexibility to follow the natural torsion of the double helix. A positively charged, small molecule with planar aromatic ring systems is an exemplary intercalator. Two contiguous base pairs form a binding slot for the intercalating molecule [57]. The biological consequences of an intercalative binding mode are versatile and complicated. By occupying the DNA sites, intercalators cause competitive inhibition of various enzymes, e.g., topoisomerase II, DNA polymerase, and RNA polymerase in addition to their ability to disturb the transcription and replication processes of DNA. Furthermore, messenger RNA (mRNA) synthesis can be impaired by frame-shift mutations. Intercalation causes DNA damage by single strand breaks [58].

Modified curcumin-conjugated Cu-complexes **17a** and **17b** were prepared to investigate the intercalative mode of curcumin complexes for the first time [59]. Knoevenagel condensates of curcumin were used as one ligand and 1,10-phenanthroline (phen) or 2,2'-bipyridyl (bpy) as the second ligand (Fig. 7).

The intercalation strength strongly correlates with the ligands phen and bpy. The phen complexes intercalated better than the bpy counterparts. By attaching the common curcumin together with a 4,7-diphenyl-1,10-phenanthroline-ligand (DIP) to the Cu center (Fig. 7), a novel complex **18** was obtained [60]. The DNA binding strength is strongly enhanced due to the DIP ligand and the mode of interaction was confirmed to be the intercalation of the complex between two base pairs of the DNA. Furthermore, it could be proven that the [CuL<sub>2</sub>] complexes (L = curcumin and its derivatives) show anticancer activity. *In vitro* studies showed a stronger inhibition of tumor growth and *in vivo* tests with tumor bearing mouse increasing the life span when treated with the Cu complexes [61,62]. It is implied that the efficacy of metallodrugs is dependent not only on the structure of one ligand and the metal itself, but rather on all subunits of the complex and their interactions. This central assumption was confirmed by a heteroligand, cyclopalladated curcumin containing complex [63]. It exhibited significant improvements in comparison to all the bis- or trischelated homoligand complexes with curcumin that came before it. Similar results were obtained

for the heteroligand mononuclear Pd-complex **19** (Fig. 8) [64]. It inhibited cell growth and induced apoptosis when tested *in vitro* with various human prostate cancer cell lines. Compared with curcumin alone, complex **19** is significantly more effective. The authors cite the dual functionality as a key reason for the enhanced efficacy as they attached two highly biologically active ligands on one complex. The advantages of the two ligands were combined and the poor bioavailability of curcumin was improved due to the formation of highly stable complex **19**. Other Pd-based curcumin complexes **20a** and **20b** demonstrated antiproliferative activity *in vitro* by inducing apoptosis in human colorectal cancer cells (Fig. 8) [65].

A ruthenium-arene complex of curcumin was synthesized and characterized by Caruso et al. [66]. Those “half-sandwich” complexes of Ru have good aqueous solubility, stability against ligand exchange under physiological conditions, and high anticancer activity *in vitro* and *in vivo*. The title compound **21** (Fig. 9) was tested against five different cancer cell lines (HCT116, MCF-7, A2780, U-87 and A549) and revealed the highest toxicity for the colorectal tumor cell line (HCT116).

The molecular structure of **21** in the crystal exhibited a two-dimensional network caused by the chlorine atom and the resulting hydrogen bonds. The DNA binding mode of the complex was investigated as well. Computer simulations and electron spray ionization mass spectrometry (ESI-MS) measurements revealed a 20° twist between the phenyl groups as well as characteristic Ru–N7-guanine binding. Previous studies indicated this stacking as intercalative and hydrophobic interactions [69]. Through investigation of the demethoxy and bisdemethoxy curcumin analog complexes, it was furthermore validated that the phenyl and methoxy groups of the curcumin do not influence the mechanism at all. This opens up entirely new possibilities for tailoring ligands to fine-tune biological properties [66]. Even a thiophene aromatic curcumin derivative conjugated version of complex **21** was prepared; it has moderate toxicity when tested against HeLa and human liver cancer cell lines [70]. To further enhance the anticancer activity of the complex **21**, the labile chloride ligand was exchanged against PTA to obtain the charged compound **22** with excellent properties

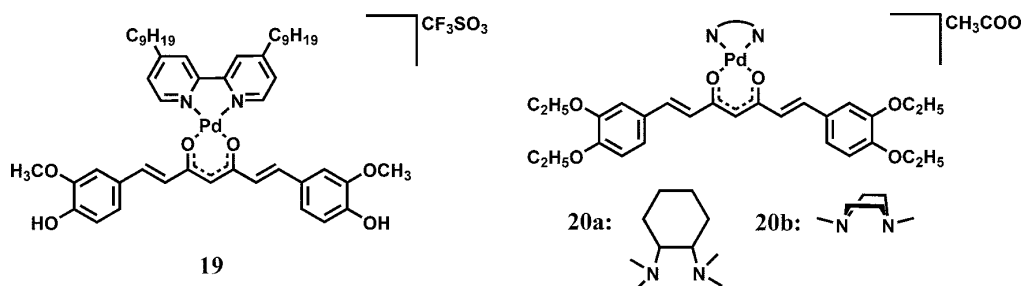


**Fig. 8.** Schematic representation of heteroligand mononuclear Pd-complexes **19** [64], **20a** and **20b** [65].



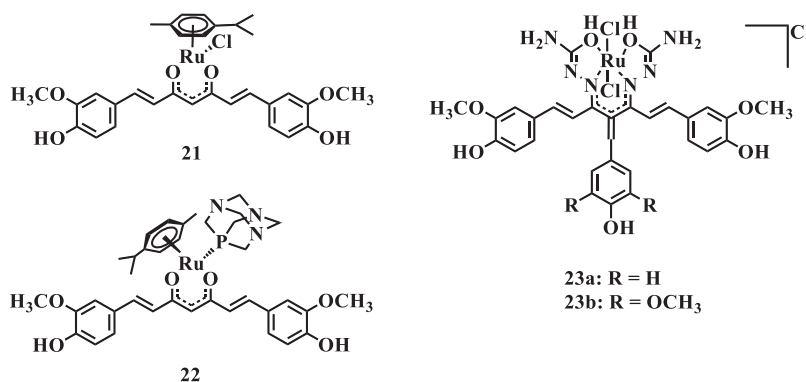


Fig. 9. Schematic representation of curcumin(oid)-conjugated Ru-complexes **21** [66], **22** [67] (anions omitted), **23a** and **23b** [68] as DNA interactive agents.

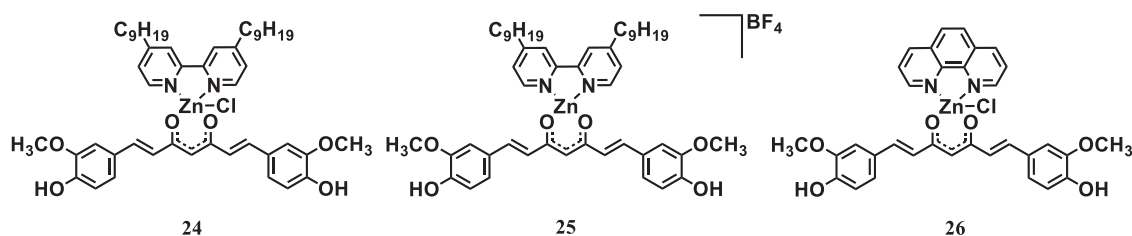


Fig. 10. Schematic representation of curcumin-bearing Zn complexes with different ancillary ligands and counterions (**24** [72], **25** and **26** [73]).

(Fig. 9) [67]. Most of these RAPTA-C like complexes show a very high toxicity in A2780 cells, which is comparable to cisplatin. The IC<sub>50</sub> values for cisplatin-resistant ovarian cancer cells are ca. 100-fold smaller than for cisplatin, offering real alternatives to platinum-based anticancer agents. Furthermore, they are less toxic to HEK293 cells, possess superior solubility and are not strongly influenced by modification of the benzyl ring or the curcumin methoxy groups, which could be used to attach relevant biomolecules for targeting. Unfortunately, the exact interaction mechanism is not yet known. The previously mentioned Knoevenagel condensates of curcumin were used to obtain two novel ruthenium complexes **23a** and **23b** (Fig. 9) [68]. The DNA interactions were identified as intercalative and non-covalent binding modes. Regarding the different ligands, there was no recognizable trend, emphasizing the complexity of the interactions. The complexes and ligands were tested against human red blood cells and revealed lower toxicity than letrozole, one drug for the treatment of cervical cancer. Furthermore, out of the four cell lines tested they show the highest toxicity against HeLa cells, making them to candidates for further developments.

Since 2011, some Zn(II) complexes (Fig. 10) of curcumin have been described [71–74].

As in other modified curcumin compounds, the complexation of curcumin overcomes its easy degradation and introduces a fluorescent entity as well. A maximum emission at  $\lambda = 540$  nm and a good quantum yield ( $\Phi = 0.204$ ) offers fluorescent techniques for investigation [74]. Complex **24** was even more active than curcumin in LAN-5 neuroblastoma cells and showed the strongest growth inhibition in all cell lines [72]. The interaction mode of the fluorescent groups revealed their perpendicular alignment to the helices as a mixture of intercalating and groove interaction. Another common anticancer strategy is to reactivate tumor specific p53 mutations. This can be performed by Zn (II), supporting the overall toxicity of the complex even more. *In vivo* tests exhibited the ability of the complex to pass the blood-tumor barrier of glioblastoma cells [71]. The same research group continued their work to further improve the strategy. The authors investigated a tetra-coordinated analog as well as different *N,N*-ligands, counterions and a dimeric complex. Two complexes (**25** and **26**) possessed

much higher cytotoxicity in human neuroblastoma cells compared with the other modified complexes or to the reference complex itself (Fig. 10). The improved intercalation ability is probably based on the ionic character of complex **25** and on the enhanced rigidity and planarity of the aromatic region in the case of complex **26**. As a result, the treated cells underwent apoptosis involving the activation of JNK, caspase-3, and changes in mitochondrial membrane potential [73].

### 3.3. Complexes with other modes of action

The following few examples of metal complexes of curcumin and its derivatives show interaction modes besides intercalation or radical-producing pathways and offer, therefore, new approaches for the development of anticancer agents. Strongly modified complexes of Cu and Zn with another ancillary ligand have been synthesized and could lead to curcumin-containing drugs for cancer therapy [75]. Complex **27** contains a 1,7-(di-9-anthracene-1,6-heptadiene-3,5-dione) ligand (9Accm) and does not interact with DNA by intercalation (Fig. 11). There is rather a mixture of different mechanisms, including weak electrostatic interactions and an accumulation in vacuoles outside the nucleus. It revealed very high activity against various cancer cell lines, even higher than cisplatin. The assumed mechanism of action is the exchange of the chloride under physiological conditions, resulting in a more soluble species due to the resulting charge.

The modification of the curcumin skeleton at the central carbon atom was also successfully accomplished. A Fc moiety, for instance (Fig. 11), has been used to push the potential of this compound class toward alternative anticancer strategies [76]. The organometallic moiety clearly enhanced the biological activity, e.g., higher cytotoxicity in B16 cells, stronger tubulin polymerization and rounding up of endothelial cells. The biological efficacy depends on the linker unit between curcumin and the Fc group and emphasizes the multitargeting properties. Like other polyphenols [77], curcumin can inhibit the proteasome function which heavily influences several biological processes such as cell-cycle regulation and apoptosis. The exchange of the *p*-cymene group in compound **21** against benzene overcomes the mentioned biological restrictions while

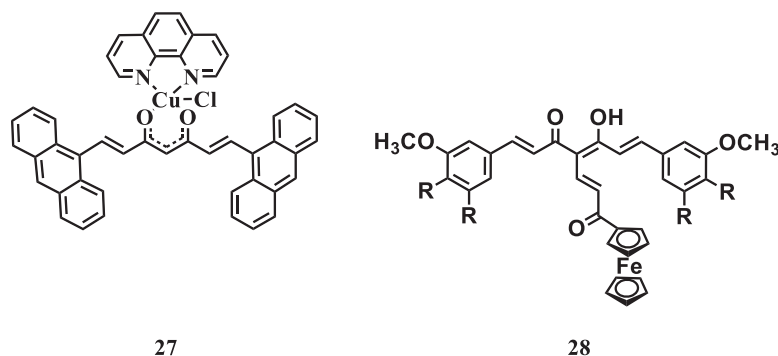


Fig. 11. Schematic representation of 9Accm-conjugated Cu-complex **27** [75] and Fc-modified curcumin skeleton **28** [76].

maintaining the proteasome inhibition of curcumin [78]. The complexation seems to play for this compound another role. Instead of direct metal proteasome interactions, the complex enhances the stability of curcumin and keeps the activity at the same time. This could be a new strategy to overcome the limitations of chemotherapy in drug-resistant tumors.

#### 4. Conclusions

Curcumin is one promising natural compound with a large variety of biological targets and interactions, linked to a number of diseases. Unfortunately, its clinical application is restricted by its the poor solubility in water, low absorption and bioavailability, high metabolism rate, light sensitivity, and the rapid clearance. To overcome these limitations, curcumin and its derivatives have been modified, attached to phospholipids, micelles, nanoparticles, liposomes and so forth. The complexation of curcumin with different metals changes the activity in comparison with the free ligands or can mitigate some disadvantageous properties. Many metals were used, resulting in potential candidates for application in experimental biology or medicine.  $\text{Gd}^{3+}$ ,  $^{99\text{m}}\text{Tc}^{+}$ ,  $\text{Re}^{+}$  and  $^{68}\text{Ga}^{2+}$  are suitable candidates for modern imaging techniques, such as fluorescence imaging, MRI, SPECT or PET.  $\text{VO}^{2+}$  in particular, but also  $\text{Cu}^{2+}$ ,  $\text{Ni}^{2+}$ , and other metal complexes were tested to explore their phototoxicity whereas  $\text{Ru}^{2+}$  and  $\text{Pd}^{2+}$  complexes act as intercalating agents. Further, some complexes revealed that the complexation does not have to take place at the  $\beta$ -diketo-moiety. The modification of the curcumin skeleton results in the ability to fine-tune the compound's properties. For instance, the introduction of electron-donating groups shifts the fluorescence to higher wavelengths while glycosylated ligands enhance the water solubility. Moreover, some heteroligand systems might be more effective than homoligands. The combination of the beneficial properties of different ligand systems could lead to new classes of anticancer or imaging agents. However, the biological activity and profile of metal complexes of curcumin and its derivatives is highly complex and depends on a variety of factors, e.g., the selected metal, curcumin skeleton and its modifications, ancillary ligand(s), the shape of the resulting complex, exchange capability of the ligands, charge, and more. Therefore, in the near future, a continuous interest in the development of novel curcumin-bearing metal complexes for medical applications is expected. There is still a significant potential for growth in this area due to the relatively small amount of reported curcumin-conjugated metal complexes. Curcumin could, for example, be a promising candidate to maintain the required cis-coordination of platinum-based anticancer agents together while enhancing their selectivity. Additionally, RAPTA-C-like Ru-curcumin complexes could afford a new level of biological activity by modification of the curcumin structure. Furthermore, the attachment of biomolecules could enhance the selectivity of

the complexes for imaging to distinguish between healthy and pathological structures. In any case, this area has only begun to be explored and future developments will reveal the true potential of metal complexes of curcumin and its derivatives.

#### Acknowledgements

The Carl-Zeiss-Foundation (JCSM Strukturantrag) and the Thüringer Ministerium für Wirtschaft, Wissenschaft und Digitale Gesellschaft (TMWWDG) are gratefully acknowledged for financial support.

#### References

- [1] M. Heger, R.F. van Golen, M. Broekgaarden, M.C. Michel, *Pharmacol. Rev.* 66 (2014) 222–307.
- [2] V. Lampe, J. Milobedzka, *Berichte der deutschen chemischen Gesellschaft* 46 (1913) 2235–2240.
- [3] S.C. Gupta, S. Patchva, W. Koh, B.B. Aggarwal, *Clin. Exp. Pharmacol. Physiol.* 39 (2012) 283–299.
- [4] K. Bairwa, J. Grover, M. Kania, S.M. Jachak, *RSC Adv.* 4 (2014) 13946–13978.
- [5] P. Anand, A.B. Kunnumakkara, R.A. Newman, B.B. Aggarwal, *Mol. Pharm.* 4 (2007) 807–818.
- [6] G. Shoba, D. Joy, T. Joseph, M. Majeed, R. Rajendran, P.S.S.R. Srinivas, *Planta Med.* 64 (1998) 353–356.
- [7] S. Bisht, G. Feldmann, S. Soni, R. Ravi, C. Karikar, A. Maitra, A. Maitra, *J. Nanobiotechnol.* 5 (2007) 3.
- [8] L. Li, F.S. Braiteh, R. Kurzrock, *Cancer* 104 (2005) 1322–1331.
- [9] Z. Ma, A. Shayeganpour, D.R. Brocks, A. Lavasanifar, J. Samuel, *Biomed. Chromatogr.* 21 (2007) 546–552.
- [10] Y.-J. Wang, M.-H. Pan, A.-L. Cheng, L.-I. Lin, Y.-S. Ho, C.-Y. Hsieh, J.-K. Lin, *J. Pharm. Biomed. Anal.* 15 (1997) 1867–1876.
- [11] K. Priyadarsini, *Molecules* 19 (2014) 20091.
- [12] A. Vyas, P. Dandawate, S. Padhye, A. Ahmad, F. Sarkar, *Curr. Pharm. Des.* 19 (2013) 2047–2069.
- [13] W.-H. Lee, C.-Y. Loo, M. Bebaawy, F. Luk, R.S. Mason, R. Rohanizadeh, *Curr. Neuropharm.* 11 (2013) 338–378.
- [14] S. Padhye, D. Chavan, S. Pandey, J. Deshpande, K.V. Swamy, F.H. Sarkar, *Mini-Rev. Med. Chem.* 10 (2010) 372–387.
- [15] A. de Fatima, L.V. Modolo, A.T.M. Neres, C.V. Ferreira, A.C.S. de Souza, *Curr. Bioact. Compd.* 4 (2008) 189–199.
- [16] F. Kühnlein, K. Polborn, W. Beck, *Z. Anorg. Allg. Chem.* 623 (1997) 1211–1219.
- [17] M.H.M. Leung, T. Harada, T.W. Kee, *Curr. Pharm. Des.* 19 (2013) 2070–2083.
- [18] B.S. Mendiguchia, I. Aiello, A. Crispini, *Dalton Trans.* 44 (2015) 9321–9334.
- [19] S. Wanninger, V. Lorenz, A. Subhan, F.T. Edelmann, *Chem. Soc. Rev.* 44 (2015) 4986–5002.
- [20] M. Rak, M.R. Del Bigio, S. Mai, D. Westaway, K. Gough, *Biopolymers* 87 (2007) 207–217.
- [21] K. Balasubramanian, *J. Agric. Food Chem.* 54 (2006) 3512–3520.
- [22] D. Bandyopadhyay, *FCHEM* 2 (2014).
- [23] S.L. Pimlott, A. Sutherland, *Chem. Soc. Rev.* 40 (2011) 149–162.
- [24] C.F. Ramogida, C. Orvig, *Chem. Commun.* 49 (2013) 4720–4739.
- [25] R.T.M. de Rosales, J. Label, *Compd. Radiopharm.* 57 (2014) 298–303.
- [26] S.M. Vithanaratchchi, M.J. Allen, *Chem. Commun. (Cambridge, U. K.)* 49 (2013) 4148–4150.
- [27] M. Sagnou, D. Benaki, C. Triantis, T. Tsotakos, V. Psycharis, C.P. Raptopoulou, I. Pirmettis, M. Papadopoulos, M. Pelecanou, *Inorg. Chem.* 50 (2011) 1295–1303.
- [28] C. Triantis, T. Tsotakos, C. Tsoukalas, M. Sagnou, C. Raptopoulou, A. Terzis, V. Psycharis, M. Pelecanou, I. Pirmettis, M. Papadopoulos, *Inorg. Chem.* 52 (2013) 12995–13003.

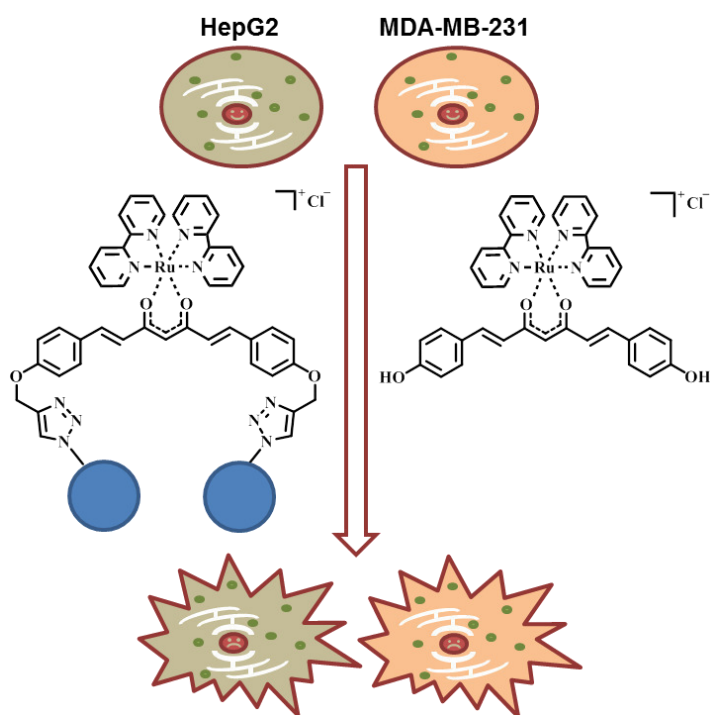
- [29] P. Caravan, C.T. Farrar, L. Frullano, R. Uppal, *Contrast Media Mol. Imaging* 4 (2009) 89–100.
- [30] M. Asti, E. Ferrari, S. Croci, G. Atti, S. Rubagotti, M. Iori, P.C. Capponi, A. Zerbini, M. Saladini, A. Versari, *Inorg. Chem.* 53 (2014) 4922–4933.
- [31] C. Ran, X. Xu, S.B. Raymond, B.J. Ferrara, K. Neal, B.J. Bacskaï, Z. Medarova, A. Moore, *J. Am. Chem. Soc.* 131 (2009) 15257–15261.
- [32] G. Bai, C. Yu, C. Cheng, E. Hao, Y. Wei, X. Mu, L. Jiao, *Org. Biomol. Chem.* 12 (2014) 1618–1626.
- [33] E.E. Nesterov, J. Skoch, B.T. Hyman, W.E. Klunk, B.J. Bacskaï, T.M. Swager, *Angew. Chem. Int. Ed.* 44 (2005) 5452–5456.
- [34] A. Felouat, A. D'Aleo, F. Fages, *J. Org. Chem.* 78 (2013) 4446–4455.
- [35] G. Xu, J. Wang, T. Liu, M. Wang, S. Zhou, B. Wu, M. Jiang, *J. Mater. Chem. B* 2 (2014) 3659–3666.
- [36] S.S. Zhou, X. Xue, B. Jiang, Y.P. Tian, *Sci. China: Chem.* 55 (2012) 334–340.
- [37] S.-S. Zhou, X. Xue, J.-F. Wang, Y. Dong, B. Jiang, D. Wei, M.-L. Wan, Y. Jia, *J. Mater. Chem.* 22 (2012) 22774–22780.
- [38] Z. Pi, J. Wang, B. Jiang, G. Cheng, S. Zhou, *Mater. Sci. Eng. C* 46 (2015) 565–571.
- [39] N. Hasima, B.B. Aggarwal, *Int. J. Biochem. Mol. Biol.* 3 (2012) 328–351.
- [40] P. Agostinis, K. Berg, K.A. Cengel, T.H. Foster, A.W. Girotti, S.O. Gollnick, S.M. Hahn, M.R. Hamblin, A. Juzenienė, D. Kessel, M. Korbelik, J. Moan, P. Mroz, D. Nowis, J. Piette, B.C. Wilson, J. Golab, *CA. Cancer J. Clin.* 61 (2011) 250–281.
- [41] L.B. Josefsen, R.W. Boyle, *Met-Based Drugs* 2008 (2008).
- [42] T. Qian, L. Kun, B. Gao, R. Zhu, X. Wu, S. Wang, *Spectrochim. Acta, Part A* 116 (2013) 6–12.
- [43] Q.-M. Huang, S.-W. Wang, Q. Li, W. Pan, P.-X. Deng, H. Zhou, Z.-Q. Pan, *Chem. J. Chin. U* 33 (2012) 732–737.
- [44] T.K. Goswami, S. Gadadhar, B. Gole, A.A. Karande, A.R. Chakravarty, *Eur. J. Med. Chem.* 63 (2013) 800–810.
- [45] M.I. Khalil, A.M. Al-Zahem, M.M. Qunaibit, *Med. Chem. Res.* 23 (2014) 1683–1689.
- [46] K.H. Thompson, K. Böhmerle, E. Polishchuk, C. Martins, P. Toleikis, J. Tse, V. Yuen, J.H. McNeill, C. Orvig, *J. Inorg. Biochem.* 98 (2004) 2063–2070.
- [47] S. Banerjee, P. Prasad, A. Hussain, I. Khan, P. Kondaiah, A.R. Chakravarty, *Chem. Commun.* 48 (2012) 7702–7704.
- [48] B. Balaji, B. Balakrishnan, S. Perumalla, A.A. Karande, A.R. Chakravarty, *Eur. J. Med. Chem.* 85 (2014) 458–467.
- [49] B. Balaji, K. Somyajit, B. Banik, G. Nagaraju, A.R. Chakravarty, *Inorg. Chim. Acta* 400 (2013) 142–150.
- [50] S. Banerjee, P. Prasad, I. Khan, A. Hussain, P. Kondaiah, A.R. Chakravarty, *Z. Anorg. Allg. Chem.* 640 (2014) 1195–1204.
- [51] S. Banerjee, A. Dixit, A.A. Karande, A.R. Chakravarty, *Eur. J. Inorg. Chem.* 2015 (2015) 447–457.
- [52] B. Banik, K. Somyajit, G. Nagaraju, A.R. Chakravarty, *Dalton Trans.* 43 (2014) 13358–13369.
- [53] P. Prasad, I. Pant, I. Khan, P. Kondaiah, A.R. Chakravarty, *Eur. J. Inorg. Chem.* (2014) 2420–2431.
- [54] A.K. Renfrew, N.S. Bryce, T.W. Hambley, *Chem. Sci.* 4 (2013) 3731–3739.
- [55] T. Sarkar, S. Banerjee, A. Hussain, *RSC Adv.* 5 (2015) 16641–16653.
- [56] A. Hussain, K. Somyajit, B. Banik, S. Banerjee, G. Nagaraju, A.R. Chakravarty, *Dalton Trans.* 42 (2013) 182–195.
- [57] B.A. Armitage, in: M. Waring, J. Chaires (Eds.), *DNA Binders and Related Subjects*, Springer, Berlin, Heidelberg, 2005, pp. 55–76.
- [58] A. Mukherjee, W.D. Sasikala, in: K.-C. Tatyana (Ed.), *Advances in Protein Chemistry and Structural Biology*, Academic Press, 2013, pp. 1–62.
- [59] J. Annaraj, S. Srinivasan, K.M. Ponvel, P.R. Athappan, *J. Inorg. Biochem.* 99 (2005) 669–676.
- [60] N. Shahabadi, M. Falsafi, N.H. Moghadam, *J. Photochem. Photobiol. B: Biol.* 122 (2013) 45–51.
- [61] J. Wang, D. Wei, B. Jiang, T. Liu, J. Ni, S. Zhou, *Trans. Metal Chem.* 39 (2014) 553–558.
- [62] D.J. Valapatukutikadan, K. Krishnankutty, *Trans. Metal Chem.* 30 (2005) 229–233.
- [63] D. Pucci, R. Bloise, A. Bellusci, S. Bernardini, M. Ghedini, S. Pirillo, A. Valentini, A. Crispini, *J. Inorg. Biochem.* 101 (2007) 1013–1022.
- [64] A. Valentini, F. Conforti, A. Crispini, A. De Martino, R. Condello, C. Stellitano, G. Rotilio, M. Ghedini, G. Federici, S. Bernardini, D. Pucci, *J. Med. Chem.* 52 (2009) 484–491.
- [65] N. Miklašová, E. Fischer-Fodor, R. Mikláš, L. Kucková, J. Kožíšek, T. Liptaj, O. Soritau, J. Valentová, F. Devinsky, *Inorg. Chem. Commun.* 46 (2014) 229–233.
- [66] F. Caruso, M. Rossi, A. Benson, C. Opazo, D. Freedman, E. Monti, M.B. Gariboldi, J. Shaulky, F. Marchetti, R. Pettinari, C. Pettinari, *J. Med. Chem.* 55 (2012) 1072–1081.
- [67] R. Pettinari, F. Marchetti, F. Condello, C. Pettinari, G. Lupidi, R. Scopelliti, S. Mukhopadhyay, T. Riedel, P.J. Dyson, *Organometallics* 33 (2014) 3709–3715.
- [68] I. Ali, K. Saleem, D. Wesselinova, A. Haque, *Med. Chem. Res.* 22 (2013) 1386–1398.
- [69] H. Chen, J.A. Parkinson, S. Parsons, R.A. Coxall, R.O. Gould, P.J. Sadler, *J. Am. Chem. Soc.* 124 (2002) 3064–3082.
- [70] X. Lei, W. Su, P. Li, Q. Xiao, S. Huang, Q. Qian, C. Huang, D. Qin, H. Lan, *Polyhedron* 81 (2014) 614–618.
- [71] A. Garufi, D. Trisciuglio, M. Porru, C. Leonetti, A. Stoppacciaro, V. D'Orazi, M. Avantaggiati, A. Crispini, D. Pucci, G. D'Orazi, *J. Exp. Clin. Cancer Res.* 32 (2013) 72–83.
- [72] D. Pucci, T. Bellini, A. Crispini, I. D'Agnano, P.F. Liguori, P. Garcia-Orduna, S. Pirillo, A. Valentini, G. Zanchetta, *MedChemComm* 3 (2012) 462–468.
- [73] D. Pucci, A. Crispini, B.S. Mendiguchia, S. Pirillo, M. Ghedini, S. Morelli, L. De Bartolo, *Dalton Trans.* 42 (2013) 9679–9687.
- [74] L. Ricciardi, D. Pucci, S. Pirillo, M. La Deda, J. Lumin. 151 (2014) 138–142.
- [75] N. Aliaga-Alcalde, P. Marques-Gallego, M. Kraaijkamp, C. Herranz-Lancho, H. den Dulk, H. Gerner, O. Roubeau, S.J. Teat, T. Weyhermüller, J. Reedijk, *Inorg. Chem.* 49 (2010) 9655–9663.
- [76] A. Arezki, G.G. Chabot, L. Quentin, D. Scherman, G. Jaouen, E. Brule, *MedChem-Comm* 2 (2011) 190–195.
- [77] M. Shen, T.H. Chan, Q.P. Dou, *Anticancer Agents Med. Chem.* 12 (2012) 891–901.
- [78] L. Bonfili, R. Pettinari, M. Cuccioloni, V. Cecarini, M. Mozzicafreddo, M. Angeletti, G. Lupidi, F. Marchetti, C. Pettinari, A.M. Eleuteri, *ChemMedChem* 7 (2012) 2010–2020.

## Publication 2

### Synthesis and *in vitro* toxicity of D-glucose and D-fructose conjugated curcumin–ruthenium complexes

M. Pröhl, T. Bus, J. A. Czaplewska, A. Traeger, M. Deicke, H. Weiss,  
W. Weigand, U. S. Schubert, M. Gottschaldt

*Eur. J. Inorg. Chem.* **2016**, 5197-5204



## Cytotoxic Complexes

# Synthesis and in vitro Toxicity of D-Glucose and D-Fructose Conjugated Curcumin–Ruthenium Complexes

Michael Pröhl,<sup>[a,b]</sup> Tanja Bus,<sup>[a,b]</sup> Justyna A. Czaplewska,<sup>[a,b]</sup> Anja Traeger,<sup>[a,b]</sup> Michael Deicke,<sup>[c]</sup> Henning Weiss,<sup>[c]</sup> Wolfgang Weigand,<sup>[b,c]</sup> Ulrich S. Schubert,<sup>[a,b]</sup> and Michael Gottschaldt<sup>\*[a,b]</sup>

**Abstract:** A series of carbohydrate-conjugated bis(demethoxy)curcumin (BDC) ligands were synthesized by using the Huisgen copper(I)-catalyzed cycloaddition between azido-functionalized D-glucose and D-fructose as well as propargyl-modified BDC. The unprotected sugar ligands were treated with Ru(bpy)<sub>2</sub>Cl<sub>2</sub> to form curcumin-conjugated Ru complexes of general formula Ru(bpy)<sub>2</sub>(L)Cl. The ligands as well as Ru complexes were analyzed by NMR, IR, UV/Vis, and fluorescence spectroscopy, mass spectrometry as well as by elemental analysis (EA).

Incubation of L929, HepG2 and the breast cancer cell line MDA-MB-231 revealed lower cytotoxicity of all carbohydrate-conjugated ligands compared with BDC. The Ru complexes exhibited higher cytotoxicity than the parent ligands, in particular against HepG2 cells, whereas the noncancerous L929 cell line remained unaffected. Unexpectedly, the D-fructose-conjugated ligand and its corresponding Ru complex did not show any significant toxicity against MDA-MB-231 cells.

## Introduction

In the last decades, medicinal inorganic chemistry has attracted increased attention in disease therapy (e.g., cisplatin for cancer treatment) as well as in disease diagnosis (e.g., <sup>99m</sup>Tc in SPECT).<sup>[1]</sup> In addition to platinum-based drugs, other transition-metal compounds also offer advantageous properties. Ru-based complexes could overcome resistance problems often linked to platinum-containing drugs or could diminish the extent of side effects.<sup>[2]</sup> Further beneficial properties, such as easy access to oxidation states +II and +III and the resulting possibility to obtain low-reactive prodrugs, led to early clinical trials of ruthenium-based anticancer agents such as NAMI-A and promising Ru<sup>III</sup> prodrugs such as RAPTA-T.<sup>[2]</sup> However, to improve the therapeutic index, selectivity plays a major role. The current approach aims to target specific cell structures, which vary in comparison to healthy cells, e.g., transport proteins, antigens or receptors on the membrane surface, and which interact with the potential drug. This is often realized by conjugation of the metal complex to targeting moieties.<sup>[3]</sup>

Carbohydrates, as a major energy source and substrates of lipid and protein metabolism, are taken up into cells by highly selective transport proteins.<sup>[4]</sup> Beside transporters for glucose (the major carbohydrate) there are carriers such as GLUT5 for fructose. GLUT5 is one of thirteen members of the known saccharide transporters (GLUTs), and its structure was determined recently.<sup>[5]</sup> It is found in the membrane in the small intestine and kidney cells, but is also reported to be overexpressed in 85 % of 33 tested breast cancer cell lines,<sup>[6]</sup> although another group reported contradictory results.<sup>[7]</sup> The latter study concludes that there is no overexpression of GLUT5 in breast cancer tissue. However, it was shown that structural modifications of D-fructose at the C1 and C6 position seems to be tolerated by the GLUT5 transporter.<sup>[8]</sup> Based on that, dyes,<sup>[9]</sup> polymers,<sup>[10]</sup> and nanoparticles<sup>[11]</sup> were functionalized with D-fructose to successfully target breast cancer cells. Another approach to study the possibility of GLUT5 targeting is the determination of cell internalization of metal complexes modified with fructose residues.<sup>[12]</sup> For instance, a fructose-conjugated Ir<sup>III</sup> complex revealed a 3.6 times higher uptake into MCF-7 cells compared with noncancerous HEK293T cells, whereas the corresponding nonfunctionalized Ir<sup>III</sup> complex did not show any significant differences in terms of cell-specific uptake.<sup>[12a]</sup> Another study exhibited the enhanced accumulation of a fructose-conjugated Re complex in breast cancer cells MDA-MB-231 and MCF-7 compared with all other studied cancerous and noncancerous cell lines. Uptake competition experiments with D-fructose indicated the involvement of the GLUT5 transporter.<sup>[12b]</sup> Additionally, the hydrophilicity of sugar moieties reduces the toxicity and increases the solubility in water and therewith in the plasma.<sup>[13]</sup> This offers the possibility to overcome disadvanta-

[a] Laboratory of Organic and Macromolecular Chemistry (IOMC), Friedrich Schiller University Jena, Humboldtstraße 10, 07743 Jena, Germany  
E-mail: michael.gottschaldt@uni-jena.de  
www.schubert-group.com

[b] Jena Center for Soft Matter (JCSM), Friedrich Schiller University Jena, Philosophenweg 7, 07743 Jena, Germany

[c] Institute of Inorganic and Analytical Chemistry, Friedrich Schiller University Jena, Humboldtstraße 8, Lessingstraße 8, 07743 Jena, Germany

Supporting information for this article is available on the WWW under <http://dx.doi.org/10.1002/ejic.201600801>.



geous properties of potentially biological active compounds and to enhance the selectivity at the same time.

Besides a large number of other polyphenols, the diaryl-hepanoid curcumin is a highly bioactive compound that is contained in the roots of turmeric. It interacts with a large number of molecular targets linked to major diseases of modern societies.<sup>[14]</sup> It is reported to possess beneficial properties such as antimicrobial, antiinflammatory and chemopreventive effects and low toxicity up to high dosages.<sup>[15]</sup> Unfortunately, medical applications of curcumin and its derivatives are limited by some major drawbacks such as rapid metabolism and poor solubility in water. In the last decades many strategies have been tested to overcome these disadvantages; for example, the use of piperine as concomitant, nanoparticle-based systems or micellar formulations.<sup>[16]</sup> Currently, metal complexes of curcumin and its derivatives are a focus of the scientific community.<sup>[17]</sup> Curcumin-conjugated metal complexes were found to have superior properties such as enhanced solubility in water,<sup>[18]</sup> higher photocytotoxicity<sup>[19]</sup> or increased cytotoxicity by intercalation.<sup>[20]</sup> In particular, a RAPTA-type complex of curcumin exhibited outstanding properties such as an approximate 100 times smaller IC<sub>50</sub> value compared with that of cisplatin against cisplatin-resistant ovarian cancer cells.<sup>[18]</sup> Furthermore, the attachment of glucose to the curcumin skeleton in an oxovanadium complex enhances both the solubility in water and the cellular uptake in cancer cells.<sup>[21]</sup>

A powerful tool to append biomolecules to different structures is “click” chemistry.<sup>[22]</sup> It combines a few types of reactions with several advantages including high yields, stereospecificity, easily available starting materials, and gentle product isolation.<sup>[23]</sup> In particular, the Cu<sup>I</sup>-catalyzed Huisgen 1,3-dipolar cycloaddition (CuAAC) between terminal alkynes and azides is used for the synthesis of five-membered heterocyclic systems.<sup>[24]</sup>

Herein, we describe the synthesis, characterization, and evaluation of the cytotoxicity of two sugar-conjugated curcumin ligands and their corresponding Ru(bpy)<sub>2</sub> complexes.

## Results and Discussion

### Synthesis and Characterization

The synthesis of altered curcuminoids by using aldehydes in a double aldol condensation with acetylacetone is well known and offers the possibility to introduce functionalities to the curcuminoid skeleton (Figure 1).<sup>[25]</sup> Compound **1** was obtained by using a modification of a reported procedure: BF<sub>3</sub>·Et<sub>2</sub>O-promoted one-pot synthesis with acetylacetone and 4-(propargyloxy)benzaldehyde in toluene. Subsequent recrystallization resulted in the isolation of the desired product in high yield and purity. Compound **1** was characterized by <sup>1</sup>H, <sup>13</sup>C and <sup>19</sup>F NMR spectroscopy and HRMS (ESI) as well as by elemental analysis to confirm the purity of the compound. The IR spectrum reveals a strong band at  $\tilde{\nu} = 3290\text{ cm}^{-1}$  resulting from the monosubstituted alkyne functionality (see the Supporting Information, Figure S5). The azide-functionalized sugar moieties were also synthesized according to reported procedures.<sup>[25]</sup>

Bis(demethoxy)curcumin (BDC, **2**) was synthesized in high yields as previously reported.<sup>[26]</sup> Ligands **3a** and **3b** were prepared according to the “Huisgen” 1,3-dipolar cycloaddition between compound **1** and **2** equiv. of the azido-sugars with CuSO<sub>4</sub> and sodium ascorbate as catalyst-forming pair. The yields of both reactions were relatively low (42 % for **3a** and 52 % for **3b**). Thin-layer chromatography (TLC) revealed byproducts: the copper complex of the ligands, the one-site-clicked product, and the corresponding copper complex of it. The copper could not be removed completely by extraction with ethylenediaminetetraacetic acid (EDTA), probably because of the stability of copper–curcumin complexes.<sup>[27]</sup> Flash column chromatography led to the pure ligands. The <sup>1</sup>H NMR spectra of the ligands clearly revealed the disappearance of the ethynyl singlet of the starting material at  $\delta = 3.63\text{ ppm}$  and the appearance of a signal for the triazole protons at  $\delta = 8.11\text{ ppm}$  for **3a** and  $\delta = 8.20\text{ ppm}$  for **3b** (see the Supporting Information, Figures S8 and S14). Furthermore, cleavage of the BF<sub>2</sub> group was confirmed by the disappearance of the peak at  $\delta = -138.14\text{ ppm}$  in the <sup>19</sup>F NMR spectra and the strong shift to lower fields of all curcuminoid-related peaks in the <sup>1</sup>H NMR spectra. ESI-MS identified the ligands as [M + X]<sup>+</sup> (X = H, Na, K). To form ligand **4a** the acetyl groups of compound **3a** were cleaved under basic conditions by using sodium methoxide in anhydrous methanol under argon. The reaction mixture was neutralized with ion exchange resin DOWEX (H<sup>+</sup>) and dialyzed in water for 1 week to remove low-molar-mass impurities. The product was obtained in good yield without any side products. The structure of the ligand was established by HRMS (ESI) as [M + Na]<sup>+</sup> (error: 1.4 ppm) and by elemental analysis. The disappearance of the carbonyl band of the acetyl groups in the IR spectrum as well as of the four singlets ( $\delta = 1.89\text{--}2.02\text{ ppm}$ ) in the <sup>1</sup>H NMR spectra and of the eight signals ( $\delta = 168.97\text{--}170, 20.21\text{--}20.49\text{ ppm}$ ) in the <sup>13</sup>C NMR spectra confirmed the success of the reaction (see the Supporting Information, Figures S20–23). The signals in the NMR spectra remained sharp and well separated. Due to the glycosidic linkage, the glucose units are still present in the pyranoid structure and, therefore, no stereoisomers are observable. The cleavage of the isopropylidene groups of compound **3b** was problematic. Neither standard acidic cleavage procedures<sup>[28]</sup> nor acidic ion exchange resins could be successfully applied.<sup>[29]</sup> Given the high sensitivity of the curcuminoid skeleton towards acids (as well as bases and light),<sup>[31]</sup> formic acid was chosen to replace the isopropylidene groups under relatively mild conditions.<sup>[30]</sup> The solution was stirred at room temperature for 1 week, and the progress was monitored by MS (ESI). The absence of all *m/z* peaks derived from the ligands substituted with isopropylidene groups indicated the full conversion. After removing the excess of formic acid in vacuo, the resulting formic acid esters were cleaved under basic conditions with aqueous 0.1 M NaOH. The crude product was dialyzed to remove the formed sodium formate, then analyzed by HRMS (ESI) as [M + Na]<sup>+</sup> (error: 4.7 ppm) and by elemental analysis to confirm the absence of any salts such as sodium formate or NaCl. The <sup>1</sup>H as well as the <sup>13</sup>C NMR spectra confirmed the disappearance of the isopropylidene peaks (see the Supporting Information, Figures S26–28). The NMR spectra

clearly reveal the presence of different ligand species due to the fructose isomers. The interaction between the hydroxy groups of the sugar units and the curcuminoid enol moieties or sugar hydroxy groups of neighboring molecules could stabilize different forms of the sugar, resulting in wider peaks and more complex NMR spectra. When measured in deuterated dimethyl sulfoxide (DMSO), broad peaks between  $\delta = 4.5$  and 6.5 ppm in the  $^1\text{H}$  NMR spectrum only appear to be coupling with the sugar ring proton signals in 2D-COSY experiments. The signals could be attributed to fructose hydroxy groups formed during deprotection. Furthermore, there are at least three peaks for each carbon atom of the fructose residues with different intensities in the  $^{13}\text{C}$  NMR spectrum of compound **4b**, confirming the existence of stereoisomers. However, the ESI-MS revealed only two major peaks ( $[\text{M} + \text{Na}]^+$  and  $[\text{M} - \text{H} + 2 \text{Na}]^+$ ), thus establishing the identity of the ligand. Complexes **5a–c** were synthesized in methanol (**5a**) or a mixture of anhydrous methanol and *N,N*-dimethylformamide (DMF) (**5b** and **5c**) with sodium methoxide as a base (Figure 2). The mixtures were heated under argon at 60 °C for 12 h. Excess  $\text{Ru}(\text{bpy})_2\text{Cl}_2$  was used to complete the reaction of the ligands. For **5a** and **5b**, the reaction mixture was concentrated, and the remaining excess of precursor was filtered off after redissolving the crude product in pure water. The remaining salts were removed from the aqueous layer by dialysis against water. HRMS (ESI) showed the pure complex **5a** without signals of precursor or ligand as  $[\text{M} - \text{Cl}]^+$  (error: 0.5 ppm) and  $[\text{M} - \text{Cl} + \text{Na}]^{2+}$ . The  $^1\text{H}$  NMR spectrum shows eight additional peaks in the aromatic region fitting to the bipyridine (bpy) units of the product with a shift to lower ppm values in comparison to the  $^1\text{H}$  NMR spectrum of **4a** (see the Supporting Information, Figures S32–34). The structure of **5b** was challenging to validate because of the instability during mass spectrometric measurements. HRMS (ESI) under soft conditions with an orbitrap mass analyzer combined with LC-MS experiments showed, next to product peak  $[\text{M} - \text{Cl}]^+$  (error: 1.8 ppm), different fragments; for example fragments without fructose unit(s) or without triazole unit(s). MS/MS experiments

of the product ion identified the fragments as being generated as a result of cleavage of the parent ion under the applied conditions (see the Supporting Information, Figures S41–S42). The  $^1\text{H}$  NMR spectrum shows an even higher complexity compared to that of the ligand. Signals in the aromatic region appear that can be clearly distinguished from  $\text{Ru}(\text{bpy})_2\text{Cl}_2$  precursor peaks. Furthermore, 2D-COSY and HSQC NMR measurements prove the attachment of fructose. Figure 3 shows the  $^1\text{H}$ - $^{13}\text{C}$ -HSQC experiments of **4b** in comparison to **5b**. The area between  $\delta = 3$  and 4 ppm in the  $^1\text{H}$  NMR spectrum, and between  $\delta = 50$  and 100 ppm in the  $^{13}\text{C}$  NMR spectrum shows the occurrence of proton and carbon peaks of various forms of fructose units in the ligand as well as in the complex. The observed pattern differs, which suggests the presence of different ratios of fructose isomers. It is known that in aqueous solution of D-fructose at pH 7, various forms exist and that the percentage of each form is strongly dependent on temperature, salts, and other conditions.<sup>[31]</sup> It was also shown that certain isomers can be stabilized; for example the presence of human serum albumin (HSA) resulted in the stabilization of the open-chain D-fructose by the  $\text{NH}_2$  functionalities of the Lys199 residue.<sup>[32]</sup> In contrast, in a D-fructose-decorated glycopolymer, the pyranose form dominates, but also furanose forms were observable.<sup>[10]</sup>

The synthesis of **5c** was performed as mentioned before, but due to the high polarity and low solubility in water of compound **5c** it was neither suitable for normal-phase silica chromatography nor convenient for dialysis with water. Therefore, the crude product was purified by size-exclusion chromatography using Sephadex LH-20 and methanol as eluent to obtain the pure complex. The  $^1\text{H}$  NMR spectrum revealed a shift of all proton signals to lower fields, and additional peaks appeared in the aromatic region fitting to the bpy units of the formed complex (see the Supporting Information, Figure S45). HRMS (ESI) confirmed the structure as  $[\text{M} - \text{Cl}]^+$  (error: 1.5 ppm).

The absorbance and emission spectra of all compounds were measured in aerated methanol. Due to the polarity of methanol,

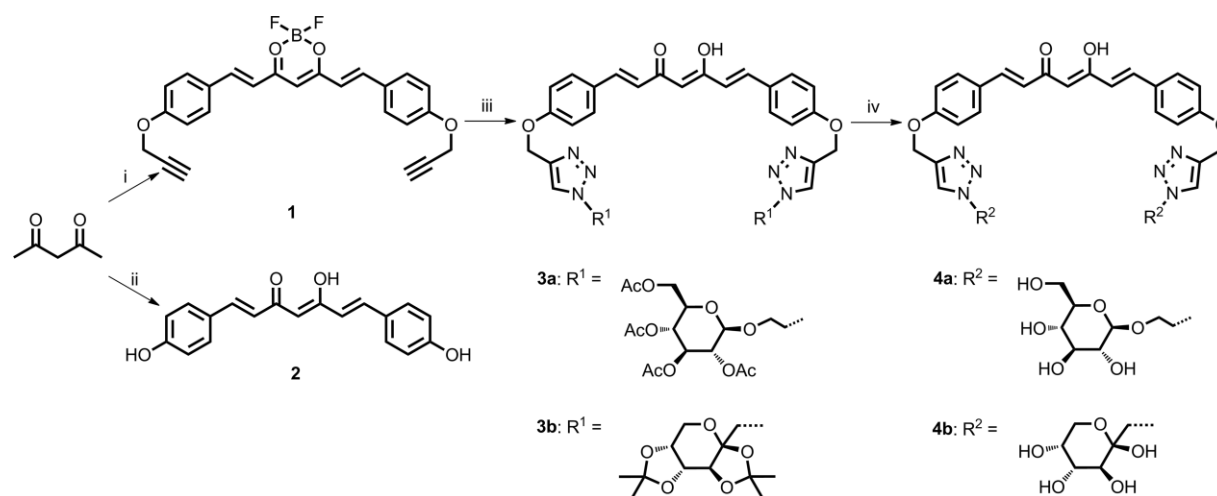


Figure 1. Schematic representation of the ligand synthesis. Reagents and conditions: (i)  $\text{BF}_3 \cdot \text{Et}_2\text{O}$ , *p*-(propargyloxy)benzaldehyde, tributyl borate, *n*-butylamine,  $\text{N}_2$ , 65 °C, toluene, 18 h; (ii) (1)  $\text{BF}_3 \cdot \text{Et}_2\text{O}$ , *p*-hydroxybenzaldehyde, tributyl borate, *n*-butylamine,  $\text{N}_2$ , 65 °C, toluene, 6 h; (2) NaOH, 70 °C,  $\text{CH}_3\text{OH}/\text{H}_2\text{O}$ , 5 h; (iii) azido-sugar,  $\text{Cu}^{10}\text{SO}_4 \cdot 5\text{H}_2\text{O}$ , sodium ascorbate, Ar, 50 °C, THF/ $\text{H}_2\text{O}$ , 12 h; (iv) **3a**  $\rightarrow$  **4a**: (1) NaOMe, Ar, room temp., MeOH, 0.5 h; (2) DOWEX H<sup>+</sup>; **3b**  $\rightarrow$  **4b**: (1) formic acid, room temp., 1 week; (2) 0.1 M NaOH, room temp., THF/ $\text{H}_2\text{O}$ , 1 h.

the vibrational structure of the excitation and emission spectra is not visible, and the absorption band is bathochromically shifted compared to those recorded in more apolar solvents.<sup>[33]</sup>

The cleavage of the boron difluoride group results in an absorption band at  $\lambda_{\text{max}} = 410$  nm for compounds **3a** and **3b**, hypsochromically shifted compared with  $\lambda_{\text{max}} = 477$  nm of **1**. Emis-

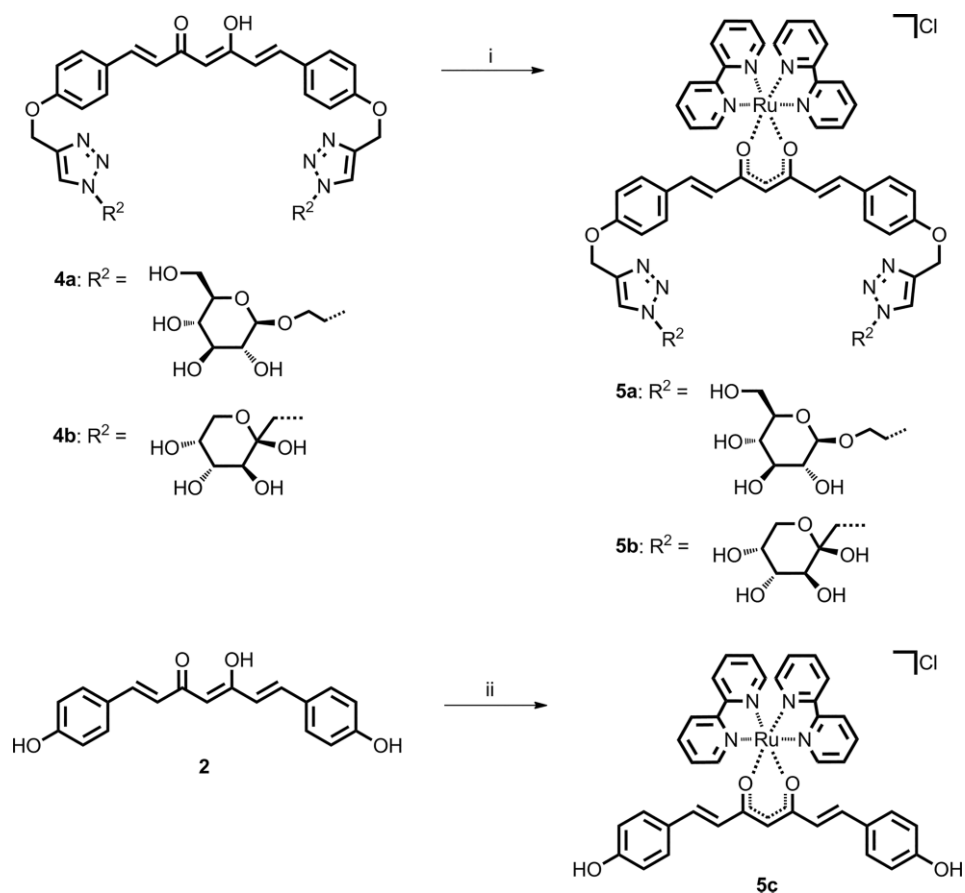


Figure 2. Schematic representation of the complex synthesis. Reagents and conditions: (i), (ii) NaOMe, Ru(bpy)<sub>3</sub>Cl<sub>2</sub>, Ar, MeOH/DMF, 60 °C, 12 h.

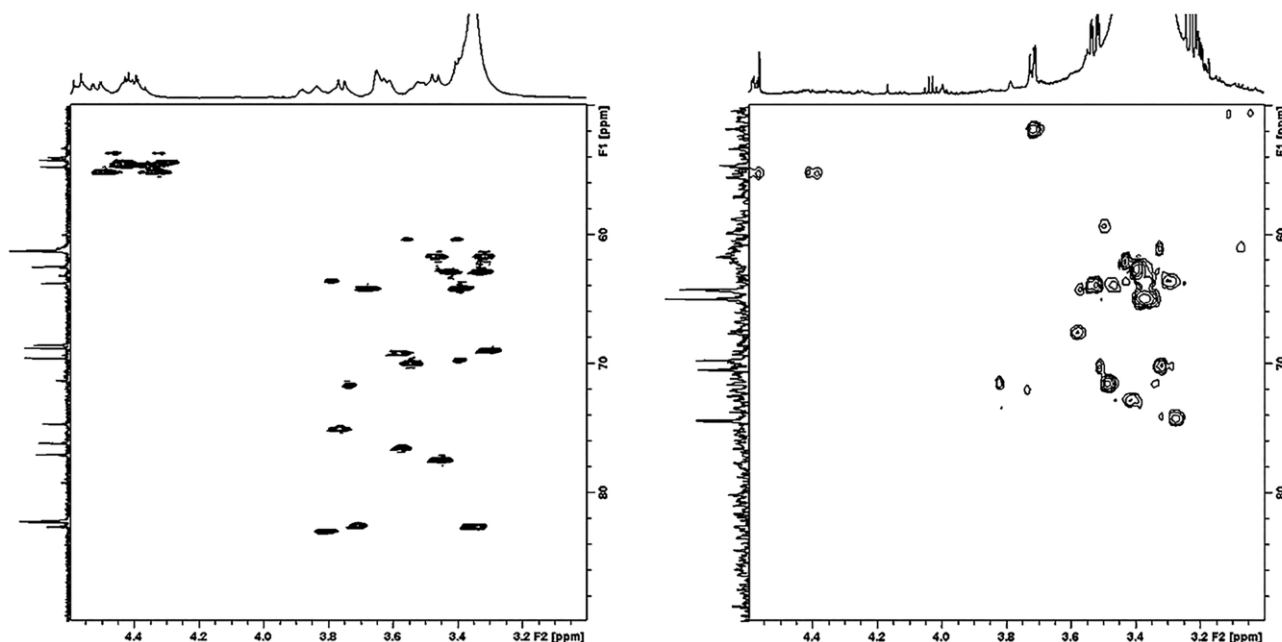


Figure 3. <sup>1</sup>H-<sup>13</sup>C-HSQC spectra of **4b** and **5b** (in [D<sub>6</sub>]DMSO) focusing on the area between  $\delta = 3$  and 4 ppm in the <sup>1</sup>H NMR spectrum, and between  $\delta = 50$  and 100 ppm in the <sup>13</sup>C NMR spectrum.



sion spectra of compound **3a** and **3b** ( $\lambda_{\text{max}} = 509 \text{ nm}$ ) and **1** ( $\lambda_{\text{max}} = 541 \text{ nm}$ ) revealed the same behavior. The appearing absorption bands for compounds **5a–c** fit to  $\pi \rightarrow \pi^*$  transition of the bpy ligands ( $\lambda_{\text{max}} = 296 \text{ nm}$ ) and metal to ligand charge transfer (MLCT) transition ( $\lambda_{\text{max}} = 517 \text{ nm}$ ). The complexes revealed fluorescence in methanol in the visible region at  $\lambda_{\text{max}} = 585 \text{ nm}$  when irradiated at  $\lambda = 296 \text{ nm}$ . Furthermore, a smaller emission maximum is observable at  $\lambda \approx 450 \text{ nm}$ , indicating two separate chromophore systems. As also previously reported,<sup>[34]</sup> fluorescence of the Ru complexes was quenched in water, and therefore complexes **5a–c** did not show any emission when measured in aqueous solution.

### Cytotoxicity Studies

Recent studies based on fluorescence using flow cytometry indicated an increased uptake of D-fructose-conjugated luminescent metal complexes into breast cancer cells.<sup>[12]</sup> Given that complexes **5a–c** show no fluorescence in water or cell media due to quenching effects<sup>[34]</sup> the uptake behavior could not be studied by spectroscopic methods. To evaluate the cytotoxicity of the ligands and complexes, the inhibitory effect on the cellular metabolic activity of different cell types was investigated by using a resazurin-based assay (alamarBlue, Thermo Fisher). The noncancerous cell line L929, the liver cancer cell line HepG2 as well as the breast cancer cell line MDA-MB-231 were treated with ligands **2**, **4a–b**, and metal complexes **5a–c** at varying concentrations for 24 h (see the Supporting Information, Figures S51–S53). None of the tested compounds induced a significant reduction in cell viability in noncancerous cell line L929. Carbohydrate-conjugated metal complexes **5a** and **5b** revealed only a slight inhibitory effect on the metabolic activity of MDA-MB-231 cells, which might be attributed to the lipophilic properties of the bipyridyl groups of the complexes, allowing for elevated diffusion through the cell or nucleic membrane in comparison to the more polar ligands **4a** and **4b**. Sugar-decorated ligands **4a** and **4b** had no influence on MDA-MB-231 cells. Fructose-conjugated complex **5b** revealed no specific cytotoxicity against MDA-MB-231 cells. A concentration-dependent reduction of cell viability was observed for the sugar-free ligand **2** and complex **5c**, which could be attributed to its increased hydrophobicity due to missing hydrophilic sugar units. As a consequence, a GLUT5-independent pathway seems to be likely. In contrast to that, HepG2 cells exhibited sensitivity against glucose- and fructose-conjugated metal complexes independent of tested concentration, as demonstrated by the decrease of cell viability below 50 % after 24 h. HepG2 remained unaffected after treatment with carbohydrate-conjugated ligands as well as for the metal complex **5c**. Previous studies already revealed a selective uptake of glucose-substituted ruthenium complexes in HepG2 cells, which could contribute to the enhanced cytotoxic effects seen in our investigations.<sup>[35]</sup> Furthermore, increased cytotoxicity of curcumin as well as curcumin-conjugated metal complexes against HepG2 cells is consistent with previous reports.<sup>[36]</sup> Correlation between cytotoxicity and specific uptake of D-fructose-conjugated compounds requires further investigations.

### Conclusions

The conjugation of protected D-glucose and D-fructose to BDC was achieved by using the click reaction between sugar azides and a propargyl-modified curcumin derivative. Deprotection procedures resulted in carbohydrate-conjugated ligands, which were successfully treated with  $\text{Ru}(\text{bpy})_2\text{Cl}_2$  to form novel complexes of the general formula  $\text{Ru}(\text{bpy})_2(\text{L})\text{Cl}$ . All compounds were extensively analyzed by  $^1\text{H}$  and  $^{13}\text{C}$  NMR, IR, UV/Vis, and fluorescence spectroscopy, mass spectrometry as well as by elemental analysis. Sugar-decorated ligands and complexes induced a decrease in cell viability of HepG2 and only a slight cytotoxicity for MDA-MB-231. However, BDC-based complex **5c** showed an increased cytotoxicity in breast cancer cell line, whereas most HepG2 cells remained unaffected for all tested concentrations, indicating a carbohydrate-independent pathway. Increased cytotoxicity of fructose-conjugated compounds in breast cancer cells was not observable in this study.

### Experimental Section

**Materials and General Experimental Details:** All reagents and solvents were commercial products purchased from Aldrich, Sigma, Fluka, Across Organics, Strem, VWR or Alfa Aesar and were used without further purification. Chromatographic separations were performed with NP Silica RediSep Cartridges by Teledyne Isco. The progress of reactions was monitored by thin-layer chromatography (TLC) using glass plates precoated with silica gel 60 (Merck). Dialyses were performed using Biotech CE membranes (MWCO 500–1000 Da) from Spectrum Labs. Cell cultivation was performed at  $37^\circ\text{C}$  in a humidified 5 %  $\text{CO}_2$  atmosphere. L929 (CCL-1, ATCC) and MDA-MB231 (HTB-26, ATCC) cells were cultured in Dulbecco's MEM (DMEM, Lonza) supplemented with 10 % fetal calf serum (FCS, Capricorn Scientific),  $100 \mu\text{g mL}^{-1}$  streptomycin, and  $100 \text{ IU mL}^{-1}$  penicillin (Biochrom, Merck). HepG2 cells (HB-8065, ATCC) were routinely cultured in DMEM/F12 media (Biochrom, Merck Millipore). Consumables for cell culture such as pipettes and cell culture plates (96 well) were obtained from Corning (USA) and Greiner Bio-one (Austria/Germany).

**Instrumentation:**  $^1\text{H}$  and  $^{13}\text{C}$  NMR spectra were measured with Bruker spectrometers (600, 300 and 250 MHz). IR spectra were recorded with Nicolet AVATAR 370 DTGS and Bruker Tensor 37 spectrometers. UV/Vis absorption spectra were measured with Thermo Unicam UV500 and analytikjena Specord250 spectrometers, and fluorescence was recorded with a Jasco FP 6500 and an Infinite M200 PRO microplate reader (298 K, methanol,  $1 \times 10^{-4}$  to  $2 \times 10^{-6} \text{ M}$  solutions). High-resolution electron spray ionization mass spectrometry [HRMS (ESI)] was measured with a Bruker MicroQToF and a Thermo QExactive plus Orbitrap mass spectrometer coupled to an ESI source. Elemental analyses were performed with a Leco CHN-932. The alamarBlue cell viability assay (Thermo Fisher) was performed with an Infinite M200 PRO microplate reader (Tecan) according to the supplier's instructions.

**Synthesis of the Curcuminoid Compounds:** The synthesis of **1** was carried out according a modification of a reported procedure, and **2** was synthesized as reported.<sup>[24]</sup>

**Synthesis of the Azido-Sugars:** 2-Azidoethyl 2,3,4,6-tetra-O-acetyl- $\beta$ -D-glucopyranoside<sup>[25a]</sup> and 1-azido-1-deoxy-2,3,4,5-di-O-isoprop-

ylidene- $\beta$ -D-fructopyranoside were synthesized as previously reported.<sup>[25b]</sup>

**Compound 1:** 2,4-Pentanedione (0.64 mL, 6.2 mmol) and  $\text{BF}_3 \cdot \text{Et}_2\text{O}$  (1.16 mL, 9.4 mmol) were dissolved in anhydrous toluene (5 mL) and stirred at 65 °C for 2 h. 4-(Propargyloxy)benzaldehyde (2 g, 12.5 mmol) in anhydrous toluene (40 mL) was added to the solution. After the addition of tributyl borate (3.9 mL, 15.6 mmol), the resulting black mixture was stirred at 65 °C for 30 min. *n*-Butylamine (0.43 mL, 4.34 mmol) was added dropwise until the color of the solution changed to red, and stirring was continued at 65 °C overnight. After cooling to room temperature, the precipitated solid was collected by filtration and washed with small amounts of cold toluene and water. The crude product was dissolved in acetone, and water was added slowly to precipitate **1** (2.575 g, 5.96 mmol) as a red solid, isolated by filtration, washed with water and dried in vacuo. Yield: 96 %.  $^1\text{H}$  NMR (300 MHz,  $[\text{D}_6]\text{DMSO}$ ):  $\delta$  = 8.02 (d,  $^3J$  = 15.69 Hz, 2 H, 3-H), 7.88 (d,  $^3J$  = 8.59 Hz, 4 H, 6-H), 7.12 (m, 6 H, 4-H, 7-H), 6.53 (s, 1 H, 1-H), 4.92 (s, 4 H, 9-H), 3.63 (s, 2 H, 11-H) ppm.  $^{13}\text{C}$  NMR (75 MHz,  $[\text{D}_6]\text{DMSO}$ ):  $\delta$  = 179.33 (C-2), 160.37 (C-8), 146.27 (C-3), 131.61 (C-6), 127.53 (C-5), 119.17 (C-4), 115.61 (C-7), 101.73 (C-1), 78.75 (C-10, C-11), 55.74 (C-9) ppm.  $^{19}\text{F}$  NMR (188 MHz,  $[\text{D}_6]\text{DMSO}$ ):  $\delta$  = -138.14 ppm. HRMS (ESI): calcd. for  $\text{C}_{25}\text{H}_{19}\text{BF}_2\text{NaO}_4$   $[\text{M} + \text{Na}]^+$  455.1237; found 455.1219 (error: 4.8 ppm).  $\text{C}_{25}\text{H}_{19}\text{BF}_2\text{O}_4$  (432.23): calcd. C 69.47, H 4.43; found C 69.44, H 4.56. IR (KBr):  $\tilde{\nu}$  = 667 ( $\delta_{\text{CH}}$ ), 3290 ( $\nu_{\text{CH}}$ )  $\text{cm}^{-1}$ . UV/Vis:  $\lambda$  ( $\epsilon \times 10^{-3}$ ) = 477 (50.55), 458 (48.1), 254 (11.8  $\text{M}^{-1} \text{cm}^{-1}$ ) nm. FL ( $\text{CH}_3\text{OH}$ ,  $\lambda_{\text{ex}}$  = 477 nm):  $\lambda$  = 541 nm.

**Compound 3a:** 2-Azidoethyl 2,3,4,6-tetra-*O*-acetyl- $\beta$ -D-glucopyranoside (3.863 g, 9.26 mmol) and **1** (2 g, 4.63 mmol) were dissolved in degassed THF (150 mL), and sodium ascorbate (1.5 g, 7.57 mmol) and  $\text{CuSO}_4$  (0.24 g, 0.96 mmol) in degassed, pure water (5 mL) were added, and the mixture was heated at 50 °C under Ar for 12 h. When TLC (NP silica; EtOAc) indicated that no starting material had remained, the solvent was evaporated, the crude product was dissolved in  $\text{CHCl}_3$  and washed thrice with saturated, aqueous EDTA solution and thrice with pure water. The organic layer was dried with  $\text{Na}_2\text{SO}_4$ , the solvent evaporated, and the product was purified by flash column chromatography (NP silica, EtOAc) to obtain the pure product (2.388 g, 1.96 mmol, 42 %).  $^1\text{H}$  NMR (600 MHz,  $[\text{D}_6]\text{DMSO}$ ):  $\delta$  = 8.11 (s, 2 H, 11-H), 7.71 (d,  $^3J$  = 8.82 Hz, 4 H, 6-H), 7.62 (d,  $^3J$  = 15.78 Hz, 2 H, 3-H), 7.12 (d,  $^3J$  = 8.88 Hz, 4 H, 7-H), 6.82 (d,  $^3J$  = 15.90 Hz, 2 H, 4-H), 6.10 (s, 1 H, 1-H), 5.25–5.18 (m, 6 H, 3'-H, 9-H), 4.92 (t,  $^3J$  = 9.72 Hz, 2 H, 4'-H), 4.84 (d,  $^3J$  = 8.04 Hz, 2 H, 1'-H), 4.76–4.73 (m, 2 H, 2'-H), 4.62–4.53 (m, 4 H, 1-H<sub>spacer</sub>), 4.19 (dd,  $^2J$  = 12.30,  $^3J$  = 5.04 Hz, 2 H, 6'-H), 4.14–4.1 (m, 2 H, 2-H<sub>spacer</sub>), 4.06 (dd,  $^2J$  = 12.24,  $^3J$  = 2.28 Hz, 2 H, 6''-H), 3.99–3.92 (m, 4 H, 5'-H, 2-H<sub>spacer</sub>), 2.02–1.89 (4s, 12 H, acetyl H) ppm.  $^{13}\text{C}$  NMR (75 MHz,  $[\text{D}_6]\text{DMSO}$ ):  $\delta$  = 183.21 (C-2), 170.05–168.97 (acetyl C=O), 159.85 (C-8), 142.18 (C-10), 139.95 (C-3), 130.14 (C-6), 127.67 (C-5), 124.94 (C-11), 122.04 (C-4), 115.19 (C-7), 101.29 (C-1), 99.15 (C-1'), 71.91 (C-3'), 70.66 (C-5'), 70.57 (C-2'), 68.09 (C-4'), 67.41 (C-2<sub>spacer</sub>), 61.65 (C-6'), 61.26 (C-9), 49.34 (C-1<sub>spacer</sub>), 20.49–20.21 (acetyl  $\text{CH}_3$ ) ppm. MS (ESI): calcd. for  $\text{C}_{57}\text{H}_{66}\text{N}_6\text{NaO}_{24}$   $[\text{M} + \text{Na}]^+$  1241.4; found 1241.3; calcd. for  $\text{C}_{57}\text{H}_{67}\text{N}_6\text{O}_{24}$   $[\text{M} + \text{H}]^+$  1219.42; found 1219.41; calcd. for  $\text{C}_{57}\text{H}_{66}\text{KN}_6\text{O}_{24}$   $[\text{M} + \text{K}]^+$  1257.38; found 1257.3.  $\text{C}_{57}\text{H}_{66}\text{N}_6\text{O}_{24}$  (1219.17): calcd. C 56.15, H 5.46, N 6.89; found C 56.44, H 5.65, N 6.73. IR (KBr):  $\tilde{\nu}$  = 1755 ( $\nu_{\text{CO}}$ ), 2887 ( $\nu_{\text{CH}}$ ), 2958 ( $\nu_{\text{CH}_2}$ ), 3145 ( $\nu_{\text{CH}}$ )  $\text{cm}^{-1}$ . UV/Vis ( $\text{CH}_3\text{OH}$ ):  $\lambda$  ( $\epsilon \times 10^{-3}$ ) = 410 (39.25), 243 (13.55  $\text{M}^{-1} \text{cm}^{-1}$ ) nm. FL ( $\text{CH}_3\text{OH}$ ,  $\lambda_{\text{ex}}$  = 410 nm):  $\lambda$  = 509 nm.

**Compound 3b:** 1-Azido-1-deoxy-2,3,4,5-di-*O*-isopropylidene- $\beta$ -D-fructopyranoside (1.74 g, 6.1 mmol) and **1** (1.318 g, 3.05 mmol) were dissolved in degassed THF (100 mL), and sodium ascorbate

(1 g, 5.05 mmol) and  $\text{CuSO}_4$  (0.15 g, 0.6 mmol) in degassed water (5 mL) were added, and the mixture was heated at 50 °C under Ar for 12 h. When TLC (NP silica; EtOAc/*n*-hexane, 2:1, v/v) indicated that no starting material had remained, the solvent was evaporated, and the crude product was dissolved in  $\text{CHCl}_3$  and washed thrice with saturated, aqueous EDTA solution and thrice with pure water. The organic layer was dried with  $\text{Na}_2\text{SO}_4$ , the solvent was evaporated, and the product was purified by flash column chromatography (NP silica; EtOAc/*n*-hexane, 2:1, v/v) to give the pure product (1.503 g, 1.57 mmol, 52 %).  $^1\text{H}$  NMR (600 MHz,  $[\text{D}_6]\text{DMSO}$ ):  $\delta$  = 8.20 (s, 2 H, 11-H), 7.69 (d,  $^3J$  = 8.82 Hz, 4 H, 6-H), 7.61 (d,  $^3J$  = 15.78 Hz, 2 H, 3-H), 7.12 (d,  $^3J$  = 8.82 Hz, 4 H, 7-H), 6.82 (d,  $^3J$  = 15.90 Hz, 2 H, 4-H), 6.09 (s, 1 H, 1-H), 5.22 (s, 4 H, 9-H), 4.66 (m, 6 H, 1'-H, 1''-H, 4'-H), 4.43 (d,  $^3J$  = 2.26 Hz, 2 H, 3'-H), 4.27 (d,  $^3J$  = 8.7 Hz, 2 H, 5'-H), 3.75 (dd,  $^4J$  = 1.59,  $^2J$  = 12.99 Hz, 2 H, 6'-H), 3.64 (d,  $^2J$  = 12.84 Hz, 2 H, 6''-H), 1.41–0.81 (4 s, 12 H, isopropylidene H) ppm.  $^{13}\text{C}$  NMR (75 MHz,  $[\text{D}_6]\text{DMSO}$ ):  $\delta$  = 183.18 (C-2), 159.79 (C-8), 142.10 (C-3), 139.93 (C-10), 130.08 (C-6), 127.60 (C-5), 127.03 (C-11), 121.98 (C-4), 115.23 (C-7), 108.60 (isopropylidene C), 108.29 (isopropylidene C), 101.26 (C-1), 100.43 (C-2'), 70.33 (C-3'), 69.82 (C-5'), 69.32 (C-4'), 60.97 (C-9, C-6'), 54.84 (C-1'), 26.02–24.00 (isopropylidene  $\text{CH}_3$ ) ppm. HRMS (ESI): calcd. for  $\text{C}_{49}\text{H}_{58}\text{N}_6\text{NaO}_{14}$   $[\text{M} + \text{Na}]^+$  977.3903; found 977.3875 (error: 2.8 ppm).  $\text{C}_{49}\text{H}_{58}\text{N}_6\text{O}_{14} \cdot 0.5\text{H}_2\text{O}$  (964.04): C 61.05, H 6.17, N 8.72; found C 61.15, H 6.18, N 8.71. FTIR (GA):  $\tilde{\nu}$  = 613 ( $\nu_{\text{C-isopropylidene}}$ ), 1087 ( $\nu_{\text{COH}}$ ), 1755 ( $\nu_{\text{CO}}$ ), 2941 ( $\nu_{\text{CH}}$ ), 2987 ( $\nu_{\text{CH}_2}$ )  $\text{cm}^{-1}$ . UV/Vis ( $\text{CH}_3\text{OH}$ ):  $\lambda$  ( $\epsilon \times 10^{-3}$ ) = 410 (37), 243 (11.95  $\text{M}^{-1} \text{cm}^{-1}$ ) nm. FL ( $\text{CH}_3\text{OH}$ ,  $\lambda_{\text{ex}}$  = 410 nm):  $\lambda$  = 508 nm.

**Compound 4a:** Compound **3a** (400 mg, 0.32 mmol) was dissolved in  $\text{CH}_3\text{OH}/\text{CHCl}_3$  (1:2, v/v; 10 mL) under Ar, and sodium methoxide was added up to ca. pH 9. After 30 min, no protected ligand had remained (monitored by TLC: NP silica; EtOAc), and DOWEX ( $\text{H}^+$ ) was added to reach ca. pH 7. The resin was filtered off and the solvent removed. The residue was dissolved in water, filtered and dialyzed for 1 week against water to obtain the pure product (180 mg, 0.20 mmol, 63 %).  $^1\text{H}$  NMR (600 MHz,  $[\text{D}_6]\text{DMSO}$ ):  $\delta$  = 8.32 (s, 2 H, 3-H), 7.71 (d,  $^3J$  = 8.10 Hz, 4 H, 6-H), 7.62 (d,  $^3J$  = 15.78 Hz, 2 H, 3-H), 7.13 (d,  $^3J$  = 8.58 Hz, 4 H, 7-H), 6.82 (d,  $^3J$  = 15.12 Hz, 2 H, 4-H), 6.11 (s, 1 H, 1-H), 5.20 (s, 4 H, 9-H), 5.11 (d,  $^3J$  = 4.86 Hz, 2 H, 2'-OH), 4.98 (d,  $^3J$  = 4.80 Hz, 2 H, 3'-OH), 4.94 (d,  $^3J$  = 5.34 Hz, 2 H, 4'-OH), 4.61 (m, 4 H, 1-H<sub>spacer</sub>), 4.54 (m, 2 H, HO-6'), 4.25 (d,  $^3J$  = 7.80 Hz, 2 H, 1'-H), 4.11 (m, 2 H, 2-H<sub>spacer</sub>), 3.94 (m, 2 H, 2-H<sub>spacer</sub>), 3.69 (m, 2 H, 6'-H), 3.44 (m, 2 H, 6''-H), 3.17–3.12 (m, 4 H, 3'-H, 5'-H), 3.06 (m, 2 H, 4'-H), 2.99 (m, 2 H, 2'-H) ppm.  $^{13}\text{C}$  NMR (75 MHz,  $[\text{D}_6]\text{DMSO}$ ):  $\delta$  = 183.23 (C-12'), 159.91 (C-6''), 142.12 (C-4''), 139.99 (C-11''), 130.17 (C-8''), 127.66 (C-9''), 125.60 (C-3''), 122.05 (C-10''), 115.26 (C-7''), 102.94 (C-1), 101.34 (C-13''), 77.01 (C-5), 76.62 (C-3), 73.34 (C-2), 70.04 (C-4), 67.34 (C-1''), 61.28 (C-5''), 61.10 (C-6), 49.78 (C-2'') ppm. HRMS (ESI): calcd. for  $\text{C}_{41}\text{H}_{50}\text{N}_6\text{NaO}_{16}$   $[\text{M} + \text{Na}]^+$  905.3176; found 905.3163 (error: 1.4 ppm).  $\text{C}_{41}\text{H}_{50}\text{N}_6\text{O}_{16} \cdot 2.5\text{H}_2\text{O}$  (927.9): calcd. C 53.07, H 5.97, N 9.06; found C 53.25, H 5.58, N 8.84. IR (KBr):  $\tilde{\nu}$  = 3352 ( $\nu_{\text{OH}}$ )  $\text{cm}^{-1}$ . UV/Vis ( $\text{CH}_3\text{OH}$ ):  $\lambda$  ( $\epsilon \times 10^{-3}$ ) = 408 (18.45), 243 (13.55  $\text{M}^{-1} \text{cm}^{-1}$ ) nm. FL ( $\text{CH}_3\text{OH}$ ,  $\lambda_{\text{ex}}$  = 408 nm):  $\lambda$  = 509 nm.

**Compound 4b:** Compound **3b** (175 mg, 0.183 mmol) was dissolved in formic acid/water (17:3, v/v; 10 mL) and stirred at room temperature for 1 week. When no isopropylidene groups had remained (monitored by ESI-MS), formic acid was coevaporated with water and the residue was dried. The crude product was dissolved in THF/water mixture (1:1, v/v; 5 mL), and aqueous 0.1 M NaOH solution was added to reach ca. pH 9. The solution was neutralized with 2.5 M HCl, freeze-dried, redissolved in water and dialyzed for 1 week against water to obtain the pure product (84 mg, 0.106 mmol, 58 %).  $^1\text{H}$  NMR (600 MHz,  $[\text{D}_6]\text{DMSO}$ ):  $\delta$  = 8.09 (s, 1 H, 11-H), 7.71

(d,  $^3J = 8.46$  Hz, 4 H, 6-H), 7.62 (d,  $^3J = 15.84$  Hz, 2 H, 3-H), 7.13 (d,  $^3J = 8.52$  Hz, 4 H, 7-H), 6.82 (d,  $^3J = 15.84$  Hz, 2 H, 4-H), 6.10 (s, 1 H, 1-H), 5.22 (m, 4 H, 9-H), 4.59–4.37 (m, 4 H, 1'-H, 1''-H), 3.88–3.41 (m, 10 H, 3-H, 4-H, 5-H, 6-H, 6'-H).  $^{13}\text{C}$  NMR (75 MHz,  $[\text{D}_6]\text{DMSO}$ ):  $\delta = 183.24$  (C-2), 159.97 (C-8), 141.98 (C-10), 140.01 (C-9), 130.17 (C-6), 127.65 (C-5), 125.94 (C-11), 122.03 (C-4), 115.28 (C-7), 102.70 (C-2'), 101.32 (C-1), 100.24 (C-2'), 96.67 (C-2'), 82.60 (C-3'), 82.21 (C-3'), 77.01 (C-5'), 76.10 (C-5'), 74.61 (C-5'), 69.55 (C-4'), 68.76 (C-4'), 68.53 (C-4'), 63.77 (C-6'), 62.49 (C-6'), 61.32 (C-6'), 61.25 (C-9), 54.75 (C-1'), 54.22 (C-1'), 54.04 (C-1') ppm. HRMS (ESI):  $m/z$  calcd. for  $\text{C}_{49}\text{H}_{58}\text{N}_6\text{O}_{14}\text{Na}$   $[\text{M} + \text{Na}]^+$ : 817.2651; found 817.2613 (error: 4.7 ppm).  $\text{C}_{37}\text{H}_{42}\text{N}_6\text{O}_{14} \cdot 2.5\text{H}_2\text{O}$  (839.81): calcd. C 52.92, H 5.64, N 10.01; found C 52.70, H 5.24, N 10.04. IR (KBr):  $\tilde{\nu} = 3352$  ( $\nu_{\text{OH}}$ )  $\text{cm}^{-1}$ . UV/Vis ( $\text{CH}_3\text{OH}$ ):  $\lambda$  ( $\epsilon \times 10^{-3}$ ) = 409 (8.75), 286 (4.10  $\text{M}^{-1} \text{cm}^{-1}$ ) nm. FL ( $\text{CH}_3\text{OH}$ ,  $\lambda_{\text{ex}} = 408$  nm):  $\lambda = 510$  nm.

**Compound 5a:** Compound **4a** (135 mg, 0.15 mmol) was dissolved in anhydrous methanol under Ar, and sodium methoxide solution (0.5 M in MeOH, 310  $\mu\text{L}$ , 0.15 mmol) was added dropwise. The solution was stirred for 1 h, and  $[\text{Ru}(\text{bpy})_2\text{Cl}_2]$  (81.7 mg, 0.17 mmol) in methanol was slowly added. The mixture was heated to reflux under Ar at 60 °C for 12 h. When TLC (NP silica;  $\text{CH}_3\text{CN}/\text{H}_2\text{O}/\text{satd. aq. KNO}_3$ , 40:4:1, v/v/v) indicated that no starting material had remained, the solvent was evaporated. The crude product was dissolved in water, filtered and dialyzed for 1 week against water to obtain the pure complex (191 mg, 0.14 mmol, 93 %).  $^1\text{H}$  NMR (600 MHz,  $[\text{D}_6]\text{DMSO}$ ):  $\delta = 8.80$  (d,  $^3J = 8.28$  Hz, 2 H, 3- $\text{H}_{\text{bpy}}$ ), 8.70 (d,  $^3J = 8.22$  Hz, 2 H, 3'- $\text{H}_{\text{bpy}}$ ), 8.65 (d,  $^3J = 5.28$  Hz, 2 H, 6- $\text{H}_{\text{bpy}}$ ), 8.30 (s, 2 H, 11-H), 8.18 (t,  $^3J = 7.80$  Hz, 2 H, 4- $\text{H}_{\text{bpy}}$ ), 7.93 (t,  $^3J = 7.83$  Hz, 2 H, 4'- $\text{H}_{\text{bpy}}$ ), 7.79 (m, 4 H, 6'- $\text{H}_{\text{bpy}}$ , 5- $\text{H}_{\text{bpy}}$ ), 7.47 (d,  $^3J = 8.76$  Hz, 4 H, 6-H), 7.31 (t,  $^3J = 6.69$  Hz, 2 H, 5'- $\text{H}_{\text{bpy}}$ ), 7.01 (m, 6 H, 3-H, 7-H), 6.63 (d,  $^3J = 15.84$  Hz, 2 H, 4-H), 5.93 (s, 1 H, 1-H), 5.13 (s, 4 H, 9-H), 4.58 (m, 4 H, 1- $\text{H}_{\text{spacer}}$ ), 4.24 (d,  $^3J = 7.86$  Hz, 2 H, 1'-H), 4.09 (m, 2 H, 2- $\text{H}_{\text{spacer}}$ ), 3.92 (m, 2 H, 2- $\text{H}_{\text{spacer}}$ ), 3.68 (dd,  $^2J = 11.76$ ,  $^3J = 1.80$  Hz, 2 H, 6'-H), 3.45 (q,  $^3J = 5.92$  Hz, 2 H, 6''-H), 3.17–3.10 (m, 4 H, 3'-H, 5'-H), 3.06 (t,  $^3J = 9.18$  Hz, 2 H, 4'-H), 2.98 (t,  $^3J = 9.18$  Hz, 2 H, 2'-H) ppm.  $^{13}\text{C}$  NMR (75 MHz,  $[\text{D}_6]\text{DMSO}$ ):  $\delta = 177.63$  (C-2), 158.89 (C-2 $_{\text{bpy}}$ ), 158.76 (C-2' $_{\text{bpy}}$ ), 157.39 (C-8), 152.84 (C-6' $_{\text{bpy}}$ ), 149.41 (C-6 $_{\text{bpy}}$ ), 142.13 (C-10), 136.63 (C-4 $_{\text{bpy}}$ ), 135.33 (C-7), 135.00 (C-4' $_{\text{bpy}}$ ), 129.08 (C-6), 128.31 (C-5), 126.79 (C-4), 126.49 (C-5 $_{\text{bpy}}$ ), 125.72 (C-5' $_{\text{bpy}}$ ), 125.53 (C-11), 123.44 (C-3 $_{\text{bpy}}$ , C-3' $_{\text{bpy}}$ ), 115.10 (C-3), 102.92 (C-1'), 102.06 (C-1), 77.03 (C-5'), 76.61 (C-3'), 73.32 (C-2'), 70.02 (C-4'), 67.27 (C-2 $_{\text{spacer}}$ ), 61.13 (C-9), 61.05 (C-6'), 49.72 (C-1 $_{\text{spacer}}$ ) ppm. HRMS (ESI): calcd. for  $\text{C}_{61}\text{H}_{65}\text{N}_{10}\text{O}_{16}\text{Ru}$   $[\text{M} - \text{Cl}]^+$  1295.3618; found 1295.3629 (error: 0.5 ppm). IR (KBr):  $\tilde{\nu} = 1425$  ( $\nu_{\text{CH}}$ ), 768 ( $\delta_{\text{oop}}$ )  $\text{cm}^{-1}$ . UV/Vis ( $\text{CH}_3\text{OH}$ ):  $\lambda$  ( $\epsilon \times 10^{-3}$ ) = 517 (9.85), 410 (31.4), 391 (34.7), 296 (46.7), 245 (27.1  $\text{M}^{-1} \text{cm}^{-1}$ ) nm. FL ( $\text{CH}_3\text{OH}$ ,  $\lambda_{\text{ex}} = 296$  nm):  $\lambda = 586$  nm.

**Compound 5b:** Compound **4b** (26 mg, 32.7  $\mu\text{mol}$ ) was dissolved in anhydrous DMF (5 mL) under Ar, and sodium methoxide solution (0.5 M in MeOH, 75  $\mu\text{L}$ , 37.5  $\mu\text{mol}$ ) was added dropwise. The solution was stirred for 1 h, and  $[\text{Ru}(\text{bpy})_2\text{Cl}_2]$  (18 mg, 37.2  $\mu\text{mol}$ ) in anhydrous DMF (4 mL) was slowly added. The mixture was heated to reflux under Ar at 60 °C for 12 h. When TLC (NP silica;  $\text{CH}_3\text{CN}/\text{H}_2\text{O}/\text{satd. aq. KNO}_3$ , 40:4:1, v/v/v) indicated that no starting material had remained, the solvent was evaporated. The crude product was dissolved in water, filtered and dialyzed for 1 week against water to obtain the pure complex (28 mg, 22.5  $\mu\text{mol}$ , 69 %).  $^1\text{H}$  NMR (600 MHz,  $[\text{D}_6]\text{DMSO}$ ):  $\delta = 8.89$  (d,  $^3J = 5.79$  Hz, 2 H, 3- $\text{H}_{\text{bpy}}$ ), 8.78 (d,  $^3J = 8.12$  Hz, 2 H, 3'- $\text{H}_{\text{bpy}}$ ), 8.63 (d,  $^3J = 8.04$  Hz, 2 H, 6- $\text{H}_{\text{bpy}}$ ), 8.15 (t,  $^3J = 7.81$  Hz, 2 H, 4- $\text{H}_{\text{bpy}}$ ), 8.06–7.97 (m, 2 H, 11-H), 7.85 (t,  $^3J = 6.60$  Hz, 2 H, 4'- $\text{H}_{\text{bpy}}$ ), 7.79 (t,  $^3J = 7.81$  Hz, 4 H, 6'- $\text{H}_{\text{bpy}}$ , 5- $\text{H}_{\text{bpy}}$ ), 7.63–7.58 (m, 6 H, 6-H, 3-H), 7.39 (m, 2 H, 5'- $\text{H}_{\text{bpy}}$ ), 7.21 (m, 4 H, 7-

H), 6.76 (d,  $^3J = 8.63$  Hz, 2 H, 4-H), 6.28–6.22 (m, 1 H, 1-H), 5.13–4.82 (m, 4 H, 9-H), 4.59–4.56 (m, 4 H, 1'-H, 1''-H), 3.72 (d,  $^3J = 2.76$  Hz, 2 H, 4'-H), 3.54–3.51 (m, 4 H, 6'-H, 6''-H), 3.30–3.17 (m, 4 H, 3'-H, 5'-H) ppm.  $^{13}\text{C}$  NMR (75 MHz,  $[\text{D}_6]\text{DMSO}$ ):  $\delta = 176.03$  (C-2), 159.95 (C-8), 158.14 (C-2 $_{\text{bpy}}$ ), 157.75 (C-2' $_{\text{bpy}}$ ), 153.10 (C-6' $_{\text{bpy}}$ ), 149.51 (C-6 $_{\text{bpy}}$ ), 139.11 (C-10), 137.62 (C-4' $_{\text{bpy}}$ ), 135.76 (C-4 $_{\text{bpy}}$ ), 134.11 (C-7), 130.62, 129.18 (C-6), 128.35 (C-5), 126.98 (C-4), 126.17 (C-11), 123.84 (C-3 $_{\text{bpy}}$ ), 123.58 (C-3' $_{\text{bpy}}$ ), 115.27 (C-3), 80.12 (C-2'), 74.36 (C-5'), 70.43 (C-4'), 69.69 (C-3'), 64.95 (C-6', C-6''), 64.22 (C-1'), 61.71 (C-1'', C-9) ppm. HRMS (ESI Orbitrap): calcd. for  $\text{C}_{57}\text{H}_{57}\text{N}_{10}\text{O}_{16}\text{Ru}$   $[\text{M} - \text{Cl}]^+$  1207.3110; found 1207.3112 (error: 1.7 ppm). FTIR (GA):  $\tilde{\nu} = 3360$  ( $\nu_{\text{OH}}$ ), 3307 ( $\nu_{\text{OH}}$ ), 2920 ( $\nu_{\text{CH}}$ ), 2850 ( $\nu_{\text{CH}_2}$ ), 1632 ( $\nu_{\text{C}=\text{C}}$ )  $\text{cm}^{-1}$ . UV/Vis ( $\text{CH}_3\text{OH}$ ):  $\lambda$  ( $\epsilon \times 10^{-3}$ ) = 499 (3.96), 349 (4.89), 294 (29.78), 245 (12.89  $\text{M}^{-1} \text{cm}^{-1}$ ) nm. FL ( $\text{CH}_3\text{OH}$ ,  $\lambda_{\text{ex}} = 296$  nm):  $\lambda = 536$  nm.

**Compound 5c:** Compound **1** (45 mg, 0.15 mmol) was dissolved in anhydrous methanol (30 mL) under Ar, and sodium methoxide solution (0.5 M in MeOH, 0.17 mmol, 350  $\mu\text{L}$ ) was added. The solution was stirred for 1 h, and  $[\text{Ru}(\text{bpy})_2\text{Cl}_2]$  (71 mg, 0.15 mmol) in anhydrous DMF (30 mL) was added dropwise. The mixture was heated under Ar at 60 °C for 12 h. When TLC (NP silica;  $\text{CH}_3\text{CN}/\text{H}_2\text{O}/\text{satd. aq. KNO}_3$ , 40:4:1, v/v/v) indicated that no starting material had remained, the solvent was evaporated. The crude product was dissolved in methanol, filtered and purified by size-exclusion chromatography (Sephadex LH-20) to obtain the pure complex (41 mg, 0.05 mmol, 37 %).  $^1\text{H}$  NMR (600 MHz,  $[\text{D}_6]\text{DMSO}$ ):  $\delta = 8.79$  (d,  $^3J = 8.22$  Hz, 2 H, 3- $\text{H}_{\text{bpy}}$ ), 8.69 (d,  $^3J = 8.22$  Hz, 2 H, 3'- $\text{H}_{\text{bpy}}$ ), 8.64 (d,  $^3J = 5.04$  Hz, 2 H, 6- $\text{H}_{\text{bpy}}$ ), 8.17 (m, 2 H, 4- $\text{H}_{\text{bpy}}$ ), 7.92 (m, 2 H, 4'- $\text{H}_{\text{bpy}}$ ), 7.78 (m, 4 H, 6'- $\text{H}_{\text{bpy}}$ , 5- $\text{H}_{\text{bpy}}$ ), 7.32 (m, 6 H, 6-H, 5'- $\text{H}_{\text{bpy}}$ ), 6.93 (d,  $^3J = 15.72$  Hz, 2 H, 3-H), 6.72 (d,  $^3J = 8.40$  Hz, 2 H, 7-H), 6.52 (d,  $^3J = 15.78$  Hz, 2 H, 4-H), 5.86 (s, 1 H, 1-H) ppm.  $^{13}\text{C}$  NMR (150 MHz,  $[\text{D}_6]\text{DMSO}$ ):  $\delta = 177.68$  (C-2), 158.97 (C-2 $_{\text{bpy}}$ ), 158.80 (C-2' $_{\text{bpy}}$ ), 157.40 (C-8), 152.81 (C-6' $_{\text{bpy}}$ ), 149.40 (C-6 $_{\text{bpy}}$ ), 136.55 (C-4 $_{\text{bpy}}$ ), 135.92 (C-3), 134.92 (C-4' $_{\text{bpy}}$ ), 129.21 (C-6), 126.45 (C-5), 126.25 (C-5 $_{\text{bpy}}$ ), 125.70 (C-5' $_{\text{bpy}}$ ), 125.47 (C-4), 123.43 (C-3 $_{\text{bpy}}$ , C-3' $_{\text{bpy}}$ ), 115.84 (C-7), 101.75 (C-1) ppm. HRMS (ESI): calcd. for  $\text{C}_{39}\text{H}_{31}\text{N}_4\text{O}_4\text{Ru}$   $[\text{M} - \text{Cl}]^+$  721.1405; found 721.1383 (error: 1.5 ppm). UV/Vis ( $\text{CH}_3\text{OH}$ ):  $\lambda$  ( $\epsilon \times 10^{-3}$ ) = 516.5 (14.55), 412.5 (48.1), 395 (49.9), 296 (58.35), 245 (34.8  $\text{M}^{-1} \text{cm}^{-1}$ ) nm. FL ( $\text{CH}_3\text{OH}$ ,  $\lambda_{\text{ex}} = 296$  nm):  $\lambda = 585$  nm.

**Determination of Cytotoxicity:** Cytotoxicity studies were performed with the mouse fibroblast cell line L929, as well as with HepG2 and MDA-MB-231 cells. In detail, cells were seeded at  $10^4$  cells per well in a 96-well plate and incubated for 24 h. Afterwards, the test substances (**2**, **4a**, **4b**, **5a–c**) at indicated concentrations (25, 50, 100  $\mu\text{M}$ ) were added to the cells, and the plates were incubated for a further 24 h. Subsequently, the medium was replaced with a mixture of fresh culture medium and alamarBlue solution (Thermo Fisher), prepared according to the manufacturer's instructions. After a further incubation of 4 h at 37 °C, the fluorescence was measured at  $\lambda_{\text{em}} = 570$  nm/ $\lambda_{\text{ex}} = 610$  nm, with untreated cells on the same well plate serving as negative controls. The negative control was standardized as 0 % of metabolism inhibition and referred to as 100 % viability. Data are expressed as mean  $\pm$  SD of three independent determinations.

## Acknowledgments

The authors gratefully thank Prof. Dr. Sven Rau for providing  $\text{Ru}(\text{bpy})_2\text{Cl}_2$  precursor and Gabi Sentis for NMR measurements. The Carl-Zeiss Foundation (JCSM Strukturantrag) and the German Federal Ministry of Education & Research (BMBF) (#031A518B Vectura) are gratefully acknowledged for financial support.



**Keywords:** Carbohydrates · Metal complexes · Curcumin · Ruthenium · Click chemistry

- [1] L. Chiang, M. R. Jones, S. L. Ferreira, T. T. Storr, *Curr. Med. Chem.* **2012**, *12*, 122–144.
- [2] A. Bergamo, C. Gaiddon, J. H. M. Schellens, J. H. Beijnen, G. Sava, *J. Inorg. Biochem.* **2012**, *106*, 90–99.
- [3] X. Wang, Z. Guo, *Chem. Soc. Rev.* **2013**, *42*, 202–224.
- [4] F. Q. Zhao, A. F. Keating, *Curr. Genomics* **2007**, *8*, 113–128.
- [5] N. Nomura, G. Verdon, H. J. Kang, T. Shimamura, Y. Nomura, Y. Sonoda, S. A. Hussien, A. A. Qureshi, M. Coincon, Y. Sato, H. Abe, Y. Nakada-Nakura, T. Hino, T. Arakawa, O. Kusano-Arai, H. Iwanari, T. Murata, T. Kobayashi, T. Hamakubo, M. Kasahara, S. Iwata, D. Drew, *Nature* **2015**, *526*, 397–401.
- [6] A. Godoy, V. Ulloa, F. Rodríguez, K. Reinicke, A. J. Yañez, M. d. I. A. García, R. A. Medina, M. Carrasco, S. Barberis, T. Castro, F. Martínez, X. Koch, J. C. Vera, M. T. Poblete, C. D. Figueroa, B. Peruzzo, F. Pérez, F. Nualart, *J. Cell. Physiol.* **2006**, *207*, 614–627.
- [7] G. Gowrishankar, S. Zitzmann-Kolbe, A. Junutula, R. Reeves, J. Levi, A. Srinivasan, K. Bruus-Jensen, J. Cyr, L. Dinkelborg, S. S. Gambhir, *PLoS One* **2011**, *6*, e26902.
- [8] a) A. Tatibouët, J. Yang, C. Morin, G. D. Holman, *Bioorg. Med. Chem.* **2000**, *8*, 1825–1833; b) J. Yang, J. Dowden, A. Tatibouët, Y. Hatanaka, G. D. Holman, *Biochem. J.* **2002**, *367*, 533–539.
- [9] J. Levi, Z. Cheng, O. Gheysens, M. Patel, C. T. Chan, Y. Wang, M. Namavari, S. S. Gambhir, *Bioconjugate Chem.* **2007**, *18*, 628–634.
- [10] C. von der Ehe, A. Rinkenauer, C. Weber, D. Szamosvari, M. Gottschaldt, U. S. Schubert, *Macromol. Biosci.* **2016**, *16*, 508–521.
- [11] J. Zhao, K. Babiuch, H. Lu, A. Dag, M. Gottschaldt, M. H. Stenzel, *Chem. Commun.* **2014**, *50*, 15928–15931.
- [12] a) K. K.-W. Lo, W. H.-T. Law, J. C.-Y. Chan, H.-W. Liu, K. Y. Zhang, *Metallomics* **2013**, *5*, 808–812; b) K. Yin Zhang, K. Ka-Shun Tso, M.-W. Louie, H.-W. Liu, K. Kam-Wing Lo, *Organometallics* **2013**, *32*, 5098–5102.
- [13] M. Gottschaldt, U. S. Schubert, *Chem. Eur. J.* **2009**, *15*, 1548–1557.
- [14] S. C. Gupta, S. Patchva, W. Koh, B. B. Aggarwal, *Clin. Exp. Pharmacol. Physiol.* **2012**, *39*, 283–299.
- [15] K. Bairwa, J. Grover, M. Kania, S. M. Jachak, *RSC Adv.* **2014**, *4*, 13946–13978.
- [16] a) P. Anand, A. B. Kunnumakkara, R. A. Newman, B. B. Aggarwal, *Mol. Pharm.* **2007**, *4*, 807–818; b) G. Shoba, D. Joy, T. Joseph, M. Majeed, R. Rajendran, P. S. S. R. Srinivas, *Planta Med.* **1998**, *64*, 353–356.
- [17] a) S. Wanninger, V. Lorenz, A. Subhan, F. T. Edelmann, *Chem. Soc. Rev.* **2015**, *44*, 4986–5002; b) S. Banerjee, A. R. Chakravarty, *Acc. Chem. Res.* **2015**, *48*, 2075–2083; c) M. Pröhl, U. S. Schubert, W. Weigand, M. Gottschaldt, *Coord. Chem. Rev.* **2016**, *307*, Part 1, 32–41.
- [18] R. Pettinari, F. Marchetti, F. Condello, C. Pettinari, G. Lupidi, R. Scopelliti, S. Mukhopadhyay, T. Riedel, P. J. Dyson, *Organometallics* **2014**, *33*, 3709–3715.
- [19] T. K. Goswami, S. Gadadhar, B. Gole, A. A. Karande, A. R. Chakravarty, *Eur. J. Med. Chem.* **2013**, *63*, 800–810.
- [20] D. Pucci, T. Bellini, A. Crispini, I. D'Agnano, P. F. Liguori, P. Garcia-Orduna, S. Pirillo, A. Valentini, G. Zanchetta, *MedChemComm* **2012**, *3*, 462–468.
- [21] S. Banerjee, P. Prasad, I. Khan, A. Hussain, P. Kondaiah, A. R. Chakravarty, *Z. Anorg. Allg. Chem.* **2014**, *640*, 1195–1204.
- [22] a) K. Nwe, M. W. Brechbiel, *Cancer Biother. Radiopharm.* **2009**, *24*, 289–302; b) B. Schulze, U. S. Schubert, *Chem. Soc. Rev.* **2014**, *43*, 2522–2571.
- [23] H. C. Kolb, M. G. Finn, K. B. Sharpless, *Angew. Chem. Int. Ed.* **2001**, *40*, 2004–2021; *Angew. Chem.* **2001**, *113*, 2056.
- [24] N. V. Sokolova, V. G. Nenajdenko, *RSC Adv.* **2013**, *3*, 16212–16242.
- [25] a) C. Kieburg, K. Sadalapure, T. K. Lindhorst, *Eur. J. Org. Chem.* **2000**, 2035–2040; b) B. E. Maryanoff, D. F. McComsey, M. J. Costanzo, C. Hochman, V. Smith-Swintosky, R. P. Shank, *J. Med. Chem.* **2005**, *48*, 1941–1947.
- [26] K. Liu, J. Chen, J. Chojnacki, S. Zhang, *Tetrahedron Lett.* **2013**, *54*, 2070–2073.
- [27] B. Zebib, Z. Mouloungui, V. Noirot, *Bioinorg. Chem. Appl.* **2010**, DOI: 10.1155/2010/292760.
- [28] a) T. J. Dickerson, N. Yamamoto, D. I. Ruiz, K. D. Janda, *J. Am. Chem. Soc.* **2004**, *126*, 11446–11447; b) A. A. Kolender, S. C. Parajon Puenzo, O. Varela, *ARKIVOC* **2011**, *7*, 237–244.
- [29] G. Wulff, H. Diederichs, *Macromol. Chem. Phys.* **1998**, *199*, 141–147.
- [30] C. Weber, J. A. Czaplewski, A. Baumgaertel, E. Altuntas, M. Gottschaldt, R. Hoogenboom, U. S. Schubert, *Macromolecules* **2012**, *45*, 46–55.
- [31] a) M. Cockman, D. G. Kubler, A. S. Oswald, L. Wilson, *J. Carbohydr. Chem.* **1987**, *6*, 181–201; b) F. Franks, *Pure Appl. Chem.* **1987**, *59*, 1189–1202; c) W. J. Goux, *J. Am. Chem. Soc.* **1985**, *107*, 4320–4327.
- [32] Y. Wang, H. Yu, X. Shi, Z. Luo, D. Lin, M. Huang, *J. Biol. Chem.* **2013**, *288*, 15980–15987.
- [33] D. Patra, C. Barakat, *Spectrochim. Acta, Part A* **2011**, *79*, 1034–1041.
- [34] G. Sprintschnik, H. W. Sprintschnik, P. P. Kirsch, D. G. Whitten, *J. Am. Chem. Soc.* **1976**, *98*, 2337–2338.
- [35] M. Gottschaldt, U. S. Schubert, S. Rau, S. Yano, J. G. Vos, T. Kroll, J. Clement, I. Hilger, *ChemBioChem* **2010**, *11*, 649–652.
- [36] a) I. Ali, K. Saleem, D. Wesselinova, A. Haque, *Med. Chem. Res.* **2013**, *22*, 1386–1398; b) H. Fan, W. Tian, X. Ma, *Targ. Oncol.* **2014**, *9*, 279–286; c) C. Syng-ai, A. L. Kumari, A. Khar, *Mol. Cancer Ther.* **2004**, *3*, 1101–1108.

Received: July 6, 2016

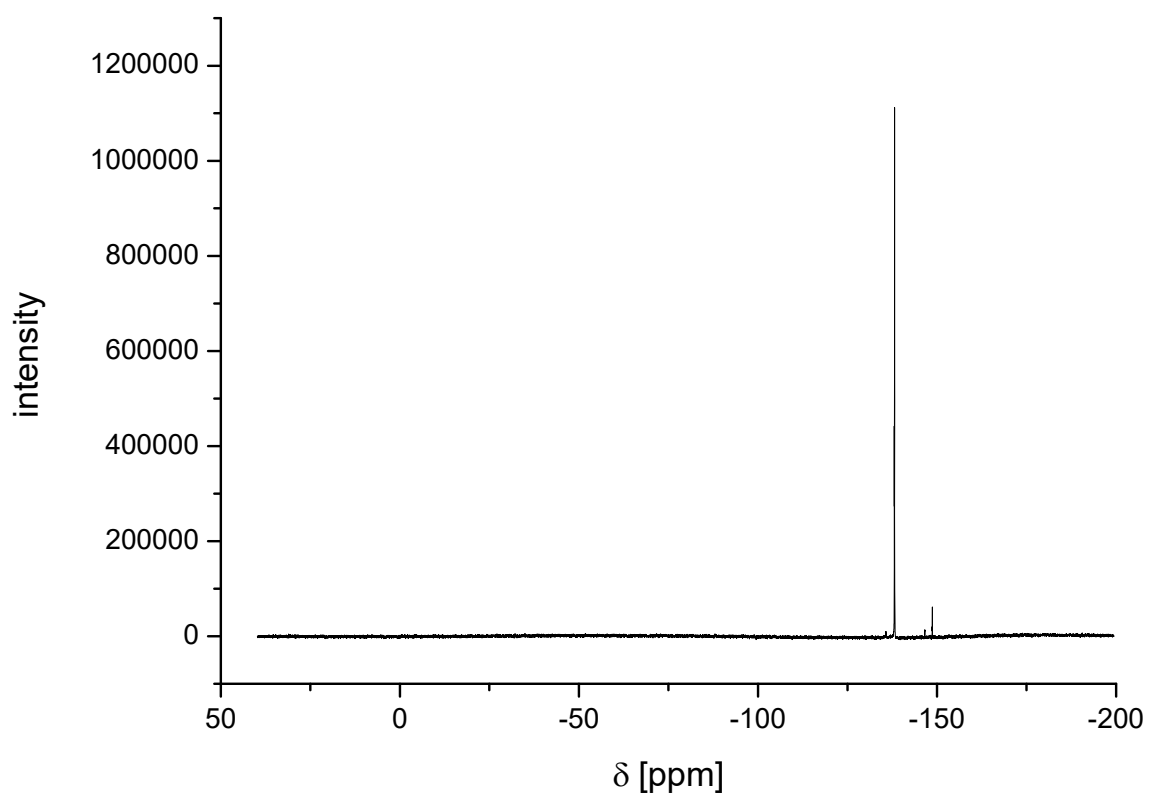
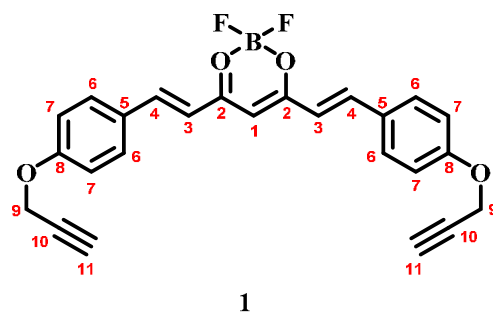
Published Online: October 19, 2016

**SUPPORTING INFORMATION**

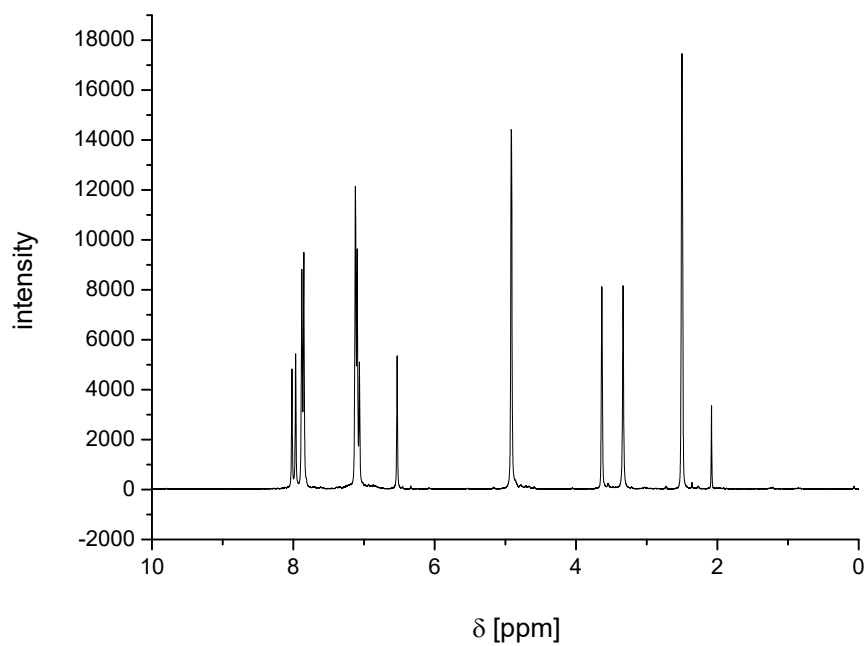
**DOI:** 10.1002/ejic.201600801

**Title:** Synthesis and in vitro Toxicity of D-Glucose and D-Fructose Conjugated Curcumin–Ruthenium Complexes

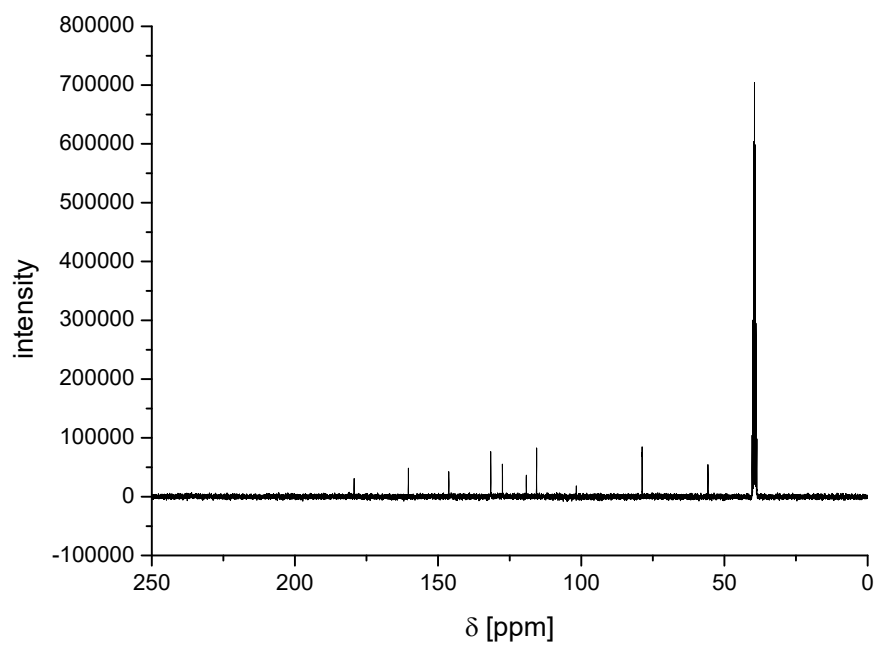
**Author(s):** Michael Pröhl, Tanja Bus, Justyna A. Czaplewska, Anja Traeger, Michael Deicke, Henning Weiss, Wolfgang Weigand, Ulrich S. Schubert, Michael Gottschaldt\*



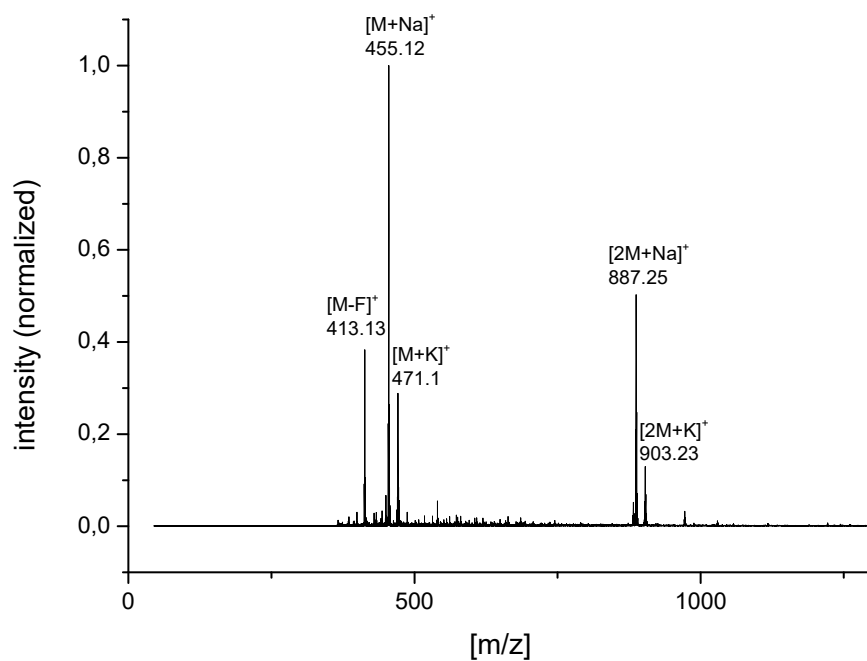
**Figure S1.** <sup>19</sup>F-NMR spectrum of **1** in DMSO-d<sub>6</sub>.



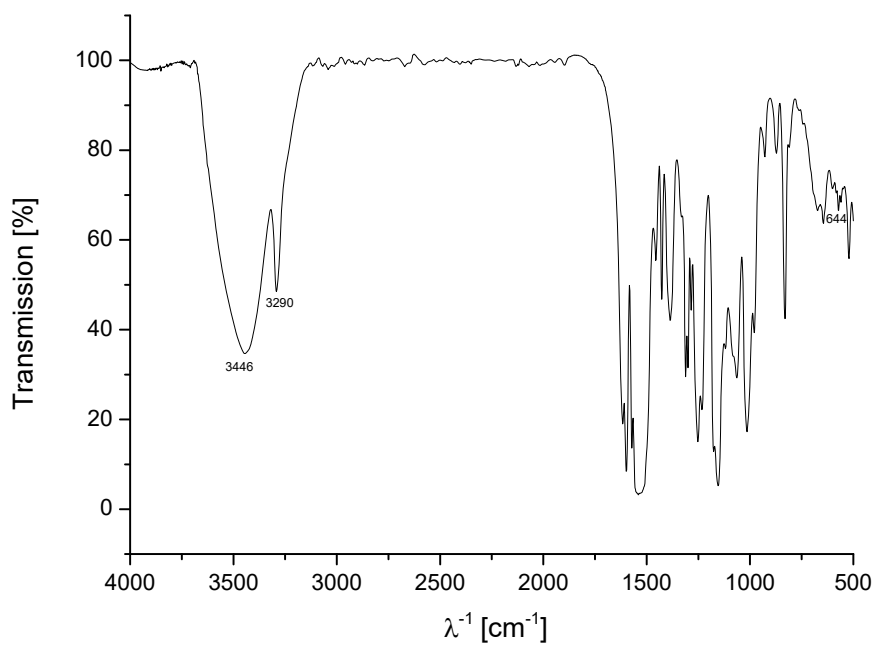
**Figure S2.**  $^1\text{H}$ -NMR spectrum of **1** in  $\text{DMSO-d}_6$ .



**Figure S3.**  $^{13}\text{C}$ -NMR spectrum of **1** in  $\text{DMSO-d}_6$ .

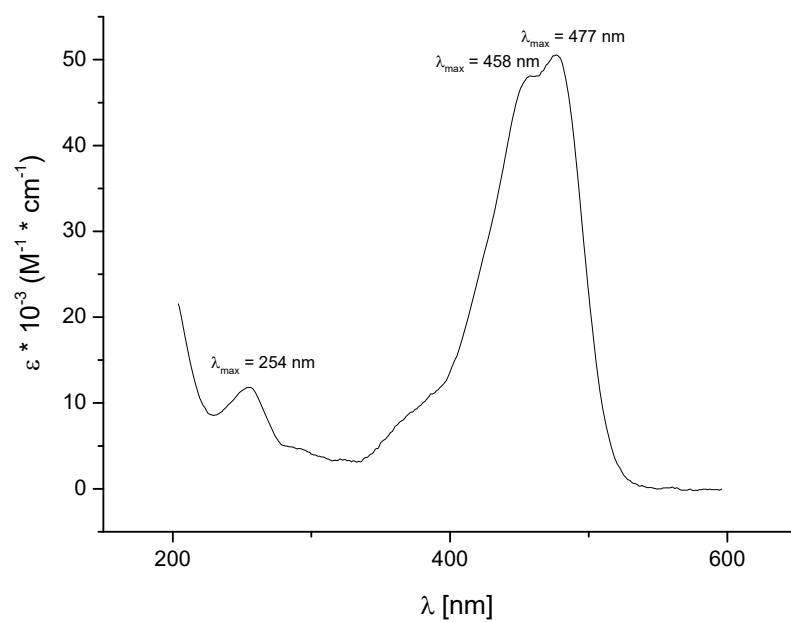


**Figure S4.** ESI-TOF-MS of **1** in acetonitrile.

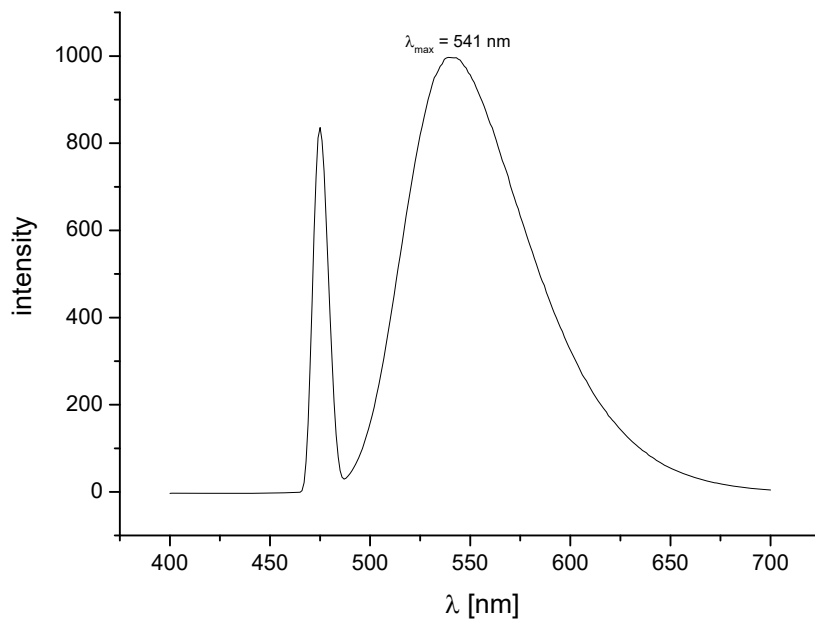


**Figure S5.** IR spectrum of **1**.

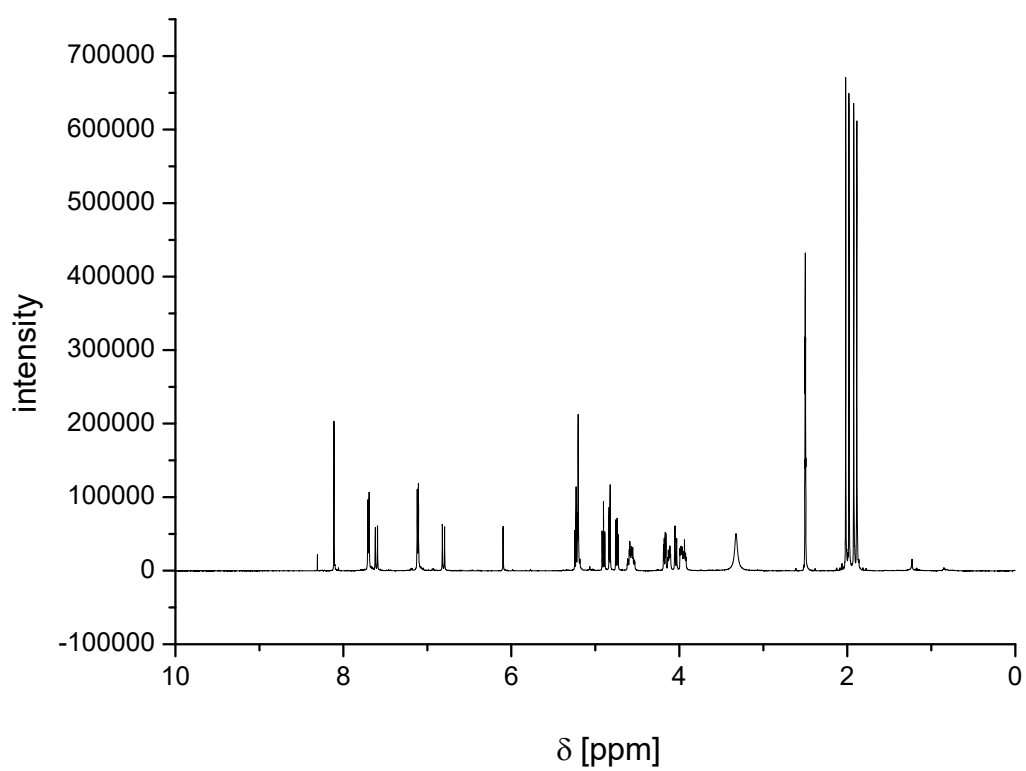
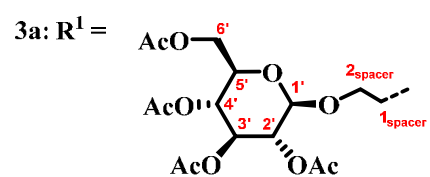
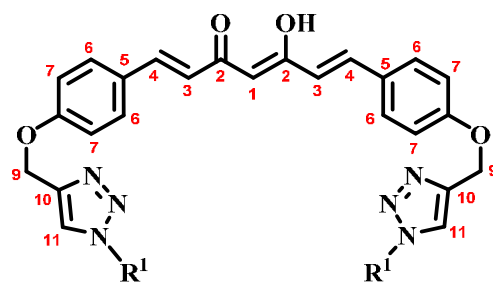




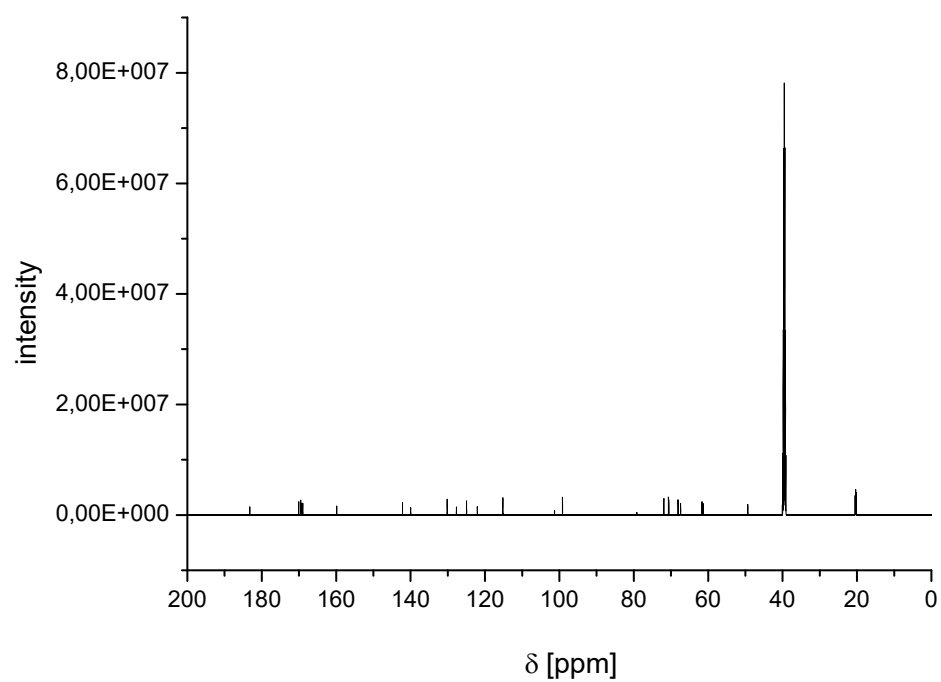
**Figure S6.** UV-Vis spectrum of **1** ( $2 \times 10^{-5} \text{ M}$ , aerated  $\text{CH}_3\text{OH}$ ).



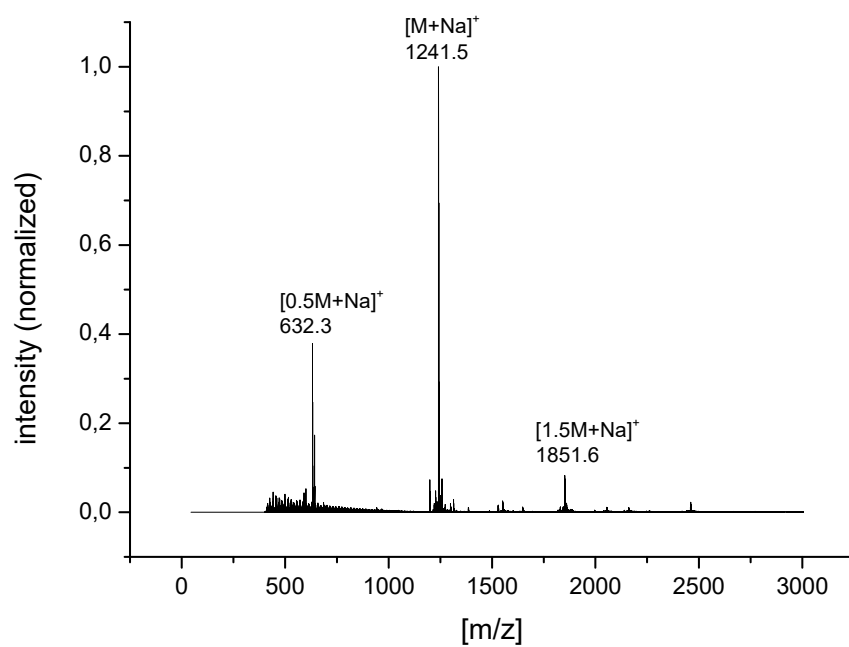
**Figure S7.** Emission spectrum of **1** ( $\lambda_{\text{ex}} = 477 \text{ nm}$ ,  $2 \times 10^{-6} \text{ M}$ , aerated  $\text{CH}_3\text{OH}$ ).



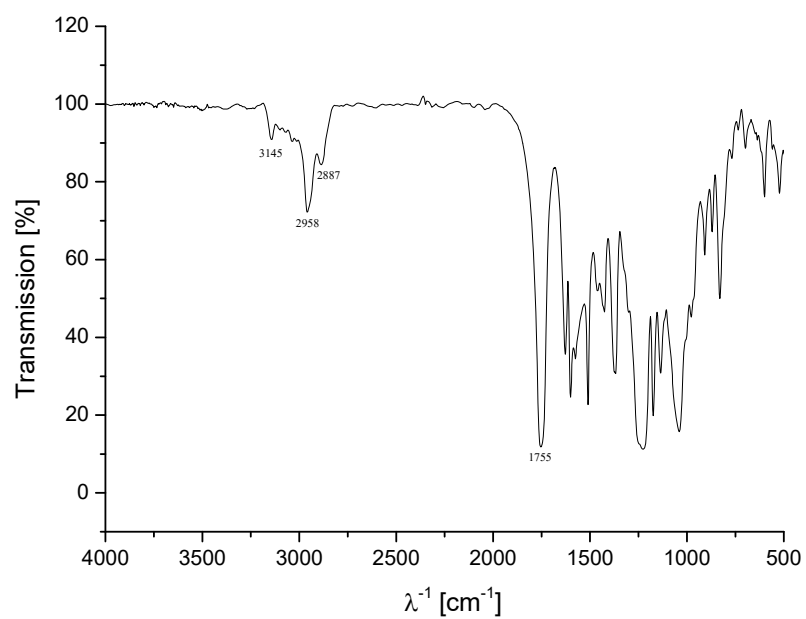
**Figure S8.** <sup>1</sup>H-NMR spectrum of **3a** in DMSO-d<sub>6</sub>.



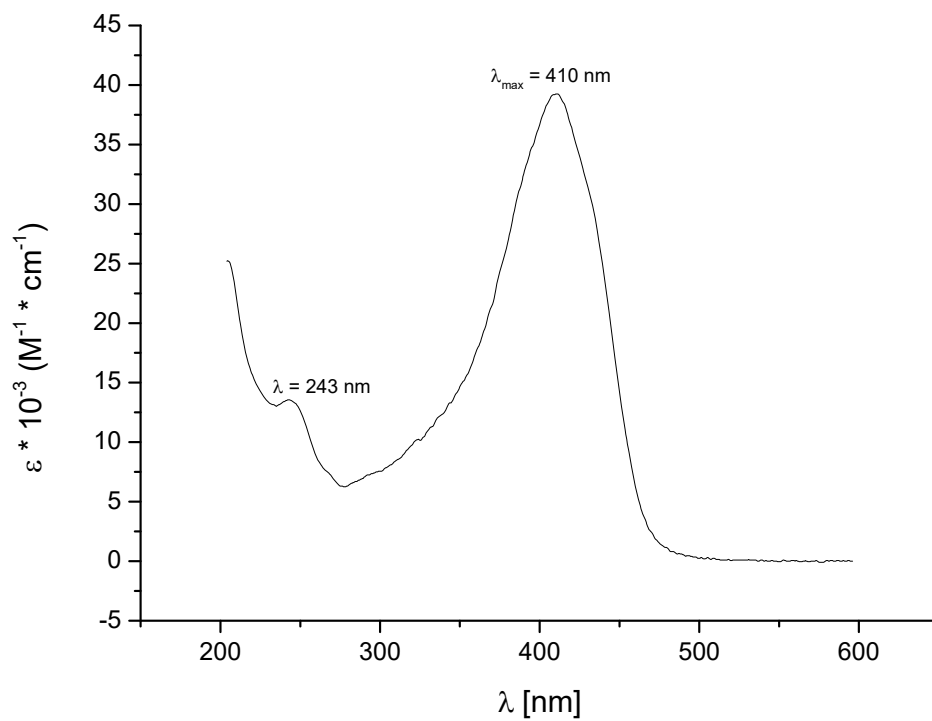
**Figure S9.**  $^{13}\text{C}$ -NMR spectrum of **3a** in  $\text{DMSO-d}_6$ .



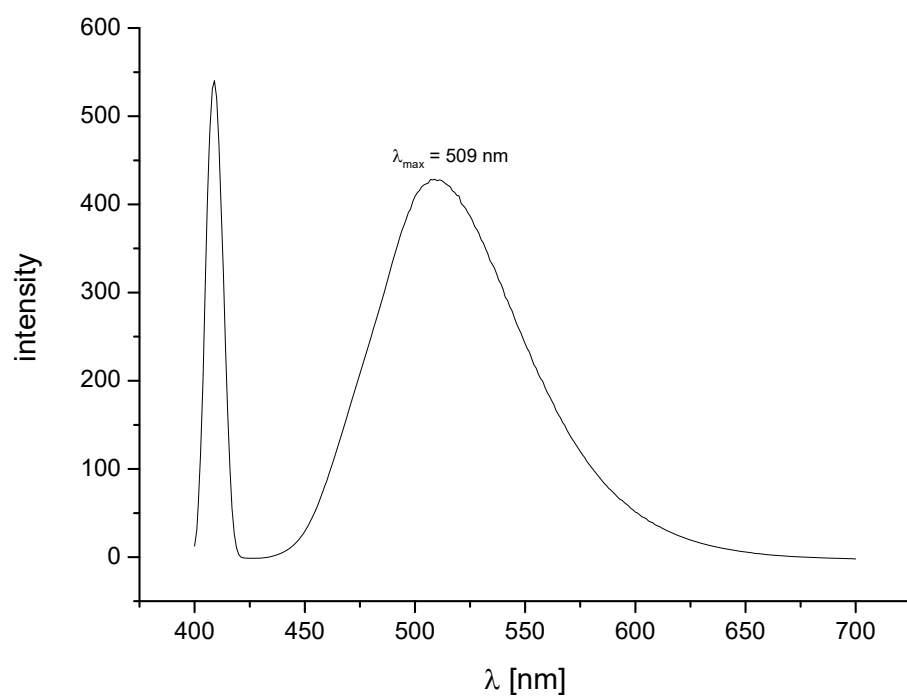
**Figure S10.** ESI-TOF-MS of **3a** in acetonitrile.



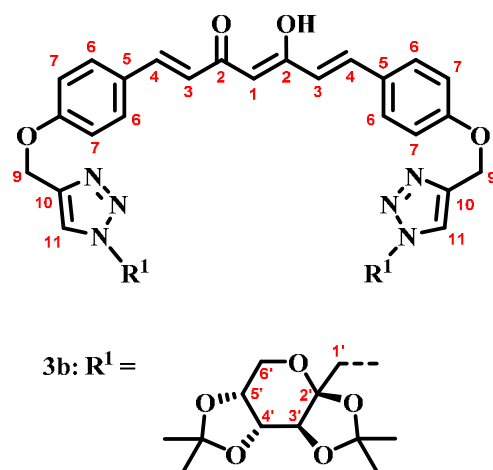
**Figure S11.** IR spectrum of **3a**.

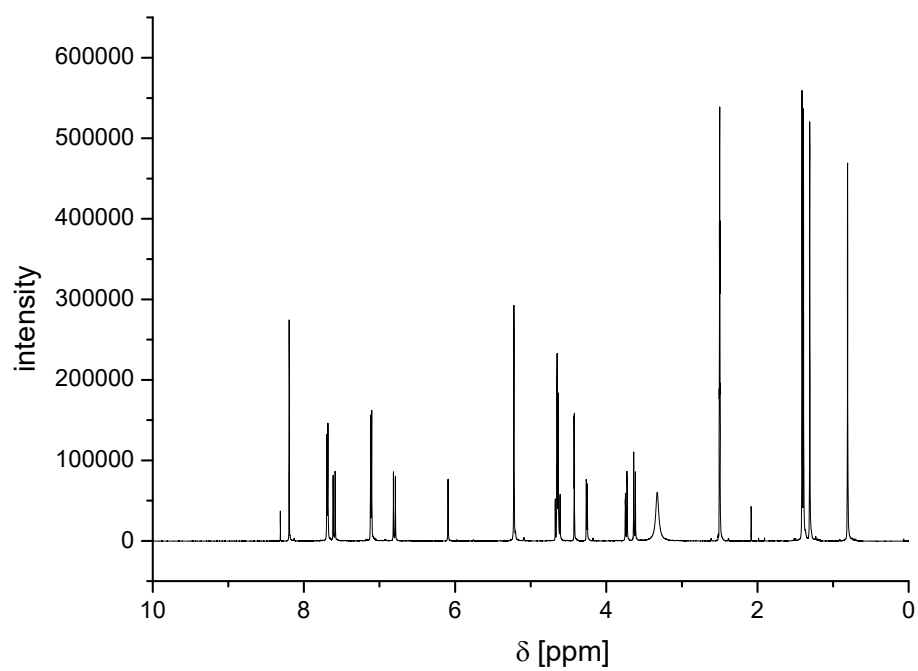


**Figure S12.** UV-Vis spectrum of **3a** ( $2 \times 10^{-5} \text{ M}$ , aerated  $\text{CH}_3\text{OH}$ ).

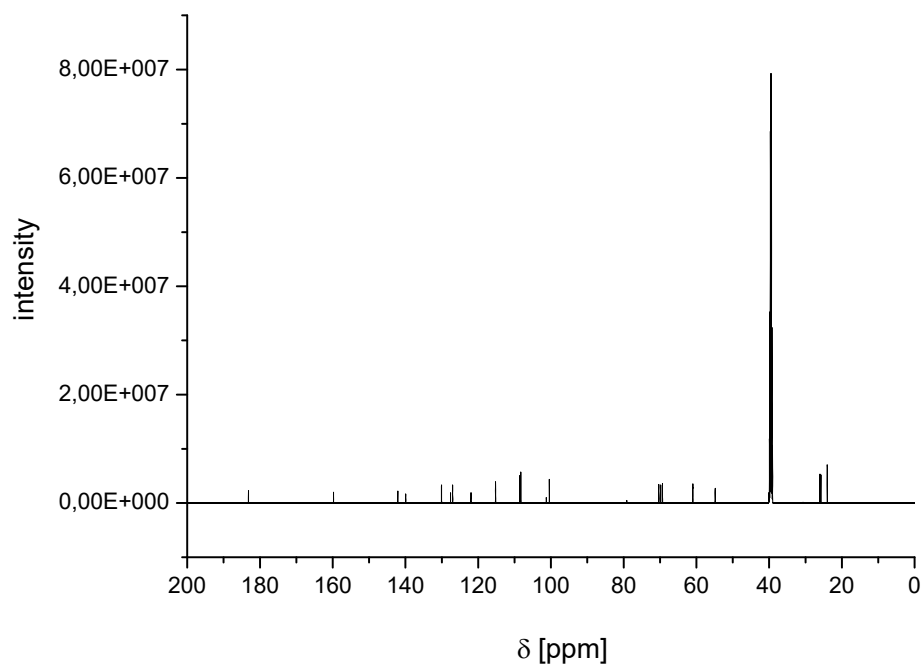


**Figure S13.** Emission spectrum of **3a** ( $\lambda_{\text{ex}} = 410 \text{ nm}$ ,  $2 \times 10^{-6} \text{ M}$ , aerated  $\text{CH}_3\text{OH}$ ).

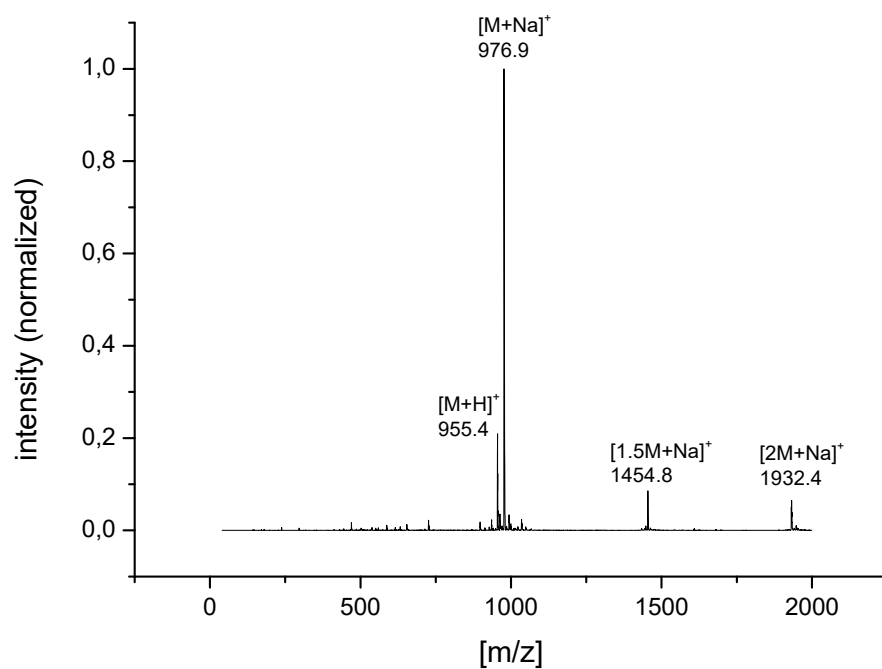




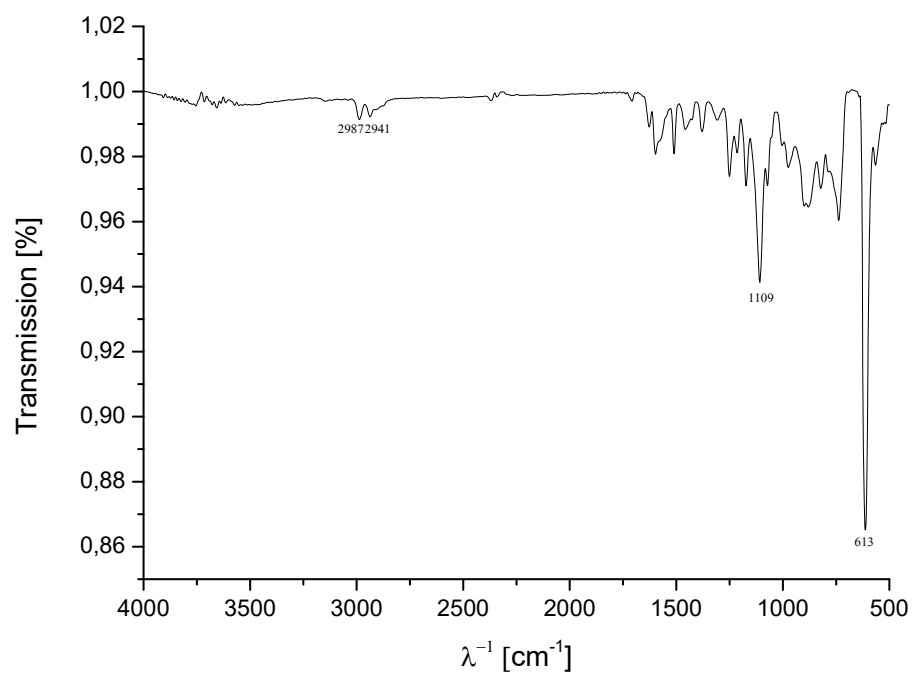
**Figure S14.** <sup>1</sup>H-NMR spectrum of **3b** in DMSO-d<sub>6</sub>.



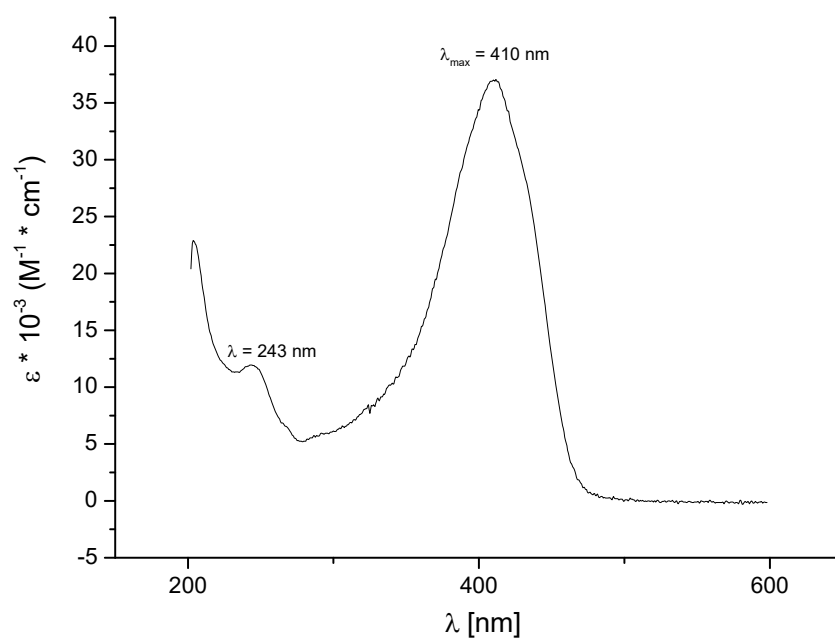
**Figure S15.** <sup>13</sup>C-NMR spectrum of **3b** in DMSO-d<sub>6</sub>.



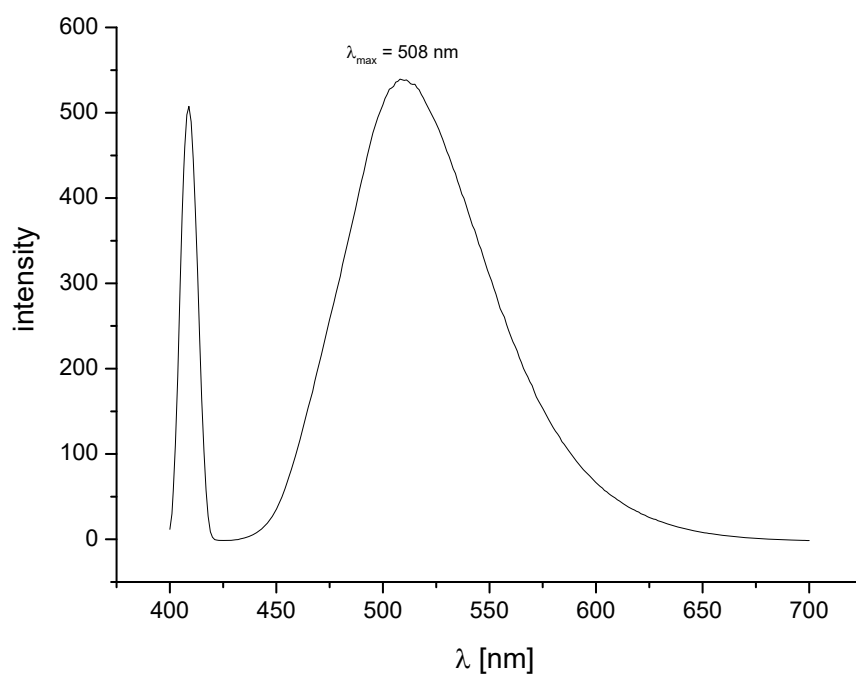
**Figure S16.** ESI-TOF-MS of **3b** in acetonitrile.



**Figure S17.** IR spectrum of **3b**.

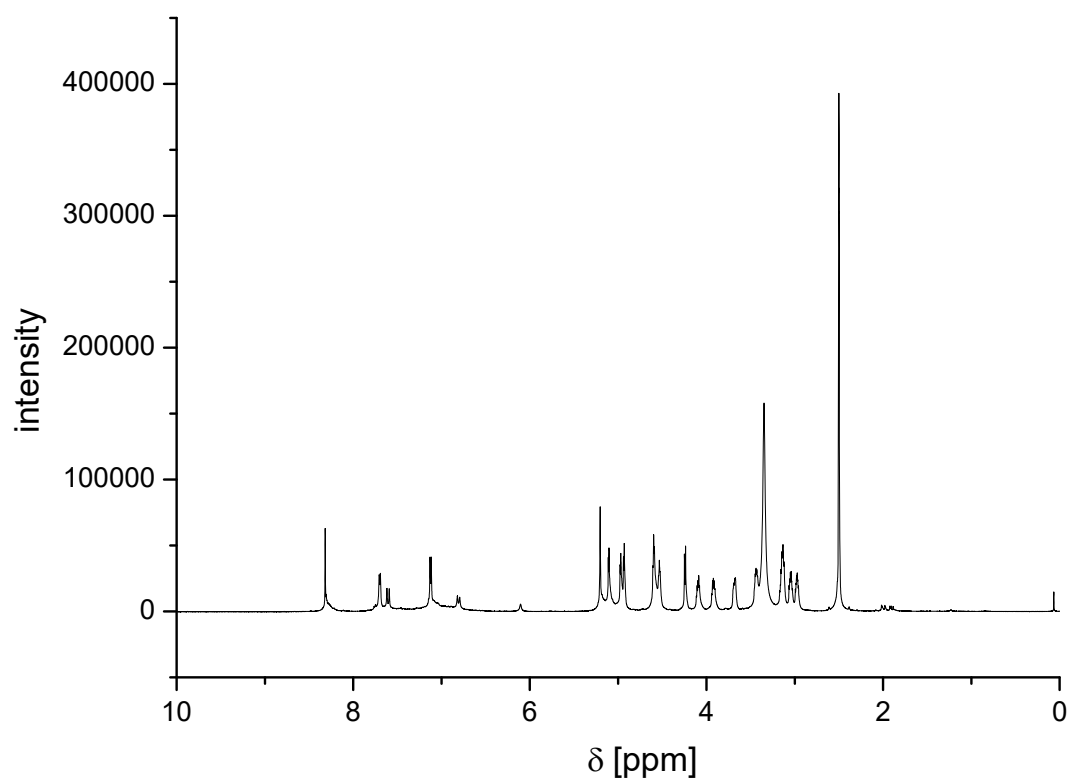
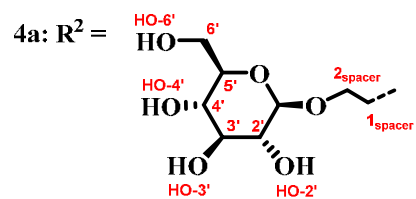
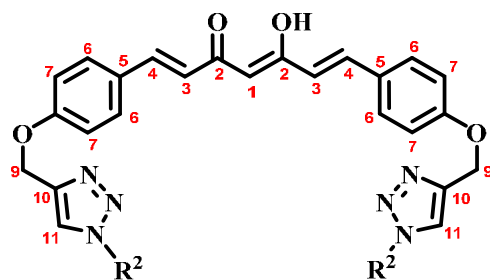


**Figure S18.** UV-Vis spectrum of **3b** ( $2 \times 10^{-5} \text{ M}$ , aerated  $\text{CH}_3\text{OH}$ ).

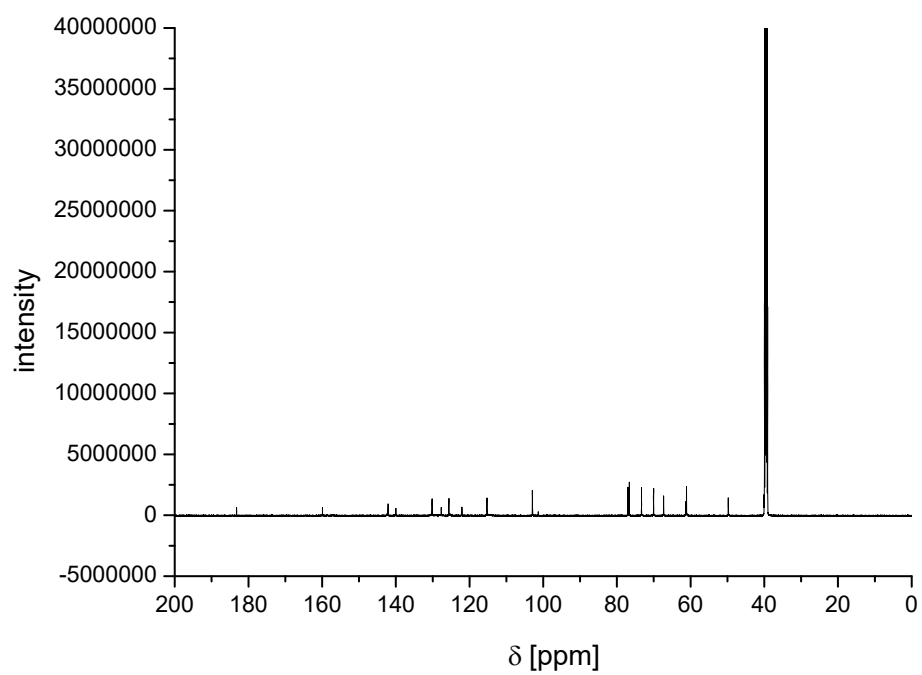


**Figure S19.** Emission spectrum of **3b** ( $\lambda_{\text{ex}} = 410 \text{ nm}$ ,  $2 \times 10^{-6} \text{ M}$ , aerated  $\text{CH}_3\text{OH}$ ).

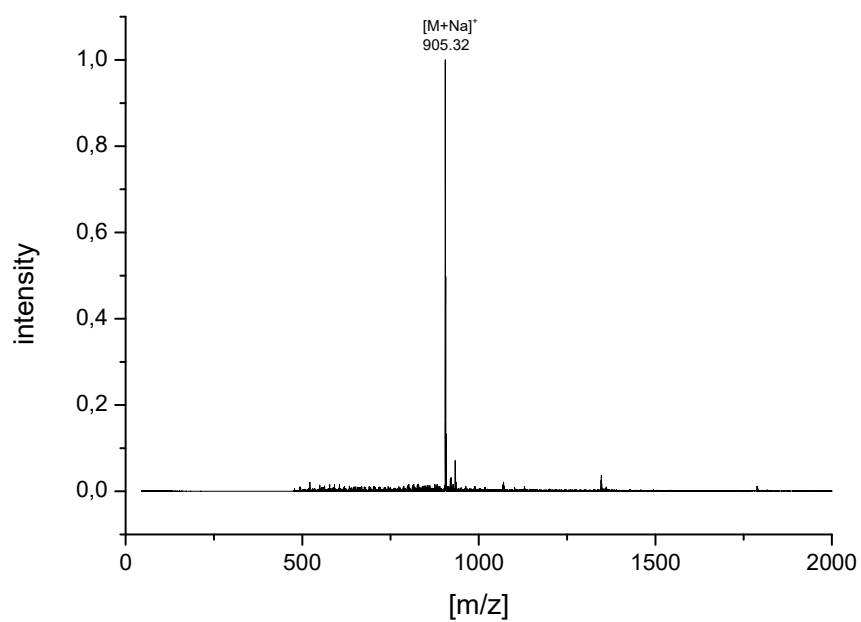




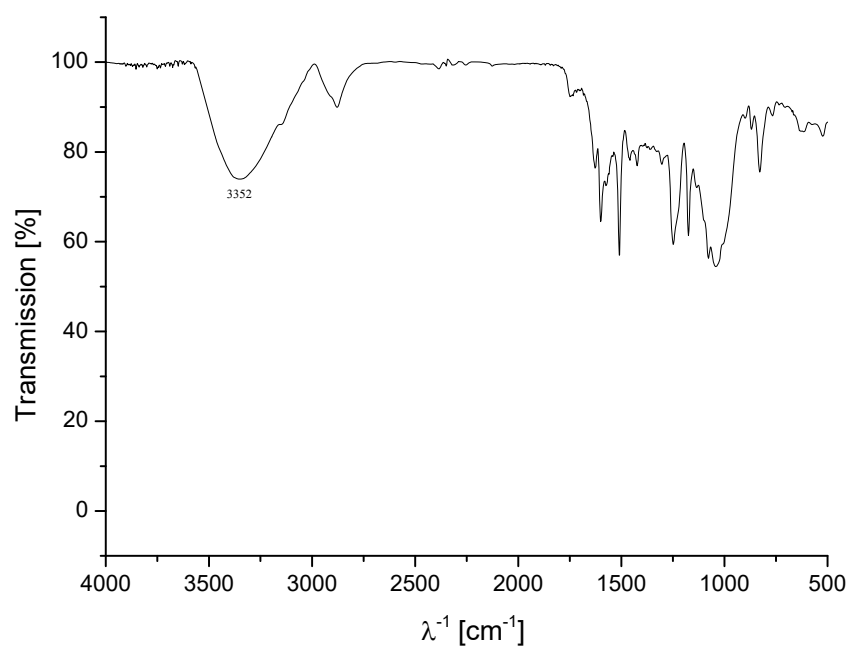
**Figure S20.** <sup>1</sup>H-NMR spectrum of **4a** in DMSO-d<sub>6</sub>.



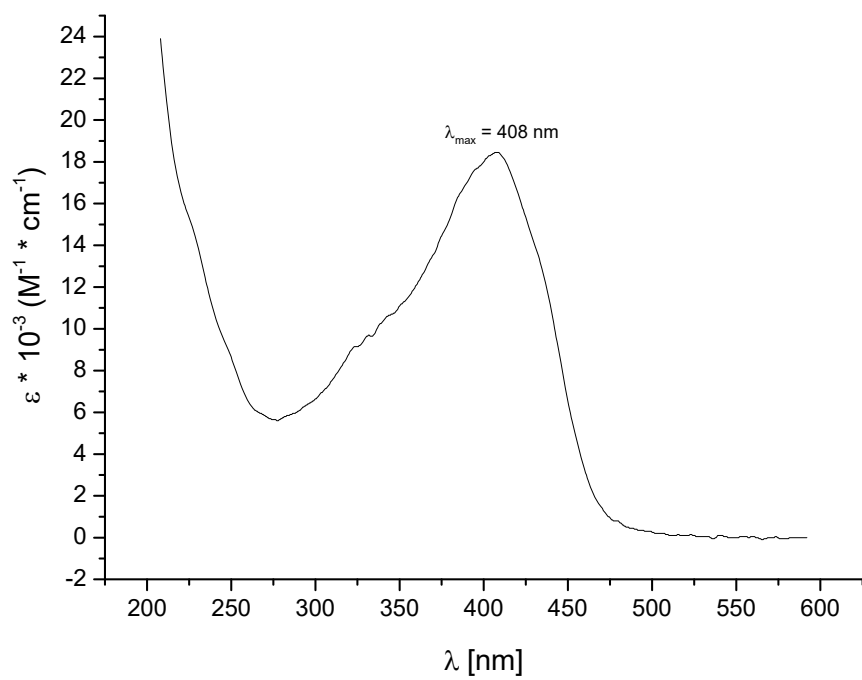
**Figure S21.**  $^{13}\text{C}$ -NMR spectrum of **4a** in  $\text{DMSO-d}_6$ .



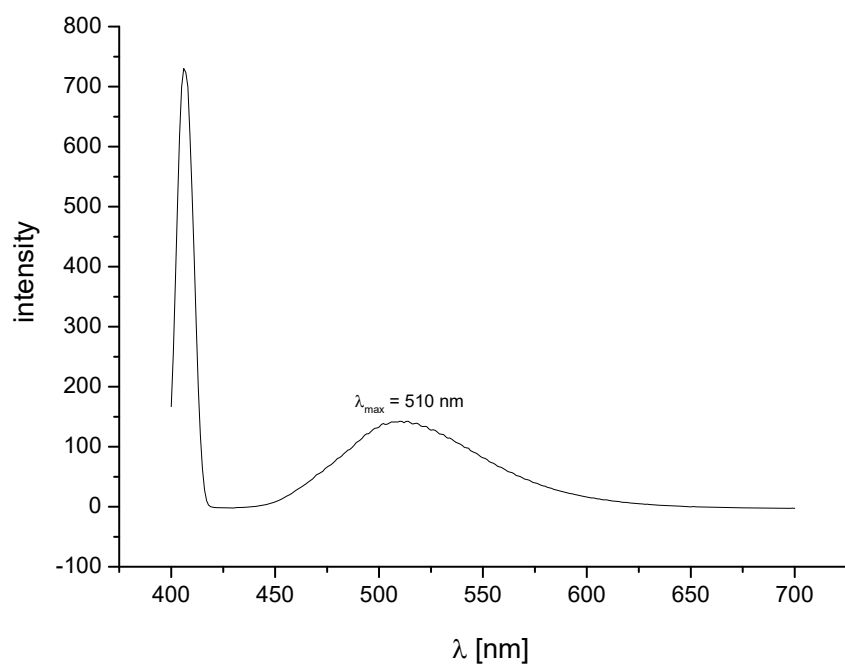
**Figure S22.** ESI-TOF-MS of **4a** in acetonitrile.



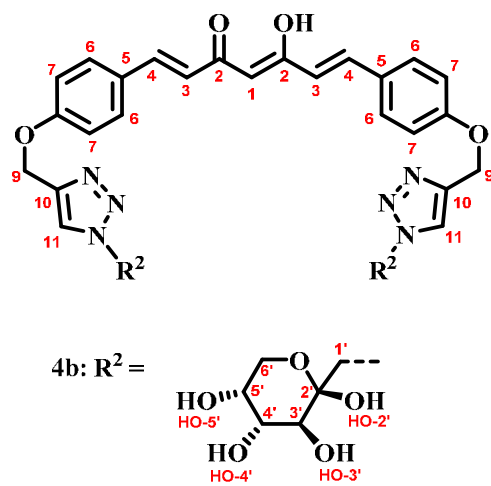
**Figure S23.** IR spectrum of **4a**.

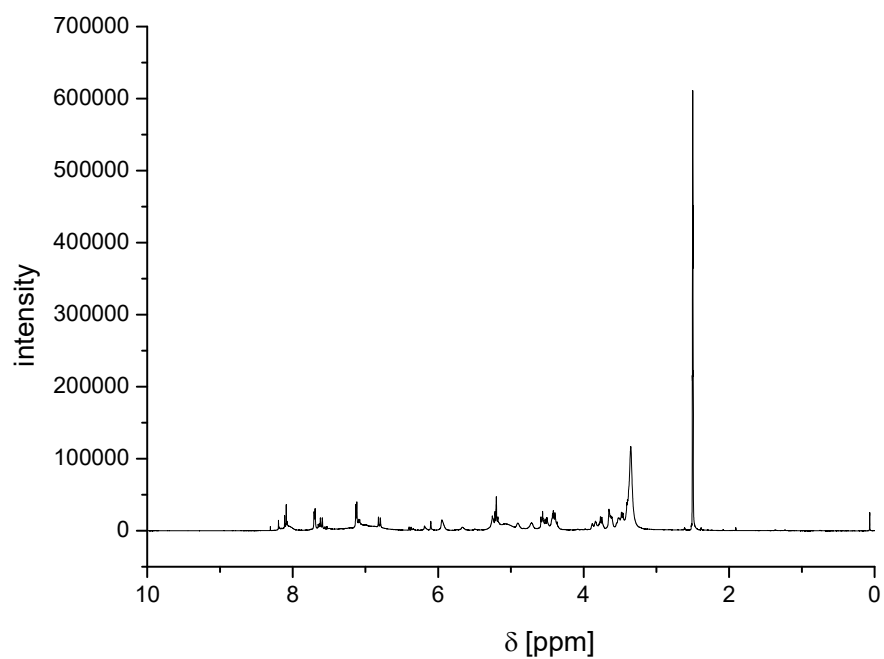


**Figure S24.** UV-Vis spectrum of **4a** ( $2 \times 10^{-5} \text{ M}$ , aerated  $\text{CH}_3\text{OH}$ ).

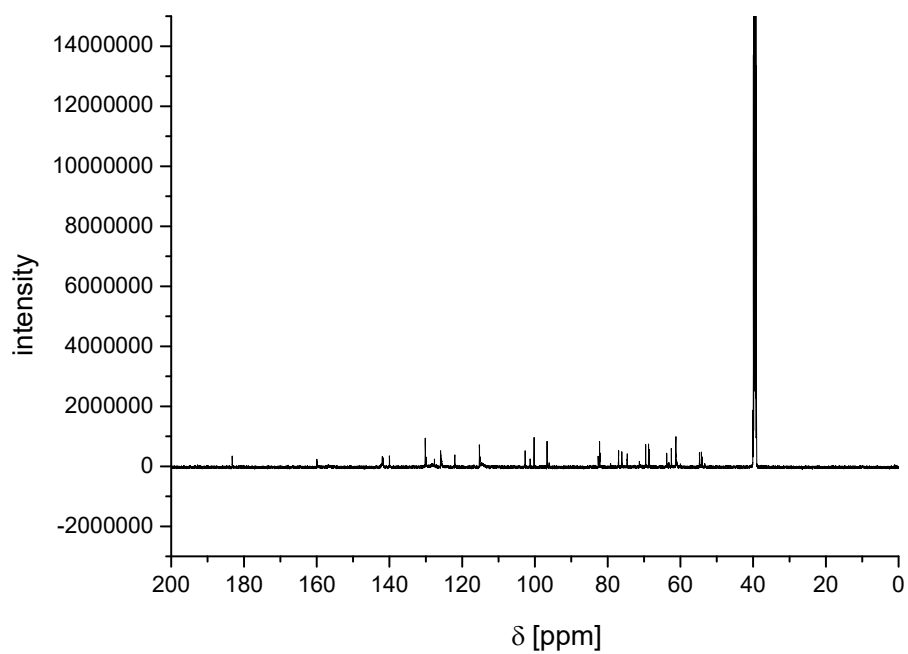


**Figure S25.** Emission spectrum of **4a** ( $\lambda_{\text{ex}} = 408 \text{ nm}$ ,  $2 \times 10^{-6} \text{ M}$ , aerated  $\text{CH}_3\text{OH}$ ).

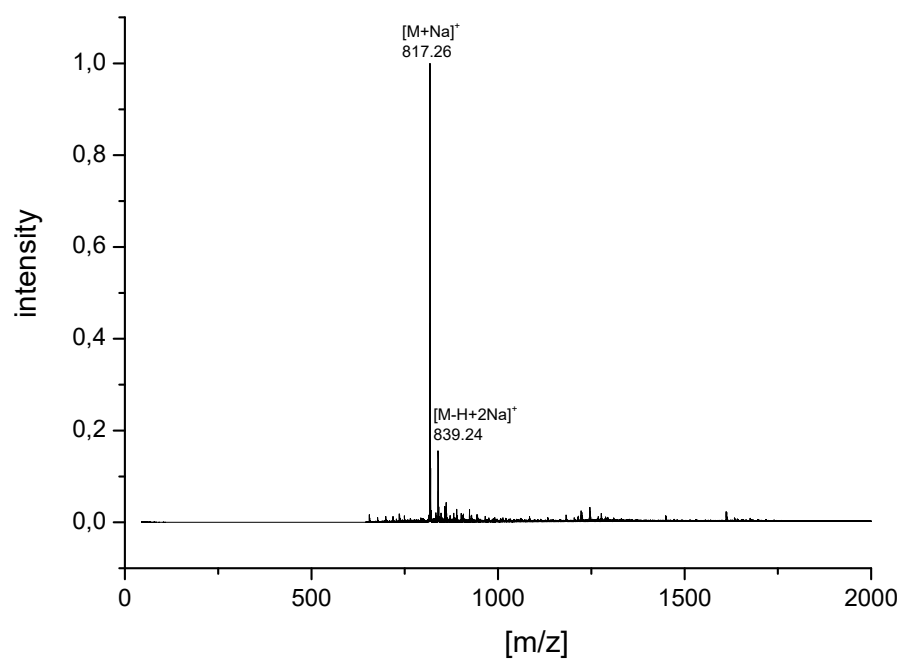




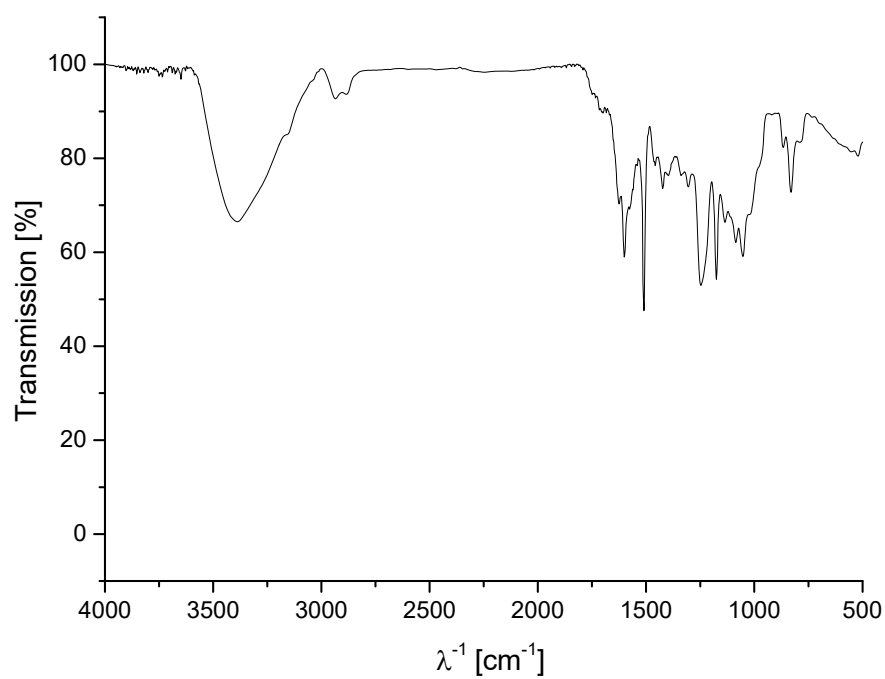
**Figure S26.**  $^1\text{H}$ -NMR spectrum of **4b** in  $\text{DMSO-d}_6$ .



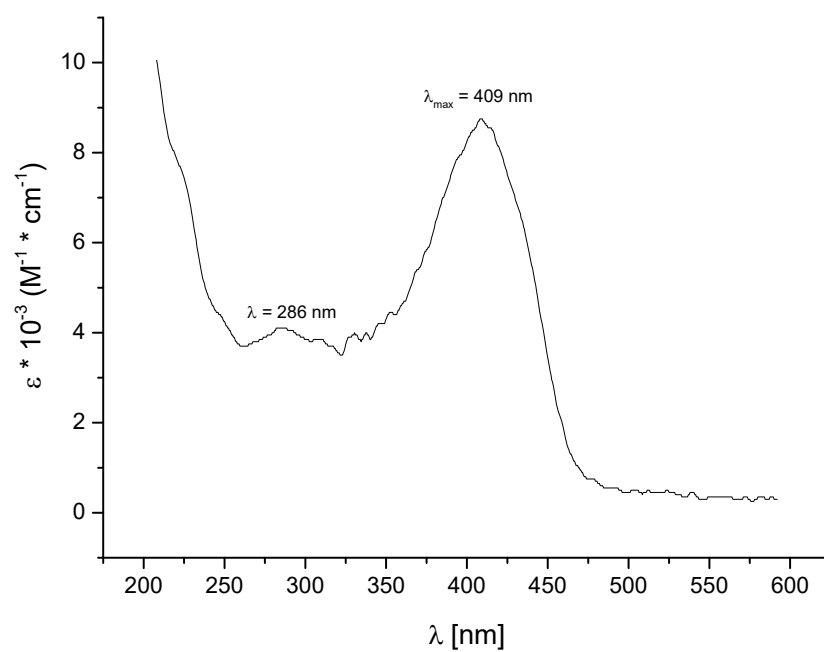
**Figure S27.**  $^{13}\text{C}$ -NMR spectrum of **4b** in  $\text{DMSO-d}_6$ .



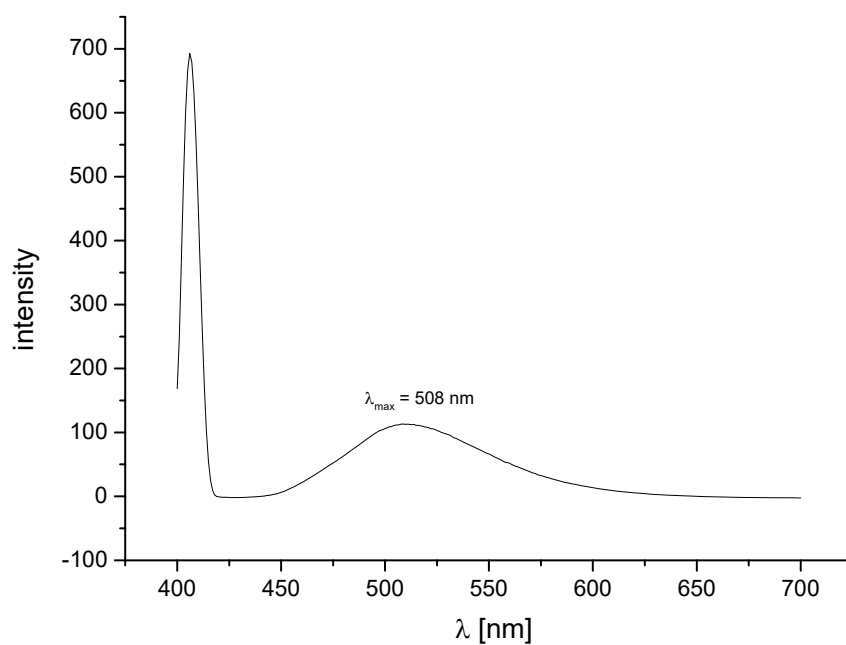
**Figure S28.** ESI-TOF-MS of **4b** in acetonitrile.



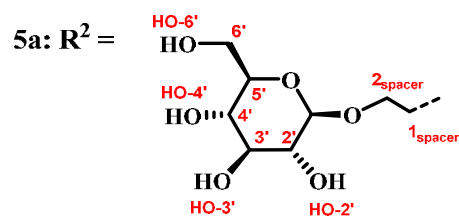
**Figure S29.** IR spectrum of **4b**.



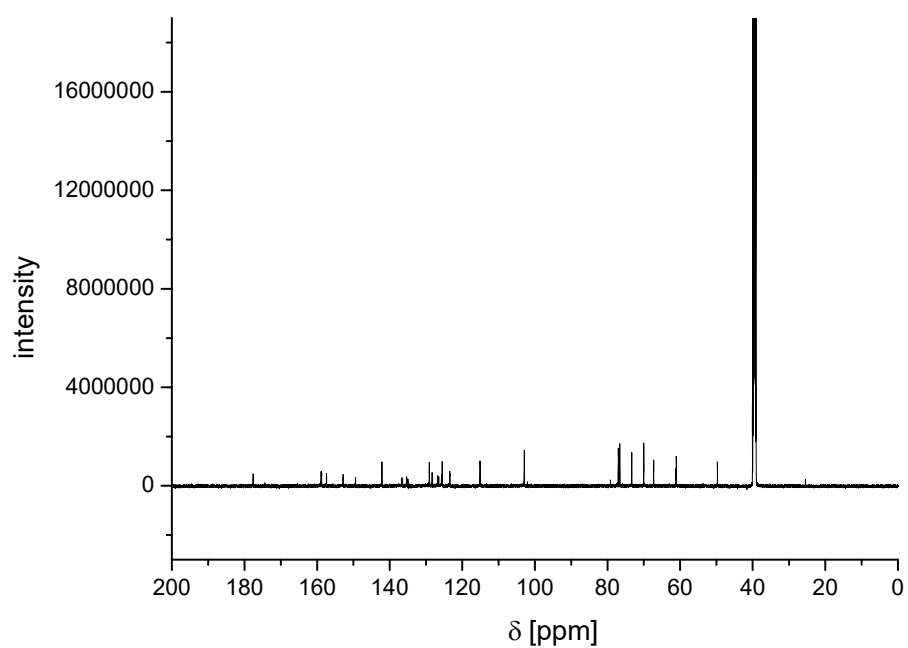
**Figure S30.** UV-Vis spectrum of **4b** ( $2 \times 10^{-5} \text{ M}$ , aerated  $\text{CH}_3\text{OH}$ ).



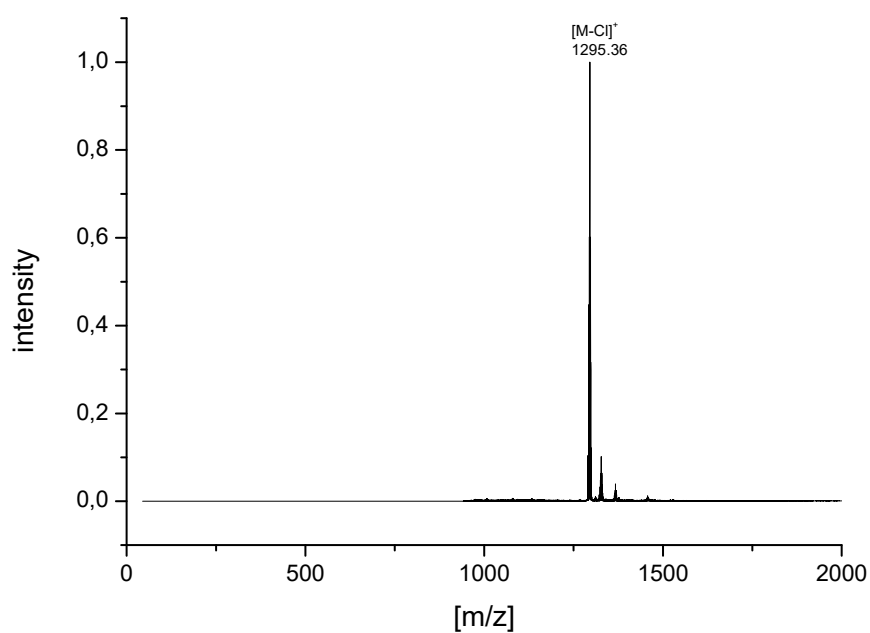
**Figure S31.** Emission spectrum of **4b** ( $\lambda_{\text{ex}} = 408 \text{ nm}$ ,  $2 \times 10^{-6} \text{ M}$ , aerated  $\text{CH}_3\text{OH}$ ).



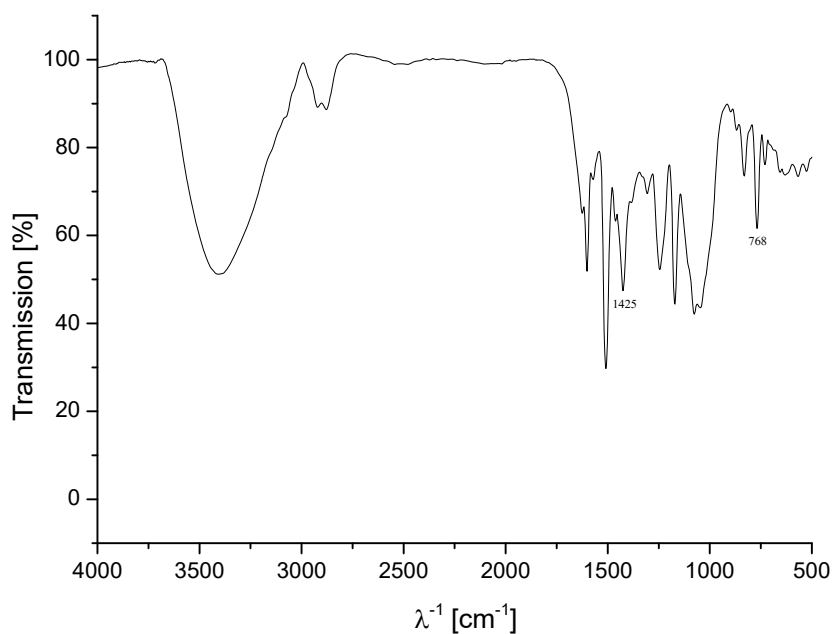




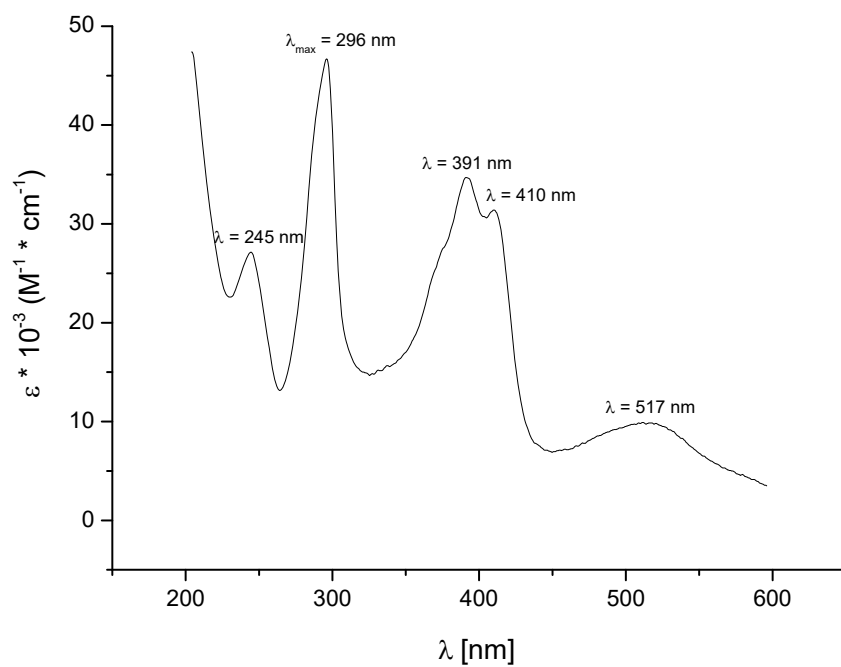
**Figure S33.**  $^{13}\text{C}$ -NMR spectrum of **5a** in  $\text{DMSO-d}_6$ .



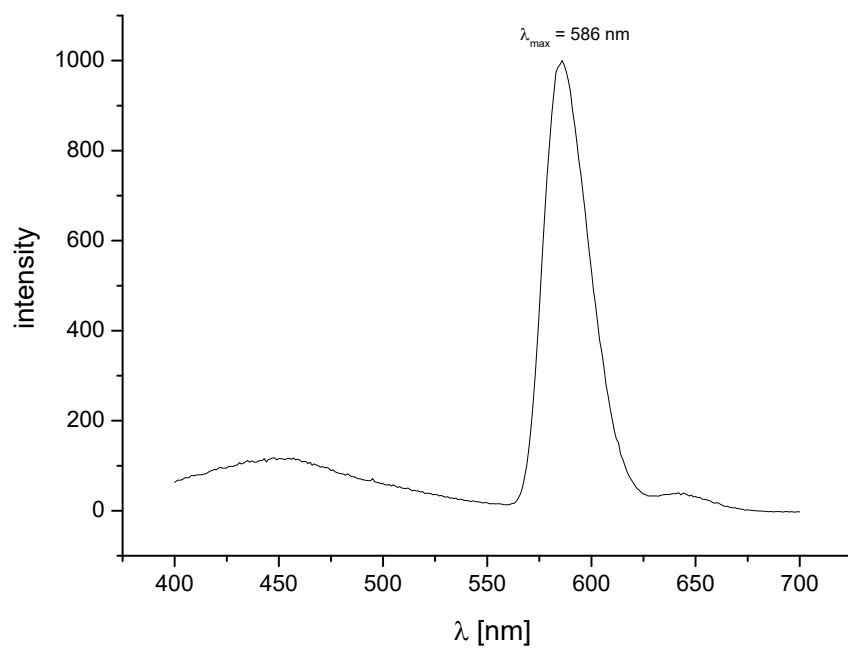
**Figure S34.** ESI-TOF-MS of **5a** in acetonitrile.



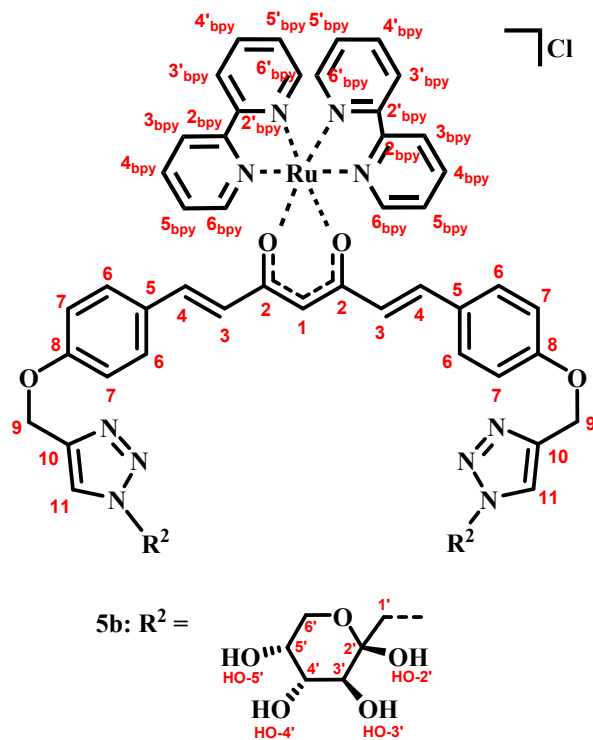
**Figure S35.** IR spectrum of **5a**.

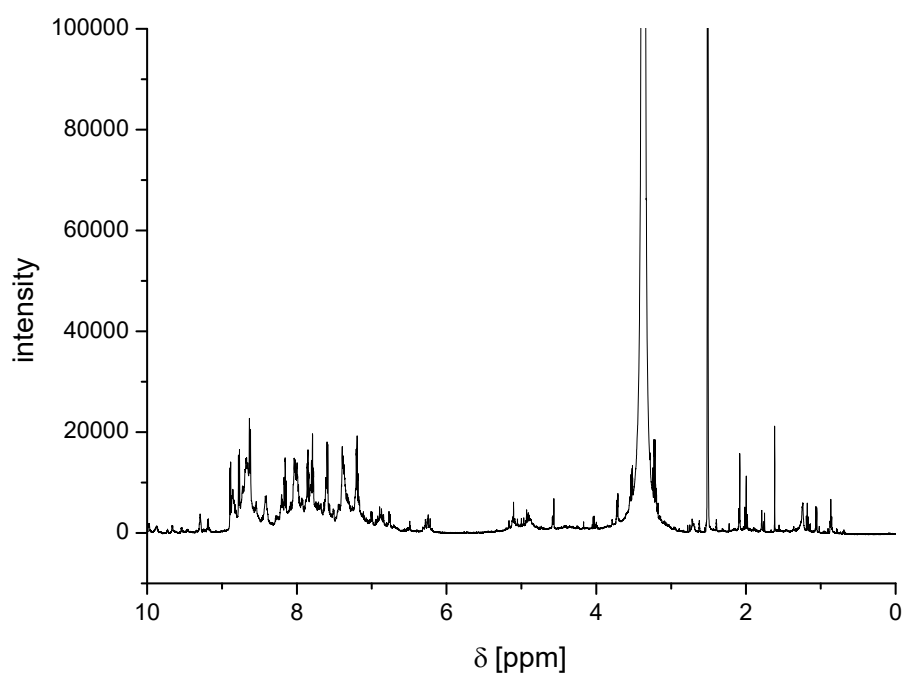


**Figure S36.** UV-Vis spectrum of **5a** ( $2 \times 10^{-5} \text{ M}$ , aerated  $\text{CH}_3\text{OH}$ ).

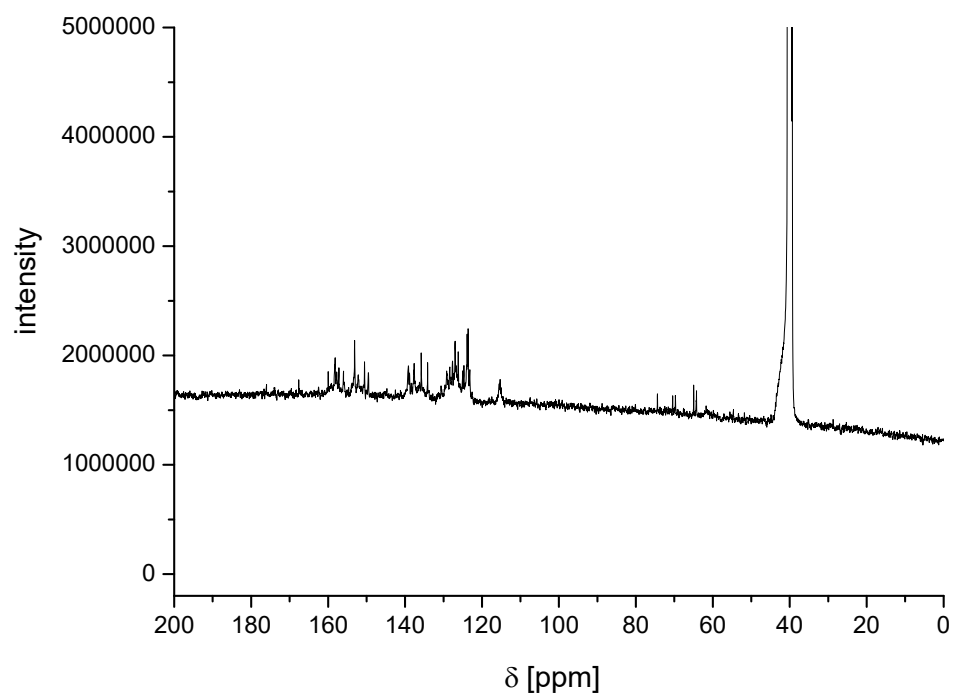


**Figure S37.** Emission spectrum of **5a** ( $\lambda_{\text{ex}} = 296 \text{ nm}$ ,  $2 \times 10^{-6} \text{ M}$ , aerated  $\text{CH}_3\text{OH}$ ).

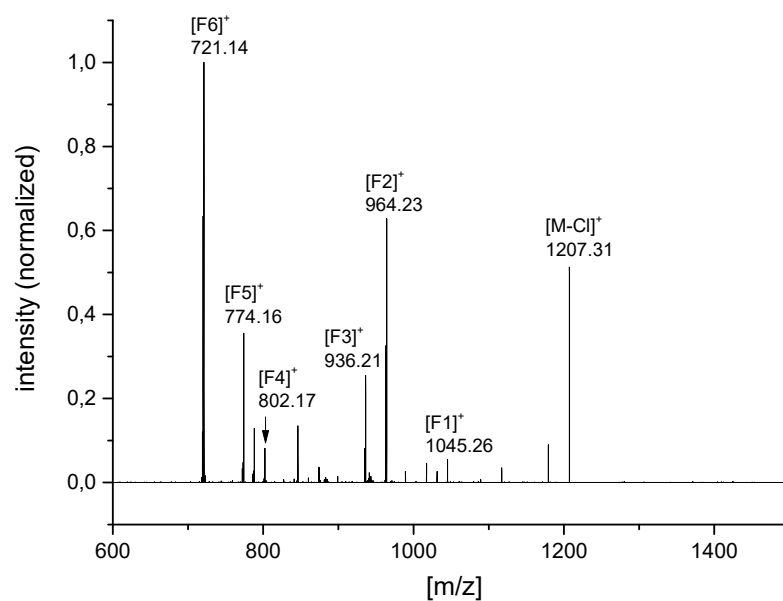




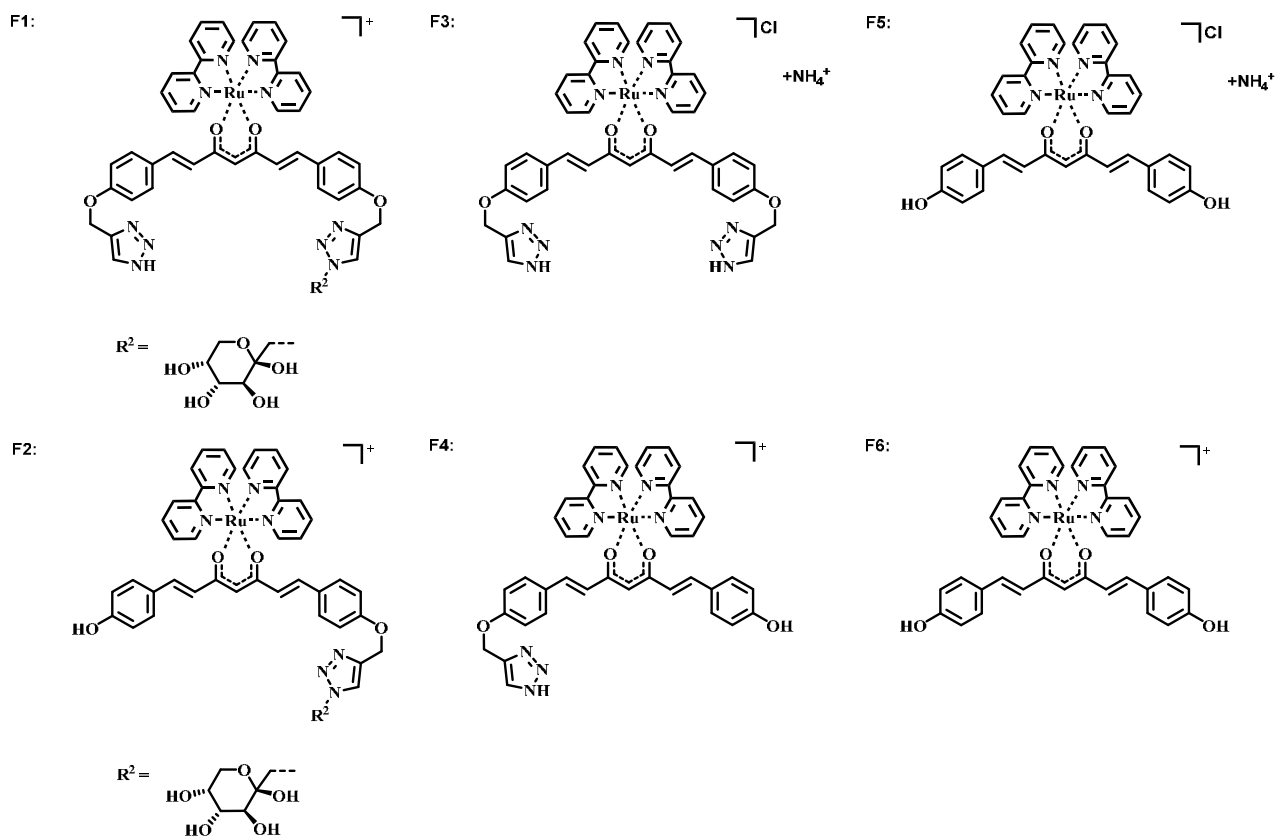
**Figure S38.**  $^1\text{H}$ -NMR spectrum of **5b** in  $\text{DMSO-d}_6$ .



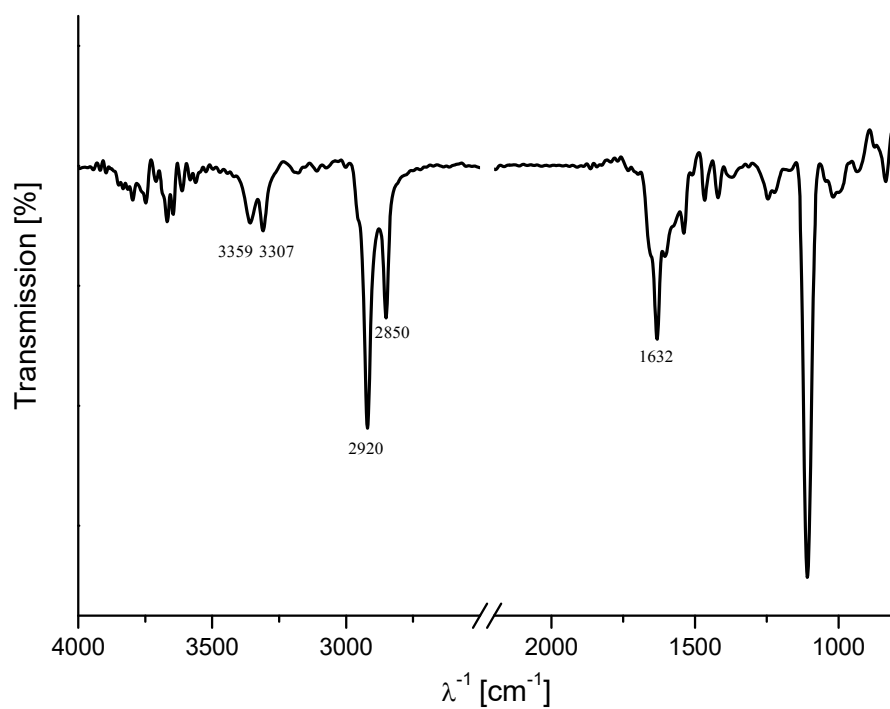
**Figure S39.**  $^{13}\text{C}$ -NMR spectrum of **5b** in  $\text{DMSO-d}_6$ .



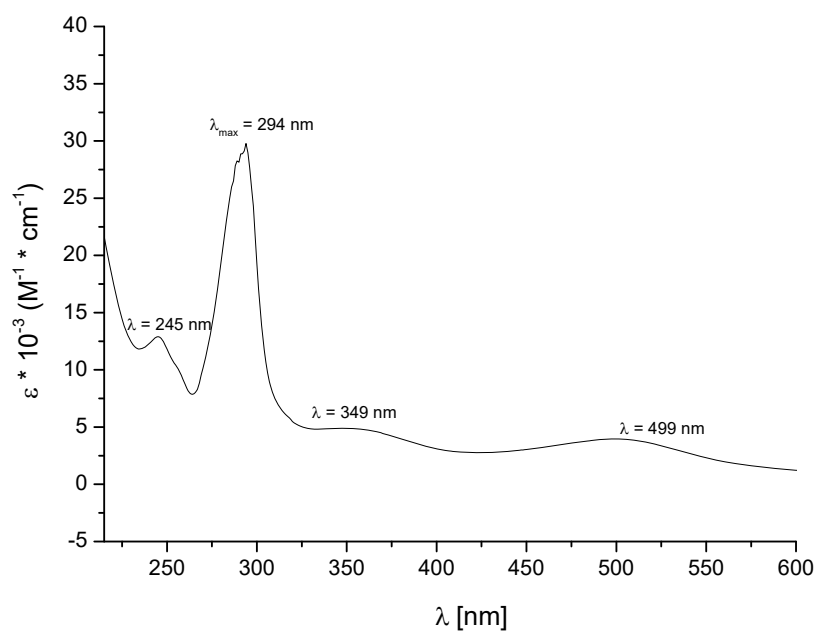
**Figure S40.** ESI-Orbitrap-MS of **5b** with various fragments **F1-F6**.



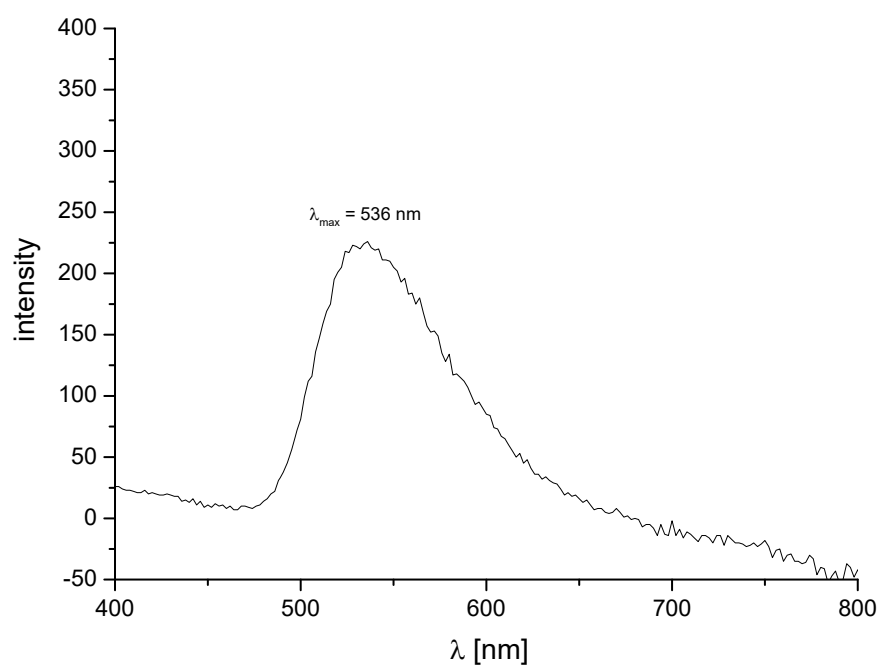
**Figure S41.** Schematic representation of fragments **F1-F6** resulting from the parent ion of **5b**.



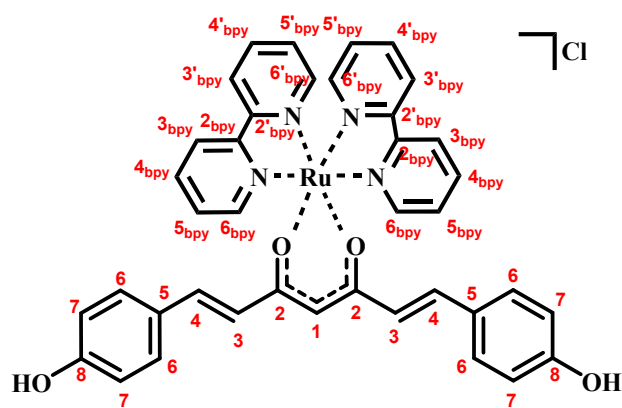
**Figure S42.** IR spectrum of **5b**.



**Figure S43.** UV-Vis spectrum of **5b** ( $1 \times 10^{-4} \text{ M}$ , aerated  $\text{CH}_3\text{OH}$ ).



**Figure S44.** Emission spectrum of **5b** ( $\lambda_{\text{ex}} = 296 \text{ nm}$ ,  $10^{-6} \text{ M}$ , aerated  $\text{CH}_3\text{OH}$ ).



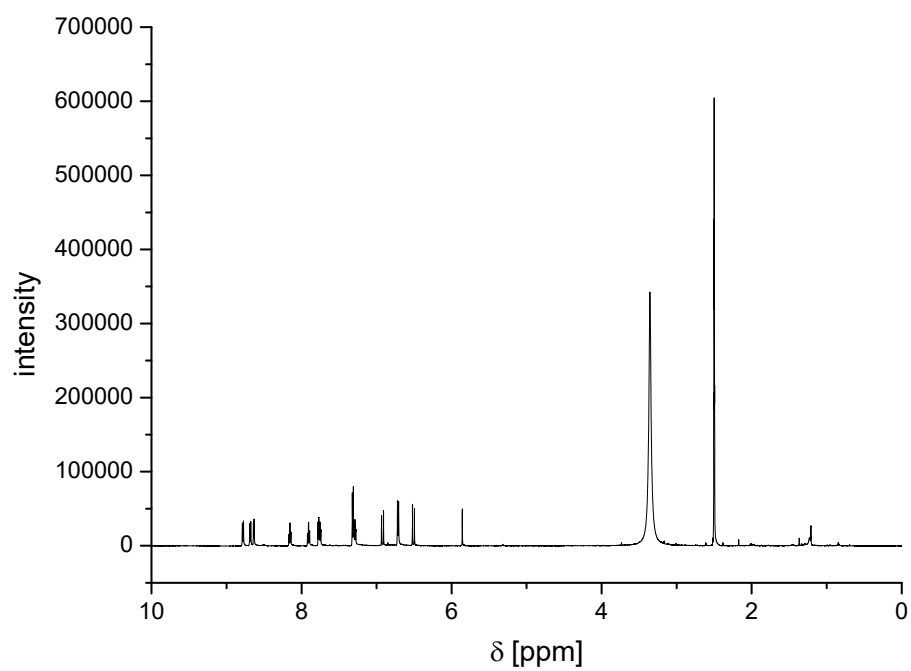


**Figure S45.**  $^1\text{H}$ -NMR spectrum of **5c** in  $\text{DMSO-d}_6$ .

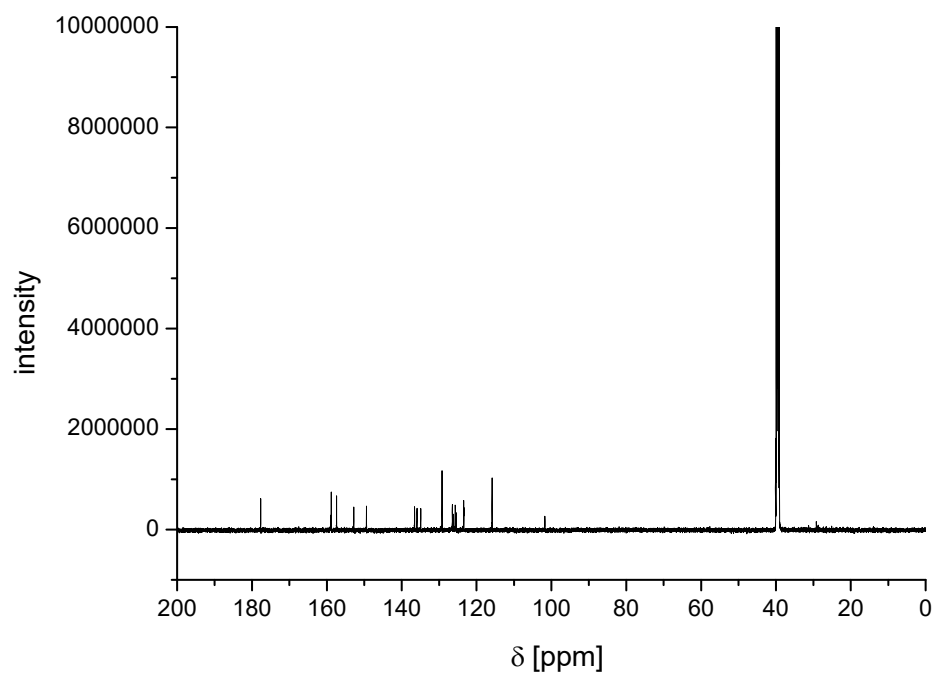


**Figure S46.**  $^{13}\text{C}$ -NMR spectrum of **5c** in  $\text{DMSO-d}_6$ .



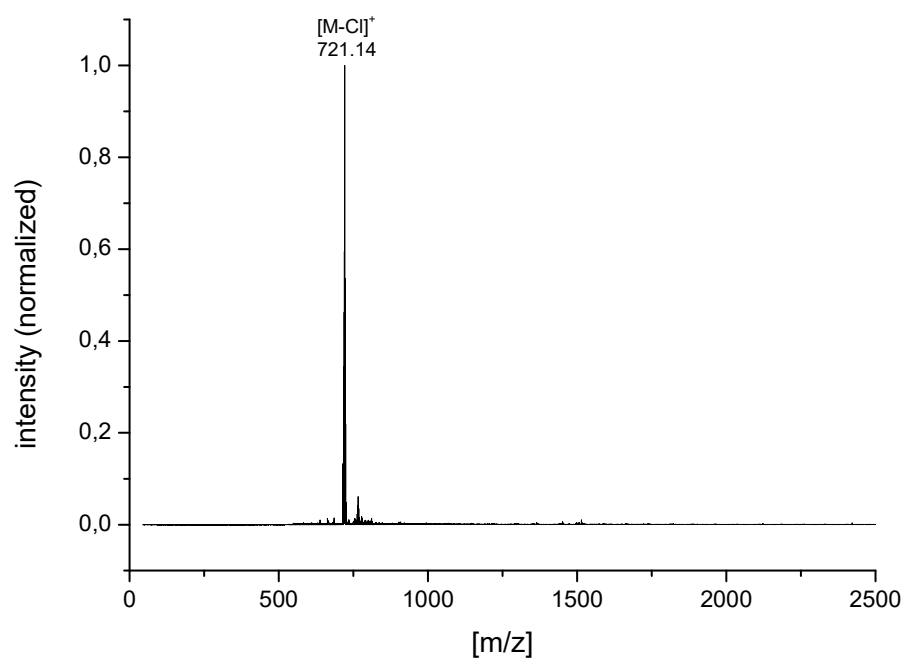


**Figure S47.** ESI-TOF-MS of **5c** in acetonitrile.

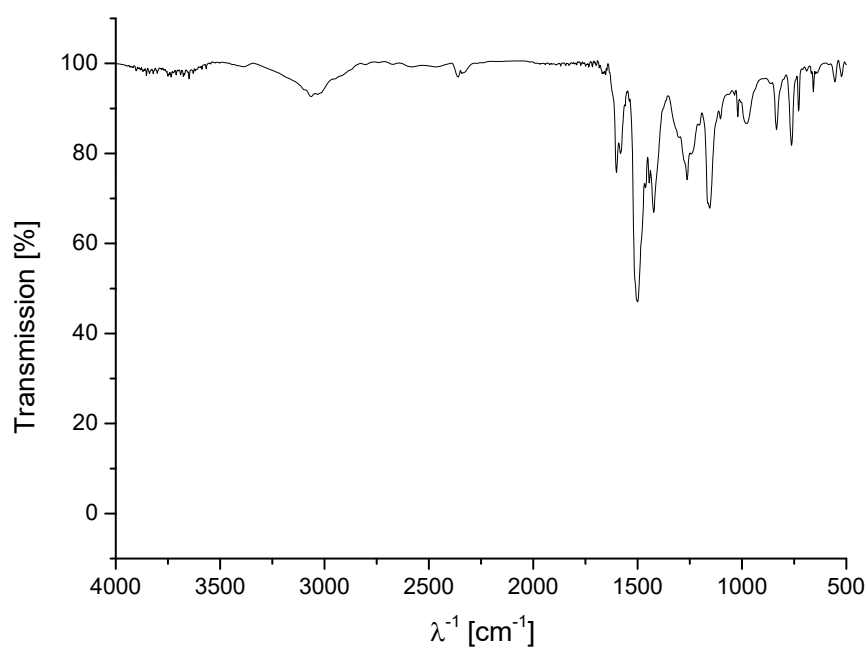


**Figure S48.** IR spectrum of **5c**.

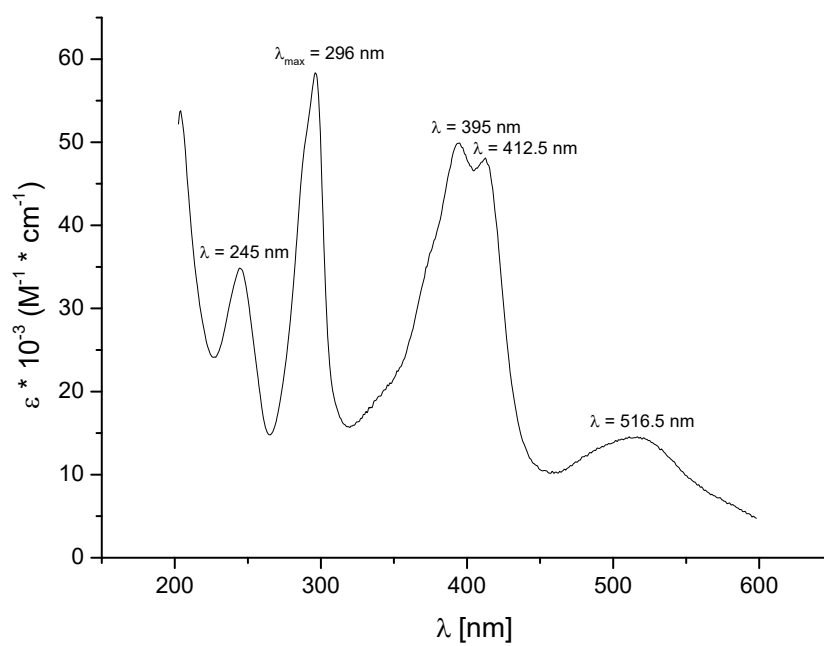


**Figure S49.** UV-Vis spectrum of **5c** ( $2 \times 10^{-5} \text{ M}$ , aerated  $\text{CH}_3\text{OH}$ ).

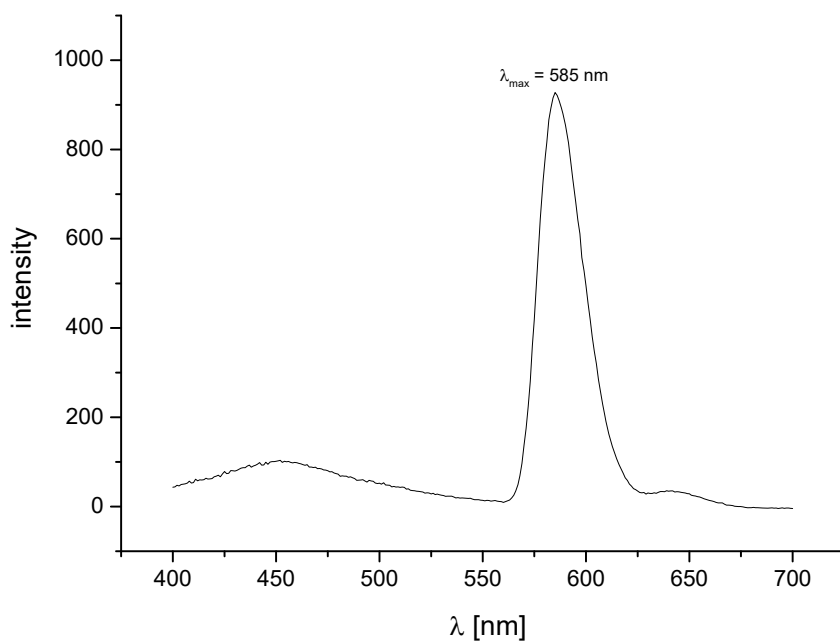


**Figure S50.** Emission spectrum of **5c** ( $\lambda_{\text{ex}} = 296 \text{ nm}$ ,  $10^{-6} \text{ M}$ , aerated  $\text{CH}_3\text{OH}$ ).

### Determination of cytotoxicity

To determine the cytotoxic potential of the corresponding complexes on different cell types, the inhibitory effect on the cellular metabolic activity was investigated *via* a resazurin based assay (alamarBlue, Thermo Fisher). For this purpose, the non-cancer cell line L929, the liver cancer cell line HepG2 as well as the breast cancer cell line MDA-MB-231 were used.

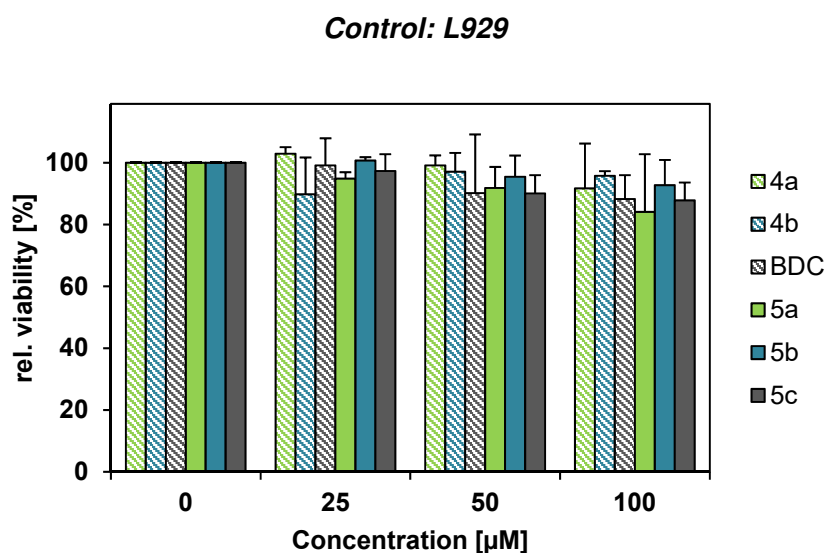


**Figure S51.** Relative viability of L929 cells (mouse fibroblasts) after 24 h incubation with the complexes at indicated concentrations. Values represent the mean  $\pm$  S.D. (n=3).

**Liver cancer: HepG2**

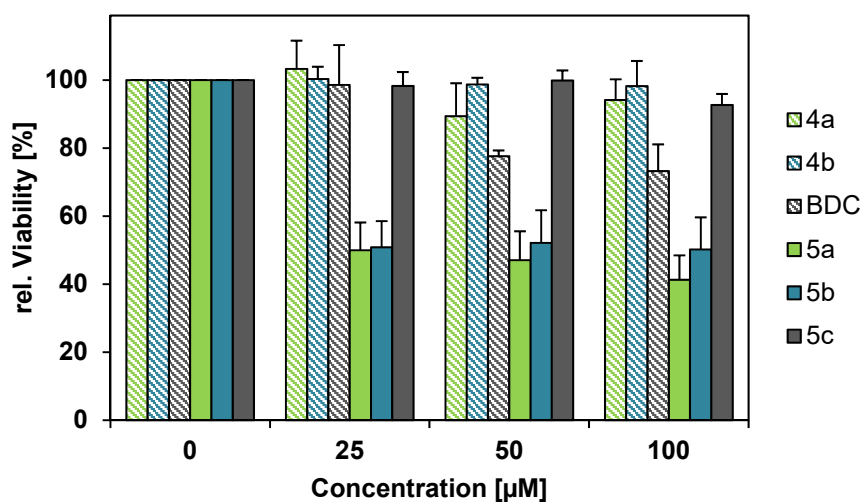


**Figure S52.** Relative viability of HepG2 cells after 24 h incubation with the complexes at indicated concentrations. Values represent the mean  $\pm$  S.D. (n=3).

**Breast cancer: MDA-MB-231**

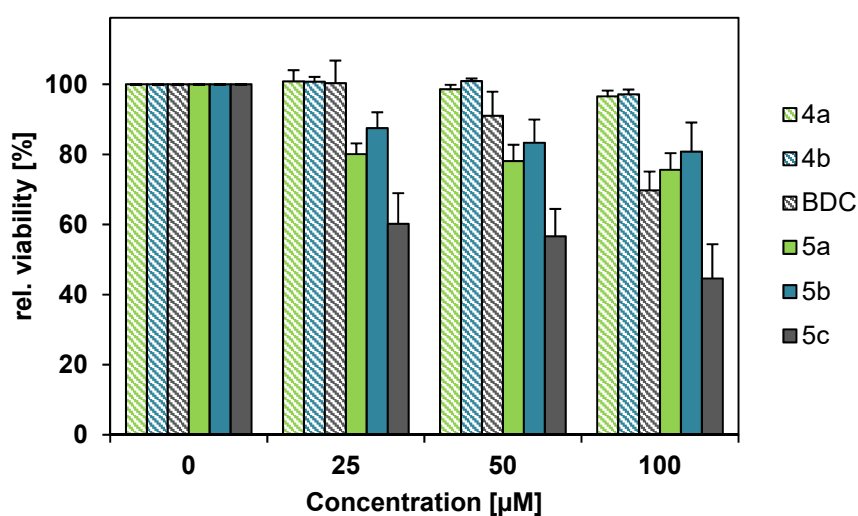


**Figure S53.** Relative viability of MDA-MB-231 after 24 h incubation with the complexes at indicated concentrations. Values represent the mean  $\pm$  S.D. (n=3).

**Table S1.** Absorption spectra, absorption coefficients and emission spectra of all compounds

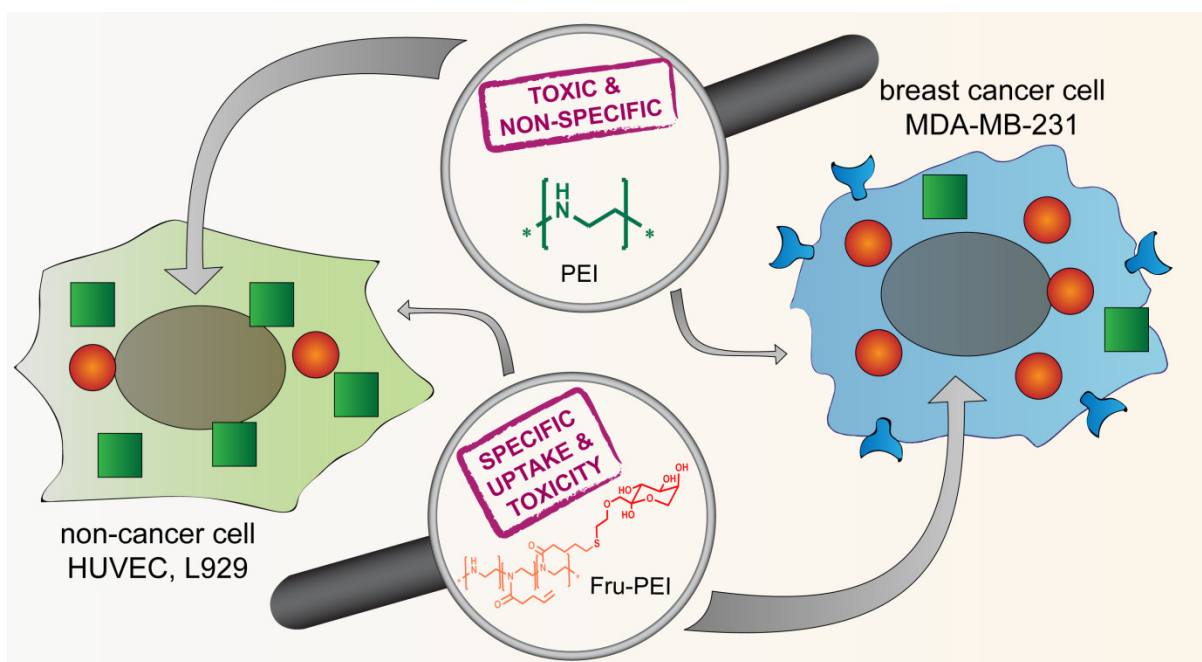
Abrev	Absorption wavelength $\lambda$ / nm	Absorption coefficient $\varepsilon \times 10^{-3} / \text{M}^{-1} \text{cm}^{-1}$	Emission wavelength $\lambda$ / nm (irradiation wavelength $\lambda_{\text{ex}}$ / nm)
<b>1</b>	477; 458; 254	50.55; 48.10; 11.80	541 (477)
<b>3a</b>	410; 243	39.25; 13.55	509 (410)
<b>3b</b>	410; 243	37.00; 11.95	508 (410)
<b>4a</b>	408; 243	18.45; 13.55	509 (408)
<b>4b</b>	409; 286	8.75; 4.10	510 (408)
<b>5a</b>	517; 410; 391; 296; 245	9.85; 31.40; 34.70; 46.70; 27.10	586 (296)
<b>5b</b>	499; 349; 294; 245	3.96; 4.89; 29.78; 12.89	536 (296)
<b>5c</b>	516.5; 412.5 395; 296; 245	14.55; 48.10; 49.90; 58.35; 34.80	585 (296)

### Publication 3

## D-Fructose-decorated poly(ethylene imine) for human breast cancer cell targeting

C. Englert, M. Pröhl, J. A. Czaplewska, C. Fritzsche, E. Preußger, U. S. Schubert,  
A. Traeger, M. Gottschaldt

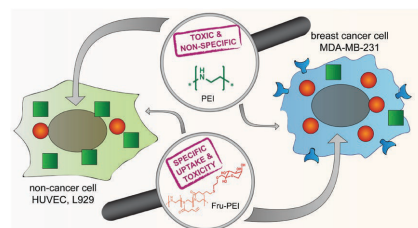
*Macromol. Biosci.* **2017**, *17*, 1600502



# D-Fructose-Decorated Poly(ethylene imine) for Human Breast Cancer Cell Targeting

Christoph Englert, Michael Pröhl, Justyna A. Czaplewska, Carolin Fritzsche, Elisabeth Preußger, Ulrich S. Schubert, Anja Traeger, Michael Gottschaldt\*

The high affinity of GLUT5 transporter for D-fructose in breast cancer cells has been discussed intensely. In this contribution, high molar mass linear poly(ethylene imine) (LPEI) is functionalized with D-fructose moieties to combine the selectivity for the GLUT5 transporter with the delivery potential of PEI for genetic material. The four-step synthesis of a thiol-group bearing D-fructose enables the decoration of a cationic polymer backbone with D-fructose via thiol-ene photoaddition. The functionalization of LPEI is confirmed by 2D NMR techniques, elemental analysis, and size exclusion chromatography. Importantly, a D-fructose decoration of 16% renders the polymers water-soluble and eliminates the cytotoxicity of PEI in noncancer L929 cells, accompanied by a reduced unspecific cellular uptake of the genetic material. In contrast, the cytotoxicity as well as the cell specific uptake is increased for triple negative MDA-MB-231 breast cancer cells. Therefore, the introduction of D-fructose shows superior potential for cell targeting, which can be assumed to be GLUT5 dependent.



## 1. Introduction

With around 1.65 million new cases of cancer and around 590 thousand deaths resulted from cancer in 2015 in the United States, human breast cancer represents the second leading death cause after heart diseases. Among them, 230 thousand new cases derive from breast cancer from which around 41 thousand ended deadly.<sup>[1]</sup> It is described as a highly heterogeneous type of cancer with manifold

grades and types.<sup>[2]</sup> The number of specific targets is high, in which 60%–80% of all cases are hormone receptors of the human epidermal growth factor receptor (HER) family that can be targeted by endocrine therapy.<sup>[3]</sup> By lacking progesterone and estrogen receptor overexpression as well as amplification of HER2 genes at the same time, a tumor type with a shorter median time from relapse to death was identified in 1987 and is nowadays treated with Trastuzumab, a monoclonal antibody.<sup>[4]</sup> Triple-negative tumors are described by the lack of hormone receptor expression as well as HER2 receptors, an aggressive type with insufficient therapy options and poor prognosis, which represents roughly 15% of all breast cancer tumors.<sup>[3]</sup> Besides the treatment with the monoclonal antibody Bevacizumab, that blocks angiogenesis by inhibiting vascular endothelial growth factor A, there are more than 50 clinical trials ongoing, which address various targets such as the epidermal growth factor,<sup>[5]</sup> Src tyrosine kinase,<sup>[6]</sup> and heat shock protein 90 to develop strategies against this aggressive kind of breast cancer.<sup>[7]</sup>

Another target, which is controversially discussed in the present literature, is the GLUT5 transporter, a highly affine D-fructose transporter.<sup>[8]</sup> While Gowrishankar

C. Englert, M. Pröhl, Dr. J. A. Czaplewska, C. Fritzsche, E. Preußger, Prof. U. S. Schubert, Dr. A. Traeger, Dr. M. Gottschaldt  
Laboratory of Organic and Macromolecular Chemistry (IOMC)  
Friedrich Schiller University Jena  
Humboldtstrasse 10, 07743 Jena, Germany  
E-mail: michael.gottschaldt@uni-jena.de  
C. Englert, M. Pröhl, Dr. J. A. Czaplewska, C. Fritzsche, E. Preußger, Prof. U. S. Schubert, Dr. A. Traeger, Dr. M. Gottschaldt  
Jena Center for Soft Matter (JCSM)  
Friedrich Schiller University Jena  
Philosophenweg 7, 07743 Jena, Germany

et al. declined the overexpression of GLUT5 in all breast cancer tissues,<sup>[9]</sup> Nualart and co-workers claimed GLUT5 as overexpressed in 85% of 33 tested breast cancer cell lines,<sup>[10]</sup> also confirmed for estrogen-receptor positive MCF-7 and triple-negative MDA-MB-231 breast cancer cell lines.<sup>[11]</sup> Nevertheless, that implies a possible enhanced selectivity of anticancer agents by the attachment of D-fructose and its derivatives. Previous studies revealed that modifications at C1- and C6-position of the sugar are tolerated by the GLUT5 transporter.<sup>[12]</sup> For this reason, D-fructose was successfully attached to dyes,<sup>[13]</sup> metal complexes,<sup>[14]</sup> polymers,<sup>[15]</sup> and nanoparticles<sup>[16]</sup> and tested with various breast cancer cell lines, revealing an increased uptake for the D-fructose conjugated compounds and structures.

Nowadays, one opportunity of cancer treatment is the manipulation of the pathways in tumors on the level of the cellular genetic information, e.g., by the introduction of genetic material. This promising anticancer approach has gained increasing interest over the last decade and various potential carriers have been investigated.<sup>[15]</sup> Since viral vectors possess considerable cytotoxicities and immunological concerns, nonviral vectors like cationic cell penetrating peptides,<sup>[17]</sup> antibodies<sup>[18]</sup> and lipid-based carriers<sup>[19]</sup> have been intensively investigated. Cationic polymers, e.g., poly(ethylene imine) (PEI), represent another class of suitable candidates to complex genetic material by electrostatic interactions.<sup>[20]</sup> Due to its superior buffering ability leading to endosomal escape ("proton sponge effect"), PEI is known as the gold standard of polymeric carriers for gene delivery.<sup>[21]</sup> However, its full potential is restricted through its high cytotoxicity and non-biodegradability.<sup>[22]</sup> One useful strategy to overcome these limitations is the modification of the PEI backbone<sup>[23]</sup> and/or the introduction of side chains. The latter approach has been extensively studied, e.g., by functionalization of PEI with various carbohydrates<sup>[24]</sup> or stealth polymers, like poly(ethylene glycol).<sup>[25]</sup>

Herein, we focused on the installation of D-fructose moieties at side chains of high molar mass linear PEI to combine the selectivity for the GLUT5 transporter and the delivery potential of genetic material. To remain a defined quantity of cationic ethylene imine units, a post-polymerization functionalization using *N*-succinimidyl-4-pentenatate was chosen. This enables the synthesis of glycopolymer structures<sup>[26]</sup> by the reaction with thiol sugars utilizing the metal-free thiol-ene photoaddition. The designed copolymer and respective precursors were investigated concerning their bio- and hemocompatibility, their affinity for binding and release of genetic material (exemplified for plasmid DNA) and their specific cellular uptake (MDA-MB231 breast cancer vs. noncancer L929 and primary human umbilical vein endothelial cells, HUVEC).

## 2. Experimental Section

### 2.1. Materials

2-Ethyl-2-oxazoline (EtOx) and methyl tosylate were obtained from Acros Organics, distilled (over barium oxide (BaO) in the case of EtOx), and stored under argon atmosphere. Pyridine, methanol, dichloromethane, 4-*N,N*-dimethylamino-pyridine (DMAP), 2,2-dimethoxy-2-phenylacetophenone (DMPA) and rhodamine B isothiocyanate were obtained from Sigma-Aldrich (Steinhausen, Germany) and are of analytical grade and are used without further purification. Acetonitrile was purified on a MBraun solvent purification system (MB SPS-800). *N*-Succinimidyl-4-pentenatate was prepared according to literature procedures.<sup>[27]</sup> Ethidium bromide solution (1%, 10 mg mL<sup>-1</sup>) was purchased from Carl Roth (Karlsruhe, Germany). AlamarBlue, YOYO-1 iodide, Hoechst 33342 trihydrochloride, heparin and Cy5 dye were obtained from Thermo Fisher (Germany). Plasmid pEGFP-N1 (4.7 kb, Clontech, USA encoding green fluorescent protein (EGFP) was isolated with the Giga Plasmid Kit provided by Qiagen (Hilden, Germany). If not stated otherwise, cell culture materials, cell culture media and solutions were obtained from Biochrom (Berlin, Germany).

### 2.2. General Methods and Instrumentation

The polymerizations as well as the hydrolysis of poly(2-ethyl-2-oxazoline) were performed under microwave irradiation in an Initiator Sixty single-mode microwave synthesizer from Biotage, equipped with a noninvasive IR sensor (accuracy 2%). Chromatographic separations were performed using normal phase (NP) silica RediSep Cartridges by Teledyne Isco. The reaction progress was monitored by thin-layer chromatography (TLC) using glass plates precoated with silica gel 60 (Merck).

Proton (<sup>1</sup>H) nuclear magnetic resonance (NMR) spectra were recorded at room temperature using spectrometers from Bruker (300, 600 MHz). <sup>13</sup>C NMR was recorded at 100 MHz. Chemical shifts ( $\delta$ ) are expressed in parts per million relative to tetramethylsilane (TMS).

Size exclusion chromatographic (SEC) investigations were performed on an Agilent Technologies 1200 Series gel permeation chromatography system equipped with a G1329A auto sampler, a G131A isocratic pump, a G1362A refractive index detector, and both a PSS Gram 30 and a PSS Gram 1000 column placed in series. As eluent a 0.21% LiCl solution in *N,N*-dimethylacetamide (DMAc) was used at 1 mL min<sup>-1</sup> flow rate and a column oven temperature of 40 °C. Molar masses were calculated using poly(styrene) standards. High-resolution electron spray ionization mass spectrometry (HR-ESI-MS) was measured with a Bruker MicroQToF and elemental analysis were measured with a Leco CHN-932.

#### 2.2.1. Synthesis of 1-(2-(Benzyloxy)ethyl)-2,3,4,5-di-O-isopropylidene- $\beta$ -D-fructopyranoside (2)

6.5 g (25 mmol) of 2,3,4,5-di-O-isopropylidene- $\beta$ -D-fructopyranoside **1** was dissolved in 150 mL of dry THF, 4 g NaH (166.7 mmol) were added and the mixture stirred for 20 min under nitrogen. Subsequently, benzyl 2-bromoethyl ether (10 g, 43.6 mmol) was added dropwise and reaction was conducted for 7 d (controlled during this time with TLC). After no starting material had remained (TLC,



SiO<sub>2</sub>, EtOAc/cyclohexane, v/v, 1:2), 50 mL of methanol were slowly added and the reaction mixture was evaporated. The crude product was dissolved in 200 mL of ethyl acetate and washed twice with each 200 mL of saturated NaHCO<sub>3</sub> solution and once with 200 mL of water. The organic phase was dried with Na<sub>2</sub>SO<sub>4</sub> and the solvent was removed. The product **2** was purified by column chromatography (SiO<sub>2</sub>, EtOAc/cyclohexane, v/v, 1:2) and collected as light yellow oil. Yield: 8.69 g (70%).

<sup>1</sup>H-NMR (300 MHz, CDCl<sub>3</sub>, δ): 7.39–7.24 (m, 5H, Bn), 4.62–4.58 (dd, *J* = 7.92 Hz, 2.61 Hz, 1H, H-4), 4.56 (s, 2H, Bn-CH<sub>2</sub>), 4.44 (d, *J* = 2.6 Hz, 1H, H-3), 3.92 (dd, *J* = 7.9 Hz, 1.1 Hz, 1H, H-5), 3.81 (dd, *J* = 13 Hz, *J* = 1.85 Hz, 1H, H-6), 3.77–3.68 (m, 3H, H-1, H-1', H-6'), 3.67–3.58 (m, 4H, CH<sub>2</sub>), 1.54, 1.47, 1.43, 1.35 (4s, 12H, CH<sub>3</sub>); <sup>13</sup>C-NMR (CDCl<sub>3</sub>, 75 MHz, δ): 138.26 (Bn-C<sub>q</sub>), 128.33, 127.66, 127.56 (Bn), 108.90 (isopropylidene-C<sub>q</sub>), 108.54 (isopropylidene-C<sub>q</sub>), 102.72 (C2), 73.23 (Bn-CH<sub>2</sub>), 72.47 (CH<sub>2</sub>), 71.38 (C1), 71.03 (C5), 70.22 (C4), 69.99 (C3), 69.37 (CH<sub>2</sub>), 61.01 (C6), 26.56, 25.87, 25.29, 24.03 (CH<sub>3</sub>). MS (ESI) *m/z*: [M+Na]<sup>+</sup> calcd for C<sub>21</sub>H<sub>30</sub>O<sub>7</sub>Na, 417.19; found, 417.18; [M+K]<sup>+</sup> calcd for C<sub>21</sub>H<sub>30</sub>O<sub>7</sub>K, 433.16; found, 433.16. Anal. calcd. for C<sub>21</sub>H<sub>30</sub>O<sub>7</sub>: C 63.94, H 7.67; found: C 63.90, H 7.69.

### 2.2.2. Synthesis of 1-(2-(Hydroxyl)ethyl)-2,3:4,5-di-O-isopropylidene-β-D-fructopyranoside (**3**)

8.38 g (21.2 mmol) of **2** were dissolved in 300 mL of methanol and 0.23 g of palladium on charcoal (3 wt%) were added to the reaction mixture. The reaction flask was evacuated and refilled with hydrogen several times. After stirring for 48 h, the catalyst was filtered off and the solvent was evaporated to obtain the product as colorless oil. Yield: 6.03 g (95%).

<sup>1</sup>H-NMR (300 MHz, CDCl<sub>3</sub>, δ): 4.62–4.56 (dd, *J* = 8.0 Hz, 2.5 Hz, 1H, H-4), 4.35 (d, *J* = 2.5 Hz, 1H, H-3), 4.26–4.21 (dd, *J* = 8.0 Hz, 1.1 Hz, 1H, H-5), 3.90 (dd, *J* = 13.0 Hz, *J* = 1.8 Hz, 1H, H-6), 3.80–3.56 (m, 5H, H-6, H-1, H-1', CH<sub>2</sub>), 2.18 (s, 1H, OH), 1.53, 1.49, 1.41, 1.34 (4s, 12H, CH<sub>3</sub>); <sup>13</sup>C-NMR (CDCl<sub>3</sub>, 75 MHz, δ): 108.98 (C<sub>q</sub>), 108.44 (C<sub>q</sub>), 102.59 (C2), 73.26 (CH<sub>2</sub>), 72.20 (C1), 70.76 (C5), 70.69 (C3), 70.14 (C4), 61.49 (CH<sub>2</sub>), 60.97 (C6), 26.44, 25.70, 25.18, 23.89 (CH<sub>3</sub>). MS (ESI) *m/z*: [M+Na]<sup>+</sup> calcd for C<sub>14</sub>H<sub>24</sub>O<sub>7</sub>Na, 327.14; found, 327.14; [M+K]<sup>+</sup> calcd for C<sub>14</sub>H<sub>24</sub>O<sub>7</sub>K, 343.12; found, 343.12; [2M+Na]<sup>+</sup> calcd for C<sub>28</sub>H<sub>48</sub>O<sub>14</sub>Na, 631.29; found, 631.29. Anal. calcd. for C<sub>14</sub>H<sub>24</sub>O<sub>7</sub>: C 55.25, H 7.95; found: C 55.24, H 8.14.

### 2.2.3. Synthesis of 1-(2-(Methanesulfonyl)ethyl)-2,3:4,5-di-O-isopropylidene-β-D-fructopyranoside (**4**)

5 g (16.4 mmol) of **3** were dissolved in 30 mL of CH<sub>2</sub>Cl<sub>2</sub> and 6.825 mL (49.24 mmol) of Et<sub>3</sub>N and 20 mg 4-DMAP (0.16 mmol) were added. The reaction mixture was cooled to 0 °C and 3 mL (38.8 mmol) of mesyl chloride were added dropwise to the solution.<sup>[28]</sup> The reaction mixture was left to slowly warm to room temperature and stirred for 2 h. After no starting material had remained (TLC, SiO<sub>2</sub>, EtOAc/cyclohexane, v/v, 2:1), 50 mL CH<sub>2</sub>Cl<sub>2</sub> were added and the mixture was washed thrice with each 200 mL of water and twice with each 200 mL of saturated, aqueous NaHCO<sub>3</sub> solution. The organic layer was dried over Na<sub>2</sub>SO<sub>4</sub> and the solvent was removed. The crude product was dissolved in 10 mL of ethyl acetate, filtered over silica gel and collected as yellowish oil.

Yield: 5.78 g (92%). <sup>1</sup>H-NMR (CDCl<sub>3</sub>, 300 MHz, δ): 4.63–4.58 (dd, *J* = 7.9 Hz, 2.6 Hz, 1H, H-4), 4.40–4.33 (m, 3H, H-3, CH<sub>2</sub>),

4.26–4.21 (dd, *J* = 7.9 Hz, 0.9 Hz, 1H, H-5), 3.94–3.64 (m, 6H, H-1, H-1', H-6, H-6', CH<sub>2</sub>), 3.05 (s, 3H, SCH<sub>3</sub>), 1.54, 1.47, 1.42, 1.34 (4s, 12H, CH<sub>3</sub>); <sup>13</sup>C-NMR (CDCl<sub>3</sub>, 75 MHz, δ): 108.95 (C<sub>q</sub>), 108.68 (C<sub>q</sub>), 102.38 (C2), 72.84 (CH<sub>2</sub>), 70.91 (C5), 70.11 (C4, C3), 69.70 (C1), 68.61 (CH<sub>2</sub>), 61.06 (C6), 37.34 (SCH<sub>3</sub>), 29.33 (CH<sub>2</sub>), 26.52, 25.88, 25.33, 24.00 (CH<sub>3</sub>). MS (ESI) *m/z*: [M+Na]<sup>+</sup> calcd for C<sub>15</sub>H<sub>26</sub>O<sub>9</sub>Na, 405.12; found, 405.12. Anal. calcd. for C<sub>15</sub>H<sub>26</sub>O<sub>9</sub>S: C 47.11, H 6.85, S 8.38; found: C 47.22, H 6.96, S 8.25.

### 2.2.4. Synthesis of 1-O-(2-Mercapto-ethyl)-2,3:4,5-di-O-isopropylidene-β-D-fructopyranoside (**5**)

1.311 g (3.43 mmol) of **4** was dissolved in 15 mL 2-butanone, 0.78 g (10.25 mmol) thiourea was added, and the mixture was heated to 95 °C under reflux for 7 h.<sup>[29]</sup> After no starting material had remained (TLC, SiO<sub>2</sub>, EtOAc/cyclohexane, v/v, 2:1), the solvent was evaporated, 15 mL CH<sub>2</sub>Cl<sub>2</sub>, 15 mL H<sub>2</sub>O and 0.874 g K<sub>2</sub>S<sub>2</sub>O<sub>5</sub> (3.93 mmol) were added and the mixture was heated to reflux for 12 h. The organic layer was washed thrice with each 200 mL of water, dried with anhydrous Na<sub>2</sub>SO<sub>4</sub>, filtered, and evaporated to effort after column chromatography (SiO<sub>2</sub>, EtOAc/cyclohexane, v/v, 1:1) the pure product.

Yield: 0.842 g (76.7%). <sup>1</sup>H-NMR (600 MHz, CDCl<sub>3</sub>, δ): 4.61 (dd, *J* = 7.92 Hz, 2.58 Hz, 1H, H-4), 4.39 (d, *J* = 2.58 Hz, 1H, H-3), 4.23 (dd, *J* = 7.92 Hz, 1.32 Hz, 1H, H-5), 3.90 (dd, *J* = 12.99 Hz, *J* = 1.83 Hz, 1H, H-6), 3.74–3.70 (m, 2H, H-6', H-1), 3.65–3.56 (m, 3H, H-1', CH<sub>2</sub>), 2.71–2.68 (m, 2H, CH<sub>2</sub>), 1.59 (t, *J* = 8.25 Hz, 1H, SH), 1.53–1.34 (4s, 12H, CH<sub>3</sub>); <sup>13</sup>C-NMR (150 MHz, CDCl<sub>3</sub>, δ): 109.07 (C<sub>q</sub>), 108.71 (C<sub>q</sub>), 102.64 (C2), 73.62 (CH<sub>2</sub>), 72.36 (C1), 71.11 (C5), 70.30 (C4), 70.23 (C3), 61.16 (C6), 26.69, 26.02, 25.52, 24.27 (CH<sub>3</sub>), 24.14 (CH<sub>2</sub>). HRMS (ESI) *m/z*: [M+Na]<sup>+</sup> calcd for C<sub>14</sub>H<sub>24</sub>O<sub>6</sub>Na, 343.1186; found, 343.1200. Anal. calcd. for C<sub>14</sub>H<sub>24</sub>O<sub>6</sub>S: C 52.48, H 7.55, S 10.01; found: C 52.77, H 7.64, S 10.39.

### 2.2.5. Synthesis of Linear Poly(ethylene imine) (**P1**)

Poly(2-ethyl-2-oxazoline) (**PEtOx**) used as starting material in this study was synthesized according to literature procedures.<sup>[30]</sup> The monomer 2-ethyl-2-oxazoline (3.965 g) and the initiator methyl tosylate (12.42 mg, 0.067 mmol) were dissolved in dry acetonitrile (6.0 mL) under inert conditions in a glovebox. After stirring for a few minutes the microwave vial was heated in a microwave synthesizer for 128 min at 140 °C. The polymerization mixture was diluted with 5 mL dichloromethane and precipitated in 250 mL ice-cold diethyl ether. Subsequently, the precipitate was filtered off and lyophilized (yield: 3.720 g, 94%).

Accordingly, **PEtOx** (degree of polymerization (DP) = 575, 2.7 g) was treated with an excess of 6 M aqueous hydrochloric acid (250 mL) at 100 °C for 16 h under reflux.<sup>[31]</sup> The excess of hydrochloric acid and the resulting propionic acid were removed under reduced pressure. The residue was dissolved in water followed by the addition of 3 M NaOH to reach pH = 8. Precipitation occurred and the precipitated, hydrolyzed linear poly(ethylene imine) was filtered off. The residue was redissolved in 10 mL of *N,N*-dimethylformamide and precipitated two times into 300 mL ice-cold diethyl ether. The obtained product was dried in vacuo at 85 °C. The degree of hydrolysis of the resulting linear poly(ethylene imine) **P1** was determined by <sup>1</sup>H NMR spectroscopy (yield: 1.0 g, 85%).

**PEtOx:** DP = 575.  $^1\text{H}$  NMR (300 MHz,  $\text{D}_2\text{O}$ ,  $\delta$ ): 3.70–3.20 (–NR–CH<sub>2</sub>–CH<sub>2</sub>), 2.41–2.08 (CH<sub>2</sub>–CH<sub>3</sub>), 1.09–0.79 (CH<sub>2</sub>–CH<sub>3</sub>). SEC (DMAc, LiCl):  $M_n$  = 69 000 g mol<sup>–1</sup>,  $\bar{D}$  = 1.3.

**P1:** EtOx:EI [%] = 2:98.  $^1\text{H}$  NMR (300 MHz, MeOD,  $\delta$ ): 3.58–3.41 (NR–CH<sub>2</sub>–CH<sub>2</sub>), 2.91–2.61 (NH–CH<sub>2</sub>–CH<sub>2</sub>), 2.56–2.36 (CH<sub>2</sub>–CH<sub>3</sub>), 1.18–1.06 (CH<sub>2</sub>–CH<sub>3</sub>).

## 2.2.6. Synthesis of P(EI-stat-ButEnOx) (P2)

**P1** (500 mg) and the catalyst 4-*N,N*-dimethylamino-pyridine (DMAP, 50 mg, 0.41 mmol) were dissolved in pyridine (5 mL) at 80 °C. A defined quantity of *N*-succinimidyl-4-pentenate (465 mg) was dissolved in pyridine (5 mL) and heated up to 80 °C. The two solutions were combined and 2 mL pyridine added to obtain a 3 wt% mixture of **P1** and stirred for 16 h at 80 °C. Afterward, the mixture was filtered and precipitated into 300 mL ice-cold diethyl ether (Et<sub>2</sub>O). The precipitated copolymer was filtered off and washed with 30 mL of diethyl ether. The purified product **P2** was dried under reduced pressure (yield: 860 mg, 89%).

EI:ButEnOx [%] = 73:27.  $^1\text{H}$  NMR (600 MHz, DMSO-*d*<sub>6</sub>,  $\delta$ ): 5.89–5.74 (HC=CH<sub>2</sub>), 5.06–4.91 (HC=CH<sub>2</sub>), 3.58–3.20 (NR–CH–CH<sub>2</sub>), 2.80–2.45 (NH–CH<sub>2</sub>–CH<sub>2</sub>), 2.44–2.34 (CH<sub>2</sub>–CH<sub>2</sub>–C<sub>2</sub>H<sub>5</sub>), 2.27–2.16 (CH<sub>2</sub>–CH<sub>2</sub>–C<sub>2</sub>H<sub>5</sub>). SEC (DMAc, LiCl, polystyrene):  $M_n$  = 8000 g mol<sup>–1</sup>,  $\bar{D}$  = 1.3. Anal. calcd. for C<sub>1927</sub>H<sub>3811</sub>N<sub>575</sub>O<sub>155</sub>: C 61.69, H 10.24, N 21.47; found: C 60.90, H 10.43, N 22.91.

## 2.2.7. Synthesis of P(EI-stat-ButEnOx-stat-isoFruButOx) via Thiol-Ene Photoaddition (isoP3)

**P2** (558 mg) was dissolved in 5 mL methanol. In a second vial, the photoinitiator DMPA (6.5 mg, 0.025 mmol) and a 1.2-fold excess per double bond of **5** (840 mg) were dissolved in methanol (5 mL). The combined solution (5 wt% of **P2**) was deoxygenated with argon for 20 min and stirred in a UV chamber ( $\lambda$  = 365 nm) for 18 h. Subsequently, the copolymer was precipitated two times in 300 mL ice-cold diethyl ether. After filtration, the copolymer was dried under reduced pressure at 40 °C (yield: 980 mg, 70%).

EI:ButEnOx:isoFruButOx [%] = 73:11:16.  $^1\text{H}$  NMR (600 MHz, DMSO-*d*<sub>6</sub>,  $\delta$ ): 5.90–5.74 (HC=CH<sub>2</sub>), 5.07–4.88 (HC=CH<sub>2</sub>), 4.57 (H-4), 4.27 (H-3), 4.22 (H-5), 3.73 (H-6), 3.66 (–CH<sub>2</sub>), 3.55 (H-6, –CH<sub>2</sub>), 3.48 (H-1), 3.43 (H-1), 3.40–3.12 (NR–CH<sub>2</sub>–CH<sub>2</sub>), 2.78–2.46 (NH–CH<sub>2</sub>–CH<sub>2</sub>), 2.42–2.16 (CH<sub>2</sub>–CH<sub>2</sub>–C<sub>2</sub>H<sub>5</sub>), 1.53 (CH<sub>2</sub>–CH<sub>2</sub>–C<sub>2</sub>H<sub>5</sub>), 1.47–1.26 (isopropylidene). SEC (DMAc, LiCl):  $M_n$  = 11 600 g mol<sup>–1</sup>,  $\bar{D}$  = 1.9. Anal. calcd. for C<sub>3123</sub>H<sub>5835</sub>N<sub>575</sub>O<sub>707</sub>S<sub>92</sub>: C 57.09, H 8.95, N 12.26, S 4.49; found: C 57.39, H 9.23, N 13.35, S 4.18.

## 2.2.8. Synthesis of P(EI-stat-ButEnOx-stat-FruButOx) via Deprotection (P3)

The cleavage of the isopropylidene groups was performed under acidic conditions.<sup>[32]</sup> The copolymer **isoP3** (685 mg) was dissolved in a THF/H<sub>2</sub>O mixture (22.5/22.5 mL) and acidified with 2 M hydrochloric acid (6.75 mL). The solution was heated to 40 °C for 12 h. Subsequently, the mixture was neutralized with 1.2 g NaHCO<sub>3</sub> and THF as well as formed acetone were evaporated under reduced pressure. Purification of the deprotected D-fructose conjugate was performed by dialysis against water using a Spectra/Por 3 dialysis membrane (3500 g mol<sup>–1</sup> cutoff).

Finally, the product was lyophilized and obtained as a yellowish powder (yield: 324 mg, 53%). EI:ButEnOx:FruButOx [%] = 73:11:16. SEC (DMAc, LiCl):  $M_n$  = 9800 g mol<sup>–1</sup>,  $\bar{D}$  = 1.2. Anal. calcd. for C<sub>2571</sub>H<sub>5099</sub>N<sub>575</sub>O<sub>707</sub>S<sub>92</sub>: C 52.94, H 8.81, N 13.81, S 5.06; found: C 53.60, H 9.13, N 14.91, S 4.66.

## 2.3. Polymer Labeling with Cy5 (P1-Cy5)

**P1** (40 mg) and triethylamine (360  $\mu\text{L}$ ) were dissolved in methanol (10 mL). After addition of the cyanine-5-NHS-ester (1 mg) the reaction was stirred at room temperature overnight. The labeled polymer was precipitated in 250 mL ice-cold diethyl ether, filtered, and redissolved in methanol (15 mL). Further purification was performed by dialysis against a mixture of water/methanol using a Spectra/Por 3 dialysis membrane (3500 g mol<sup>–1</sup> cutoff). Finally, the product was dried under reduced pressure (yield: 15 mg, 37%; labeling efficiency: 2.0% of dye).

## 2.4. Copolymer Labeling with Rhodamine (P2-Rho, P3-Rho)

The copolymer (**P2**: 35 mg, **P3**: 40 mg) and triethylamine (200  $\mu\text{L}$ ) were dissolved in DMF (4 mL). After addition of Rhodamine B isothiocyanate (0.7 mg) the reaction was stirred at room temperature for 18 h. Purification was performed by dialysis against water using a Spectra/Por 3 dialysis membrane (3500 g mol<sup>–1</sup> and subsequently 6–8000 g mol<sup>–1</sup> cutoff). Finally, the product was lyophilized and obtained as a reddish powder. The calculated labeling efficiency (via UV–vis spectroscopy) for conjugation was 1.4% of dye for the **P2-Rho** (yield: 23 mg, 66%) and 30.4% of dye for the labeled **P3** (yield: 26 mg, 65%). To achieve comparable fluorescence intensities, the labeled **P3** was mixed with the unlabeled **P3** (1:19) to obtain **P3-Rho** (new label efficiency: 1.5% of dye).

## 2.5. Polyplex Preparation

Polyplexes of plasmid desoxyribonucleic acid (pDNA) and selected polymers were prepared by mixing stock solutions of 15  $\mu\text{g mL}^{-1}$  pDNA and the respective polymers (1 mg mL<sup>–1</sup>) in different amounts to obtain various N/P ratios (nitrogen of polymer to phosphate of pDNA) in HBG (HEPES buffered glucose) buffer (20  $\times 10^{-3}$  M 4-(2-hydroxyethyl) piperazine-1-ethanesulfonic acid and 5% (w/v) glucose, pH 7.2). The solutions were vortexed for 10 s at maximal speed and incubated at room temperature for 20 min to ensure a complex formation.

## 2.6. Determination of Cytotoxicity

Cytotoxicity studies were performed with the mouse fibroblast cell line L929 (CCL-1, ATCC), as recommended by ISO10993-5. Furthermore, the breast cancer cell line MDA-MB-231 and the HUVEC cells were used. The cells were routinely cultured in Dulbecco's modified eagle's medium (Lonza, Basel) supplemented with 10% fetal calf serum (FCS), 100 U mL<sup>–1</sup> penicillin, and 100  $\mu\text{g mL}^{-1}$  streptomycin at 37 °C in a humidified 5% (v/v) CO<sub>2</sub> atmosphere. HUVEC cells were cultured in M199 Medium (Lonza, Basel) supplemented with 17.5% FCS, 680  $\times 10^{-6}$  M L-glutamin, 25  $\mu\text{g mL}^{-1}$

heparin, 7.5 g mL<sup>-1</sup> endothelial mitogenic, Vitamin C (5 µg mL<sup>-1</sup>), human serum and 100 U mL<sup>-1</sup> penicillin, and 100 µg mL<sup>-1</sup> streptomycin at 37 °C in a humidified 5% (v/v) CO<sub>2</sub> atmosphere. In detail, cells were seeded at 1 × 10<sup>4</sup> cells per well in a 96-well plate and incubated for 24 h, whereas no cells were seeded in the outer wells. Subsequently, **P1**, **P2**, and **P3** were added to the cells in fresh media at indicated concentrations and the plates were incubated for 24 h. Control cells were incubated only with fresh culture medium. Subsequently, media was replaced by a mixture of fresh culture medium and AlamarBlue solution, prepared according to the manufacturer's instructions. After a further incubation of 4 h at 37 °C, the fluorescence was measured at  $E_x$  570 nm/ $E_m$  610 nm, with untreated cells on the same well plate serving as negative controls. The negative control was set as 0% of metabolism inhibition and referred as 100% viability. Cell viability below 70% was considered indicative of cytotoxicity. Data are expressed as mean ± standard deviation (SD) of three independent determinations of six data points each.

## 2.7. Hemocompatibility and Erythrocyte Aggregation

The interaction of polymers with cellular membranes was investigated by analyzing the release of hemoglobin from erythrocytes. Blood from sheep, collected in heparinized tubes, was provided by the Institute of Laboratory Animal Science and Animal Welfare, Friedrich Schiller University Jena. The blood was centrifuged at 4500 × *g* for 5 min, and the pellet was washed three times with cold 1.5 × 10<sup>-3</sup> M phosphate buffered saline (PBS, pH 7.4). After dilution of erythrocytes with PBS in a ratio of 1:7, aliquots of erythrocyte suspension were mixed 1:1 with the indicated polymer solution up to 100 µg mL<sup>-1</sup> and incubated in a water bath at 37 °C for 60 min. After centrifugation at 2400 × *g* for 5 min, the hemoglobin release into the supernatant was determined spectrophotometrically at a wavelength of 544 nm using a microplate reader (TECAN Infinite M200 Pro, Crailsheim, Germany). Complete hemolysis (100%) was achieved using 1% Triton X-100 serving as positive control. Pure PBS was used as negative control (0% hemolysis). The hemolytic activity of the polycations was calculated using Equation (1)

$$\% \text{Hemolysis} = 100 \times \frac{(A_{\text{Sample}} - A_{\text{Negative control}})}{(A_{\text{Positive control}} - A_{\text{Negative control}})} \quad (1)$$

A value less than 2% hemolysis rate was classified as non-hemolytic, 2%–5% as slightly hemolytic and >5% as hemolytic. Experiments were run in triplicates and were performed with three different batches of donor blood.

To study the influence of aggregation, erythrocytes were isolated as described above. The erythrocyte suspensions were mixed 1:1 with the polymer solutions (100 µL total volume) in a clear flat bottomed 96-well plate. The cells were incubated at 37 °C for 2 h, and the absorbance was measured at 645 nm in a microplate reader. Cells, which were treated with PBS, served as negative control and 25 kDa branched PEI (BPEI) (50 µg mL<sup>-1</sup>, Sigma-Aldrich) was used as positive control. Absorbance values of the test solutions lower than the negative control were regarded as aggregation. Experiments were run in triplicates and were performed with three different batches of donor blood.

## 2.8. Ethidium Bromide Quenching Assay (EBA)

The formation of polyplexes with pDNA was examined by quenching of the ethidium bromide fluorescence. Briefly, 15 µg mL<sup>-1</sup> pDNA in a total volume of 100 µL HBG buffer were incubated with ethidium bromide (0.4 µg mL<sup>-1</sup>) for 10 min at room temperature. Subsequently, polyplexes with different amounts of polymer (various N/P ratios) were prepared in black 96-well plates (Nunc Thermo Fisher). The samples were incubated at room temperature for 15 min before fluorescence measurements. The fluorescence of the samples was measured at an excitation wavelength of 525 nm and an emission wavelength of 605 nm using a Tecan Genios Pro fluorescence plate reader (Tecan, Crailsheim, Germany). A sample containing only pDNA and ethidium bromide was used to calibrate the device to 100% fluorescence against a background of 0.4 µg mL<sup>-1</sup> of ethidium bromide in HBG solution. The percentage of dye displaced upon polyplex formation was calculated using Equation (2)

$$\text{RFU} [\%] = \frac{F_{\text{sample}}}{F_{\text{pDNA}}} \times 100 \quad (2)$$

Here, RFU is the relative fluorescence and  $F_{\text{sample}}$  and  $F_{\text{pDNA}}$  are the fluorescence intensities of a given sample and the ethidium bromide intercalated into pDNA alone.

## 2.9. Heparin Dissociation Assay

To investigate the release of pDNA from polyplexes, the heparin dissociation assay was performed. Polyplexes with an N/P ratio of 30 were prepared as described above in a total volume of 100 µL HBG buffer containing ethidium bromide (0.4 µg mL<sup>-1</sup>). After incubation in the dark at room temperature for 15 min, the polyplexes were transferred into a black 96-well plate, and heparin solutions of indicated concentrations were added. The solutions were mixed and incubated for further 30 min at 37 °C in the dark. The fluorescence of ethidium bromide was measured at  $E_x$  525 nm/ $E_m$  605 nm with a Tecan microplate reader. The percentage of intercalated ethidium bromide was calculated as described above.

## 2.10. Dynamic and Electrophoretic Light Scattering (ELS)

Dynamic light scattering was performed on a Zetasizer Nano ZS (Malvern Instruments, Herrenberg) with an He-Ne laser operating at a wavelength of  $\lambda = 633$  nm. All measurements (30 runs, triplicate) were carried out at 25 °C after an equilibration time of 120 s. The counts were detected at an angle of 173°. The mean particle size was approximated as the effective (*z*-average) diameter and the width of the distribution as the polydispersity index of the particles (PDI) obtained by the cumulants method assuming a spherical shape. ELS was used to measure the zeta potential ( $\zeta$ ). The measurement was performed on a Zetasizer Nano ZS (Malvern Instruments, Herrenberg, Germany) by applying laser Doppler velocimetry. For each measurement, 20 runs were carried out using the slow-field reversal and the fast-field reversal mode at 150 V. Each experiment was performed in triplicate at 25 °C. The zeta potential was calculated



from the electrophoretic mobility ( $\mu$ ) according to the Henry's equation. Henry coefficient  $f(ka)$  was calculated according to Oshima.

### 2.11. Uptake Studies

For uptake studies, cells were cultured as described above. Subsequently, cells were seeded at a density of  $10^5$  (HUVEC,  $3 \times 10^5$ ) cells per mL in 24-well plates and cultured for 24 h. One hour prior to the addition of the polyplexes, the medium was changed to OptiMEM (Life Technologies, Darmstadt, Germany). The polyplexes were prepared as described above and at least 50  $\mu$ L polyplex solution of N/P 50 were added to the cells cultured with 500  $\mu$ L media. The plates were incubated for 1 h at 37 °C under 5% CO<sub>2</sub> atmosphere.

For flow cytometry studies the pDNA (pEGFP-N1) was labeled with YOYO-1 iodide prior to the polyplex preparation. For labeling of 1  $\mu$ g pDNA, 0.026  $\mu$ L of 1 M YOYO-1 solution was mixed with pDNA and incubated for 20 min at 4 °C protected from light. Afterward, HBG buffer and polymers were added at the indicated N/P ratio and the polyplexes were formed as described previously. The cells were washed and harvested after 1 h and 10% trypan blue was added to quench the outer fluorescence of the cells. To determine the relative uptake of the polyplexes, 10 000 cells were measured by flow cytometry using a Cytomics FC 500 (Beckman Coulter) and the amount of viable cells showing YOYO-1 signal (FL1) were gated. Dead cells were identified via counterstaining with propidium iodide. The experiments were performed at least three times independently.

Live cell imaging was performed for uptake studies. In detail, cells ( $10^5$  cells mL<sup>-1</sup>) were seeded on glass-bottomed dishes (Greiner, Germany) and cultivated for 24 h in a humidified atmosphere. One hour prior to the polymer addition, the cells were rinsed with PBS and the medium was changed to OptiMEM. The polyplexes were formed with **P1-Cy5**, or **P2-Rho**, and **P3-Rho**, added to the cells, and incubated for one additional hour. Subsequently, the medium was replaced by fresh culture medium or PBS supplemented with Hoechst 33342 for nucleus staining. Imaging was performed with LSM880, Elyra PS.1 system (Zeiss, Oberkochen, Germany) applying a 63 $\times$  1.4 NA plan apochromat oil objective.

### 2.12. Transfection Studies

For transfection studies HUVEC cells were seeded at a density of  $2 \times 10^5$  cells mL<sup>-1</sup> in 24-well plates 1 d before transfection. One hour prior to transfection, cells were rinsed with PBS and supplemented with 1 mL of OptiMEM (Life Technologies). Polyplexes (50  $\mu$ L) were added to the cells and the plates were incubated for 4 h in the incubator. Afterward, the supernatant was replaced by 1 mL of fresh growth medium and the cells were further incubated for 20 h. For analysis, adherent cells were harvested by trypsinization. The relative expression of EGFP fluorescence of  $10^4$  cells was quantified via flow cytometry using a Cytomics FC 500 (Beckman Coulter). For determination of the transfection efficiency viable cells expressing EGFP were gated.

## 3. Results and Discussion

To conjugate a D-fructose derivative to a cationic polymer backbone, the thiol-ene photoaddition was utilized as the method of choice since it can be performed under mild conditions (low temperature, no toxic metal catalysts) in high yields.<sup>[33]</sup> Previous studies revealed that overexpressed D-fructose receptors of various breast cancer cell lines tolerate only defined positions of the introduced functional groups.<sup>[12]</sup> Several modifications at the C1 position of fructopyranose have been reported to be tolerated by GLUT5.<sup>[13,14,34]</sup> Since 1-deoxy-1-mercapto-fructopyranose did not react with the respective copolymers by thiol-ene photoaddition, an ethyl spacer had to be installed at the C1 position between the D-fructose moiety and the thiol group.

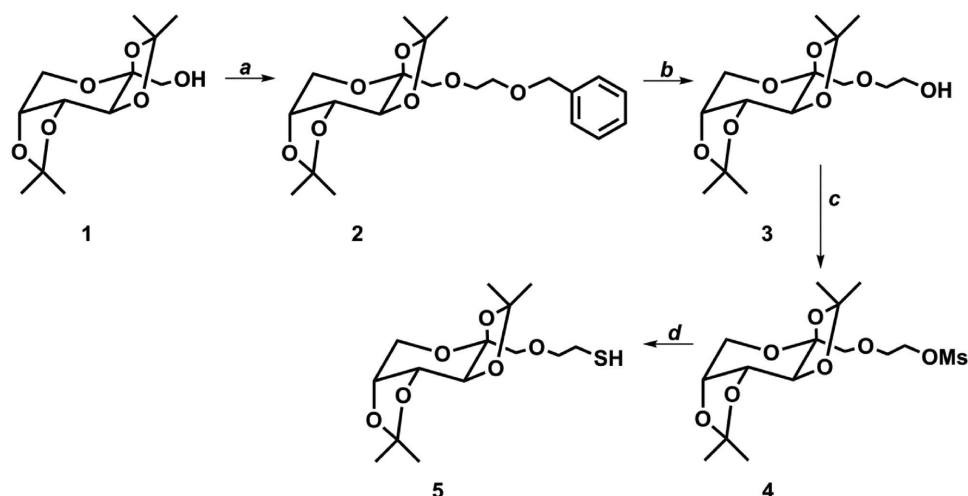
### 3.1. Synthesis of Thio-Functionalized D-Fructose

The D-fructose derivative bearing a thiol-group was obtained in a four-step synthesis from commercially available 2,3:4,5-di-*O*-isopropylidene- $\beta$ -D-fructopyranoside (**1**). First, a benzyl ether group was introduced by the conversion of **1** with benzyl-2-bromoethyl ether (Scheme 1) resulting in 1-(2-(benzyloxy)ethyl)-2,3:4,5-di-*O*-isopropylidene- $\beta$ -D-fructopyranoside (**2**). In a second step, the benzyl group of **2** was cleaved under standard conditions with H<sub>2</sub>/palladium on activated charcoal to obtain **3** in high yield (95%). The OH-group was transformed into a leaving group by mesylation with mesyl chloride under argon atmosphere analog to a literature procedure.<sup>[28]</sup> In a substitution reaction, the thiol functionality was introduced stepwise by transformation to the isothioronium salt and, subsequently, hydrolysis to yield the product 1-*O*-(2-mercaptoethyl)-2,3:4,5-di-*O*-isopropylidene- $\beta$ -D-fructopyranoside (**5**).

Characterization of the synthesis pathway by <sup>1</sup>H NMR spectroscopy for the compounds **1–5** is illustrated in Figure 1. The successful introduction of the “benzyl ethyl” substituent (**1–2**) can be followed by the proton signals in the aromatic region (7.24–7.39 ppm), the benzylic CH<sub>2</sub> signal (4.56 ppm), and the disappearance of the OH-quadruplet (2.09 ppm). After cleavage of the benzyl group (**3**), the disappearance of the aromatic and the benzylic CH<sub>2</sub> signals is observed. The successful substitution with mesyl chloride is characterized by the appearance of a sharp singlet at 3.02 ppm (**4**). The disappearance of the mesyl singlet and the appearance of a quadruplet (1.58 ppm) confirm the successful introduction of the thiol group (**5**). For the subsequent polymer modification, the protected thio-fructose **5** was used.

### 3.2. Synthesis of a D-Fructose Bearing Cationic Copolymer

The homopolymer poly(2-ethyl-2-oxazoline) (PEtOx) was synthesized according to a literature procedure by



**Scheme 1.** Schematic representation of the four-step synthesis of 1-*O*-(2-mercapto-ethyl)-2,3:4,5-di-*O*-isopropylidene- $\beta$ -D-fructopyranoside: a) benzyl-2-bromoethyl ether, NaH, THF, rt; b) H<sub>2</sub>/Pd, CH<sub>3</sub>OH, rt; c) mesyl chloride, Et<sub>3</sub>N, 4-DMAP, CH<sub>2</sub>Cl<sub>2</sub>, 0 °C; d) (1) thiourea, butanone, 95 °C, (2) K<sub>2</sub>S<sub>2</sub>O<sub>5</sub>, CH<sub>2</sub>Cl<sub>2</sub>/H<sub>2</sub>O, 50 °C.

microwave supported cationic ring-opening polymerization.<sup>[30]</sup> Before purification, the NMR signals of tosylate protons of the initiator MeOTos were used to calculate the degree of polymerization (575). This high molar mass homopolymer was used as starting material for the subsequent synthesis of linear poly(ethylene imine) (**P1**). For this

purpose, **PEtOx** was hydrolyzed in half concentrated hydrochloric acid (see Scheme 2).<sup>[35]</sup>

The formed ethylene imine units were functionalized with *N*-succinimidyl-4-pentenate to introduce double bonds to the polymer.<sup>[36]</sup> The resulting copolymer P(EI-*stat*-ButEnOx) (**P2**) revealed an ethylene imine content

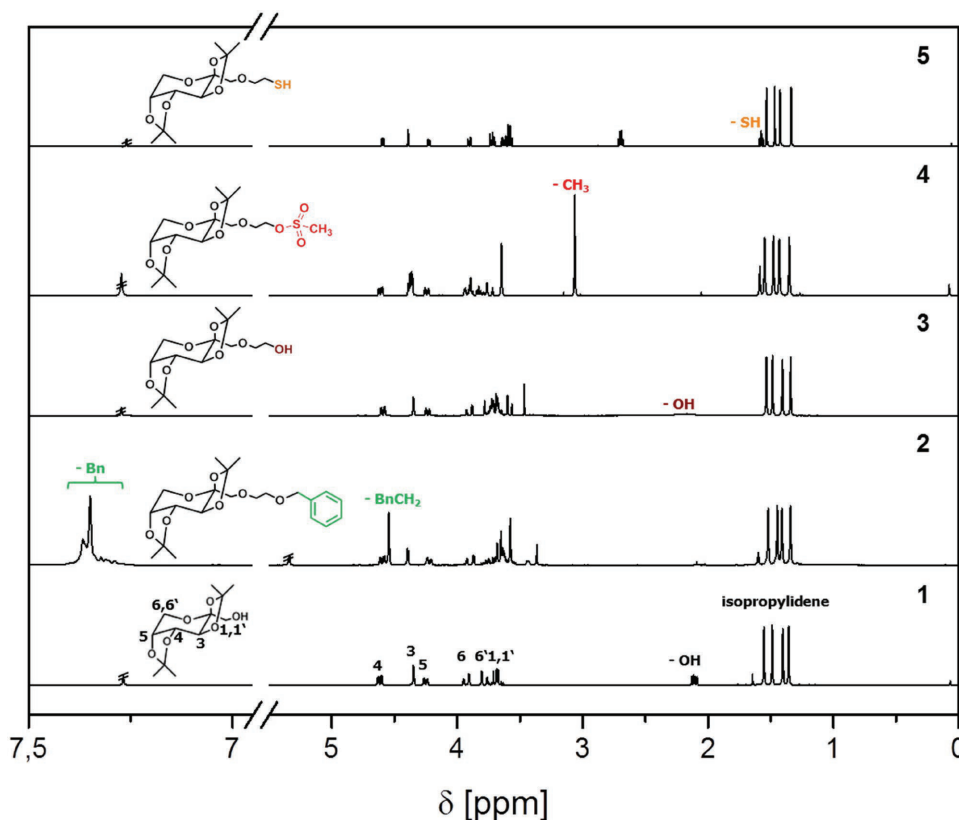


**Figure 1.** <sup>1</sup>H NMR of D-fructose derivatives 1–5 (300 and 600 MHz CDCl<sub>3</sub>/CD<sub>2</sub>Cl<sub>2</sub>).



**Scheme 2.** Schematic representation of the synthesis of P(EI-*stat*-ButEnOx-*stat*-FruButOx): a) 6 M HCl, 100 °C under reflux; b) pyridine, 4-*N,N*-dimethylamino-pyridine, *N*-succinimidyl-4-pentenat, 80 °C; c) D-fructose derivative (**5**), methanol, 2,2-dimethoxy-2-phenylacetophenone, room temperature, UV = 365 nm; d) THF/H<sub>2</sub>O, 2 M HCl, 40 °C.

of 73% (referring to the repeating units) to enable an effective binding of genetic material (Table 1). The introduction of the functionalized D-fructose was performed by thiol-ene photoaddition which represents a mild and metal-free reaction type. For this purpose, the corresponding precursor **P2** was converted with the protected thio-fructose **5** under UV irradiation at room temperature to yield the copolymer P(EI-*stat*-ButEnOx-*stat*-isoFruButOx) (**isoP3**). Surprisingly, a full conversion of the double bonds was not possible even after stepwise photoaddition using an excess of protected thio-fructose. Steric hindrance by the bulky side chains (including the isopropylidene protecting groups) could be one possible explanation. However, a high functionalization with carbohydrates rather hinders a stable polyplex formation.<sup>[24a]</sup> Subsequent deprotection of the isopropylidene groups resulted in P(EI-*stat*-ButEnOx-*stat*-FruButOx) (**P3**) revealing 16% of repeating units functionalized with D-fructose. Interestingly, this content of D-fructose modification rendered the final polymer **P3** water soluble.

Characterization by <sup>1</sup>H NMR confirms the presence of 2-butenyl-2-oxazoline (ButEnOx) and ethylene imine (EI) units in **P2** (Figure 2), proven by the appearance of proton signals of the double bond at 5.9 ppm (–HC=CH<sub>2</sub>, A) and 5.0 ppm (–HC=CH<sub>2</sub>, B). To calculate the composition of the obtained copolymer, the integral of the signals of the double bond (5.9 ppm) was compared to the integral

of the ethylene imine backbone (2.9–2.5 ppm). Since the ethylene imine units are not used for further modification, their content remains constant, representing 73% of repeating units of the copolymer. The successful functionalization of **P2** with **5** is shown by the appearance of D-fructose related signals between 4.6 and 3.4 ppm after photoaddition (**isoP3**, Figure 2). Furthermore, four singlets of the isopropylidene groups appear between 1.5 and 1.1 ppm. After treatment with hydrochloric acid, neutralization, and dialysis against water (cutoff: 3500 g mol<sup>–1</sup>) the signals of the protecting groups disappeared, indicating the successful deprotection of **isoP3** and, consequently, the formation of P(EI-*stat*-ButEnOx-*stat*-FruButOx) (**P3**). The isopropylidene cleavage results in the formation of a hemiketal structure and, therefore, in an equilibrium of pyranoses, furanoses, and an open-chained form, which can be distinguished via 2D NMR spectroscopy according to literature.<sup>[34]</sup> Since the ring proton signals of D-fructose are covered in the <sup>1</sup>H NMR spectra by the signals of the polymer backbone (Figure 2, **P3**), heteronuclear single quantum coherence (HSQC) NMR spectroscopy was used to prove their presence beneath the signals of the copolymer backbone as well as the successful formation of deprotected D-fructose moieties at the polymer (Figure 3).

The successful photoaddition, resulting in a single (polymeric) species (**P3**) and, hence, the absence of degradation, was further confirmed utilizing diffusion-ordered

**Table 1.** Composition and molar masses for PETox and P1–P3.

Abbreviation	Name	NMR <sup>a)</sup>	SEC <sup>b)</sup>		Sugar content <sup>c)</sup>
		<i>M<sub>n</sub></i> (theo) [g mol <sup>–1</sup> ]	<i>M<sub>n</sub></i> [g mol <sup>–1</sup> ]	<i>Đ</i>	
PETox	PETox <sub>575</sub>	57 000	69 000	1.3	–
P1	LPEI <sub>575</sub>	24 800	–	–	–
P2	P(EI <sub>73%</sub> - <i>stat</i> -ButEnOx <sub>27%</sub> )	37 500	8000	1.3	–
isoP3	P(EI <sub>73%</sub> - <i>stat</i> -ButEnOx <sub>11%</sub> - <i>stat</i> -isoFruButOx <sub>16%</sub> )	67 000	11 600	1.9	11
P3	P(EI <sub>73%</sub> - <i>stat</i> -ButEnOx <sub>11%</sub> - <i>stat</i> -FruButOx <sub>16%</sub> )	59 600	9800	1.2	12

<sup>a)</sup>Determined by <sup>1</sup>H NMR (calculated from tosylate signals of MeOTos before purification; <sup>b)</sup>SEC: DMAc, 0.21% LiCl, polystyrene calibration; <sup>c)</sup>Determined by elemental analysis.

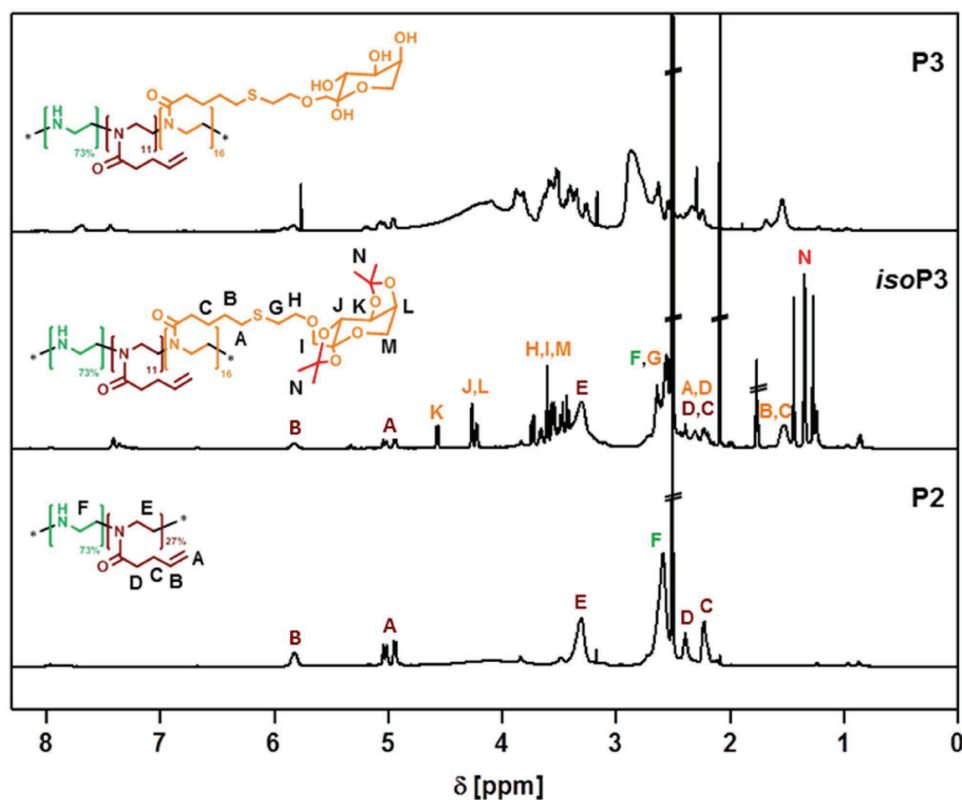


Figure 2. Comparison of  $^1\text{H}$  NMR spectra of the precursor copolymer **P2**, the protected D-fructose copolymer **isoP3** and the final product **P3** (600 MHz,  $\text{DMSO}-d_6$ ).

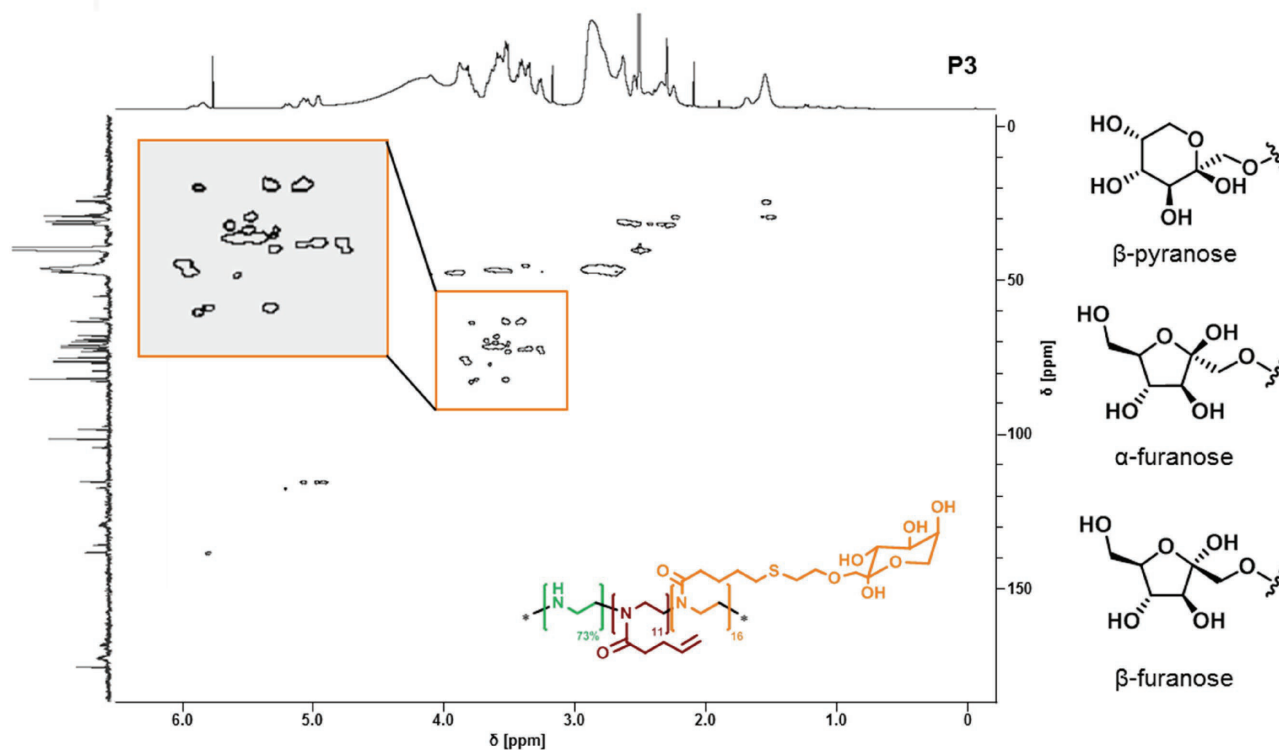
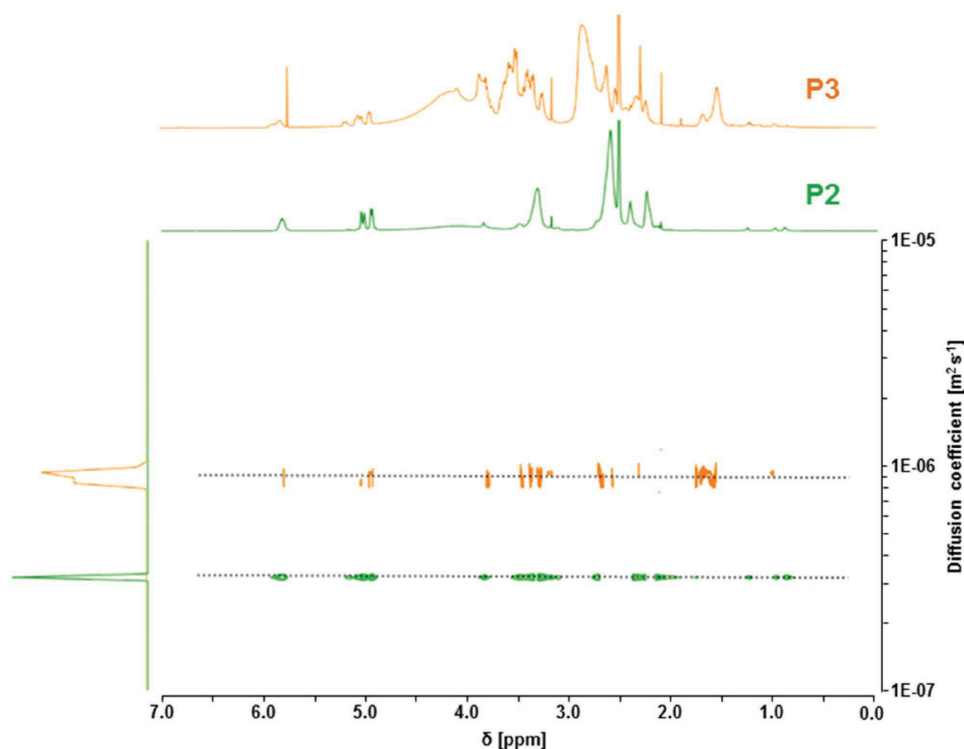


Figure 3. HSQC NMR of the copolymer **P3** ( $\text{DMSO}-d_6$ , 600 MHz).



■ Figure 4. DOSY NMR of the precursor **P2** (green) and the final copolymer **P3** (orange) (DMSO- $d_6$ , 600 MHz, 25 °C).

NMR spectroscopy (DOSY NMR) (Figure 4). The diffusion coefficient of **P3** is larger than for the precursor copolymer **P2**, indicating a decrease of the hydrodynamic radius of the polymer in solution.

A comparison of the composition and molar masses of the prepared copolymers obtained by size exclusion chromatography (SEC) is depicted in Table 1. The cationic polymers **P1–P3** show undesired interactions with the column and a change in the elution behavior. Furthermore, an SEC calibration for cationic polymers is not available, which complicates the determination of meaningful accurate molar masses with this technique. For this reason, a meaningful determination of molar masses of the copolymers by size exclusion measurements was not possible. However, for the modified poly(ethylene imine)s a trend is clearly visible. After the photoaddition of the protected thio-fructose the signal of *isoP3* is observed at lower elution volumes indicating an increased hydrodynamic volume. Deprotection results in a slight shift to higher elution volumes, and, therefore, to lower molar masses.

To enable a more detailed insight into the uptake in noncancer (L929) and triple negative breast cancer cells (MDA-MB-231) via microscopy, the precursor **P2** and the final copolymer **P3** were labeled using one equivalent of Rhodamine B isothiocyanate per polymer chain. For comparison with the nontargeted standard polymer, **Cy5–P1** was used.

### 3.3. Bio- and Hemocompatibility

Recently, cationic polymers such as PEI have been used extensively as nonviral vectors to deliver genetic material into mammalian cells. The cytotoxicity of the polymers represents a major drawback for potential applications. Former studies revealed increased biocompatibility of linear PEI (LPEI) compared to branched PEI.<sup>[37]</sup> Furthermore, cytotoxicity strongly depends on the molar mass and the cationic charge density.<sup>[22a]</sup> This study aimed to investigate the impact of functionalization with D-fructose (**P3**) in noncancerous fibroblast cell line L929, routinely used for toxicity screenings, in HUVEC cell line and in breast cancer cell line MDA-MB-231 compared to linear PEI (**P1**) and the precursor polymer **P2**.

**P1** exhibits a concentration-dependent cytotoxicity in the cell lines observed using the AlamarBlue assay (Figure 5). Increased concentrations result in reduced cell viability, as reported before for LPEI of the respective molecular mass.<sup>[38]</sup> Treatment with 5  $\mu\text{g mL}^{-1}$  decreases the cell viability to 15.8% in L929 cells, 2.8% in HUVEC and 1% in MDA-MB-231 cells, respectively. **P2** causes a dramatically reduced viability of breast cancer cells MDA-MB-231 ( $\text{IC}_{50} < 10 \mu\text{g mL}^{-1}$ ). In contrast, **P2** shows an increased biocompatibility in HUVEC cells ( $\text{IC}_{50} = 205 \mu\text{g mL}^{-1}$ ) and over the entire concentration range in L929 cells ( $\text{IC}_{50} > 500 \mu\text{g mL}^{-1}$ ). The D-fructose-conjugated polymer **P3** displays even improved biological properties. No significant reduction of the viability in mouse fibroblast



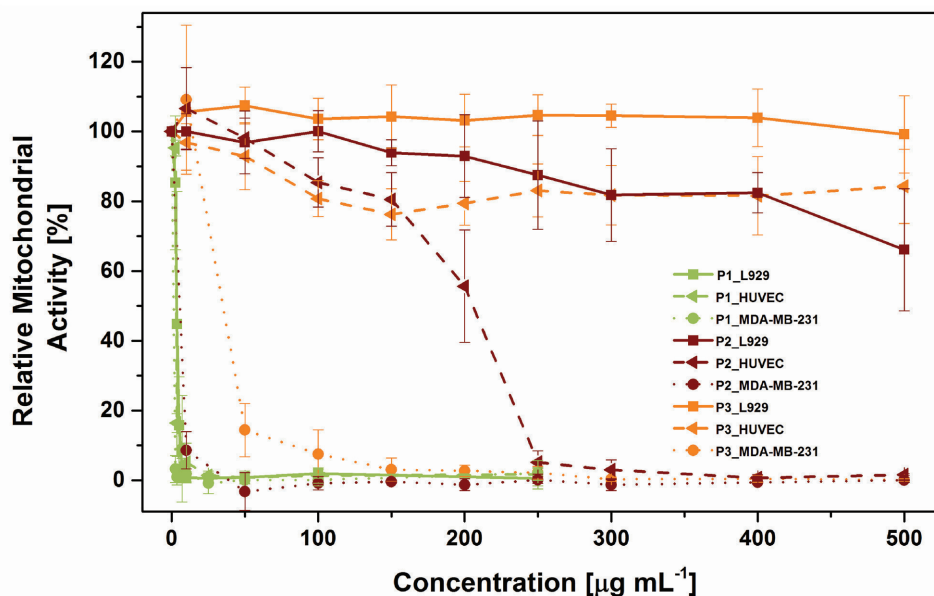


Figure 5. Cell-type-dependent cytotoxicity assay of **P1–P3** using AlamarBlue. Nontreated cells served as 100% relative viability. Cells were treated 24 h with the indicated concentrations of the polymers.

L929 cells and in the primary human endothelial HUVEC cells was observed after 24 h treatment with **P3** for all tested concentrations ( $IC_{50} > 500 \mu\text{g mL}^{-1}$ ). The cytotoxicity of **P3** ( $IC_{50} = 35 \mu\text{g mL}^{-1}$ ) toward breast cancer cells is concentration dependent, comparable to **P2**. As a consequence, D-fructose-conjugated polymer **P3** combines strongly enhanced biocompatibility for the noncancer cell line L929 as well as primary human cells HUVEC on the one hand and selective toxicity for breast cancer cell line MDA-MB-231.

Red blood cells (RBC) aggregates are naturally formed by plasma proteins, which is a reversible process.<sup>[39]</sup> In the presence of various polymers irreversible erythrocyte aggregation can occur due to membrane interactions forming bridges between the polymers and the erythrocytes, which increases the blood viscosity and can be dangerous for vital organs.<sup>[40]</sup> The erythrocyte aggregation caused by polymers **P1**, **P2**, and **P3** was studied using BPEI as positive control (Figure 6A). None of the investigated polymers revealed a membrane perturbing activity up to  $100 \mu\text{g mL}^{-1}$  and therefore no formation of erythrocyte aggregation was observable. The disruption of the RBC membrane and the detection of hemoglobin, another known side effect of cationic polymers, were measured for all investigated polymers (Figure 6B). As a general trend, it was found that cell release of hemoglobin of **P3** was lower when compared to **P1** or **P2** for all measured concentrations ( $100 \mu\text{g mL}^{-1}$ , 2.4%). **P1** and **P2** caused only slight hemolysis (2%–5%) up to  $100 \mu\text{g mL}^{-1}$ . However, **P3** reveals a very high hemocompatibility regarding irreversible RBC aggregation and hemolytic potential. Therefore, it offers outstanding properties for advanced uptake studies.

### 3.4. Characterization of Polyplexes

To investigate the binding of the D-fructose-bearing copolymers with genetic material, pDNA was utilized for model studies. The efficient delivery of nucleic acids into cells comes along with several requirements. Among others, this comprises the condensation of genetic material in a compact mode as well as the dissociation from the vector after it has been transferred into the cellular cytoplasm or nucleus.<sup>[38]</sup>

To investigate the condensation of pDNA with **P1**, **P2**, and **P3**, the EBA was used. For this purpose, the oligonucleotides were preincubated with ethidium bromide (EB) resulting in a fluorescent DNA-EB complex. Subsequently, increasing amounts of polymers were added to form polyplexes at different nitrogen (polymer) to phosphate (DNA) ratios (N/P). It should be noted that the N/P calculations are based on all nitrogens (N) of the polymer, also the ones showing no activity for complex formation (amides in the backbone of, e.g., ButEnOx). The electrostatic and hydrophobic interactions between the polymers and the nucleic acid lead to the displacement of EB and, hence, to a reduction of the fluorescence intensity that correlates with the affinity for complexation.<sup>[41]</sup> The modified polymers (**P2** and **P3**) as well as linear poly(ethylene imine) (**P1**) revealed decreasing fluorescence intensity of ethidium bromide showing an interaction with the DNA (Figure 7A). For **P1**, a stable polyplex formation is observed for N/P ratios between 10 and 40 ( $\approx 25\%$  RFU). The polymers **P2** and **P3** revealed a decreased fluorescence intensity plateau between N/P 15 and 40 (57% RFU at N/P 40). The smaller content of ethylene imine

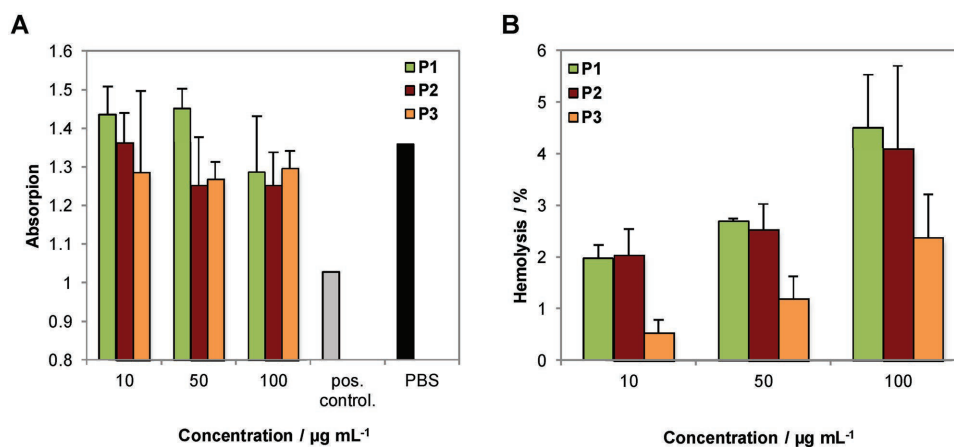


**Figure 6.** A) Erythrocyte aggregation assay of polymers at indicated concentrations. BPEI served as positive control and PBS as negative control. B) Hemolysis assay of erythrocytes after incubation with polymers at indicated concentrations. Triton X-100 served as positive control (100% hemolysis) and PBS as negative control (1.99%). A value less than 2% hemolysis rate is classified as nonhemolytic, 2%–5% as slightly hemolytic and >5% as hemolytic. Values represent the mean  $\pm$  SD ( $n = 3$ ).

units (73%) combined with steric challenging side chains (ButEnOx) that hinders a tight attachment to the DNA might be reasons for the higher fluorescence level. However, polymers **P2** and **P3** were able to form polyplexes by complexation with pDNA, as this RFU was also reported for other transfection polymers.<sup>[42]</sup>

The heparin dissociation assay was used to analyze the formed polyplexes concerning DNA release. Heparin is a sulfated glycosaminoglycan with multiple negative charges in the polymer chain, which competes with the nucleic acid of the polyplex. Increasing amounts of heparin displace the pDNA of the polyplexes. Ethidium bromide is added (in the same concentration as for the EBA)

and intercalates into the free pDNA again. As the result, an increase of fluorescence intensity can be observed (Figure 7B). For **P2** and **P3**, the pDNA was released rapidly to nearly 100% (10 U mL<sup>-1</sup> heparin) whereas **P1** required increased amounts of anionic competitor (40 U mL<sup>-1</sup> heparin) for a full dissociation, indicating a less pronounced releasing profile. This correlates well with the data determined by the EBA (Figure 7A).

The size of the polyplexes is of crucial importance since they are usually internalized into cells via endocytic pathways. In literature, critical sizes of polymeric nanocarriers up to a maximum of 200 nm are recommended for efficient delivery.<sup>[43]</sup> As depicted in Table 2, all polyplexes

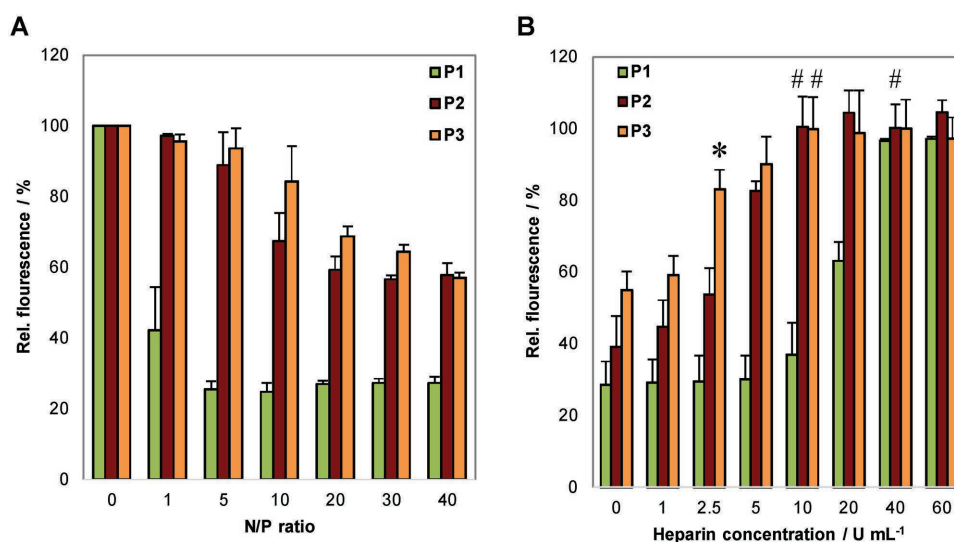


**Figure 7.** Polyplex formation and stability with plasmid DNA using the polymers **P1**, **P2**, and **P3**. A) Affinity of complexation of respective polymers at indicated N/P ratios (ethidium bromide quenching assay). B) Dissociation assay of polyplexes formed at N/P 20 using heparin (0–60 U mL<sup>-1</sup>). Values represent the mean  $\pm$  SD ( $n = 3$ ); \* represents a significant ( $p < 0.01$ ) difference between **P2** and **P3**; # indicates no significant difference ( $p < 0.05$ ) to 100% relative fluorescence.

**Table 2.** Size and zeta potential of pDNA polyplexes of **P1–P3** at N/P 20 in HBG buffer measured by dynamic and electrophoretic light scattering.

Polymeric system	z-Average [d nm <sup>-1</sup> ]	PDI	Number-weighted size [d nm <sup>-1</sup> ]	Zeta potential [mV]
<b>P1</b>	217 ± 8	0.47	71 ± 13	24.0 ± 0.4
<b>P2</b>	264 ± 11	0.35	109 ± 33	24.3 ± 1.1
<b>P3</b>	165 ± 1	0.26	83 ± 29	17.6 ± 0.4

are in the nanometer scale with a positive zeta potential; the polyplexes formed of **P1**, **P2**, and **P3** revealed favorable sizes smaller than 200 nm. The slightly increased sizes of the polyplexes formed with the modified polymers **P2** and **P3** can be explained by the introduction of polymeric side chains with bulky groups not interacting with the genetic material. These results show the complexation of large pDNA molecules (300–400 nm pure pDNA) into compact polyplex structures, a central prerequisite for gene delivery.

### 3.5. Cell-Type-Dependent Uptake Efficiency

Beside complexation and protection of the genetic material, one major challenge is the cellular uptake of the polyplexes. For nontargeted cationic polyplexes, internalization into cells by endocytosis, followed by the endosomal release of the pDNA into the cytosol, is reported.<sup>[44]</sup> The functionalization of cationic polymers with targeting units such as D-fructose can change the interaction with cells depending on the interaction with cell type specific receptors. This interaction as well as usually fast and specific internalization of polyplexes can be visualized and quantified by microscopy as well as flow cytometry,

respectively. For this purpose, pDNA was preincubated with YOYO-1, a DNA specific dye with high fluorescence intensity once intercalated with no displacement during polyplex formation. The cellular uptake into noncancerous L929 as well as HUVEC and breast cancer MDA-MB-231 cells after 1 h (a time point at which no cytotoxicity had been observed) at different concentrations measured by flow cytometry is depicted in Figure 8. **P1** showed a strong uptake in all tested cell types indicating no cell specificity. At N/P 10, **P2** and **P3** revealed no uptake in all three cell lines. **P2** polyplexes at N/P 20 can be detected in MDA-MB-231 and HUVEC cells, higher N/P values induce pDNA uptake in all tested cells. **P3** polyplexes were only detectable in MDA-MB-231 cells at N/P value 20. At N/P 50 the amount of pDNA is even increased compared to **P1** in MDA-MB-231 cells. In contrast to this, the uptake of genetic material into the control cells is reduced. These results indicate a positive influence of D-fructose units toward cell specific uptake of polyplexes into breast cancer cells. Non-cancerous L929 and HUVEC cells efficiently take up polyplexes formed with **P1** and **P2**, but less efficient with **P3**. In contrast, D-fructose targeted **P3** enables the uptake of pDNA polyplexes at N/P ratio of 50 into MDA-MB-231 cells in a concentration-dependent manner.

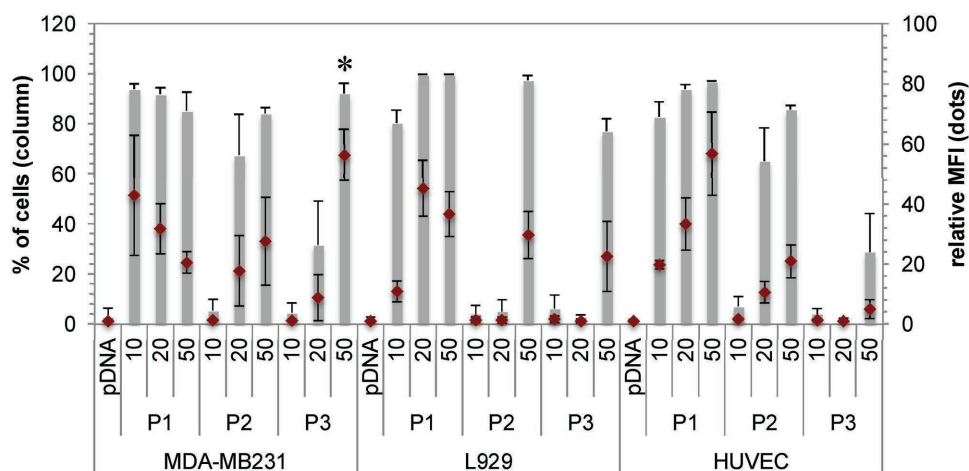


**Figure 8.** Uptake study. Polyplexes formed with YOYO-1 labeled pDNA were incubated with L929, HUVEC, and MDA-MB-231 cells in OptiMEM for 1 h with the polyplexes of the copolymers **P1–P3** at indicated N/P ratios. The amount of cells (%), which have taken up pDNA polyplexes relative, as well as the mean fluorescence intensity (MFI) of all viable cells compared to pDNA control without polymers were depicted. Values represent the mean ± SD ( $n \geq 3$ ); \* represents statistical significant difference in MFI to **P3** N/P 50 of L929 and HUVEC, ANOVA,  $p$ -value < 0.01.

To support these findings and to rule out that polyplexes sticking to the cell membrane influence the data from flow cytometry, the uptake of polyplexes with labeled polymers was visualized by live cell confocal laser scanning microscopy (CLSM) (Figure 9). To further investigate cell morphologies, also transmitted light and nuclei staining (Hoechst 33342, blue) was plotted. It can be clearly observed that all cells have taken up polyplexes/polymers, which supports the results of the flow cytometry. Furthermore, some aggregates can be detected in case of **P2** in all cell lines, but to a higher extent in MDA-MB-231. **P3** is also taken up by all investigated cell lines, but the intensity is considerably higher in MDA-MB-231 cells, further supporting the results obtained by flow cytometry.

### 3.6. Transfection Efficiency

To investigate, whether an increased cell-specific uptake of genetic material results in enhanced transfection efficiency, the delivery and expression of a protein coded on a plasmid DNA was tested (Figure 10). Interestingly, 20%–30% of cells were expressing EGFP if **P1** polyplexes were used, but over 40% were reached in the case of **P2** polyplexes (as it can be found in literature)<sup>[45]</sup> and only 1% for **P3** polyplexes. Even an increase in the N/P value did not result in an increased transfection efficiency of **P3**. The same trend **P2** > **P1** > **P3** could be observed, if the amount of EGFP is considered (mean fluorescence intensity, MFI).

This indicates that **P3** has to be further optimized not just only to deliver genetic material but also to transfect the targeted cells.

Transfection efficiency is the result of some more events than just successful uptake. Besides the uptake, the endosomal release of the polyplexes usually mediated by the proton sponge effect represents another important parameter. In our case, the latter step might be hindered by the amount of coupled fructose residues. Even if the transfection investigations for **P3** failed, the described modification of cationic polymers can be used to further develop the concept of D-fructose conjugated cationic polymers. Potential approaches for future research to increase the transfection efficiencies are the synthesis of different polymer compositions varying the ethylene imine/sugar ratio and, additionally, the introduction of amino functionalities to the side chains (analog to Ref.<sup>[38]</sup>).

## 4. Conclusions

A novel thiol-functionalized D-fructose derivative **5** was synthesized starting from commercially available protected D-fructose **1** in a four-step synthesis. Thiol-ene photoaddition of **5** to double bond containing copolymer P(EI-stat-ButEnOx) **P2** resulted in the isopropylidene bearing D-fructose conjugated polymer **iso-P3**. Deprotection under acidic conditions led to water soluble polymer

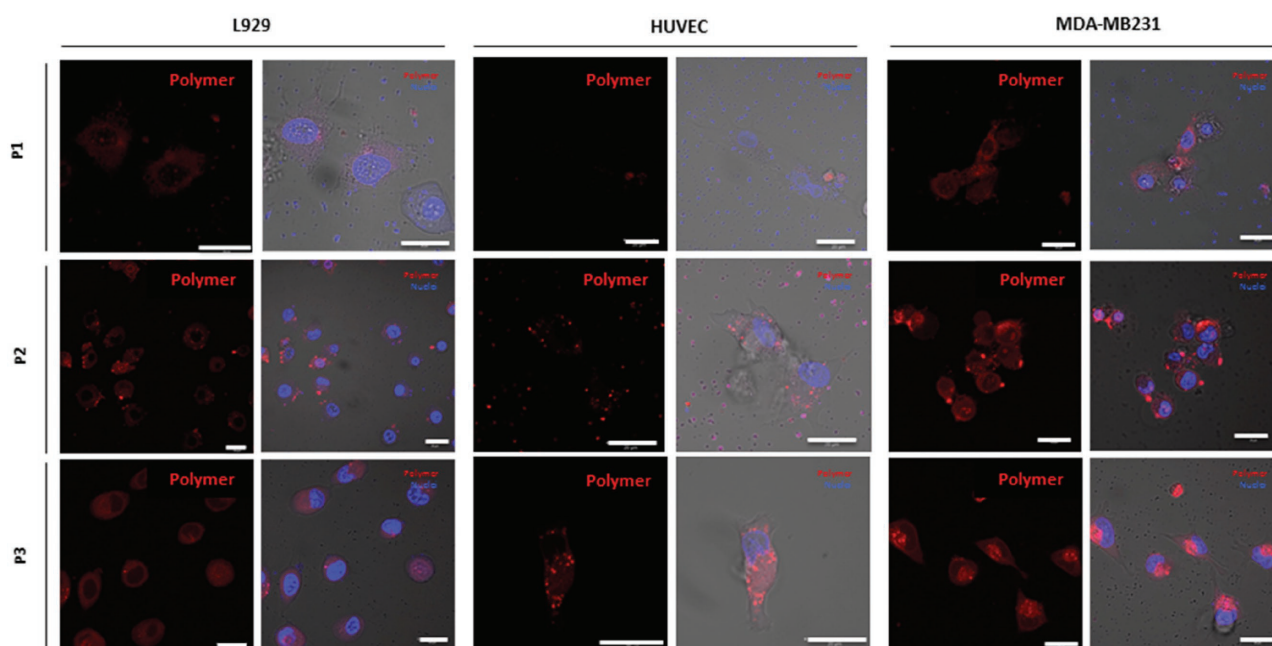


**Figure 9.** Live cell uptake studies. Polyplexes formed at N/P 50 with labeled polymers (red) **P1-Cy5**, **P2-Rho**, and **P3-Rho** were added to L929, HUVEC, and MDA-MB-231 cells. The cells were analyzed after 1 h via confocal laser scanning microscopy (CLSM) using the same laser settings for each cell line. The cell nucleus was stained with Hoechst 33342 (blue). Scale bar: 20  $\mu\text{m}$ .



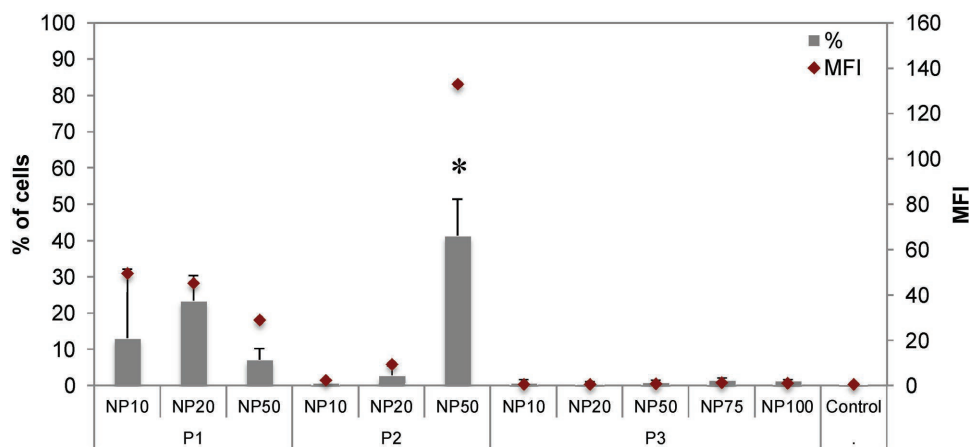


**Figure 10.** Transfection efficiency measured by the expression of EGFP. Polyplexes formed at N/P 50 with indicated polymers **P1–P3** at increasing N/P values. The amount (%) and the mean fluorescence intensity (MFI) of viable cells expressing EGFP were plotted. \* indicates significant difference ( $p < 0.05$ ) to amount of EGFP positive cells observed with **P1**.

**P3.** To evaluate GLUT5 targeting of D-fructose conjugated polymer **P3** in comparison to sugar-free polymers **P1** and **P2** cytotoxicity, uptake and transfection studies were performed. Cytotoxicity assays of **P3** revealed almost no toxicity against fibroblast cells (L929) as well as human primary HUVEC cells in the tested concentration range (up to  $500 \mu\text{g mL}^{-1}$ ), but a very pronounced cytotoxicity for breast cancer cells (MDA-MB-231). Furthermore, no irreversible RBC aggregation and a low hemolytic potential was observed for **P3**. Condensation experiments with pDNA exhibited stable polyplexes of **P3** at an N/P ratio  $> 15$ . When treated with anionic competitor heparin ( $10 \text{ U mL}^{-1}$ ), polyplexes of **P3** offered a rapid release of pDNA to nearly 100%. Additionally, the polymers were labeled with dyes to obtain **P1-Cy5**, **P2-Rho**, and **P3-Rho**. After the formation of labeled polyplexes, the cell-type-dependent uptake via flow cytometry and live cell CLSM was investigated. At N/P 50, MFI for **P3** was low in L929 or HUVEC and high for MDA-MB-231 cell line, whereas **P1** and **P2** revealed a reverse trend. Results of live cell imaging are in accordance with the results from flow cytometry, indicating cell-type-dependent interaction of D-fructose conjugated polymer **P3**. These findings might be attributed to D-fructose conjugation and therefore to GLUT5 mediated transport into cells.

The determination of the transfection efficiencies revealed unexpected low EGFP expressions, in particular for **P3**. The modification of LPEI only represents one example to install D-fructose on a cationic polymer. To achieve appropriate transfection efficiencies it is necessary to investigate the influence of different polymer compositions comprising varying ethylene imine and D-fructose contents. Further approaches comprise the introduction of different cationic functionalities in the side chains of various polymer classes.

**Acknowledgements:** C.E. and M.P. contributed equally to this work. The authors would like to thank Matthias Hartlieb for synthesis of poly(2-ethyl-2-oxazoline). This project was funded by the Thüringer Ministerium für Wirtschaft, Wissenschaft, und Digitale Gesellschaft (TMWWDG, ProExzellenzII, NanoPolar). The funding of the collaborative research center ChemBioSys (SFB 1127) by the Deutsche Forschungsgemeinschaft (DFG) is highly acknowledged. A.T. is grateful for the financial support from Carl Zeiss Stiftung and M.G. is grateful for the funding by the DFG (GO 1100/4-1). The LSM880 ELYRA PS.1 was further funded with a grant from the DFG. The authors also would like to thank Alexander S. Mosig for providing HUVEC cells. Primary cell donors were informed about the aim of the study and gave written informed consent. The study and experimental protocols used therein were approved by the ethics committee of the Jena University Hospital (assigned study number 3939-12/13).

Received: November 29, 2016; Revised: February 3, 2017;  
Published online: ; DOI: 10.1002/mabi.201600502

**Keywords:** cell-type specific uptake; D-fructose, poly(ethylene imine); nonviral gene delivery; triple-negative MDA-MB-231 breast cancer

- [1] R. L. Siegel, K. D. Miller, A. Jemal, *Ca-Cancer J. Clin.* **2015**, *65*, 5.
- [2] B. Weigelt, J. S. Reis-Filho, *Nat. Rev. Clin. Oncol.* **2009**, *6*, 718.
- [3] R. Chacon, M. Costanzo, *Breast Cancer Res.* **2010**, *12*, S3.
- [4] a) J. S. Ross, J. A. Fletcher, K. J. Bloom, G. P. Linette, J. Stec, W. F. Symmans, L. Pusztai, G. N. Hortobagyi, *Mol. Cell. Proteomics* **2004**, *3*, 379; b) F. Tomao, A. Papa, E. Zaccarelli, L. Rossi, D. Caruso, M. Minozzi, P. Vici, L. Frati, S. Tomao, *OncoTargets Ther.* **2015**, *8*, 177.
- [5] D. Gholam, A. Chebib, D. Hauteville, M. P. Bralet, C. Jasmin, *Anticancer Drugs* **2007**, *18*, 835.
- [6] R. S. Finn, J. Dering, C. Ginther, C. A. Wilson, P. Glaspy, N. Tchekmedyian, D. J. Slamon, *Breast Cancer Res. Treat.* **2007**, *105*, 319.

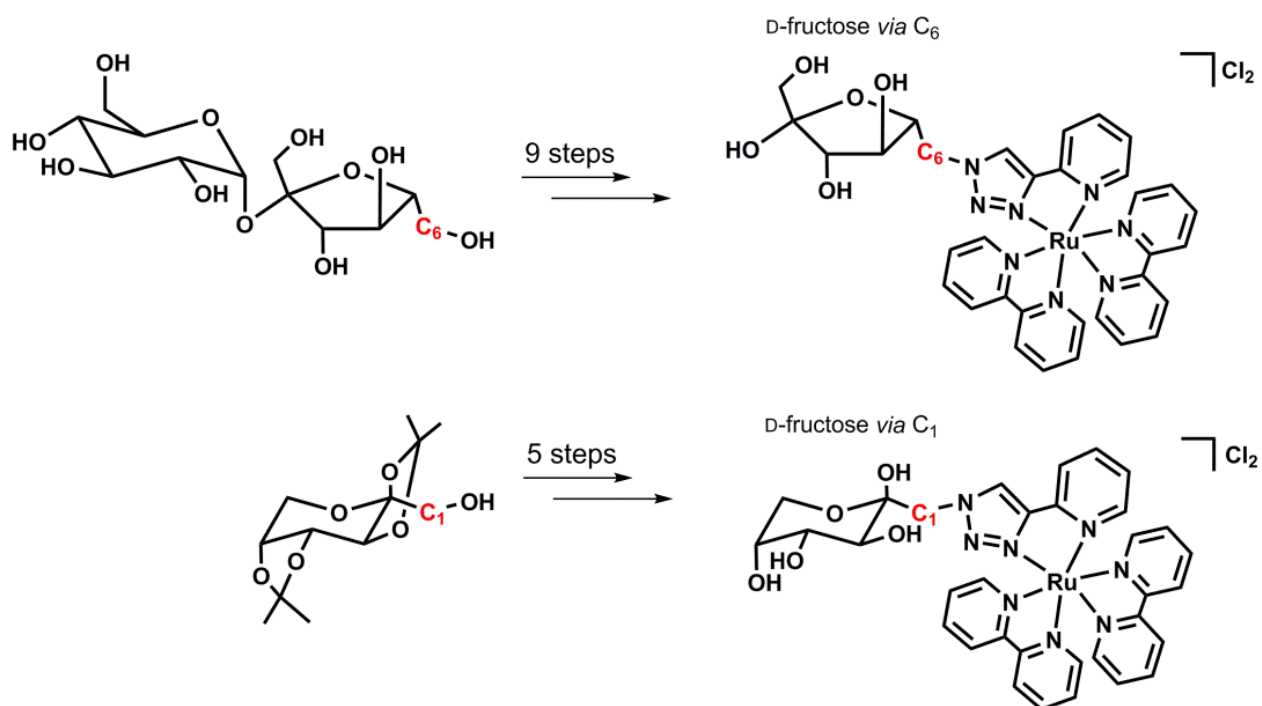
- [7] E. Caldas-Lopes, L. Cerchietti, J. H. Ahn, C. C. Clement, A. I. Robles, A. Rodina, K. Moullick, T. Taldone, A. Gozman, Y. Guo, N. Wu, E. de Stanchina, J. White, S. S. Gross, Y. Ma, L. Varticovski, A. Melnick, G. Chiosis, *Proc. Natl. Acad. Sci. USA* **2009**, *106*, 8368.
- [8] K. Miyamoto, S. Tatsumi, A. Morimoto, H. Minami, H. Yamamoto, K. Sone, Y. Taketani, Y. Nakabou, T. Oka, E. Takeda, *Biochem. J.* **1994**, *303*, 877.
- [9] G. Gowrishankar, S. Zitzmann-Kolbe, A. Junutula, R. Reeves, J. Levi, A. Srinivasan, K. Bruus-Jensen, J. Cyr, L. Dinkelborg, S. S. Gambhir, *PLoS One* **2011**, *6*, e26902.
- [10] A. Godoy, V. Ulloa, F. Rodríguez, K. Reinicke, A. J. Yañez, M. L. García, R. A. Medina, M. Carrasco, S. Barberis, T. Castro, F. Martínez, X. Koch, J. C. Vera, M. T. Poblete, C. D. Figueroa, B. Peruzzo, F. Pérez, F. Nualart, *J. Cell. Physiol.* **2006**, *207*, 614.
- [11] K. K. Chan, J. Y. W. Chan, K. K. W. Chung, K.-P. Fung, *J. Cell. Biochem.* **2004**, *93*, 1134.
- [12] a) A. Tatibouët, J. Yang, C. Morin, G. D. Holman, *Bioorg. Med. Chem.* **2000**, *8*, 1825; b) J. Yang, J. Dowden, A. Tatibouët, Y. Hatanaka, G. D. Holman, *Biochem. J.* **2002**, *367*, 533.
- [13] J. Levi, Z. Cheng, O. Gheysens, M. Patel, C. T. Chan, Y. Wang, M. Namavari, S. S. Gambhir, *Bioconjugate Chem.* **2007**, *18*, 628.
- [14] a) K. K.-W. Lo, W. H.-T. Law, J. C.-Y. Chan, H.-W. Liu, K. Y. Zhang, *Metallomics* **2013**, *5*, 808; b) K. Y. Zhang, K. K.-S. Tso, M.-W. Louie, H.-W. Liu, K. K.-W. Lo, *Organometallics* **2013**, *32*, 5098; c) M. Pröhl, T. Bus, J. A. Czaplewski, A. Traeger, M. Deicke, H. Weiss, W. Weigand, U. S. Schubert, M. Gottschaldt, *Eur. J. Inorg. Chem.* **2016**, *2016*, 5197.
- [15] a) C. von der Ehe, A. Rinkenauer, C. Weber, D. Szamosvari, M. Gottschaldt, U. S. Schubert, *Macromol. Biosci.* **2016**, *16*, 508; b) A. Abdolmaleki, S. Mallakpour, M. Rostami, *High Perform. Polym.* **2015**, *27*, 903; c) S. Ganda, Y. Jiang, D. S. Thomas, J. Eliezar, M. H. Stenzel, *Macromolecules* **2016**, *49*, 4136; d) A. Dag, M. Callari, H. Lu, M. H. Stenzel, *Polym. Chem.* **2016**, *7*, 1031; e) J. Zhao, H. Lu, P. Xiao, M. H. Stenzel, *ACS Appl. Mater. Interfaces* **2016**, *8*, 16622; f) J. Zhao, H. Lai, H. Lu, C. Barner-Kowollik, M. H. Stenzel, P. Xiao, *Biomacromolecules* **2016**, *17*, 2946.
- [16] J. Zhao, K. Babiuch, H. Lu, A. Dag, M. Gottschaldt, M. H. Stenzel, *Chem. Commun.* **2014**, *50*, 15928.
- [17] N. Unnamalai, B. G. Kang, W. S. Lee, *FEBS Lett.* **2004**, *566*, 307.
- [18] E. Song, P. Zhu, S.-K. Lee, D. Chowdhury, S. Kussman, D. M. Dykxhoorn, Y. Feng, D. Palliser, D. B. Weiner, P. Shankar, W. A. Marasco, J. Lieberman, *Nat. Biotechnol.* **2005**, *23*, 709.
- [19] J. Halder, A. A. Kamat, C. N. Landen, L. Y. Han, S. K. Lutgendorf, Y. G. Lin, W. M. Merritt, N. B. Jennings, A. Chavez-Reyes, R. L. Coleman, D. M. Gershenson, R. Schmandt, S. W. Cole, G. Lopez-Berestein, A. K. Sood, *Clin. Cancer Res.* **2006**, *12*, 4916.
- [20] J. Wang, Z. Lu, M. G. Wientjes, J. L.-S. Au, *AAPS J.* **2010**, *12*, 492.
- [21] O. Boussif, F. Lezoualch, M. A. Zanta, M. D. Mergny, D. Scherman, B. Demeneix, J.-P. Behr, *Proc. Natl. Acad. Sci. USA* **1995**, *92*, 7297.
- [22] a) J. H. Jeong, S. H. Song, D. W. Lim, H. Lee, T. G. Park, *J. Controlled Release* **2001**, *73*, 391; b) Y. Yue, F. Jin, R. Deng, J. Cai, Z. Dai, M. C. M. Lin, H.-F. Kung, M. A. Matthebjerg, T. L. Andresen, C. Wu, *J. Controlled Release* **2011**, *152*, 143.
- [23] C. Englert, M. Hartlieb, P. Bellstedt, K. Kempe, C. Yang, S. K. Chu, X. Ke, J. M. García, R. J. Ono, M. Fevre, R. J. Wojtecki, U. S. Schubert, Y. Y. Yang, J. L. Hedrick, *Macromolecules* **2015**, *48*, 7420.
- [24] a) K. Kunath, A. von Harpe, D. Fischer, T. Kissel, *J. Controlled Release* **2003**, *88*, 159; b) D. Appelhans, H. Komber, M. A. Quadir, S. Richter, S. Schwarz, J. van der Vlist, A. Aigner, M. Müller, K. Loos, J. Seidel, K.-F. Arndt, R. Haag, B. Voit, *Biomacromolecules* **2009**, *10*, 1114; c) W. Cheng, C. Yang, J. L. Hedrick, D. F. Williams, Y. Y. Yang, P. G. Ashton-Rickardt, *Biomaterials* **2013**, *34*, 3697; d) C. Englert, M. Fevre, R. J. Wojtecki, W. Cheng, Q. Xu, C. Yang, X. Ke, M. Hartlieb, K. Kempe, J. M. García, R. J. Ono, U. S. Schubert, Y. Y. Yang, J. L. Hedrick, *Polym. Chem.* **2016**, *7*, 5862.
- [25] M. Ogris, S. Brunner, S. Schuller, R. Kirchheis, E. Wagner, *Gene Ther.* **1999**, *6*, 595.
- [26] S. Slavin, J. Burns, D. M. Haddleton, C. R. Becer, *Eur. Polym. J.* **2011**, *47*, 435.
- [27] A. Gress, A. Völkel, H. Schlaad, *Macromolecules* **2007**, *40*, 7928.
- [28] G. Adiwidjaja, J.-S. Brunck, K. Polchow, J. Voss, *Carbohydr. Res.* **2000**, *325*, 237.
- [29] B. D. Johnston, B. M. Pinto, *J. Org. Chem.* **2000**, *65*, 4607.
- [30] M. Bauer, C. Lautenschlaeger, K. Kempe, L. Tauhardt, U. S. Schubert, D. Fischer, *Macromol. Biosci.* **2012**, *12*, 986.
- [31] J. C. Fernandes, X. Qiu, F. M. Winnik, M. Benderdour, X. Zhang, K. Dai, Q. Shi, *Int. J. Nanomed.* **2013**, *8*, 4091.
- [32] T. J. Dickerson, N. Yamamoto, D. I. Ruiz, K. D. Janda, *J. Am. Chem. Soc.* **2004**, *126*, 11446.
- [33] H. C. Kolb, M. G. Finn, K. B. Sharpless, *Angew. Chem., Int. Ed. Engl.* **2001**, *40*, 2004.
- [34] C. von der Ehe, A. Rinkenauer, C. Weber, D. Szamosvari, M. Gottschaldt, U. S. Schubert, *Macromol. Biosci.* **2016**, *16*, 508.
- [35] H. M. L. Lambermont-Thijs, F. S. van der Woerd, A. Baumgaertel, L. Bonami, F. E. Du Prez, U. S. Schubert, R. Hoogenboom, *Macromolecules* **2010**, *43*, 927.
- [36] C. Englert, L. Tauhardt, M. Hartlieb, K. Kempe, M. Gottschaldt, U. S. Schubert, *Biomacromolecules* **2014**, *15*, 1124.
- [37] S. Ferrari, A. Pettenazzo, N. Garbati, F. Zacchello, J. P. Behr, M. Scarpa, *Biochim. Biophys. Acta, Gene Struct. Expression* **1999**, *1447*, 219.
- [38] T. Bus, C. Englert, M. Reifarh, P. Borchers, M. Hartlieb, A. Vollrath, S. Hoepfner, A. Traeger, U. S. Schubert, *J. Mater. Chem. B* **2017**, *5*, 1258.
- [39] M. I. Ul-Haq, B. F. L. Lai, R. Chapanian, J. N. Kizhakkedathu, *Biomaterials* **2012**, *33*, 9135.
- [40] M. Jawanda, B. F. L. Lai, J. N. Kizhakkedathu, K. Ishihara, R. Narain, *Polym. Chem.* **2013**, *4*, 3140.
- [41] a) J. B. Lepecq, C. Paoletti, *J. Mol. Biol.* **1967**, *27*, 87; b) A. J. Geall, I. S. Blagbrough, *J. Pharm. Biomed. Anal.* **2000**, *22*, 849.
- [42] A. C. Rinkenauer, L. Tauhardt, F. Wendler, K. Kempe, M. Gottschaldt, A. Traeger, U. S. Schubert, *Macromol. Biosci.* **2015**, *15*, 414.
- [43] a) R. Luxenhofer, G. Sahay, A. Schulz, D. Alakhova, T. K. Bronich, R. Jordan, A. V. Kabanov, *J. Controlled Release* **2011**, *153*, 73; b) J. Rejman, V. Oberle, I. S. Zuhorn, D. Hoekstra, *Biochem. J.* **2004**, *377*, 159.
- [44] a) A. C. Rinkenauer, S. Schubert, A. Traeger, U. S. Schubert, *J. Mater. Chem. B* **2015**, *3*, 7477; b) U. Lächelt, E. Wagner, *Chem. Rev.* **2015**, *115*, 11043.
- [45] C. Englert, A.-K. Trützschler, M. Raasch, T. Bus, P. Borchers, A. S. Mosig, A. Traeger, U. S. Schubert, *J. Controlled Release* **2016**, *241*, 1.

## Publication 4

### Synthesis of D-fructose conjugated ligands *via* C<sub>6</sub> and C<sub>1</sub> and their corresponding [Ru(bpy)<sub>2</sub>(L)]Cl<sub>2</sub> complexes

M. Pröhl, P. D. Moser, J. A. Czaplewska, P. Hoffmann, T. Bus, A. Traeger,  
H. Görls, U. S. Schubert, M. Gottschaldt

*Carbohydr. Res.* **2017**, 446-447, 19-27





# Synthesis of D-fructose conjugated ligands *via* C6 and C1 and their corresponding [Ru(bpy)<sub>2</sub>(L)]Cl<sub>2</sub> complexes

Michael Pröhl<sup>a, b</sup>, Pascal D. Moser<sup>a, b</sup>, Justyna A. Czaplewska<sup>a, b</sup>, Patrick Hoffmann<sup>a, b</sup>,  
Tanja Buš<sup>a, b</sup>, Anja Traeger<sup>a, b</sup>, Helmar Goerls<sup>c</sup>, Ulrich S. Schubert<sup>a, b</sup>,  
Michael Gottschaldt<sup>a, b, \*</sup>

<sup>a</sup> Laboratory of Organic and Macromolecular Chemistry (IOMC), Friedrich Schiller University Jena, Humboldtstraße 10, 07743 Jena, Germany

<sup>b</sup> Jena Center for Soft Matter (JCSM), Friedrich Schiller University Jena, Philosophenweg 7, 07743 Jena, Germany

<sup>c</sup> Institute for Inorganic and Analytical Chemistry, Friedrich Schiller University Jena, Humboldtstraße 8, 07743 Jena, Germany

## ARTICLE INFO

### Article history:

Received 13 February 2017

Received in revised form

24 April 2017

Accepted 24 April 2017

Available online 27 April 2017

### Keywords:

D-fructose

Sucrose

Carbohydrates

Metal complexes

Click chemistry

## ABSTRACT

A pyridyl triazole (pyta) modified sucrose ligand was prepared in a seven step synthesis using D-glucose as the protection group for D-fructose and starting from commercially available sucrose. After complexation with Ru(bpy)<sub>2</sub>Cl<sub>2</sub> precursor, the sucrose-conjugated Ru complex of the general formula [Ru(bpy)<sub>2</sub>(L)]Cl<sub>2</sub> was formed. Acidic cleavage of the D-glucose unit led to the first D-fructose conjugated metal complex *via* D-fructose C6 in literature. Additionally, pyta-modified D-fructose *via* C1 and the corresponding Ru complex were synthesized. All compounds were analyzed by R<sub>f</sub> values, specific rotation, NMR, IR, UV/Vis and fluorescence spectroscopy, mass spectrometry and elemental analysis.

© 2017 Elsevier Ltd. All rights reserved.

## 1. Introduction

The attachment of carbohydrates represents a strategy to enhance the hydrophilicity and selectivity of the corresponding metal complexes due to their interaction with various biological structures [1]. Among a diversity of sugars, which are extensively used for biomedical applications, D-fructose gained interest for the targeting of the GLUT5 receptor. In general, carbohydrates are entering into the cells by highly selective transport proteins (GLUTs) [2]. Among the thirteen known saccharide transporters, GLUT5 is specific for D-fructose and its structure was confirmed recently [3]. The incidence of GLUT5 is controversially discussed in literature. Next to the existence in the kidney, colon and adrenal cells, it is supposed to be overexpressed in more than 85% of 33 tested breast cancer cell lines [4], whereas another group claimed there is no GLUT5 overexpression in any breast cancer tissue [5].

Additionally, the GLUT5 receptor might be overexpressed in acute myeloid leukemia cells [6]. Since it is known that structural modifications of the C1 as well as of the C6 position of the D-fructose are tolerated by the GLUT5 transporter [7,8], there is intensive research in chemical modification of D-fructose, the attachment of these derivatives to various structures and in their biological properties. Therefore, nanoparticulate formulations [9,10] as well as dyes [11], micelles [12,13] and polymers [14–16] have been successfully functionalized with D-fructose to address breast cancer cell lines. Also, low molar mass metal complexes conjugated with various D-fructose residues were used to investigate their interactions with the GLUT5 transporter. For instance, Re complexes were functionalized with D-fructose and their phosphorescence was used to show the selective accumulation in breast cancer cell lines MCF-7 and MDA-MB-231 mediated by GLUT5 [17]. A D-fructose conjugated Ir(III) complex exhibited a 3.7 times higher uptake in MCF-7 than in non-cancerous cells. In contrast to that, the D-fructose-free complex did not display any selectivity [18]. Also, the natural compound bisdemethoxycurcumin was successfully labeled with D-fructose by using Cu(I)-catalyzed “click” reaction between azides and alkynes and then complexed to Ru. Incubation of L929, HepG2 and MDA-MB-231 revealed a high biocompatibility of these compounds due

\* Corresponding author. Laboratory of Organic and Macromolecular Chemistry (IOMC), Friedrich Schiller University Jena, Humboldtstraße 10, 07743 Jena, Germany.

E-mail address: [michael.gottschaldt@uni-jena.de](mailto:michael.gottschaldt@uni-jena.de) (M. Gottschaldt).



to the curcumin moiety, but unfortunately, detailed uptake studies were not performed [19].

The importance of the substitution position was shown very recently for a set of D-glucose conjugated platinum complexes. The C2-substituted D-glucose Pt complex showed an enhanced accumulation in various cancer cell lines, whereas the C3-substituted analogue was the least active complex [20]. Since the C1 and the C3 position of D-fructopyranose are easy to address due to commercially available starting materials with protection groups, all presented studies focused on compounds, which were covalently bound to these positions of the D-fructose moiety, whereas modifications of the C6 position of D-fructose are rarely discussed. Sucrose was used as a starting point, since it contains a unit of D-glucose, which is  $\alpha(1-2)$  covalently bound to D-fructofuranose (Fig. 1).

The glycosidically linked D-glucose avoids ring opening reactions of the D-fructofuranose and, therefore, enables the selective modification of the C6'-position of the sucrose molecule. Sucrose is cultivated in sugar beets to produce crystalline sugar [21]. Additionally, it is used for macroporous alumina ceramics [22], dye sensitized solar cells [23] and hollow carbon nanospheres [24]. Due to the renewable and biocompatible properties of sucrose, it was also investigated regarding its use for the synthesis of polymers [25–27], nanoparticles [28] and low molar mass bioactive compounds [29].

The Cu(I)-catalyzed “click” reaction between azides and alkynes provides a very effective tool for the synthesis of five-membered

heterocyclic systems, with good tolerance of other functional groups, simple reaction conditions and a high selectivity [30]. The formation of 1,4-substituted triazoles enables various features like hydrogen bonding and the attendance in dipole-dipole interactions, render them to isosteres of amides, a key structure in biological molecules [31]. Synthetic protocols of carbohydrate chemists can easily introduce azide or alkyne functionalities into sugar residues [32]. The formation of carbohydrate-conjugated triazoles can result in beneficial properties such as anticancerous and antiviral effects as well as in fluorescent glycoprobe for diagnostics [33,34]. Additionally, click reactions with other N-alkynes such as 2-ethynyl pyridine result in potentially bidentate chelators and, therefore, the possibility to form various metal complexes [35,36].

Here we present the synthesis of pyridyl triazole (pyta) conjugated sugars using Cu(I) catalyzed click reactions between azides and alkynes. In particular, the pyta group was introduced to D-fructose via C1 in a four step synthesis and to the C6' position of sucrose (which represents the C6 position of the D-fructofuranose) in a seven step synthesis. The ligands were reacted with Ru(bpy)<sub>2</sub>Cl<sub>2</sub> to form complexes of the general formula [Ru(bpy)<sub>2</sub>(L)]Cl<sub>2</sub> and in the case of sucrose-conjugated Ru complex, the D-glucose unit was cleaved to form the first D-fructose-conjugated complex at C6. The cytotoxicity and uptake of the complexes was evaluated as well.

## 2. Results and discussion

### 2.1. Synthesis and characterization

The aim was the synthesis of novel D-fructose derivatives substituted at C6. For modification of this position of D-fructose, sucrose was chosen as the starting molecule. At first, D-fructose-moiety in sucrose had to be modified selectively at the C6' position (Fig. 2). Starting from acetylated and C6'-tert-butyl-diphenyl-silyl (TBDPS)-protected sucrose **1** [37,38], the silylether was cleaved by a fluoride source. For this, TBAF was used to form a hydroxyl group at C6' to avoid HF or HF-pyridine as cleaving agent [38]. Due to the migration and fluorolysis of the acetyl groups by using only TBAF, acetic acid was added to eliminate these side reactions [39].

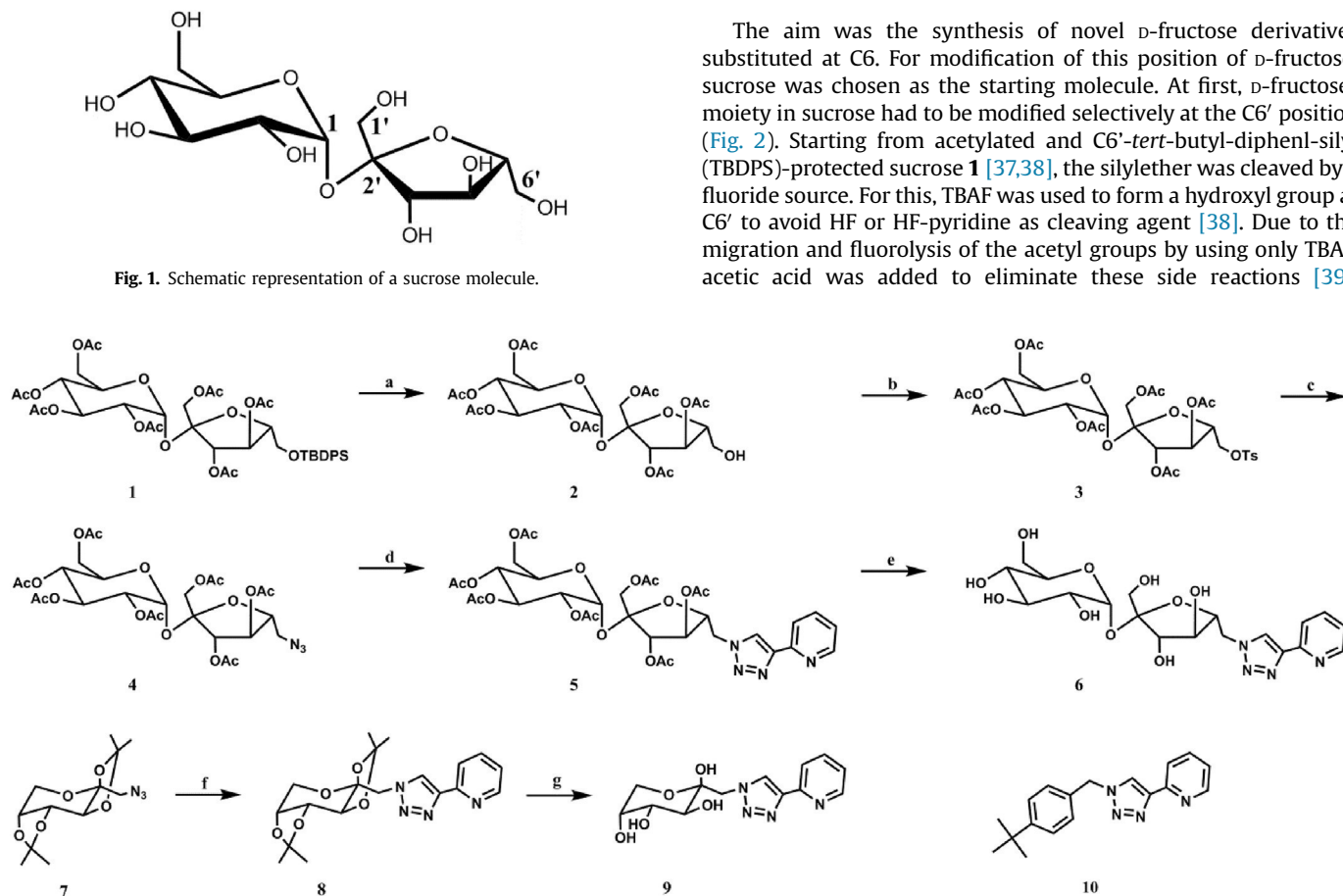


Fig. 1. Schematic representation of a sucrose molecule.

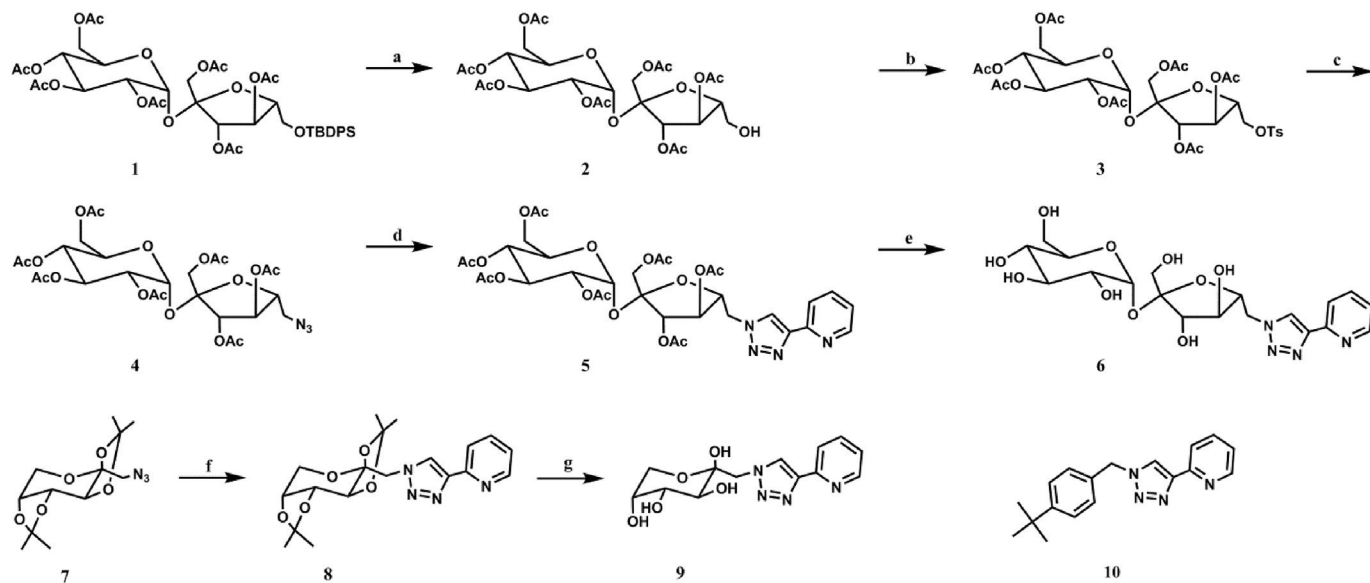
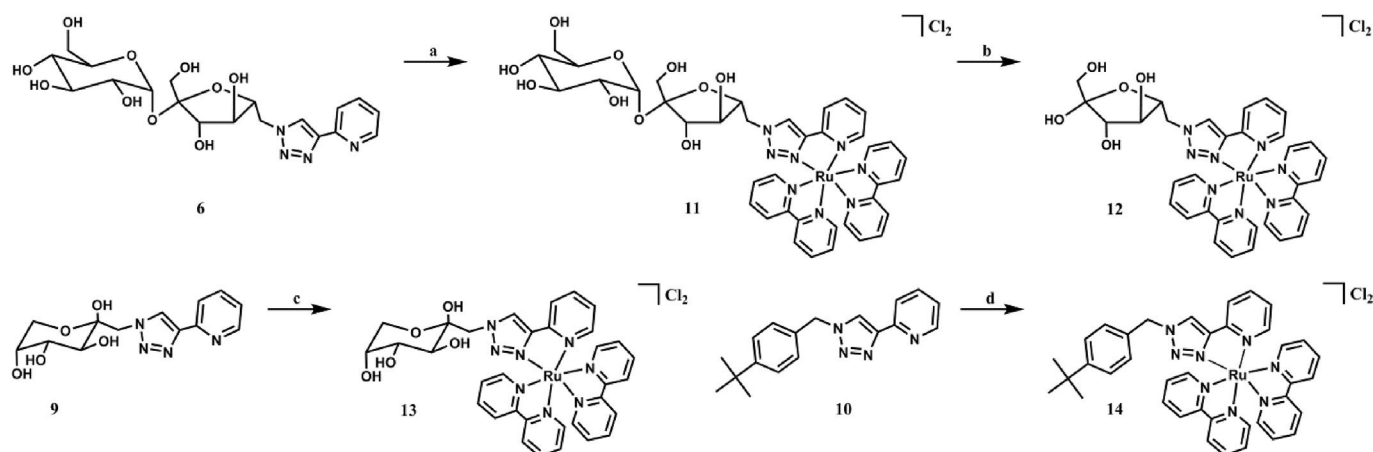


Fig. 2. Schematic representation of the synthesis of the ligands. a) TBAF, CH<sub>3</sub>COOH, DMF/H<sub>2</sub>O, rt, 24 h; b) *p*-toluenesulfonyl chloride, Et<sub>3</sub>N, CH<sub>2</sub>Cl<sub>2</sub>, 0 °C, 2 h; c) NaN<sub>3</sub>, 120 °C, 10 min (mw); d) 2-ethynyl-pyridine, Cu(I)SO<sub>4</sub> × 5H<sub>2</sub>O, sodium ascorbate, *tert*-BuOH/H<sub>2</sub>O, 60 °C, 25 min (mw); e) 1. NaOMe, CH<sub>3</sub>OH, rt, 24 h, 2. DOWEX H<sup>+</sup> to pH = 7; f) 2-ethynyl-pyridine, Cu(II)SO<sub>4</sub> × 5H<sub>2</sub>O, sodium ascorbate, THF/H<sub>2</sub>O, 60 °C, 2 d; g) 2 M HCl, EtOH/H<sub>2</sub>O, 1. 40 °C 12 h, 2. rt, 24 h.



**Fig. 3.** Schematic representation of the complex syntheses. a)  $\text{Ru}(\text{bpy})_2\text{Cl}_2$ ,  $\text{Et}_3\text{N}$ ,  $\text{CH}_3\text{OH}$ ,  $60^\circ\text{C}$ , 12 h; b) 2 M  $\text{HCl}$ ,  $\text{H}_2\text{O}$ ,  $40^\circ\text{C}$ , 16 h; c)  $\text{Ru}(\text{bpy})_2\text{Cl}_2$ ,  $\text{DMF}$ ,  $125^\circ\text{C}$ , 2 h (mw); d)  $\text{Ru}(\text{bpy})_2\text{Cl}_2$ ,  $\text{CH}_3\text{OH}$ ,  $60^\circ\text{C}$ , 12 h.

Following this procedure, the desired product **2** was obtained in moderate yield (66%). Success of the reaction is shown by the disappearance of the *tert*-butyl ( $\delta = 1.07$  ppm) and the aromatic signals ( $\delta = 7.30\text{--}7.78$  ppm) in the  $^1\text{H}$  NMR spectrum as well as by the appearance of  $[\text{M}+\text{Na}]^+$  peak in the mass spectrum and the crystal structure (SI, Figs. S1 and S3). Reaction of mesylated sucrose derivative [38] with  $\text{NaN}_3$  in  $\text{DMF}$  at  $80^\circ\text{C}$  did not result in the desired product. Due to long reaction time, poor yield and partial cleavage of protection groups, when applying  $80^\circ\text{C}$  in  $\text{DMF}$ , the route for the synthesis of  $\text{N}_3$ -functionalized sucrose was changed. Tosyl chloride was chosen to form tosylated sucrose derivative **3** in quantitative yield. Appearance of signals in the  $^1\text{H}$  NMR at  $\delta = 2.46$  ppm ( $\text{CH}_3$ ) and  $\delta = 7.36\text{--}7.8$  ppm (phenyl moiety) as well as the  $[\text{M}+\text{Na}]^+$  signal in HR-MS (error: 3.4 ppm) proved the successful introduction of the tosyl group (SI, Figs. S6 and S8). Reaction with an excess of sodium azide led to  $\text{N}_3$ -functionalized sucrose derivative **4** in quantitative yield. Disappearance of four tosyl-related peaks in the  $^{13}\text{C}$  NMR ( $\delta = 128\text{--}146$  ppm and  $\delta = 21.66$  ppm) proved success of the reaction (SI, Fig. S12).  $\text{Cu}(\text{I})$ -catalyzed “click” reaction between sucrose-azide and 2-ethynylpyridine resulted in the sucrose derivative **5** with pyridyl triazole (pyta) functionality. Like for previously reported procedures [38], microwave irradiation of a mixture of *tert*-butanol and water as solvent and  $\text{Cu}(\text{II})\text{SO}_4 \times 5\text{H}_2\text{O}$  and sodium ascorbate as catalyst forming pair offers a fast and easy approach for the synthesis. Triazole proton signal detected in  $^1\text{H}$  NMR spectrum at  $\delta = 8.26$  ppm as well as  $[\text{M}+\text{Na}]^+$  signal in HR-MS (error: 0.3 ppm) confirms the structure of **5** (SI, Figs. S15 and S17). Standard deprotection procedure with  $\text{NaOMe}$  in methanol resulted in water soluble pyta-functionalized sucrose **6** in quantitative yield. Cleavage of the acetyl groups was proven by the disappearing of the signals in  $^1\text{H}$  NMR ( $\delta = 2.01\text{--}2.18$  ppm) and  $^{13}\text{C}$  NMR spectra ( $\delta = 20.48\text{--}20.67$  ppm). Furthermore, the structure of the ligand was confirmed by the  $[\text{M}+\text{Na}]^+$  peak in HR-MS with an error of 4.0 ppm (SI, Figs. S20–S22). To cleave off the  $\text{D}$ -glucose, compound **6** was stirred with 2M  $\text{HCl}$  at  $40^\circ\text{C}$  in water for 12 h. Unfortunately, in this way only products of decomposition were observed. The alternative synthesis strategy was the cleavage of the  $\text{D}$ -glucose after conjugation to the Ru complex (Fig. 3).

The synthesis of pyta-functionalized  $\text{D}$ -fructose via C1 was utilized in a two-step synthesis started from 1-azido-1-deoxy-2,3:4,5-di-*O*-isopropylidene- $\beta$ - $\text{D}$ -fructopyranose [40].  $\text{Cu}(\text{I})$ -catalyzed “click” reaction between azido-fructose **7** and 2-ethynylpyridine resulted in the pyta-conjugated  $\text{D}$ -fructose derivative **8** in high yield

(92%). Success of the reaction is proven by the appearance of signals in the aromatic region in the  $^1\text{H}$  NMR spectrum, which correspond to the triazole and pyridine protons (SI, Fig. S25). Additionally, the  $[\text{M}+\text{H}]^+$  signal in the HR-MS spectrum (error: 0.3 ppm) confirms the structure of the desired compound (SI, Fig. S27). Acidic cleavage of the isopropylidene groups of sugar **8** was performed by stirring with 2 M  $\text{HCl}$  in the presence of water. The crude product was extracted with dry acetonitrile to remove most of the  $\text{NaCl}$ , which was formed by neutralization with aqueous  $\text{NaHCO}_3$  solution. Disappearance of signals related to isopropylidene groups in  $^1\text{H}$  NMR ( $\delta = 0.87\text{--}1.50$  ppm) as well as in  $^{13}\text{C}$  NMR spectra ( $\delta = 109.31\text{--}109.52$  ppm and  $24.05\text{--}26.35$  ppm) and the  $[\text{M}+\text{H}]^+$  signal in HR-MS (error: 2.5 ppm) confirm the formation of the desired compound **9** (SI, Figs. S30–S32).

Ligands **6**, **9** and **10** were reacted with  $\text{Ru}(\text{bpy})_2\text{Cl}_2$  to form complexes of the general formula  $[\text{Ru}(\text{bpy})_2(\text{L})]\text{Cl}_2$  (Fig. 3), which are soluble in water, methanol and polar solvents.

Complexation reaction of **6** with  $\text{Ru}(\text{bpy})_2\text{Cl}_2$  was carried out in  $\text{CH}_3\text{OH}$  at  $60^\circ\text{C}$  and resulted in complex **11** in moderate yield. Triethylamine was added to avoid partial cleavage of  $\text{D}$ -glucose from the sucrose ligand. Due to the charged character of the formed complex, a size exclusion column (Sephadex LH-20 in  $\text{H}_2\text{O}$ ) was used to purify compound **11**. Aromatic signals, which belong to the bpy-ligands of the complex, appear in  $^1\text{H}$  ( $\delta = 7\text{--}9$  ppm) and  $^{13}\text{C}$  NMR spectra ( $\delta = 120\text{--}160$  ppm). Additionally, another signal with the same intensity is appearing for each signal in  $^1\text{H}$  as well as in  $^{13}\text{C}$  NMR spectra, indicating the existence of  $\lambda$ - and  $\Delta$ -isomers (Fig. 4).

Furthermore, the structure of complex **11** was proven by HR-MS as  $[\text{M}-2\text{Cl}]^{2+}$  with an error of 2.9 ppm (SI, Figs. S36–S38). Stirring at  $\text{pH} = 2$  in water for 16 h at  $40^\circ\text{C}$  resulted in the  $\text{D}$ -fructose conjugated Ru complex **12** via C6 in high yield. The structure of the desired complex was confirmed by the disappearance of the  $\text{D}$ -glucose-related signals by  $^1\text{H}$  NMR ( $\delta = 5.23$  ppm and  $\delta = 4.99$  ppm) as well as by HR-MS as  $[\text{M}-2\text{Cl}]^{2+}$  with an error of 1.9 ppm (SI, Figs. S42 and S44). Due to the cleavage of the  $\text{D}$ -glucose unit, the C2 position of the  $\text{D}$ -fructose moiety is changed from full to semi acetal structure. This results in the existence of stereoisomers of the  $\text{D}$ -fructose, in particular the  $\alpha$ - and  $\beta$ - $\text{D}$ -fructofuranose and the open-chained form, which is clearly visible in the appearance of additional signals in the  $^{13}\text{C}$  NMR spectrum between 60 and 85 ppm, when measured in deuterated water (SI, Fig. S43). Those results are in accordance to literature, where various  $\text{D}$ -fructose conjugated compounds revealed this behavior in NMR [14,19].

The reaction of **9** with  $\text{Ru}(\text{bpy})_2\text{Cl}_2$  in a similar manner to that of

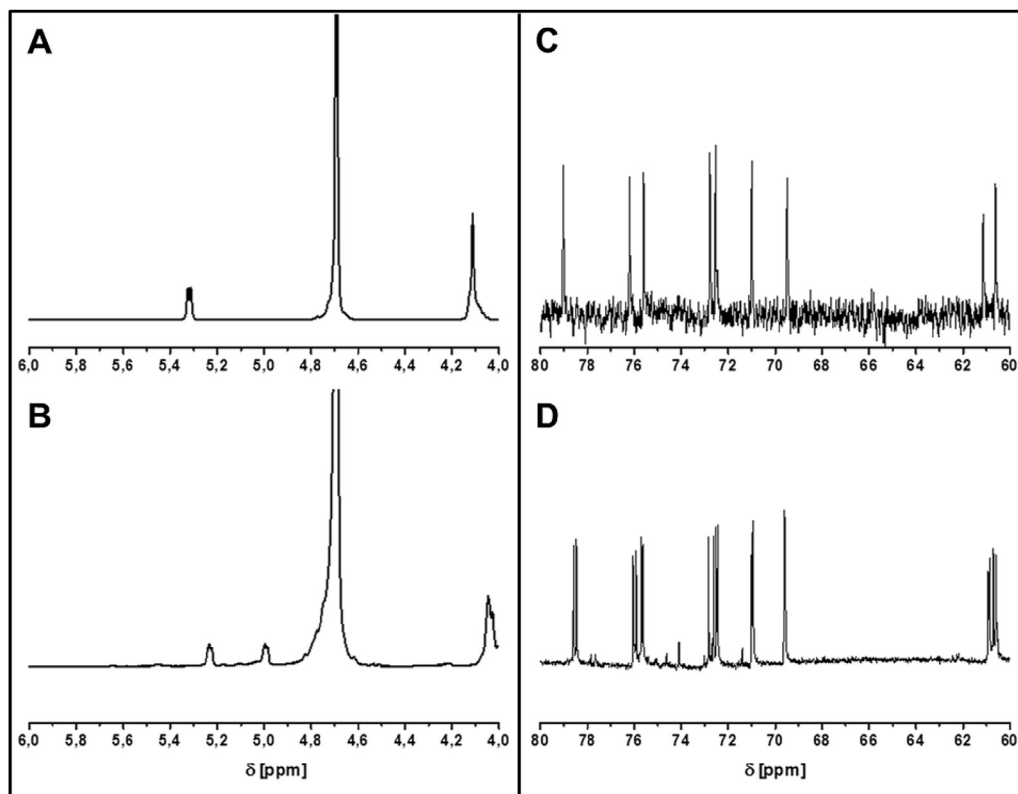


**Fig. 4.** Details of A)  $^1\text{H}$  NMR spectrum of compound **11** in  $\text{D}_2\text{O}$ ; B)  $^1\text{H}$  NMR spectrum of compound **12** in  $\text{D}_2\text{O}$ ; C)  $^{13}\text{C}$  NMR spectrum of compound **11** in  $\text{D}_2\text{O}$ ; D)  $^{13}\text{C}$  NMR spectrum of compound **12** in  $\text{D}_2\text{O}$ .

sucrose complex **11** was not satisfying due to long reaction time ( $>1$  week) and formation of side products. Hence, complexation reaction of **9** was carried out in DMF at  $125^\circ\text{C}$  for 2 h under microwave irradiation. After purification *via* size exclusion column (Sephadex LH-20, water), complex **13** was obtained in moderate yield and high purity. Next to the product signal in HR-MS ( $[\text{M}-2\text{Cl}]^{2+}$ , error: 0.2 ppm), additional signals in  $^1\text{H}$  NMR as well as in  $^{13}\text{C}$  NMR spectra in the aromatic region in comparison to spectra of ligand **9** prove the successful formation of the desired complex (SI, Figs. S48, S50 and S51). The appearance of signals between  $\delta = 9.3$  ppm and 9.7 ppm for the triazole proton of the pyta ligand (H-5<sub>ta</sub>) in  $^1\text{H}$  NMR spectrum showed the presence of different forms of the D-fructose in solution and the existence of  $\lambda$ - and  $\Delta$ -isomers (SI, Fig. S49). For compound **13**, when dissolved in deuterated DMSO, an approximate amount of 37.5%  $\beta$ -D-fructopyranose, 27%  $\beta$ -D-fructofuranose, 27%  $\alpha$ -D-fructofuranose and 8.5% of the open-chain D-fructose was detected by  $^1\text{H}$  measurements. The equilibrium between the different forms is strongly dependent from pH, temperature, solvent, presence of salts and others [41–43].

Since the rhenium (I) tricarbonyl complex of ligand **10** exhibited remarkable cytotoxicity in HepG2 cells [36], the corresponding Ru complex of **10** was synthesized. Complex **14** was prepared and purified in a similar manner to that of sucrose complex **11**. Success of the reaction is shown by the appearance of signals in  $^1\text{H}$  NMR as well as in  $^{13}\text{C}$  NMR spectrum, which belong to bipyridine groups of the complex (SI, Figs. S55 and S56).

The absorbance and emission spectra of all compounds were measured in aerated methanol and are summarized in the supporting information (Table S1). The absorption bands of compounds **5**, **6**, **8** and **9** at  $\lambda_{\text{max}} = 280$  nm were associated with  $\pi \rightarrow \pi^*$  transitions of the ligands. For the Ru complexes **11** to **14** an additional absorption maximum at around  $\lambda_{\text{max}} = 440$  nm was

observed, which fits to the metal to ligand charge transfer (MLCT) transition. The complexes revealed fluorescence in the visible region at around  $\lambda_{\text{max}} = 600$  nm and when excited at around  $\lambda_{\text{ex}} = 440$  nm.

Additionally, dynamic light scattering (DLS) experiments were conducted and revealed the formation of particles with average sizes of  $500 \pm 37$  nm (PDI = 0.146) for complex **14** dissolved in water, whereas for all other complexes no well-defined correlation function was observable, indicating no particle formation.

## 2.2. Cytotoxicity and cell-type dependent uptake studies

To investigate the compounds regarding their cytotoxicity, non-cancerous cell line L929 and breast cancer cell lines MCF-7 and MDA-MB-231 were treated with ligands **6**, **9** and **10** and metal complexes **11** to **14** at varying concentrations for 24 h in serum-containing media. As expected, none of the tested compounds revealed significant cytotoxicity for the tested cell lines using these conditions (SI, Figs. S61–S63).

Since studies showed an enhanced uptake of D-fructose conjugated metal complexes into breast cancer cells [17,18], complexes **11** to **14** were also tested for their uptake behavior using flow cytometry and live-cell CLSM (SI, Figs. S64 and S65). As also previously reported [19,44], the fluorescence of these kind of complexes was quenched in aqueous media and therefore, no meaningful results regarding their uptake could be obtained by these measurements (SI, Fig. S60). To quantify the uptake of the complexes into cells ICP-MS experiments were performed (SI, Fig. S66). ICP-MS revealed an increased, unspecific uptake of sugar-free complex **14** in comparison to the other complexes into all tested cell lines. This might be attributed to the formation of particles in water and the resulting enhanced uptake into cells. The

uptake of D-fructose conjugated complexes **12** and **13** into breast cancer cell lines MDA-MB-231 and MCF-7 was not significantly increased in comparison to sucrose bearing complex **11**. In contrast to other studies [17,18], the results here show that for this type of D-fructose substituted metal complexes an enhanced GLUT5 mediated uptake is not observable.

### 3. Conclusion

In this work we presented the modification of sucrose in a seven step synthesis to modify the C6 position of the D-fructose unit exclusively with a pyridyl triazole (pyta) group. The D-glucose unit acts as protection group of the D-fructofuranose. Using this approach, C6-modified D-fructose derivatives are accessible in high yields, since up to now D-fructose derivatives were modified exclusively at the C1 or C3 position. Additionally, pyridyl triazole modified D-fructose *via* C1 was prepared in four-step synthesis, starting from commercially available isopropylidene-protected D-fructose. For both pyridyl triazole D-fructose derivatives as well as for pyta sucrose, Ru complexes of the general formula  $[\text{Ru}(\text{bpy})_2(\text{L})]\text{Cl}_2$  were prepared. All compounds were analyzed by  $R_f$  values, specific rotation,  $^1\text{H}$  NMR and  $^{13}\text{C}$  NMR, IR, UV/Vis and fluorescence spectroscopy, mass spectrometry as well as by elemental analysis. No cytotoxic effects could be detected for concentrations up to  $100\ \mu\text{mol} \times \text{L}^{-1}$  against L929, MDA-MB-231 or MCF-7 cells.

### 4. Experimental part

#### 4.1. Materials and general experimental details

All reagents and solvents were commercial products purchased from Sigma-Aldrich, Fluka, Across Organics, Strem, VWR or Alfa Aesar and were used without further purification. Chromatographic separations were performed with NP silica RediSep Cartridges from Teledyne Isco. The progress of the reactions was monitored by thin-layer chromatography (TLC) using glass plates precoated with silica gel 60 (Merck). Microwave-assisted syntheses were performed in a Initiator Sixty single-mode microwave synthesizer from Biotage equipped with a noninvasive IR sensor. FT-IR measurements were conducted utilizing a Brewster angle setup. Samples were prepared on clean double side polished silicon wafers (p-type silicon wafers (100), resistivity 10–20  $\Omega\ \text{cm}$  obtained from Siegart Wafer). Samples were dropcasted onto the wafer and the solvent was allowed to dry. Spectra were obtained at a resolution of  $4\ \text{cm}^{-1}$  and 32 spectra were measured for each sample for averaging purposes. Spectra were baseline corrected by the Bruker analysis software OPUS 5.5. The alamarBlue solution for cytotoxicity studies was purchased from Thermo Fisher. Cell cultivation was performed at  $37\ ^\circ\text{C}$  in a humidified 5%  $\text{CO}_2$  atmosphere. L929 (CCL-1, ATCC), MDA-MB231 (HTB-26, ATCC) and MCF-7(ATCC) cells were cultured in Dulbecco's MEM (DMEM, Biochrom) supplemented with 10% fetal calf serum (FCS, Capricorn Scientific),  $100\ \mu\text{g}\ \text{mL}^{-1}$  streptomycin and  $100\ \text{IU}\ \text{mL}^{-1}$  penicillin (Biochrom, Merck). HUVEC cells were kindly provided by the Institute of Biochemistry, Friedrich Schiller University, group of Prof. Mosig. Consumables for cell culture, like pipettes and cell culture plates (96-well) were obtained from Corning (USA) and Greiner Bio-one (Austria/Germany). Crystallographic data were corrected for Lorentz and polarization effects; absorption was taken into account on a semi-empirical basis using multiple-scans [45,46] The structures were solved by direct methods (SHELXS) and refined by full-matrix least squares techniques against  $\text{Fo}^2$  (SHELXL-97) [47]. All hydrogen atoms (with exception of the methylene group of C23 from compound **3**) were located by difference Fourier synthesis and refined isotropically. The hydrogen atoms of the methylene group were

included at calculated positions with fixed thermal parameters. All non-hydrogen atoms were refined anisotropically [47]. Crystallographic data as well as structure solution and refinement details are summarized in Table S2. MERCURY was used for structure representations [48]. Dynamic light scattering experiments were carried out at  $25\ ^\circ\text{C}$  ( $\lambda = 633\ \text{nm}$ ) after an equilibration time of 120 s. The counts were detected at an angle of  $173^\circ$ . Each measurement was performed in triplicate. The mean particle size was approximated as the effective (Z-average) diameter and the width of the distribution as the polydispersity index of the particles (PDI) obtained by the cumulants method assuming a spherical shape of the particles.

#### 4.2. Instrumentation

$^1\text{H}$  NMR and  $^{13}\text{C}$  NMR spectra were measured with Bruker spectrometers (600, 500, 300 and 250 MHz). IR spectra were recorded with a Bruker Tensor 37 FT-IR spectrometer. UV/Vis absorption spectra were measured with an AnalytikJenaAG Specord250 spectrometer and fluorescence was recorded with a Jasco FP 6500 (298 K, methanol,  $10^{-5}\ \text{M}$  solutions). High Resolution electron spray ionization mass spectrometry (HR-ESI-MS) was measured with a Bruker MicroQToF. Elemental analysis was performed with a Leco CHN-932. The alamarBlue cell viability assay (Thermo Fisher) was performed with an Infinite M200 PRO microplate reader (Tecan) according to supplier's instructions. Specific rotation was measured in a Jasco P-2000 polarimeter. Crystallographic data was collected on a Nonius KappaCCD diffractometer using graphite-monochromated  $\text{Mo-K}_\alpha$  radiation. For the uptake studies of HUVEC, MCF-7 and MDA-MB-231 cells a flow cytometer (Cytomics FC 500; Beckman Coulter, Krefeld, Germany) and a confocal laser scanning microscope ELYRA PS1 LSM880 (Carl Zeiss, Jena, Germany) were used (see below). ICP-MS measurements were performed using a XSeriesII (Thermo Fisher). Dynamic light scattering was performed on a Zetasizer Nano ZS (Malvern Instruments, Herrenberg, Germany).

#### 4.3. Synthesis of the ligands

##### 4.3.1. 6'-O-tert-butylidiphenylsilyl-1',2,3,3',4,4',6-hepta-O-acetyl-sucrose (**1**)

Silylated sucrose derivative was synthesized according to literature procedures [37,38].

##### 4.3.2. 1',2,3,3',4,4',6-Hepta-O-acetyl-sucrose (**2**)

19 g (21.72 mmol) of **1** were dissolved in 380 mL DMF and a solution of 5.679 g (21.72 mmol) TBAF and 1.242 mL (21.72 mmol)  $\text{CH}_3\text{COOH}$  in 27 mL  $\text{H}_2\text{O}$  was added dropwise. The reaction mixture was stirred for 24 h at room temperature. After TLC ( $\text{SiO}_2$ , EtOAc:n-hexane, v/v 2:1) indicated that no silylated sucrose was left, the solvent was evaporated. The crude product was re-dissolved in 300 mL EtOAc, washed thrice with brine and the organic layer was dried with  $\text{Na}_2\text{SO}_4$ . Purification by column chromatography ( $\text{SiO}_2$ , EtOAc:n-hexane, v/v 2:1) resulted in 9.165 g (14.40 mmol) of a colorless oil. Yield: 66%. Crystals were obtained by slow diffusion of n-hexane in a solution of the ligand in  $\text{CHCl}_3$ .  $R_f$  0.75 ( $\text{SiO}_2$ , EtOAc);  $[\alpha]_D^{20} = +139.8$  (c 0.1,  $\text{CHCl}_3$ ); IR:  $\tilde{\nu} = 2961$  ( $\nu_{\text{CH}}$ ), 1749 ( $\nu_{\text{CO}}$ )  $\text{cm}^{-1}$ ;  $^1\text{H}$  NMR (300 MHz,  $\text{CDCl}_3$ ):  $\delta$  5.66 (s, 1H, H-1), 5.48–5.37 (m, 3H, H-4, H-3, H-3'), 5.10 (t, 1H,  $J_3$  9.51 Hz, H-5), 4.87 (d, 1H,  $J_3$  10.41 Hz, H-2), 4.26–4.03 (m, 6H, H-6, H-1', H-4', H-5'), 3.84 (dd, 2H,  $J_2$  12.81 Hz, H-6'), 2.16–1.99 (m, 21H, H-Ac).  $^{13}\text{C}$  NMR (75 MHz,  $\text{CDCl}_3$ ):  $\delta$  170.68–169.47 (CO), 103.3 (C-2'), 90.07 (C-1), 81.64 (C-1'), 76.11 (C-3), 73.66 (C-3'), 70.25 (C-2), 69.37 (C-4), 68.74 (C-6), 67.96 (C-5), 63.89 (C-5'), 61.41 (C-4'), 61.14 (C-6'), 20.73–20.55 ( $\text{CH}_3$ ). Calcd. for  $\text{C}_{26}\text{H}_{36}\text{O}_{18}$  (636.56  $\text{g} \times \text{mol}^{-1}$ ): C, 49.06; H, 5.70. Found: C, 49.23; H, 5.71. ESI-MS found  $[\text{2M}+\text{K}]^+$  (7.5%) 1311.32,  $[\text{2M}+\text{Na}]^+$  (33.6%)



1295.35,  $[M+K]^+$  (71.9%) 675.15,  $[M+Na]^+$  (100%) 659.18.

#### 4.3.3. 1',2,3,3',4,4',6-Hepta-O-acetyl-6'-O-tosyl-sucrose (**3**)

7.35 g (10.99 mmol) of **2** were dissolved in 60 mL dry  $CH_2Cl_2$ , 8 mL (57.71 mmol) of  $Et_3N$  were added and a solution of 2.39 g (12.54 mmol) *p*-toluenesulfonyl chloride in 20 mL dry  $CH_2Cl_2$  was added dropwise at 0 °C under Ar. After 2 h stirring at room temperature, TLC ( $SiO_2$ , EtOAc:*n*-hexane, *v/v* 2:1) indicated that no starting material remained. The solution was washed thrice with saturated, aqueous  $NaHCO_3$  solution, dried with  $Na_2SO_4$  and purified by column chromatography ( $SiO_2$ , EtOAc:*n*-hexane, *v/v* 2:1) to obtain 8.8 g (11.13 mmol) of a colorless oil. Yield: 96%. Crystals were obtained by slow diffusion of *n*-hexane into a solution of the ligand in  $CHCl_3$ ,  $R_f$  0.23 ( $SiO_2$ , EtOAc:*n*-hexane, *v/v* 1:1);  $[\alpha]_D^{20} = +168.2$  (c 0.1,  $CHCl_3$ ); IR:  $\tilde{\nu} = 1751$  ( $\nu_{CO}$ ), 820 ( $\delta_{CH}$ )  $cm^{-1}$ ;  $^1H$  NMR (600 MHz,  $CDCl_3$ ):  $\delta$  7.80 (d, 2H,  $J_3$  8.22 Hz, H-2''), 7.36 (d, 2H,  $J_3$  8.28 Hz, H-3''), 5.42 (d, 1H,  $J_3$  6.12 Hz, H-1), 5.39–5.36 (m, 2H, H-3', H-3), 5.22 (t, 1H,  $J_3$  5.82 Hz, H-4'), 4.98 (t, 1H,  $J_3$  9.90 Hz, H-4), 4.79 (dd, 1H,  $J_3$  10.44 Hz, 3.60 Hz, H-2), 4.32–4.19 (m, 4H, H-5, H-6, H-1'), 4.11–4.03 (m, 4H, H-5', H-1', H-6'), 2.46 (s, 3H, H-5''), 2.13–2.00 (m, 21H, H-Ac).  $^{13}C$  NMR (100 MHz,  $CDCl_3$ ):  $\delta$  170.69–169.58 (CO), 145.18 (C-1''), 132.66 (C-4''), 129.94 (C-3''), 128.08 (C-2''), 103.86 (C-2'), 89.85 (C-1), 78.81 (C-1'), 75.23 (C-3), 74.78 (C-3'), 70.03 (C-2), 69.47 (C-4), 69.33 (C-6), 68.47 (C-5), 68.26 (C-5'), 62.53 (C-4'), 62.23 (C-6'), 21.66 (C-5''), 20.67–20.45 ( $CH_3$ ). Calcd. for  $C_{33}H_{42}O_{20}S$  (790.74 g  $\times$  mol $^{-1}$ ): C, 50.12; H, 5.35; S, 4.06. Found: C, 50.29; H, 5.38; S, 4.16. HR-ESI-MS *m/z* calcd. for  $C_{33}H_{42}O_{20}SNa$   $[M+Na]^+$ : 813.1882; found: 813.1855 (error: 3.4 ppm).

#### 4.3.4. 1',2,3,3',4,4',6-Hepta-O-acetyl-6'-azido-6'-deoxy-sucrose (**4**)

5.673 g (7.17 mmol) of **3** were dissolved in 10 mL DMF, 2.8 g (43.07 mmol) of  $NaN_3$  were added and the suspension was stirred for 10 min in the microwave at 120 °C. After cooling to room temperature the solvent was removed and the crude product re-dissolved in 200 mL EtOAc. The organic layer was washed thrice with saturated, aqueous  $NaHCO_3$  solution, dried with  $Na_2SO_4$  and purified by column chromatography ( $SiO_2$ , EtOAc:*n*-hexane, *v/v* 3:2) to obtain 4.704 g (7.11 mmol) of a colorless oil. Yield: 99%.  $R_f$  0.32 ( $SiO_2$ , EtOAc:*n*-hexane, *v/v* 1:1);  $[\alpha]_D^{20} = +108$  (c 0.1,  $CHCl_3$ ); IR:  $\tilde{\nu} = 2104$  ( $\nu_{azide}$ ), 1753 ( $\nu_{CO}$ )  $cm^{-1}$ ;  $^1H$  NMR (300 MHz,  $CDCl_3$ ):  $\delta$  5.63 (d, 1H,  $J_3$  3.60 Hz, H-1), 5.50–5.43 (m, 2H, H-3', H-3), 5.31 (t, 1H,  $J_3$  6.17 Hz, H-4'), 5.09 (t, 1H,  $J_3$  9.80 Hz, H-4), 4.91 (dd, 1H,  $J_3$  10.41 Hz, 3.63 Hz, H-2), 4.31–4.10 (m, 6H, H-5, H-6, H-5', H-1'), 3.74–3.47 (m, 2H, H-6'), 2.16–2.01 (m, 21H, H-Ac).  $^{13}C$  NMR (75 MHz,  $CDCl_3$ ):  $\delta$  170.67–169.56 (CO), 103.89 (C-2'), 90.35 (C-1), 80.15 (C-5'), 75.73 (C-3'), 61.99 (C-2), 70.20 (C-6), 69.42 (C-3), 68.56 (C-5), 68.24 (C-4), 62.73 (C-1'), 64.99 (C-6), 52.88 (C-6'), 20.70–20.48 ( $CH_3$ ). Calcd. for  $C_{33}H_{42}O_{20}S$  (661.57 g  $\times$  mol $^{-1}$ ): C, 47.20; H, 5.33; N, 6.35. Found: C, 47.49; H, 5.37; N, 5.96. ESI-MS found  $[M+K]^+$  (26.9%) 700.16,  $[M+Na]^+$  (100%) 684.18.

#### 4.3.5. 1',2,3,3',4,4',6-Hepta-O-acetyl-6'-deoxy-6'-(4-(2-pyridyl)-1,2,3-triazole-1-yl) sucrose (**5**)

4.704 g (7.11 mmol) of **4** and 1.077 mL (10.7 mmol) 2-ethynylpyridine were dissolved in 5 mL degassed *tert*-butanol under Ar. 585 mg (2.95 mmol) of sodium ascorbate and 383 mg (1.53 mmol) of  $Cu(II)SO_4 \times 5H_2O$  in each 2.5 mL degassed  $H_2O$  were added and the mixture was heated at 60 °C for 25 min under microwave irradiation. After TLC ( $SiO_2$ , EtOAc:*n*-hexane, *v/v* 1:1) indicated that no starting material remained, the solvent was evaporated and the crude product was re-dissolved in 250 mL of EtOAc and washed thrice with each 100 mL of aqueous ammonia solution (25%) and once with 200 mL brine. The organic layer was dried with  $Na_2SO_4$  and purified by column chromatography ( $SiO_2$ , EtOAc) to obtain 4.493 g (5.88 mmol) of a colorless oil. Yield: 83%.  $R_f$  0.57 ( $SiO_2$ ,

EtOAc);  $[\alpha]_D^{20} = +119.8$  (c 0.1,  $CHCl_3$ ); UV–Vis:  $\lambda$  ( $CH_3OH$ ,  $\epsilon \times 10^{-3}/M^{-1} cm^{-1}$ ): 280 (14.97) nm; IR:  $\tilde{\nu} = 1751$  ( $\nu_{CO}$ )  $cm^{-1}$ .  $^1H$  NMR (300 MHz,  $CDCl_3$ ):  $\delta$  8.58 (d, 1H,  $J_3$  4.29 Hz, H-6<sub>py</sub>), 8.26 (s, 1H, H-5<sub>ta</sub>), 8.17 (d, 1H,  $J_3$  7.92 Hz, H-3<sub>py</sub>), 7.80 (t, 1H,  $J_3$  7.74 Hz, H-4<sub>py</sub>), 7.25 (m, 1H, H-5<sub>py</sub>), 5.65 (d, 1H,  $J_3$  3.54 Hz, H-1), 5.56–5.41 (m, 3H, H-3', H-3, H-4), 5.08 (t, 1H,  $J_3$  9.86 Hz, H-4'), 4.97–4.75 (m, 3H, H-2, H-6), 4.54–4.49 (m, 1H, H-5), 4.35–4.29 (m, 1H, H-5'), 4.25–3.93 (m, 4H, H-1', H-6'), 2.18–2.01 (m, 21H, H-Ac).  $^{13}C$  NMR (75 MHz,  $CDCl_3$ ):  $\delta$  170.51–169.53 (CO), 150.00 (C-6<sub>py</sub>), 149.31 (C-2<sub>py</sub>), 148.37 (C-4<sub>ta</sub>), 137.00 (C-5<sub>py</sub>), 123.33 (C-5<sub>ta</sub>), 122.94 (C-3<sub>py</sub>), 120.34 (C-4<sub>py</sub>), 103.79 (C-2'), 90.26 (C-1), 79.53 (C-5'), 75.51 (C-3), 74.93 (C-3'), 69.94 (C-2), 69.35 (C-4'), 69.04 (C-5), 68.32 (C-4), 62.63 (C-1'), 62.31 (C-6), 53.04 (C-6'), 20.67–20.48 ( $CH_3$ ). Calcd. for  $C_{33}H_{40}N_4O_{17}$  (764.69 g  $\times$  mol $^{-1}$ ): C, 51.83; H, 5.27; N, 7.33. Found: C, 51.96; H, 5.43; N, 7.16. HR-ESI-MS *m/z* calcd. for  $C_{33}H_{40}N_4O_{17}Na$   $[M+Na]^+$ : 787.2281; found: 787.2278 (error: 0.3 ppm).

#### 4.3.6. 6'-Deoxy-6'-(4-(2-pyridyl)-1,2,3-triazole-1-yl) sucrose (**6**)

4.493 g (5.88 mmol) of **5** were dissolved in 100 mL dry  $CH_3OH$  and 76.4 mL of a 0.5 M NaOMe solution (38.2 mmol) in  $CH_3OH$  were slowly added under argon. The mixture was stirred for 24 h at room temperature and Amberlite IR-120 ( $H^+$ ) resin was added until the pH value changed to 7. The resin was filtered, washed with  $CH_3OH$  and the solvent was evaporated. The crude product was re-dissolved in water and washed thrice with  $CHCl_3$ . Then, the aqueous layer was freeze-dried to obtain 2.72 g (5.78 mmol) of a colorless oil. Yield: 98%.  $R_f$  0.22 ( $SiO_2$ ,  $CH_3CN:H_2O:KNO_3(aq)$ , *v/v*, 40:4:1);  $[\alpha]_D^{20} = +69.6$  (c 0.1,  $CH_3OH$ ); UV–Vis:  $\lambda$  ( $CH_3OH$ ,  $\epsilon \times 10^{-3}/M^{-1} cm^{-1}$ ): 281 (13.19) nm. IR:  $\tilde{\nu} = 3333$  ( $\nu_{OH}$ )  $cm^{-1}$ .  $^1H$  NMR (300 MHz,  $CDCl_3$ ):  $\delta$  8.45–8.08 (m, 2H, H-5<sub>ta</sub>, H-6<sub>py</sub>), 7.85–7.57 (m, 2H, H-3<sub>py</sub>, H-4<sub>py</sub>), 7.22 (s, 1H, H-5<sub>py</sub>), 5.32 (d, 1H,  $J_3$  3.60 Hz, H-1), 4.8–4.6 (m, 2H, H-3, H-4), 4.19–4.00 (m, 3H, H-4', H-6), 3.86–3.40 (m, 7H, H-5, H-1', H-3', H-5', H-6'), 3.31 (t, 1H,  $J_3$  9.45 Hz, H-2).  $^{13}C$  NMR (75 MHz,  $CDCl_3$ ):  $\delta$  148.91 (C-2<sub>py</sub>), 144.68 (C-6<sub>py</sub>), 138.39 (C-3<sub>py</sub>, C-4<sub>py</sub>, C-5<sub>py</sub>), 124.46 (C-4<sub>ta</sub>, C-5<sub>ta</sub>), 104.05 (C-2'), 92.22 (C-1), 79.02 (C-5'), 76.19 (C-3), 75.60 (C-3'), 72.77 (C-2), 72.53 (C-4'), 70.99 (C-5), 69.48 (C-4), 61.14 (C-1'), 60.61 (C-6), 52.98 (C-6'). Calcd. for  $C_{19}H_{26}N_4O_{10} \times 2.5 H_2O$  (515.48 g  $\times$  mol $^{-1}$ ): C, 44.27; H, 6.06; N, 10.87. Found: C, 44.44; H, 5.77; N, 10.84. HR-ESI-MS *m/z* calcd. for  $C_{19}H_{26}N_4O_{10}Na$   $[M+Na]^+$ : 493.1501; found: 493.1481 (error: 4.0 ppm).

#### 4.3.7. 1-Azido-1-deoxy-2,3:4,5-di-O-isopropylidene- $\beta$ -D-fructopyranose (**7**)

The azide was synthesized as previously reported [40].

#### 4.3.8. 1-(4-(2-Pyridyl)-1,2,3-triazole-1-yl)-1-deoxy-2,3:4,5-di-O-isopropylidene- $\beta$ -D-fructopyranose (**8**)

6.777 g (23.8 mmol) of **7** and 2.88 mL of 2-ethynyl pyridine (28.5 mmol) were dissolved in 100 mL degassed THF. 471 mg (2.4 mmol) of sodium ascorbate and 297 mg (1.2 mmol) of  $Cu(II)SO_4 \times 5H_2O$  in each 5 mL degassed  $H_2O$  were added and the mixture was heated to 60 °C for two days. After TLC ( $SiO_2$ , EtOAc:*n*-hexane, *v/v* 1:2) indicated that no starting material remained, the solvent was evaporated and the crude product was re-dissolved in 300 mL EtOAc and washed thrice with each 100 mL of aqueous ammonia solution (25%) and once with 200 mL of brine. The organic layer was dried with  $Na_2SO_4$ , filtered and the solvent was evaporated. The crude product was re-crystallized from a mixture of EtOAc and *n*-hexane (EtOAc:*n*-hexane, *v/v* 1:4) to obtain 8.521 g (5.88 mmol) of a colorless oil. Yield: 92%.  $R_f$  0.22 ( $SiO_2$ , EtOAc:*n*-hexane, *v/v* 1:1);  $[\alpha]_D^{20} = +42$  (c 0.1,  $CHCl_3$ ); UV–Vis:  $\lambda$  ( $CH_3OH$ ,  $\epsilon \times 10^{-3}/M^{-1} cm^{-1}$ ): 279 (8.90); 238 (14.79) nm. IR:  $\tilde{\nu} = 3159$  ( $\nu_{CH}$ ); 1605 ( $\nu_{C=C}$ ); 1421 ( $\delta_{CH}$ ); 1045 ( $\delta_{CH}$ ); 1011 ( $\delta_{CH}$ ); 980 ( $\delta_{CH}$ )  $cm^{-1}$ .  $^1H$  NMR (300 MHz,  $CDCl_3$ ):  $\delta$  8.60 (d, 1H,  $J_3$  4.80 Hz, H-

6<sub>py</sub>), 8.30 (s, 1H, H-5<sub>ta</sub>), 8.19 (d, 1H, J<sub>3</sub> 7.96 Hz, H-3<sub>py</sub>), 7.80 (td, 1H, J<sub>3</sub> 1.68 Hz, 1H, H-4<sub>py</sub>), 7.24 (m, 1H, H-5<sub>py</sub>), 4.81 (d, 1H, J<sub>2</sub> 14.31 Hz, H-1), 4.68–4.60 (m, 2H, H-4, H-1), 4.52 (d, 1H, J<sub>3</sub> 2.73 Hz, H-3), 4.27 (m, 1H, H-5), 3.95–3.78 (m, 2H, H-6), 1.50–0.87 (4s, 12H, CH<sub>3</sub>). <sup>13</sup>C NMR (75 MHz, CDCl<sub>3</sub>): δ 150.32 (C-6<sub>py</sub>), 149.40 (C-2<sub>py</sub>), 148.16 (C-4<sub>ta</sub>), 136.81 (C-4<sub>py</sub>), 124.80 (C-5<sub>ta</sub>), 122.77 (C-5<sub>py</sub>), 120.29 (C-3<sub>py</sub>), 109.52 (C<sub>q</sub>), 109.31 (C<sub>q</sub>), 100.81 (C-2), 70.78 (C-3), 70.58 (C-5), 70.11 (C-4), 61.89 (C-6), 55.34 (C-1), 26.35–24.05 (CH<sub>3</sub>). Calcd. for C<sub>33</sub>H<sub>40</sub>N<sub>4</sub>O<sub>17</sub> (388.42 g × mol<sup>-1</sup>): C, 58.75; H, 6.23; N, 14.42. Found: C, 58.80; H, 6.27; N, 14.46. HR-ESI-MS *m/z* calcd. for C<sub>19</sub>H<sub>25</sub>N<sub>4</sub>O<sub>5</sub> [M+H]<sup>+</sup>: 389.1819; found: 389.1818 (error: 0.3 ppm).

#### 4.3.9. 1-(4-(2-Pyridyl)-1,2,3-triazole-1-yl)-1-deoxy-β-D-fructopyranose (**9**)

515 mg of **8** (1.33 mmol) were dissolved in 10 mL of ethanol and 5 mL of an aqueous 2 M HCl solution were added slowly. After 10 mL of water were added, the solution was heated to 40 °C for 12 h and stirred at rt for additional 24 h. After TLC (SiO<sub>2</sub>, EtOAc) indicated that no starting material remained, the solution was neutralized with NaHCO<sub>3</sub> and lyophilized. The crude residue was thrice suspended in 100 mL of dry acetonitrile and filtered. The organic layers were combined and the solvent was evaporated to obtain 360 mg (1.17 mmol) of a colorless oil. Yield: 88%. R<sub>f</sub> 0.42 (SiO<sub>2</sub>, CH<sub>3</sub>CN:H<sub>2</sub>O:KNO<sub>3</sub>(aq), v/v, 40:4:1); [α]<sub>D</sub><sup>20</sup> = -24 (c 0.1, CH<sub>3</sub>OH); UV–Vis: λ (CH<sub>3</sub>OH, ε × 10<sup>-3</sup>/M<sup>-1</sup> cm<sup>-1</sup>): 280 (36.38); 240 (57.27) nm. IR: ν̄ = 3537 (ν<sub>OH</sub>), 3493 (ν<sub>OH</sub>), 3360 (ν<sub>OH</sub>), 3176 (ν<sub>OH</sub>) cm<sup>-1</sup>. <sup>1</sup>H NMR (250 MHz, DMSO-d<sub>6</sub>): δ 8.60 (d, 1H, J<sub>3</sub> 2.04 Hz, H-6<sub>py</sub>), 8.51–8.37 (m, 1H, H-5<sub>ta</sub>), 8.05 (d, 1H, J<sub>3</sub> 8.04 Hz, H-3<sub>py</sub>), 7.92 (t, 1H, J<sub>3</sub> 7.69 Hz, H-4<sub>py</sub>), 7.35 (t, 1H, J<sub>3</sub> 5.80 Hz, H-5<sub>py</sub>), 6.22–4.75 (m, 4H, 2-OH, 3-OH, 4-OH, 5-OH), 4.68–4.41 (m, 2H, H-1), 3.91–3.35 (m, 5H, H-3, H-4, H-5, H-6). <sup>13</sup>C NMR (75 MHz, DMSO-d<sub>6</sub>): δ 150.67 (C-2<sub>py</sub>), 150.60 (C-2<sub>py</sub>), 150.48 (C-2<sub>py</sub>), 150.04 (C-6<sub>py</sub>), 150.01 (C-6<sub>py</sub>), 147.38 (C-4<sub>ta</sub>), 147.26 (C-4<sub>ta</sub>), 147.17 (C-4<sub>ta</sub>), 137.64 (C-4<sub>py</sub>), 137.61 (C-4<sub>py</sub>), 124.77 (C-5<sub>ta</sub>), 124.67 (C-5<sub>ta</sub>), 124.62 (C-5<sub>ta</sub>), 123.36 (C-5<sub>py</sub>), 123.27 (C-5<sub>py</sub>), 123.23 (C-5<sub>py</sub>), 119.81 (C-3<sub>py</sub>), 119.77 (C-3<sub>py</sub>), 103.19 (C-2), 100.67 (C-2), 97.17 (C-2), 96.60 (C-2), 83.09 (C-3), 82.75 (C-3), 82.53 (C-3), 77.50 (C-5), 76.58 (C-5), 75.16 (C-5), 69.98 (C-4), 69.20 (C-4), 68.78 (C-4), 64.24 (C-6), 63.10 (C-6), 61.69 (C-6), 55.22 (C-1), 54.78 (C-1), 54.61 (C-1). Calcd. for C<sub>13</sub>H<sub>16</sub>N<sub>4</sub>O<sub>5</sub> (308.29 g × mol<sup>-1</sup>): C, 50.65; H, 5.23; N, 18.17; found: C, 50.37; H, 5.15; N, 18.15. HR-ESI-MS *m/z* calcd. for C<sub>13</sub>H<sub>17</sub>N<sub>4</sub>O<sub>5</sub> [M+H]<sup>+</sup>: 309.1193; found: 309.1186 (error: 2.5 ppm).

#### 4.3.10. 2-(1-(4-(tert-Butyl)benzyl)-1H-1,2,3-triazole-4-yl)pyridine (**10**)

The ligand was synthesized like previously reported [49]. Crystals were obtained by slow diffusion of *n*-hexane into a solution of the ligand in CHCl<sub>3</sub>.

### 4.4. Synthesis of the complexes

#### 4.4.1. 6'-Deoxy-6'-(4-(2-pyridyl)-1,2,3-triazole-1-yl) sucrose bis(2,2'-bipyridine) ruthenium(II) dichloride (**11**)

To a solution of 200 mg (0.43 mmol) of **6** in 25 mL CH<sub>3</sub>OH, 206 mg (0.43 mmol) of Ru(bpy)<sub>2</sub>Cl<sub>2</sub> in 25 mL CH<sub>3</sub>OH and 60 μL (0.43 mmol) Et<sub>3</sub>N were added. The mixture was stirred for 12 h at 60 °C. After cooling to room temperature the mixture was concentrated and was purified by a sephadex LH-20 column in H<sub>2</sub>O to obtain 198 mg (0.25 mmol) of a red oil. Yield: 58%. R<sub>f</sub> 0.1 (SiO<sub>2</sub>, CH<sub>3</sub>CN:H<sub>2</sub>O:KNO<sub>3</sub>(aq), v/v, 40:4:1); [α]<sub>D</sub><sup>20</sup> = +60.2 (c 0.1, CH<sub>3</sub>OH); UV–Vis: λ (CH<sub>3</sub>OH, ε × 10<sup>-3</sup>/M<sup>-1</sup> cm<sup>-1</sup>): 444 (11.97), 287 (54.07) nm. Fluorescence (CH<sub>3</sub>OH, λ<sub>ex</sub> = 444 nm): λ<sub>em</sub> = 599 nm. IR: ν̄ = 3343 (ν<sub>OH</sub>), 1643 (ν<sub>C=N</sub>) cm<sup>-1</sup>. <sup>1</sup>H NMR (300 MHz, D<sub>2</sub>O): δ 8.81 (m, 2H, H-5<sub>ta</sub>), 8.43 (m, 8H, H-3<sub>bpy</sub>, H-3'<sub>bpy</sub>), 8.08 (m, 2H, H-6<sub>py</sub>), 7.96–7.71 (m, 18H, H-3<sub>py</sub>, H-4<sub>bpy</sub>, H-4'<sub>bpy</sub>, H-6<sub>bpy</sub>, H-6'<sub>bpy</sub>), 7.62 (m,

2H, H-4<sub>py</sub>), 7.36–7.10 (m, 10H, H-5<sub>py</sub>, H-5<sub>bpy</sub>, H-5'<sub>bpy</sub>), 5.23 (m, 1H, H-1), 4.99 (m, 1H, H-1), 4.11–3.14 (m, 26H, H-2, H-3, H-4, H-5, H-6, H-1', H-3', H-4', H-5', H-6'). <sup>13</sup>C NMR (125 MHz, D<sub>2</sub>O): δ 157.61–156.95 (C-2<sub>bpy</sub>, C-2'<sub>bpy</sub>), 152.04–151.43 (C-6<sub>py</sub>, C-6'<sub>py</sub>), 150.59 (C-2<sub>py</sub>), 148.20 (C-6<sub>py</sub>), 148.17 (C-6<sub>py</sub>), 137.94 (C-4<sub>ta</sub>), 137.65–137.32 (C-4<sub>py</sub>, C-4<sub>bpy</sub>, C-4'<sub>bpy</sub>), 127.16–125.65 (C-3<sub>py</sub>, C-3<sub>bpy</sub>, C-3'<sub>bpy</sub>), 123.94 (C-5<sub>ta</sub>), 123.66–122.63 (C-5<sub>py</sub>, C-5<sub>bpy</sub>, C-5'<sub>bpy</sub>), 103.98 (C-2'), 103.83 (C-2'), 92.18 (C-1), 91.86 (C-1), 78.59 (C-5'), 78.47 (C-5'), 76.04 (C-3), 75.92 (C-3), 75.69 (C-3'), 75.63 (C-3'), 72.83 (C-2), 72.62 (C-2), 72.51 (C-4'), 72.44 (C-4'), 70.99 (C-5), 70.93 (C-5), 69.60 (C-4), 69.57 (C-4), 60.93 (C-1'), 60.87 (C-1'), 60.71 (C-6), 60.59 (C-6), 54.37 (C-6'), 54.26 (C-6'). HR-ESI-MS *m/z* calcd. for C<sub>39</sub>H<sub>42</sub>N<sub>8</sub>O<sub>10</sub>Ru [M-2Cl]<sup>2+</sup>: 442.1028; Found: 442.1021 (error: 2.9).

#### 4.4.2. 6'-(4-(2-Pyridyl)-1,2,3-triazole-1-yl)-6'-deoxy-D-fructofuranose bis(2,2'-bipyridine) ruthenium(II) dichloride (**12**)

118 mg (0.12 mmol) of **11** were dissolved in 40 mL H<sub>2</sub>O and 20 mL 2 M HCl were added and the resulting mixture was stirred for 16 h at 40 °C. After TLC (SiO<sub>2</sub>, CH<sub>3</sub>CN:H<sub>2</sub>O:KNO<sub>3</sub>(aq), v/v, 40:4:1) indicated that no starting material remained, the solution was neutralized with aqueous 2 M NaOH solution. The solution was concentrated and purified by a Sephadex LH-20 column in H<sub>2</sub>O to obtain 50 mg (0.06 mmol) of a red oil. Yield: 51%. R<sub>f</sub> 0.14 (SiO<sub>2</sub>, CH<sub>3</sub>CN:H<sub>2</sub>O:KNO<sub>3</sub>(aq), v/v, 40:4:1); [α]<sub>D</sub><sup>20</sup> = +39.2 (c 0.1, CH<sub>3</sub>OH); UV–Vis: λ (CH<sub>3</sub>OH, ε × 10<sup>-3</sup>/M<sup>-1</sup> cm<sup>-1</sup>): 443 (12.26), 286 (56.24), 239 (31.20) nm. Fluorescence (CH<sub>3</sub>OH, λ<sub>ex</sub> = 444 nm): λ<sub>em</sub> = 600 nm. IR: ν̄ = 3379 (ν<sub>OH</sub>), 1607 (ν<sub>C=N</sub>), 779 (δ<sub>bpy</sub>) cm<sup>-1</sup>. <sup>1</sup>H NMR (500 MHz, D<sub>2</sub>O): δ 8.89 (m, 2H, H-5<sub>ta</sub>), 8.46–8.34 (m, 8H, H-3<sub>bpy</sub>, H-3'<sub>bpy</sub>), 8.1 (m, 2H, H-6<sub>py</sub>), 8.01–7.69 (m, 18H, H-3<sub>py</sub>, H-4<sub>bpy</sub>, H-4'<sub>bpy</sub>, H-6<sub>bpy</sub>, H-6'<sub>bpy</sub>), 7.61 (t, <sup>3</sup>J = 4.63 Hz, 2H, H-4<sub>py</sub>), 7.39–7.15 (m, 10H, H-5<sub>py</sub>, H-5<sub>bpy</sub>, H-5'<sub>bpy</sub>), 4.67–2.60 (m, 14H, H-1', H-3', H-4', H-5', H-6'). <sup>13</sup>C NMR (125 MHz, D<sub>2</sub>O): δ 157.47–156.93 (C-2<sub>bpy</sub>, C-2'<sub>bpy</sub>), 151.89–151.43 (C-6<sub>bpy</sub>, C-6'<sub>bpy</sub>), 150.62–150.56 (C-2<sub>py</sub>), 147.92 (C-6<sub>py</sub>), 147.88 (C-6<sub>py</sub>), 137.94 (C-4<sub>ta</sub>), 137.72–137.31 (C-4<sub>py</sub>, C-4<sub>bpy</sub>, C-4'<sub>bpy</sub>), 127.31–126.47 (C-3<sub>py</sub>, C-3<sub>bpy</sub>, C-3'<sub>bpy</sub>), 125.65 (C-5<sub>ta</sub>), 123.96–122.66 (C-5<sub>py</sub>, C-5<sub>bpy</sub>, C-5'<sub>bpy</sub>), 105.12 (C-2'), 104.61 (C-2'), 102.15 (C-2'), 101.97 (C-2'), 81.26 (C-5'), 81.11 (C-5'), 79.24 (C-3'), 78.42 (C-3'), 77.86 (C-5'), 77.68 (C-5'), 77.16 (C-4'), 76.60 (C-4'), 75.13 (C-3'), 75.06 (C-3'), 74.64 (C-4'), 74.62 (C-4'), 62.86 (C-1'), 62.45 (C-1'), 62.27 (C-1'), 62.20 (C-1'), 53.50 (C-6'), 52.71 (C-6'), 52.33 (C-6'), 46.66 (C-6'). HR-ESI-MS *m/z* calcd. for C<sub>33</sub>H<sub>32</sub>N<sub>8</sub>O<sub>5</sub>Ru [M-2Cl]<sup>2+</sup>: 361.0764; found: 361.0775 (error: 1.9 ppm).

#### 4.4.3. 1-(4-(2-Pyridyl)-1,2,3-triazole-1-yl)-1-deoxy-β-D-fructopyranose bis(2,2'-bipyridine) ruthenium(II) dichloride (**13**)

85 mg of **9** (0.28 mmol) and 134 mg of Ru(bpy)<sub>2</sub>Cl<sub>2</sub> (0.28 mmol) were dissolved in 15 mL DMF and were stirred at 125 °C for 2 h in the microwave. After cooling to room temperature, the solvent was evaporated *in vacuo*. The crude product was redissolved in 3 mL of H<sub>2</sub>O, filtered and was purified by a Sephadex LH-20 column in H<sub>2</sub>O to obtain 106 mg (0.13 mmol) of a red oil. Yield: 48%. R<sub>f</sub> 0.14 (SiO<sub>2</sub>, CH<sub>3</sub>CN:H<sub>2</sub>O:KNO<sub>3</sub>(aq), v/v, 40:4:1); [α]<sub>D</sub><sup>20</sup> = -21 (c 0.1, CH<sub>3</sub>OH); UV–Vis: λ (CH<sub>3</sub>OH, ε × 10<sup>-3</sup>/M<sup>-1</sup> cm<sup>-1</sup>): 440 (9.14); 285 (53.24); 240 (24.92) nm. Fluorescence (CH<sub>3</sub>OH, λ<sub>ex</sub> = 439 nm): λ<sub>em</sub> = 604 nm. IR: ν̄ = 3402 (ν<sub>OH</sub>), 1603 (ν<sub>C=N</sub>), 779 (δ<sub>bpy</sub>) cm<sup>-1</sup>. <sup>1</sup>H NMR (400 MHz, DMSO-d<sub>6</sub>): δ 9.67–9.37 (m, 2H, H-5<sub>ta</sub>), 8.94–8.48 (m, 10H, H-6<sub>py</sub>, H-3<sub>bpy</sub>, H-3'<sub>bpy</sub>), 8.23–8.07 (m, 10H, H-3<sub>py</sub>, H-6<sub>bpy</sub>, H-6'<sub>bpy</sub>), 7.91–7.39 (m, 20H, H-4<sub>py</sub>, H-5<sub>py</sub>, H-4<sub>bpy</sub>, H-4'<sub>bpy</sub>, H-5<sub>bpy</sub>, H-5'<sub>bpy</sub>), 6.55–6.18 (m, 2H, 3-OH), 5.98–5.67 (m, 2H, 5-OH), 5.46–5.34 (m, 4H, 5-OH, 4-OH), 5.11–4.99 (m, 2H, 4-OH), 4.96–4.68 (m, 2H, 2-OH), 4.69–4.33 (m, 4H, H-1), 4.02–3.21 (m, 10H, H-3, H-4, H-5, H-6). <sup>13</sup>C NMR (75 MHz, CDCl<sub>3</sub>): δ 157.74–157.08 (C-2<sub>bpy</sub>, C-2'<sub>bpy</sub>), 152.23–151.58 (C-6<sub>bpy</sub>, C-6'<sub>bpy</sub>), 151.29 (C-2<sub>py</sub>), 151.11 (C-2<sub>py</sub>), 147.19 (C-6<sub>py</sub>), 147.07 (C-6<sub>py</sub>), 138.80 (C-4<sub>ta</sub>), 138.32–138.09 (C-4<sub>py</sub>, C-4<sub>bpy</sub>, C-4'<sub>bpy</sub>), 128.26–126.61 (C-3<sub>py</sub>, C-3<sub>bpy</sub>, C-3'<sub>bpy</sub>), 126.52 (C-

5<sub>ta</sub>), 125.02 (C-5<sub>ta</sub>), 124.89–123.22 (C-5<sub>py</sub>, C-5<sub>bpy</sub>, C-5'<sub>bpy</sub>), 102.72 (C-2), 102.54 (C-2), 100.34 (C-2), 100.11 (C-2), 96.84 (C-2), 96.40 (C-2), 83.58 (C-3), 82.99 (C-3), 82.59 (C-3), 82.36 (C-3), 82.17 (C-3), 79.09 (C-5), 78.49 (C-5), 76.63 (C-5), 75.35 (C-5), 70.16 (C-4), 70.00 (C-4), 69.46 (C-4), 69.30 (C-4), 69.10 (C-4), 64.43 (C-6), 62.99 (C-6), 61.42 (C-6), 61.19 (C-6), 57.99 (C-1), 57.38 (C-1), 57.17 (C-1), 56.86 (C-1). HR-ESI-MS *m/z* calcd. for C<sub>33</sub>H<sub>32</sub>N<sub>8</sub>O<sub>5</sub>Ru [M-2Cl]<sup>2+</sup>: 361.0764; Found: 361.0769 (error: 0.2 ppm).

#### 4.4.4. 2-(1-(4-(tert-Butyl)benzyl)-1H-1,2,3-triazole-4-yl)pyridine bis(2,2'-bipyridine) ruthenium(II) dichloride (**14**)

195 mg (0.40 mmol) of Ru(bpy)<sub>2</sub>Cl<sub>2</sub> precursor complex were dissolved in 10 mL CH<sub>3</sub>OH and 118 mg (0.40 mmol) of ligand **10** in 20 mL CH<sub>3</sub>OH were slowly added. The mixture was stirred for 12 h at 60 °C. After cooling to room temperature the mixture was concentrated and purified by a Sephadex LH-20 column in CH<sub>3</sub>OH to obtain 262 mg (0.34 mmol) of a red oil. Yield: 85%. R<sub>f</sub> 0.42 (SiO<sub>2</sub>, CH<sub>3</sub>CN:H<sub>2</sub>O:KNO<sub>3</sub>(aq), v/v, 40:4:1); [α]<sub>D</sub><sup>20</sup> = −7.2 (c 0.1, CH<sub>3</sub>OH); UV–Vis: λ (CH<sub>3</sub>OH, ε × 10<sup>−3</sup>/M<sup>−1</sup> cm<sup>−1</sup>): 443 (12.11); 287 (54.57) nm. Fluorescence (CH<sub>3</sub>OH, λ<sub>ex</sub> = 444 nm): λ<sub>em</sub> = 600 nm. IR:  $\tilde{\nu}$  = 1608 ( $\nu_{C=N}$ ), 777 ( $\delta_{bpy}$ ) cm<sup>−1</sup>. <sup>1</sup>H NMR (500 MHz, DMF-d<sub>7</sub>): δ 10.05 (s, 1H, H-5<sub>ta</sub>), 9.16 (m, 2H, H-3<sub>bpy</sub>), 9.08 (m, 2H, H-3'<sub>bpy</sub>), 8.72 (d, 1H, J<sub>3</sub> 7.90 Hz, H-6<sub>py</sub>), 8.31 (m, 3H, H-4<sub>bpy</sub>, H-4'<sub>bpy</sub>), 8.24 (t, 1H, J<sub>3</sub> 3.43 Hz, H-4'<sub>bpy</sub>), 8.19 (m, 3H, H-6<sub>bpy</sub>, H-6'<sub>bpy</sub>), 8.10 (d, 1H, J<sub>3</sub> 5.45 Hz, H-3<sub>py</sub>), 8.04 (d, 1H, J<sub>3</sub> 4.88 Hz, H-5<sub>py</sub>), 7.88 (d, 1H, J<sub>3</sub> 5.49 Hz, H-6<sub>bpy</sub>), 7.68 (m, 3H, H-5<sub>bpy</sub>, H-4<sub>py</sub>), 7.60 (m, 1H, H-5'<sub>bpy</sub>), 7.53 (m, 1H, H-5'<sub>bpy</sub>), 7.40 (m, 2H, H-3<sub>Bn</sub>), 7.21 (m, 2H, H-2<sub>Bn</sub>), 5.89 (q, 2H, J<sub>3</sub> 24.01 Hz, CH<sub>2</sub>), 1.29 (s, 9H, CH<sub>3</sub>) ppm. <sup>13</sup>C NMR (125 MHz, DMF-d<sub>7</sub>): δ 157.98 (C-2<sub>bpy</sub>), 157.62 (C-2<sub>bpy</sub>), 157.53 (C-4<sub>Bn</sub>), 157.28 (C-1<sub>Bn</sub>), 152.37 (C-5<sub>py</sub>), 152.29 (C-6<sub>bpy</sub>), 152.00 (C-3<sub>py</sub>), 151.79 (C-6<sub>bpy</sub>), 151.51 (C-2<sub>py</sub>), 151.16 (C-2'<sub>bpy</sub>), 148.07 (C-5<sub>ta</sub>), 138.46 (C-6'<sub>bpy</sub>), 138.07 (C-5<sub>py</sub>), 137.87 (C-4'<sub>bpy</sub>), 131.89 (C-4<sub>ta</sub>), 127.91 (C-4<sub>py</sub>), 127.84 (C-2<sub>Bn</sub>), 127.44, 127.16 (C-5<sub>bpy</sub>), 126.28 (C-5'<sub>bpy</sub>), 125.81 (C-3<sub>Bn</sub>), 124.94 (C-5<sub>bpy</sub>), 124.89 (C-3<sub>bpy</sub>), 124.44 (C-3'<sub>bpy</sub>), 124.15 (C-3'<sub>bpy</sub>), 123.26 (C-6<sub>py</sub>), 54.85 (CH<sub>2</sub>), 48.78 (C<sub>q</sub>), 30.80 (CH<sub>3</sub>).

### 4.5. Biological studies

#### 4.5.1. Determination of cytotoxicity

Cytotoxicity studies were performed with L929, MCF-7 and MDA-MB-231 cells. Cells were seeded at 10<sup>4</sup> cells per well in a 96-well plate and incubated for 24 h. Afterwards, the test substances (**6** and **9** to **14**) at indicated concentrations (25, 50, 100 μmol L<sup>−1</sup>) were added to the cells and the plates were incubated for further 24 h. Subsequently, the medium was replaced by a mixture of fresh culture medium and alamarBlue solution (Thermo Fisher), prepared according to the manufacturer's instructions. After a further incubation of 4 h at 37 °C, the fluorescence was measured at λ<sub>ex</sub> = 570 nm/λ<sub>em</sub> = 610 nm, with untreated cells on the same well plate serving as negative controls. The negative control was standardized as 0% of metabolism inhibition and referred as 100% viability. Data are expressed as mean ± SD of three independent determinations.

#### 4.5.2. Uptake studies

HUVEC, MCF-7 and MDA-MB-231 cells were cultured as described above. Subsequently, cells were seeded at a density of 10<sup>5</sup> cells per mL in 24-well plates and cultured for 24 h. One hour prior to the addition of the complexes, the medium was replaced by fresh culture medium. The plates were incubated for 1 h at 37 °C under 5% CO<sub>2</sub> atmosphere. Metal complexes were added to the cells at indicated concentrations for 1 h. Afterwards the cells were washed, harvested and 10% trypan blue was added to quench the outer fluorescence of the cells. To determine the relative uptake of the metal complexes, 10,000 cells were measured by flow

cytometry using a Cytomics FC 500 (Beckman Coulter). The experiments were performed at least three times independently. Live cell imaging was additionally performed for uptake studies. In detail, cells (10<sup>5</sup> cells mL<sup>−1</sup>) were seeded on glass-bottomed dishes (Greiner, Germany) and cultivated for 24 h in a humidified atmosphere. One hour prior to the metal complex addition, the cells were rinsed with phosphate buffered saline (PBS) and the medium was changed to fresh culture medium. The metal complexes were added to the cells and incubated for one additional hour. Imaging was performed with LSM880, ELYRA PS.1 system (Zeiss, Oberkochen, Germany) applying a 63 × 1.4 NA plan apochromat oil objective. The excitation wavelength was λ<sub>ex</sub> = 488 nm and the fluorescence was detected from λ = 553–650 nm. Since the complexes showed no measurable fluorescence in aqueous media, ICP-MS studies were performed. Cells were grown to 50% confluency in a 6-well plate. Unless specified, the cells were incubated with the Ru complexes **11** to **14** (50 μM) in D-fructose-free medium at 37 °C under a 5% CO<sub>2</sub> atmosphere for 1 h. The medium was then removed and cells were washed gently with PBS. The cells were trypsinized and harvested. The harvested cells were digested with 65% HNO<sub>3</sub> at 60 °C in an ultrasonic bath for 1 h and afterwards incubated at room temperature over night to ensure complete digestion. The samples were then diluted with ultrapure water (Millipore Merck) to a final concentration of 2% HNO<sub>3</sub> and measured by ICP-MS.

### Acknowledgement

The authors gratefully thank Carolin Fritzsche for the accomplishment of the cytotoxicity assays, Gabi Sentis for NMR measurements and Dr. Dirk Merten for ICP-MS measurements. This project was funded by the German Federal Ministry of Education & Research (BMBF, #031A518B Vectura) and by the German Research Council (DFG, GO 1100/4-1). Furthermore, the Carl Zeiss Foundation (JCSM Strukturantrag, 0563-2.8/335/4) is gratefully acknowledged for financial support. The LSM880 ELYRA PS.1 was further funded with a grant from the German Research Council (DFG, INST 275/315-1).

### Appendix A. Supplementary data

Supplementary data related to this article can be found at <http://dx.doi.org/10.1016/j.carres.2017.04.020>.

### References

- [1] M. Gottschaldt, U.S. Schubert, *Chem. Eur. J.* 15 (2009) 1548–1557.
- [2] F.Q. Zhao, A.F. Keating, *Curr. Genomics* 8 (2007) 113–128.
- [3] N. Nomura, G. Verdon, H.J. Kang, T. Shimamura, Y. Nomura, Y. Sonoda, S.A. Hussien, A.A. Qureshi, M. Coincon, Y. Sato, H. Abe, Y. Nakada-Nakura, T. Hino, T. Arakawa, O. Kusano-Arai, H. Iwanari, T. Murata, T. Kobayashi, T. Hamakubo, M. Kasahara, S. Iwata, D. Drew, *Nature* 526 (2015) 397–401.
- [4] A. Godoy, V. Ulloa, F. Rodríguez, K. Reinicke, A.J. Yañez, M. d. I. A. García, R.A. Medina, M. Carrasco, S. Barberis, T. Castro, F. Martínez, X. Koch, J.C. Vera, M.T. Poblete, C.D. Figueroa, B. Peruzzo, F. Pérez, F. Nualart, *J. Cell. Physiol.* 207 (2006) 614–627.
- [5] G. Gowrishankar, S. Zitzmann-Kolbe, A. Junutula, R. Reeves, J. Levi, A. Srinivasan, K. Bruus-Jensen, J. Cyr, L. Dinkelborg, S.S. Gambhir, *PLoS One* 6 (2011) e26902.
- [6] W.-L. Chen, Y.-Y. Wang, A. Zhao, L. Xia, G. Xie, M. Su, L. Zhao, J. Liu, C. Qu, R. Wei, C. Rajani, Y. Ni, Z. Cheng, Z. Chen, S.-J. Chen, W. Jia, *Cancer Cell* 30 (2016) 779–791.
- [7] A. Tatibouët, J. Yang, C. Morin, G.D. Holman, *Bioorg. Med. Chem.* 8 (2000) 1825–1833.
- [8] J. Yang, J. Dowden, A. Tatibouët, Y. Hatanaka, G.D. Holman, *Biochem. J.* 367 (2002) 533–539.
- [9] J. Zhao, K. Babich, H. Lu, A. Dag, M. Gottschaldt, M.H. Stenzel, *Chem. Commun.* 50 (2014) 15928–15931.
- [10] A. Dag, M. Callari, H. Lu, M.H. Stenzel, *Polym. Chem.* 7 (2016) 1031–1036.
- [11] J. Levi, Z. Cheng, O. Gheysens, M. Patel, C.T. Chan, Y. Wang, M. Namavari, S.S. Gambhir, *Bioconjug. Chem.* 18 (2007) 628–634.
- [12] S. Ganda, Y. Jiang, D.S. Thomas, J. Eliezar, M.H. Stenzel, *Macromolecules* 49

- (2016) 4136–4146.
- [13] J. Zhao, H. Lu, P. Xiao, M.H. Stenzel, *ACS Appl. Mater. Interfaces* 8 (2016) 16622–16630.
  - [14] C. von der Ehe, A. Rinkenauer, C. Weber, D. Szamosvari, M. Gottschaldt, U.S. Schubert, *Macromol. Biosci.* 16 (2016) 508–521.
  - [15] X. Zhou, X. Qin, T. Gong, Z.-R. Zhang, Y. Fu, *Macromol. Biosci.* (2017), <http://dx.doi.org/10.1002/mabi.201600502>.
  - [16] C. Englert, M. Pröhl, J.A. Czaplewski, C. Fritzsche, E. Preußger, U.S. Schubert, A. Traeger, M. Gottschaldt, *Macromol. Biosci.* (2017), <http://dx.doi.org/10.1002/mabi.201600529>.
  - [17] K. Yin Zhang, K. Ka-Shun Tso, M.-W. Louie, H.-W. Liu, K. Kam-Wing Lo, *Organometallics* 32 (2013) 5098–5102.
  - [18] K.K.-W. Lo, W.H.-T. Law, J.C.-Y. Chan, H.-W. Liu, K.Y. Zhang, *Metalomics* 5 (2013) 808–812.
  - [19] M. Pröhl, T. Bus, J.A. Czaplewski, A. Traeger, M. Deicke, H. Weiss, W. Weigand, U.S. Schubert, M. Gottschaldt, *Eur. J. Inorg. Chem.* 2016 (2016) 5197–5204.
  - [20] M. Patra, S.G. Awuah, S.J. Lippard, *J. Am. Chem. Soc.* 138 (2016) 12541–12551.
  - [21] L. Pan, Q. Zhu, R. Lu, J.M. McGrath, *Food Chem.* 167 (2015) 264–271.
  - [22] K. Mohanta, A. Kumar, O. Parkash, D. Kumar, *J. Eur. Ceram. Soc.* 34 (2014) 2401–2412.
  - [23] R. Kumar, V. More, S.P. Mohanty, S.S. Nemala, S. Mallick, P. Bhargava, *J. Colloid Interface Sci.* 459 (2015) 146–150.
  - [24] R. Atchudan, S. Perumal, T.N. Jebakumar Immanuel Edison, Y.R. Lee, *Mater. Lett.* 166 (2016) 145–149.
  - [25] K.T. Petrova, T.M. Potewar, O.S. Ascenso, M.T. Barros, *Carbohydr. Polym.* 110 (2014) 38–46.
  - [26] M.T. Barros, K.T. Petrova, R.P. Singh, *Int. J. Mol. Sci.* 11 (2010) 1792.
  - [27] M.T. Barros, K.T. Petrova, *Eur. Polym. J.* 45 (2009) 295–301.
  - [28] C.I.C. Crucho, M.T. Barros, *J. Mater. Chem. B* 2 (2014) 3946–3955.
  - [29] K.T. Petrova, T.M. Potewar, P. Correia-da-Silva, M.T. Barros, R.C. Calhelha, A. Ćirić, M. Soković, I.C.F.R. Ferreira, *Carbohydr. Res.* 417 (2015) 66–71.
  - [30] N.V. Sokolova, V.G. Nenajdenko, *RSC Adv.* 3 (2013) 16212–16242.
  - [31] V.K. Tiwari, B.B. Mishra, K.B. Mishra, N. Mishra, A.S. Singh, X. Chen, *Chem. Rev.* 116 (2016), 3086–3240.
  - [32] Z. Györgydeák, L. Szilágyi, H. Paulsen, *J. Carbohydr. Chem.* 12 (1993) 139–163.
  - [33] X.-P. He, Y.-L. Zeng, Y. Zang, J. Li, R.A. Field, G.-R. Chen, *Carbohydr. Res.* 429 (2016) 1–22.
  - [34] H.-L. Zhang, X.-L. Wei, Y. Zang, J.-Y. Cao, S. Liu, X.-P. He, Q. Chen, Y.-T. Long, J. Li, G.-R. Chen, K. Chen, *Adv. Mater.* 25 (2013) 4097–4101.
  - [35] S.B. Deepthi, R. Trivedi, P. Sujitha, C.G. Kumar, B. Sridhar, S.K. Bhargava, *J. Chem. Sci.* 124 (2012) 1405–1413.
  - [36] J.A. Czaplewski, F. Theil, E. Altuntas, T. Niksch, M. Freesmeyer, B. Happ, D. Pretzel, H. Schäfer, M. Obata, S. Yano, U.S. Schubert, M. Gottschaldt, *Eur. J. Inorg. Chem.* 2014 (2014) 6290–6297.
  - [37] M.T. Barros, K.T. Petrova, A.M. Ramos, *J. Org. Chem.* 69 (2004) 7772–7775.
  - [38] T.M. Potewar, K.T. Petrova, M.T. Barros, *Carbohydr. Res.* 379 (2013) 60–67.
  - [39] S. Higashibayashi, K. Shinko, T. Ishizu, K. Hashimoto, H. Shirahama, M. Nakata, *Synlett* (2000) 1306–1308.
  - [40] B.E. Maryanoff, D.F. McComsey, M.J. Costanzo, C. Hochman, V. Smith-Swintosky, R.P. Shank, *J. Med. Chem.* 48 (2005) 1941–1947.
  - [41] M. Cockman, D.G. Kubler, A.S. Oswald, L. Wilson, *J. Carbohydr. Chem.* 6 (1987) 181–201.
  - [42] F. Franks, *Pure Appl. Chem.* 59 (1987) 1189–1202.
  - [43] W.J. Goux, *J. Am. Chem. Soc.* 107 (1985) 4320–4327.
  - [44] G. Sprintschnik, H.W. Sprintschnik, P.P. Kirsch, D.G. Whitten, *J. Am. Chem. Soc.* 98 (1976) 2337–2338.
  - [45] Hooft, R. Nonius BV, Delft, The Netherlands 1998.
  - [46] Z. Otwinowski, W. Minor, in: *Methods Enzymol*, Academic Press, 1997, pp. 307–326.
  - [47] G. Sheldrick, *Acta Cryst. A* 64 (2008) 112–122.
  - [48] C.F. Macrae, P.R. Edgington, P. McCabe, E. Pidcock, G.P. Shields, R. Taylor, M. Towler, J. van de Streek, *J. Appl. Crystallogr.* 39 (2006) 453–457.
  - [49] B. Happ, C. Friebe, A. Winter, M.D. Hager, R. Hoogenboom, U.S. Schubert, *Chem. Asian J.* 4 (2009) 154–163.



# **Supporting Information**

## **Synthesis of D-fructose conjugated ligands *via* C6 and C1 and their corresponding [Ru(bpy)<sub>2</sub>(L)]Cl<sub>2</sub> complexes**

Michael Pröhl,<sup>†,‡</sup> Pascal D. Moser,<sup>†,‡</sup> Justyna A. Czaplewska,<sup>†,‡</sup> Patrick Hoffmann,<sup>†,‡</sup> Tanja Bus,<sup>†,‡</sup> Anja Traeger,<sup>†,‡</sup> Helmar Görls,<sup>§</sup> Ulrich S. Schubert,<sup>†,‡</sup> Michael Gottschaldt<sup>†,‡,\*</sup>

† Laboratory of Organic and Macromolecular Chemistry (IOMC), Friedrich Schiller University Jena, Humboldtstraße 10, 07743 Jena, Germany

‡ Jena Center for Soft Matter (JCSM), Friedrich Schiller University Jena, Philosophenweg 7, 07743 Jena, Germany

§ Institute for Inorganic and Analytical Chemistry, Friedrich Schiller University Jena, Humboldtstraße 8, 07743 Jena, Germany

\*corresponding author: michael.gottschaldt@uni-jena.de

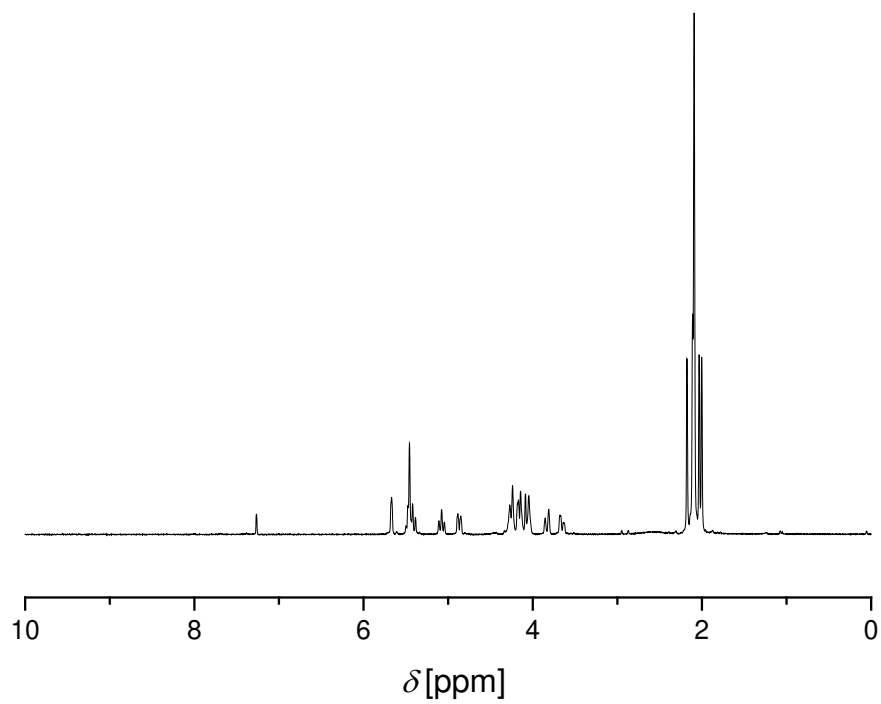
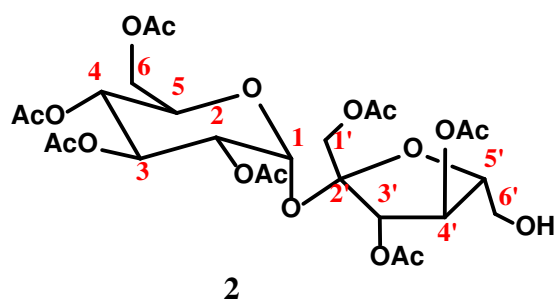


**Figure S1.**  $^1\text{H}$  NMR spectrum of **2** in  $\text{CDCl}_3$ .

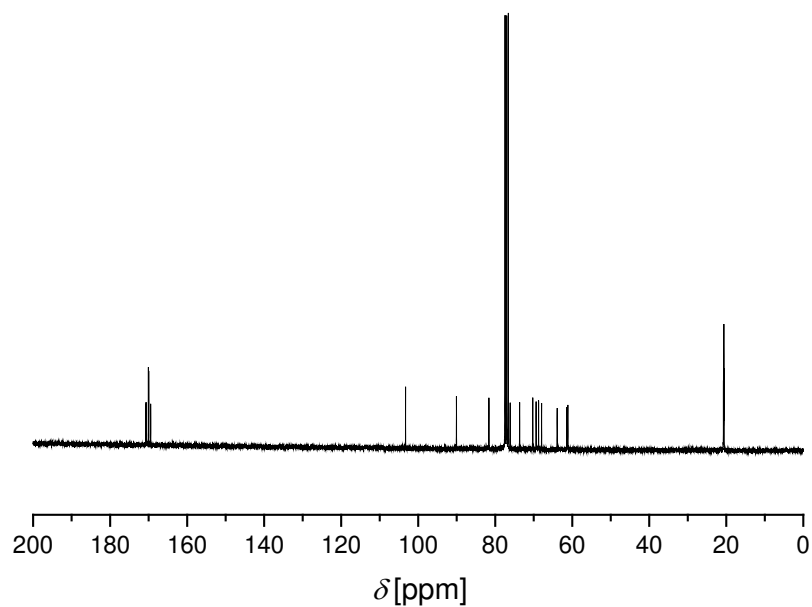


**Figure S2.**  $^{13}\text{C}$  NMR spectrum of **2** in  $\text{CDCl}_3$ .

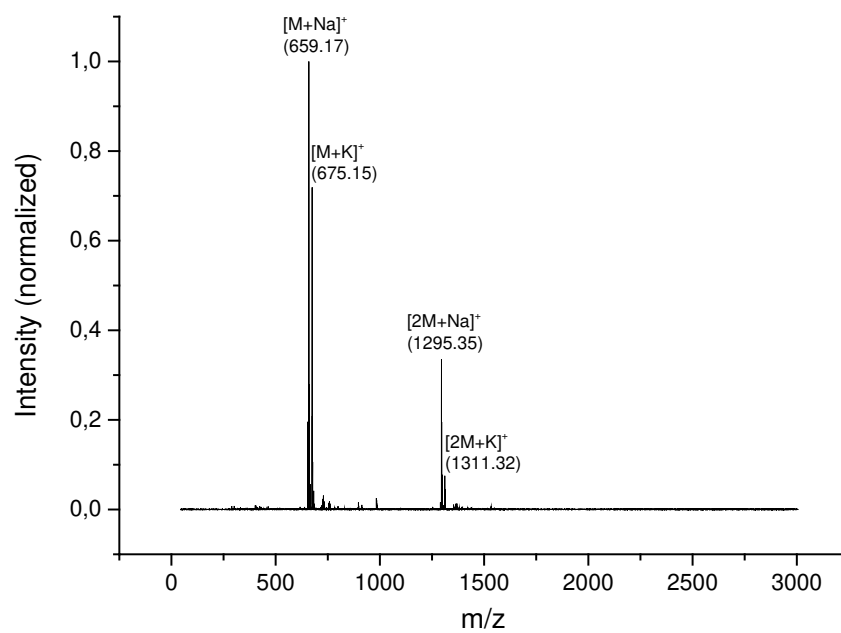


**Figure S3.** ESI-TOF-MS spectrum of **2** in acetonitrile.

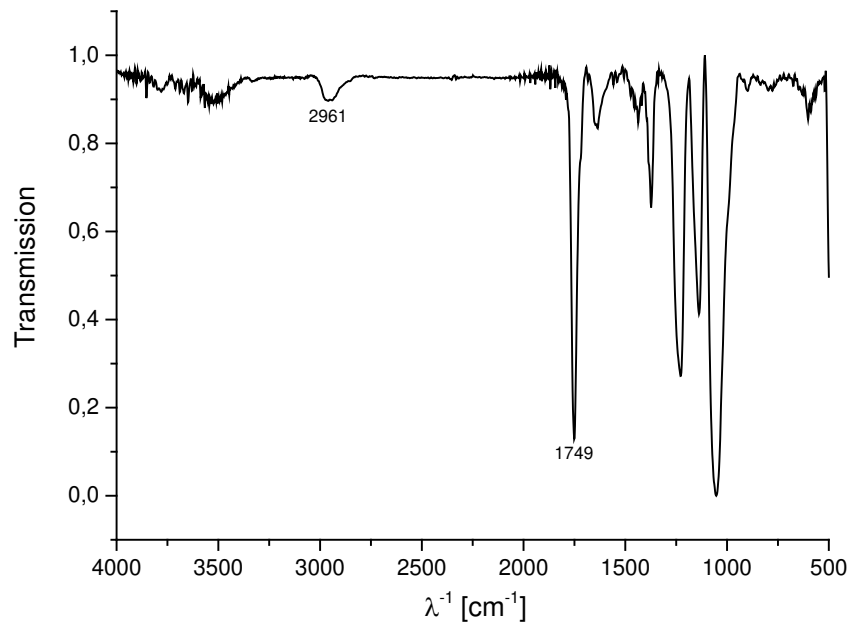


**Figure S4.** IR spectrum of **2**.

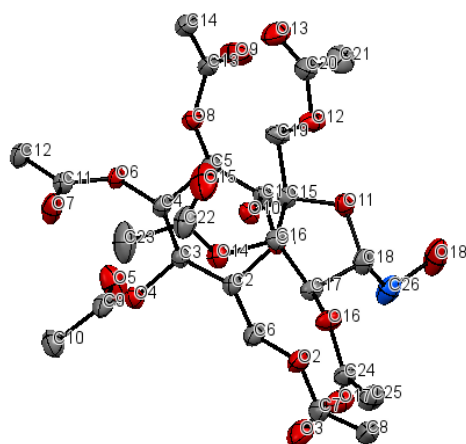


**Figure S5.** Molecular structure of **2**. Crystals were obtained by diffusion of *n*-hexane into a solution of **2** in  $\text{CHCl}_3$ . Thermal ellipsoids are drawn at 50% probability and hydrogen atoms are omitted for clarity. Blue-colored carbon C26 represents the C6' position of the sucrose derivative.

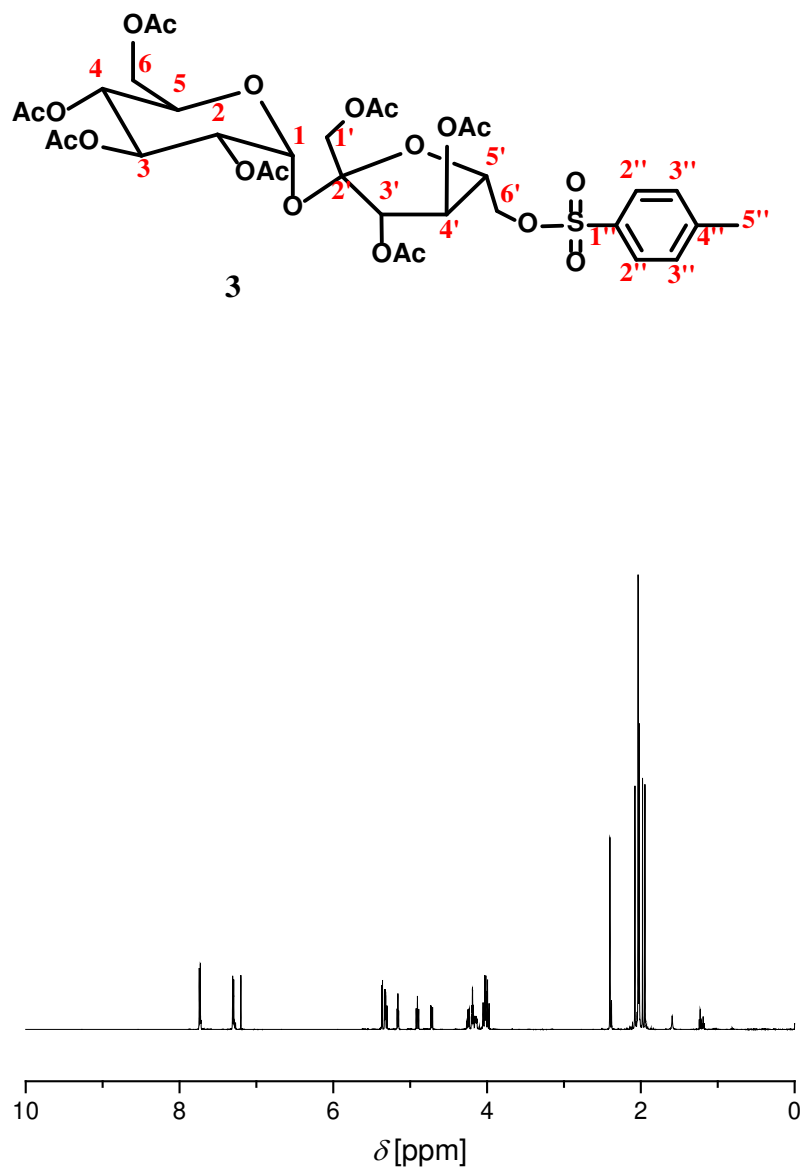


**Figure S6.**  $^1\text{H}$  NMR spectrum of **3** in  $\text{CDCl}_3$ .

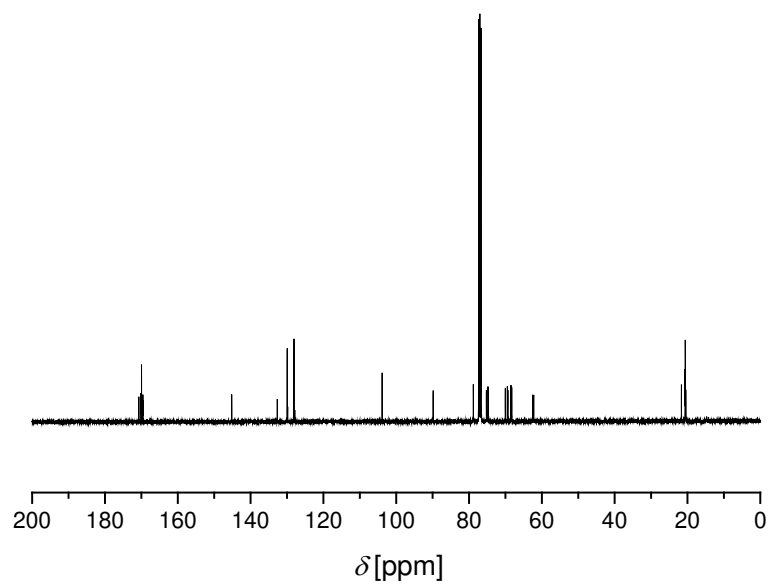


**Figure S7.**  $^{13}\text{C}$  NMR spectrum of **3** in  $\text{CDCl}_3$ .

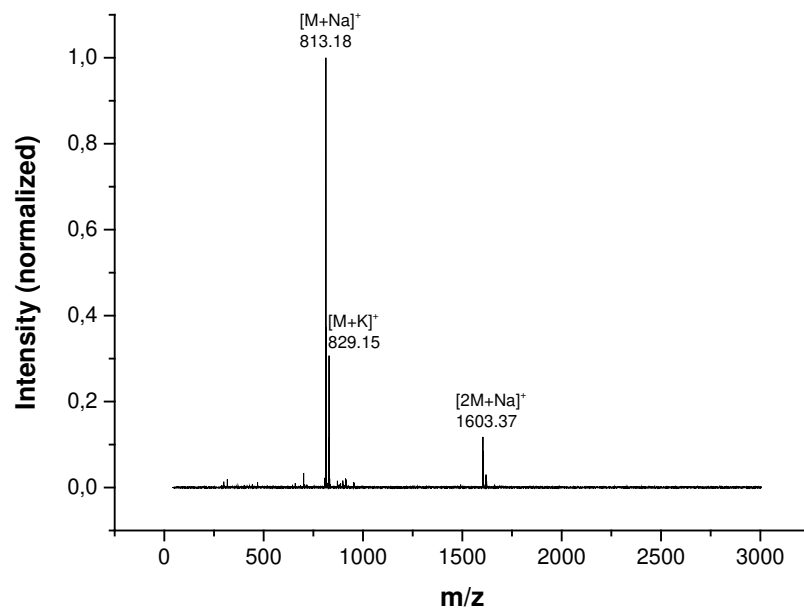


**Figure S8.** ESI-TOF-MS spectrum of **3** in acetonitrile.

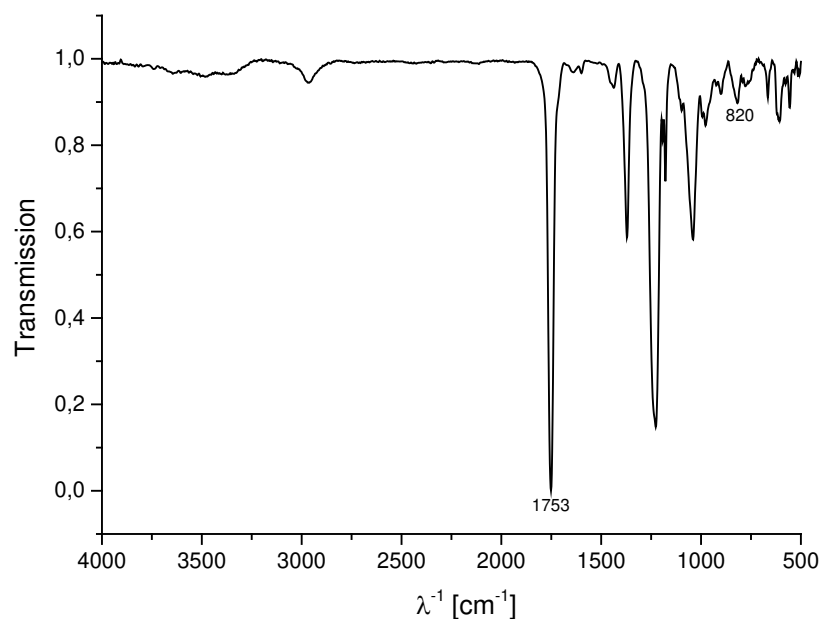


**Figure S9.** IR spectrum of **3**.

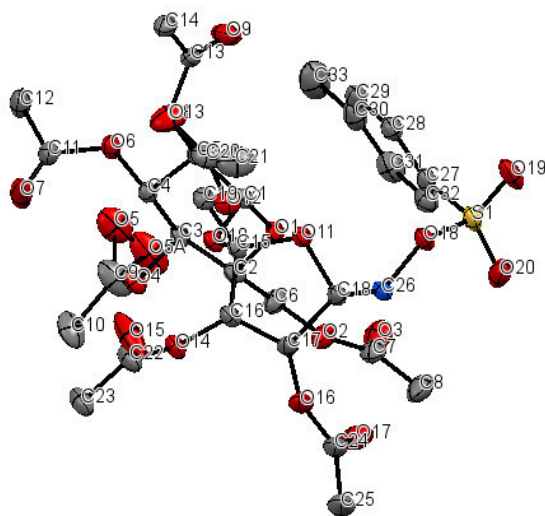


**Figure S10.** Molecular structure of **3**. Crystals were obtained by diffusion of *n*-hexane into a solution of **3** in  $\text{CHCl}_3$ . Thermal ellipsoids are drawn at 50% probability and hydrogen atoms are omitted for clarity. Blue-colored carbon C26 represents the C6' position of the sucrose derivative.

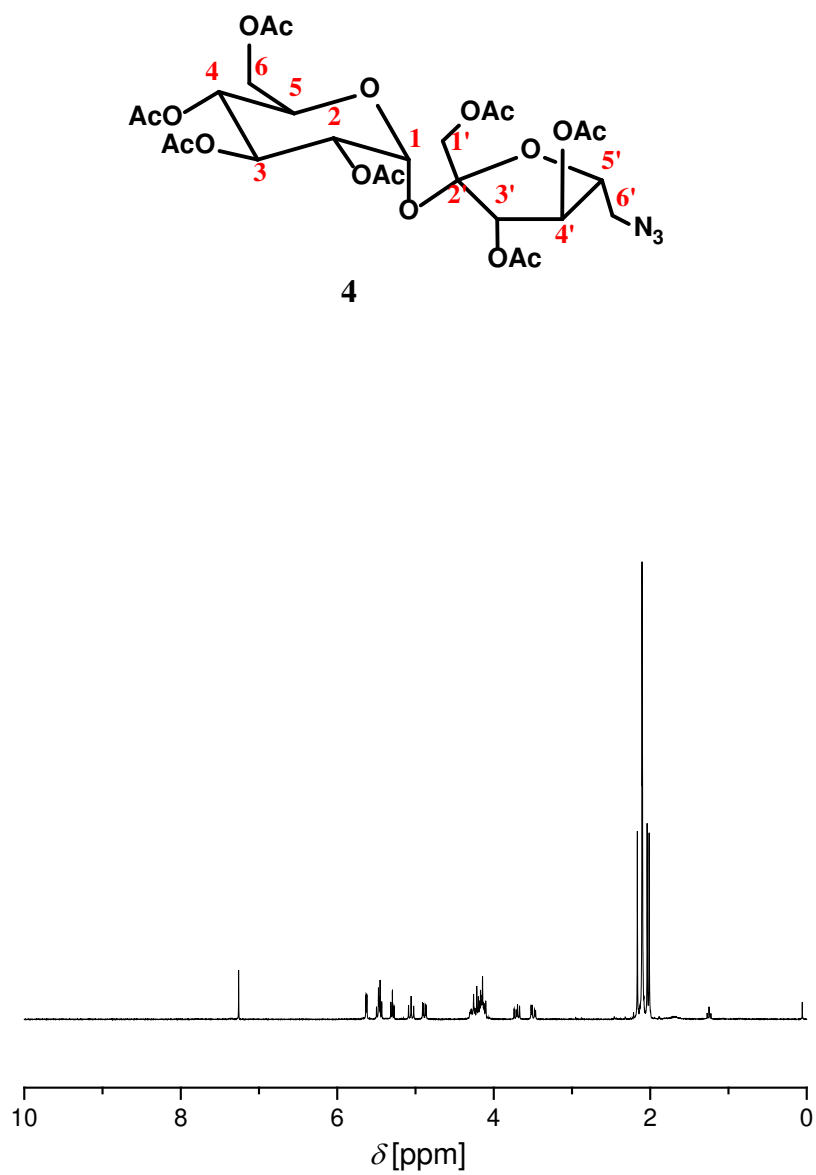


**Figure S11.**  $^1\text{H}$  NMR spectrum of **4** in  $\text{CDCl}_3$ .



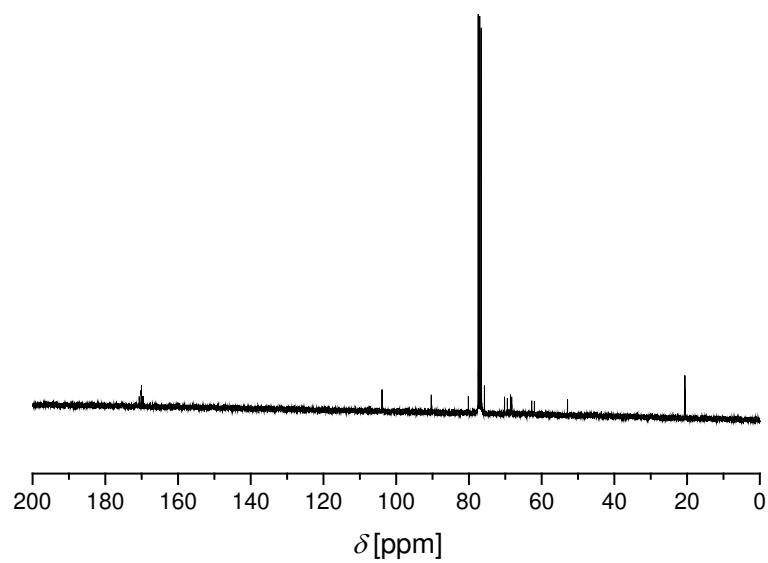


**Figure S12.**  $^{13}\text{C}$  NMR spectrum of **4** in  $\text{CDCl}_3$ .

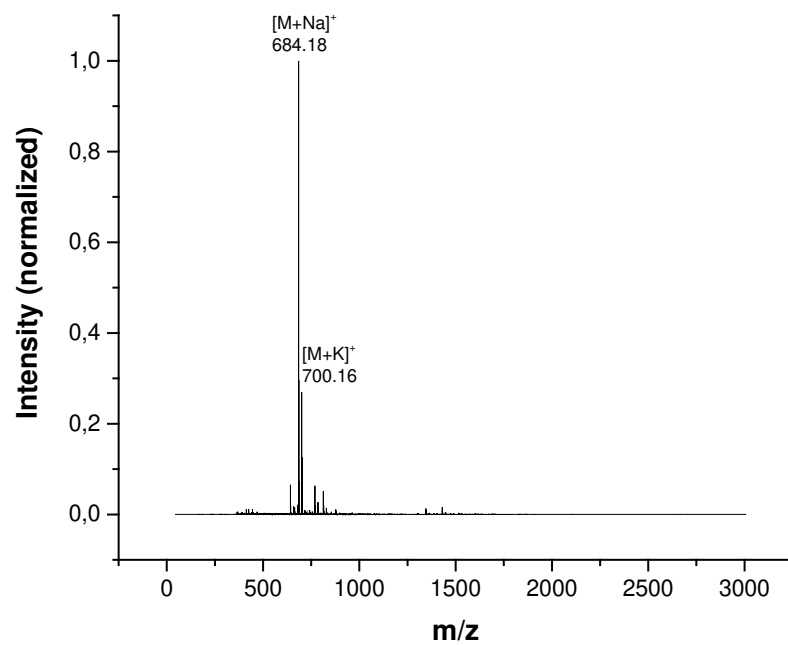


**Figure S13.** ESI-TOF-MS spectrum of **4** in acetonitrile.

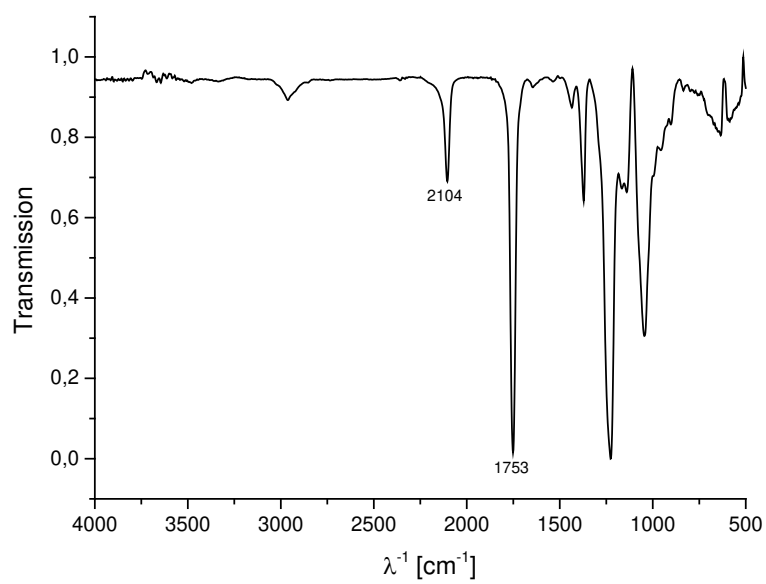


**Figure S14.** IR spectrum of **4**.

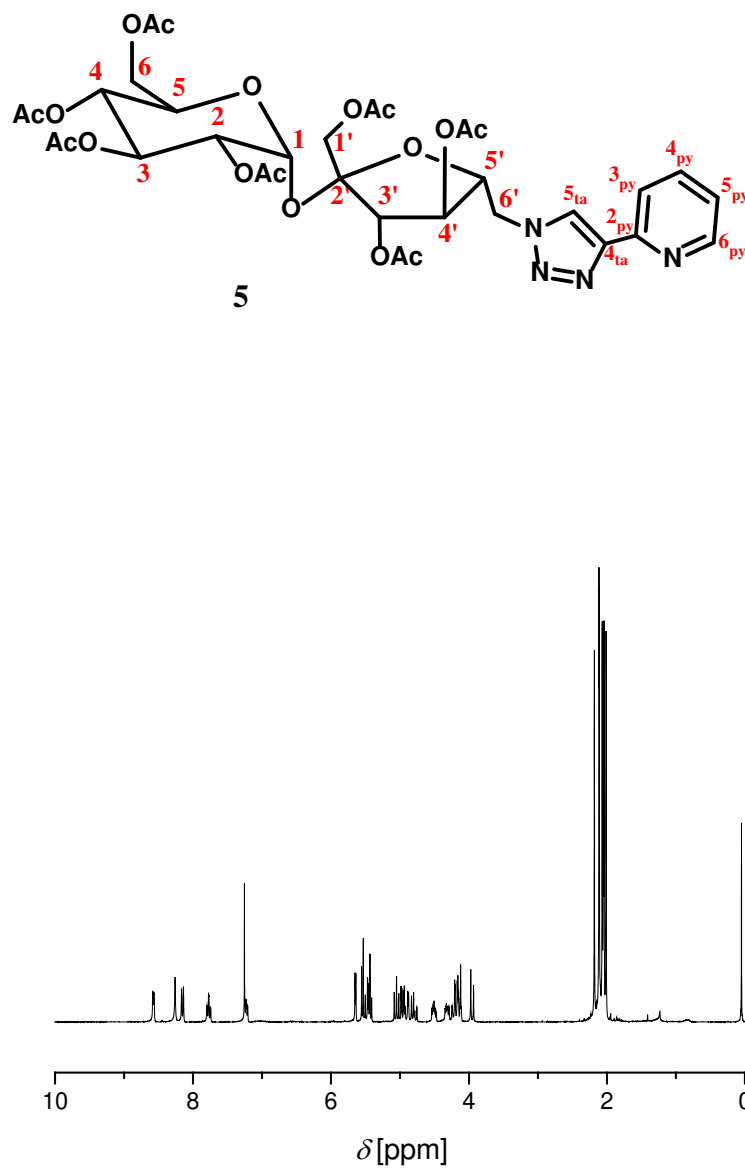


**Figure S15.**  $^1\text{H}$  NMR spectrum of **5** in  $\text{CDCl}_3$ .

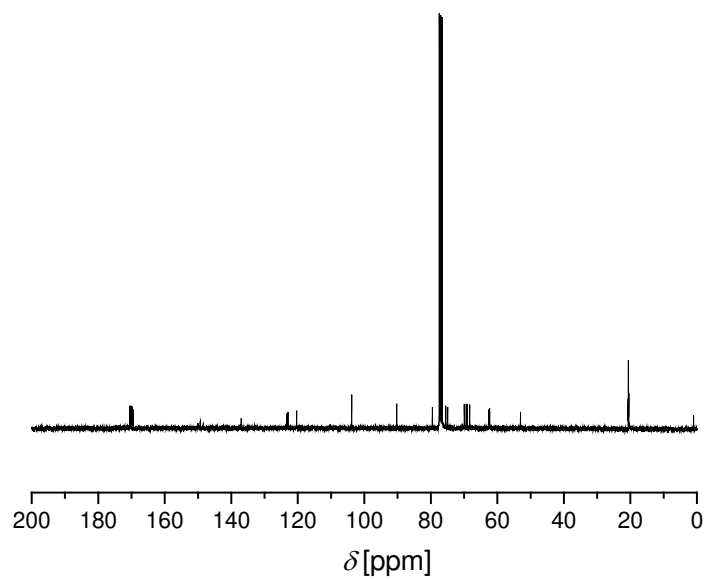


**Figure S16.**  $^{13}\text{C}$  NMR spectrum of **5** in  $\text{CDCl}_3$ .

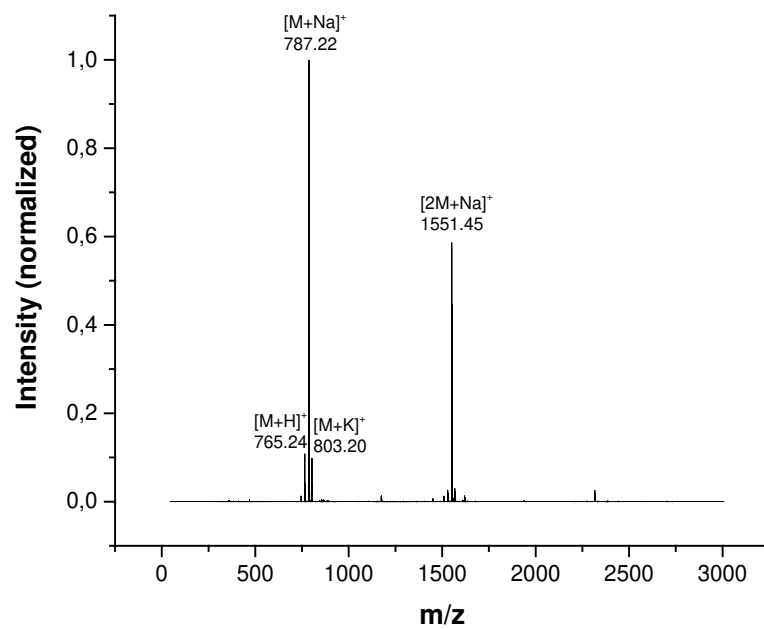


**Figure S17.** ESI-TOF-MS spectrum of **5** in acetonitrile.

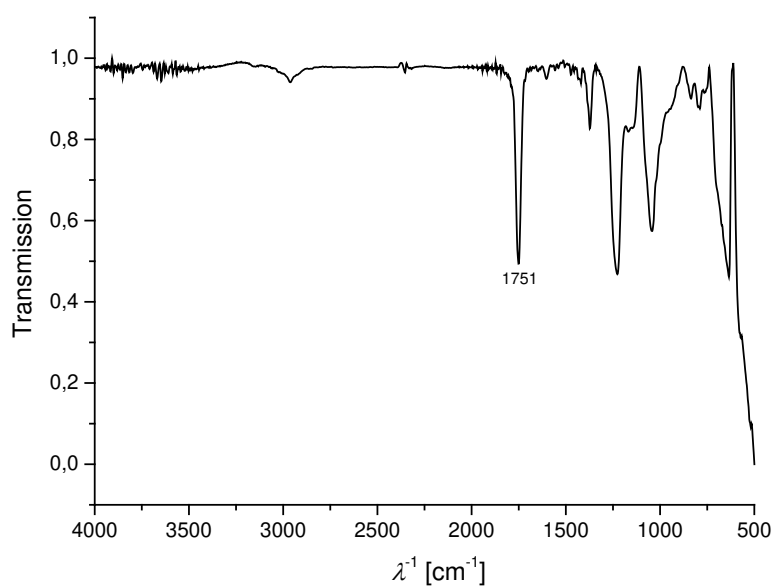


**Figure S18.** IR spectrum of **5**.

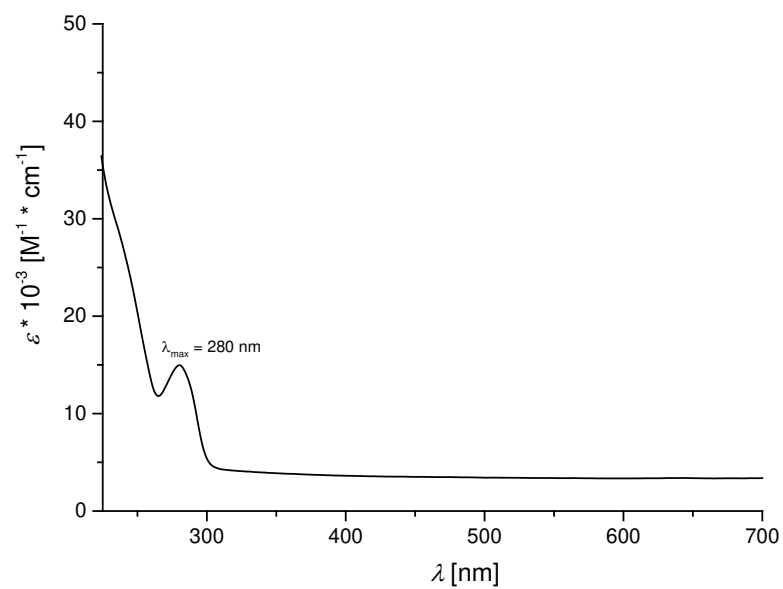


**Figure S19.** UV-Vis spectrum of **5** ( $10^{-5} \text{ M}$ , aerated  $\text{CH}_3\text{OH}$ ).

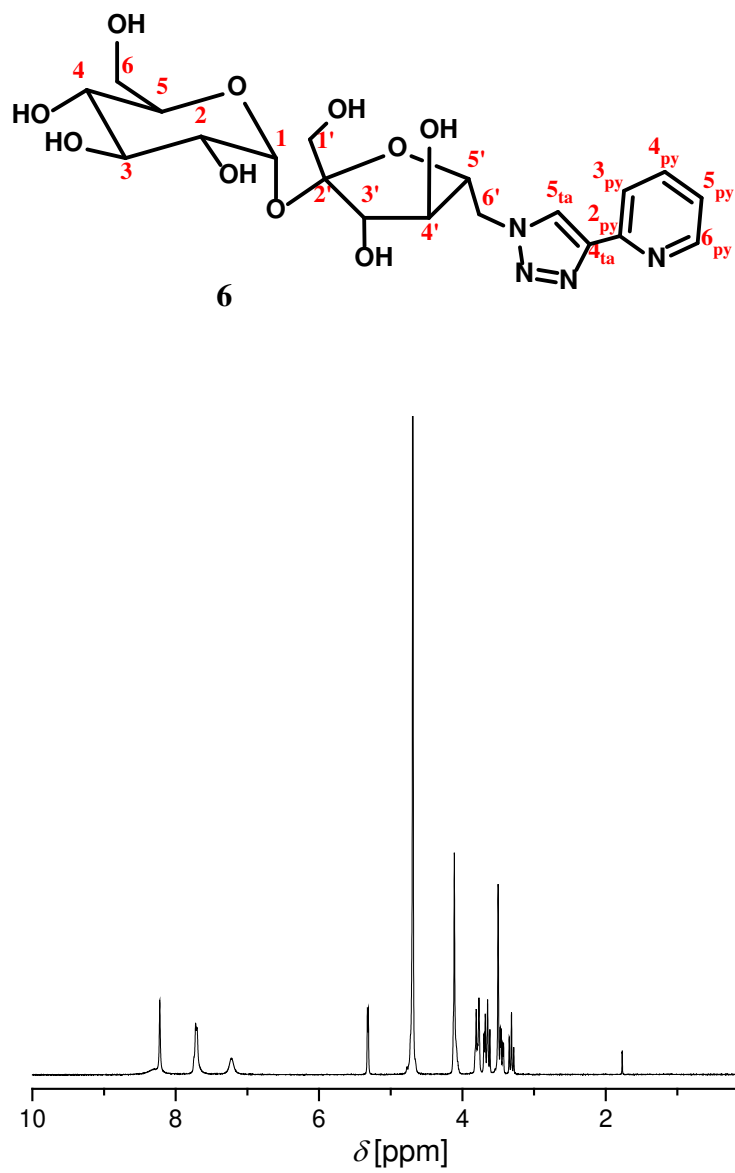


**Figure S20.**  $^1\text{H}$  NMR spectrum of **6** in  $\text{D}_2\text{O}$ .

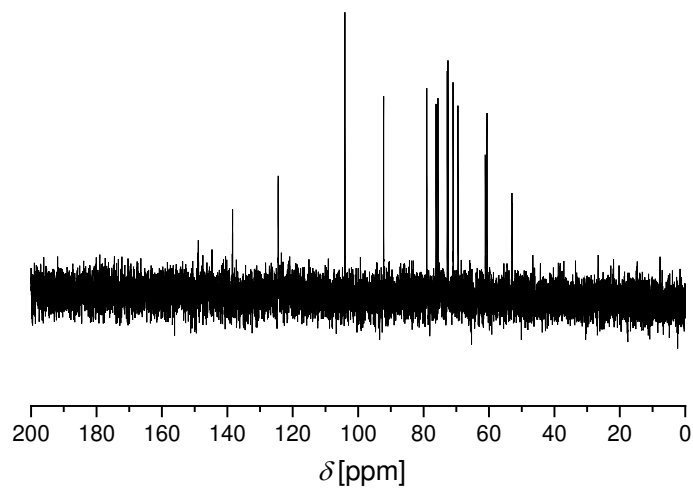


**Figure S21.**  $^{13}\text{C}$  NMR spectrum of **6** in  $\text{D}_2\text{O}$ .

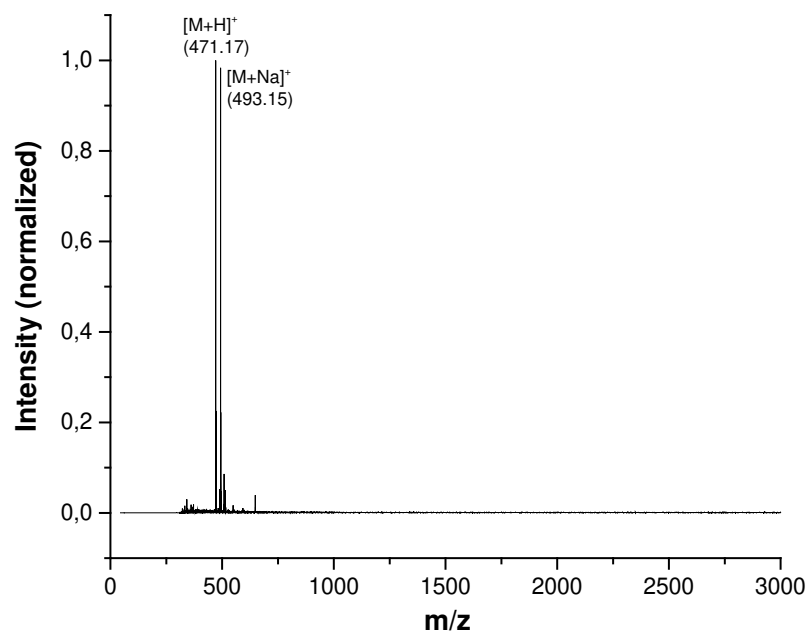


**Figure S22.** ESI-TOF-MS spectrum of **6** in acetonitrile.

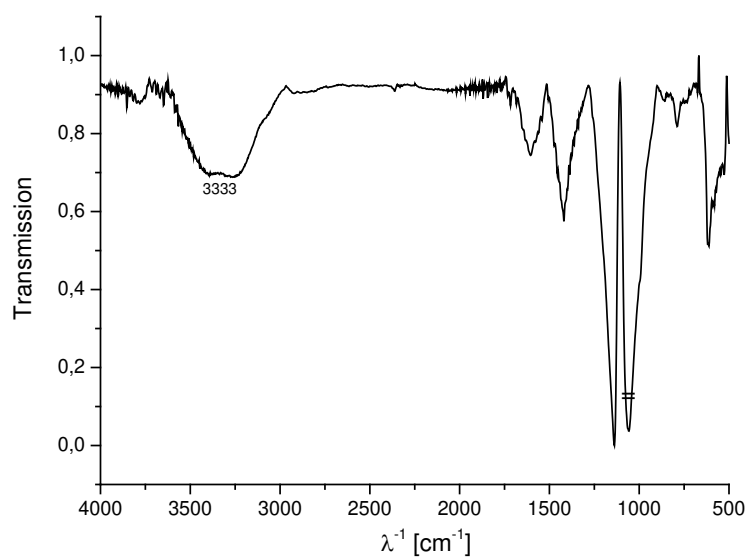


**Figure S23.** IR spectrum of **6**.

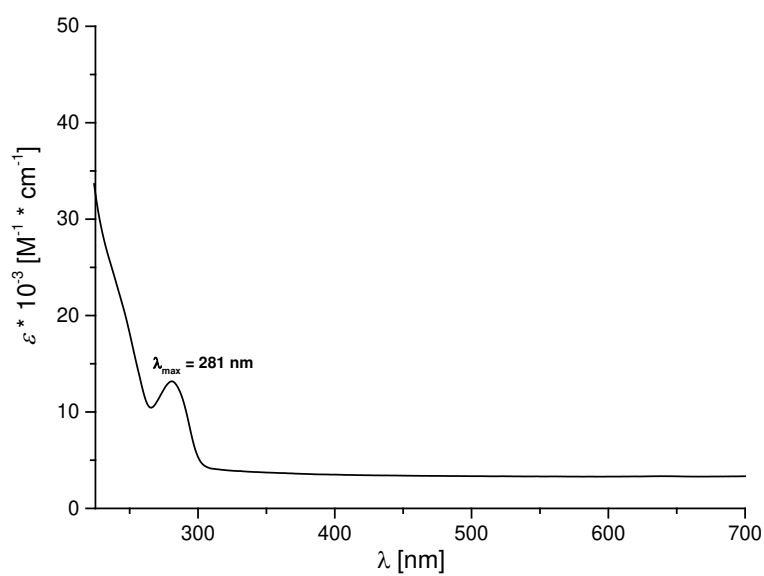


**Figure S24.** UV-Vis spectrum of **6** ( $10^{-5} \text{ M}$ , aerated  $\text{CH}_3\text{OH}$ ).



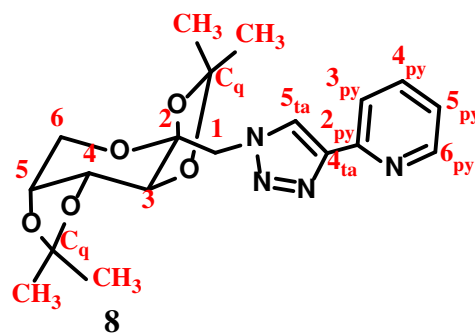


**Figure S25.**  $^1\text{H}$  NMR spectrum of **8** in  $\text{CDCl}_3$ .

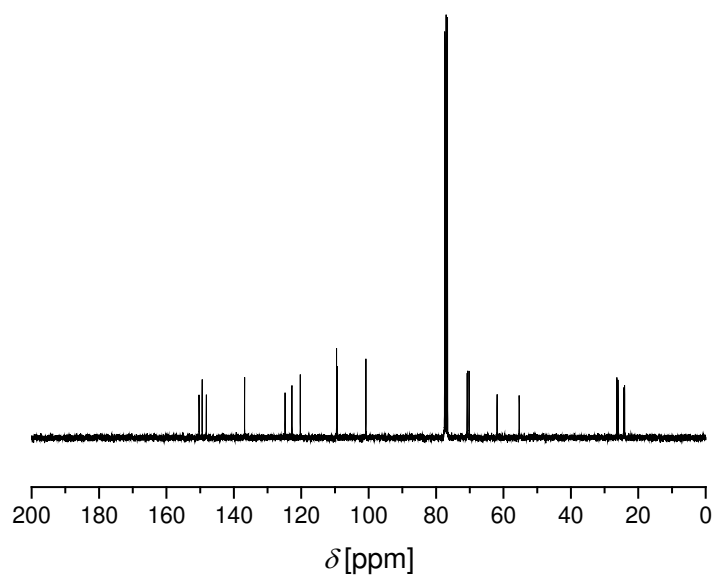


**Figure S26.**  $^{13}\text{C}$  NMR spectrum of **8** in  $\text{CDCl}_3$ .

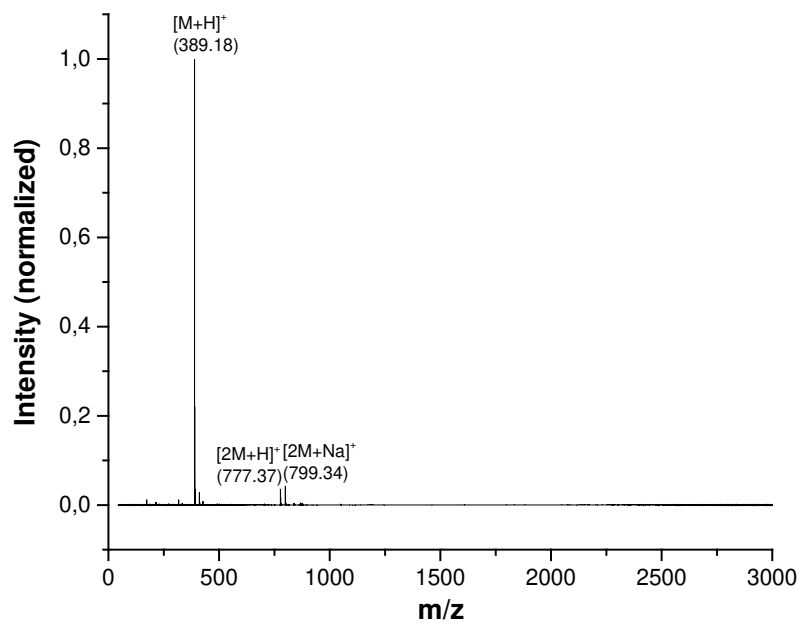


**Figure S27.** ESI-TOF-MS spectrum of **8** in acetonitrile.

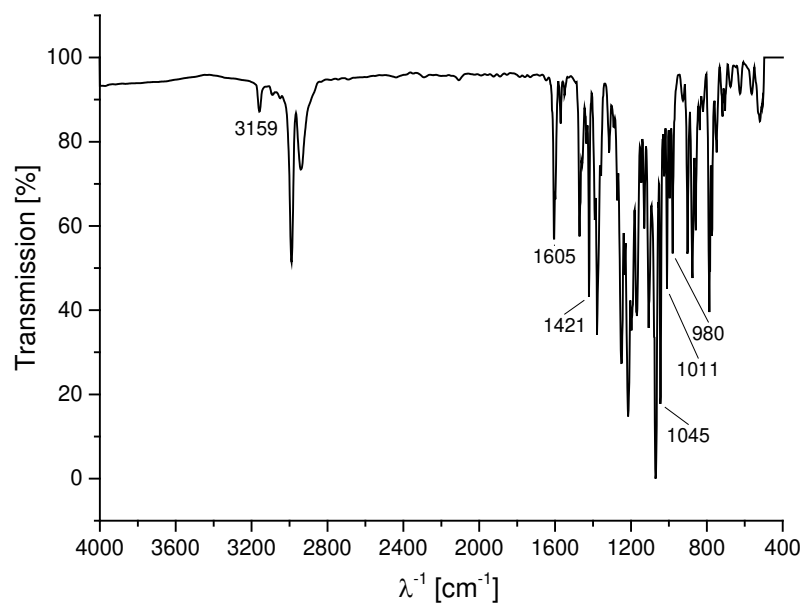


**Figure S28.** IR spectrum of **8**.

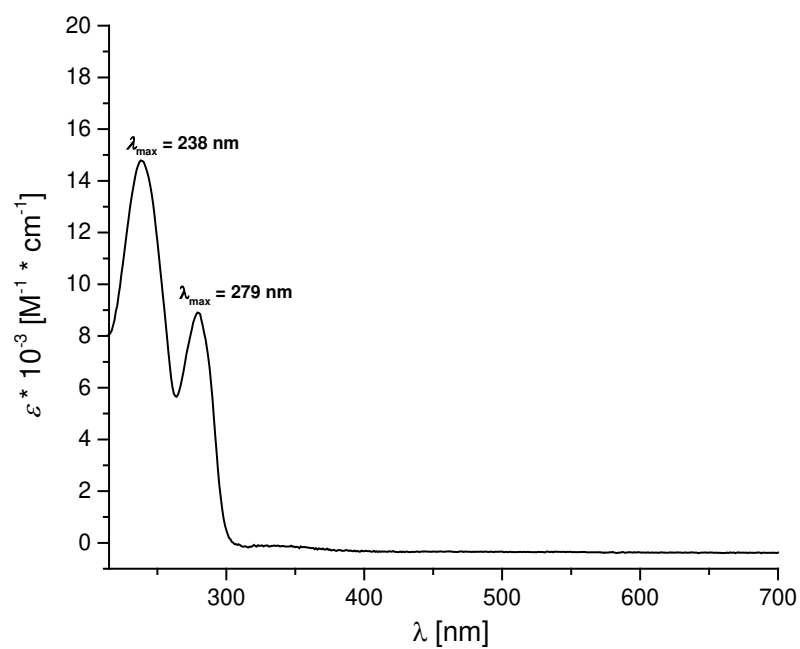


**Figure S29.** UV-Vis spectrum of **8** ( $10^{-5} \text{ M}$ , aerated  $\text{CH}_3\text{OH}$ ).

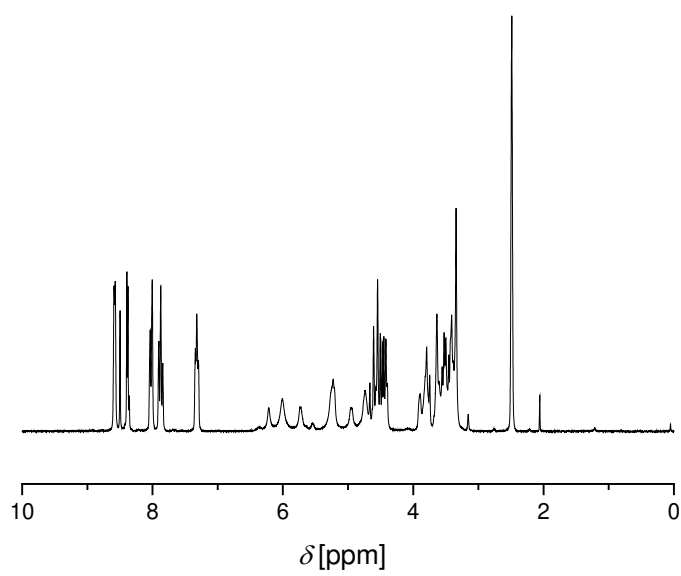
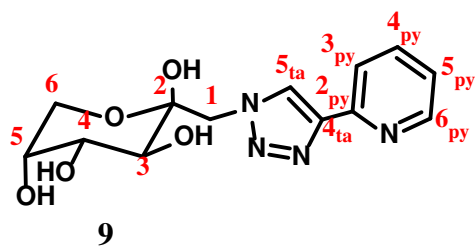


**Figure S30.**  $^1\text{H}$  NMR spectrum of **9** in  $\text{DMSO-d}_6$ .

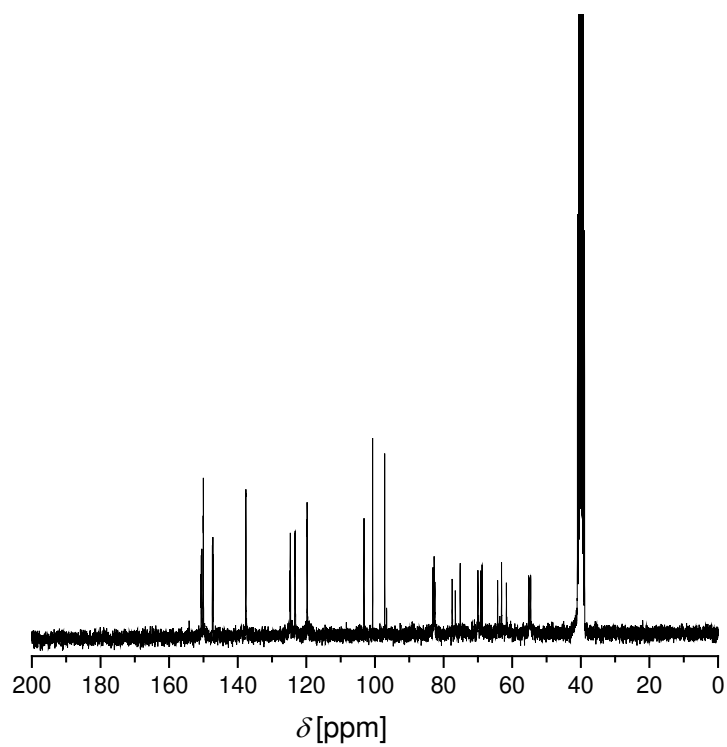


**Figure S31.**  $^{13}\text{C}$  NMR spectrum of **9** in DMSO- $d_6$ .

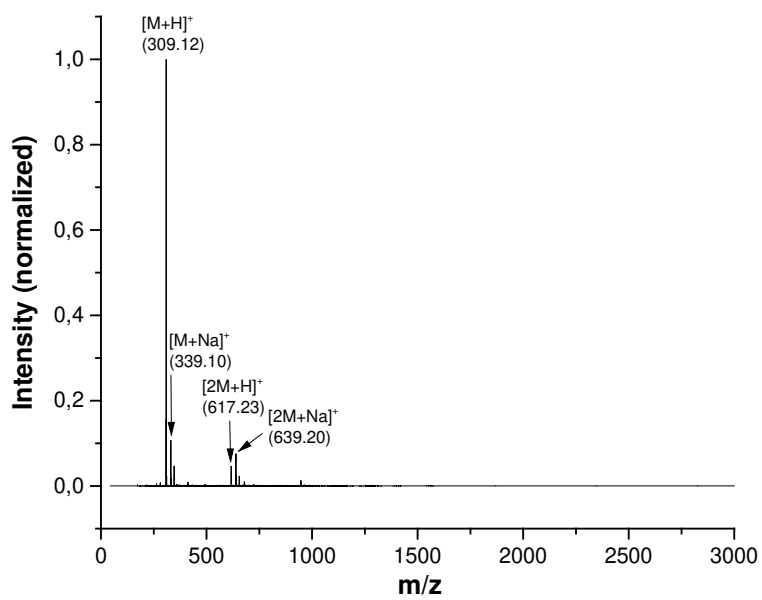


**Figure S32.** ESI-TOF-MS spectrum of **9** in acetonitrile.

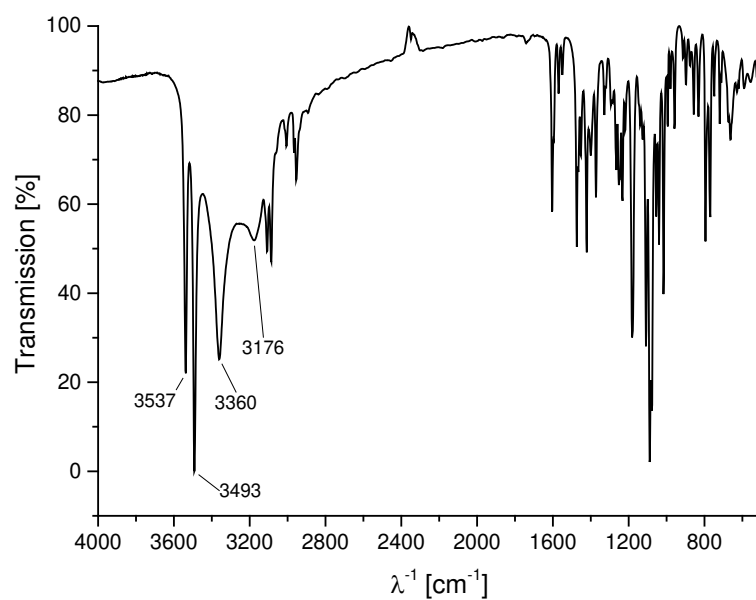


**Figure S33.** IR spectrum of **9**.

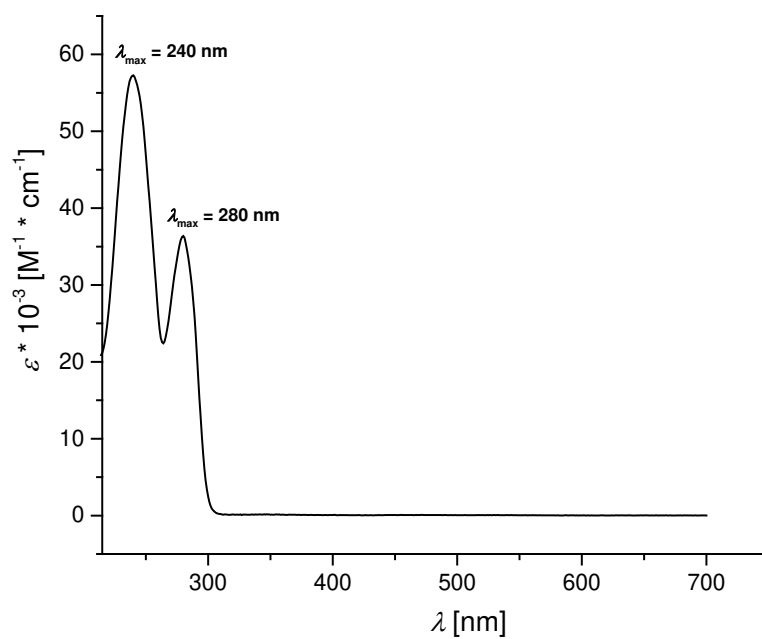


**Figure S34.** UV-Vis spectrum of **9** ( $10^{-5} \text{ M}$ , aerated  $\text{CH}_3\text{OH}$ ).

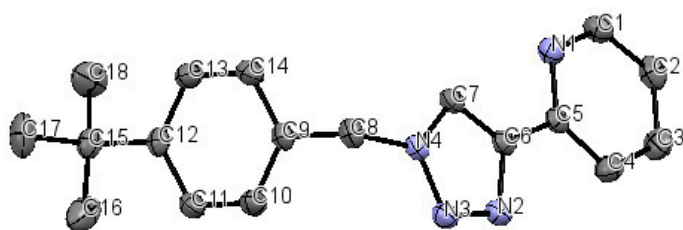
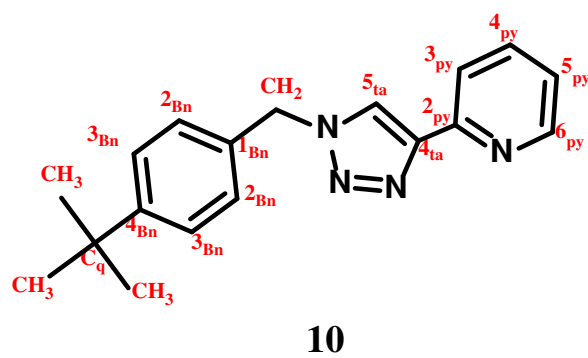


**Figure S35.** Molecular structure of **10**. Crystals were obtained by diffusion of *n*-hexane into a solution of **3** in CHCl<sub>3</sub>. Thermal ellipsoids are drawn at 50% probability and hydrogen atoms are omitted for clarity.

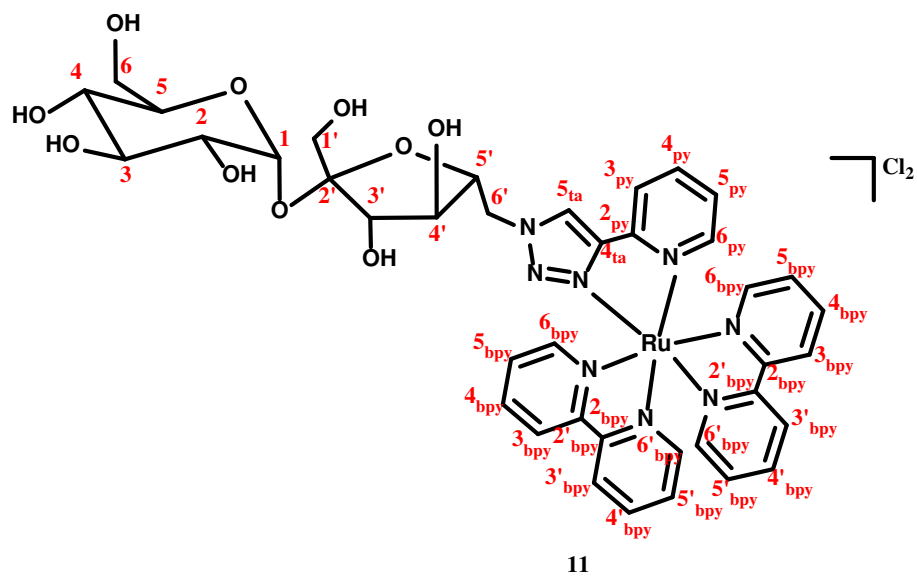


**Figure S36.**  $^1\text{H}$  NMR spectrum of **11** in  $\text{D}_2\text{O}$ .



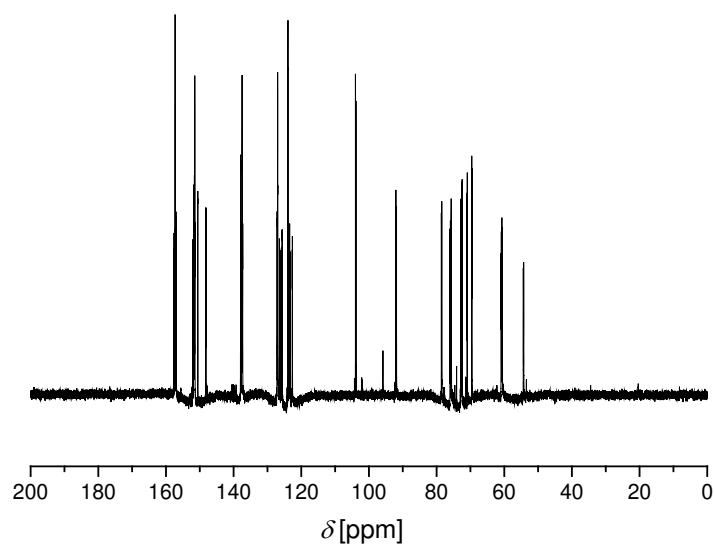


**Figure S37.**  $^{13}\text{C}$  NMR spectrum of **11** in  $\text{D}_2\text{O}$ .

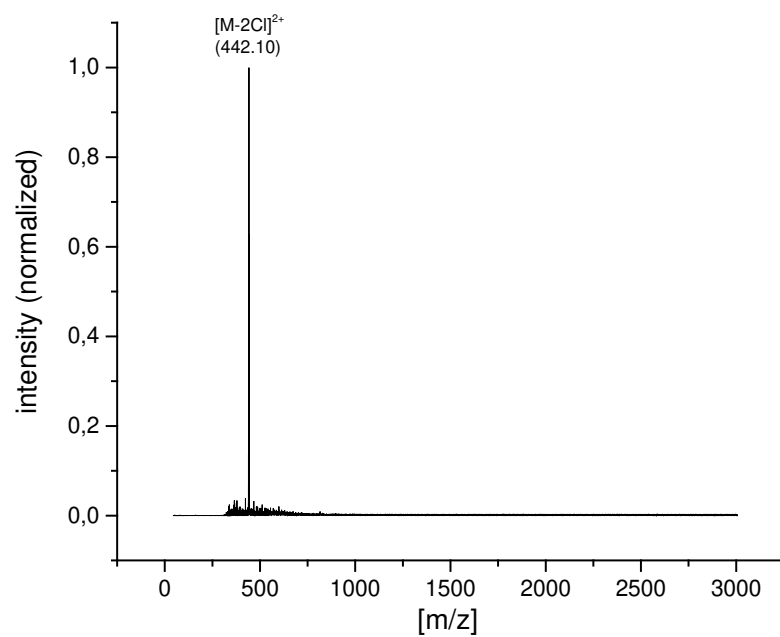


**Figure S38.** ESI-TOF-MS spectrum of **11** in acetonitrile.

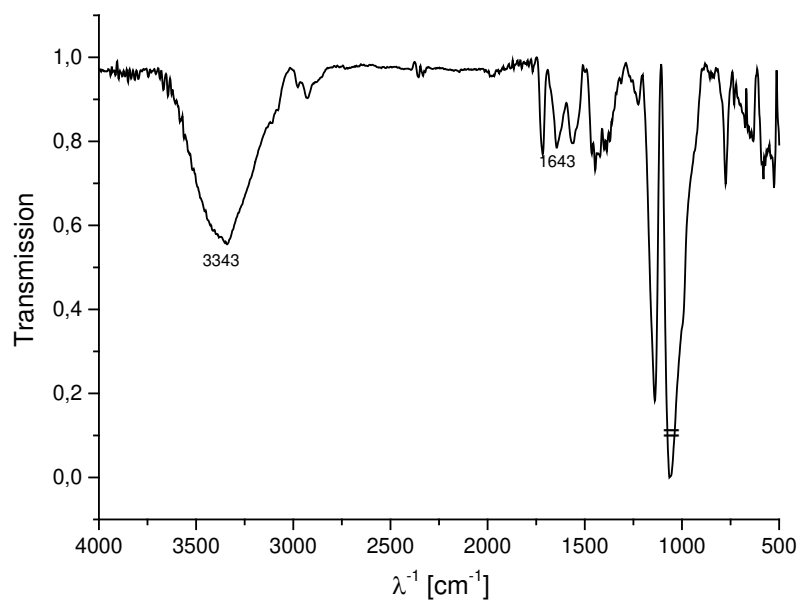


**Figure S39.** IR spectrum of **11**.

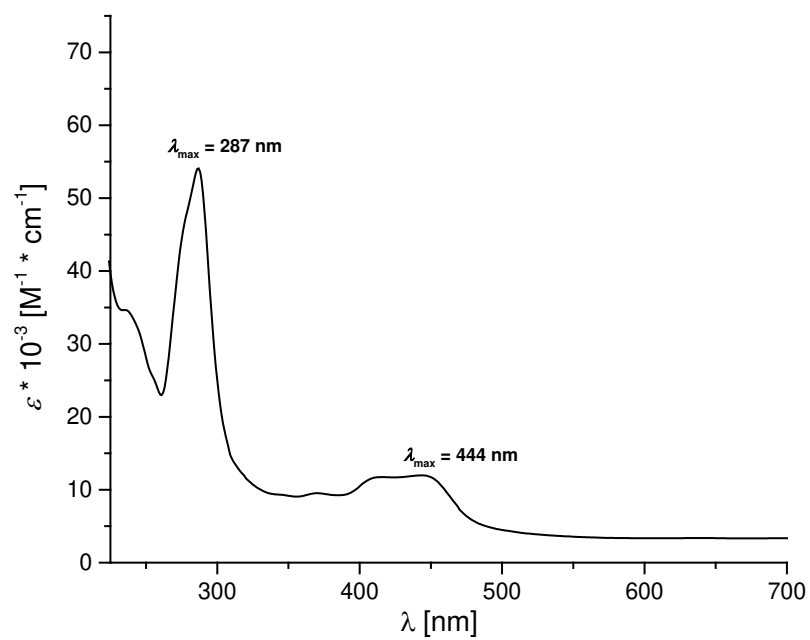


**Figure S40.** UV-Vis spectrum of **11** ( $10^{-5} \text{ M}$ , aerated  $\text{CH}_3\text{OH}$ ).

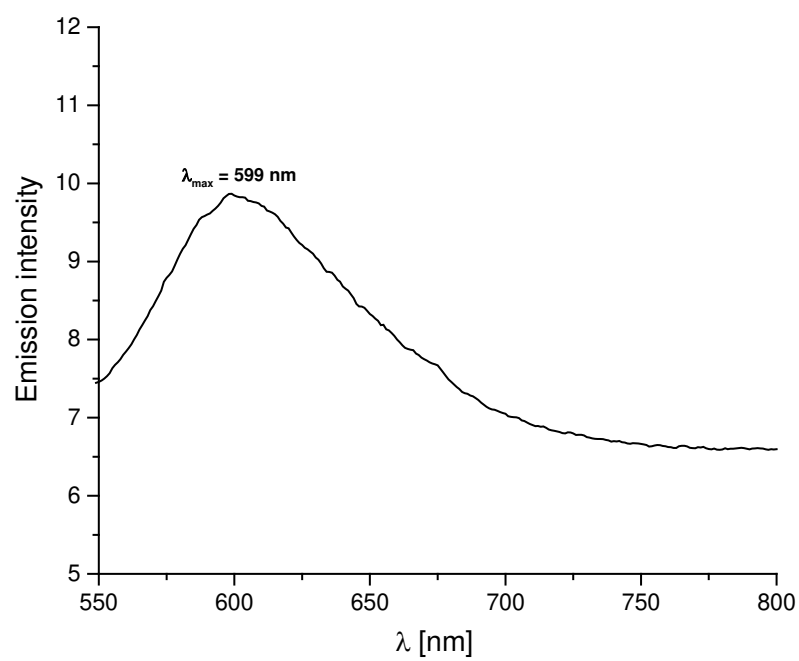


**Figure S41.** Emission spectrum of **11** ( $10^{-5}$  M, aerated  $\text{CH}_3\text{OH}$ ,  $\lambda_{\text{ex}} = 444$  nm).

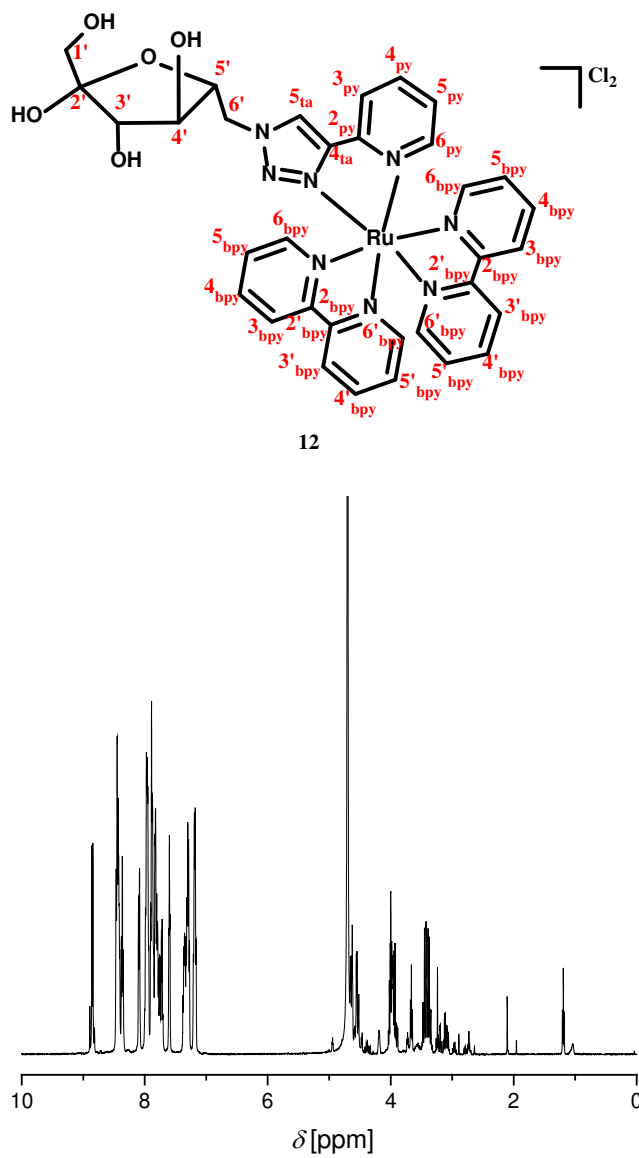


**Figure S42.**  $^1\text{H}$  NMR spectrum of **12** in  $\text{D}_2\text{O}$ .

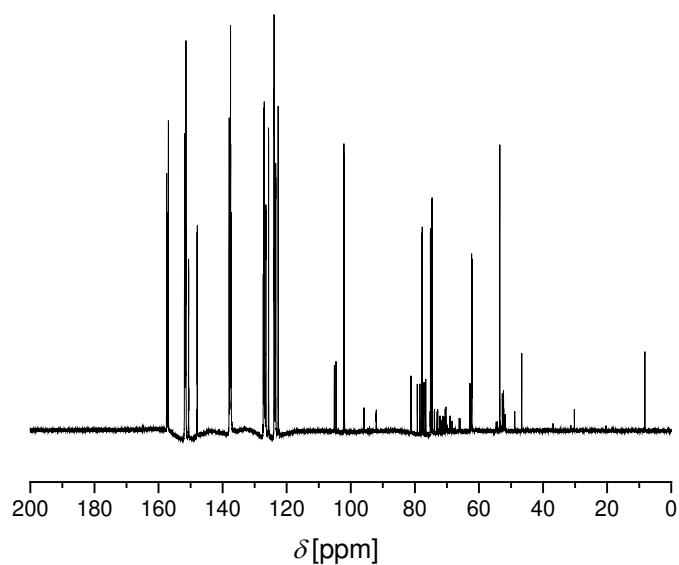


**Figure S43.**  $^{13}\text{C}$  NMR spectrum of **12** in  $\text{D}_2\text{O}$ .

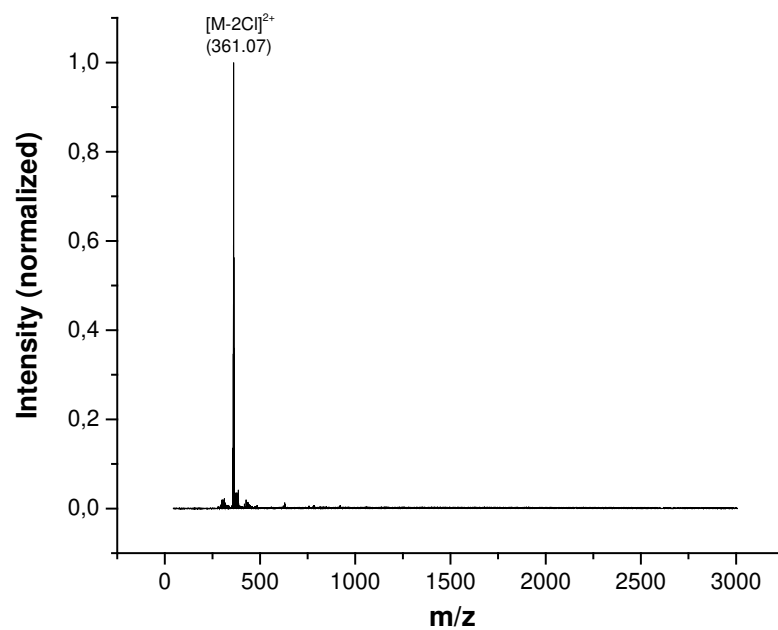


**Figure S44.** ESI-TOF-MS spectrum of **12** in acetonitrile.

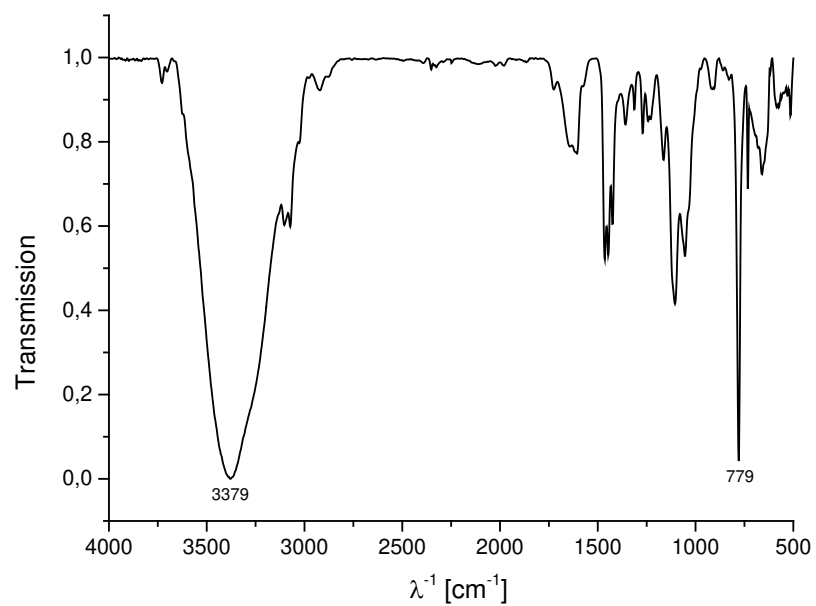


**Figure S45.** IR spectrum of **12**.

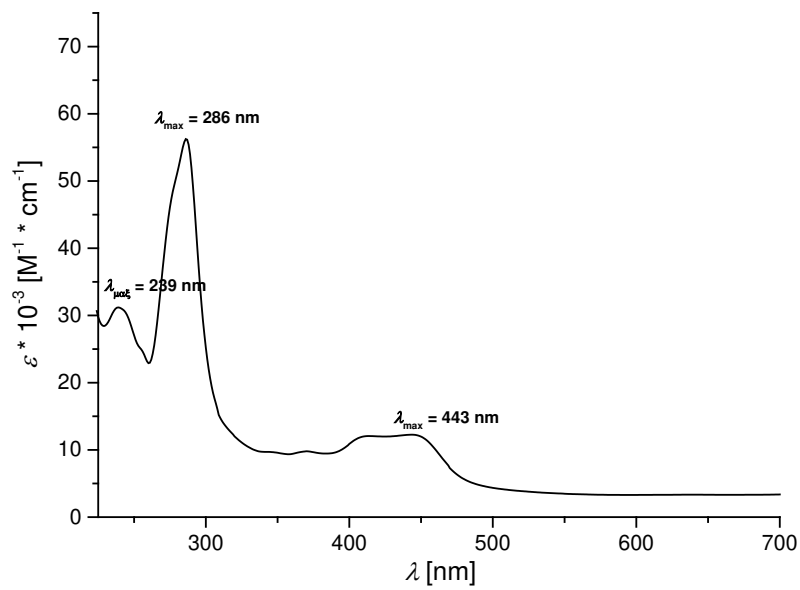


**Figure S46.** UV-Vis spectrum of **12** ( $10^{-5} \text{ M}$ , aerated  $\text{CH}_3\text{OH}$ ).

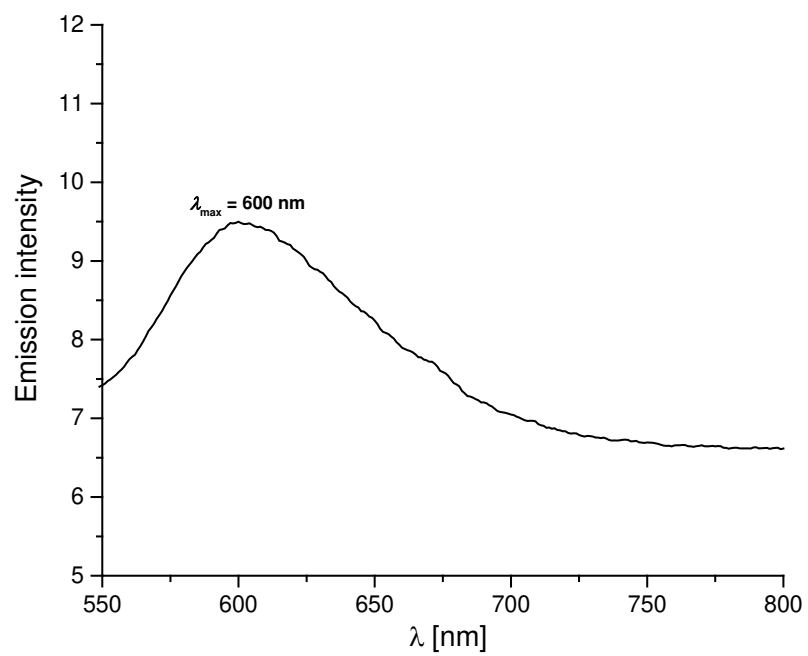


**Figure S47.** Emission spectrum of **12** ( $10^{-5}$  M, aerated  $\text{CH}_3\text{OH}$ ,  $\lambda_{\text{ex}} = 444 \text{ nm}$ ).

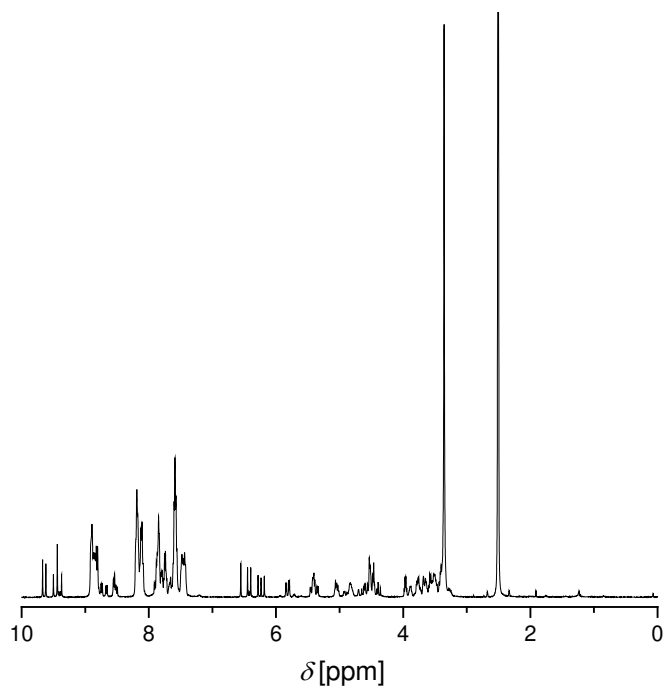
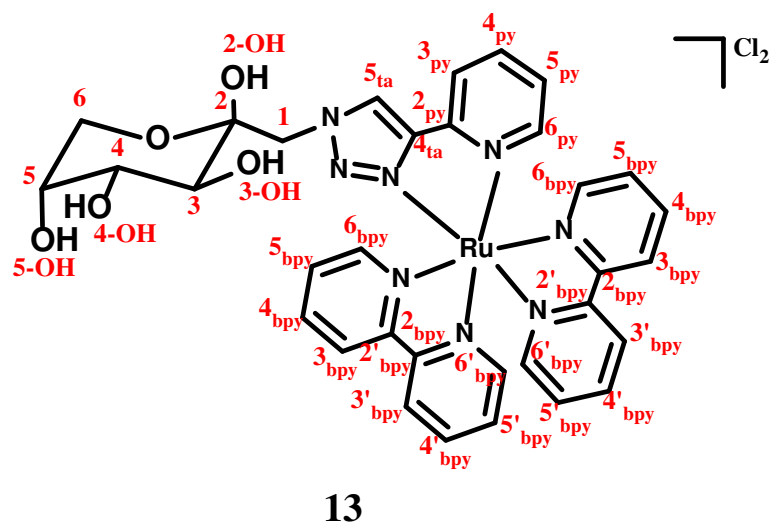


**Figure S48.** <sup>1</sup>H NMR spectrum of **13** in DMSO-d<sub>6</sub>.



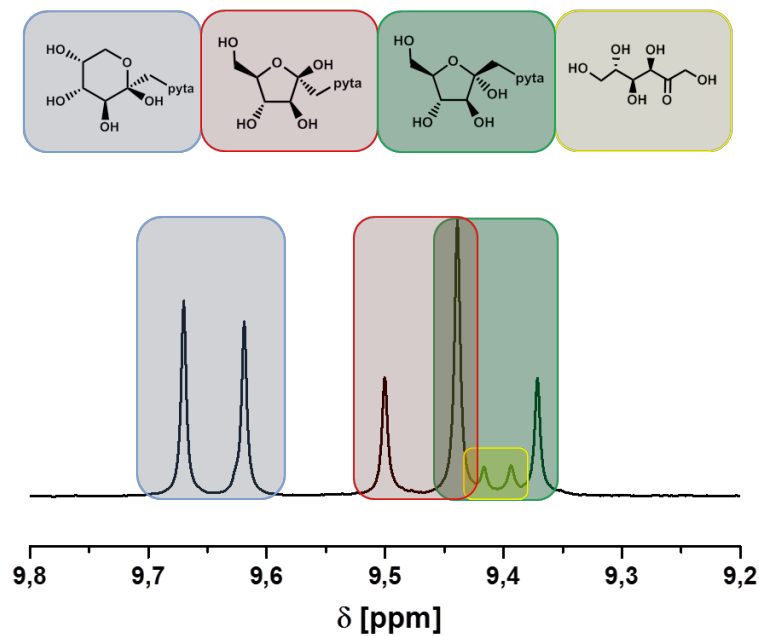


**Figure S49.** Assignment of different forms of D-fructose to signals in  $^1\text{H}$  NMR spectrum of **13**.

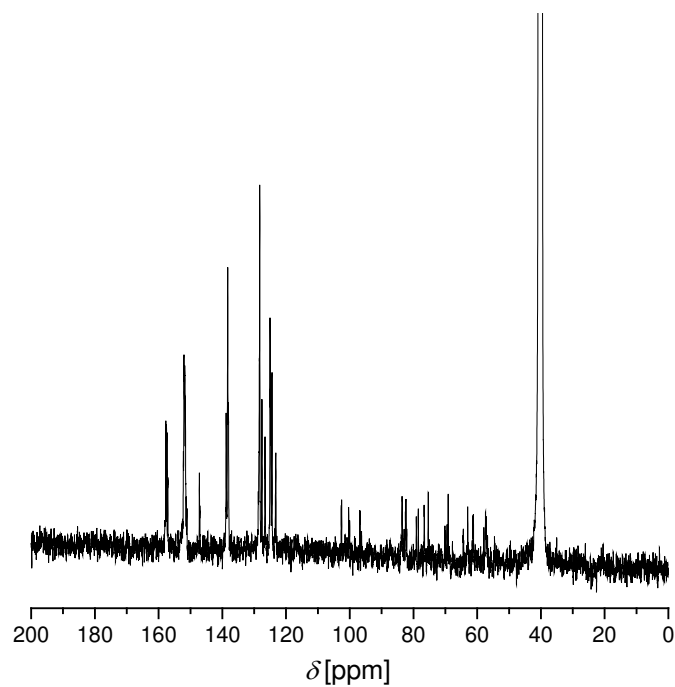


**Figure S50.**  $^{13}\text{C}$  NMR spectrum of **13** in  $\text{DMSO-d}_6$ .

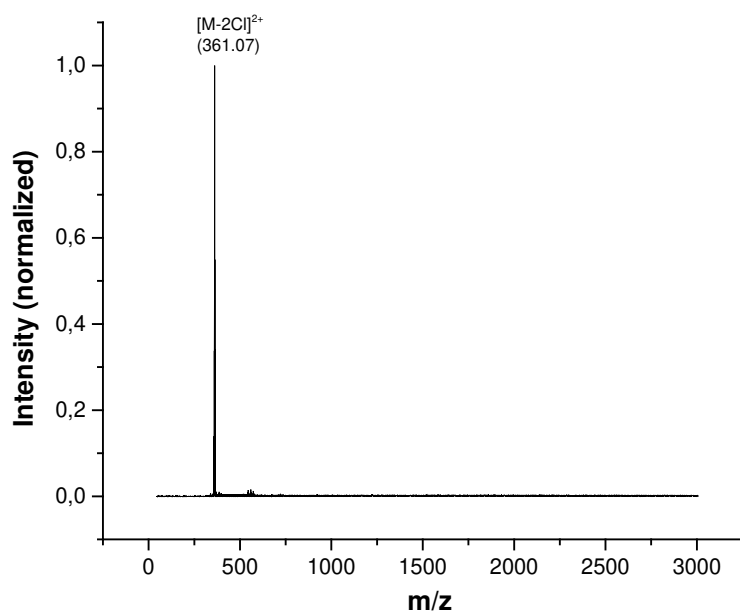


**Figure S51.** ESI-TOF-MS spectrum of **13** in acetonitrile.

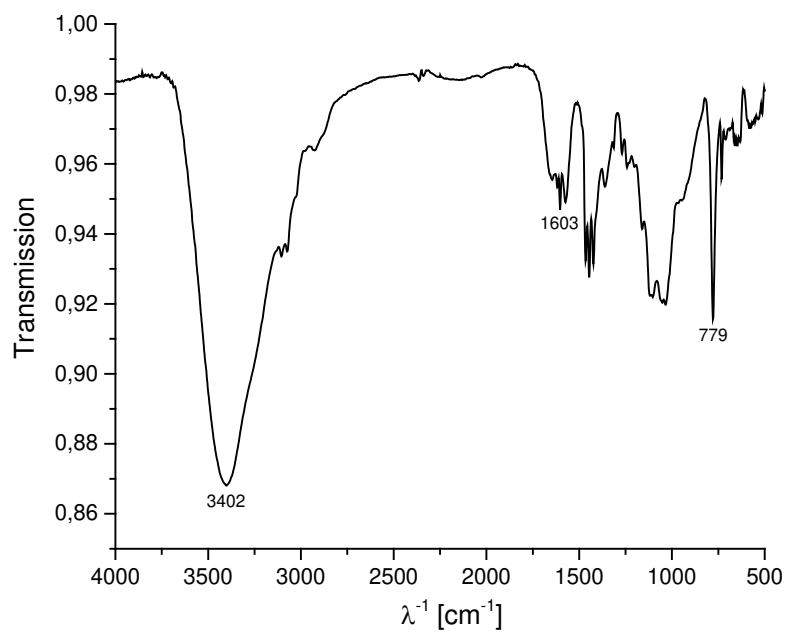


**Figure S52.** IR spectrum of **13**.

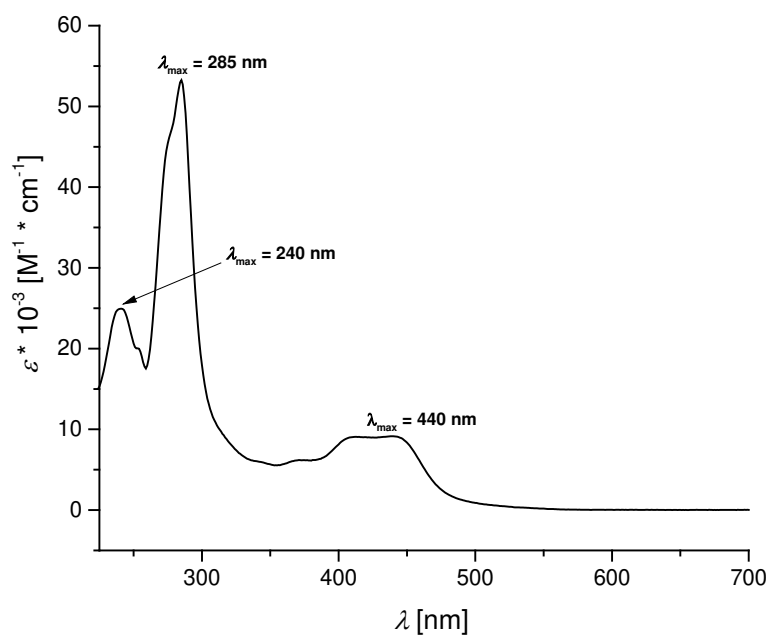


**Figure S53.** UV-Vis spectrum of **13** ( $10^{-5} \text{ M}$ , aerated  $\text{CH}_3\text{OH}$ ).

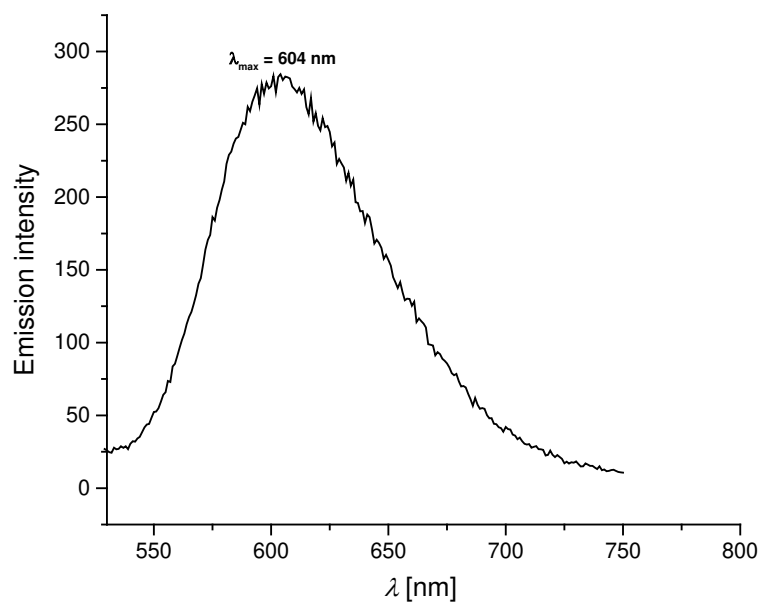


**Figure S54.** Emission spectrum of **13** ( $10^{-5} \text{ M}$ , aerated  $\text{CH}_3\text{OH}$ ,  $\lambda_{\text{ex}} = 439 \text{ nm}$ ).

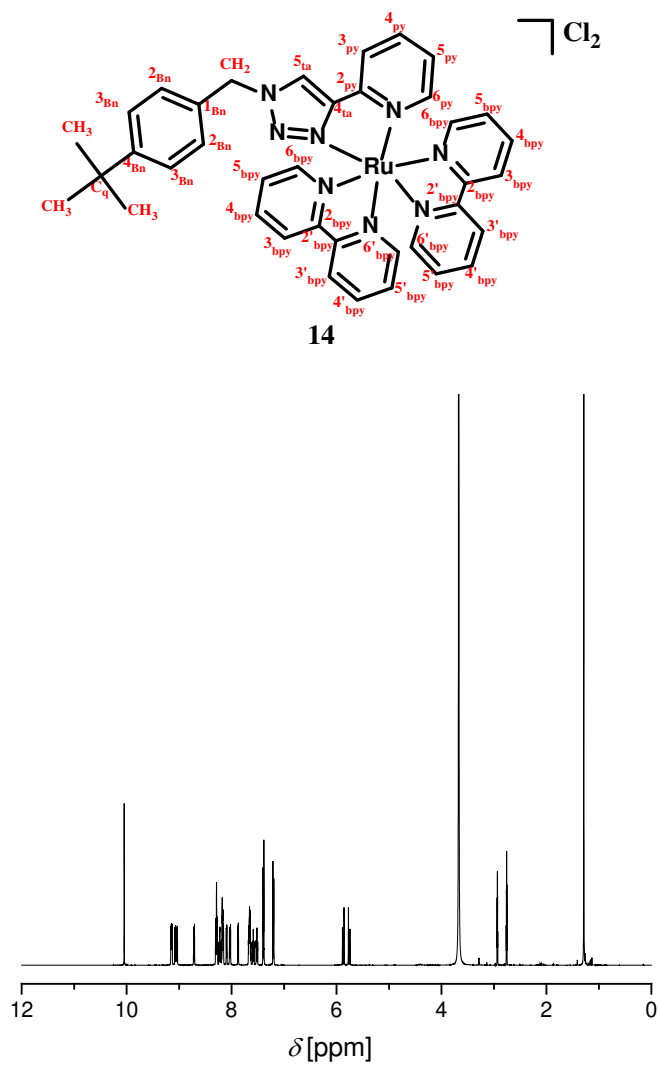


**Figure S55.**  $^1\text{H}$  NMR spectrum of **14** in  $\text{DMF-d}_7$ .

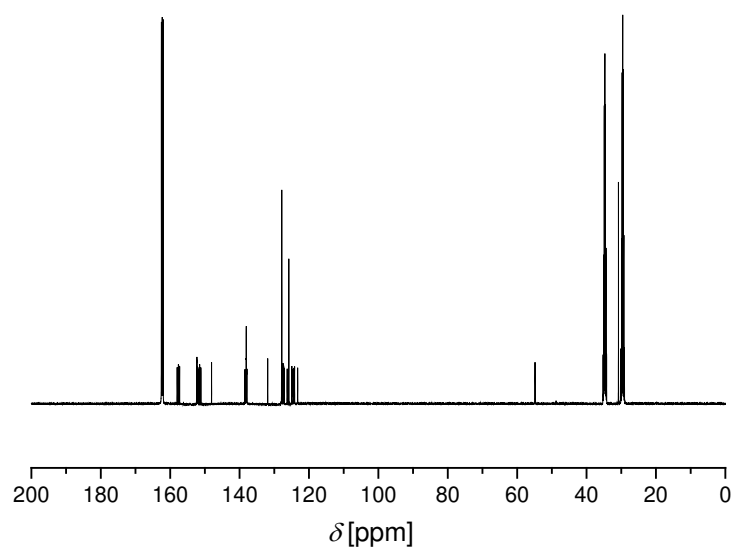


**Figure S56.**  $^{13}\text{C}$  NMR spectrum of **14** in  $\text{DMF-d}_7$ .

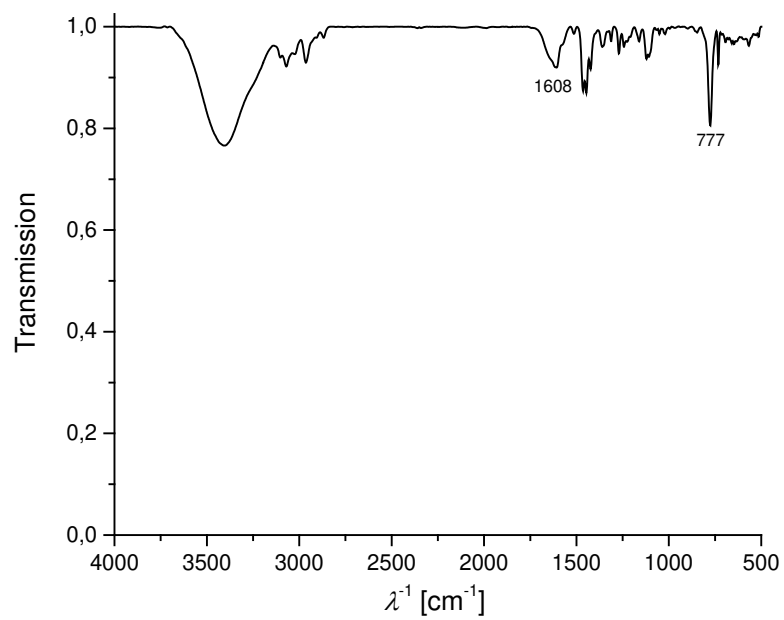


**Figure S57.** IR spectrum of **14**.

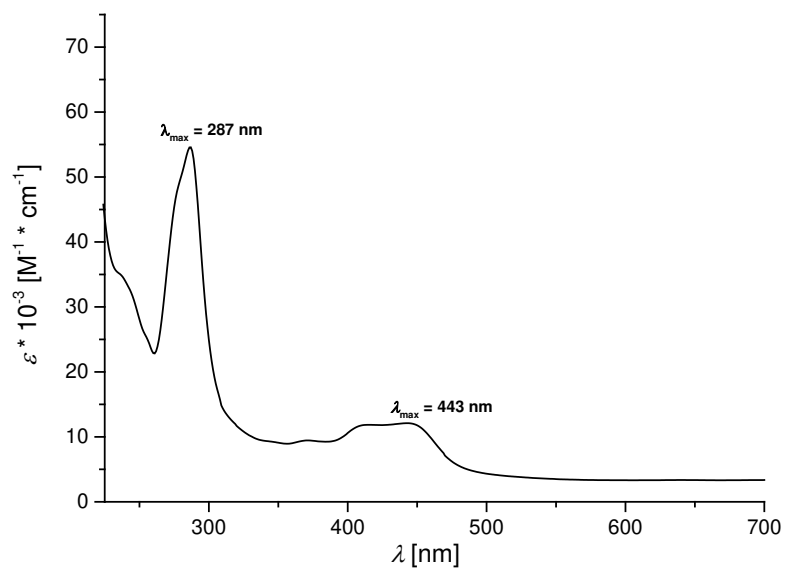


**Figure S58.** UV-Vis spectrum of **14** ( $10^{-5} \text{ M}$ , aerated  $\text{CH}_3\text{OH}$ ).

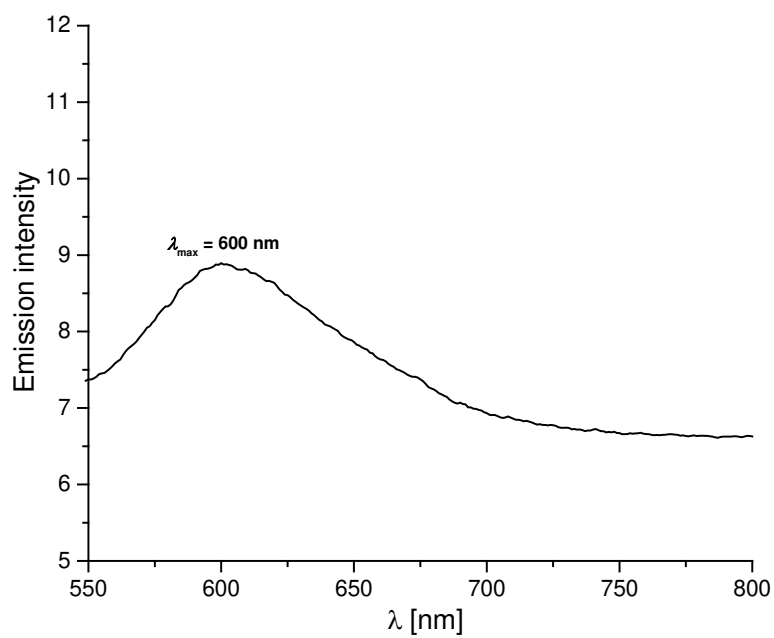


**Figure S59.** Emission spectrum of **14** ( $10^{-5} \text{ M}$ , aerated  $\text{CH}_3\text{OH}$ ,  $\lambda_{\text{ex}} = 444 \text{ nm}$ ).

**Table S1.** Summarized absorption emission data of all measured compounds.

Compound	Absorption wavelength $\lambda$ / nm	Extinction coefficient $\varepsilon \times 10^{-3} / \text{M}^{-1} \text{cm}^{-1}$	Emission wavelength $\lambda$ / nm (excitation wavelength $\lambda_{\text{ex}}$ / nm)
<b>5</b>	280	14.97	-
<b>6</b>	281	13.19	-
<b>8</b>	279; 238	8.90; 14.79	-
<b>9</b>	280; 240	36.38; 57.27	-
<b>11</b>	444; 287	11.97; 54.07	599 (444)
<b>12</b>	443; 286; 239	12.26; 56.24; 31.20	600 (444)
<b>13</b>	440, 285, 240	9.14; 53.24; 24.92	604 (439)
<b>14</b>	443; 287	12.11; 54.57	600 (444)

**Table S2.** Crystal data and refinement details for the X-ray structure determinations of the compounds **2**, **3** and **10**.

Compound	<b>2</b>	<b>3</b>	<b>10</b>
formula	C <sub>26</sub> H <sub>36</sub> O <sub>18</sub>	C <sub>33</sub> H <sub>42</sub> O <sub>20</sub> S	C <sub>18</sub> H <sub>20</sub> N <sub>4</sub>
fw (g·mol <sup>-1</sup> )	636.55	790.73	292.38
T/°C	-140(2)	-140(2)	-140(2)
crystal system	monoclinic	orthorhombic	triclinic
space group	P 2 <sub>1</sub>	P 2 <sub>1</sub> 2 <sub>1</sub> 2 <sub>1</sub>	P $\bar{1}$
a/ Å	13.2532(3)	12.9943(1)	5.9855(2)
b/ Å	8.3392(2)	13.7547(1)	11.2424(4)
c/ Å	13.8749(4)	21.6137(2)	12.3320(4)
$\alpha$ /°	90	90	101.426(2)
$\beta$ /°	92.726(1)	90	100.763(2)
$\gamma$ /°	90	90	97.072(2)
V/Å <sup>3</sup>	1531.73(7)	3863.07(5)	787.96(5)
Z	2	4	2
$\rho$ (g·cm <sup>-3</sup> )	1.380	1.360	1.232
$\mu$ (cm <sup>-1</sup> )	1.18	1.64	.76
measured data	11782	23896	7827
data with $I > 2\sigma(I)$	5796	8394	2962
unique data ( $R_{\text{int}}$ )	6747/0.0322	8856/0.0236	3567/0.0259
$wR_2$ (all data, on $F^2$ ) <sup>a)</sup>	0.0957	0.0782	0.1249
$R_1$ ( $I > 2\sigma(I)$ ) <sup>a)</sup>	0.0508	0.0326	0.0524
$S$ <sup>b)</sup>	1.135	1.070	1.036
Res. dens./e·Å <sup>-3</sup>	0.263/-0.187	0.342/-0.253	0.241/-0.212
Flack-parameter	-0.4(9)	-0.01(5)	-
absorpt method	multi-scan	multi-scan	multi-scan
absorpt corr $T_{\text{min}}/T_{\text{max}}$	0.6830/0.7456	0.7141/0.7456	0.6949/0.7456
CCDC No.	1527070	1527071	1527071

<sup>a)</sup> Definition of the  $R$  indices:  $R_1 = (\sum ||F_o| - |F_c||) / \sum |F_o|$ ;  $wR_2 = \{\sum [w(F_o^2 - F_c^2)^2] / \sum [w(F_o^2)^2]\}^{1/2}$  with  $w^{-1} = \frac{1}{\sigma^2(F_o^2)} + \frac{1}{(aP)^2 + bP}$ ;  $P = [2F_c^2 + \text{Max}(F_o^2)/3]$ ; <sup>b)</sup>  $s = \{\sum [w(F_o^2 - F_c^2)^2] / (N_o - N_p)\}^{1/2}$ .



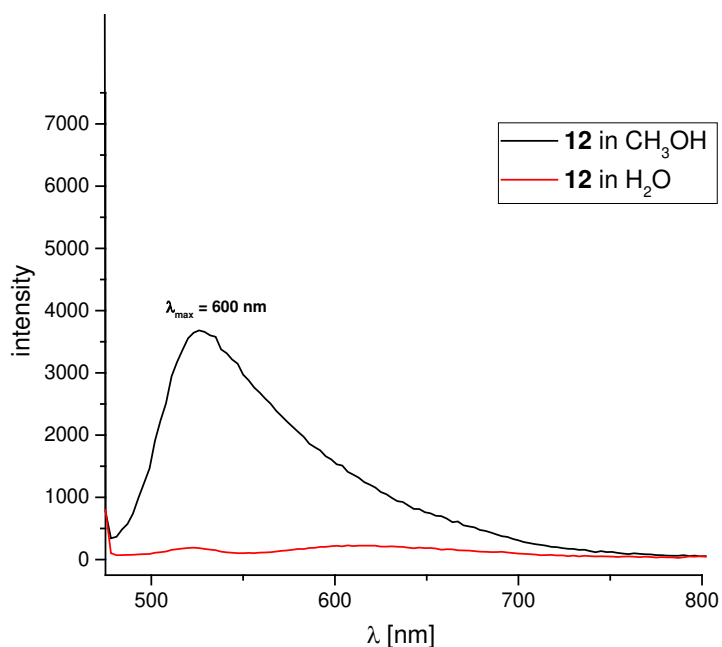


**Figure S60.** Emission spectrum of **12** in CH<sub>3</sub>OH and H<sub>2</sub>O after excitation at  $\lambda_{\text{ex}} = 444 \text{ nm}$  ( $10^{-5} \text{ M}$ ). Fluorescence in water is quenched.

#### Determination of cytotoxicity

To determine the cytotoxic potential of the corresponding complexes on different cell types, the inhibitory effect on the cellular metabolic activity was investigated via a resazurin based assay (alamarBlue, Thermo Fisher). For this purpose, the non-cancerous cell line L929 and the breast cell lines MDA-MB-231 and MCF-7 were used.

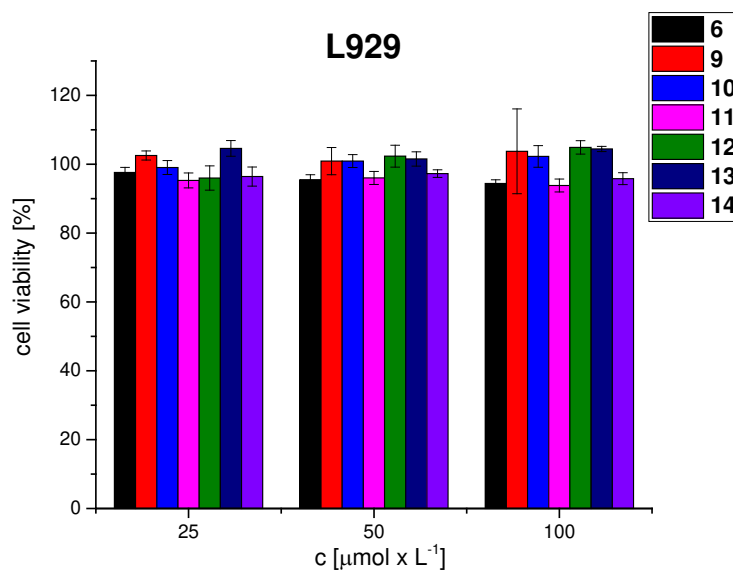


**Figure S61.** Relative viability of L929 cells after 24 h incubation with the complexes at indicated concentrations in serum-containing media. Values represent the mean  $\pm$  S.D. ( $n=3$ ).

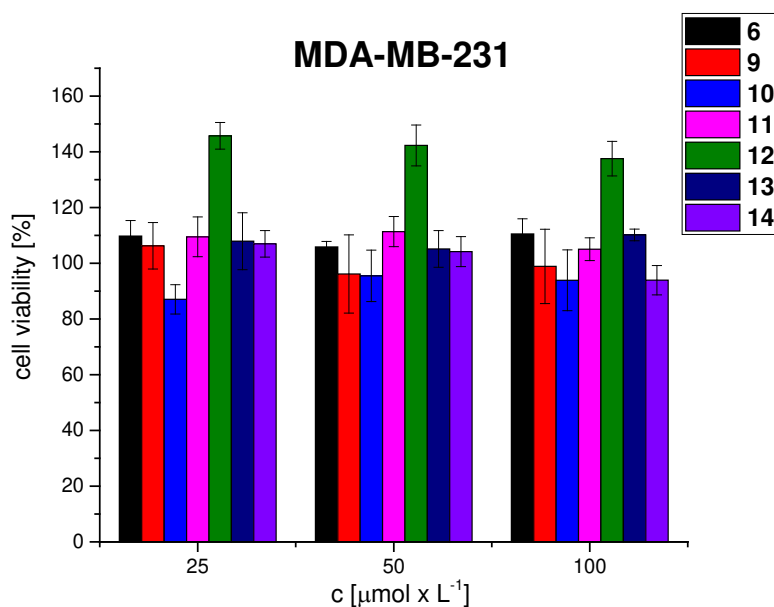


**Figure S62.** Relative viability of MDA-MB-231 cells after 24 h incubation with the complexes at indicated concentrations in serum-containing media. Values represent the mean  $\pm$  S.D. (n=3).

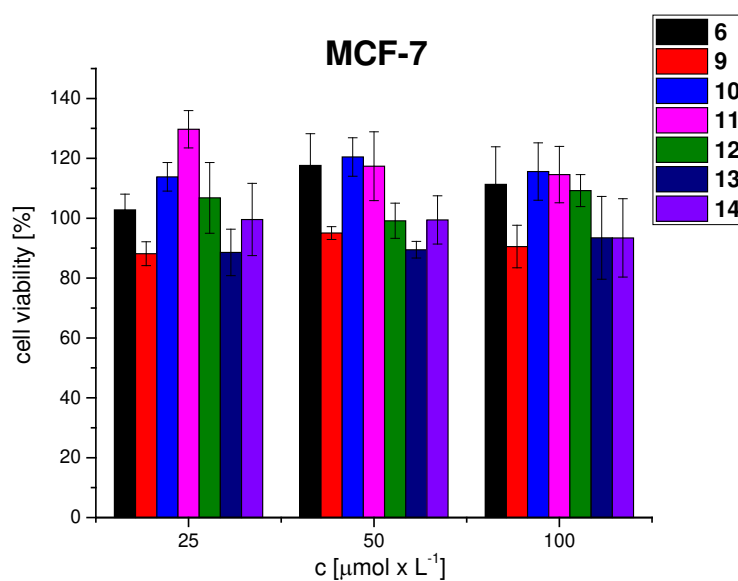


**Figure S63.** Relative viability of MCF-7 cells after 24 h incubation with the complexes at indicated concentrations in serum-containing media. Values represent the mean  $\pm$  S.D. (n=3).

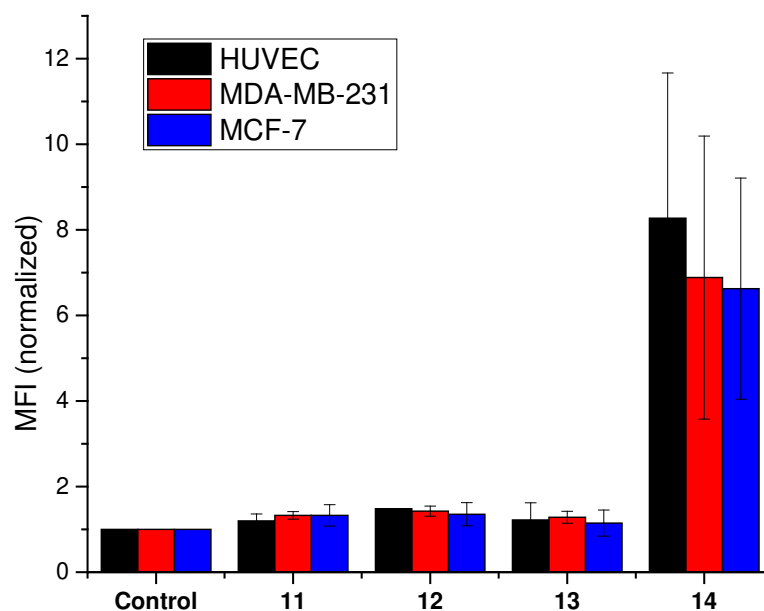


**Figure S64.** Complexes **11** to **14** were incubated with HUVEC, MCF-7 and MDA-MB-231 cells in serum-containing media. The mean fluorescence intensity (MFI) of all viable cells is visualized. Values represent the mean  $\pm$  S.D. ( $n \geq 3$ ). Complexes **11** to **13** show no significant increased MFI values. Complex **14** revealed increased MFI which might be due to particle formulation. This was also verified by DLS measurements.

Dynamic light scattering was performed on a Zetasizer Nano ZS (Malvern Instruments, Herrenberg, Germany). After an equilibration time of 180 s, 3×30 s runs were carried out at 25 °C ( $\lambda = 633$  nm). The counts were detected at an angle of 173°. Each measurement was performed in triplicate. The mean particle size was approximated as the effective (Z-average) diameter and the width of the distribution as the polydispersity index of the particles (PDI) obtained by the cumulants method assuming a spherical shape of the particles.

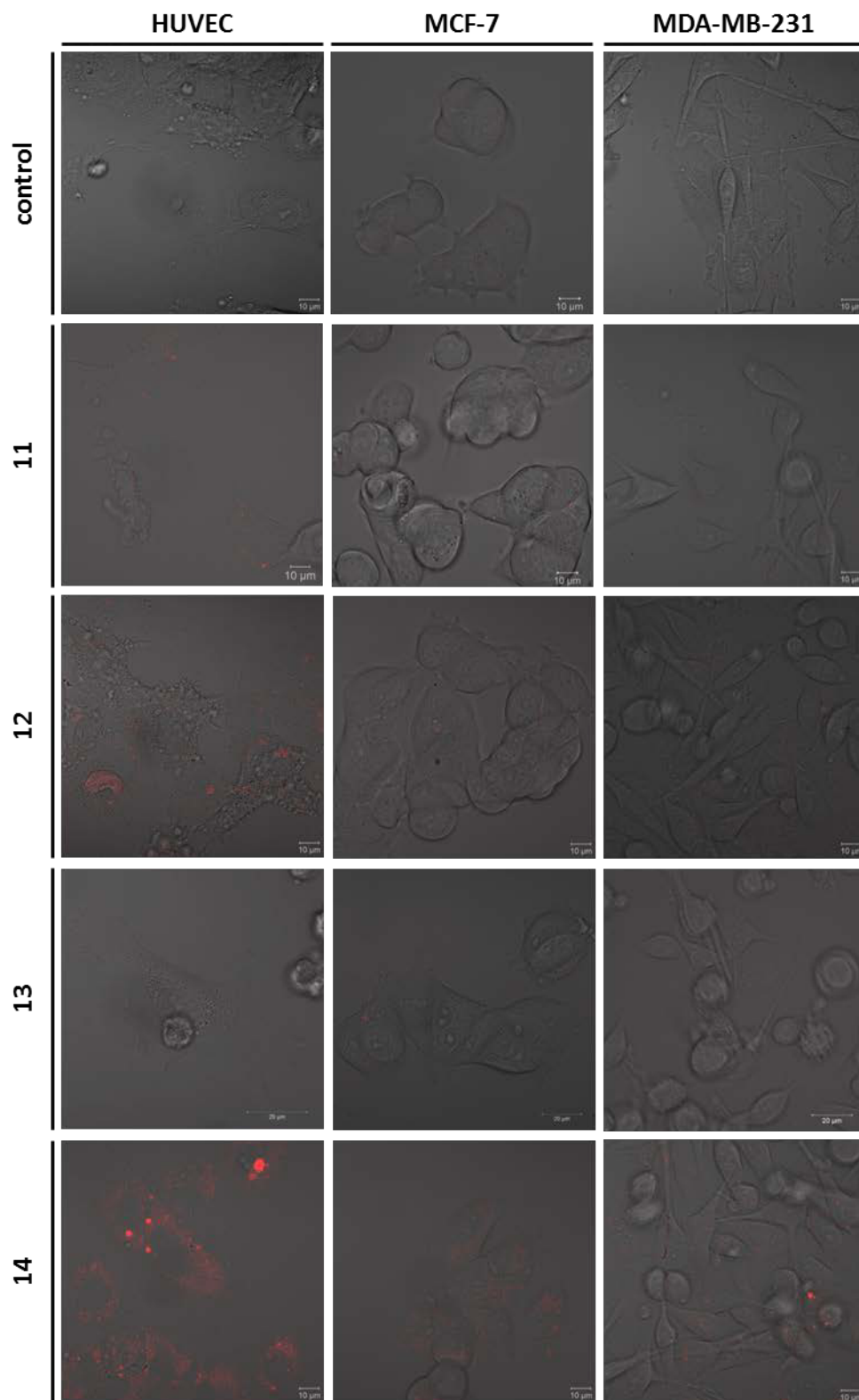


**Figure S65.** Complexes **11** to **14** were incubated with HUVEC, MCF-7 and MDA-MB-231 cells in serum containing media and analyzed after 24 h.

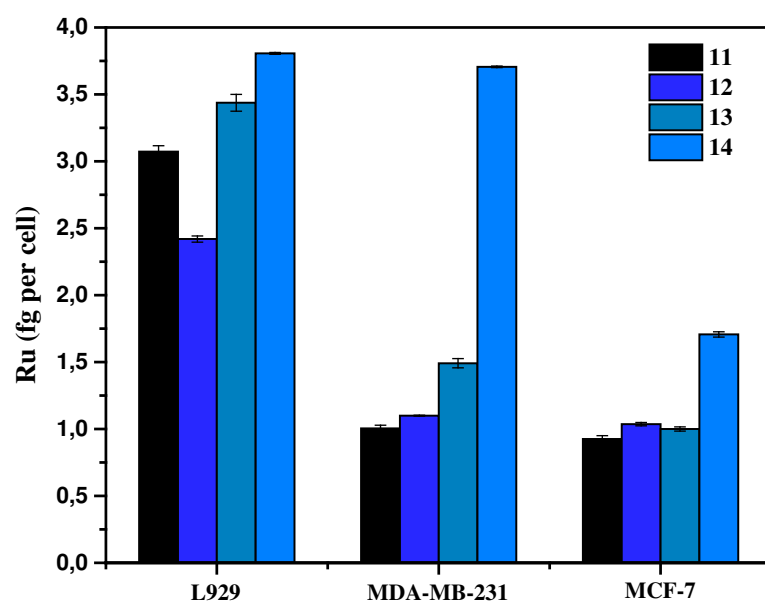


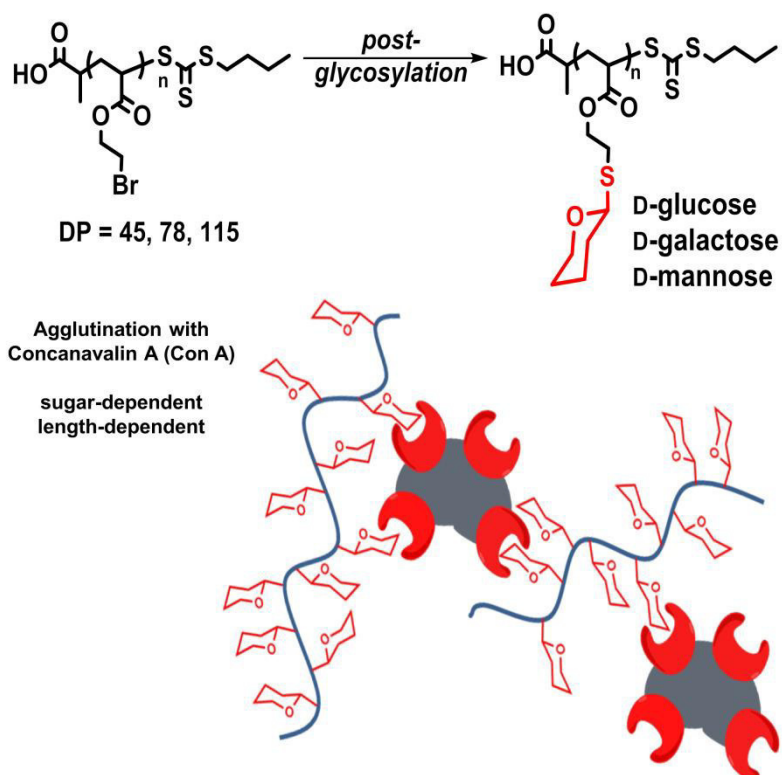
**Figure S66.** Uptake of complexes **11** to **14** (Ru in fg per cell). L929, MDA-MB-231 and MCF-7 cells were incubated at 50  $\mu$ M for 1 h. The uptake was determined by ICP-M. For controls not incubated with complexes, no Ru content was determined (Ru < 0.03 fg / cell).

## Publication 5

# RAFT polymerization and thio-bromo substitution: an efficient way towards well-defined, large glycopolymers

M. Pröhl, C. Englert, M. Gottschaldt, U. S. Schubert, J. C. Brendel

*J. Polym. Sci. A Polym. Chem.* **2017**, DOI: 55, 3617-3626.



# RAFT Polymerization and Thio-Bromo Substitution: An Efficient Way towards Well-Defined Glycopolymers

Michael Pröhl,<sup>1,2</sup> Christoph Englert,<sup>1,2</sup> Michael Gottschaldt,<sup>1,2</sup> Johannes C. Brendel <sup>1,2</sup>,  
Ulrich S. Schubert<sup>1,2</sup>

<sup>1</sup>Laboratory of Organic and Macromolecular Chemistry (IOMC), Friedrich Schiller University Jena, Humboldtstraße 10, Jena 07743, Germany

<sup>2</sup>Jena Center for Soft Matter (JCSM), Friedrich Schiller University Jena, Philosophenweg 7, Jena 07743, Germany

Correspondence to: U. S. Schubert (E-mail: ulrich.schubert@uni-jena.de) or J. C. Brendel (E-mail: johannes.brendel@uni-jena.de)

Received 15 June 2017; accepted 18 July 2017; published online 00 Month 2017

DOI: 10.1002/pola.28745

**ABSTRACT:** Despite an increasing effort to design well-defined glycopolymers, the convenient synthesis of polymers with higher DPs (>100) and without tedious protection and deprotection steps remains a challenge. Combining the reversible addition fragmentation transfer (RAFT) polymerization and the efficient substitution of primary bromo groups by thiols, we were able to synthesize a set of well-defined glycopolymers with DPs of up to 115. With the polymerization of the highly reactive monomer (2-bromoethyl)-acrylate polymers with low dispersities were obtained that could efficiently be functionalized with various sugar thiol(ate)s. In particular, derivatives of D-glucose, D-galactose, and D-mannose gave excellent degrees of functionalization close to quantitative conversion using only

a slight excess of the thiol. This atom efficient synthesis can even be applied for copolymers with acid or base labile components due to the use of unprotected sugar moieties and, hence, the lack of further deprotection steps. Binding studies with the lectin concanavalin A and the subsequent competition studies with  $\alpha$ -D-methyl-mannopyranose ( $\alpha$ MeMan) proved the effective binding of these derivatives and revealed a DP- and carbohydrate-dependent clustering and dissolution. © 2017 Wiley Periodicals, Inc. *J. Polym. Sci., Part A: Polym. Chem.* 2017, 00, 000–000

**KEYWORDS:** carbohydrates; glycosylation; lectins; nucleophilic substitution; polymers; postmodification; RAFT

**INTRODUCTION** Synthetic, carbohydrate-functionalized polymers gained increased interest in biological sciences due to the crucial role of natural glycoconjugates in cell-cell recognition processes. The main interactions of living organisms are saccharide-protein, protein-protein, and protein-antibody interactions and include binding possibilities in a multivalent manner caused by hydrophobic and electrostatic interactions as well as by hydrogen bonding.<sup>1</sup> The saccharide-protein interactions were found to play important roles in cell adhesion and cell differentiation, but also in inflammations, viral replications, and parasitic infections.<sup>2</sup>

Biological events are often related to the interaction between carbohydrates and lectins. Lectins are binding proteins with high stereo-specificity for carbohydrates. A single saccharide reveals only a low affinity for its natural ligand, whereas multivalent interactions between a single or more lectins with one or more of the corresponding carbohydrate units are highly prevalent in nature.<sup>3</sup> The so-called “cluster-effect”<sup>4</sup> strongly influences the design of well-defined glycopolymer architectures.

Early glycopolymer synthesis was conducted by Kobayashi *et al.* in 1985, who prepared lactose and D-maltose conjugated styrene polymers, offering strong interactions with hepatocytes and D-galactose selective lectins.<sup>5</sup> Since then, various polymers with defined architectures can be obtained due to the use of modern polymerization techniques and available sugar derivatives. In general, there are two ways to obtain carbohydrate-conjugated polymers: Polymerization of carbohydrate-conjugated monomers (glycomonomers) or postpolymerization conjugation of a suitable, reactive polymer. Many attempts were performed to polymerize glycomonomers in a controlled manner by anionic<sup>6</sup> and cationic,<sup>7</sup> controlled radical,<sup>8</sup> ring-opening,<sup>9</sup> and other polymerization techniques.<sup>10</sup> However, the synthesis of glycomonomers usually requires various steps and the functional groups of unprotected glycomonomers reveal incompatibility with most controlled polymerization techniques.<sup>11</sup> Additionally, high molar mass polymers with a narrow distribution are still challenging to obtain by polymerizing glycomonomers. To postmodify polymers with carbohydrates, a reactive

Additional Supporting Information may be found in the online version of this article.

© 2017 Wiley Periodicals, Inc.

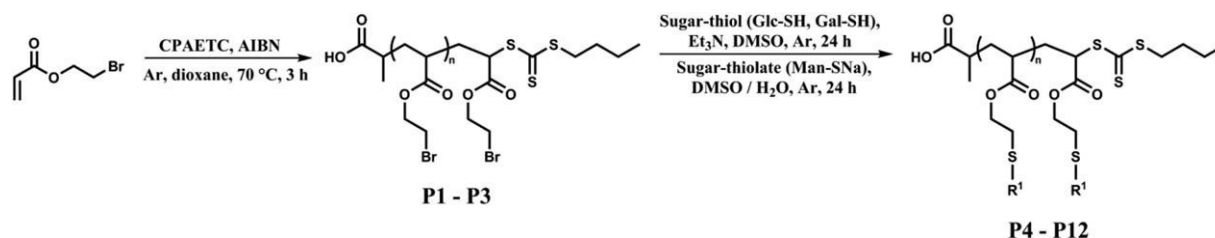


**FIGURE 1** Schematic representation of the polymers **P1** to **P12** obtained via RAFT with subsequent postglycosylation.

polymer backbone is required. For this purpose, many functional groups are reported, including 4-nitrophenyl carbonate,<sup>12</sup> *para*-fluoro-phenyl,<sup>13</sup> alkynyl,<sup>14</sup> alkenyl,<sup>15</sup> and others.<sup>11</sup>

A relatively unexplored reaction for the postmodification of polymers represents the nucleophilic substitution of various alkyl halides with suitable nucleophiles. Mainly used in metal-catalyzed polymerizations, the use of halide-containing polymers obtained by reversible deactivation radical polymerization (RDRP) techniques is limited. This is primarily attributed to the sensitivity of alkyl halides towards abstraction by radicals, which is intentionally used in iodine transfer polymerization.<sup>16</sup> However, only a few examples using RDRP for alkyl halide monomers are reported and even less are applied for the synthesis of glycopolymers. Stenzel and coworkers reported the synthesis of star shaped glycopolymers derived from poly(vinyl benzylchloride) (PVBC) via reversible addition-fragmentation polymerization (RAFT).<sup>17</sup> The polymers were reacted with equimolar amounts of 1-deoxy-1-thio- $\beta$ -D-glucopyranose sodium salt in DMSO for 110 h without any catalyst. Also poly(epichlorohydrin) obtained via cationic ring-opening polymerization (CROP) was postmodified with 1-deoxy-1-thio- $\beta$ -D-glucopyranose to obtain bristle-like polymers with moderate dispersity ( $\bar{D} = 1.68$ ).<sup>18</sup> Recently, the Perrier group demonstrated the versatility of poly(bromoethyl acrylate) (PBEA), which was polymerized via RAFT.<sup>19</sup> Various nucleophiles were used to yield efficient substitution of the bromides, which resulted in polymers with a wide range of functionalities including already a D-glucose derivative. However, a rather large excess of the nucleophile 1-deoxy-1-thio- $\beta$ -D-glucopyranose sodium salt was used to form the D-glucosylated acrylate. To the best of our knowledge, there is no systematic study, which shows the synthesis of glyco-homopolymers by controlled radical polymerization techniques with low dispersities and DPs exceeding 100 units comparing different sugar residues.

Based on these results, we attempted to further exploit the reaction based on PBEA to synthesize a whole library of various glycopolymers and to test their suitability for selective binding to well-known lectins (Fig. 1). For this purpose, polymers with lengths ranging from 45 to 115 repeating units were prepared by RAFT polymerization and subsequently modified with various sugar residues (D-glucose, D-galactose, D-mannose). All these polymers were finally tested for their affinity to the binding-protein concanavalin A (Con A).

## EXPERIMENTAL

### Materials and Methods

All reagents and solvents were commercial products purchased from Sigma-Aldrich (triethylamine, dioxan, AIBN, Con A), Roth (DMSO, Zellutrans dialysis tube), or Carbosynth ( $\alpha$ -D-thiomannose sodium salt) and were used without further purification. (4-Cyanopentanoic acid)ylethyl trithiocarbonate (CPAETC) was synthesized as previously reported.<sup>19,20</sup> HBS buffer (0.10 M HEPES, 0.9 M NaCl, 1 mM CaCl<sub>2</sub>, 1 mM MgCl<sub>2</sub>, and 1 mM MnCl<sub>2</sub>) was prepared with Milli-Q water as the solvent.

### Equipment

<sup>1</sup>H NMR spectra were measured with a Bruker spectrometer (300 MHz). Elemental analysis was performed with a Leco CHN-932. Size-exclusion chromatography (SEC) of polymers **P1** to **P3** was performed on a Agilent system (series 1200) equipped with a G1310A pump, a G1362A refractive index detector and a PSS GRAM column with DMAc (+ 0.21 wt % LiCl) as eluent. The column oven was set to 40 °C and a polystyrene (PS) standard was used for calibration. SEC of polymers **P4** to **P12** was performed on a Jasco system equipped with a PU-980 pump, a RI-2031 Plus refractive index detector and a PSS SUPREMA column with H<sub>2</sub>O (+ 0.1 M NaNO<sub>3</sub> and 0.05% NaN<sub>3</sub>) as eluent. The column oven was set to 30 °C and a pullulan standard was used for calibration. UV/Vis absorbance spectra were measured with an Analytik Jena AG Specord250 spectrometer. Quartz cuvettes were purchased from Hellma Analytics.

### Syntheses of the Thio-Sugars

1-Deoxy-1-thio- $\beta$ -D-glucopyranose and 1-deoxy-1-thio- $\beta$ -D-galactopyranose were synthesized according to literature procedures.<sup>21</sup>

### Synthesis of 2-Bromoethyl Acrylate (BEA)

The BEA monomer was synthesized according to a modified literature procedure.<sup>19</sup> Thirty-eight milliliter of acryloyl chloride (0.54 mol) were dissolved in 250 mL dry CH<sub>2</sub>Cl<sub>2</sub> under an Ar atmosphere and 82 mL of Et<sub>3</sub>N (0.59 mol) were added. The mixture was cooled to 0 °C and 53 mL of 2-bromoethanol (0.66 mol) dissolved in 40 mL CH<sub>2</sub>Cl<sub>2</sub> were added dropwise. The reaction mixture was allowed to stir for 18 h at room temperature. Subsequently, the solution was filtered and the organic layer was washed thrice with saturated, aqueous NaHCO<sub>3</sub> solution. Additionally, the organic layer was stirred with 250 mL of 0.1 M NaOH<sub>(aq)</sub>



solution for 24 h separated and dried with  $\text{Na}_2\text{SO}_4$ . The solution was filtered and the organic solvent was evaporated *in vacuo* to obtain the crude product as a colorless oil. Ten milligram of 2,6-di-tert-butyl-4-methylphenol were added and the product was subjected a fractionated distillation under vacuum to yield 34.97 g (0.2 mol) of the desired product in highest purity and 37% yield. bp 55 °C (4.5 mmHg).  $\delta\text{H}$  (300 MHz;  $\text{CDCl}_3$ ) 6.49 (m, 1H,  $\text{CH}_2=\text{CH}$ ), 6.19 (m, 1H,  $\text{CH}_2=\text{CH}$ ), 5.90 (m, 1H,  $\text{CH}_2=\text{CH}$ ), 4.48 (t, 2H,  $^3J$  6.2,  $\text{CH}_2\text{CH}_2\text{Br}$ ), and 4.48 (t, 2H,  $^3J$  6.2,  $\text{CH}_2\text{CH}_2\text{Br}$ ).

### General Procedure for the Syntheses of PBEA Homopolymers

CPAETC, BEA, and AIBN were dissolved in dioxane and the reaction mixture was deoxygenated with Ar for 10 min and stirred at 65 °C for 4 h. After completion, the solution was cooled to room temperature, opened to air, and precipitated in diethyl ether to give PBEA homopolymers **P1** to **P3**.

#### P1

$^1\text{H}$  NMR (300 MHz;  $\text{CDCl}_3$ ,  $\delta$  ppm) 4.99–4.88 (1 H, m), 4.42 (2n H, br s), 3.57 (2n H, br s), 3.40 (2 H, t,  $^3J$  7.4), 2.49 (2n H, br s), 2.05 (2n H, br s), 1.94–1.50 (2n + 1 H, m), 1.48–1.41 (3 H, m), 0.95 (3 H, t,  $^3J$  7.3). SEC (DMAc + 0.21 wt % LiCl, PS standard):  $M_n$  = 8,800 g mol $^{-1}$ ,  $M_w$  = 9,600 g mol $^{-1}$ ,  $\bar{D}$  = 1.10.

#### P2

$^1\text{H}$  NMR (300 MHz;  $\text{CDCl}_3$ ,  $\delta$  ppm) 4.98–4.88 (1 H, m), 4.43 (2n H, br s), 3.57 (2n H, br s), 3.39 (2 H, t,  $^3J$  7.2), 2.47 (2n H, br s), 2.15–1.97 (2n H, br s), 1.90–1.39 (2n H, m), 0.96 (3 H, t,  $^3J$  7.4). SEC (DMAc + 0.21 wt % LiCl, PS standard):  $M_n$  = 11,200 g mol $^{-1}$ ,  $M_w$  = 13,500 g mol $^{-1}$ ,  $\bar{D}$  = 1.21.

#### P3

$^1\text{H}$  NMR (300 MHz;  $\text{CDCl}_3$ ,  $\delta$  ppm) 4.98–4.88 (1 H, m), 4.42 (2n H, br s), 3.57 (2n H, br s), 3.38 (2 H, t,  $^3J$  6.4), 2.47 (2n H, br s), 2.14–1.96 (2n H, m), 1.92–1.39 (2n H, m), 0.95 (3 H, t,  $^3J$  7.3). SEC (DMAc + 0.21 wt % LiCl, PS standard):  $M_n$  = 18,000 g mol $^{-1}$ ,  $M_w$  = 20,000 g mol $^{-1}$ ,  $\bar{D}$  = 1.11.

### General Procedure for the Postpolymerization Modification with Glc and Gal

One hundred milligram of the precursor polymer was dissolved in 1 mL DMSO and a solution of the desired carbohydrate (DP-1.1 equiv.) in 1 mL DMSO was added. The solution was deoxygenated with Ar for 30 min and 1 equiv. (based on the carbohydrate) dry triethylamine was added dropwise. The reaction mixture was stirred at room temperature for one day and dialyzed against water for one week (CE, MWCO: 3.5 kDa). The dialyzed solution was freeze-dried to obtain the desired polymer.

#### P4

$^1\text{H}$  NMR (300 MHz;  $\text{D}_2\text{O}$ ,  $\delta$  ppm) 4.49 (n H, d,  $^3J$  9.8,  $\text{H}_{\text{Glc}}-1$ ), 4.24 (2n H, br s), 3.85–3.69 (n H, m), 3.69–3.55 (n H, m), 3.47–3.17 (4n H, m), 3.07–2.74 (2n H, m), 2.33 (2n H, br s), 2.03–1.00 (2n + 1 H, m). SEC ( $\text{H}_2\text{O}$ , 0.1 M  $\text{NaNO}_3$ , 0.05%  $\text{NaN}_3$ , pullulan standard):  $M_n$  = 10,000 g mol $^{-1}$ ,  $M_w$  = 11,800

g mol $^{-1}$ ,  $\bar{D}$  = 1.19. Anal. calcd for  $\text{C}_{503}\text{H}_{824}\text{O}_{317}\text{S}_{48}$ : C, 44.81; H, 6.16; S, 11.41; Br, 0. Found: C, 43.87; H, 6.17; S, 10.81; Br, 0.89.

#### P5

$^1\text{H}$  NMR (300 MHz;  $\text{D}_2\text{O}$ ,  $\delta$  ppm) 4.44 (n H, d,  $^3J$  9.3,  $\text{H}_{\text{Gal}}-1$ ), 4.25 (2n H, br s), 3.89 (n H, s), 3.82–3.41 (5n H, m), 3.16–2.72 (2n H, m), 2.36 (2n H, br s), 2.04–1.00 (2n + 1 H, m). SEC ( $\text{H}_2\text{O}$ , 0.1 M  $\text{NaNO}_3$ , 0.05%  $\text{NaN}_3$ , pullulan standard):  $M_n$  = 9,900 g mol $^{-1}$ ,  $M_w$  = 12,000 g mol $^{-1}$ ,  $\bar{D}$  = 1.22. Anal. calcd for  $\text{C}_{503}\text{H}_{824}\text{O}_{317}\text{S}_{48}$ : C, 44.81; H, 6.16; S, 11.41; Br, 0. Found: C, 41.88; H, 6.13; S, 11.99; Br, 1.99.

#### P7

$^1\text{H}$  NMR (300 MHz;  $\text{D}_2\text{O}$ ,  $\delta$  ppm) 4.49 (n H, d,  $^3J$  9.7,  $\text{H}_{\text{Glc}}-1$ ), 4.24 (2n H, br s), 3.85–3.70 (n H, m), 3.70–3.56 (n H, m), 3.55–3.18 (4n H, m), 3.11–2.70 (2n H, m), 2.37 (2n H, br s), 2.11–1.00 (2n + 1 H, m). SEC ( $\text{H}_2\text{O}$ , 0.1 M  $\text{NaNO}_3$ , 0.05%  $\text{NaN}_3$ , pullulan standard):  $M_n$  = 17,400 g mol $^{-1}$ ,  $M_w$  = 21,800 g mol $^{-1}$ ,  $\bar{D}$  = 1.25. Anal. calcd for  $\text{C}_{866}\text{H}_{1418}\text{O}_{548}\text{S}_{81}$ : C, 44.84; H, 6.16; S, 11.20; Br, 0. Found: C, 44.15; H, 6.18; S, 9.48; Br, 2.14.

#### P8

$^1\text{H}$  NMR (300 MHz;  $\text{D}_2\text{O}$ ,  $\delta$  ppm) 4.44 (n H, d,  $^3J$  8.9,  $\text{H}_{\text{Gal}}-1$ ), 4.24 (2n H, br s), 3.90 (n H, s), 3.83–3.41 (5n H, m), 3.17–2.71 (2n H, m), 2.38 (2n H, br s), 2.04–0.99 (2n + 1 H, m). SEC ( $\text{H}_2\text{O}$ , 0.1 M  $\text{NaNO}_3$ , 0.05%  $\text{NaN}_3$ , pullulan standard):  $M_n$  = 16,400 g mol $^{-1}$ ,  $M_w$  = 21,000 g mol $^{-1}$ ,  $\bar{D}$  = 1.28. Anal. calcd for  $\text{C}_{866}\text{H}_{1418}\text{O}_{548}\text{S}_{81}$ : C, 44.84; H, 6.16; S, 11.20; Br, 0. Found: C, 43.28; H, 6.18; S, 9.31; Br, 3.09.

#### P10

$^1\text{H}$  NMR (300 MHz;  $\text{D}_2\text{O}$ ,  $\delta$  ppm) 4.49 (n H, d,  $^3J$  9.7,  $\text{H}_{\text{Glc}}-1$ ), 4.24 (2n H, br s), 3.86–3.69 (n H, m), 3.69–3.55 (n H, m), 3.55–3.17 (4n H, m), 3.08–2.71 (2n H, m), 2.36 (2n H, br s), 2.06–1.00 (2n + 1 H, m). SEC ( $\text{H}_2\text{O}$ , 0.1 M  $\text{NaNO}_3$ , 0.05%  $\text{NaN}_3$ , pullulan standard):  $M_n$  = 23,300 g mol $^{-1}$ ,  $M_w$  = 29,300 g mol $^{-1}$ ,  $\bar{D}$  = 1.26. Anal. calcd for  $\text{C}_{1273}\text{H}_{2084}\text{O}_{807}\text{S}_{118}$ : C, 44.86; H, 6.16; S, 11.10; Br, 0. Found: C, 43.53; H, 6.20; S, 10.20; Br, 1.54.

#### P11

$^1\text{H}$  NMR (300 MHz;  $\text{D}_2\text{O}$ ,  $\delta$  ppm) 4.44 (n H, d,  $^3J$  9.1,  $\text{H}_{\text{Gal}}-1$ ), 4.24 (2n H, br s), 3.89 (n H, s), 3.83–3.41 (5n H, m), 3.22–2.72 (2n H, m), 2.37 (2n H, br s), 2.09–1.00 (2n + 1 H, m). SEC ( $\text{H}_2\text{O}$ , 0.1 M  $\text{NaNO}_3$ , 0.05%  $\text{NaN}_3$ , pullulan standard):  $M_n$  = 23,300 g mol $^{-1}$ ,  $M_w$  = 29,900 g mol $^{-1}$ ,  $\bar{D}$  = 1.28. Anal. calcd for  $\text{C}_{1273}\text{H}_{2084}\text{O}_{807}\text{S}_{118}$ : C, 44.86; H, 6.16; S, 11.10; Br, 0. Found: C, 41.73; H, 6.05; S, 10.58; Br, 2.52.

### General Procedure for the Postpolymerization Modification with Man

One hundred milligram of the precursor polymer was dissolved in 1 mL DMSO and a solution of Man-SNa (DP-1.1 equiv.) in 0.5 mL  $\text{H}_2\text{O}$  was added. The solution was deoxygenated with Ar for 30 min, stirred at room temperature for one day and dialyzed against water for one week (CE, MWCO: 3.5

**TABLE 1** Summary of BEA Polymerization

Abbrev.	[M] <sub>0</sub> /CTA	[CTA]/I <sub>0</sub>	Conv. <sup>a</sup> (%)	M <sub>n,th</sub> <sup>b</sup> (g/mol)	M <sub>n,NMR</sub> <sup>c</sup> (g/mol)	M <sub>n,SEC</sub> <sup>d</sup> (g/mol)	<i>Đ</i>
<b>P1</b>	60	10	69	7,600	8,300	8,800	1.10
<b>P2</b>	150	10	58	15,700	14,200	11,200	1.21
<b>P3</b>	300	5	42	22,700	20,800	18,000	1.11

<sup>a</sup> Determined from <sup>1</sup>H NMR of the polymerization mixture before precipitation.

<sup>b</sup> Calculated from monomer conversion.

<sup>c</sup> Determined from <sup>1</sup>H NMR end-group analysis [calculated from signal intensity of the proton of the tertiary C-atom next to trithiocarbonate

( $\delta = 4.93$  ppm) in comparison to the proton signal of the C1 atom of the acryl ester ( $\delta = 4.43$  ppm) before postmodification]. These ratios were used to calculate the DP.

<sup>d</sup> SEC: DMAc + 0.21 wt % LiCl, PS calibration.

kDa). The dialyzed solution was freeze-dried to obtain the desired polymer.

### P6

<sup>1</sup>H NMR (300 MHz; D<sub>2</sub>O,  $\delta$  ppm) 5.30 (*n* H, s, H<sub>Man</sub>-1), 4.49–4.07 (3*n* H, m), 3.97 (*n* H, s), 3.93–3.49 (4*n* H, m), 2.88 (2*n* H, s), 2.38 (2*n* H, br s), 2.11–0.93 (2*n* + 1 H, m). SEC (H<sub>2</sub>O, 0.1 M NaNO<sub>3</sub>, 0.05% NaN<sub>3</sub>, pullulan standard): M<sub>n</sub> = 3,300 g mol<sup>-1</sup>, M<sub>w</sub> = 4,800 g mol<sup>-1</sup>, *Đ* = 1.44. Anal. calcd for C<sub>503</sub>H<sub>824</sub>O<sub>317</sub>S<sub>48</sub>: C, 44.81; H, 6.16; S, 11.41; Br, 0. Found: C, 43.76; H, 6.27; S, 10.36; Br, 0.

### P9

<sup>1</sup>H NMR (300 MHz; D<sub>2</sub>O,  $\delta$  ppm) 5.30 (*n* H, s, H<sub>Man</sub>-1), 4.50–4.06 (3*n* H, m), 3.97 (*n* H, s), 3.92–3.47 (4*n* H, m), 2.88 (2*n* H, s), 2.38 (2*n* H, br s), 2.12–0.93 (2*n* + 1 H, m). SEC (H<sub>2</sub>O, 0.1 M NaNO<sub>3</sub>, 0.05% NaN<sub>3</sub>, pullulan standard): M<sub>n</sub> = 9,400 g mol<sup>-1</sup>, M<sub>w</sub> = 12,600 g mol<sup>-1</sup>, *Đ* = 1.34. Anal. calcd for C<sub>866</sub>H<sub>1418</sub>O<sub>548</sub>S<sub>81</sub>: C, 44.84; H, 6.16; S, 11.20; Br, 0. Found: C, 43.80; H, 6.14; S, 10.45; Br, 0.

### P12

<sup>1</sup>H NMR (300 MHz; D<sub>2</sub>O,  $\delta$  ppm) 5.30 (*n* H, s, H<sub>Man</sub>-1), 4.47–4.06 (3*n* H, m), 3.98 (*n* H, s), 3.93–3.46 (4*n* H, m), 2.88 (2*n* H, s), 2.38 (2*n* H, br s), 2.15–0.97 (2*n* + 1 H, m). SEC (H<sub>2</sub>O, 0.1 M NaNO<sub>3</sub>, 0.05% NaN<sub>3</sub>, pullulan standard): M<sub>n</sub> = 15,900 g mol<sup>-1</sup>, M<sub>w</sub> = 21,200 g mol<sup>-1</sup>, *Đ* = 1.33. Anal. calcd for C<sub>1273</sub>H<sub>2084</sub>O<sub>807</sub>S<sub>118</sub>: C, 44.86; H, 6.16; S, 11.10; Br, 0. Found: C, 43.83; H, 6.16; S, 10.42; Br, 0.36.

### Turbidimetry Assay

The aggregation studies with Con A were conducted as previously reported.<sup>22</sup> Con A was fully dissolved in HBS buffer (~1 mg mL<sup>-1</sup>) and diluted to a 1  $\mu$ M stock solution. 1 mL of the Con A stock solution was added to a quartz glass cuvette, which was placed in the UV-Vis spectrometer. One milliliter of a 50  $\mu$ M (50  $\mu$ M per sugar unit) stock solution of the polymer in HBS buffer was appended with a pipette to the ground of the glass cuvette and the absorbance of the mixture was immediately recorded at  $\lambda = 420$  nm for 30 min every 0.5 s. The interaction rate was calculated by using the slope of the linear fit of the steepest portion. Every experiment was conducted thrice.

### Reversal Aggregation Assay

The competition experiments with  $\alpha$ -D-methyl-mannopyranose were carried out according to literature procedure.<sup>22</sup> The solutions of the turbidimetry assay were allowed to rest for 2 h at room temperature. Following the addition of 0.2 mL of a 54 mM stock solution of methyl- $\alpha$ -D-mannopyranoside in HBS buffer, the absorbance at  $\lambda = 420$  nm was immediately recorded for 60 min every 0.5 s.

## RESULTS AND DISCUSSION

### RAFT Polymerization of BEA

Similar to the previously published procedure, the BEA monomer was polymerized using CPAETC as chain transfer agent (CTA) and AIBN as radical initiator for the RAFT process. Optimizing the synthesis and purification procedure for the monomer (see experimental section for details) we were able to increase the final DP of the polymers without the loss of control. As a consequence, various DPs could be addressed by changing the ratio [monomer]/[CTA] (Table 1).

For all polymers, low dispersity (*Đ*  $\leq$  1.2) and narrow mono-modal distributions were obtained, emphasizing the capabilities to polymerize halide-containing monomers by RDRP. In addition, we analyzed the end group fidelity using NMR analysis. The intensities of the signals at  $\delta = 0.95$  ppm for the terminal CH<sub>3</sub> group and of the signal at  $\delta = 3.38$  ppm for the CH<sub>2</sub> group next to the trithiocarbonate match well with the expectations proving the excellent retention of the RAFT end group. Recent studies showed the synthesis of a similar polymer named poly(2-bromoethyl methacrylate) by postmodification of poly(2-hydroxyethyl methacrylate) with a mixture of various chemicals.<sup>23</sup> Our study represents a more effective approach due to the lack of postbromination procedures and the introduction of the bromide directly to the monomer circumventing the requirement for additional tedious modification steps.

### Postglycosylation

With the defined precursor polymers at hand, the various carbohydrates were examined for the next step. For this purpose, the thiolated carbohydrates (1-deoxy-1-thio- $\beta$ -D-glucopyranose,<sup>21</sup> 1-deoxy-1-thio- $\beta$ -D-galactopyranose,<sup>21</sup> and commercially available 1-deoxy-1-thio- $\beta$ -D-mannopyranose sodium salt) were reacted with precursor polymers **P1** to **P3** in a S<sub>N</sub>2 reaction (Table 2). These carbohydrates were chosen for

**TABLE 2** Overview of the Glycopolymers **P4** to **P12** Prepared and Tested in This Study

Abbrev.	DP	Attached Sugar (R <sup>1</sup> )	$M_{n,th}^a$	$M_{n,SEC}^b$	$\bar{D}$
<b>P4</b>	45	Glc	13,500	10,000	1.19
<b>P5</b>	45	Gal	13,500	9,900	1.22
<b>P6</b>	45	Man	13,500	3,300	1.44
<b>P7</b>	78	Glc	23,200	17,400	1.25
<b>P8</b>	78	Gal	23,200	16,400	1.28
<b>P9</b>	78	Man	23,200	9,400	1.34
<b>P10</b>	115	Glc	34,100	23,300	1.26
<b>P11</b>	115	Gal	34,100	23,300	1.28
<b>P12</b>	115	Man	34,100	15,900	1.33

<sup>a</sup> Calculated by assuming polymers with the respective DP and full substitution of the bromide groups.

<sup>b</sup> SEC: H<sub>2</sub>O, 0.1 M NaNO<sub>3</sub>, 0.05% NaN<sub>3</sub>, Pullulan calibration.

different reasons. D-galactose (Gal) conjugated polymers were shown to bind to hepatocytes via a receptor-mediated mechanism and, therefore, representing useful targeting moieties for the development of polymers used in various biomedical fields, such as tissue engineering and drug-loaded nanoparticles.<sup>24</sup> D-Mannose (Man) is in the focus of the scientific community due to its strong interactions with the lectin Con A and with macrophages, which overexpress mannose-receptors on their surface.<sup>25</sup> D-Glucose (Glc) interacts with transport proteins like with the GLUT1 transporter, which is shown to be overexpressed in various types of cancers, such as renal cell carcinoma<sup>26</sup> or non-small cell lung carcinoma.<sup>27</sup>

D-Galactose and D-glucose were attached using only 1.1 equivalents of the deprotected  $\beta$ -1-thiol derivatives. The S<sub>N</sub>2

reactions with polymers **P1** to **P3** were conducted in DMSO and the thiol functionalities of the carbohydrates were deprotonated with one equivalent of triethyl amine. The reactions were stopped after 24 h and purified by dialysis against H<sub>2</sub>O (MWCO: 3.5 kDa) to remove low-molar mass impurities and side-products such as DMSO and formed triethyl ammoniumbromide. In the case of D-mannose attachment, 1.1 equivalents of the commercially available sodium salt of the  $\alpha$ -1-thiol derivative of D-mannose were used. Therefore, no base is required and the formation of sodium bromide as a side-product represents the driving force for the substitution reaction. The mannosylated polymers were purified in a similar manner to the gluco- and galactosylated ones. The success of the reaction can be shown by various NMR techniques as depicted for polymer **P12** in Figure 2, representative for all other polymers. All spectra of polymers **P1** to **P12** are available in the Supporting Information (Fig. S1–S47).

The substitution of the bromides in **P3** against the sugar-thiolate results in the formation of a thio-ether. This is clearly visible in the shift of the ethyl acrylate signals from  $\delta = 4.42$  ppm in **P3** to  $\delta = 4.22$  ppm in **P12**, respectively, from  $\delta = 3.57$  ppm in **P3** to  $\delta = 2.89$  ppm in **P12** in the <sup>1</sup>H NMR spectra. Additionally, the signal of the C1 proton appears nicely isolated at  $\delta = 5.30$  ppm, whereas the other D-mannose proton signals are visible between  $\delta = 3.5$  and 4.5 ppm. As also previously shown,<sup>28</sup> the attachment of carbohydrates result in water-soluble polymers **P4** to **P12**, whereas precursor polymers **P1** to **P3** revealed nonsolubility in water. Additionally, by binding D-mannose S-glycosidically to the polymer backbone, a thioether is formed, which possesses a lower rate of hydrolysis of the thioglycosidic bond by enzymatic cleavage relative to O-glycosidically coupled sugar residues.<sup>29</sup>

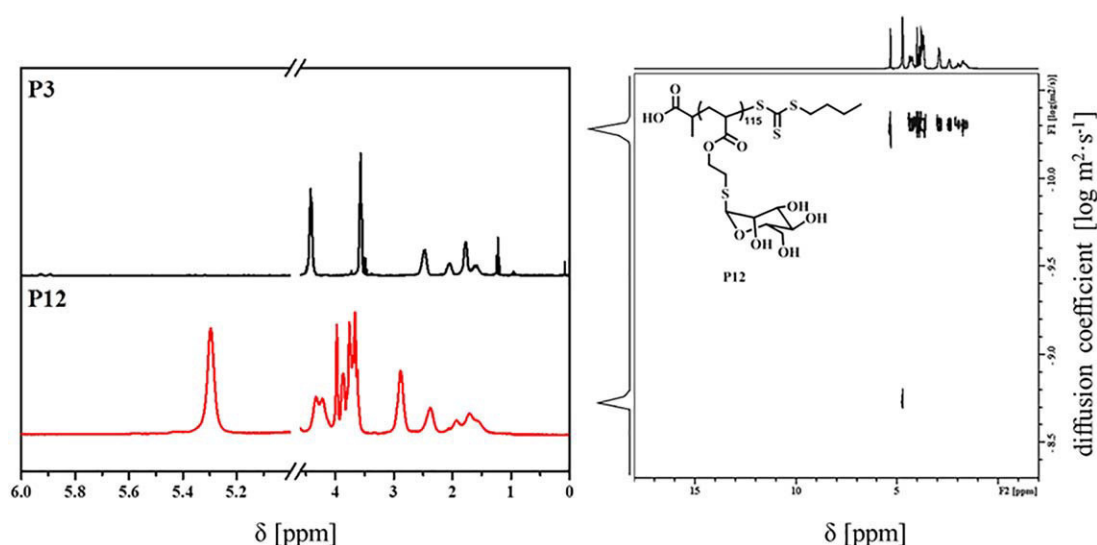


**FIGURE 2** Left: Comparison of <sup>1</sup>H NMR of compounds **P3** (measured in CDCl<sub>3</sub>) and **P12** (measured in D<sub>2</sub>O) between  $\delta = 0$  and 6 ppm. Intermittent axis between  $\delta = 4.6$  and 5 ppm was used due to solvent residue signal in the spectrum of **P12**. Right: <sup>1</sup>H diffusion-ordered NMR (DOSY) at  $T = 25$  °C of **P12**. [Color figure can be viewed at [wileyonlinelibrary.com](http://wileyonlinelibrary.com)]

**TABLE 3** Elemental Compositions of Polymers **P4** to **P12**; the Calculated DFs are Based on Theoretical Br Content of Polymers **P1** to **P3**

Abbrev.	DP	Saccharide	Elemental Composition <sup>a</sup> (%)				DF (%)
			C	H	S	Br	
<b>P1</b>	45	–	<b>33.74</b>	<b>4.00</b>	<b>1.16</b>	<b>43.35</b>	–
<b>P4</b>	45	Glc	43.87	6.17	10.81	0.89	97.9
<b>P5</b>	45	Gal	41.88	6.13	11.99	1.99	95.4
<b>P6</b>	45	Man	43.76	6.27	10.36	0	100
<b>P2</b>	78	–	<b>33.66</b>	<b>3.97</b>	<b>0.68</b>	<b>43.89</b>	–
<b>P7</b>	78	Glc	44.15	6.18	9.48	2.14	95.1
<b>P8</b>	78	Gal	43.28	6.18	9.31	3.09	93
<b>P9</b>	78	Man	43.80	6.14	10.45	0	100
<b>P3</b>	115	–	<b>33.63</b>	<b>3.96</b>	<b>0.46</b>	<b>44.12</b>	–
<b>P10</b>	115	Glc	43.53	6.20	10.20	1.54	96.5
<b>P11</b>	115	Gal	41.73	6.05	10.58	2.52	94.3
<b>P12</b>	115	Man	43.83	6.16	10.42	0.36	99.2

<sup>a</sup> Elemental composition of starting material polymers **P1** to **P3** was calculated assuming one polymer species with the depicted DP.

<sup>1</sup>H diffusion-ordered NMR (DOSY) investigations of **P12** revealed the appearance of all signals (except the signal for the solvent residue) at high diffusion constants typical for polymers ( $D = 5 \cdot 10^{-11} \text{ m}^2 \text{ s}^{-1}$ ), indicating the successful attachment of D-mannose units without the appearance of any side-products.

In contrast to the previous polymers **P1** to **P3** the end group fidelity of the RAFT group could not be determined after postpolymerization functionalization due to the overlap of the important signals in the NMR with the signals of the sugar moiety. Reinitiation experiments, however, indicated a degradation of the trithiocarbonate as no block formation is observed.

To further evaluate the quality of the substitution reaction, the elemental composition of polymers **P4** to **P12** was analyzed. The determined halogen content represents the remaining bromoethyl ester content and can be used to calculate the degree of functionalization (DF) with the following equation (Table 3).

$$\text{DF} = 1 - \frac{\text{Br content (sugar polymer)}}{\text{Br content (PBEA)}} \times 100$$

The DF ranges from 93 to 100% and some general tendencies are noticeable. D-Mannose functionalized polymers **P6**, **P9**, and **P12** showed remaining Br content between 0 and the lower detection limit (0.36%), whereas the other polymers revealed Br content between 0.89 and 3.09%. Therefore, the use of the sodium salt of the corresponding thiol-sugars, instead of the thiol-sugars and a suitable base, seems to be beneficial for the substitution reaction. This might be attributed to the decreased solubility of the formed sodium bromide in the solvent mixture of D-mannosylated polymers

in comparison to the solubility of the formed triethyl ammoniumbromide of the other polymers in DMSO. Additionally, the DF with D-galactose is generally decreased in comparison to D-glucose, which might be caused by the existence of small amounts of 1-deoxy-1-thio- $\alpha$ -D-galactopyranose, which could be sterically hindered during the substitution reaction. Due to the well resolved signals from the C1 protons of the D-mannose units in <sup>1</sup>H NMR, they can be used to validate the DF by comparing their intensity to that of the backbone signal at  $\delta = 2.9$  ppm. The obtained data is in good agreement with the results obtained from the elemental analysis of the polymers.

The polymers **P4** to **P12** were also investigated via SEC to obtain information about the increase of the molar mass of the polymers and their dispersities (Fig. 3).

The traces still show a mono-modal distribution and the dispersity remains narrow below 1.5, indicating no formation of macromolecular side-products during the  $S_N2$  reaction and the absence of previously observed chain-chain coupling due to the removal of the CTA and the subsequent disulfide formation or other side reactions.<sup>19</sup> The latter can certainly be attributed to the reduced excess of thio-sugar molecules used for the substitution. The symmetric broadening of the SEC traces and the slight increase of the dispersities relative to the precursor polymers **P1** to **P3** is most probably related to the difference in the SEC system applied for the analysis of the polymers and potential interactions of the attached sugar moieties with the column material. An indication for this phenomenon is further the later elution of D-mannosylated polymers **P6**, **P9**, and **P12** in comparison to the corresponding D-glucosylated or D-galactosylated polymers, respectively, although the absolute molar masses should be very similar. An additional effect for this shift in the elution



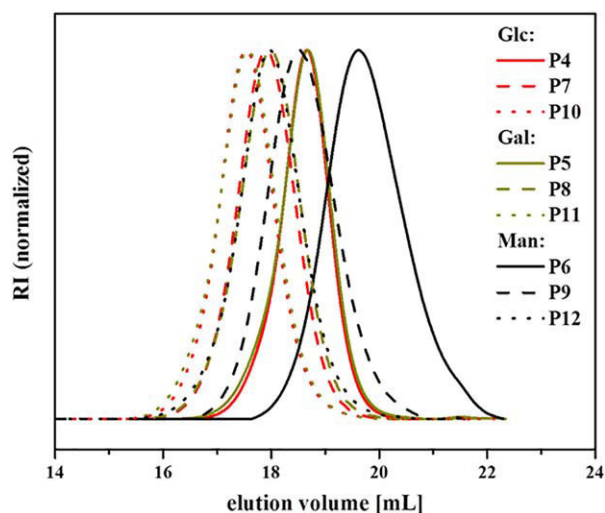


**FIGURE 3** SEC traces of polymers **P4** to **P12** ( $\text{H}_2\text{O}$ , 0.1 M  $\text{NaNO}_3$ , 0.05%  $\text{NaN}_3$ , Pullulan standard). [Color figure can be viewed at [wileyonlinelibrary.com](http://wileyonlinelibrary.com)]

volume might be the interaction between the axial C2 hydroxyl groups of the D-mannose units and the carboxylic ester functionalities on the polymer backbone, which decrease the resulting hydrodynamic radius, whereas D-glucose and D-galactose possess equatorial hydroxyl groups at their C2 atoms. Another reason could be the stronger interaction of D-mannose with the column material in comparison to the other sugars. D-Glucose conjugated polymers roughly eluted after the same volume than the D-galactosylated polymers with the same DP.

### Lectin Binding

One critical requirement for the application of glycopolymers, for example, in targeted drug delivery, is their ability to selectively bind to lectins for the respective type of sugar. To examine the binding efficacy of the glycopolymers, turbidimetry assays were performed for the polymers **P4** to **P12**

using the lectin Con A. Con A consists of aggregates of  $25,000 \text{ g mol}^{-1}$  size. While existing at pH range 5–5.6 as a dimer, Con A is predominantly aggregating into tetramers above pH = 7.<sup>30</sup> Each monomer unit is known to selectively bind to one unit of  $\alpha$ -gluco- or  $\alpha$ -mannopyranose, but no binding should be observed in the case of the galactopyranose.<sup>31</sup> The rate of clustering was monitored in real-time by measuring the absorbance at  $\lambda = 420 \text{ nm}$  over time after mixing the lectin and polymer solutions. The change in turbidity is related to the rate of receptor-receptor associations caused by the sugar-units of the polymers.<sup>32</sup> The slope of the steepest portion of the initial curve was used to represent the clustering rate, expressed in arbitrary units per second ( $\text{a.u. s}^{-1}$ ).<sup>22</sup> The initial values of the curves are correlated to the formation of isolated Con A polymer clusters, whereas interactions between the clusters occur at later points. The formation of cross-linked clusters of higher order increases over the time and, therefore, the analysis is limited to the initial portion of the curve.<sup>33</sup> The experimental results are summarized in Figure 4. All spectra of the triplicate measurements including the linear fits are available in the Supporting Information (Fig. S9, S14, S18, S23, S28, S32, S37, S42, and S46).

Polymers **P5**, **P8**, and **P11** bearing D-galactose residues did not show any aggregation with Con A over a time period of 30 min, which is in accordance to previously reported D-galactosylated polymers.<sup>14</sup> D-Glucosylated and D-mannosylated polymers exhibited the formation of Con A clusters with varying clustering rates. As a general trend, the polymers grafted with D-mannose residues revealed higher rates of Con A clustering than their D-glucosylated polymers with the same DP. This might be attributed to the higher binding affinity of the Con A tetramers to  $\alpha$ -D-mannose in comparison to D-glucose residues. Another reason could be the decreased hydrodynamic radius of D-mannosylated polymers relative to the D-glucosylated ones, which could offer beneficial shape or length of the polymers in solution in terms of Con A binding. The absorbance of D-mannose bearing polymers reached

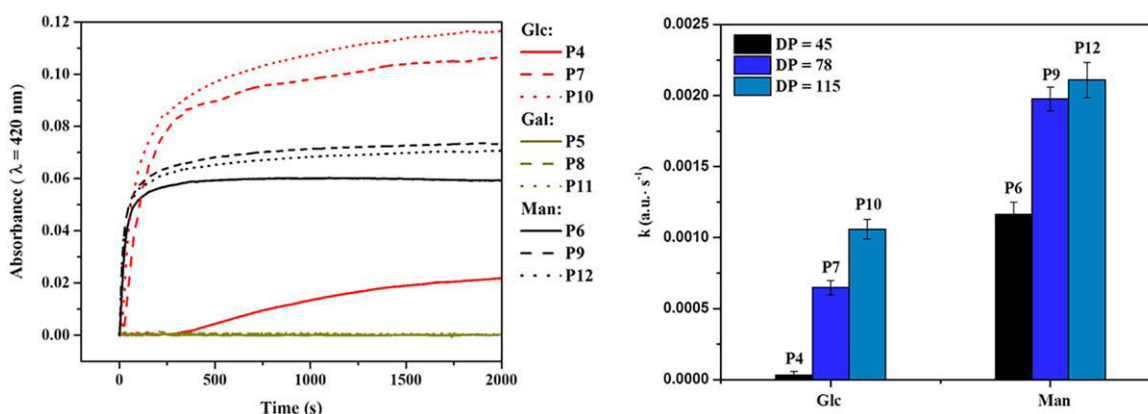


**FIGURE 4** Results of turbidimetry measurements. Left: Absorbance ( $\lambda = 420 \text{ nm}$ ) curves after adding 1 mL solution of polymers **P4** to **P12** ( $50 \mu\text{M}$  per sugar unit) to  $1 \mu\text{M}$  solutions of Con A in HBS buffer. Right: Calculated rates of clustering between Con A tetramers and D-glucosyl- or D-mannosylated polymers obtained by a linear fit of the steepest portions of the curves,  $k$  values represent the average of three replicates. [Color figure can be viewed at [wileyonlinelibrary.com](http://wileyonlinelibrary.com)]

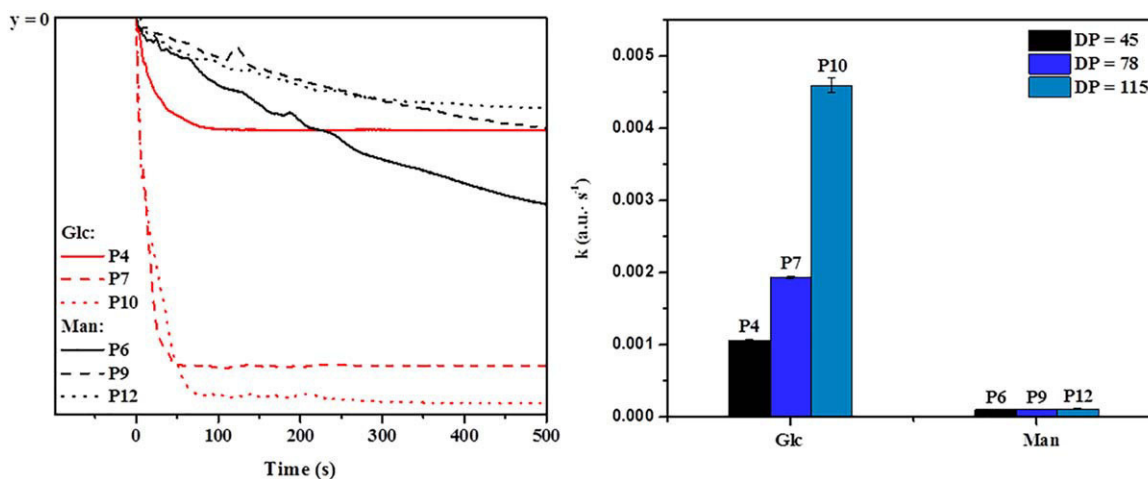


**FIGURE 5** Results of reversal aggregation measurements. Left: Absorbance ( $\lambda = 420$  nm) curves after adding 0.2 mL solution of  $\alpha$ MeMan (54 mM) to the polymer solutions (50  $\mu$ M per sugar unit) in HBS buffer. Right: Calculated rates of the reverse interaction between Con A aggregates and the competitor  $\alpha$ MeMan obtained by a linear fit of the steepest portions of the curves. [Color figure can be viewed at [wileyonlinelibrary.com](http://wileyonlinelibrary.com)]

very fast a plateau and stayed almost constant at this level for the remaining measurement, which is attributed to a rapid precipitation of most of the Con A tetramers (Fig. 4). In contrast, D-glucosylated polymers exhibited a continuous, but slower increase of the absorbance, indicating secondary interactions such as cross-linked clusters or partially soluble conjugates. In particular, the shortest D-glucose bearing polymer **P4** exhibited different clustering rates compared to all other polymers. One reason is the general decreased affinity of D-glucose to Con A relative to D-mannose. Another one is certainly the overall length of the polymer. Considering a fully stretched chain the length of **P4** can be estimated to be  $\sim 80$  Å taking into account the binding angles. The distance between two binding sites of the Con A tetramer is around 72 Å and,<sup>34</sup> therefore, the length of the polymer, which is just above the distance between the binding sites, paired with the low affinity of Con A towards D-glucose did not result in fast agglutination of the Con A clusters. In the light of this, the existence of a critical polymer length for high clustering rates of Con A aggregates is assumed, which is also in accordance to literature reports.<sup>35</sup>

Another trend is obtained by comparing the rate of clustering caused by the polymers with the same sugar residues, but with different DPs. With higher DPs (for D-glucose as well as for D-mannose bearing polymers) the precipitation of Con A clusters is promoted more rapidly. Therefore, we assume a dependency of the speed of clustering with the epitope density, which was also reported for other glycopolymers.<sup>33,35</sup> Additionally, the rate of clustering for polymers with D-mannose residues seems to approximate a constant level in dependency of the DP. A lower increase of the clustering rates for D-mannosylated polymers with higher DPs relative to **P12** in comparison to the increase between **P9** to **P12** is expected. To exactly determine the required DP, more turbidimetry investigations with D-mannosylated polymers of

higher DPs are necessary. The described polymerization and postglycosylation could be used to synthesize these polymers in future studies.

### Reversal Aggregation

In addition to the previous binding assays, the strengths and efficiencies of the interaction between glycopolymer and lectin can be evaluated by competition experiments. For this purpose, the aggregates formed during turbidimetry assays were allowed to rest for around 2 h to finish the formation of higher-order aggregates and were subsequently treated with an excessive amount of  $\alpha$ -D-methyl-mannopyranose ( $\alpha$ MeMan), a competitor for the binding sites of Con A. The absorbance at  $\lambda = 420$  nm over the time was monitored and the results are summarized in Figure 5 for D-manno- and D-glucosylated polymers. The D-galactose bearing polymers were omitted due to the inefficient binding to the lectin Con A and all spectra are available in the Supporting Information (Fig. S10, S19, S24, S33, S38, and S47).

The results of the reversal aggregation assay revealed carbohydrate-specific and length-dependent tendencies. The rates of the dissolution of the D-glucosylated polymers are strongly enhanced relative to those of the D-mannosylated polymers when treated with the monovalent competitor  $\alpha$ MeMan in large excess. The turbidity was rapidly reduced to a constant level, indicating a rather weak interaction between Con A and the D-glucose bearing polymers. Additionally, the dissolution of the D-glucose Con A clusters happened faster with increasing DP of the polymers. The dissolution of the cluster of D-mannosylated polymers was slow but continuous to a constant level, indicating higher binding affinity of the Con A tetramers to D-mannosylated polymers. Other tendencies are observable when comparing the difference of the highest and the lowest absorbance ( $\lambda = 420$  nm) after addition of Con A to the difference

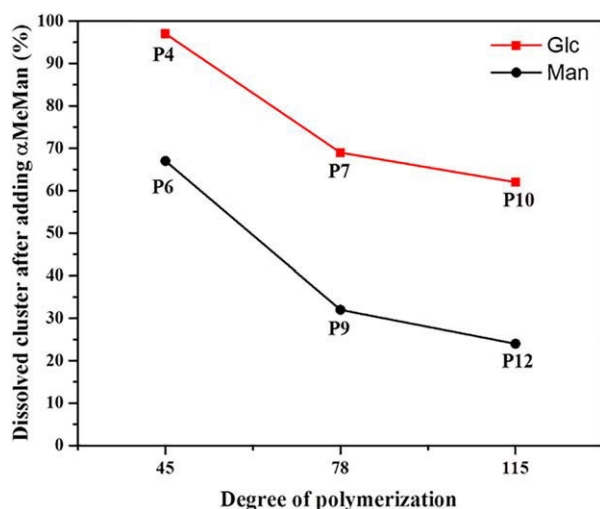


**FIGURE 6** Ratio of the dissolved Con A polymer clusters after adding  $\alpha$ MeMan relative to the DP. The values were calculated by the ratio of the moduli of the difference between the highest and lowest absorbance after adding  $\alpha$ MeMan respectively Con A to the polymer solutions. [Color figure can be viewed at [wileyonlinelibrary.com](http://wileyonlinelibrary.com)]

obtained after addition of  $\alpha$ MeMan. First of all, the Con A aggregates of D-mannosylated polymers (**P6**, **P9**, **P12**) were not completely dissolved after adding the competitor and a clear trend is that with higher DP, the amount of undissolved Con A clusters remaining in solution increases (Fig. 6, Supporting Information Table S1).

Comparing the different sugar moieties (except for the D-galactosylated polymers) all aggregates with D-glucosylated polymers revealed decreased stability relative to the respective clusters of the D-mannosylated polymers with the same DP. This is in accordance with the results we obtained for the reversal aggregation assay showing higher dissolution rates for increasing DPs of the polymers (**P4** < **P7** < **P10**). It is further noteworthy to mention that we observe an increased total stability of the D-glucosylated polymers **P7** (69%) and **P10** (62%) although Con A clusters of D-glucose are commonly fully dissolved after adding  $\alpha$ MeMan.<sup>22</sup> For the D-mannosylated polymers an even higher stability is observed despite the addition of almost 1000 equivalents of the competitor  $\alpha$ MeMan, which has the same binding motif. This could indicate beneficial properties of the presented polymers in terms of their length, the flexibility of the polymeric backbone and way of attachment of the pendant sugar moieties, which may yield in an improved binding strength to the lectin.

## CONCLUSION

In summary, this work demonstrates the high potential of the combination of RAFT polymerization and the bromo-thio substitution to create different, well-defined sugar-conjugated polymers. The basis for the reactive scaffold is the (2-bromo-ethyl)-acrylate monomer that enables excellent control in the RAFT polymerization and high DPs of up to 115

repeating units. The bromides were readily substituted in a post-glycosylation procedure by addition of almost equal amounts of sugar-thiol(ate)s, in particular D-glucose, D-galactose, and D-mannose, in an  $S_N2$  reaction. The substitution was performed directly with unprotected carbohydrates, emphasizing the versatility of this method towards potential copolymers or linker structures, which are labile under the basic or acidic conditions usually applied for the deprotection of sugar units. Furthermore, the reactions are highly atom efficient and create only nontoxic side-products (triethyl ammoniumbromide, sodium bromide). The analytics of the novel polymers revealed mono-modal distributions with narrow dispersities and excellent DF of up to 100%, which was confirmed by elemental analysis. Binding studies of Con A with the synthesized polymers as multivalent ligands prove the selective binding ability of the sugar moieties as expected for the small molecules. D-Mannosylated polymers revealed higher clustering rates than the D-glucosylated polymers, whereas D-galactose bearing polymers showed no formation of cluster with Con A at all. With the linear, high molar mass polymers at hand, we could also demonstrate that the precipitation of Con A clusters is promoted more rapidly with increasing DP of the polymers. Reverse results were obtained by treating the Con A clusters with monovalent competitor  $\alpha$ -D-methyl-mannopyranose ( $\alpha$ MeMan). The turbidity of the D-glycosylated polymer clusters was rapidly reduced to a constant level, whereas the D-mannosylated ones decreased slower but continuous. This indicates a weak interaction between the Con A binding site and the multivalent D-glucose bearing polymers. Additionally, the remaining undissolved clusters of D-glucosylated and D-mannosylated polymers indicate an excellent binding affinity of these new types of polymers, which surpasses most other reported polymers with respective sugar groups attached.

This work demonstrated the use of RAFT for the polymerization of bromide-containing monomer BEA with high control and DPs higher than 100 as well as the subsequent post-glycosylation with almost quantitative DFs by versatile  $S_N2$  reaction with thiol(ate) derivatives of various sugars. The D-mannose bearing polymers via thioether functionality revealed the formation of very stable clusters with the lectin Con A.

## ACKNOWLEDGMENTS

The authors gratefully thank Gabi Sentis and Peter Bellstedt for the conducted DOSY NMR measurements and Beate Lentvogt and Sandra Köhn for the performed determination of the elemental compositions. The funding of the collaborative research center ChemBioSys (SFB 1127) by the Deutsche Forschungsgemeinschaft (DFG) is highly acknowledged. J.C. Brendel further thanks the DFG for support (Return Grant, BR 4905/2-1).

## REFERENCES

- 1 Y. Miura, Y. Hoshino, H. Seto, *Chem. Rev.* **2016**, *116*, 1673.

- 2 (a) Y. Miura, *Polym. J.* **2012**, *44*, 679; (b) R. A. Dwek, *Chem. Rev.* **1996**, *96*, 683.
- 3 (a) R. J. Pieters, *Org. Biomol. Chem.* **2009**, *7*, 2013; (b) A. Ghadban, L. Albertin, *Polymers* **2013**, *5*, 431.
- 4 J. J. Lundquist, E. J. Toone, *Chem. Rev.* **2002**, *102*, 555.
- 5 (a) K. Kobayashi, H. Sumitomo, Y. Ina, *Polym. J.* **1985**, *17*, 567; (b) A. Kobayashi, T. Akaike, K. Kobayashi, H. Sumitomo, *Macromol. Rapid Commun.* **1986**, *7*, 645.
- 6 S. Loykulnant, A. Hirao, *Macromolecules* **2000**, *33*, 4757.
- 7 M.-P. Labeau, H. Cramail, A. Deffieux, *Macromol. Chem. Phys.* **1998**, *199*, 335.
- 8 (a) D. M. Haddleton, R. Edmonds, A. M. Heming, E. J. Kelly, D. Kukulj, *New J. Chem.* **1999**, *23*, 477; (b) K. Ohno, Y. Tsujii, T. Fukuda, *J. Polym. Sci. Part A: Polym. Chem.* **1998**, *36*, 2473.
- 9 K. Aoi, K. Tsutsumiuchi, M. Okada, *Macromolecules* **1994**, *27*, 875.
- 10 V. Ladmiral, E. Melia, D. M. Haddleton, *Eur. Polym. J.* **2004**, *40*, 431.
- 11 J. A. Burns, M. I. Gibson, C. R. Becer, *Functional Polymers by Post-Polymerization Modification*; Wiley-VCH Verlag GmbH & Co. KGaA: Weinheim, **2012**; pp. 237.
- 12 M. C. García-Oteiza, M. Sánchez-Chaves, F. Arranz, *Macromol. Chem. Phys.* **1997**, *198*, 2237.
- 13 C. R. Becer, K. Babiuch, D. Pilz, S. Hornig, T. Heinze, M. Gottschaldt, U. S. Schubert, *Macromolecules* **2009**, *42*, 2387.
- 14 V. Ladmiral, G. Mantovani, G. J. Clarkson, S. Cauet, J. L. Irwin, D. M. Haddleton, *J. Am. Chem. Soc.* **2006**, *128*, 4823.
- 15 G. Chen, S. Amajjahe, M. H. Stenzel, *Chem. Commun.* **2009**, 1198.
- 16 G. David, C. Boyer, J. Tonnar, B. Ameduri, P. Lacroix-Desmazes, B. Boutevin, *Chem. Rev.* **2006**, *106*, 3936.
- 17 Y. Chen, G. Chen, M. H. Stenzel, *Macromolecules* **2010**, *43*, 8109.
- 18 J. C. Kim, Y. Rho, G. Kim, M. Kim, H. Kim, I. J. Kim, J. R. Kim, M. Ree, *Polym. Chem.* **2013**, *4*, 2260.
- 19 T. R. Barlow, J. C. Brendel, S. Perrier, *Macromolecules* **2016**, *49*, 6203.
- 20 C. J. Ferguson, R. J. Hughes, D. Nguyen, B. T. T. Pham, R. G. Gilbert, A. K. Serelis, C. H. Such, B. S. Hawkett, *Macromolecules* **2005**, *38*, 2191.
- 21 A. Bruneau, M. Roche, A. Hamze, J.-D. Brion, M. Alami, S. Messaoudi, *Chem. Eur. J.* **2015**, *21*, 8375.
- 22 Y. Gou, J. Geng, S.-J. Richards, J. Burns, C. Remzi Becer, D. M. Haddleton, *J. Polym. Sci. Polym. Chem.* **2013**, *51*, 2588.
- 23 H. Zhou, Y. Chen, C. M. Plummer, H. Huang, Y. Chen, *Polym. Chem.* **2017**, *8*, 2189.
- 24 (a) Y. Wang, G. Jiang, T. Qiu, F. Ding, *Drug Dev. Ind. Pharm.* **2012**, *38*, 1039; (b) C. S. Cho, S. J. Seo, I. K. Park, S. H. Kim, T. H. Kim, T. Hoshiba, I. Harada, T. Akaike, *Biomaterials* **2006**, *27*, 576.
- 25 (a) S. Kawakami, A. Sato, M. Nishikawa, F. Yamashita, M. Hashida, *Gene Ther.* **2000**, *7*, 292; (b) H. Kitano, Y. Takahashi, K. Mizukami, K. Matsuura, *Colloids Surf. B* **2009**, *70*, 91.
- 26 A. Lidgren, A. Bergh, K. Grankvist, T. Rasmuson, B. Ljungberg, *BJU Int.* **2008**, *101*, 480.
- 27 M. Younes, R. W. Brown, M. Stephenson, M. Gondo, P. T. Cagle, *Cancer* **1997**, *80*, 1046.
- 28 E. L. Dane, S. L. Chin, M. W. Grinstaff, *ACS Macro Lett.* **2013**, *2*, 887.
- 29 J. R. Rich, A. Szpacenko, M. M. Palcic, D. R. Bundle, *Angew. Chem. Int. Ed.* **2004**, *43*, 613.
- 30 S. M. Dimick, S. C. Powell, S. A. McMahon, D. N. Moothoo, J. H. Naismith, E. J. Toone, *J. Am. Chem. Soc.* **1999**, *121*, 10286.
- 31 K. H. Mortell, R. V. Weatherman, L. L. Kiessling, *J. Am. Chem. Soc.* **1996**, *118*, 2297.
- 32 A. M. Puertas, F. J. de las Nieves, *J. Phys.: Condens. Matter* **1997**, *9*, 3313.
- 33 C. W. Cairo, J. E. Gestwicki, M. Kanai, L. L. Kiessling, *J. Am. Chem. Soc.* **2002**, *124*, 1615.
- 34 P. N. Kanellopoulos, K. Pavlou, A. Perrakis, B. Agianian, C. E. Vorgias, C. Mavrommatis, M. Soufi, P. A. Tucker, S. J. Hamodrakas, *J. Struct. Biol.* **1996**, *116*, 345.
- 35 C. Xiao, C. Zhao, P. He, Z. Tang, X. Chen, X. Jing, *Macromol. Rapid Commun.* **2010**, *31*, 991.



## **RAFT polymerization and thio-bromo substitution: An efficient way towards well-defined glycopolymers**

Michael Pröhl,<sup>†,‡</sup> Christoph Englert,<sup>†,‡</sup> Michael Gottschaldt,<sup>†,‡</sup> Johannes C. Brendel,<sup>†,‡,\*</sup>  
Ulrich S. Schubert<sup>†,‡,\*</sup>

† Laboratory of Organic and Macromolecular Chemistry (IOMC), Friedrich Schiller University Jena, Humboldtstraße 10, 07743 Jena, Germany

‡ Jena Center for Soft Matter (JCSM), Friedrich Schiller University Jena, Philosophenweg 7, 07743 Jena, Germany

\*corresponding authors: [ulrich.schubert@uni-jena.de](mailto:ulrich.schubert@uni-jena.de), [johannes.brendel@uni-jena.de](mailto:johannes.brendel@uni-jena.de)

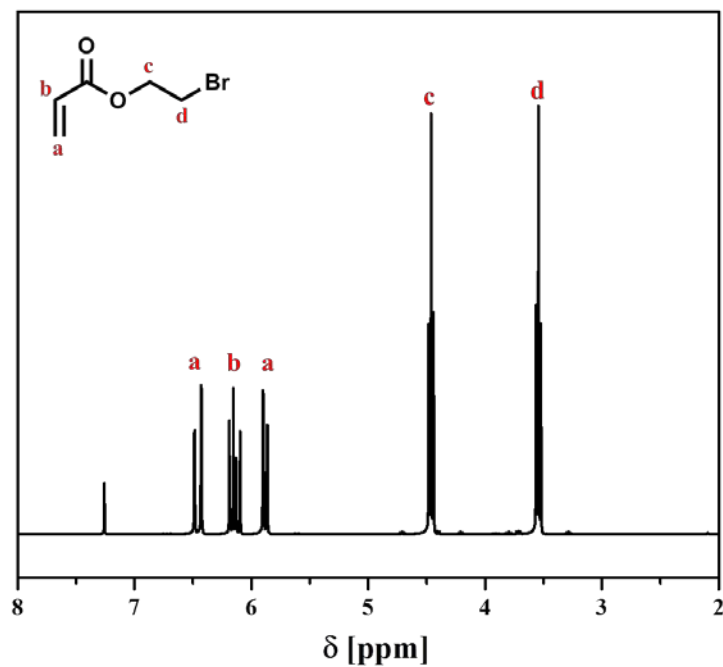


**Figure S1.**  $^1\text{H}$  NMR spectrum of 2-bromoethyl acrylate in  $\text{CDCl}_3$ .

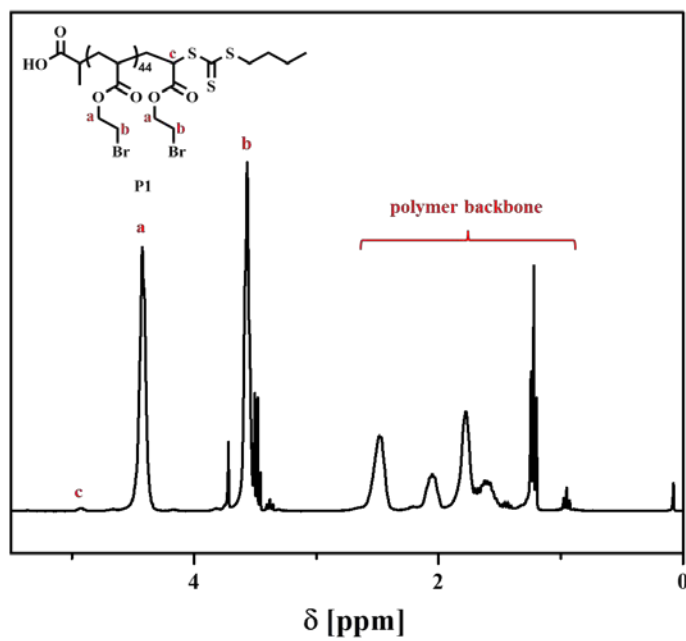


**Figure S2.**  $^1\text{H}$  NMR spectrum of **P1** in  $\text{CDCl}_3$ .

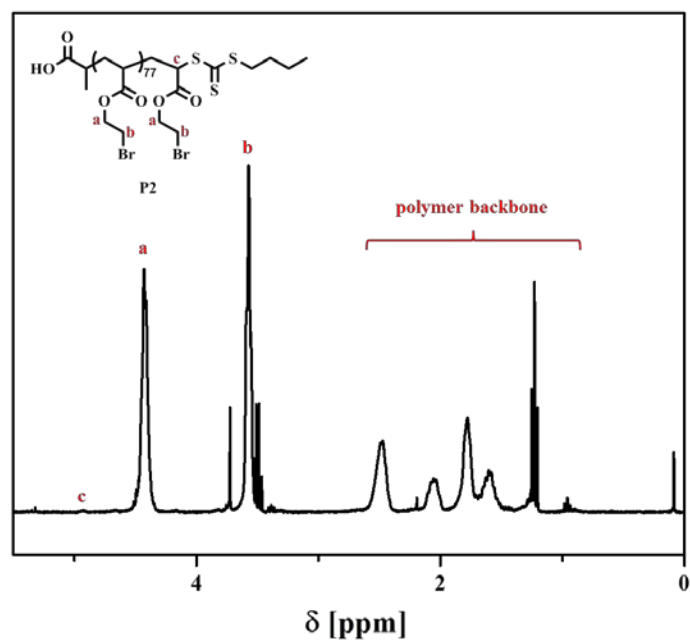


**Figure S3.** <sup>1</sup>H NMR spectrum of **P2** in CDCl<sub>3</sub>.

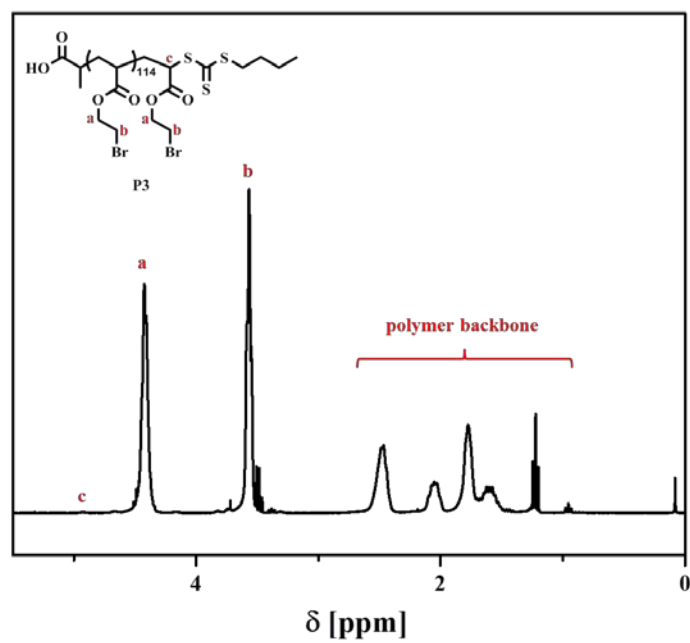


**Figure S4.** <sup>1</sup>H NMR spectrum of **P3** in CDCl<sub>3</sub>.

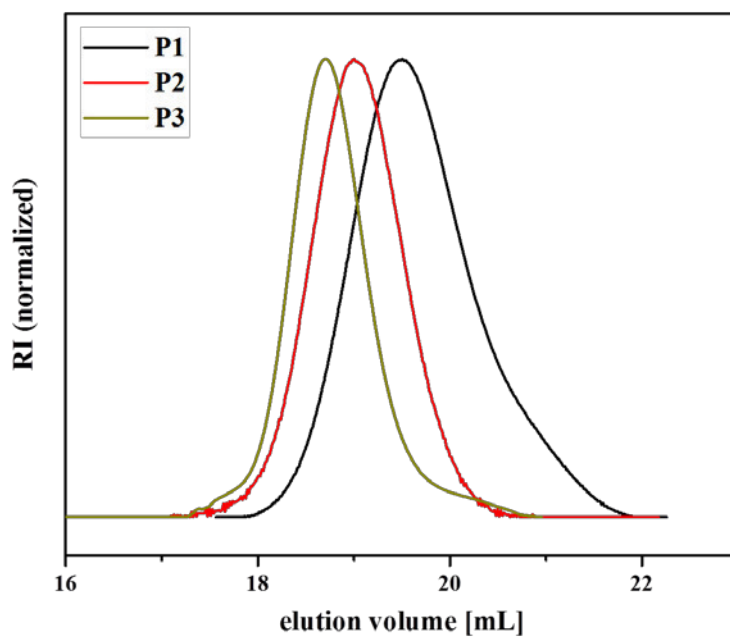


**Figure S5.** SEC trace of **P1** to **P3** (DMAc + 0.21 wt.% LiCl, PS calibration).

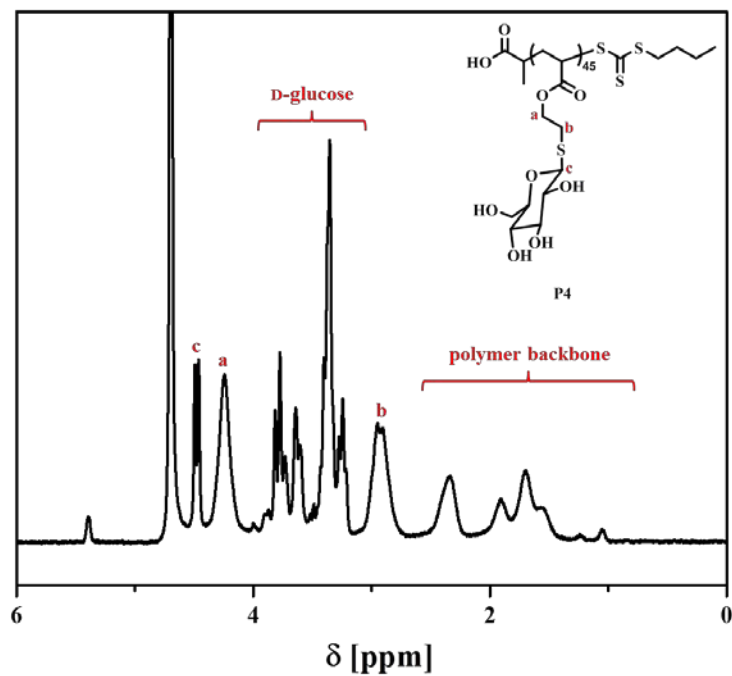


**Figure S6.**  $^1\text{H}$  NMR spectrum of **P4** in  $\text{D}_2\text{O}$ .

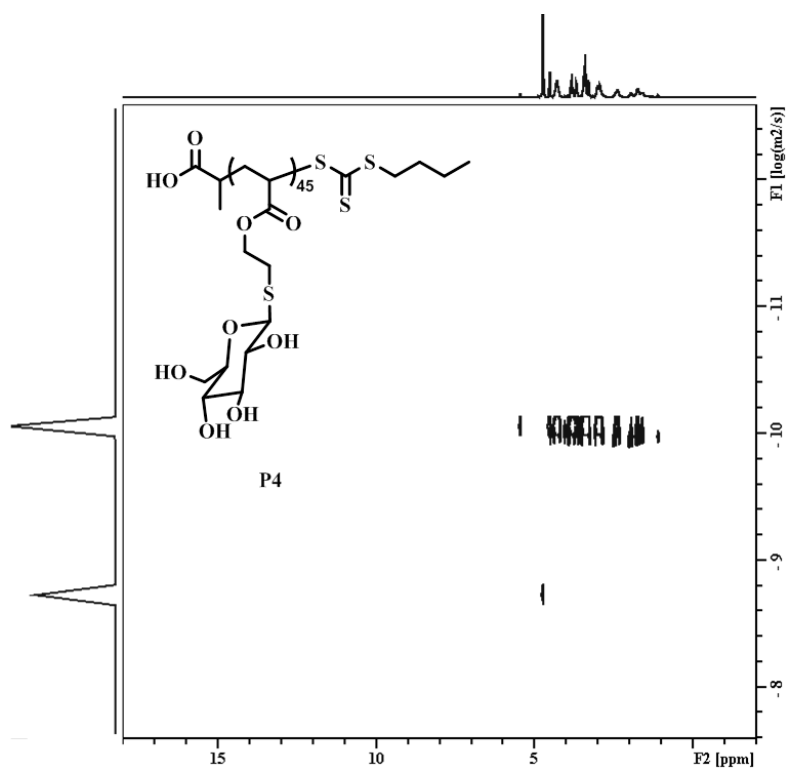


**Figure S7.**  $^1\text{H}$  DOSY NMR spectrum of **P4** in  $\text{D}_2\text{O}$ .

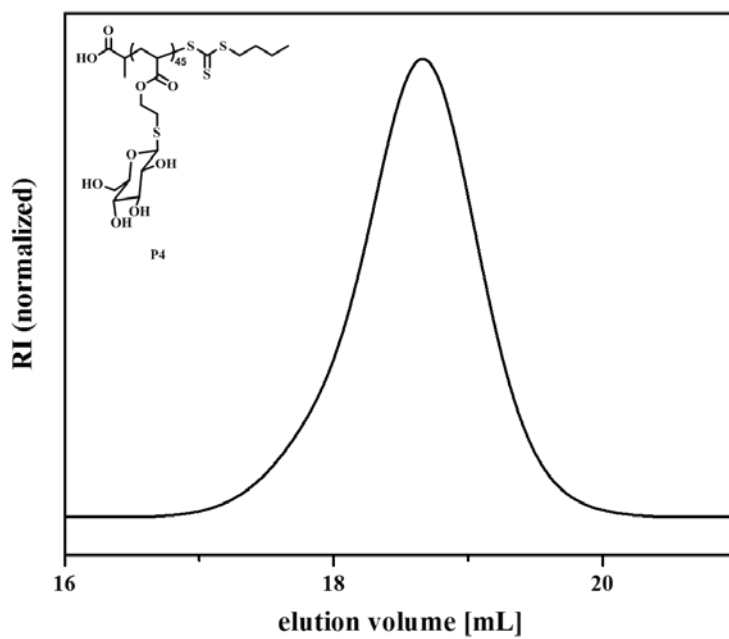


**Figure S8.** SEC trace of **P4** ( $\text{H}_2\text{O}$ , 0.1 M  $\text{NaNO}_3$ , 0.05 %  $\text{NaN}_3$ , pullulan standard).

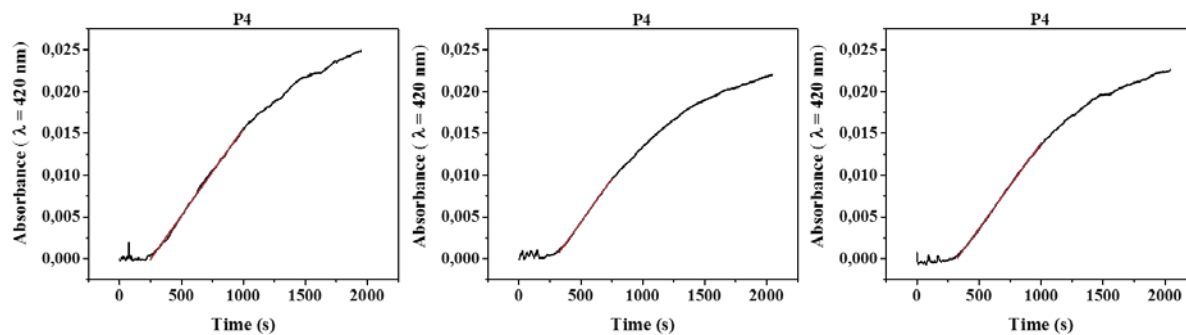


**Figure S9.** Absorbance ( $\lambda = 420$  nm) curves after adding 1 mL of 1  $\mu$ M solution of Con A in HBS buffer to the solution of the polymer **P4** (50  $\mu$ M per sugar unit, in HBS). The linear fit of the steepest portions of the curves were used to calculate the clustering rate  $k = 3,3411 \cdot 10^{-5}$  a.u. $\cdot$ s $^{-1}$ .

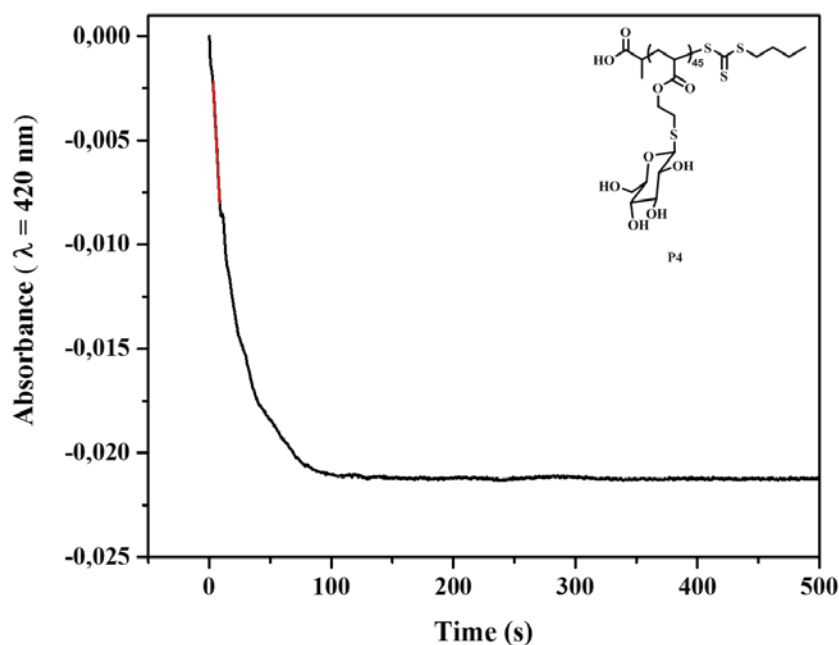


**Figure S10.** Absorbance ( $\lambda = 420$  nm) curves after adding 0.2 mL solution of  $\alpha$ MeMan (54 mM) to the Con A aggregates suspension in HBS buffer. Calculated rate of the reverse interaction between Con A aggregates and the competitor  $\alpha$ MeMan was obtained by a linear fit of the steepest portions of the curve,  $k = 1.06 \cdot 10^{-3}$  a.u. $\cdot$ s $^{-1}$ .

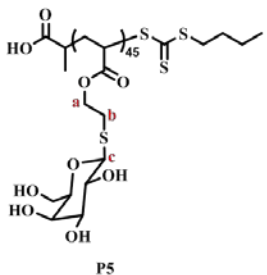


**Figure S12.**  $^1\text{H}$  DOSY NMR spectrum of **P5** in  $\text{D}_2\text{O}$ .

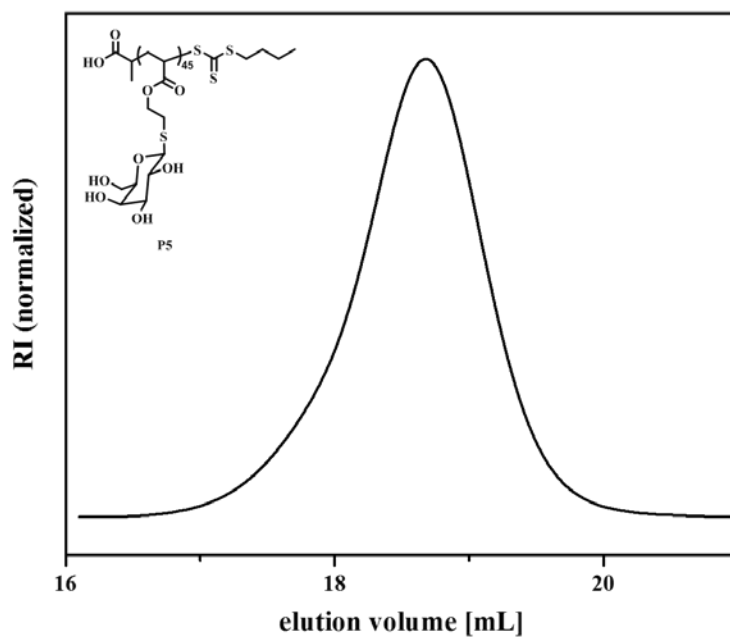


**Figure S13.** SEC trace of **P5** ( $\text{H}_2\text{O}$ , 0.1 M  $\text{NaNO}_3$ , 0.05 %  $\text{NaN}_3$ , pullulan standard).

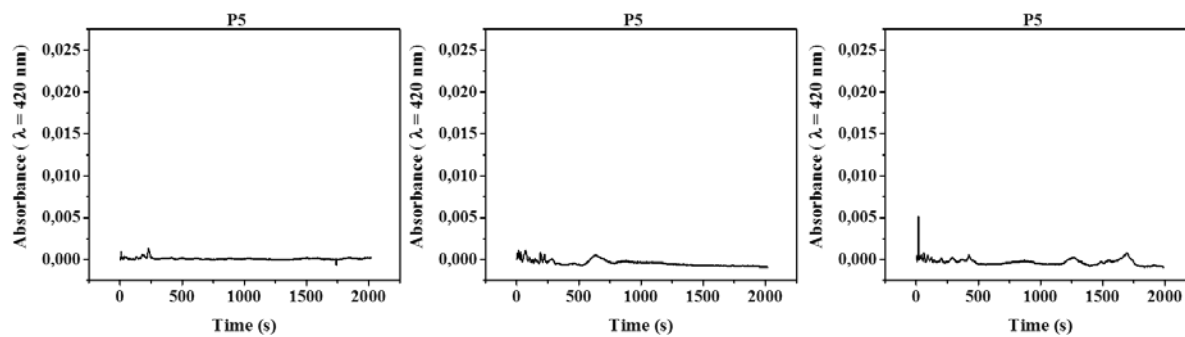


**Figure S14.** Absorbance ( $\lambda = 420 \text{ nm}$ ) curves after adding 1 mL of 1  $\mu\text{M}$  solution of Con A in HBS buffer to the solution of the polymer **P5** (50  $\mu\text{M}$  per sugar unit, in HBS).



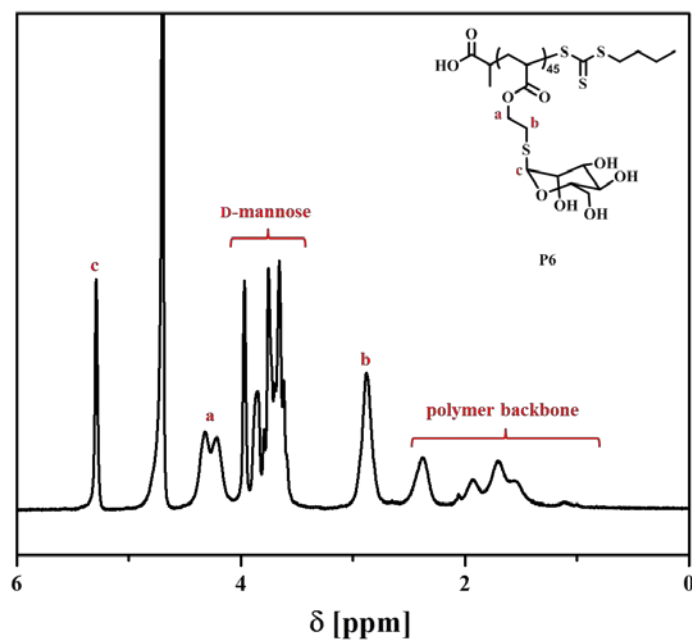


**Figure S15.**  $^1\text{H}$  NMR spectrum of **P6** in  $\text{D}_2\text{O}$ .

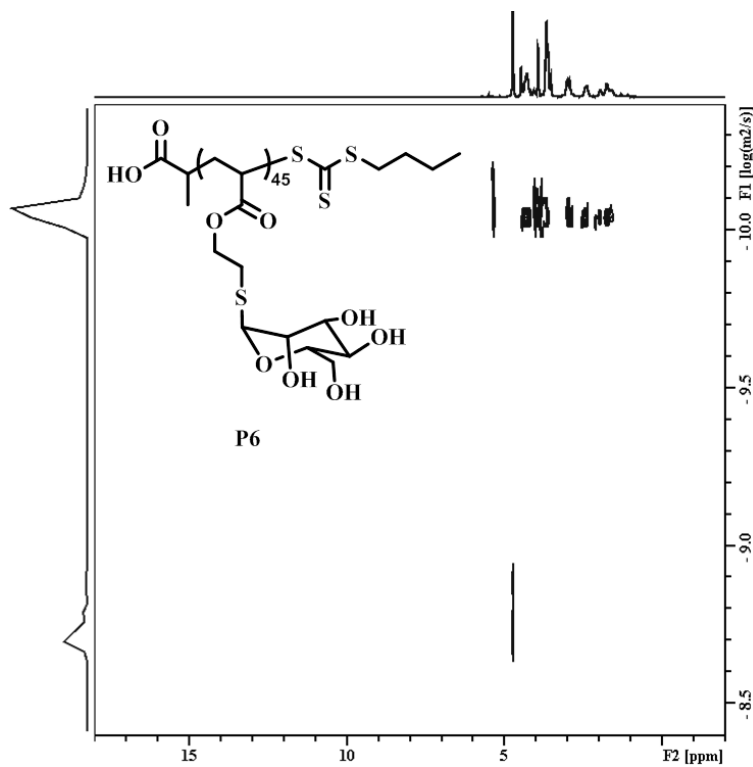


**Figure S16.**  $^1\text{H}$  DOSY NMR spectrum of **P6** in  $\text{D}_2\text{O}$ .

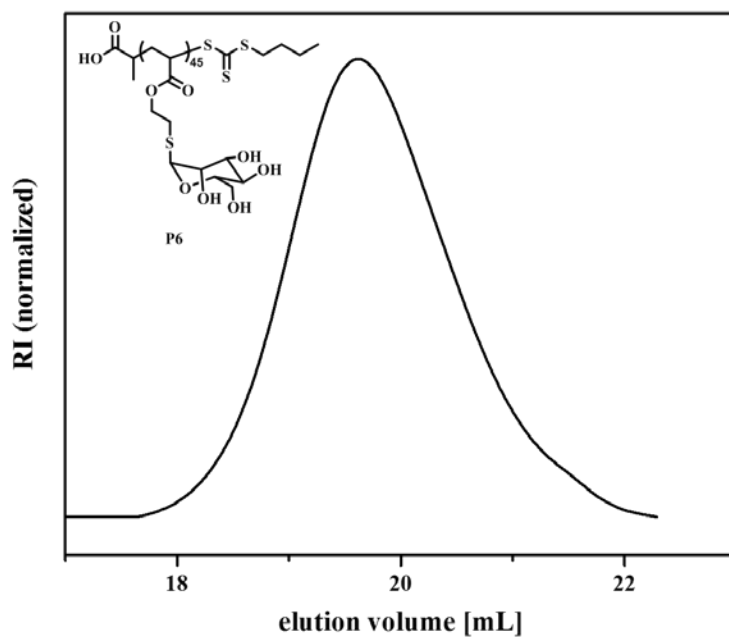


**Figure S17.** SEC trace of **P6** (H<sub>2</sub>O, 0.1 M NaNO<sub>3</sub>, 0.05 % NaN<sub>3</sub>, pullulan standard).

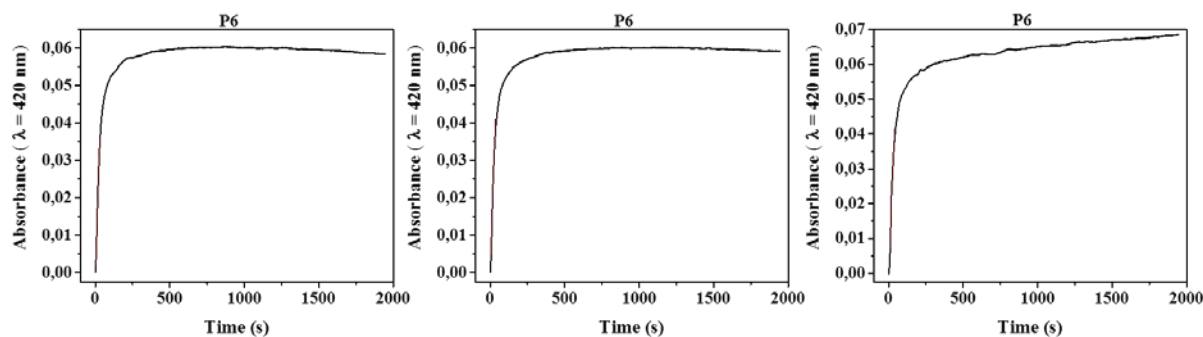


**Figure S18.** Absorbance ( $\lambda = 420$  nm) curves after adding 1 mL of 1  $\mu$ M solution of Con A in HBS buffer to the solution of the polymer **P6** (50  $\mu$ M per sugar unit, in HBS). The linear fit of the steepest portions of the curves were used to calculate the clustering rate  $k = 1.16 \cdot 10^{-3}$  a.u. $\cdot$ s<sup>-1</sup>.

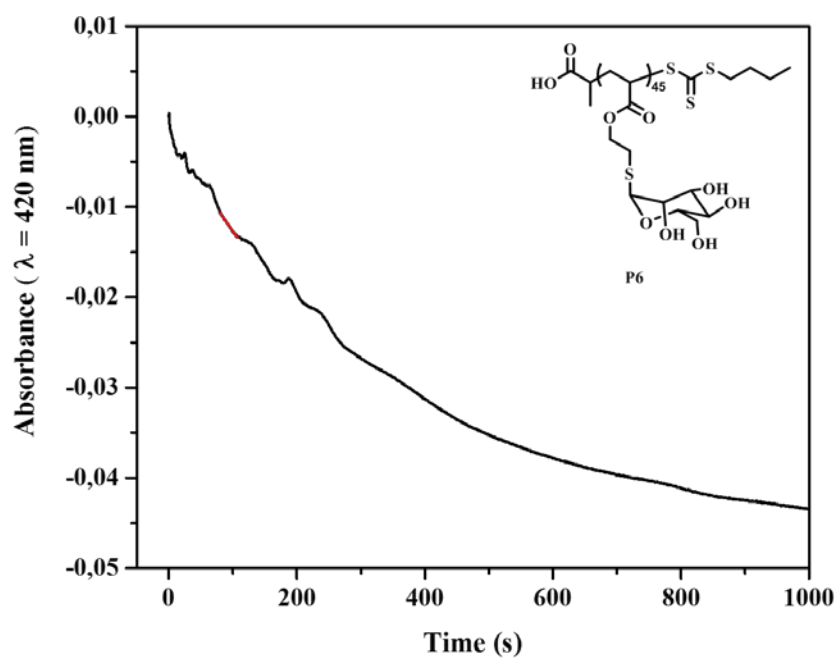


**Figure S19.** Absorbance ( $\lambda = 420$  nm) curves after adding 0.2 mL solution of  $\alpha$ MeMan (54 mM) to the Con A aggregates suspension in HBS buffer. Calculated rate of the reverse interaction between Con A aggregates and the competitor  $\alpha$ MeMan was obtained by a linear fit of the steepest portions of the curve,  $k = 1.02 \cdot 10^{-4}$  a.u. $\cdot$ s $^{-1}$ .

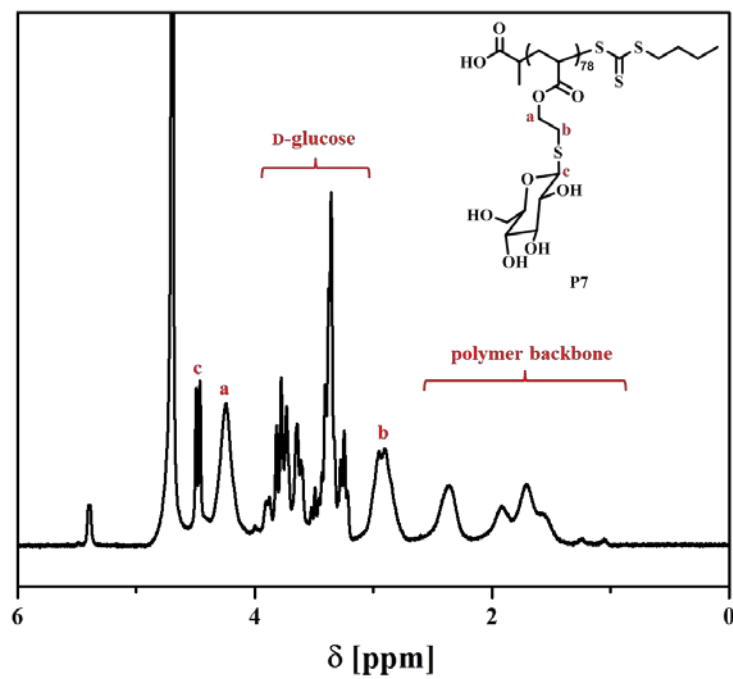


**Figure S20.**  $^1\text{H}$  NMR spectrum of **P7** in  $\text{D}_2\text{O}$ .

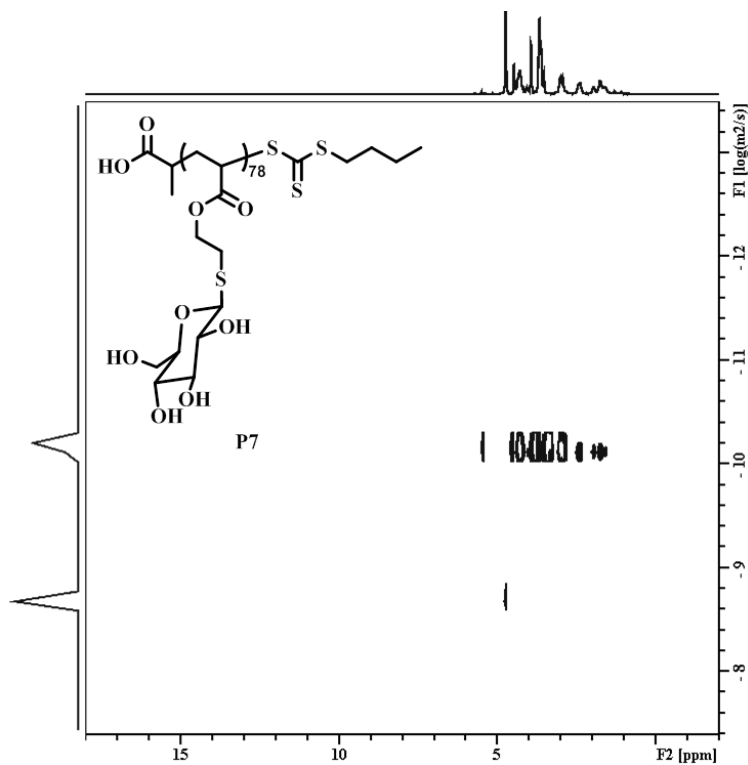


**Figure S21.**  $^1\text{H}$  DOSY NMR spectrum of **P7** in  $\text{D}_2\text{O}$ .

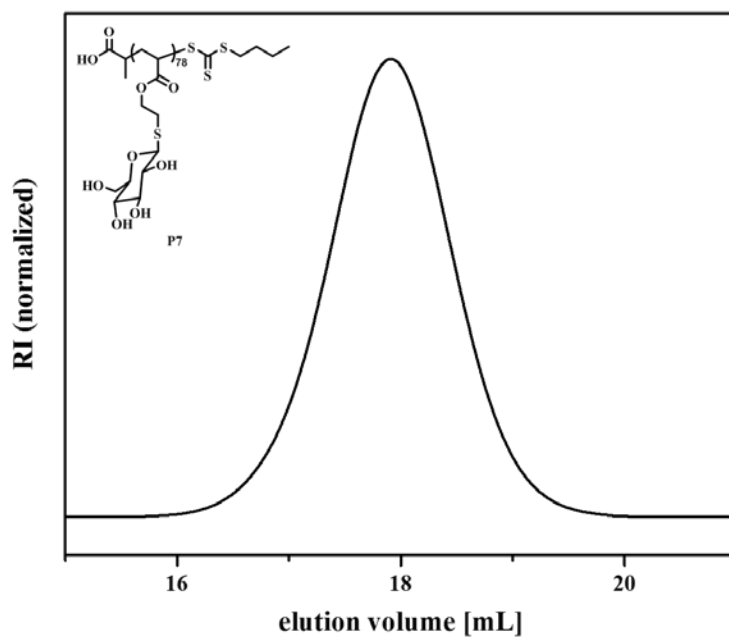


**Figure S22.** SEC trace of **P7** (H<sub>2</sub>O, 0.1 M NaNO<sub>3</sub>, 0.05 % NaN<sub>3</sub>, pullulan standard).

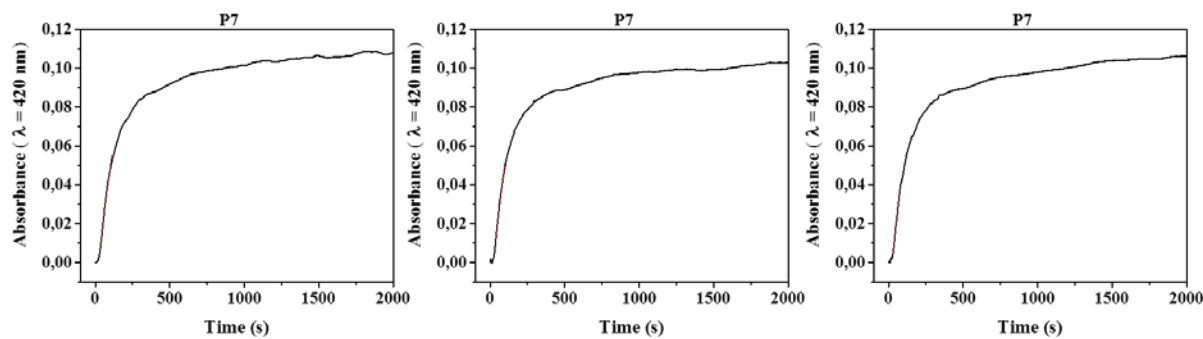


**Figure S23.** Absorbance ( $\lambda = 420$  nm) curves after adding 1 mL of 1  $\mu$ M solution of Con A in HBS buffer to the solution of the polymer **P7** (50  $\mu$ M per sugar unit, in HBS). The linear fit of the steepest portions of the curves were used to calculate the clustering

$$\text{rate } k = 6.481 \cdot 10^{-4} \text{ a.u.} \cdot \text{s}^{-1}.$$

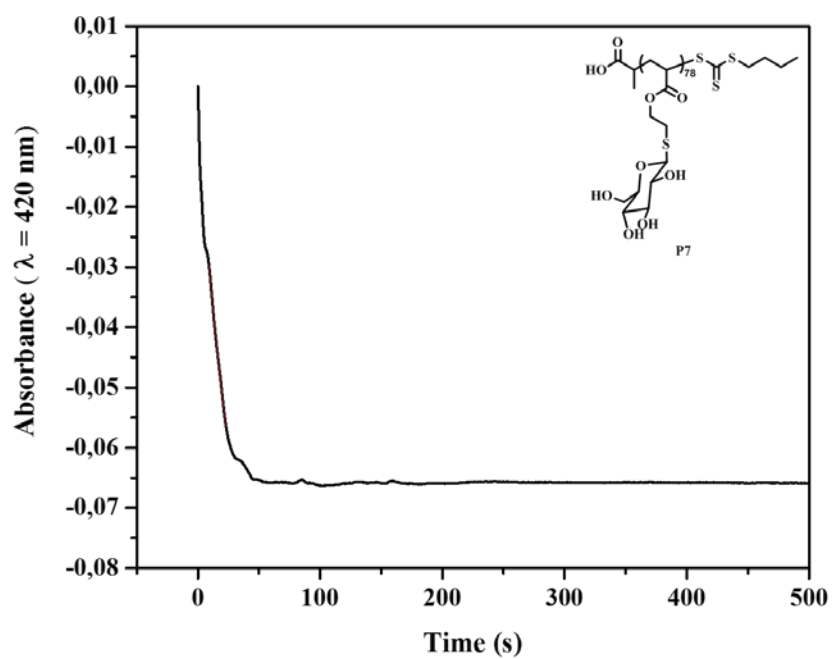


**Figure S24.** Absorbance ( $\lambda = 420$  nm) curves after adding 0.2 mL solution of  $\alpha$ MeMan (54 mM) to the Con A aggregates suspension in HBS buffer. Calculated rate of the reverse interaction between Con A aggregates and the competitor  $\alpha$ MeMan was obtained by a linear fit of the steepest portions of the curve,  $k = 1.94 \cdot 10^{-3}$  a.u. $\cdot$ s $^{-1}$ .

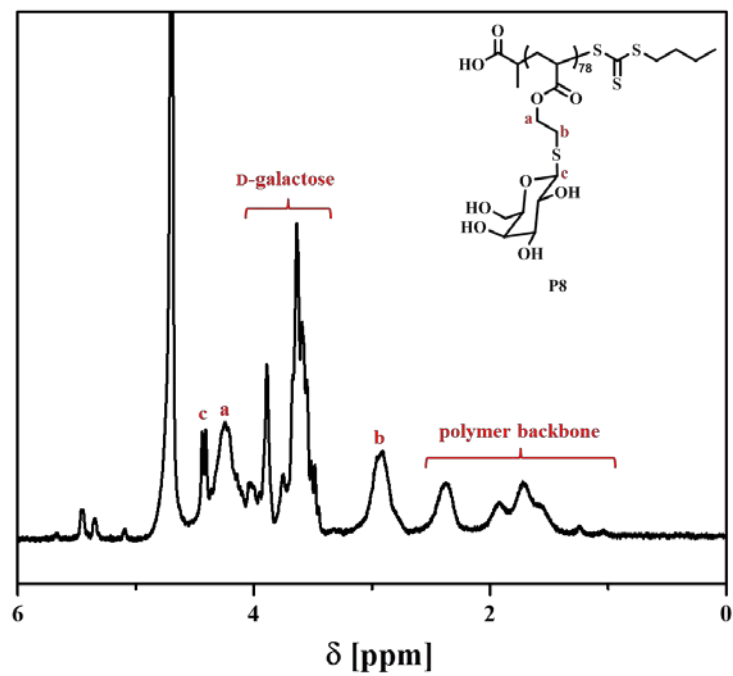


**Figure S25.**  $^1\text{H}$  NMR spectrum of **P8** in  $\text{D}_2\text{O}$ .

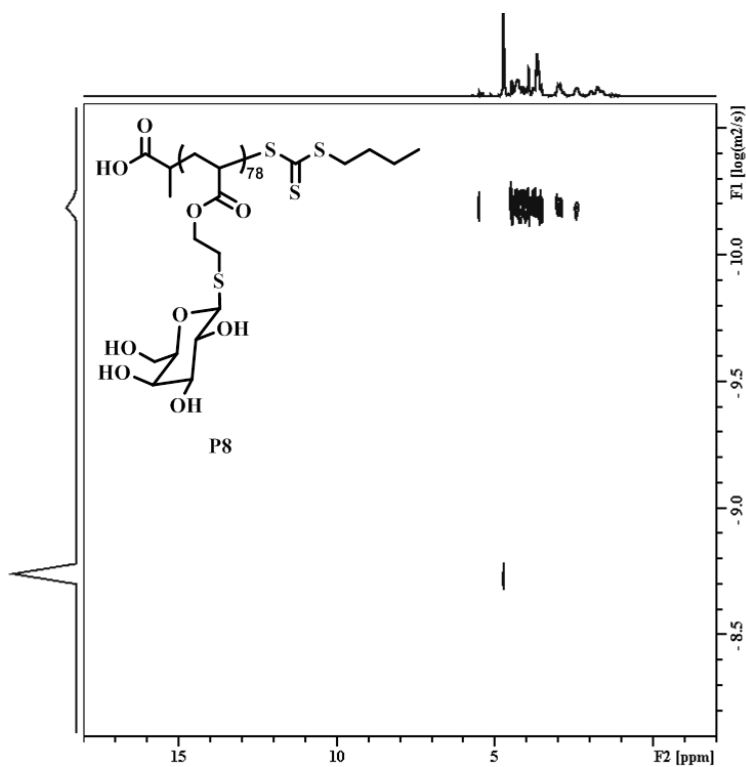


**Figure S26.**  $^1\text{H}$  DOSY NMR spectrum of **P8** in  $\text{D}_2\text{O}$ .

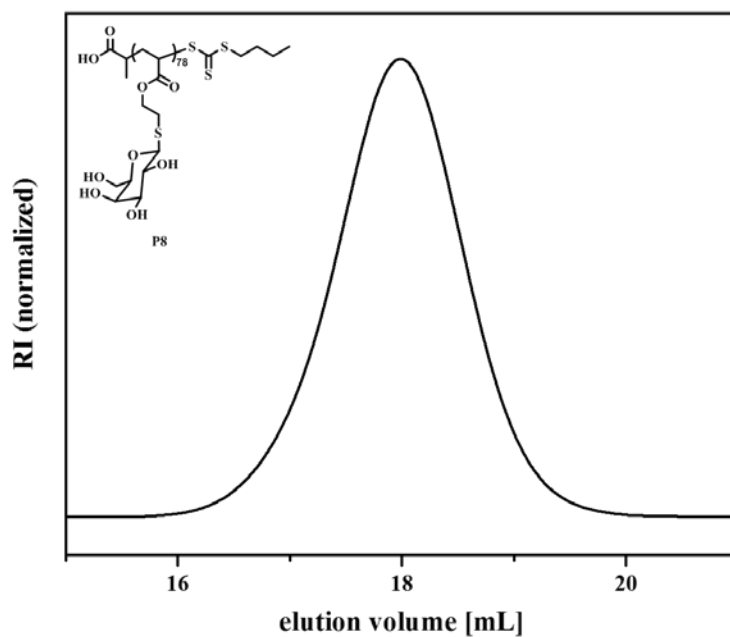


**Figure S27.** SEC trace of **P8** ( $\text{H}_2\text{O}$ , 0.1 M  $\text{NaNO}_3$ , 0.05 %  $\text{NaN}_3$ , pullulan standard).

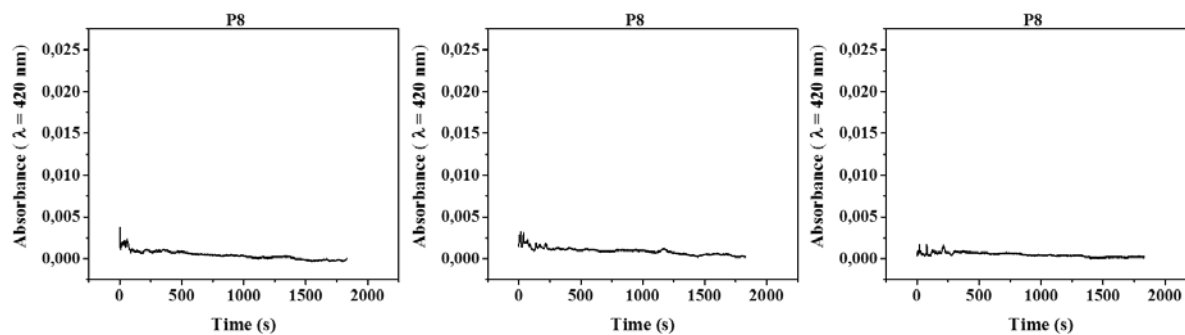


**Figure S28.** Absorbance ( $\lambda = 420 \text{ nm}$ ) curves after adding 1 mL of 1  $\mu\text{M}$  solution of Con A in HBS buffer to the solution of the polymer **P8** (50  $\mu\text{M}$  per sugar unit, in HBS).



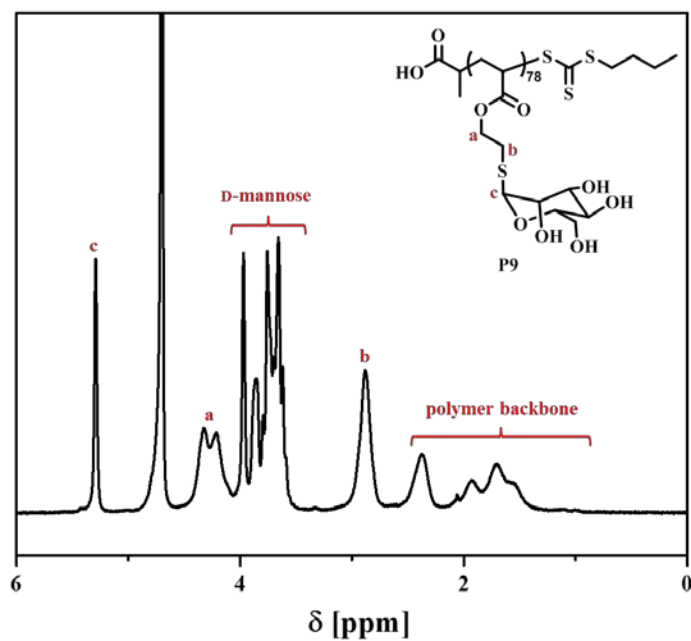


**Figure S29.**  $^1\text{H}$  NMR spectrum of **P9** in  $\text{D}_2\text{O}$ .

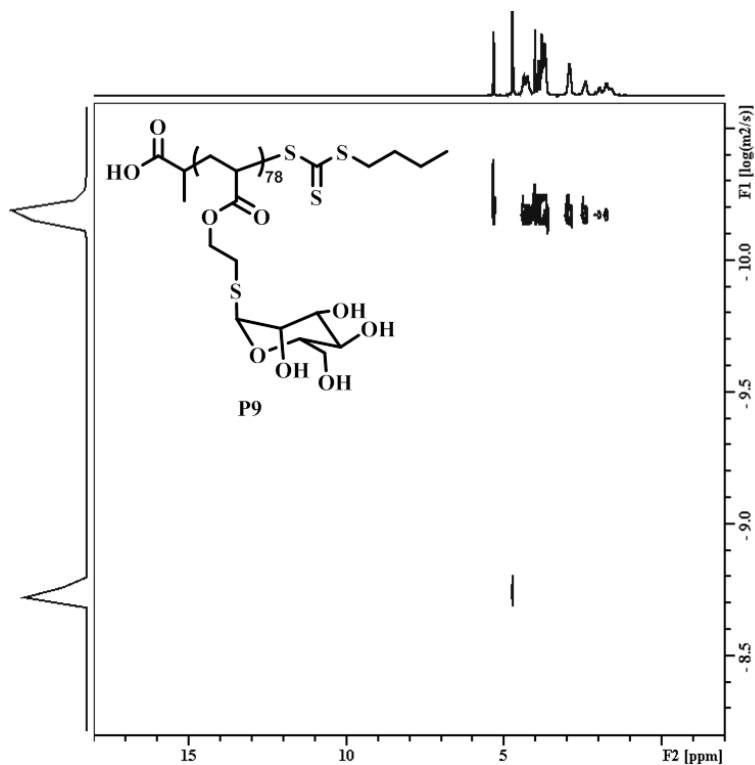


**Figure S30.**  $^1\text{H}$  DOSY NMR spectrum of **P9** in  $\text{D}_2\text{O}$ .

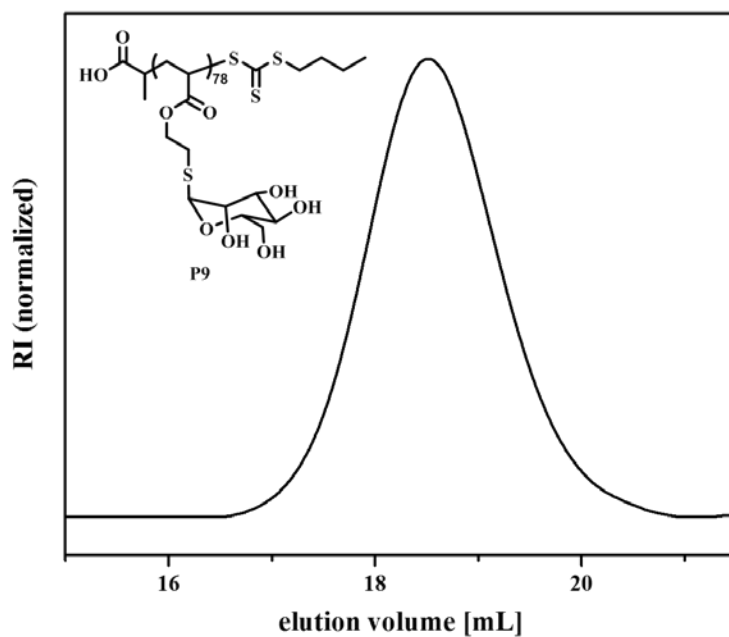


**Figure S31.** SEC trace of **P9** (H<sub>2</sub>O, 0.1 M NaNO<sub>3</sub>, 0.05 % NaN<sub>3</sub>, pullulan standard).

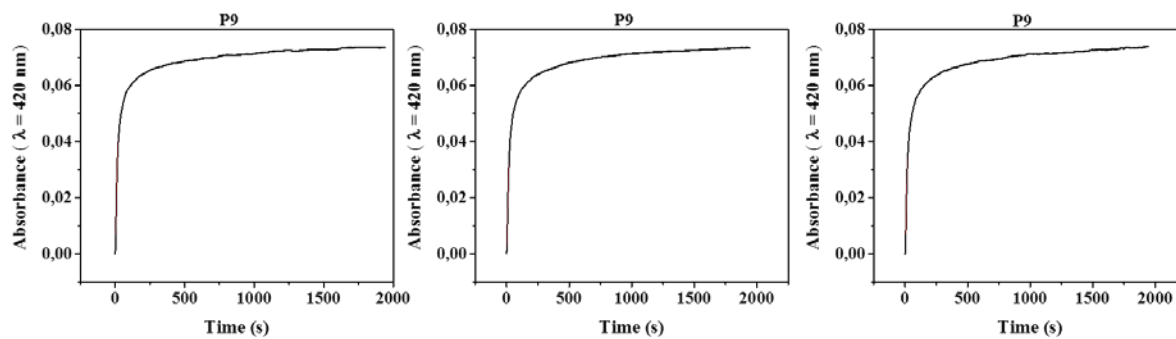


**Figure S32.** Absorbance ( $\lambda = 420$  nm) curves after adding 1 mL of 1  $\mu$ M solution of Con A in HBS buffer to the solution of the polymer **P9** (50  $\mu$ M per sugar unit, in HBS). The linear fit of the steepest portions of the curves were used to calculate the clustering rate  $k = 1.98 \cdot 10^{-3}$  a.u. $\cdot$ s<sup>-1</sup>.

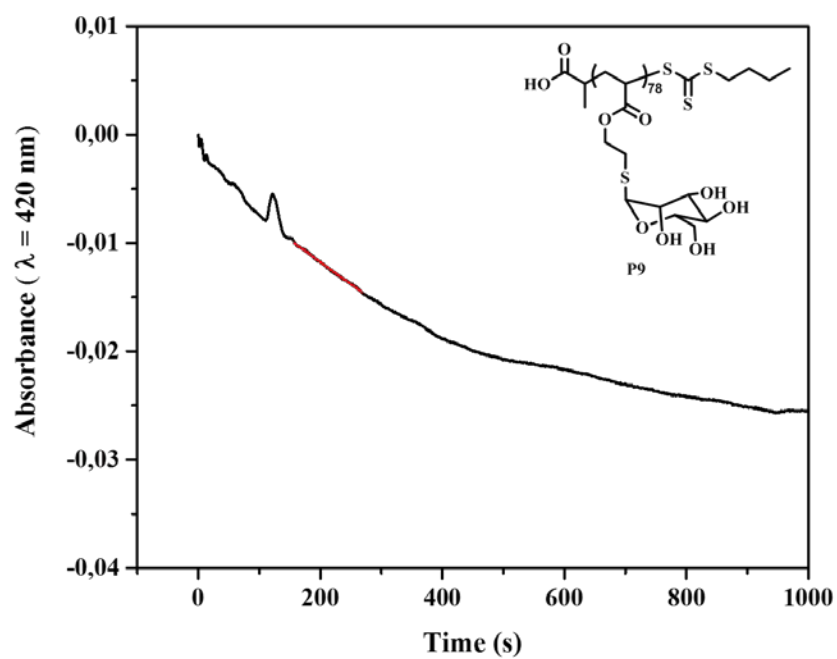


**Figure S33.** Absorbance ( $\lambda = 420 \text{ nm}$ ) curves after adding 0.2 mL solution of  $\alpha\text{MeMan}$  (54 mM) to the Con A aggregates suspension in HBS buffer. Calculated rate of the reverse interaction between Con A aggregates and the competitor  $\alpha\text{MeMan}$  was obtained by a linear fit of the steepest portions of the curve,  $k = 9.91 \cdot 10^{-5} \text{ a.u.} \cdot \text{s}^{-1}$ .

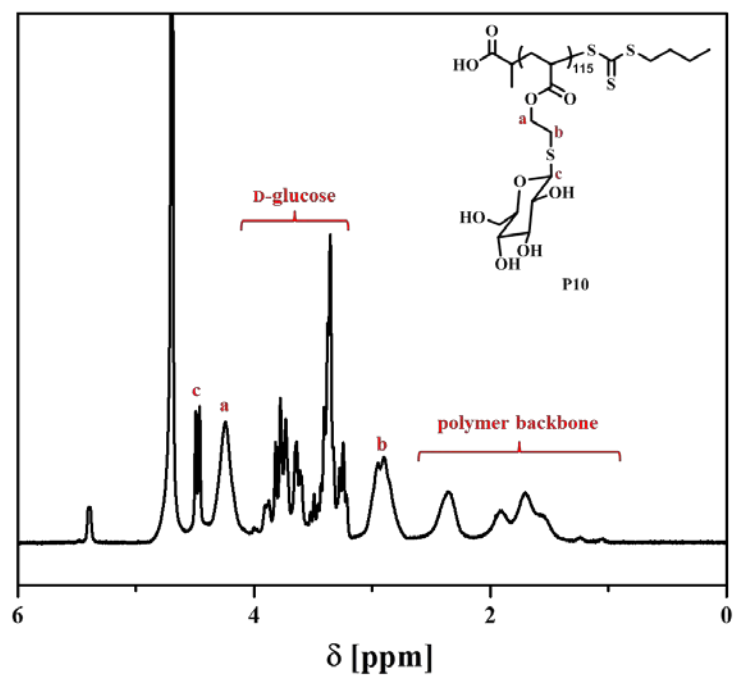


**Figure S34.**  $^1\text{H}$  NMR spectrum of **P10** in  $\text{D}_2\text{O}$ .

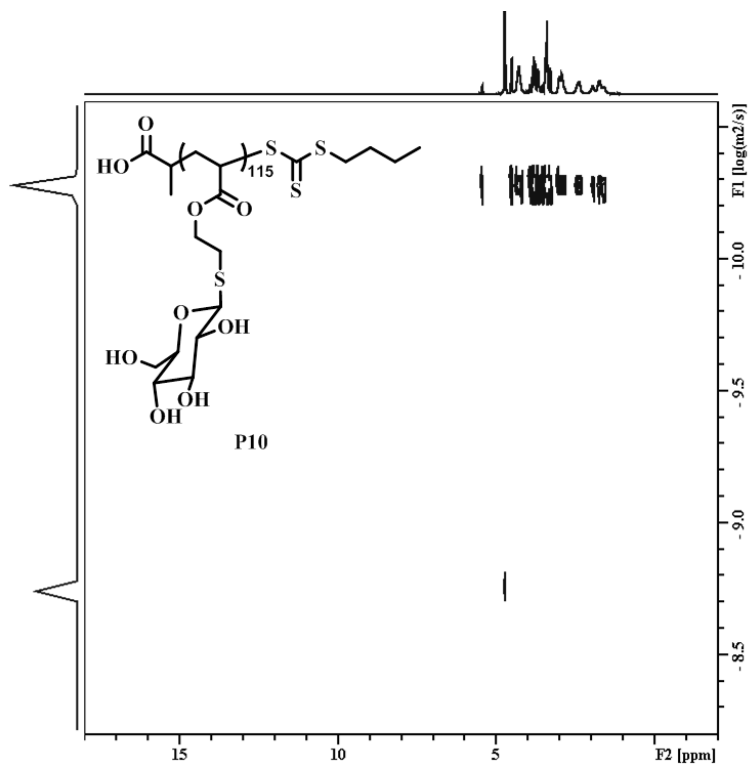


**Figure S35.**  $^1\text{H}$  DOSY NMR spectrum of **P10** in  $\text{D}_2\text{O}$ .

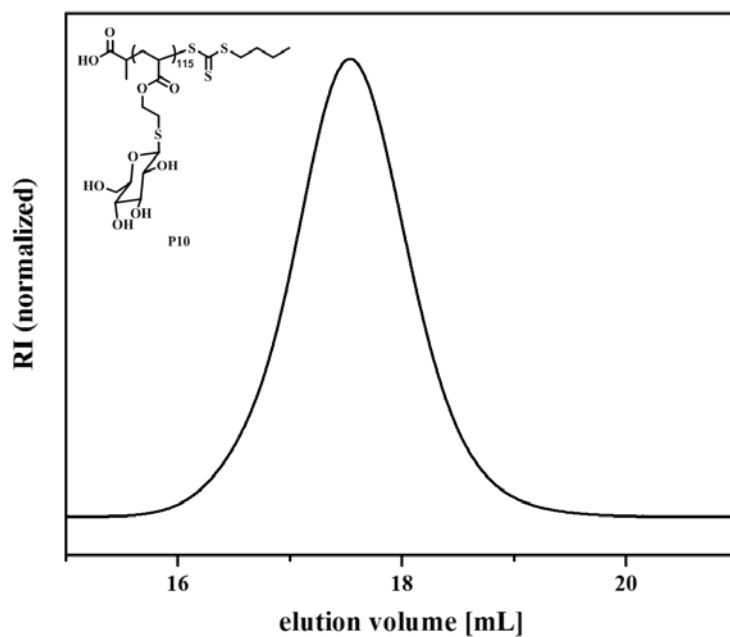


**Figure S36.** SEC trace of **P10** (H<sub>2</sub>O, 0.1 M NaNO<sub>3</sub>, 0.05 % NaN<sub>3</sub>, pullulan standard).

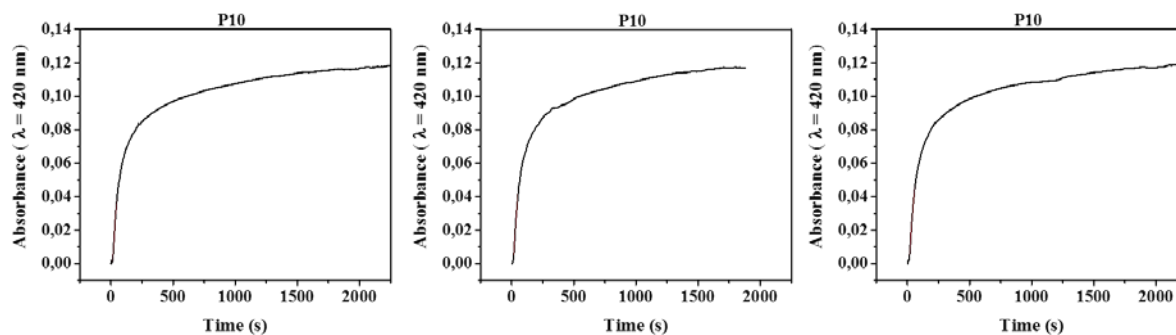


**Figure S37.** Absorbance ( $\lambda = 420$  nm) curves after adding 1 mL of 1  $\mu$ M solution of Con A in HBS buffer to the solution of the polymer **P10** (50  $\mu$ M per sugar unit, in HBS). The linear fit of the steepest portions of the curves were used to calculate the clustering

$$\text{rate } k = 1.06 \cdot 10^{-3} \text{ a.u.} \cdot \text{s}^{-1}.$$

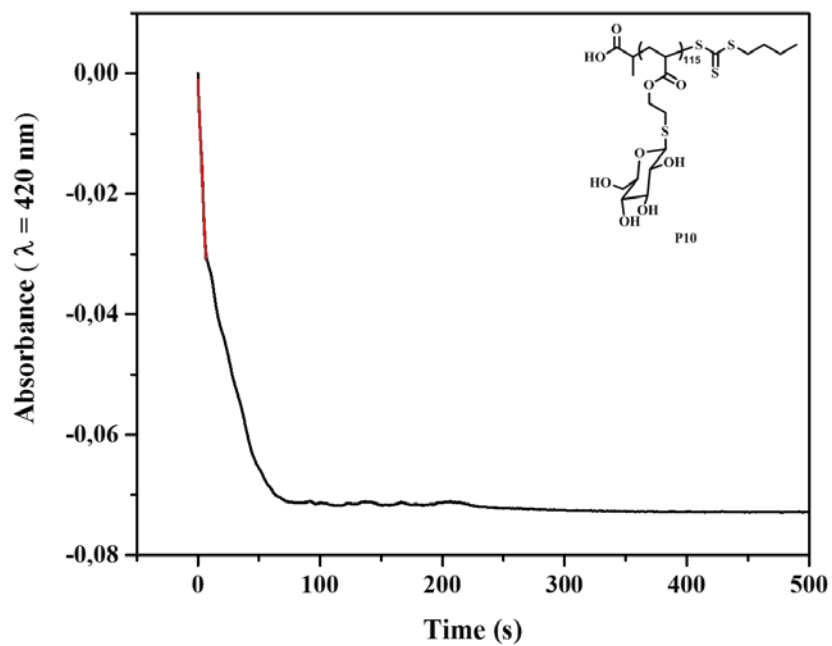


**Figure S38.** Absorbance ( $\lambda = 420$  nm) curves after adding 0.2 mL solution of  $\alpha$ MeMan (54 mM) to the Con A aggregates suspension in HBS buffer. Calculated rate of the reverse interaction between Con A aggregates and the competitor  $\alpha$ MeMan was obtained by a linear fit of the steepest portions of the curve,  $k = 4.6 \cdot 10^{-3}$  a.u. $\cdot$ s $^{-1}$ .

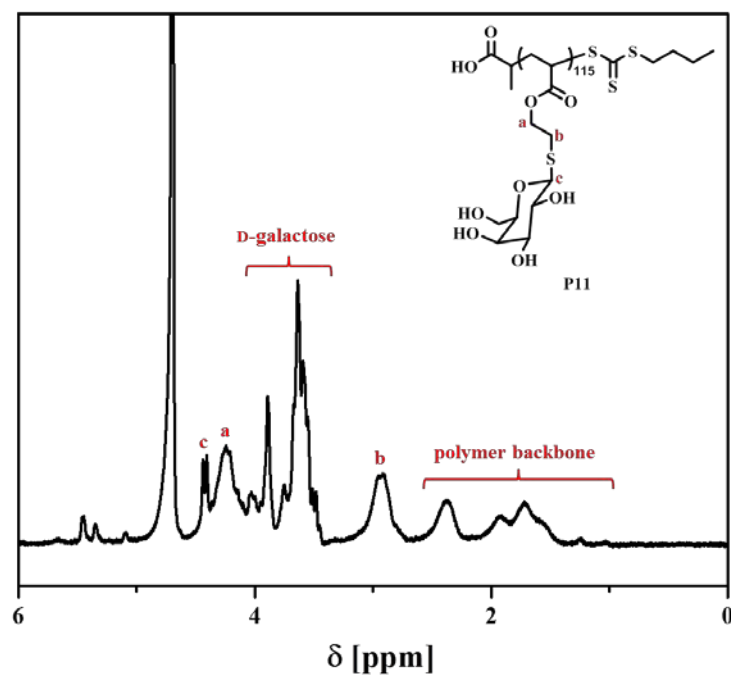


**Figure S39.**  $^1\text{H}$  NMR spectrum of **P11** in  $\text{D}_2\text{O}$ .

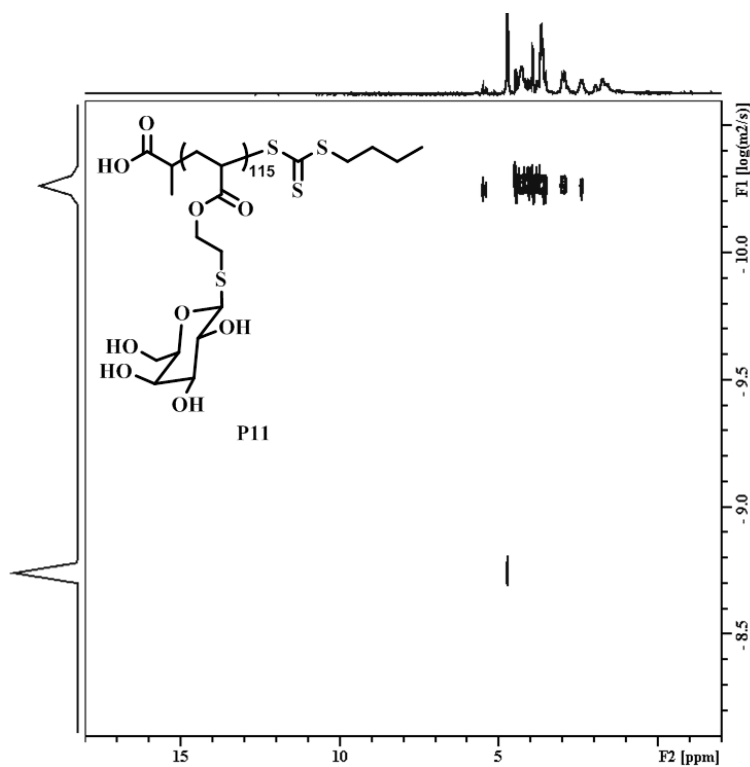


**Figure S40.**  $^1\text{H}$  DOSY NMR spectrum of **P11** in  $\text{D}_2\text{O}$ .

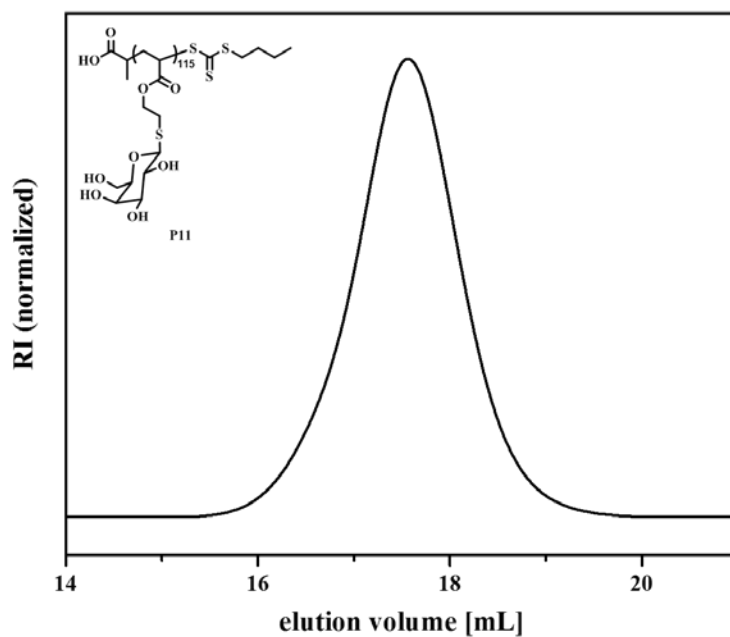


**Figure S41.** SEC trace of **P11** (H<sub>2</sub>O, 0.1 M NaNO<sub>3</sub>, 0.05 % NaN<sub>3</sub>, pullulan standard).

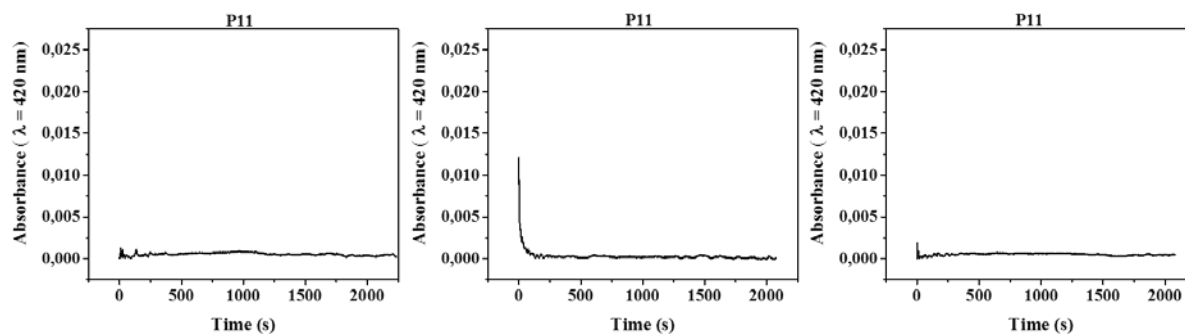


**Figure S42.** Absorbance ( $\lambda = 420$  nm) curves after adding 1 mL of 1  $\mu$ M solution of Con A in HBS buffer to the solution of the polymer **P11** (50  $\mu$ M per sugar unit, in HBS).



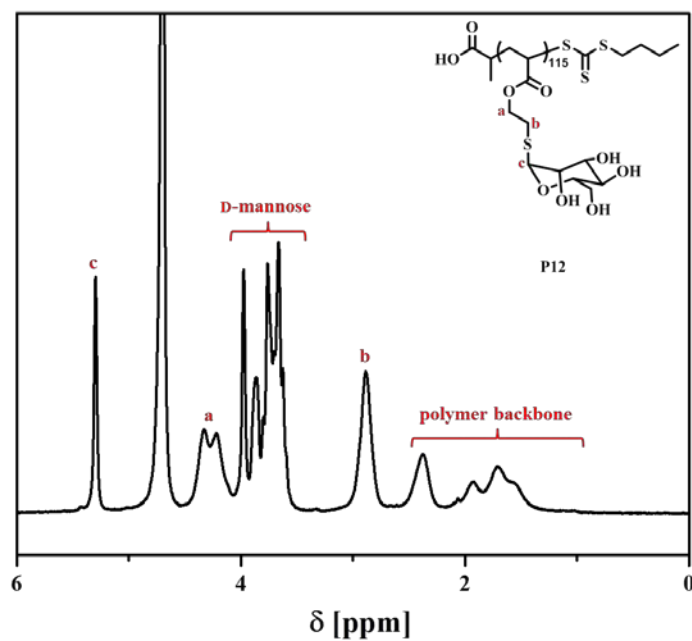


**Figure S43.**  $^1\text{H}$  NMR spectrum of **P12** in  $\text{D}_2\text{O}$ .

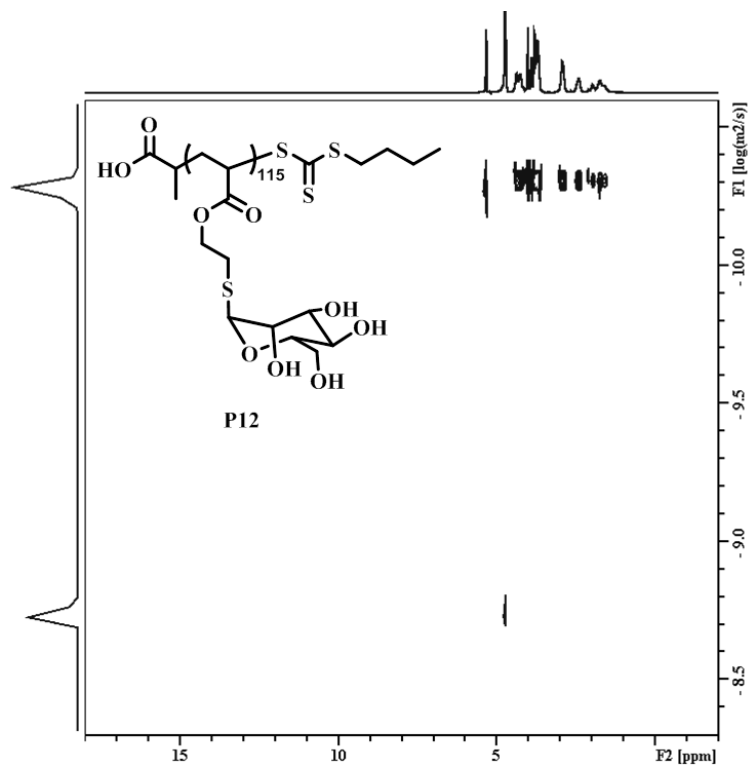


**Figure S44.**  $^1\text{H}$  DOSY NMR spectrum of **P12** in  $\text{D}_2\text{O}$ .

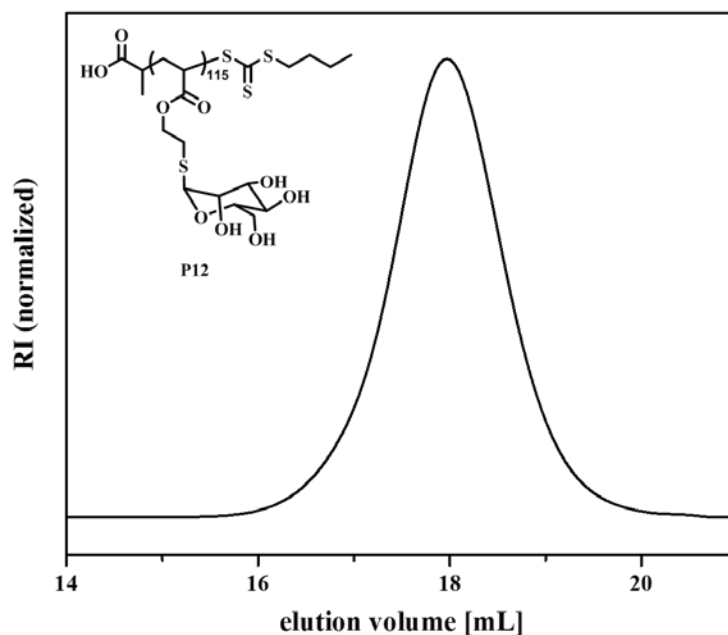


**Figure S45.** SEC trace of **P12** (H<sub>2</sub>O, 0.1 M NaNO<sub>3</sub>, 0.05 % NaN<sub>3</sub>, pullulan standard).

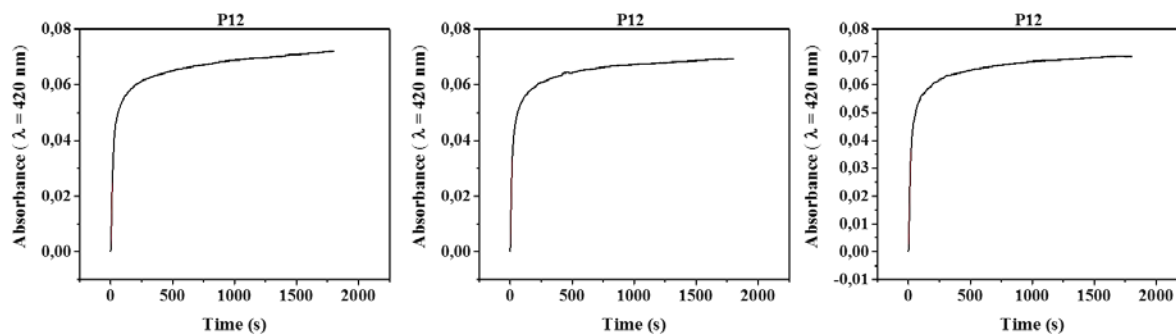


**Figure S46.** Absorbance ( $\lambda = 420$  nm) curves after adding 1 mL of 1  $\mu$ M solution of Con A in HBS buffer to the solution of the polymer **P10** (50  $\mu$ M per sugar unit, in HBS). The linear fit of the steepest portions of the curves were used to calculate the clustering

$$\text{rate } k = 2.11 \cdot 10^{-3} \text{ a.u.} \cdot \text{s}^{-1}.$$

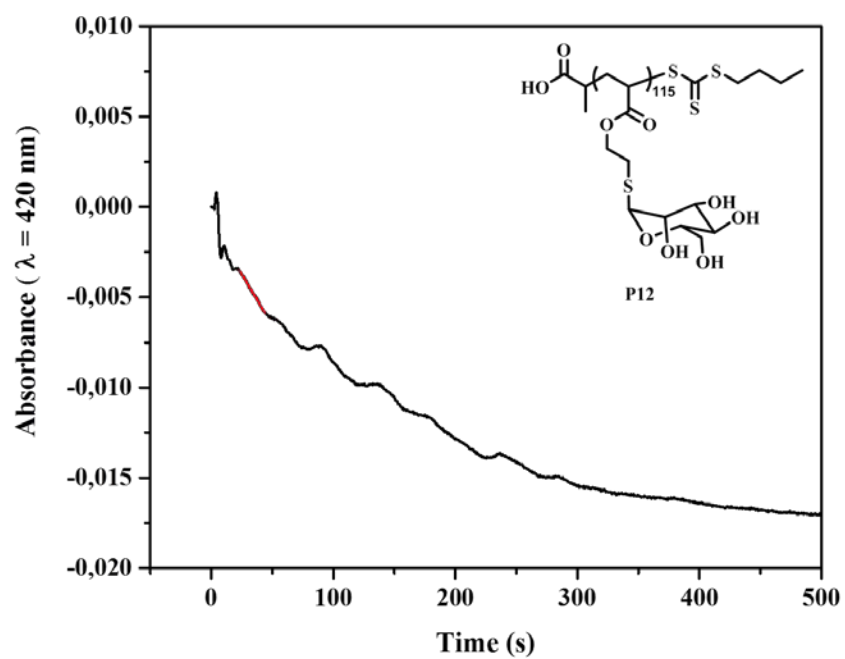


**Figure S47.** Absorbance ( $\lambda = 420$  nm) curves after adding 0.2 mL solution of  $\alpha$ MeMan (54 mM) to the Con A aggregates suspension in HBS buffer. Calculated rate of the reverse interaction between Con A aggregates and the competitor  $\alpha$ MeMan was obtained by a linear fit of the steepest portions of the curve,  $k = 1.13 \cdot 10^{-4}$  a.u. $\cdot$ s $^{-1}$ .

**Table S1.** Comparison of the total increase respectively decrease of the absorbance after adding Con A respectively  $\alpha$ MeMan to the polymer solution.

Abbrev.	Modulus of the total increase of the absorbance at $\lambda = 420$ nm after adding Con A	Modulus of the total decrease of the absorbance at $\lambda = 420$ nm after adding $\alpha$ MeMan	Percentage of dissolved Con A clusters
<b>P4</b>	0.0219	0.0212	97
<b>P6</b>	0.0600	0.0400	67
<b>P7</b>	0.1062	0.0729	69
<b>P9</b>	0.0733	0.0234	32
<b>P10</b>	0.1171	0.0729	62
<b>P12</b>	0.0706	0.0171	24

## Publication 6

### Curcuminoid-BF<sub>2</sub>-complexes: Synthesis, fluorescence and optimization of BF<sub>2</sub> group cleavage

H. Weiss, J. Reichel, H. Görls, K. R. A. Schneider, M. Micheel, M. Pröhl,  
M. Gottschaldt, B. Dietzek, W. Weigand

*Beilstein J. Org. Chem.* **2017**, *13*, 2264-2272.





# Curcuminoid–BF<sub>2</sub> complexes: Synthesis, fluorescence and optimization of BF<sub>2</sub> group cleavage

Henning Weiss<sup>1</sup>, Jeannine Reichel<sup>1</sup>, Helmar Görls<sup>1</sup>, Kilian Rolf Anton Schneider<sup>2</sup>, Mathias Micheel<sup>3</sup>, Michael Pröhl<sup>4</sup>, Michael Gottschaldt<sup>4</sup>, Benjamin Dietzek<sup>2,3</sup> and Wolfgang Weigand<sup>\*1,4</sup>

## Full Research Paper

[Open Access](#)

### Address:

<sup>1</sup>Institute for Inorganic and Analytical Chemistry, Friedrich-Schiller-Universität Jena, Humboldtstrasse 8, 07743 Jena, Germany, <sup>2</sup>Institute for Physical Chemistry, Friedrich-Schiller-Universität Jena, Helmholtzweg 4, 07743 Jena, Germany, <sup>3</sup>Leibniz Institute of Photonic Technology (IPHT), Albert-Einstein-Straße 9, 07745 Jena, Germany and <sup>4</sup>Jena Center of Soft Matter, Friedrich-Schiller-Universität Jena, Philosophenweg 7, 07743 Jena, Germany

### Email:

Wolfgang Weigand\* - wolfgang.weigand@uni-jena.de

\* Corresponding author

### Keywords:

BF<sub>2</sub> complex; curcumin; dyes; fluorescence; hydrolysis; spectroscopy

*Beilstein J. Org. Chem.* **2017**, *13*, 2264–2272.

doi:10.3762/bjoc.13.223

Received: 19 June 2017

Accepted: 28 September 2017

Published: 26 October 2017

Associate Editor: T. J. J. Müller

© 2017 Weiss et al.; licensee Beilstein-Institut.

License and terms: see end of document.

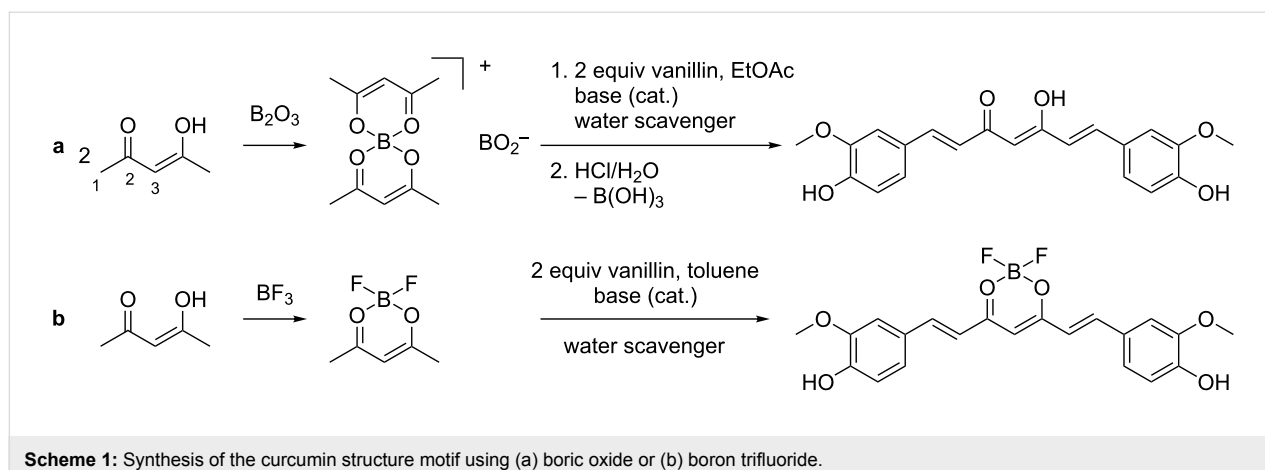
## Abstract

Eight difluoroboron complexes of curcumin derivatives carrying alkyne groups containing substituents have been synthesized following an optimised reaction pathway. The complexes were received in yields up to 98% and high purities. Their properties as fluorescent dyes have been investigated. Furthermore, a strategy for the hydrolysis of the BF<sub>2</sub> group has been established using aqueous methanol and sodium hydroxide or triethylamine.

## Introduction

In recent years curcumin, a pigment naturally occurring in *curcuma longa*, and its analogues, the curcuminoids, have attracted much attention regarding their biological activities [1]. These include antioxidant [2] and radical scavenging [3], anti-tumor [4] and anti-inflammatory [5] activities, as well as HIV inhibition [6]. Despite showing activity against several diseases and having only negligible side effects, low water solubility and fast degradation limit their potential medical application to this day [7].

The formation of the curcumin structure motif takes place by a base catalysed aldol condensation between the corresponding aldehyde and 2,4-pentanedione. To avoid a Knoevenagel condensation at the C-3 atom (Scheme 1a), the β-diketone moiety needs to be fixed into the enol form. In principle, this can be achieved by two different methods. The first one described by Pabon et al. utilises boric oxide in ethyl acetate as an intermediate agent (Scheme 1a) [8]. Boric acid esters like tri-*n*-butyl borate are normally used to scavenge water being produced



**Scheme 1:** Synthesis of the curcumin structure motif using (a) boric oxide or (b) boron trifluoride.

during the reaction, while piperidine [9] and *n*-butylamine [10,11] are typical bases used as catalysts for this type of reaction (Scheme 1). Although working well with vanillin and similar derivatives, the yields strongly decrease when employing other aldehydes [12]. This procedure also requires a rather extensive work-up including several extraction steps and chromatography [8]. A second, more recent approach first published by Rao et al. relies on boron trifluoride as the complexing agent [13]. The reaction was altered by Zhang et al. to be carried out in toluene (Scheme 1b) [14]. This reaction produces the  $BF_2$  complex of the corresponding curcuminoid in yields up to 98% and high purity as an insoluble solid, which requires only a minimum of work-up.

The  $BF_2$  complexes by themselves have attracted attention regarding their properties as fluorescent dyes with fluorescence quantum yields of up to 60% and Stokes shifts of up to  $5000\text{ cm}^{-1}$  [9]. Additionally, the incorporation of the  $BF_2$  group forces the  $\beta$ -diketone unit into the enol form, which leads to increased rigidity and enhanced photostability of the molecule [9].

Although a range of papers reports the synthesis of  $BF_2$  complexes of  $\beta$ -diketones such as curcuminoids [13,14] or dibenzoylmethanes [15,16], to our knowledge the reported procedures for the hydrolysis of these complexes are very limited and not always reproducible.

As part of our ongoing research to increase the selectivity of antitumor active metal complexes [17–22], our focus was on the synthesis of curcuminoids that could serve as building blocks to attach sugars like D-fructose or D-glucose [23]. Due to the easy accessibility to azido sugars [24,25] we decided to synthesise a range of curcuminoids bearing propargyl and pent-1-yn-5-yl ether groups as partners for “click” reactions [26]. We already observed that for the  $BF_2$  complex of bispropargyl function-

alised bisdemethoxycurcumin, the  $BF_2$  group was hydrolysed under regular “click” reaction conditions [23].

In this paper we report on the synthesis and spectroscopic characterization of the above mentioned compound as well as seven other novel curcuminoid  $BF_2$  complexes containing terminal triple bonds in their side chains. We also optimized the reaction conditions for the cleavage of the  $BF_2$  group to release the curcuminoids as an alternative synthetic route to substituted curcumins.

## Results and Discussion

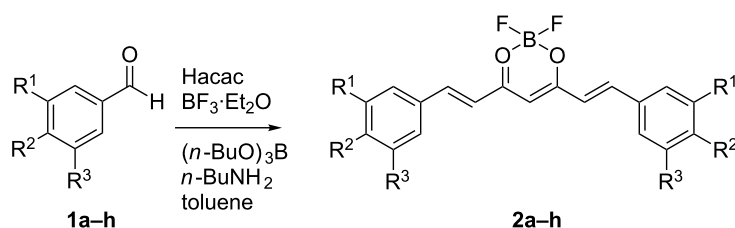
### Synthesis

#### $BF_2$ complexes

First, we prepared the aldehydes **1a–h** as the starting materials by Williamson ether synthesis of the corresponding hydroxybenzaldehydes with either propargyl bromide in dry DMF or 5-chloropent-1-yne in dry acetonitrile. As bases we used potassium carbonate for the propargyl ethers and caesium carbonate for the ethers with the longer side chains. Aqueous work-up achieved the aldehydes in excellent yields of up to 98%. NMR spectroscopic results were found to be in good accordance with the data published elsewhere [27–30].

We received the  $BF_2$  complexes **2a–h** by aldol reactions between the in situ generated  $BF_2$  complex of 2,4-pentanedione and the corresponding aromatic aldehydes **1a–h**. Following a procedure reported originally by Zhang [14], we were able to isolate **2a–h** in yields ranging from 56 to 96% (Table 1).

The amount of base required have to be increased from 0.1 to ca. 0.6 equiv due to the formation of HF, which forms *n*-butylammonium fluoride as a main impurity. Therefore, all complexes were purified by recrystallization from a mixture of acetone and water. Because most of the compounds were partially hydrolysed when heated to  $80\text{ }^\circ\text{C}$  in aqueous acetone solution,

**Table 1:** BF<sub>3</sub>·Et<sub>2</sub>O-promoted synthesis of curcuminoid–BF<sub>2</sub> complexes **2a–h**.

Entry	R <sup>1</sup>	R <sup>2</sup>	R <sup>3</sup>	Yield (%) <sup>a</sup>
<b>2a</b>	H	O-propargyl	OMe	90
<b>2b</b>	H	O-propargyl	H	96
<b>2c</b>	Br	O-propargyl	OMe	94
<b>2d</b>	Br	O-propargyl	H	65
<b>2e</b>	H	O-propargyl	O-propargyl	74
<b>2f</b>	H	OMe	O-propargyl	88
<b>2g</b>	H	OMe	O-pent-4-yn-1-yl	56
<b>2h</b>	H	O-pent-4-yn-1-yl	H	87

<sup>a</sup>Yield after recrystallization.

we carried out the purification at room temperature. The final compounds were characterized by <sup>1</sup>H, <sup>11</sup>B{<sup>1</sup>H}, <sup>13</sup>C{<sup>1</sup>H} and <sup>19</sup>F{<sup>1</sup>H} NMR spectroscopy, EI mass spectrometry, elemental analyses as well as UV–vis absorption and fluorescence spectroscopy.

The proton NMR spectra of all compounds exhibit the characteristic AB spin systems (*J* = approx. 16 Hz) occurring from the *trans*-olefinic protons in combination with a singlet at around 6.5 ppm. Signals in <sup>19</sup>F{<sup>1</sup>H} NMR appeared as sharp singlets at around –140 ppm, while <sup>11</sup>B{<sup>1</sup>H} NMR signals appear as up to 3 ppm broad singlets at about +0.9 ppm. No coupling between <sup>19</sup>F and <sup>11</sup>B nuclei was observed because of the high quadrupole moment of the <sup>11</sup>B nucleus. Due to the high relative mass difference between both naturally occurring boron isotopes, signals for the <sup>10</sup>B<sup>19</sup>F and <sup>11</sup>B<sup>19</sup>F complexes with Δδ ≈ 0.1 ppm could be found in the <sup>19</sup>F{<sup>1</sup>H} NMR spectrum. Several additional signals were observed after a few hours, as the compounds started to hydrolyse due to residual water in DMSO-*d*<sub>6</sub>. Resonances at –148.6 ppm in <sup>19</sup>F{<sup>1</sup>H} and –1.3 ppm in <sup>11</sup>B{<sup>1</sup>H} spectra (sharp singlet) could be assigned to BF<sub>4</sub><sup>–</sup> as the most common hydrolysis byproduct by comparison with HBF<sub>4</sub> in DMSO-*d*<sub>6</sub>.

### X-ray crystallography

Compounds **2f**, **2g** and **2h** were also characterized by X-ray diffraction methods. Crystals suitable for analysis were grown by slow diffusion of *n*-hexane into CH<sub>2</sub>Cl<sub>2</sub> solutions. All BF<sub>2</sub> complexes show the expected tetrahedral coordination sphere around the boron atom and the all-*trans* geometry of the olefinic

double bonds (Figure 1). Bond lengths and angles around the boron atom are in good accordance to values published for similar complexes [9]. One aromatic ring of **2f** is twisted by approx. 8° out of the plane formed by the ligand backbone and the second aromatic ring (Figure 1a). The twisting is stabilized by an intermolecular interaction between one propargyl CH<sub>2</sub> proton and a methoxy oxygen atom (see Supporting Information File 1 for intermolecular distances as well as selected bond length and angles). This interaction also induces the respective propargyl group to be turned by approximately 70° out of the plane formed by the backbone. Due to sterical intermolecular interactions in **2g**, one pent-5-yne-1-yl chain is in *gauche/anti* conformation, while the other is in the more favoured *anti/anti* conformation (Figure 1b) with the torsion angles only slightly differing from the ideal 60° or 180°, respectively. The aromatic rings are almost coplanar with the backbone. In both cases, one of the longer side chains lays mostly within the molecule plane, while the other is turned out. The structure of complex **2h** shows C<sub>2</sub> symmetry with both side chains in *gauche/anti* conformation. The deviation from the ideal angles is higher than that for **2g**. The plane formed by each phenyl ring is turned by approximately 5° out of the plane of the backbone.

### BF<sub>2</sub> cleavage

To hydrolyse the BF<sub>2</sub> complexes and release the free ligands we investigated several mixtures of organic solvents and water in 4:1 ratios as well as dry THF as a control reaction at 65 °C (Table 2). Complex **2b** was chosen as the model compound (Scheme 2) as **3b** has been previously reported in the literature [31].



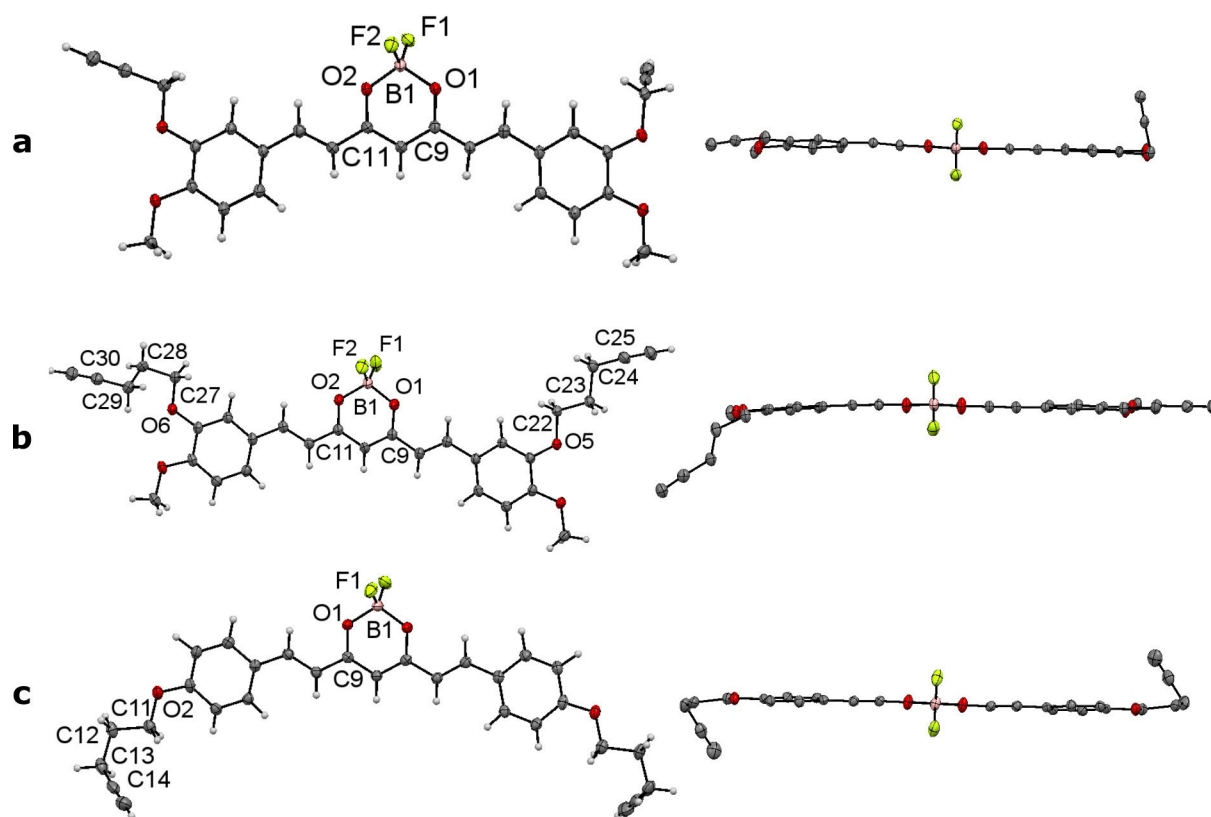
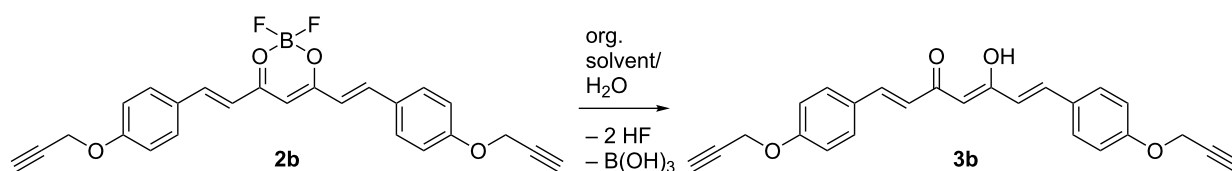


**Figure 1:** ORTEP drawings in side view (left) and top view (right) of complexes **2f** (a), **2g** (b) and **2h** (c). Hydrogen atoms are omitted from top view for clarity.



**Scheme 2:**  $\text{BF}_2$  group hydrolysis of complex **2b**.

From the solvents screened, methanol and THF containing water show the best results (Table 2). Comparison with data reported in the literature [31] as well as the absence of a  $^{19}\text{F}\{^1\text{H}\}$  NMR signal proved the success of the reaction. As expected, in the control reaction in dry THF no cleavage reaction was observed.

Interestingly, upon upscaling from 0.4 mmol to 4 mmol **2b** the yield of **3b** decreased to approx. 40%. Alterations of reaction time and temperature resulted in no significant changes.

Rao and co-worker report, that for the  $\text{BF}_2$  complex or unsubstituted curcumin a tautomeric form exists in solution, which acts as a weak acid [13]. Only the  $\text{BF}_2$  group of the deprotonated

**Table 2:** Optimization of reaction conditions for  $\text{BF}_2$  group cleavage.

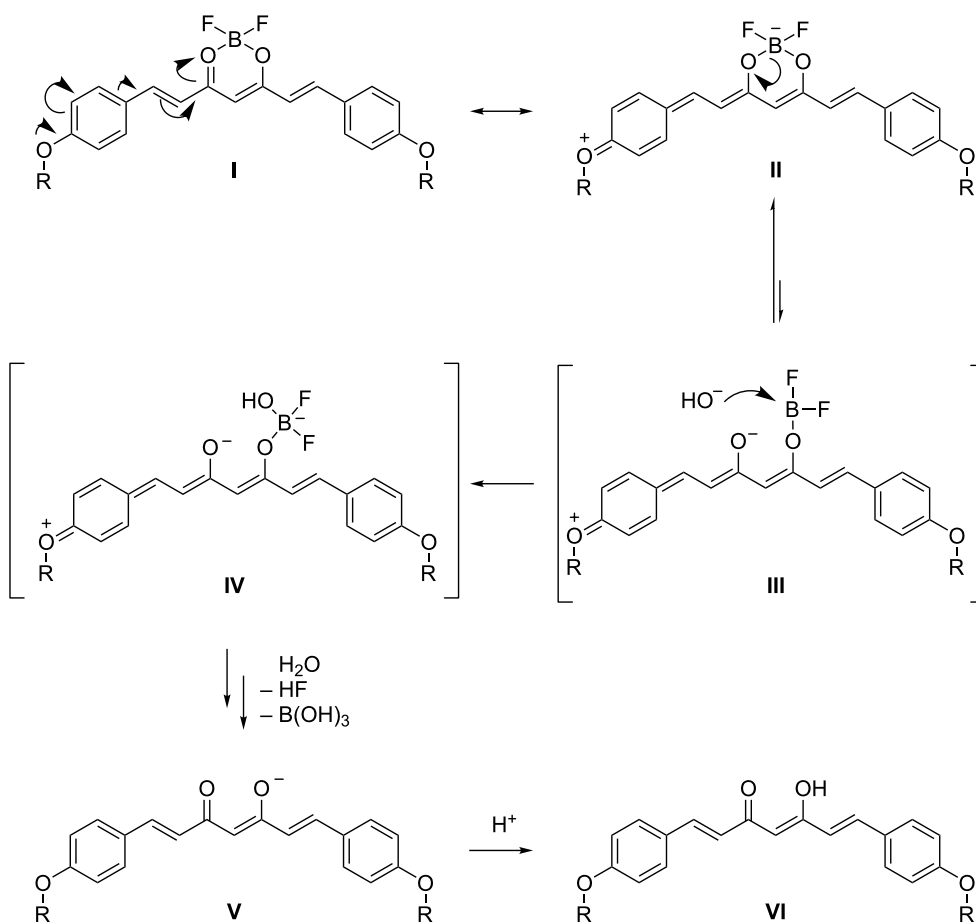
Solvent	Additive	Time (h)	Yield (%)
THF <sup>a</sup>	none	18	75 <sup>b</sup>
MeOH <sup>a</sup>	none	18	80 <sup>b</sup>
EtOH <sup>a</sup>	none	18	65 <sup>b</sup>
DMF <sup>a</sup>	none	6	30 <sup>b</sup>
dry THF	none	18	0
THF <sup>a</sup>	NaOH <sup>c</sup>	6	80 <sup>d</sup>
MeOH <sup>a</sup>	NaOH <sup>c</sup>	3.5	98 <sup>d</sup>

<sup>a</sup>Containing 20%  $\text{H}_2\text{O}$ ; <sup>b</sup>Yield after purification by column chromatography; <sup>c</sup>5 wt % in water; <sup>d</sup>Yield after recrystallization from acetone/water.

acid is able to become hydrolysed. In our case, although no free OH groups are present, we have also observed a similar pH value dependence as reported by Rao [13]. For this reason, we suggest that the possibility to form a quinoid structure is responsible for the increased stability of the  $\text{BF}_2$  complex in acidic solution (Scheme 3). At higher temperatures, there is an equilibrium between the quinoid form of the  $\text{BF}_2$  complex with a formal negative charge on the boron atom (II, “borate”) and a structure with one cleaved boron oxygen bond having the formal negative charge localized on the oxygen atom (III, best described as a difluoroboric acid ester). The ester is prone to a nucleophilic attack of a hydroxide ion, while the borate is not. After the nucleophilic attack a hydroxy difluoroborate (IV) is formed, which undergoes fast hydrolysis to boric acid, hydroxide fluoride and the corresponding curcuminoid in the anionic form (V). The latter finally becomes protonated by one equivalent of HF (VI). If no additional base is present, the hydroxide concentration decreases with ongoing hydrolysis so far, that the reaction effectively stops.

To confirm our suggestion we carried out the hydrolysis reactions of 4 mmol **2b** in 80% aq methanol or THF again with the addition of 10 mol % of NaOH. The final yields could be increased to 98 and 80%, respectively. Additionally, we could observe a much shorter reaction time. This proves the necessity for a base to be present to complete the reaction.

We were able to apply this procedure to  $\text{BF}_2$  complexes **2a–c** and **2e** to receive the curcuminoids **3** in good to excellent yields. **2d** and **2f–h** were found to possess a relatively low solubility in methanol and especially **2d** to be more sensitive to nucleophilic bases when heated in solution. To increase the solubility, most of the water added was replaced by DMSO (Table 3). This improved the solubility and did not induce any additional impurities. We also changed the base from NaOH to triethylamine for these compounds to avoid partial decomposition. The disadvantage of triethylamine was a longer reaction time of seven to eighteen hours, probably due to the lower hydroxide concentration.



**Scheme 3:** Suggested mechanism of  $\text{BF}_2$  complex hydrolysis.

**Table 3:** Hydrolysis reactions.

Entry	R <sup>1</sup>	R <sup>2</sup>	R <sup>3</sup>	Solvent (MeOH/DMSO/H <sub>2</sub> O)	Base	Yield (%) <sup>a</sup>
<b>3a</b>	H	O-propargyl	OMe	8:0:2	NaOH <sup>b</sup>	87
<b>3b</b>	H	O-propargyl	H	8:0:2	NaOH	92
<b>3c</b>	Br	O-propargyl	OMe	8:0:2	NaOH	92
<b>3d</b>	Br	O-propargyl	H	8:1.5:0.5	TEA	n/a
<b>3e</b>	H	O-propargyl	O-propargyl	8:0:2	NaOH	84
<b>3f</b>	H	OMe	O-propargyl	8:1.5:0.5	TEA	90
<b>3g</b>	H	OMe	O-pent-4-yn-1-yl	8:1.5:0.5	TEA	80
<b>3h</b>	H	O-pent-4-yn-1-yl	H	8:1.5:0.5	TEA	95

<sup>a</sup>Yield after recrystallization; <sup>b</sup>5 wt % solution in water.

Regarding the <sup>1</sup>H NMR spectra, we found that all crude products contain small amounts of decomposition products resulting from base induced cleavage of the backbone. Recrystallization from acetone or ethanol and water mixtures gave the pure products **3a–c** and **3e–h** as yellow or orange solids in good to excellent yields. They were characterized by <sup>1</sup>H and <sup>13</sup>C{<sup>1</sup>H} NMR spectroscopy, mass spectrometry, UV-visible spectroscopy and elemental analysis. For **3d** we found two sets of NMR signals in both <sup>1</sup>H and <sup>13</sup>C{<sup>1</sup>H} NMR spectra with relative intensities of 1:0.25, which could be assigned to be no starting material. These did not change upon alteration of NMR solvent or temperature. Also, no [M]<sup>+</sup> signals or any expected fragments for **3d** were found in EI or ESIMS spectra.

### Optical spectroscopy

To investigate their properties as fluorescent dyes we measured the UV–vis absorption and fluorescence spectra of the BF<sub>2</sub> complexes **2a–h**. Measurements were carried out in dichloromethane at room temperature and under ambient atmosphere. The results are shown in Figure 2.

All BF<sub>2</sub> complexes show strong absorption bands with absorption maxima between 475 and 503 nm resulting from π–π\* transitions [9]. Extinction coefficients range from roughly 9500 to over 50000 M<sup>−1</sup> cm<sup>−1</sup> (Table 4). All absorption curves show secondary maxima or shoulders at slightly shorter wavelengths.

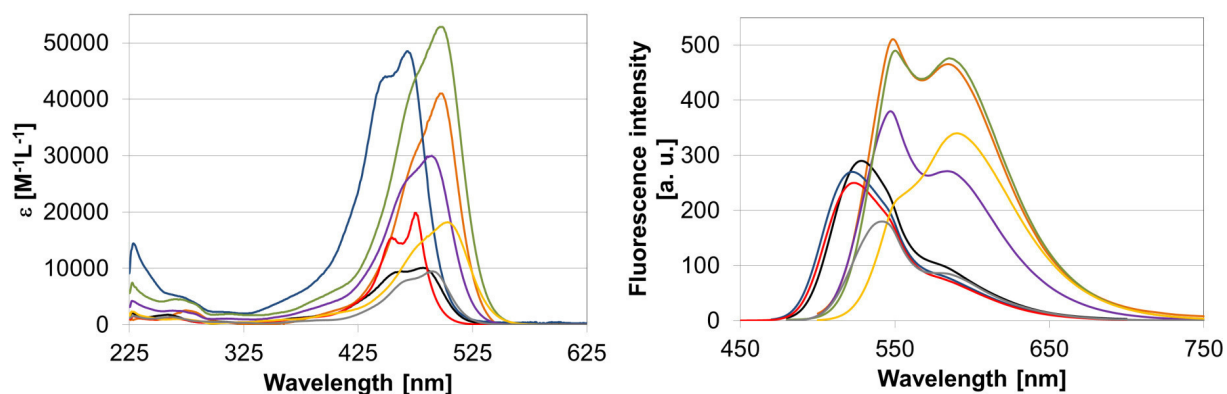


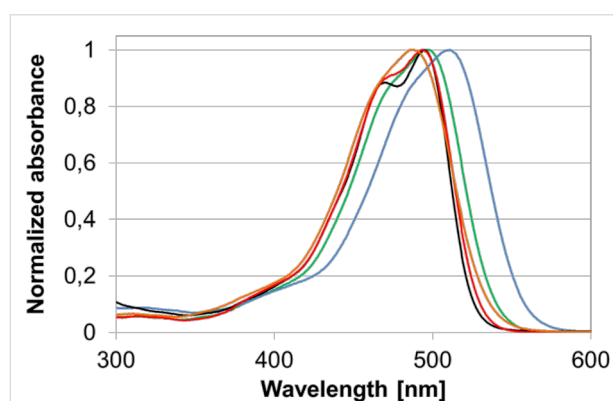
**Figure 2:** Absorbance (left) and emission (right) spectra of compounds **2a** (orange), **2b** (black), **2c** (blue), **2d** (red), **2e** (purple), **2f** (green), **2g** (yellow) and **2h** (grey) in CH<sub>2</sub>Cl<sub>2</sub>.

**Table 4:** Absorption and emission spectral properties of BF<sub>2</sub> complexes **2a–h** in CH<sub>2</sub>Cl<sub>2</sub>. See Supporting Information File 1 for details on the measurement setup.

Compound	$\lambda_{\max}^{\text{abs}}$ (nm)	$\epsilon \cdot 10^{-3}$ (M <sup>-1</sup> cm <sup>-1</sup> )	$\lambda_{\max}^{\text{em}}$ (nm)	$\Phi^a$	$\tau^b$ (ns)	Stokes-shift (cm <sup>-1</sup> )
<b>2a</b>	497	41.0	548	0.51	1.68	1873
<b>2b</b>	480	10.1	528	0.29	1.21	1894
<b>2c</b>	476	48.5	522	0.27	1.01	1851
<b>2d</b>	475	19.8	524	0.25	1.01	1969
<b>2e</b>	487	30.0	547	0.38	1.56	2252
<b>2f</b>	497	52.8	550	0.49	1.55	1939
<b>2g</b>	503	18.2	590	0.34	1.57	2932
<b>2h</b>	489	9.5	542	0.18	1.50	2000

<sup>a</sup>Fluorescence quantum yield was determined against rhodamine 6G ( $\Phi = 0.95$ ) in ethanol. <sup>b</sup>Fluorescence lifetime upon 400 nm excitation.

As solvatochromism is a known property for curcumin and its derivatives [32,33], we investigated the solvatochromism of **2b** as an example compound in five different solvents (Figure 3). Solvents were chosen by their  $E_T(30)$  values of polarity as determined by Reichardt [34]. With rising solvent polarity, the vibrational structure of the absorption band is being lost. In toluene, THF and dichloromethane the compound shows only weak solvatochromism. Interestingly, a positive solvatochromism relative to the more nonpolar solvents is appearing in DMSO, while the absorption band is slightly being shifted hypsochromically in methanol.

**Figure 3:** Absorbance spectra of **2b** in methanol (orange), tetrahydrofuran (red), toluene (black), dichloromethane (green) and dimethyl sulfoxide (blue).

In solution, upon excitation at 365 nm, green, yellow or orange fluorescence can be observed (Figure 4).

All fluorescence spectra are characterized by two maxima, one in the range of 520–550 nm and one in the range of 580–590 nm. However, there are distinct differences in the intensity ratios of these two maxima between the compounds. For **2b–d**, the lower energy maximum appears as a shoulder, for **2a** and **2e–h**, it appears as a local maximum, and for **2g** it repre-

**Figure 4:** Compounds **2a–h** in dichloromethane solution in daylight (top) and under 365 nm irradiation (bottom).

sents the global maximum of emission. This trend can be rationalized by taking the electronic structure of the compounds into account. With increasing electron density of the aromatic system, the emission intensity in the low-energy regime of the spectrum increases. It is also noteworthy, that regarding **2a** and **2f**, which are regioisomers, the second fluorescence band is more intense for **2f** than for **2a**. For the complexes containing a brominated phenyl ring, the presence of an additional electron-donating methoxy group has almost no impact on the fluorescence properties.

## Conclusion

We have synthesized a series of novel curcuminoid–BF<sub>2</sub> complexes by an improved synthetic route. All complexes were received in high yields and purities and characterized by <sup>1</sup>H, <sup>11</sup>B, <sup>13</sup>C and <sup>19</sup>F NMR spectroscopy, mass spectrometry and elemental analysis. We found the complexes to possess high absorption in the range of 475 to 500 nm and strong fluorescence between 520 and 590 nm, resulting in Stokes shifts of up to 3000 cm<sup>-1</sup>. Finally, an effective strategy to hydrolyse the

BF<sub>2</sub> group and release the curcuminoids could be established using aqueous methanol and mild basic conditions. In some cases, when the solubility of the substrates was low, DMSO was used as an additional solvent. These compounds can act as building blocks for the attachment of biomolecules via “click” chemistry.

## Supporting Information

### Supporting Information File 1

Experimental data, X-ray crystallographic details, selected bond lengths and angles, copies of NMR spectra.

[<http://www.beilstein-journals.org/bjoc/content/supplementary/1860-5397-13-223-S1.pdf>]

### Supporting Information File 2

CIF files for complexes **2f**, **2g** and **2h**. These data (CCDC-1526555 for **2f**, CCDC-1526556 for **2g**, and CCDC-1526557 for **2h**) can be obtained free of charge from The Cambridge Crystallographic Data Centre via [http://www.ccdc.cam.ac.uk/data\\_request/cif](http://www.ccdc.cam.ac.uk/data_request/cif).

[<http://www.beilstein-journals.org/bjoc/content/supplementary/1860-5397-13-223-S2.cif>]

## References

- Esatbeyoglu, T.; Huebbe, P.; Ernst, I. M. A.; Chin, D.; Wagner, A. E.; Rimbach, G. *Angew. Chem., Int. Ed.* **2012**, *51*, 5308–5332. doi:10.1002/anie.201107724
- Tønnesen, H. H.; Greenhill, J. V. *Int. J. Pharm.* **1992**, *87*, 79–87. doi:10.1016/0378-5173(92)90230-Y
- Anto, R.; Kuttan, G.; Babu, K. V. D.; Rajasekharan, K. N.; Kuttan, R. *Int. J. Pharm.* **1996**, *131*, 1–7. doi:10.1016/0378-5173(95)04254-7
- Kuttan, R.; Bhanumathy, P.; Nirmala, K.; George, M. C. *Cancer Lett.* **1985**, *29*, 197–202. doi:10.1016/0304-3835(85)90159-4
- Ghosh, S.; Hayden, M. S. *Nat. Rev. Immunol.* **2008**, *8*, 837–848. doi:10.1038/nri2423
- Artico, M.; Di Santo, R.; Costi, R.; Novellino, E.; Greco, G.; Massa, S.; Tramontano, E.; Marongiu, M. E.; De Montis, A.; La Colla, P. *J. Med. Chem.* **1998**, *41*, 3948–3960. doi:10.1021/jm9707232
- Ammon, H. P. T.; Wahl, M. A. *Planta Med.* **1991**, *57*, 1–7. doi:10.1055/s-2006-960004
- Pabon, H. J. *J. Recl. Trav. Chim. Pays-Bas* **1964**, *83*, 379–386. doi:10.1002/recl.19640830407
- Bai, G.; Yu, C.; Cheng, C.; Hao, E.; Wei, Y.; Mu, X.; Jiao, L. *Org. Biomol. Chem.* **2014**, *12*, 1618–1626. doi:10.1039/c3ob42201a
- Pedersen, U.; Rasmussen, P. B.; Lawesson, S.-O. *Liebigs Ann. Chem.* **1985**, 1557–1569. doi:10.1002/jlac.198519850805
- Nurfin, A. N.; Reksohadiprodjo, M. S.; Timmerman, H.; Jenie, U. A.; Sugiyanto, D.; van der Goot, H. *Eur. J. Med. Chem.* **1997**, *32*, 321–328. doi:10.1016/S0223-5234(97)89084-8
- Khan, M. A.; El-Khatib, R.; Rainsford, K. D.; Whitehouse, M. W. *Bioorg. Chem.* **2012**, *40*, 30–38. doi:10.1016/j.bioorg.2011.11.004
- Rao, E. V.; Sudheer, P. *Indian J. Pharm. Sci.* **2011**, *73*, 262–270.
- Liu, K.; Chen, J.; Chojnacki, J.; Zhang, S. *Tetrahedron Lett.* **2013**, *54*, 2070–2073. doi:10.1016/j.tetlet.2013.02.015
- Ono, K.; Yoshikawa, K.; Tsuji, Y.; Yamaguchi, H.; Uozumi, R.; Tomura, M.; Taga, K.; Saito, K. *Tetrahedron* **2007**, *63*, 9354–9358. doi:10.1016/j.tet.2007.07.004
- Hu, J.; He, Z.; Wang, Z.; Li, X.; You, J.; Gao, G. *Tetrahedron Lett.* **2013**, *54*, 4167–4170. doi:10.1016/j.tetlet.2013.05.099
- Mügge, C.; Marzo, T.; Massai, L.; Hildebrandt, J.; Ferraro, G.; Rivera-Fuentes, P.; Metzler-Nolte, N.; Merlino, A.; Messori, L.; Weigand, W. *Inorg. Chem.* **2015**, *54*, 8560–8570. doi:10.1021/acs.inorgchem.5b01238
- Mügge, C.; Liu, R.; Görls, H.; Gabbiani, C.; Michelucci, E.; Rüdiger, N.; Clement, J. H.; Messori, L.; Weigand, W. *Dalton Trans.* **2014**, *43*, 3072–3086. doi:10.1039/c3dt52284a
- Mügge, C.; Micheucci, E.; Boscaro, F.; Gabbiani, C.; Messori, L.; Weigand, W. *Metallomics* **2011**, *3*, 987–990. doi:10.1039/c1mt00069a
- Mügge, C.; Rothenburger, C.; Beyer, A.; Görls, H.; Gabbiani, C.; Casini, A.; Michelucci, E.; Landini, I.; Nobili, S.; Mini, E.; Messori, L.; Weigand, W. *Dalton Trans.* **2011**, *40*, 2006–2016. doi:10.1039/c0dt00845a
- Hildebrandt, J.; Häfner, N.; Görls, H.; Kritsch, D.; Ferraro, G.; Dürst, M.; Runnebaum, I. B.; Merlino, A.; Weigand, W. *Dalton Trans.* **2016**, *45*, 18876–18891. doi:10.1039/c6dt01388k
- Hildebrandt, J.; Görls, H.; Häfner, N.; Ferraro, G.; Dürst, M.; Runnebaum, I. B.; Weigand, W.; Merlino, A. *Dalton Trans.* **2016**, *45*, 12283–12287. doi:10.1039/c6dt02380k
- Pröhl, M.; Bus, T.; Czaplewski, J. A.; Traeger, A.; Deicke, M.; Weiss, H.; Weigand, W.; Schubert, U. S.; Gottschaldt, M. *Eur. J. Inorg. Chem.* **2016**, 5197–5204. doi:10.1002/jeic.201600801
- Kieburg, C.; Sadalapure, K.; Lindhorst, T. K. *Eur. J. Org. Chem.* **2000**, 2035–2040. doi:10.1002/1099-0690(200006)2000:11<2035::AID-EJOC2035>3.0.CO;2-V
- Maryanoff, B. E.; McComsey, D. F.; Costanzo, M. J.; Hochman, C.; Smith-Swintosky, V.; Shank, R. P. *J. Med. Chem.* **2005**, *48*, 1941–1947. doi:10.1021/jm040124c
- Rostovtsev, V. V.; Green, L. G.; Fokin, V. V.; Sharpless, K. B. *Angew. Chem., Int. Ed.* **2002**, *41*, 2596–2599. doi:10.1002/1521-3773(20020715)41:14<2596::AID-ANIE2596>3.0.CO;2-4
- Pal, M.; Parasuraman, K.; Yeleswarapu, K. R. *Org. Lett.* **2003**, *5*, 349–352. doi:10.1021/ol027382t
- Kant, R.; Kumar, D.; Agarwal, D.; Gupta, R. D.; Tilak, R.; Awasthi, S. K.; Agarwal, A. *Eur. J. Med. Chem.* **2016**, *113*, 34–49. doi:10.1016/j.ejmech.2016.02.041
- Zammit, S. C.; Cox, A. J.; Gow, R. M.; Zhang, Y.; Gilbert, R. E.; Krum, H.; Kelly, D. J.; Williams, S. J. *Bioorg. Med. Chem. Lett.* **2009**, *19*, 7003–7006. doi:10.1016/j.bmcl.2009.09.120
- Goto, H.; Nimori, S.; Akagi, K. *Synth. Met.* **2005**, *155*, 576–587. doi:10.1016/j.synthmet.2005.09.044
- Gomes, D. de C. F.; Alegrio, L. V.; Edilson Freire de Lim, M.; Leon, L. L.; Araújo, C. A. C. *Arzneim. Forsch.* **2002**, *52*, 120–124. doi:10.1055/s-0031-1299867
- Khopde, S. M.; Priyadarsini, K. I.; Palit, D. K.; Mukherjee, T. *Photochem. Photobiol.* **2000**, *72*, 625–631. doi:10.1562/0031-8655(2000)0720625EOSOTE2.0.CO2
- Barik, A.; Priyadarsini, K. I. *Spectrochim. Acta, Part A* **2013**, *105*, 267–272. doi:10.1016/j.saa.2012.12.036
- Reichardt, C. *Chem. Rev.* **1994**, *94*, 2319–2358. doi:10.1021/cr00032a005

## License and Terms

This is an Open Access article under the terms of the Creative Commons Attribution License (<http://creativecommons.org/licenses/by/4.0>), which permits unrestricted use, distribution, and reproduction in any medium, provided the original work is properly cited.

The license is subject to the *Beilstein Journal of Organic Chemistry* terms and conditions: (<http://www.beilstein-journals.org/bjoc>)

The definitive version of this article is the electronic one which can be found at:  
[doi:10.3762/bjoc.13.223](https://doi.org/10.3762/bjoc.13.223)

**Supporting Information**

**for**

**Curcuminoid–BF<sub>2</sub> complexes: Synthesis,  
fluorescence and optimization of BF<sub>2</sub> group cleavage**

Henning Weiss<sup>1</sup>, Jeannine Reichel<sup>1</sup>, Helmar Görls<sup>1</sup>, Kilian Rolf Anton Schneider<sup>2</sup>, Mathias Micheel<sup>3</sup>, Michael Pröhl<sup>4</sup>, Michael Gottschaldt<sup>4</sup>, Benjamin Dietzek<sup>2,3</sup> and Wolfgang Weigand<sup>1,4\*</sup>

<sup>4\*</sup>

Address: <sup>1</sup>Institute for Inorganic and Analytical Chemistry, Friedrich-Schiller-Universität Jena, Humboldtstrasse 8, 07743 Jena, Germany, <sup>2</sup>Institute for Physical Chemistry, Friedrich-Schiller-Universität Jena, Helmholtzweg 4, 07743 Jena, Germany, <sup>3</sup>Leibniz Institute of Photonic Technology (IPHT), Albert-Einstein-Straße 9, 07745 Jena, Germany and <sup>4</sup>Jena Center of Soft Matter, Friedrich-Schiller-Universität Jena, Philosophenweg 7, 07743 Jena, Germany

Email: Wolfgang Weigand - [wolfgang.weigand@uni-jena.de](mailto:wolfgang.weigand@uni-jena.de)

\*Corresponding author

**Experimental data, X-ray crystallographic details, selected bond lengths and angles,  
copies of NMR spectra**

## Table of contents

1. General remarks	S3
2. Synthesis of aldehydes <b>1</b> and characterization data	S4
3. Synthesis of BF <sub>2</sub> complexes <b>2</b> and characterization data	S6
4. Synthesis of curcuminoids <b>3</b> and characterization data	S11
5. X-ray crystallographic data for <b>2f</b> , <b>2g</b> and <b>2h</b>	S16
6. References	S18
7. Intermolecular interactions in <b>2f</b>	S19
8. Copies of NMR spectra for <b>2</b> and <b>3</b>	S20



## 1: General remarks:

All, except hydrolysis reactions, were carried out under nitrogen atmosphere using standard Schlenk techniques. DMF and acetonitrile were dried over calcium hydride, toluene over sodium and benzophenone, while THF was stored over KOH. All solvents were distilled prior to use. Starting materials were commercially sourced and used without further purification. 3-Bromo-4-hydroxy-5-methoxybenzaldehyde and 3-bromo-4-hydroxybenzaldehyde were received following a literature procedure [1]. NMR spectra were recorded on Bruker Avance 200, 400 or 600 spectrometers in regular borosilicate glass tubes. Chemical shifts are reported in ppm relative to external TMS for  $^1\text{H}$  and  $^{13}\text{C}\{^1\text{H}\}$ ,  $\text{FCCl}_3$  for  $^{19}\text{F}\{^1\text{H}\}$  and  $\text{BF}_3\cdot\text{OEt}_2$  for  $^{11}\text{B}\{^1\text{H}\}$  NMR, respectively. Coupling constants are reported in Hz. EI and ESI–TOF–MS were recorded on SSQ 710 and MAT95XL (Finnigan MAT) devices in positive mode. UV–vis spectra were measured on a Specord D 600 spectrometer by Analytik Jena. Fluorescence spectra were recorded on a Jasco FP-6300 fluorescence spectrometer. Relative fluorescence quantum yields were measured by comparing the areas under the fluorescence emission spectrum of dilute ( $0.02 < A < 0.06$ ) solutions of **2a–h** in dichloromethane. Rhodamine 6G in ethanol ( $\phi = 0.95$ ) was used as the standard. Final values were determined by using equations reported in the literature [2]. Spectrally resolved emission decay curves were determined employing a Hamamatsu HPDTA streak camera. Samples were excited by pulses centred at 400 nm created by frequency doubling the output of a Ti:sapphire laser (Tsunami, Newport Spectra-Physics GmbH). The repetition rate of the fundamental is reduced to 400 kHz by a pulse selector (model 3980, Newport Spectra-Physics GmbH). Emission was collected for solutions from a 1 cm cuvette in a  $90^\circ$  angle and spectrally dispersed on the detector using a CHROMEX spectrograph.

Measurements were performed with a polarizer set to magic angle, i.e., set to 54.7° with respect to the excitation polarization, in the detection path. Spectrally and time-resolved emission data was spectrally integrated and analysed using DecayFit software [1]. All decay curves could adequately fitted by a monoexponential decay model.

## 2. Synthesis of aldehydes 1 and characterization data:

Aldehydes **1** were synthesized following two general procedures. Analytical results are in good accordance to data published elsewhere [3–7].

**General procedure (1a–f):** The respective hydroxybenzaldehyde (6 mmol) was dissolved in DMF and K<sub>2</sub>CO<sub>3</sub> (3.3 g, 24 mmol) and propargyl bromide (0.63 mL, 6.6 mmol; 80 wt % in toluene) were added. The resulting suspension was stirred at room temperature overnight and poured into ice water. The precipitated solid was collected by filtration, washed with water and dried in air to receive the respective ethers as off-white solids.

**General procedure (1g–h):** The respective hydroxybenzaldehyde (6 mmol) was dissolved in acetonitrile (30 mL) and Cs<sub>2</sub>CO<sub>3</sub> (2.9 g, 9 mmol), KI (1 g, 6 mmol) and 5-chloropent-1-yne (0.7 mL, 6.6 mmol) were added. The mixture was stirred under reflux overnight and cooled to room temperature. Ethyl acetate and water (15 mL each) were added and the organic phase was extracted with water (3 × 15 mL) and brine, dried (Na<sub>2</sub>SO<sub>4</sub>) and evaporated under reduced pressure to yield the respective ethers as pale yellow solids.

**3-Methoxy-4-propargyloxybenzaldehyde (1a)** from 3-methoxy-4-hydroxybenzaldehyde: Yield 95%. <sup>1</sup>H-NMR (400 MHz, CDCl<sub>3</sub>): δ 9.85 (s, 1H); 7.45 (dd, 1H, *J*

= 8.2, 1.8 Hz); 7.41 (d, 1H  $J$  = 1.8 Hz); 7.13 (d, 1H,  $J$  = 8.2 Hz); 4.84 (d, 2H,  $J$  = 2.4 Hz); 3.92 (s, 3H); 2.56 (t, 1H,  $J$  = 2.4 Hz).

**4-Propargyloxybenzaldehyde (1b)** from 4-hydroxybenzaldehyde: Yield 99%.  $^1\text{H}$ -NMR (400 MHz,  $\text{CDCl}_3$ ):  $\delta$  9.88 (s, 1H); 7.84 (d, 2H,  $J$  = 8.8 Hz); 7.07 (d, 2H,  $J$  = 8.7 Hz); 4.76 (d, 2H,  $J$  = 2.3 Hz); 2.57 (t, 1H,  $J$  = 2.4 Hz).  $^{13}\text{C}\{^1\text{H}\}$ -NMR (101 MHz,  $\text{CDCl}_3$ ):  $\delta$  190.9; 162.5; 132.0; 130.7; 115.3; 77.6; 76.5; 56.0.

**3-Bromo-4-propargyloxy-5-methoxybenzaldehyde (1c)** from 3-bromo-4-hydroxy-5-methoxybenzaldehyde: Yield 94%.  $^1\text{H}$ -NMR (600 MHz,  $\text{CDCl}_3$ ):  $\delta$  9.84 (s, 1H); 7.65 (d, 1H  $J$  = 1.8 Hz); 7.38 (d, 1H,  $J$  = 1.7 Hz); 4.87 (d, 2H  $J$  = 2.4 Hz); 3.93 (s, 3H); 2.49 (t, 1H,  $J$  = 2.4 Hz).  $^{13}\text{C}\{^1\text{H}\}$ -NMR (151 MHz,  $\text{CDCl}_3$ ):  $\delta$  190.0; 154.3; 149.3; 133.6; 128.8; 118.8; 110.1; 78.2; 76.3; 60.3; 56.4.

**3-Bromo-4-propargyloxybenzaldehyde (1d)** from 3-bromo-4-hydroxybenzaldehyde: Yield 92%.  $^1\text{H}$ -NMR (400 MHz,  $\text{CDCl}_3$ ):  $\delta$  9.85 (s, 1H); 8.09 (d, 1H,  $J$  = 2.0 Hz, 1H); 7.82 (dd, 1H,  $J$  = 8.5, 2.0 Hz); 7.17 (d, 1H,  $J$  = 8.5 Hz); 4.87 (d, 2H,  $J$  = 2.4 Hz); 2.60 (t, 1H,  $J$  = 2.4 Hz).  $^{13}\text{C}\{^1\text{H}\}$ -NMR (101 MHz,  $\text{CDCl}_3$ ):  $\delta$  189.7; 158.7; 134.9; 131.4; 130.9; 113.3; 113.2; 77.3; 77.0; 57.0.

**3,4-Bis-(propargyloxy)benzaldehyde (1e)** from 3,4-dihydroxybenzaldehyde and 2.4 eq. of propargyl bromide: Yield 83%. The product was purified by column chromatography (silica gel, ethyl acetate / hexanes 1:2).  $^1\text{H}$ -NMR (400 MHz,  $\text{CDCl}_3$ ):  $\delta$  9.88 (s, 1H); 7.58 (d, 1H,  $J$  = 1.8 Hz); 7.53 (dd, 1H,  $J$  = 8.2, 1.8 Hz); 7.18 (d, 1H,  $J$  = 8.3 Hz); 4.86 (d, 2H,  $J$  = 2.4 Hz); 4.83 (d, 2H,  $J$  = 2.4 Hz); 2.57 (t, 1H,  $J$  = 2.4 Hz); 2.55 (t, 1H,  $J$  = 2.4 Hz).

**3-Propargyloxy-4-methoxybenzaldehyde (1f)** from isovanillin: Yield 95%.  $^1\text{H}$ -NMR (600 MHz,  $\text{CDCl}_3$ ):  $\delta$  9.78 (s, 1H); 7.46 (d, 1H  $J$  = 1.6 Hz); 7.44 (dd, 1H,  $J$  = 8.2,

1.7 Hz); 6.94 (d, 1H,  $J = 8.2$  Hz); 4.75 (d, 2H,  $J = 2.4$  Hz, 2H); 3.88 (s, 3H); 2.52 (t, 1H,  $J = 2.4$  Hz).  $^{13}\text{C}\{^1\text{H}\}$ -NMR (151 MHz,  $\text{CDCl}_3$ ):  $\delta$  190.6; 154.9; 147.2; 129.8; 127.2; 112.0; 110.9; 77.8; 76.5; 56.6; 56.1.

**3-(Ppent-4-yn-1-yloxy)-4-methoxybenzaldehyde (1g)** from isovanillin: Yield 94%.

$^1\text{H}$ -NMR (400 MHz,  $\text{CDCl}_3$ ):  $\delta$  9.84 (s, 1H); 7.45 (dd, 1H,  $J = 8.2, 1.8$  Hz); 7.42 (d, 1H,  $J = 1.8$  Hz); 6.97 (d, 1H,  $J = 8.1$  Hz); 4.18 (t, 2H,  $J = 6.3$  Hz); 3.94 (s, 3H); 2.43 (td, 2H,  $J = 6.9, 2.7$  Hz); 2.12 – 2.03 (m, 2H); 1.98 (t, 1H,  $J = 2.6$  Hz).

**4-(Pent-4-yn-1-yloxy)-benzaldehyde (1h)** from 4-hydroxybenzaldehyde: Yield 93%.

$^1\text{H}$ -NMR (400 MHz,  $\text{DMSO}-d_6$ ):  $\delta$  9.86 (s, 1H); 7.85 (d, 1H,  $J = 8.7$  Hz); 7.11 (d, 1H,  $J = 8.7$  Hz); 4.14 (t, 2H,  $J = 6.2$  Hz); 2.80 (t, 1H,  $J = 2.8$  Hz); 2.34 (td, 2H,  $J = 7.1, 2.8$  Hz); 1.97 – 1.88 (m, 2H).  $^{13}\text{C}\{^1\text{H}\}$ -NMR (101 MHz,  $\text{DMSO}-d_6$ ):  $\delta$  191.3; 163.5; 131.9; 129.7; 114.9; 83.5; 71.7; 66.6; 27.5; 14.5.

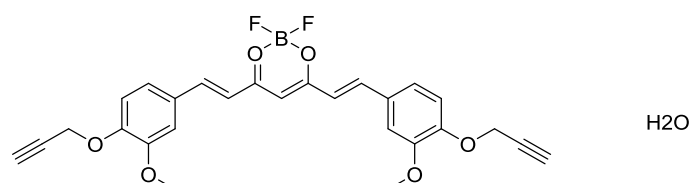
### 3. Synthesis of $\text{BF}_2$ complexes 2 and characterization data:

**General procedure** (modified from lit. [8]):

2,4-Pentanedione (0.3 mL, 3 mmol) and  $\text{BF}_3 \cdot \text{OEt}_2$  (0.55 mL, 4.4 mmol) were dissolved in toluene (5 mL) and stirred at 65 °C for 2 h. Then, the respective aldehyde (6 mmol) dissolved in the minimum amount of toluene was transferred into the solution, followed by tri-*n*-butyl borate (1.85 mL, 7.4 mmol). Stirring was continued for 30 min and *n*-butylamine (approx. 0.6 equiv) was added dropwise until a color change was observed and a solid began to precipitate. The resulting suspension was kept stirring at 65 °C overnight. After cooling to room temperature the crude product was separated by filtration and washed with small amounts of cold

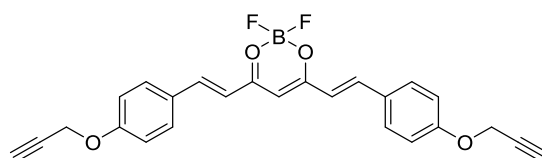
toluene and water. The isolated solid was dissolved in acetone at room temperature and water was added slowly. The resulting suspension was filtered and the isolated solid washed with water and dried in air to receive the pure product.

**2a · H<sub>2</sub>O:**



Yield 90%, purple solid. m. p.: 221.5 – 222.5 °C. <sup>1</sup>H-NMR (400 MHz, DMSO-d<sub>6</sub>): δ 7.97 (d, 2H, *J* = 15.6 Hz), 7.56 (d, 2H, *J* = 1.5 Hz), 7.52 (d, 2H, *J* = 8.4 Hz, 2,1 Hz), 7.13 (d, 2H, *J* = 8.5 Hz), 7.07 (d, 2H, *J* = 15.7 Hz), 6.55 (s, 1H), 4.88 (d, 4H, *J* = 2.2 Hz), 3.86 (s, 6H), 3.60 (t, 2H, *J* = 2.2 Hz). <sup>13</sup>C{<sup>1</sup>H}-NMR (101 MHz, DMSO-d<sub>6</sub>): δ 179.11, 152.88, 146.71, 146.65, 126.85, 125.82, 119.02, 113.53, 112.26, 101.26, 78.93, 78.56, 56.09, 55.85. <sup>11</sup>B{<sup>1</sup>H}-NMR (128 MHz, DMSO-d<sub>6</sub>): δ 0.9 (s). <sup>19</sup>F{<sup>1</sup>H}-NMR (188 MHz, DMSO-d<sub>6</sub>): δ -138.4 (s). EI-MS: *m/z* (%) = 492 (15); 387 (25); 215 (100). UV/Vis λ<sub>max</sub> [nm] (ε [M<sup>-1</sup>cm<sup>-1</sup>]): 497 (41013). Anal. calcd. for C<sub>27</sub>H<sub>23</sub>BF<sub>2</sub>O<sub>6</sub>·H<sub>2</sub>O: C (63.55); H (4.94). Found: C (63.27); H (4.72).

**2b:**

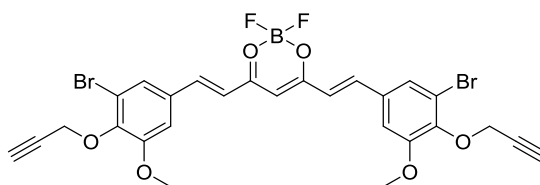


Yield 96%, red solid. m. p.: 253 – 254 °C. <sup>1</sup>H-NMR (600 MHz, DMSO-d<sub>6</sub>): δ 7.98 (d, 2H, *J* = 15.4 Hz, H-5); 7.85 (d, 4H, *J* = 8.5 Hz); 7.10 (d, 4H, *J* = 8.3 Hz); 7.07 (d, 2H, *J* = 15.4 Hz); 6.53 (s, 1H); 4.91 (s, 4H); 3.62 (s, 2H). <sup>13</sup>C{<sup>1</sup>H}-NMR (150 MHz, DMSO-d<sub>6</sub>): δ 55.8; 78.8; 101.8; 115.6; 119.2; 127.5; 131.6; 146.3; 160.4; 179.4. <sup>19</sup>F{<sup>1</sup>H}-

NMR (188 MHz, DMSO- $d_6$ ):  $\delta$  -138.1.  $^{11}\text{B}\{^1\text{H}\}$ -NMR (128 MHz, DMSO- $d_6$ ):  $\delta$  -1.26.

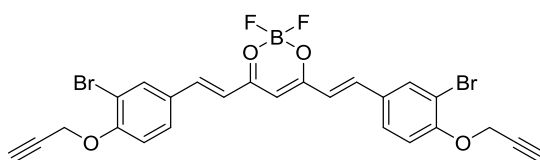
EI-MS:  $m/z$  (%) = 432 (60); 413 (20); 393 (5); 327 (35); 185 (100). UV/Vis  $\lambda_{\text{max}}$  [nm] ( $\epsilon$  [ $\text{M}^{-1}\text{cm}^{-1}$ ]): 480 (10128). Anal. calcd. for  $\text{C}_{25}\text{H}_{19}\text{BF}_2\text{O}_4$ : C (69.47); H (4.43). Found: C (69.44); H (4.56).

**2c · H<sub>2</sub>O:**



Yield 94%, orange solid. m. p.: 279.5 – 280 °C.  $^1\text{H}$ -NMR (600 MHz, DMSO- $d_6$ ):  $\delta$  7.99 (d, 2H,  $J$  = 15.7 Hz); 7.79 (d, 2H,  $J$  = 2.0 Hz); 7.61 (d, 2H,  $J$  = 2.2 Hz); 7.32 (d, 2H,  $J$  = 15.8 Hz); 6.53 (s, 1H); 4.83 (d, 4H,  $J$  = 2.6 Hz); 3.91 (s, 6H); 3.57 (t, 2H,  $J$  = 2.5 Hz).  $^{13}\text{C}\{^1\text{H}\}$ -NMR (150 MHz, DMSO- $d_6$ ):  $\delta$  179.9; 153.5; 146.0; 145.2; 131.9; 125.8; 122.2; 117.9; 113.4; 78.9; 78.7; 59.8; 56.5.  $^{19}\text{F}\{^1\text{H}\}$ -NMR (188 MHz, DMSO- $d_6$ ):  $\delta$  -137.6 (s).  $^{11}\text{B}\{^1\text{H}\}$ -NMR (193 MHz, DMSO- $d_6$ ):  $\delta$  0.90 (s). EI-MS:  $m/z$  (%) = 650 (1); 611 (5); 545 (2); 293 (2); 96 (100). UV/Vis  $\lambda_{\text{max}}$  [nm] ( $\epsilon$  [ $\text{M}^{-1}\text{cm}^{-1}$ ]): 476 (48514). Anal. calcd. for  $\text{C}_{27}\text{H}_{21}\text{BBBr}_2\text{F}_2\text{O}_6 \cdot \text{H}_2\text{O}$ : C (48.54); H (3.47). Found: C (48.49); H (3.29).

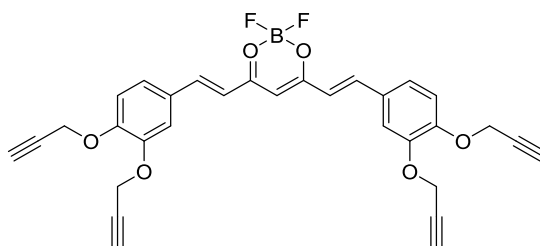
**2d:**



Yield 92%, orange solid. m. p.: 251 °C (dec.).  $^1\text{H}$ -NMR (600 MHz, DMSO- $d_6$ ):  $\delta$  8.22 (s, 2H); 7.96 (d, 2H,  $J$  = 15.7 Hz); 7.90 (d, 2H,  $J$  = 8.3 Hz); 7.29 (d, 2H,  $J$  = 8.5 Hz); 7.22 (d, 2H,  $J$  = 15.7 Hz); 6.50 (s, 1H); 5.03 (s, 4H); 3.68 (s, 2H).  $^{13}\text{C}\{^1\text{H}\}$ -NMR (150 MHz, DMSO- $d_6$ ):  $\delta$  179.9; 153.5; 146.0; 145.2; 131.9; 125.8; 122.2; 117.9; 113.4; 78.9; 78.7; 59.8; 56.5.  $^{19}\text{F}\{^1\text{H}\}$ -NMR (188 MHz, DMSO- $d_6$ ):  $\delta$  -137.6 (s).  $^{11}\text{B}\{^1\text{H}\}$ -NMR (193 MHz, DMSO- $d_6$ ):  $\delta$  0.90 (s). EI-MS:  $m/z$  (%) = 650 (1); 611 (5); 545 (2); 293 (2); 96 (100). UV/Vis  $\lambda_{\text{max}}$  [nm] ( $\epsilon$  [ $\text{M}^{-1}\text{cm}^{-1}$ ]): 476 (48514). Anal. calcd. for  $\text{C}_{27}\text{H}_{21}\text{BBBr}_2\text{F}_2\text{O}_6 \cdot \text{H}_2\text{O}$ : C (48.54); H (3.47). Found: C (48.49); H (3.29).

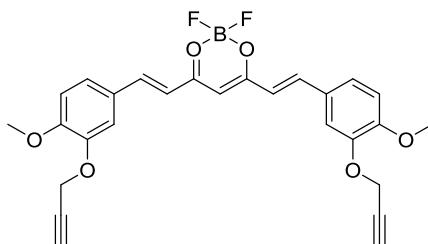
MHz, DMSO- $d_6$ ):  $\delta$  179.6; 156.2; 145.0; 133.8; 131.2; 129.0; 120.6; 114.3; 112.0; 102.4; 79.3; 78.2; 56.9.  $^{19}\text{F}\{^1\text{H}\}$ -NMR (188 MHz, DMSO- $d_6$ ):  $\delta$  = -137.8 (s).  $^{11}\text{B}\{^1\text{H}\}$ -NMR (128 MHz, DMSO- $d_6$ ):  $\delta$  = 0.88 (s). EI-MS:  $m/z$  (%) = 590 (2); 485 (2); 39 (100). UV/Vis  $\lambda_{\text{max}}$  [nm] ( $\epsilon$  [ $\text{M}^{-1}\text{cm}^{-1}$ ]): 475 (19847). Anal. calcd. for  $\text{C}_{25}\text{H}_{17}\text{BBr}_2\text{F}_2\text{O}_4$ : C (50.89); H (2.90). Found: C (50.58); H (2.83).

**2e:**



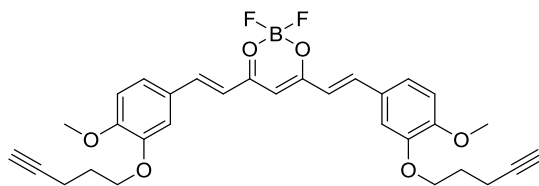
Yield 74%, purple solid. m. p.: 251.5 – 252.5 °C.  $^1\text{H}$ -NMR (400 MHz, DMSO- $d_6$ ):  $\delta$  = 7.98 (d, 2H,  $J$  = 15.6 Hz); 7.59 (d, 2H,  $J$  = 1.8 Hz); 7.52 (dd, 2H,  $J$  = 8.6 Hz,  $J$  = 1.8 Hz); 7.18 (d, 2H,  $J$  = 8.6 Hz); 7.10 (d, 2H,  $J$  = 15.7 Hz); 6.58 (s, 1H); 4.93 (d, 4H,  $J$  = 2.3 Hz); 4.90 (d, 4H,  $J$  = 2.3 Hz); 3.64 (t, 2H,  $J$  = 2.3 Hz); 3.61 (t, 2H,  $J$  = 2.3 Hz).  $^{13}\text{C}\{^1\text{H}\}$ -NMR (100 MHz, DMSO- $d_6$ ):  $\delta$  = 179.3; 150.5; 147.0; 146.6; 127.6; 125.2; 119.5; 113.9; 102.4; 78.92; 78.87; 78.7; 56.1.  $^{19}\text{F}\{^1\text{H}\}$ -NMR (188 MHz, DMSO- $d_6$ ):  $\delta$  = -138.27.  $^{11}\text{B}\{^1\text{H}\}$ -NMR (193 MHz, DMSO- $d_6$ ):  $\delta$  = -0.88. EI-MS:  $m/z$  (%) = 540 (12); 344 (48); 305 (84); 91 (55); 28 (100). UV/Vis  $\lambda_{\text{max}}$  [nm] ( $\epsilon$  [ $\text{M}^{-1}\text{cm}^{-1}$ ]): 487 (29973). Anal. calcd. for  $\text{C}_{31}\text{H}_{23}\text{BF}_2\text{O}_6$ : C (68.91); H (4.29). Found: C (68.74); H (4.37).

**2f · 0.4 H<sub>2</sub>O:**



Yield 88%, red solid. m. p.: 208.5 – 209.5 °C.  $^1\text{H}$ -NMR (400 MHz, DMSO- $d_6$ ):  $\delta$  = 7.96 (d, 2H,  $J$  = 15.6 Hz); 7.55 (s, 2H); 7.50 (d, 2H,  $J$  = 8.3 Hz); 7.11 (d, 2H,  $J$  = 8.4 Hz); 7.05 (d, 2H,  $J$  = 15.7 Hz); 6.54 (s, 1H); 4.88 (d, 4H,  $J$  = 2.6 Hz); 3.85 (s, 6H).  $^{13}\text{C}\{^1\text{H}\}$ -NMR (101 MHz, DMSO- $d_6$ ):  $\delta$  179.2, 152.9, 146.8, 146.7, 129.0, 128.3, 126.9, 125.9, 125.4, 119.1, 113.6, 112.3, 79.0, 78.6, 56.2, 55.9, 38.7.  $^{19}\text{F}\{^1\text{H}\}$ -NMR (188 MHz, DMSO- $d_6$ ):  $\delta$  = -138.3.  $^{11}\text{B}\{^1\text{H}\}$ -NMR (193 MHz, DMSO- $d_6$ ):  $\delta$  = 0.90. EI-MS:  $m/z$  (%) = 492 (60); 426 (42); 387 (44); 215 (100). UV/Vis  $\lambda_{\text{max}}$  [nm] ( $\epsilon$  [ $\text{M}^{-1}\text{cm}^{-1}$ ]): 497 (52812). Anal. calcd. for  $\text{C}_{27}\text{H}_{23}\text{BF}_2\text{O}_6 \cdot 0.4\text{H}_2\text{O}$ : C (64.93); H (4.80). Found: C (64.96); H (4.70).

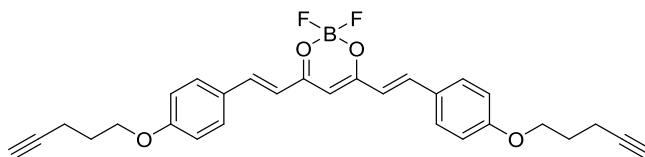
**2g · 0.25 H<sub>2</sub>O:**



Yield 56%, dark red solid. m. p.: 205 – 206 °C.  $^1\text{H}$ -NMR (400 MHz, DMSO- $d_6$ ):  $\delta$  = 7.95 (d, 2H,  $J$  = 15.7 Hz); 7.49 (d, 2H,  $J$  = 2.0 Hz); 7.45 (dd, 2H,  $J$  = 8.5, 2.0 Hz); 7.08 (d, 2H,  $J$  = 15.7 Hz); 7.07 (d, 2H,  $J$  = 15.7 Hz); 6.49 (s, 1H); 4.11 (t, 4H,  $J$  = 6.0 Hz); 3.84 (s, 6H); 2.85 (t, 2H,  $J$  = 2.4 Hz); 2.34 (td, 2H,  $J$  = 7.1, 2.8 Hz); 1.90 – 1.94 (m, 4H).  $^{13}\text{C}\{^1\text{H}\}$ -NMR (100 MHz, DMSO- $d_6$ ):  $\delta$  = 179.1; 152.7; 148.3; 146.7; 127.1; 125.2; 118.9; 112.5; 112.0; 101.3; 83.7; 71.6; 66.8; 55.8; 27.7; 14.5.  $^{19}\text{F}\{^1\text{H}\}$ -NMR (188 MHz, DMSO- $d_6$ ):  $\delta$  = -138.3.  $^{11}\text{B}\{^1\text{H}\}$ -NMR (193 MHz, DMSO- $d_6$ ):  $\delta$  = 0.90. EI-MS:  $m/z$  (%) = 548 (18); 529 (23); 482 (98); 243 (60); 177 (100). UV/Vis  $\lambda_{\text{max}}$  [nm] ( $\epsilon$  [ $\text{M}^{-1}\text{cm}^{-1}$ ]): 503 (18194). Anal. calcd. for  $\text{C}_{31}\text{H}_{31}\text{BF}_2\text{O}_6 \cdot 0.25\text{H}_2\text{O}$ : C (67.34); H (5.74). Found: C (67.28); H (5.43).



**2h · 0.5 H<sub>2</sub>O:**



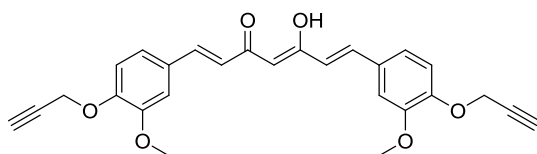
Yield 87%, orange solid. m. p.: 225 – 226 °C. <sup>1</sup>H-NMR (600 MHz, DMSO-d<sub>6</sub>): δ 7.97 (d, 2H, *J* = 15.6 Hz); 7.83 (d, 4H, *J* = 8.6 Hz); 7.06 (d, 4H, *J* = 8.4 Hz); 7.06 (d, 2H, *J* = 16.0 Hz); 6.51 (s, 1H); 4.13 (t, 4H, *J* = 6.2 Hz); 2.82 (t, 2H *J* = 3.1 Hz); 2.34 (td, 4H, *J* = 7.0, 2.9 Hz); 1.91 (p, 4H, *J* = 6.8 Hz). <sup>13</sup>C{<sup>1</sup>H}-NMR (150 MHz, DMSO-d<sub>6</sub>): δ 179.2; 161.8; 146.4; 131.8; 126.9; 118.8; 115.3; 101.6; 83.5; 71.7; 66.4; 27.6; 14.4. <sup>19</sup>F{<sup>1</sup>H}-NMR (188 MHz, DMSO-d<sub>6</sub>): δ = -138.2. <sup>11</sup>B{<sup>1</sup>H}-NMR (193 MHz, DMSO-d<sub>6</sub>): δ = 0.88. EI-MS: *m/z* (%) = 488 (63); 469 (16); 422 (36); 344 (88); 213 (100); 147 (58). UV/Vis λ<sub>max</sub> [nm] (ε [M<sup>-1</sup>cm<sup>-1</sup>]): 489 (9481). Anal. calcd. for C<sub>29</sub>H<sub>27</sub>BF<sub>2</sub>O<sub>4</sub>·0.5 H<sub>2</sub>O: C (70.04); H (5.67). Found: C (70.20); H (5.75).

#### 4. Synthesis of curcuminoids 3 and characterization data:

**General procedure (3a–c and 3e):** The respective curcuminoid–BF<sub>2</sub> complex **2** (1.5 mmol) was dissolved in methanol (40 mL) and water (10 mL). NaOH (3 mmol, 5% w/w aqueous solution) was added upon which the color turned to reddish green. The solution was stirred at 70 °C for 3 to 4 h and monitored by TLC (ethyl acetate/*n*-hexane 2:3). After the reaction was completed, the solution was cooled to room temperature and acidified with 2 M HCl. Methanol was removed under reduced pressure and the precipitated solid was collected by filtration, washed neutral with water, recrystallized from acetone/water or ethanol/water and dried in air.

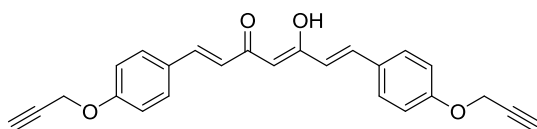
**General procedure (3d and 3f–h):** The respective curcuminoid–BF<sub>2</sub> complex **2** (0.25 mmol) was dissolved in DMSO (10 mL) and methanol (200 mL) and water (5 mL) were added subsequently. To the resulting suspension was added triethylamine (0.5 mmol) upon which the color turned to orange-green. The solution was stirred at 50 °C for 7 to 18 h and monitored by TLC (ethyl acetate/*n*-hexane 1:1). After the reaction was completed, the solution was cooled to room temperature and acidified with 2 M HCl. Methanol was removed under reduced pressure and the resulting oil was poured into ice water. The precipitated solid was isolated by filtration, washed five times with water (20 mL), recrystallized from acetone/water and dried in air.

**3a · 0.5 H<sub>2</sub>O [8]:**



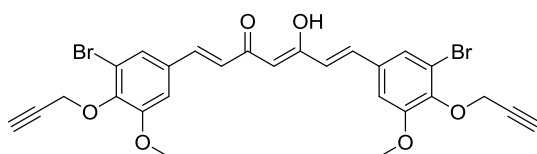
Yield 87%, orange solid. m. p.: 170 – 171 °C. <sup>1</sup>H-NMR (400 MHz, DMSO-d<sub>6</sub>): δ 7.60 (d, 2H, *J* = 15.9 Hz); 7.39 (d, 2H, *J* = 1.9 Hz); 7.28 (dd, 2H, *J* = 8.3, 1.9 Hz); 7.09 (d, 2H, *J* = 8.3 Hz); 6.87 (d, 2H, *J* = 15.9 Hz); 6.13 (s, 1H); 4.86 (d, 4H, *J* = 2.6 Hz); 3.85 (s, 6H); 3.61 (t, 2H, *J* = 2.6 Hz). <sup>13</sup>C{<sup>1</sup>H}-NMR (100 MHz, DMSO-d<sub>6</sub>): δ 183.0; 149.4; 148.5; 140.0; 128.5; 122.5; 114.0; 111.2; 100.8; 78.8; 78.2; 56.1; 55.6. EI-MS: *m/z* (%) = 444 (30); 426 (25); 405 (8); 387 (38); 215 (100). UV/Vis λ<sub>max</sub> [nm] (ε [M<sup>-1</sup>cm<sup>-1</sup>]): 414 (17254). Anal. calcd. for C<sub>27</sub>H<sub>24</sub>O<sub>6</sub>·0.5H<sub>2</sub>O: C (71.51); H (5.56). Found: C (71.18); H (5.75).

**3b · 0.25 H<sub>2</sub>O:**



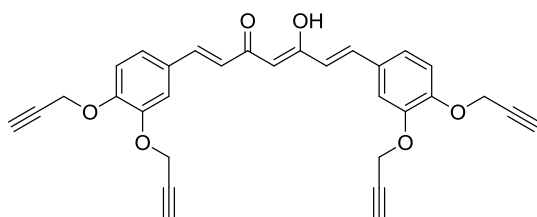
Yield 92%, brownish yellow solid. m. p.: 176 – 178 °C.  $^1\text{H}$ -NMR (400 MHz, DMSO- $d_6$ ):  $\delta$  7.70 (d, 4H,  $J$  = 8.7 Hz); 7.59 (d, 2H,  $J$  = 15.9 Hz); 7.05 (d, 4H,  $J$  = 8.7 Hz); 6.81 (d, 2H,  $J$  = 8.7 Hz); 6.11 (s, 1H); 4.87 (d, 4H,  $J$  = 2.2 Hz); 3.60 (t, 2H,  $J$  = 2.2 Hz).  $^{13}\text{C}\{^1\text{H}\}$ -NMR (100 MHz, DMSO- $d_6$ ): 183.2; 159.0; 139.9; 130.1; 128.0; 122.3; 115.4; 101.4; 79.0; 78.6; 55.6. EI-MS:  $m/z$  (%) = 384 (29); 366 (10); 345 (10); 185 (90); 180 (100). UV/Vis  $\lambda_{\text{max}}$  [nm] ( $\epsilon$  [ $\text{M}^{-1}\text{cm}^{-1}$ ]): 410 (41437). Anal. calcd. for  $\text{C}_{25}\text{H}_{20}\text{O}_4 \cdot 0.25 \text{H}_2\text{O}$ : C (77.20); H (5.31). Found: C (77.57); H (5.18).

**3c · 0.5 H<sub>2</sub>O:**



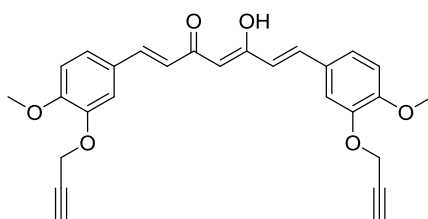
Yield 92%, yellow-orange solid. m. p.: 207.5 – 209.5 °C.  $^1\text{H}$ -NMR (400 MHz, DMSO- $d_6$ ):  $\delta$  7.61 (d, 2H,  $J$  = 2.0 Hz); 7.58 (d, 4H,  $J$  = 15.9 Hz); 7.47 (d, 2H,  $J$  = 2.0 Hz); 7.02 (d, 4H,  $J$  = 15.8 Hz); 6.14 (s, 1H); 4.78 (d, 4H,  $J$  = 2.6 Hz); 3.90 (s, 6H); 3.54 (t, 2H,  $J$  = 2.4 Hz).  $^{13}\text{C}\{^1\text{H}\}$ -NMR (100 MHz, DMSO- $d_6$ ):  $\delta$  183.1; 153.6; 144.6; 138.8; 132.7; 125.2; 124.6; 117.8; 112.0; 102.1; 78.9; 78.8; 59.7; 56.4. EI-MS:  $m/z$  (%) = 602 (18); 584 (10); 563 (17); 545 (35); 517 (13). UV/Vis  $\lambda_{\text{max}}$  [nm] ( $\epsilon$  [ $\text{M}^{-1}\text{cm}^{-1}$ ]): 405 (36739). Anal. calcd. for  $\text{C}_{27}\text{H}_{22}\text{Br}_2\text{O}_6 \cdot 0.5\text{H}_2\text{O}$ : C (53.05); H (3.79). Found: C (52.89); H (3.72).

**3e · 0.5 H<sub>2</sub>O:**



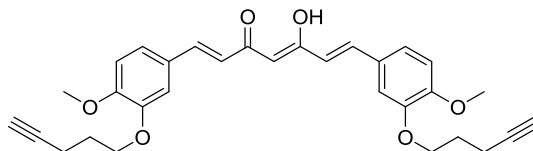
Yield 84%, yellow solid. m. p.: 153 – 154 °C.  $^1\text{H}$ -NMR (400 MHz, DMSO- $d_6$ ):  $\delta$  7.58 (d, 2H,  $J$  = 15.8 Hz); 7.45 (d, 2H,  $J$  = 1.8 Hz); 7.33 (dd, 2H,  $J$  = 8.5 Hz, 1.7 Hz); 7.12 (d, 2H,  $J$  = 8.5 Hz); 6.84 (d, 2H,  $J$  = 15.9 Hz); 6.14 (s, 1H); 4.89 (d, 4H,  $J$  = 2.4 Hz); 4.88 (d, 4H,  $J$  = 2.3 Hz); 3.60 - 3.62 (m, 4H).  $^{13}\text{C}\{^1\text{H}\}$ -NMR (100 MHz, DMSO- $d_6$ ):  $\delta$  183.2; 148.9; 147.0; 140.1; 128.2; 123.3; 122.7; 113.9; 113.0; 101.1; 79.0; 78.9; 78.7; 78.6; 56.1; 56.0. EI-MS:  $m/z$  (%) = 492 (20); 474 (8); 453 (17); 239 (100). UV/Vis  $\lambda_{\text{max}}$  [nm] ( $\epsilon$  [ $\text{M}^{-1}\text{cm}^{-1}$ ]): 405 (50732). Anal. calcd. for  $\text{C}_{31}\text{H}_{24}\text{O}_6 \cdot 0.5\text{H}_2\text{O}$ : C (74.24); H (5.02). Found: C (74.11); H (4.93).

### 3f · 0.6 H<sub>2</sub>O:



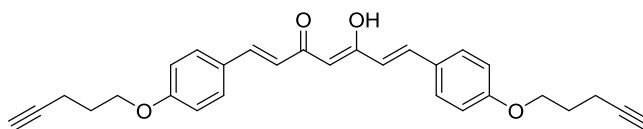
Yield 90%, yellow-orange solid. m. p.: 176 – 177 °C.  $^1\text{H}$ -NMR (400 MHz, DMSO- $d_6$ ):  $\delta$  7.58 (d, 2H,  $J$  = 15.9 Hz); 7.42 (d, 2H,  $J$  = 1.8 Hz); 7.32 (dd,  $J$  = 8.4 Hz, 1.7 Hz); 7.05 (d, 2H,  $J$  = 8.5 Hz); 6.80 (d, 2H,  $J$  = 15.9 Hz); 6.12 (s, 1H); 4.87 (d, 4H,  $J$  = 2.3 Hz); 3.82 (s, 6H); 3.57 (t, 2H,  $J$  = 2.3 Hz).  $^{13}\text{C}\{^1\text{H}\}$ -NMR: (400 MHz, DMSO- $d_6$ ):  $\delta$  = 183.2; 151.4; 146.7; 140.3; 127.4; 123.9; 122.3; 112.7; 112.2; 101.0; 79.2; 78.5; 56.1; 55.7. EI-MS:  $m/z$  (%) 444 (19); 426 (17); 405 (10); 215 (60); 188 (100); 173 (75). UV/Vis  $\lambda_{\text{max}}$  [nm] ( $\epsilon$  [ $\text{M}^{-1}\text{cm}^{-1}$ ]): 418 (25029). Anal. calcd. for  $\text{C}_{27}\text{H}_{24}\text{O}_6 \cdot 0.6\text{H}_2\text{O}$ : C (71.23); H (5.58). Found: C (71.03); H (5.26).

**3g · 0.5 H<sub>2</sub>O:**



Yield 80%, yellow-orange solid. m. p.: 132 – 133 °C. <sup>1</sup>H-NMR (400 MHz, DMSO-d<sub>6</sub>): δ = 7.56 (d, 2H, *J* = 15.6 Hz); 7.35 (d, 2H, *J* = 2.1 Hz); 7.26 (dd, 2H, *J* = 8.4, 2.1 Hz); 7.01 (d, 2H, *J* = 8.4 Hz); 6.81 (d, 2H, *J* = 15.8 Hz); 6.10 (s, 1H); 4.09 (t, 4H, *J* = 6.2 Hz); 3.81 (s, 6H); 2.82 (t, 2H, *J* = 2.7 Hz); 2.34 (td, 2H, *J* = 7.1, 2.7 Hz); 1.89 – 1.93 (m, 4H). <sup>13</sup>C{<sup>1</sup>H}-NMR (100 MHz, DMSO-d<sub>6</sub>): δ = 183.2; 151.2; 148.2; 140.3; 127.6; 123.1; 122.1; 111.9; 111.8; 83.7; 71.6; 66.8; 55.7; 27.8; 14.5. EI-MS: *m/z* (%) = 500 (49); 482 (100); 467; 404 (37); 256 (47); 232 (70); 203 (31); 178 (55). UV/Vis λ<sub>max</sub> [nm] (ε [M<sup>-1</sup>cm<sup>-1</sup>]): 405 (11036). Anal. calcd. for C<sub>31</sub>H<sub>32</sub>O<sub>6</sub>·0.5H<sub>2</sub>O: C (73.07); H (6.53). Found: C (73.15); H (6.47).

**3h:**



Yield 95%, orange solid. m. p.: 153.5 – 154.5 °C. <sup>1</sup>H-NMR (400 MHz, DMSO-d<sub>6</sub>): δ = 16.32 (br s, 1H); 7.67 (d, 4H, *J* = 8.8 Hz); 7.59 (d, 2H, *J* = 15.9 Hz); 7.00 (d, 4H, *J* = 8.8 Hz); 6.78 (d, 2H, *J* = 15.9 Hz); 6.08 (s, 1H); 4.09 (t, 4H, *J* = 6.2 Hz); 2.82 (t, 2H, *J* = 2.6 Hz); 2.34 (td, 4H, *J* = 7.1, 2.6 Hz); 2.34 (td, 2H, *J* = 7.1, 2.7 Hz); 1.90 (qui, 4H, *J* = 6.7 Hz). <sup>13</sup>C{<sup>1</sup>H}-NMR (100 MHz, DMSO-d<sub>6</sub>): δ = 183.2; 160.3; 140.0; 130.2; 127.4; 121.9; 114.9; 101.2; 83.6; 71.7; 66.2; 27.6; 14.4. EI-MS: *m/z* (%) = . UV/Vis λ<sub>max</sub> [nm]

( $\epsilon$  [ $\text{M}^{-1}\text{cm}^{-1}$ ]): 414 (29870). Anal. calcd. for  $\text{C}_{29}\text{H}_{28}\text{O}_4$ : C (79.07); H (6.41). Found: C (78.86); H (3.36).

## 5. X-ray crystallographic data for 2f, 2g and 2h

The intensity data for the compounds were collected on a Nonius KappaCCD diffractometer using graphite-monochromated  $\text{Mo-K}\alpha$  radiation. Data were corrected for Lorentz and polarization effects; absorption was taken into account on a semi-empirical basis using multiple-scans [9-11]. The structures were solved by direct methods (SHELXS [12]) and refined by full-matrix least squares techniques against  $\text{Fo}^2$  (SHELXL-97 [13]). All hydrogen atoms were located by difference Fourier synthesis and refined isotropically. All non-hydrogen atoms were refined anisotropically [12]. Crystallographic data as well as structure solution and refinement details are summarized in Table S1. MERCURY [13] was used for structure representations.

**Table S1:** Crystal data and refinement details for the X-ray structure determinations of the compounds **2f–2h**.

Compound	<b>2f</b>	<b>2g</b>	<b>2h</b>
formula	C <sub>27</sub> H <sub>23</sub> BF <sub>2</sub> O <sub>6</sub>	C <sub>31</sub> H <sub>31</sub> BF <sub>2</sub> O <sub>6</sub>	C <sub>29</sub> H <sub>27</sub> BF <sub>2</sub> O <sub>4</sub>
fw (g·mol <sup>-1</sup> )	492.26	548.37	488.32
T/°C	-140(2)	-140(2)	-140(2)
crystal system	triclinic	triclinic	monoclinic
space group	P $\bar{1}$	P $\bar{1}$	C 2/c
<i>a</i> /Å	8.5535(3)	11.1586(3)	10.7368(3)
<i>b</i> /Å	10.2782(3)	11.2846(3)	16.3081(5)
<i>c</i> /Å	14.3695(5)	11.7934(3)	14.5077(5)
$\alpha$ /°	101.013(2)	88.864(2)	90
$\beta$ /°	102.402(2)	83.361(2)	102.498(2)
$\gamma$ /°	101.684(2)	69.043(2)	90
<i>V</i> /Å <sup>3</sup>	1171.36(7)	1377.12(6)	2480.06(13)
<i>Z</i>	2	2	4
$\rho$ (g·cm <sup>-3</sup> )	1.396	1.322	1.308
$\mu$ (cm <sup>-1</sup> )	1.07	.99	.95
measured data	7699	17970	8445
data with <i>I</i> > 2 $\sigma$ ( <i>I</i> )	3677	5030	2349
unique data ( <i>R</i> <sub>int</sub> )	5140/0.0384	6282/0.0289	2741/0.0321
<i>wR</i> <sub>2</sub> (all data, on <i>F</i> <sup>2</sup> ) <sup>a)</sup>	0.1551	0.1180	0.1189
<i>R</i> <sub>1</sub> ( <i>I</i> > 2 $\sigma$ ( <i>I</i> )) <sup>a)</sup>	0.0778	0.0494	0.0456
<i>S</i> <sup>b)</sup>	1.168	1.050	1.067
Res. dens./e·Å <sup>-3</sup>	0.310/-0.310	0.326/-0.208	0.432/-0.223
absorpt method	multi-scan	multi-scan	multi-scan
absorpt corr	0.6526/0.7456	0.6925/0.7456	0.6783/0.7456
T <sub>min</sub> /max			
CCDC No.	1526555	1526556	1526557

<sup>a)</sup> Definition of the *R* indices:  $R_1 = (\sum ||F_o| - |F_c||) / \sum |F_o|$ ;  
 $wR_2 = \{\sum [w(F_o^2 - F_c^2)^2] / \sum [w(F_o^2)^2]\}^{1/2}$  with  $w^{-1} = \sigma^2(F_o^2) + (aP)^2 + bP$ ;  $P = [2F_c^2 + \text{Max}(F_o^2)]/3$ ;  
<sup>b)</sup>  $s = \{\sum [w(F_o^2 - F_c^2)^2] / (N_o - N_p)\}^{1/2}$ .

## 6. References:

1. Nakhjiri, M.; Safavi, M.; Alipour, E.; Emami, S.; Atash, A. F.; Jafari-Zavareh, M.; Ardestani, S. K.; Khoshneviszadeh, M.; Foroumadi, A.; Shafiee, A. *Eur. J. Med. Chem.* **2012**, *50*, 113–123.
2. Williams, A.; Winfield, S. *Analyst* **1983**, *108*, 1067–1071.
3. DecayFit - Fluorescence Decay Analysis Software 1.3, FluorTools, [www.fluortools.com](http://www.fluortools.com)
3. Pal, M.; Parasuraman, K.; Yeleswarapu, K. R. *Org. Lett.* **2003**, *5*, 349–352.
4. Kant, R.; Kumar, D.; Agarwal, D.; Gupta, R. D.; Tilak, R.; Awasthi, S. K.; Agarwal, A. *Eur. J. Med. Chem.* **2016**, *113*, 34–49.
5. Zammit, S. C.; Cox, A. J.; Gow, R. M.; Zhang, Y.; Gilbert, R. E.; Krum, H.; Kelly, D. J.; Williams, S. J. *Bioorg. Med. Chem. Lett.* **2009**, *19*, 7003–7006.
6. Goto, H.; Nimori, S.; Akagi, K. *Synt. Met.* **2005**, *155*, 576–587.
7. Liu, K.; Chen, J.; Chojnacki, J.; Zhang, S. *Tetrahedron Lett.* **2013**, *54*, 2070–2073.
8. Gomes, D.; Alegrio, L.; Lim, M.; Leon, L.; Araújo, C. *Arzneim. Forsch.* **2002**, *52*, 120–124.
9. *COLLECT*, Data Collection Software; Nonius B. V., Netherlands, 1998.
10. Otwinowski, Z.; Minor, W. Processing of X-Ray Diffraction Data Collected in Oscillation Mode. In *Methods in Enzymology*; Carter, C. W., Sweet, R. M., Eds.; Macromolecular Crystallography, Part A, Vol. 276, Academic Press, 1997, pp. 307–326. doi:10.1016/S0076-6879(97)76066-X
11. *SADABS 2.10*, Bruker-AXS inc., Madison, WI, U.S.A., 2002.
12. Sheldrick, G. M. *Acta Cryst.* **2008**, *A64*, 112–122. doi:10.1107/S0108767307043930
13. Macrae C. F.; Edgington P. R.; McCabe P.; Pidcock E.; Shields G. P.; Taylor R., Towler M., van de Streek J. *J. Appl. Cryst.* **2006**, *39*, 453. doi:10.1107/S002188980600731X



## 7. Intermolecular interactions in 2f:

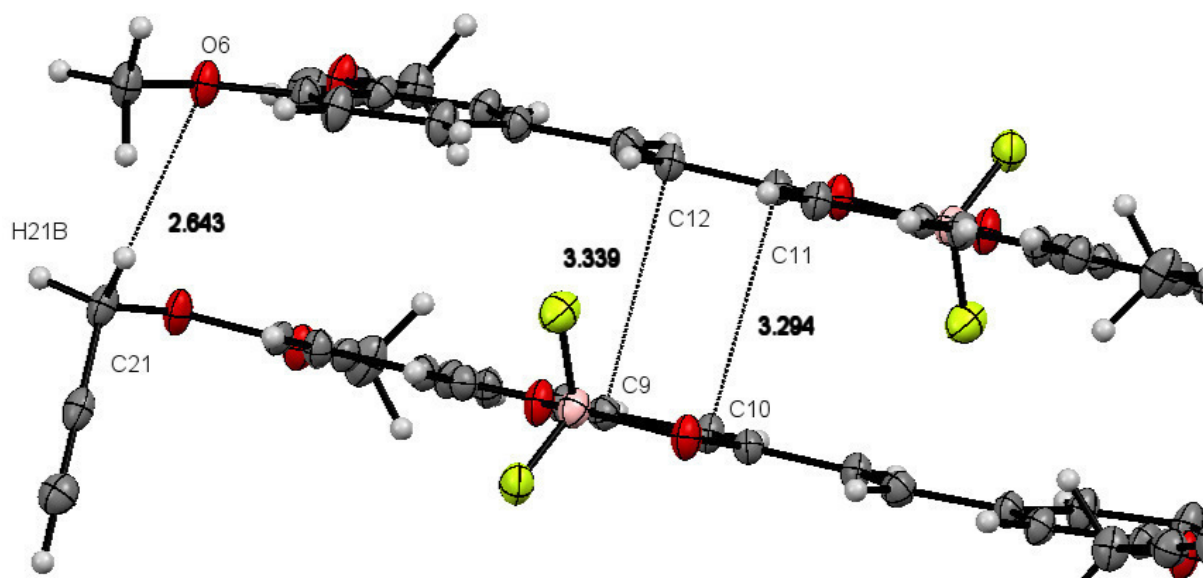


**Figure S1:** ORTEP drawing showing intermolecular interactions between two molecules of **2f**. Calculated distances are given in Å.

## 8. NMR spectra for compounds 2 and 3

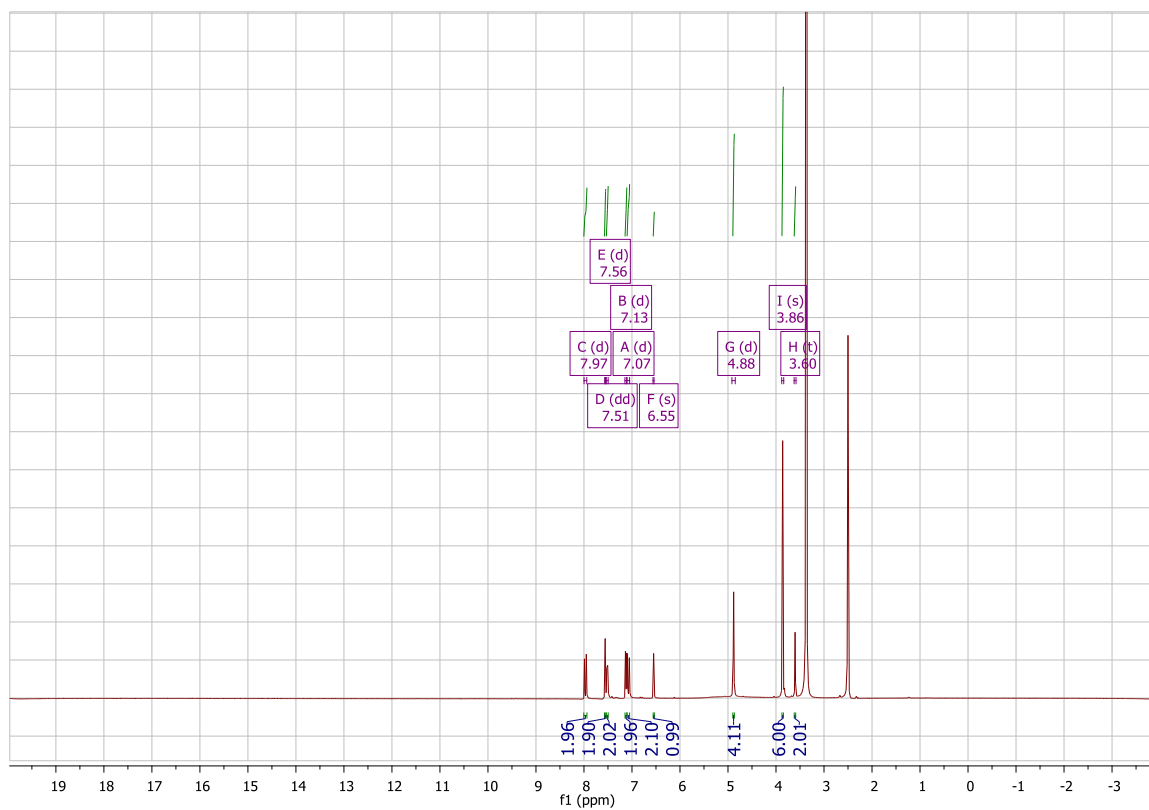


**Figure S2:**  $^1\text{H}$  NMR spectrum (400 MHz,  $\text{DMSO}-d_6$ ) of **2a**.

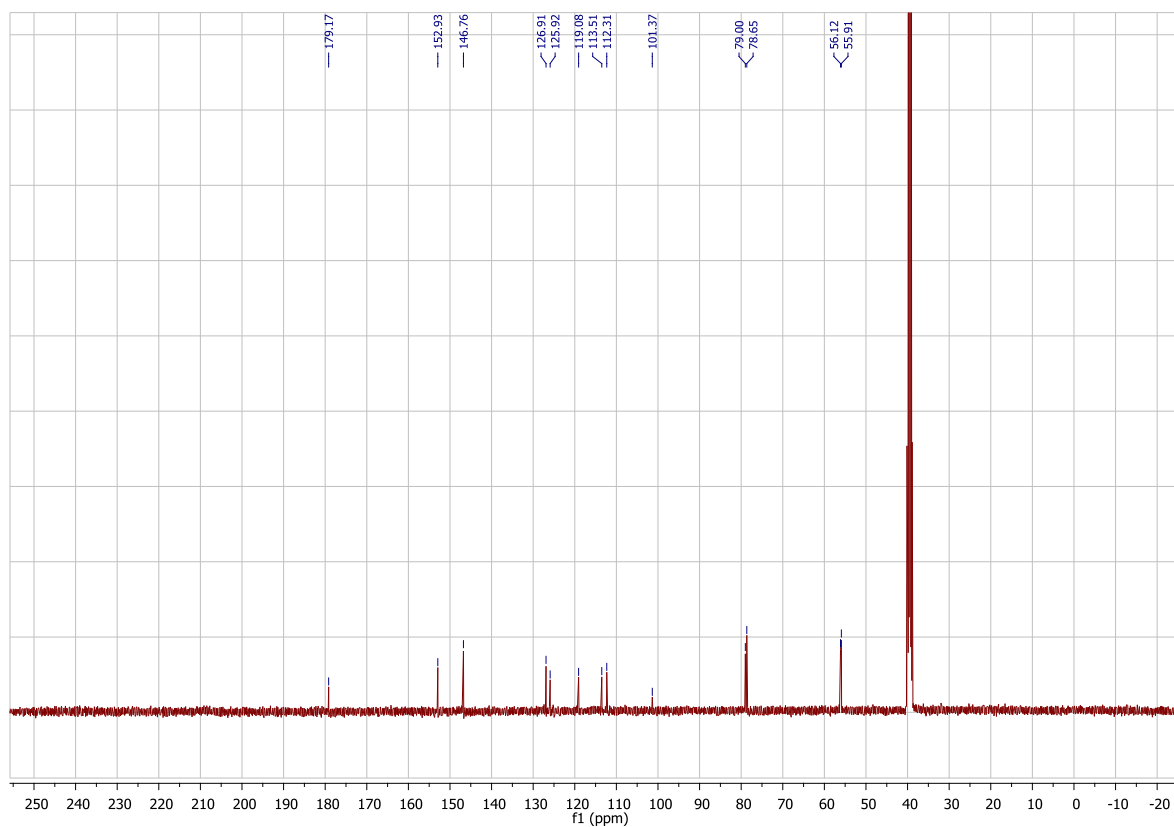


**Figure S3:**  $^{13}\text{C}\{^1\text{H}\}$  NMR spectrum (100 MHz,  $\text{DMSO}-d_6$ ) of **2a**.

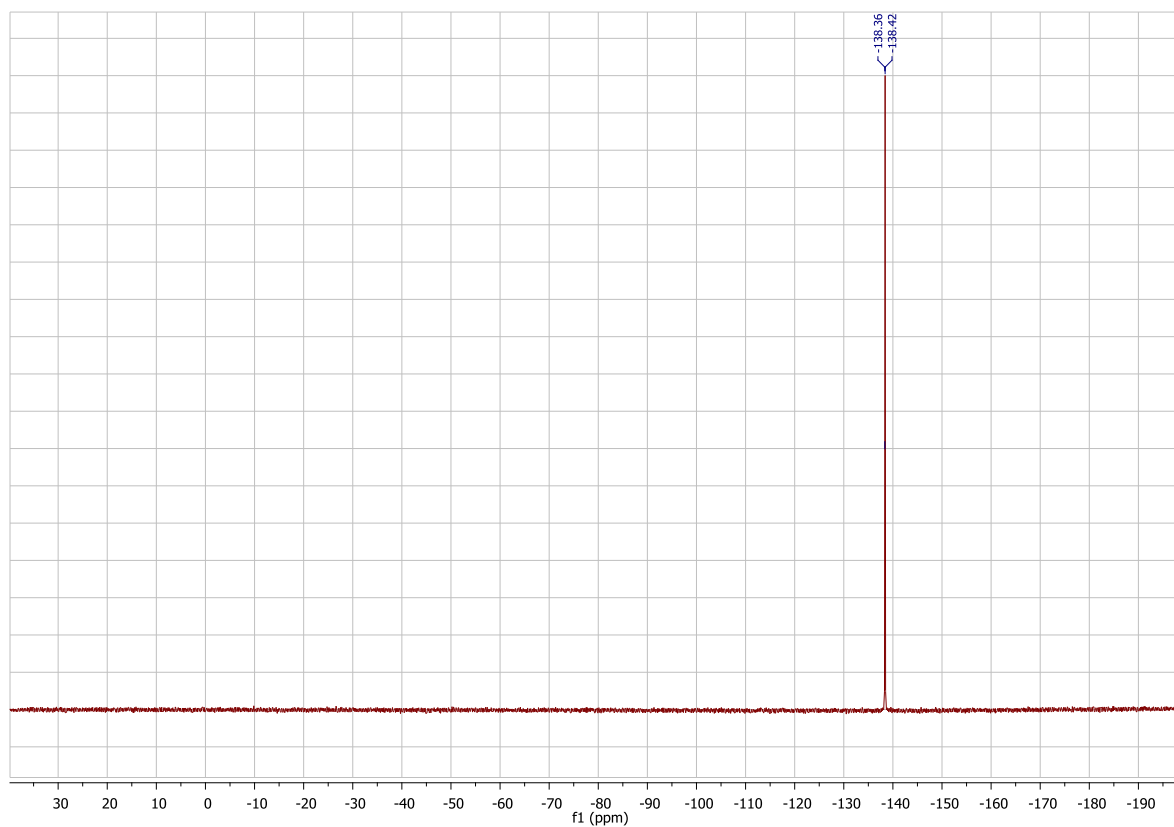


**Figure S4:**  $^{19}\text{F}\{^1\text{H}\}$  NMR spectrum (188 MHz,  $\text{DMSO}-d_6$ ) of **2a**.

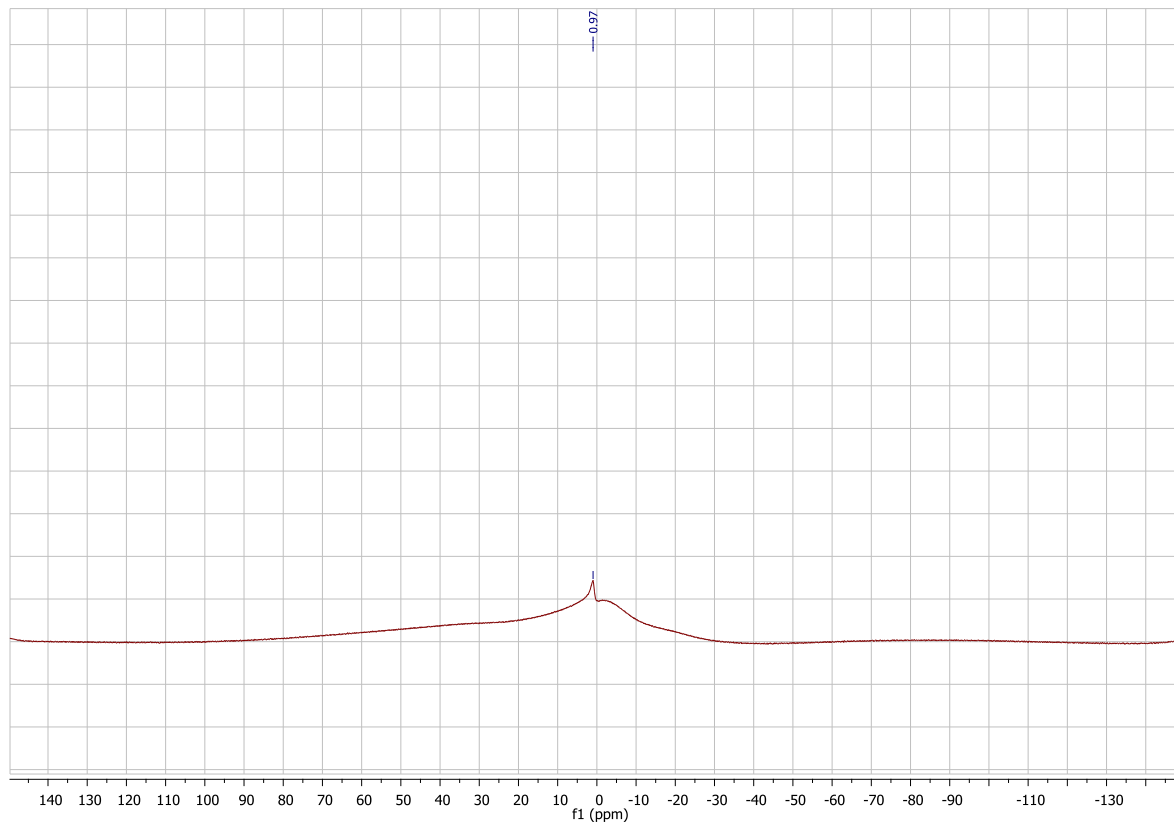


**Figure S5:**  $^{11}\text{B}\{^1\text{H}\}$  NMR spectrum (128 MHz,  $\text{DMSO}-d_6$ ) of **2a**.

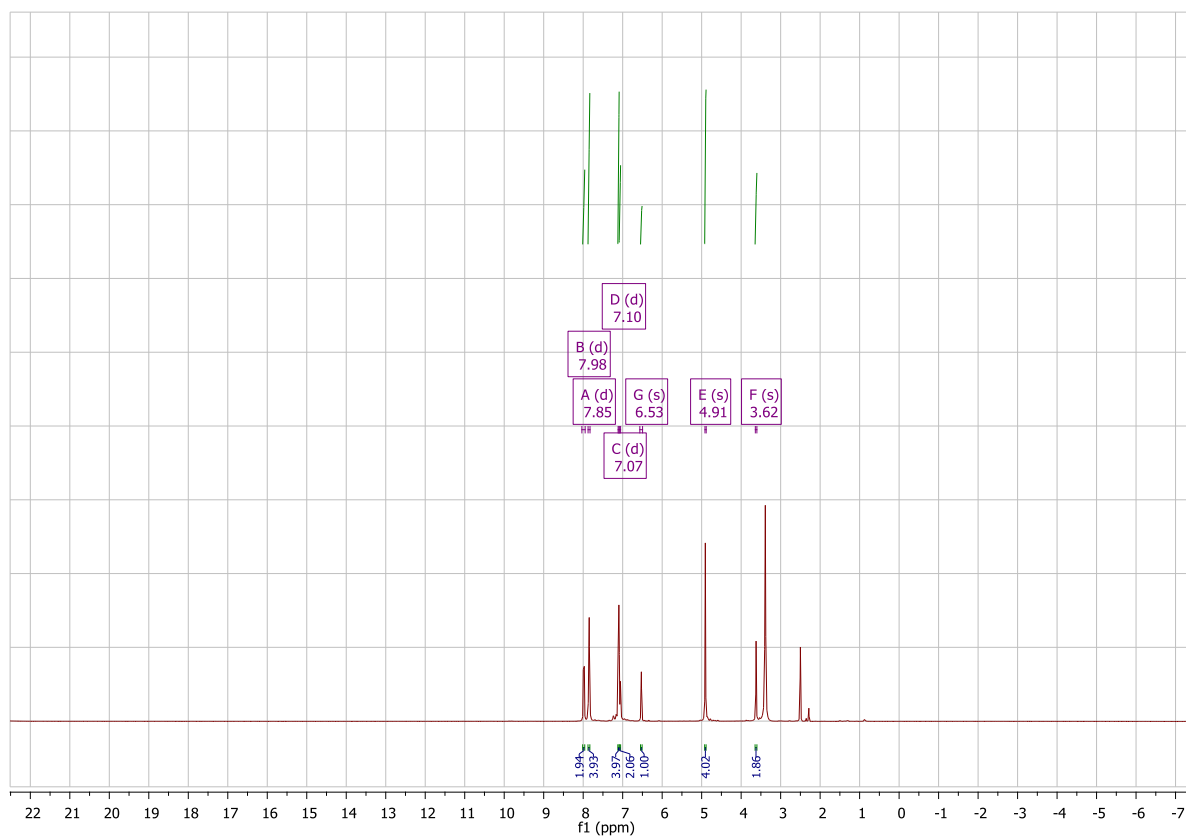


**Figure S6:** <sup>1</sup>H NMR spectrum (400 MHz, DMSO-*d*<sub>6</sub>) of **2b**.

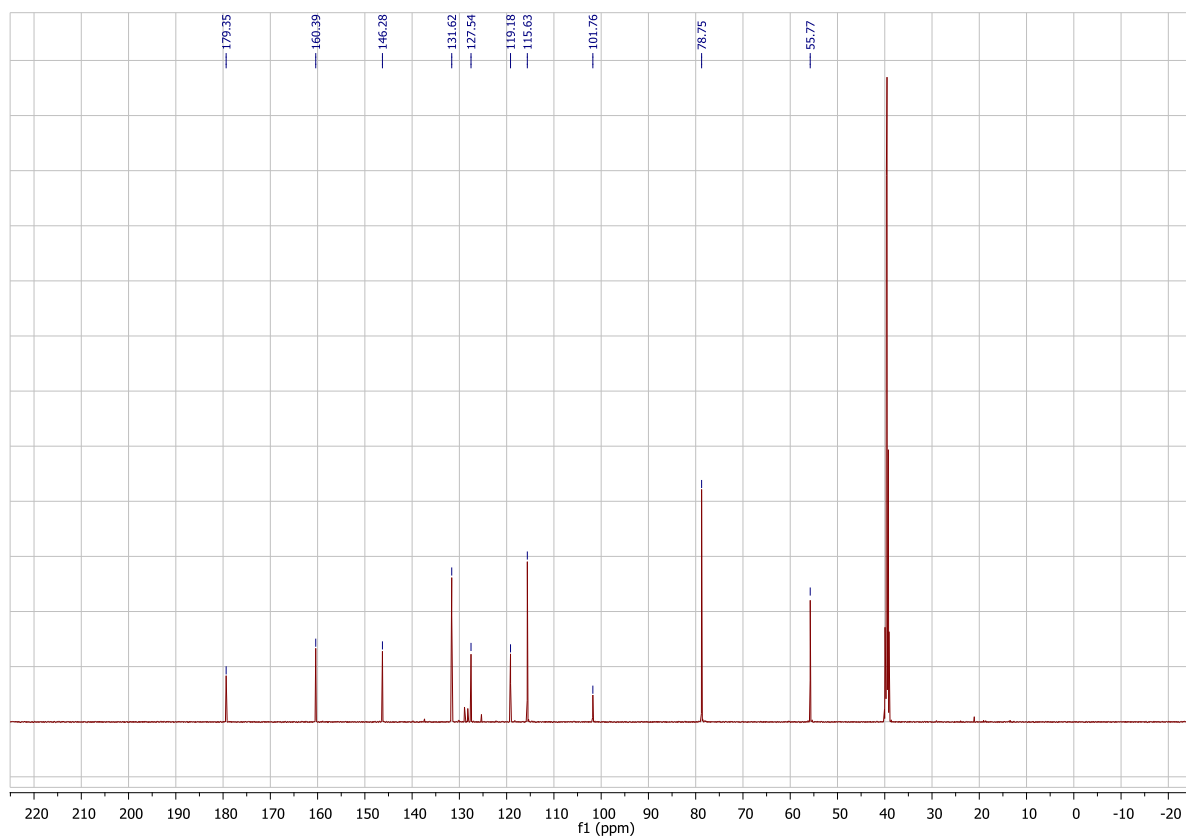


**Figure S7:** <sup>13</sup>C{<sup>1</sup>H} NMR spectrum (100 MHz, DMSO-*d*<sub>6</sub>) of **2b**.

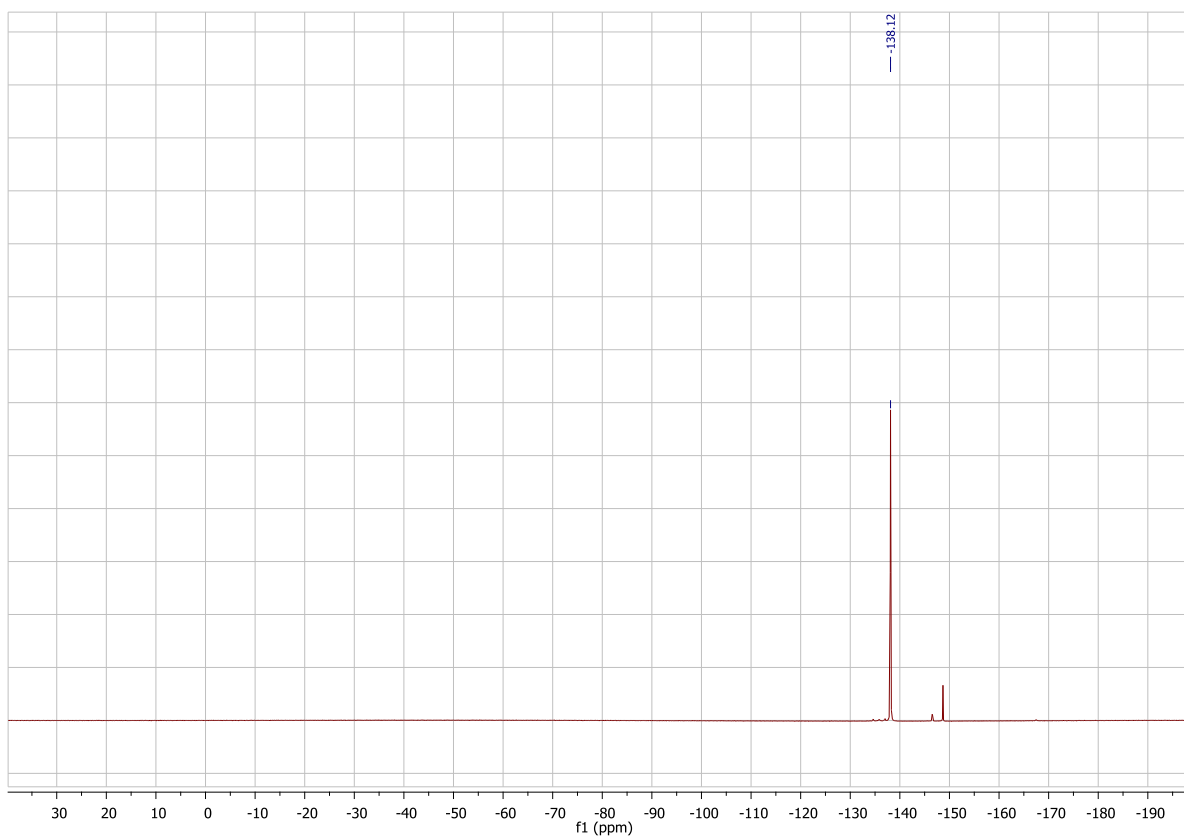


**Figure S8:**  $^{19}\text{F}\{^1\text{H}\}$  NMR spectrum (188 MHz,  $\text{DMSO}-d_6$ ) of **2b**.

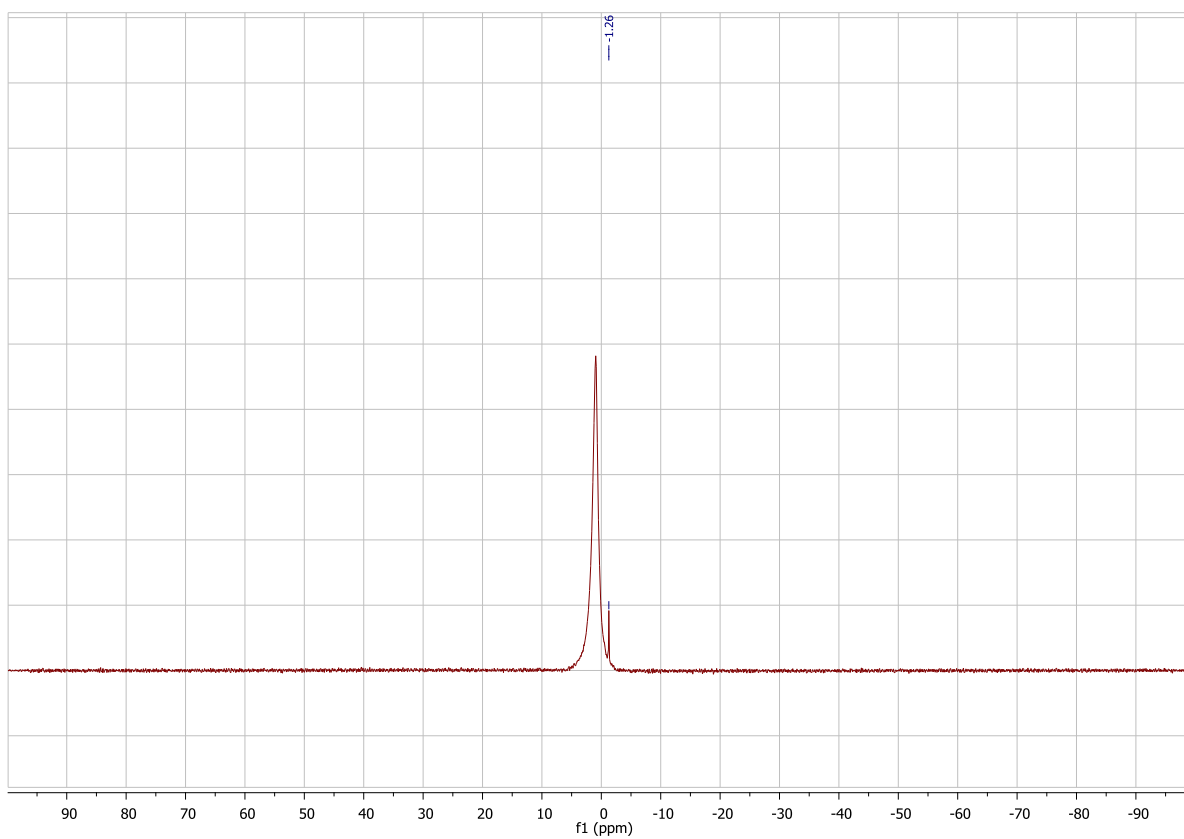


**Figure S9:**  $^{11}\text{B}\{^1\text{H}\}$  NMR spectrum (128 MHz,  $\text{DMSO}-d_6$ ) of **2b**.

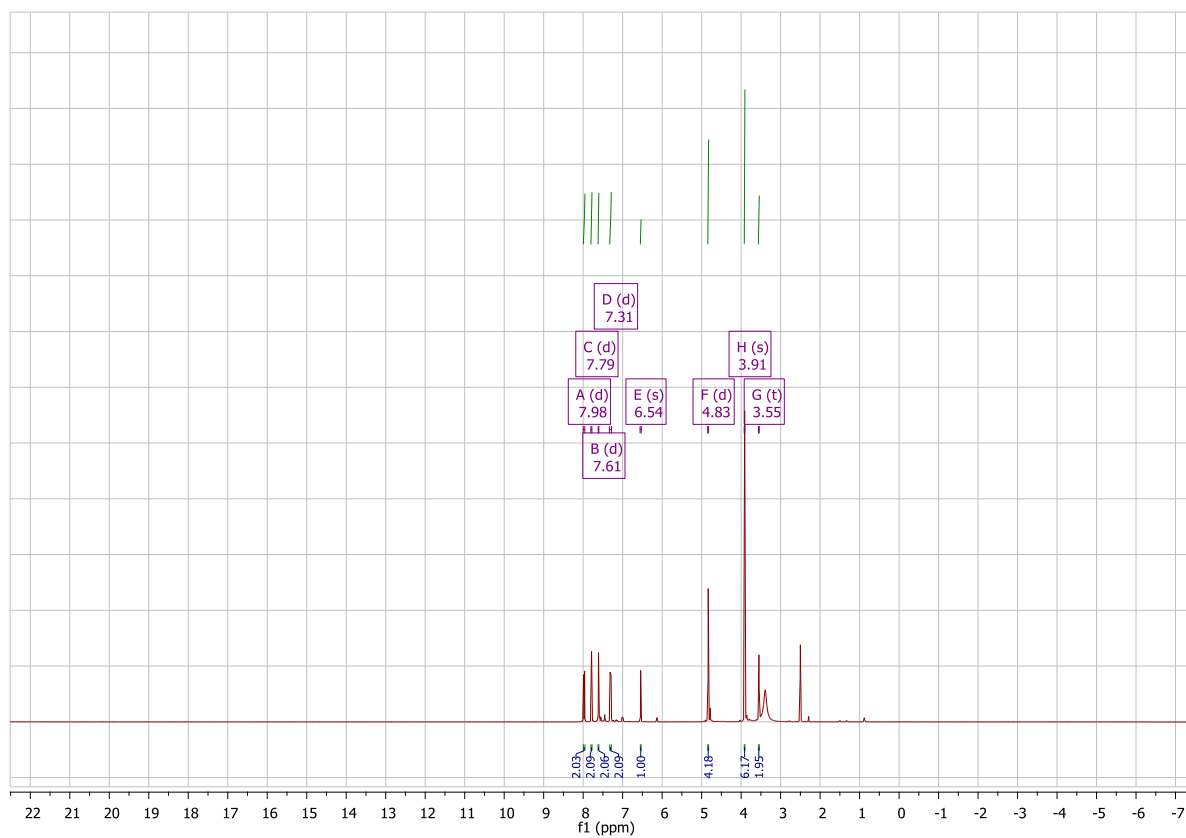


**Figure S10:** <sup>1</sup>H NMR spectrum (600 MHz, DMSO-*d*<sub>6</sub>) of **2c**.

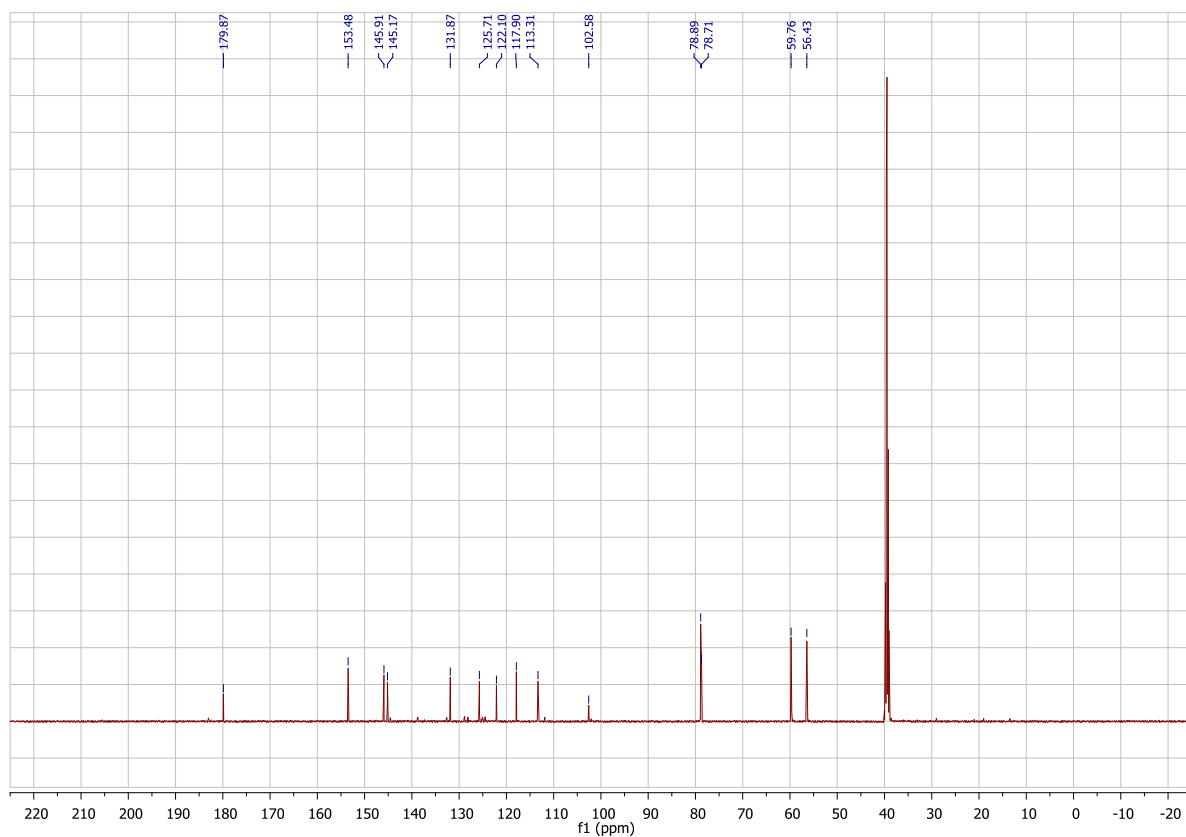


**Figure S11:** <sup>13</sup>C{<sup>1</sup>H} NMR spectrum (150 MHz, DMSO-*d*<sub>6</sub>) of **2c**.

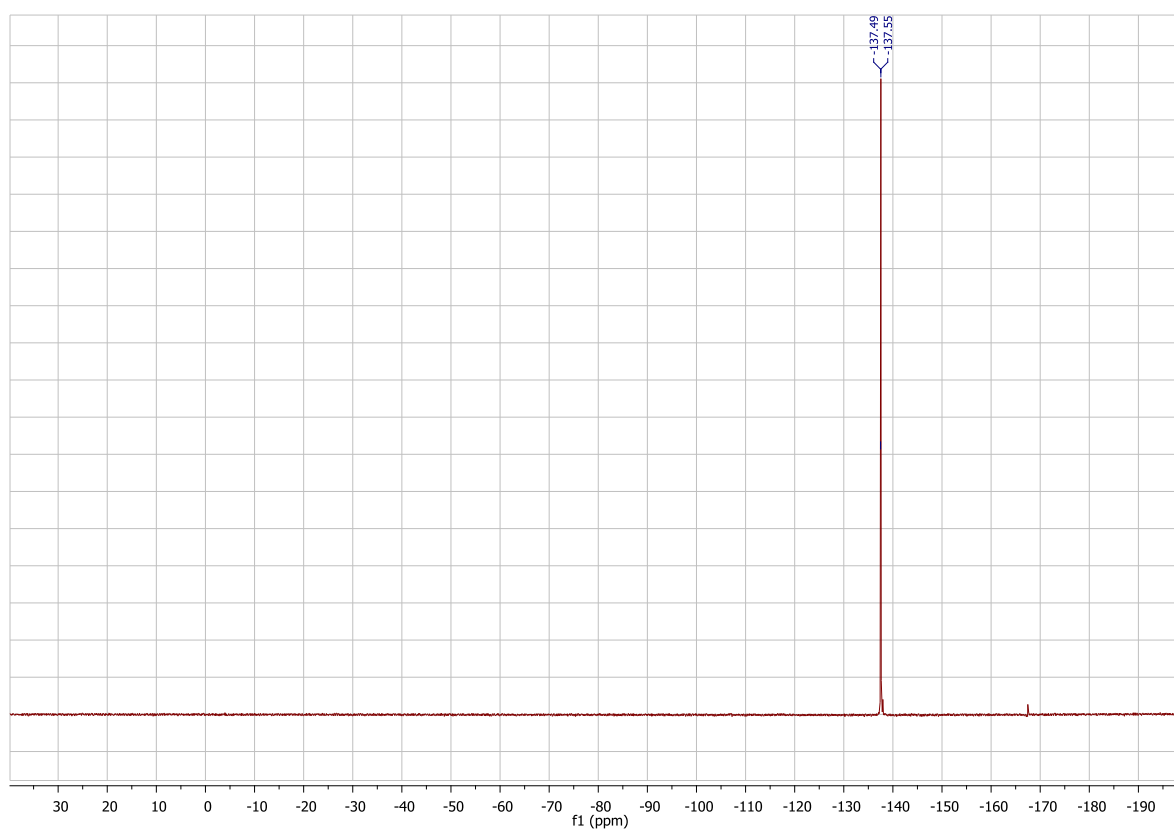


**Figure S12:**  $^{19}\text{F}\{^1\text{H}\}$  NMR spectrum (188 MHz,  $\text{DMSO}-d_6$ ) of **2c**.

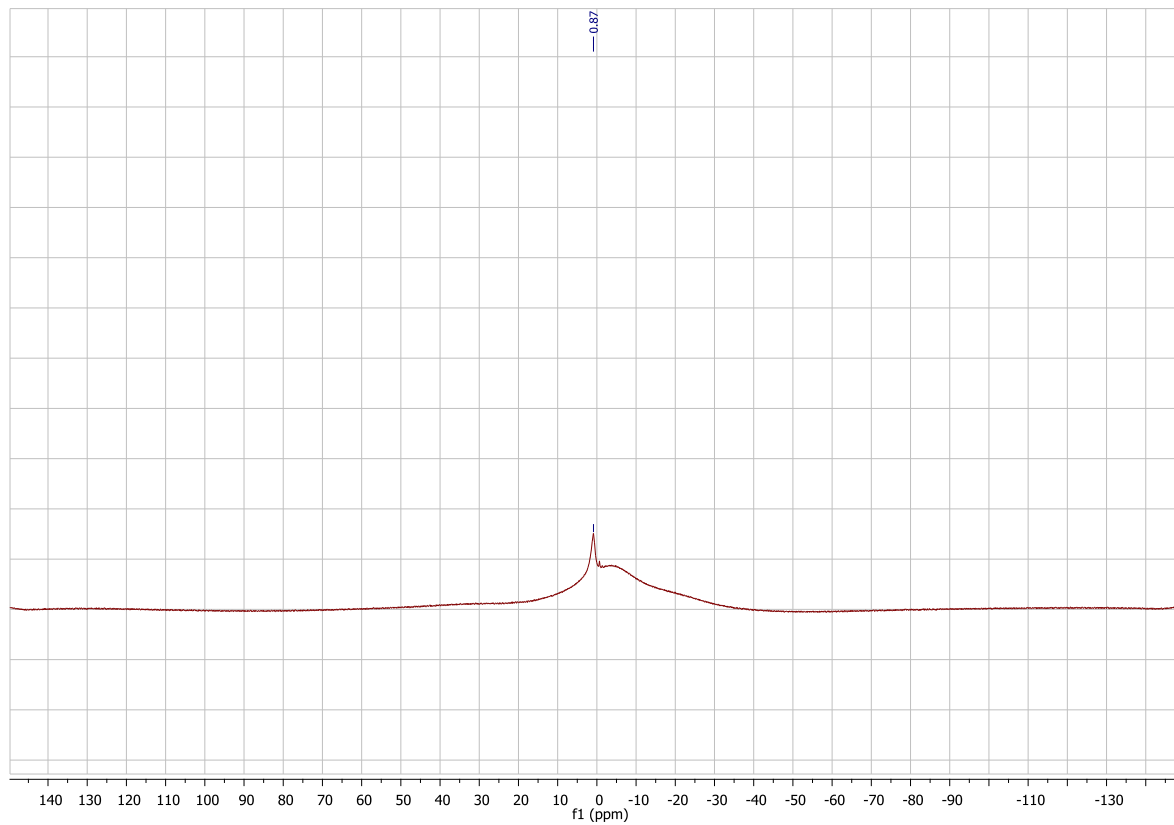


**Figure S13:**  $^{11}\text{B}\{^1\text{H}\}$  NMR spectrum (128 MHz,  $\text{DMSO}-d_6$ ) of **2c**.

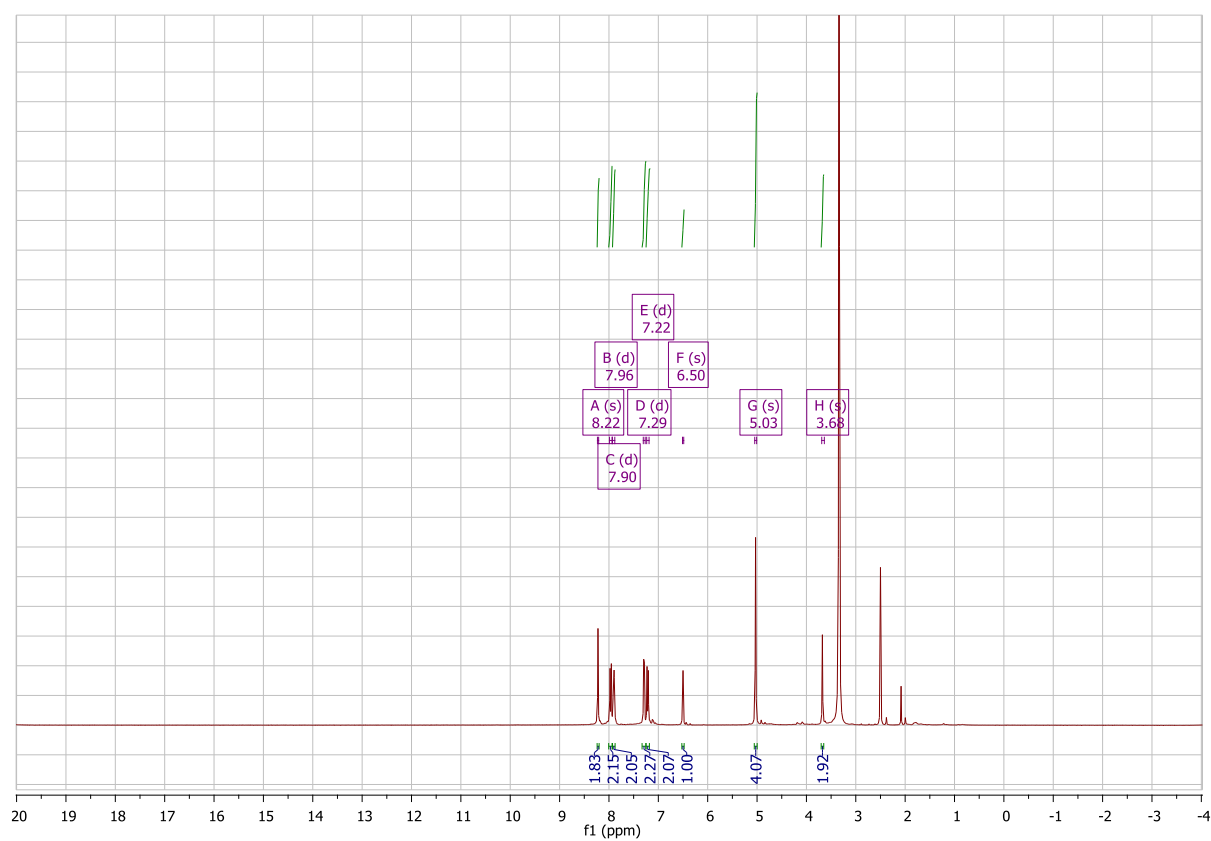


**Figure S14:** <sup>1</sup>H NMR spectrum (600 MHz, DMSO-*d*<sub>6</sub>) of **2d**.

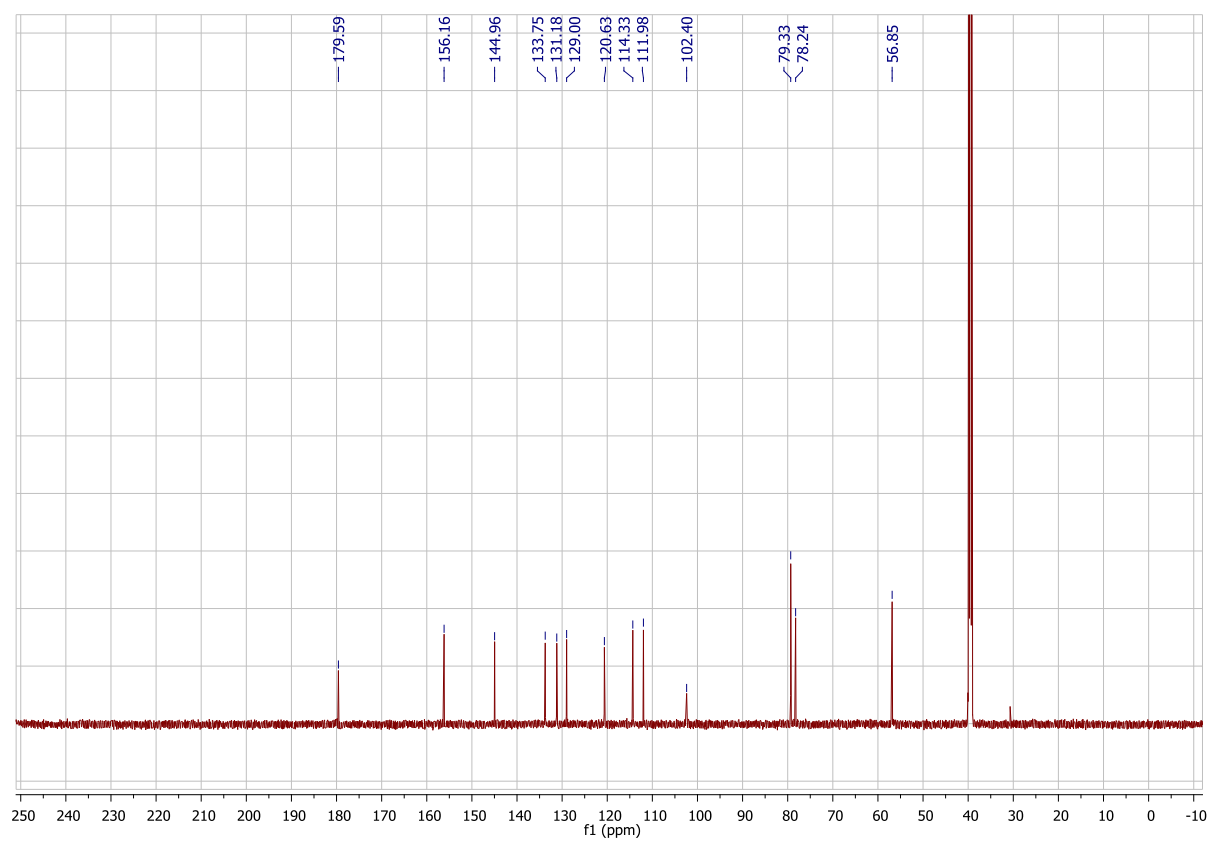


**Figure S15:** <sup>13</sup>C{<sup>1</sup>H} NMR spectrum (150 MHz, DMSO-*d*<sub>6</sub>) of **2d**.



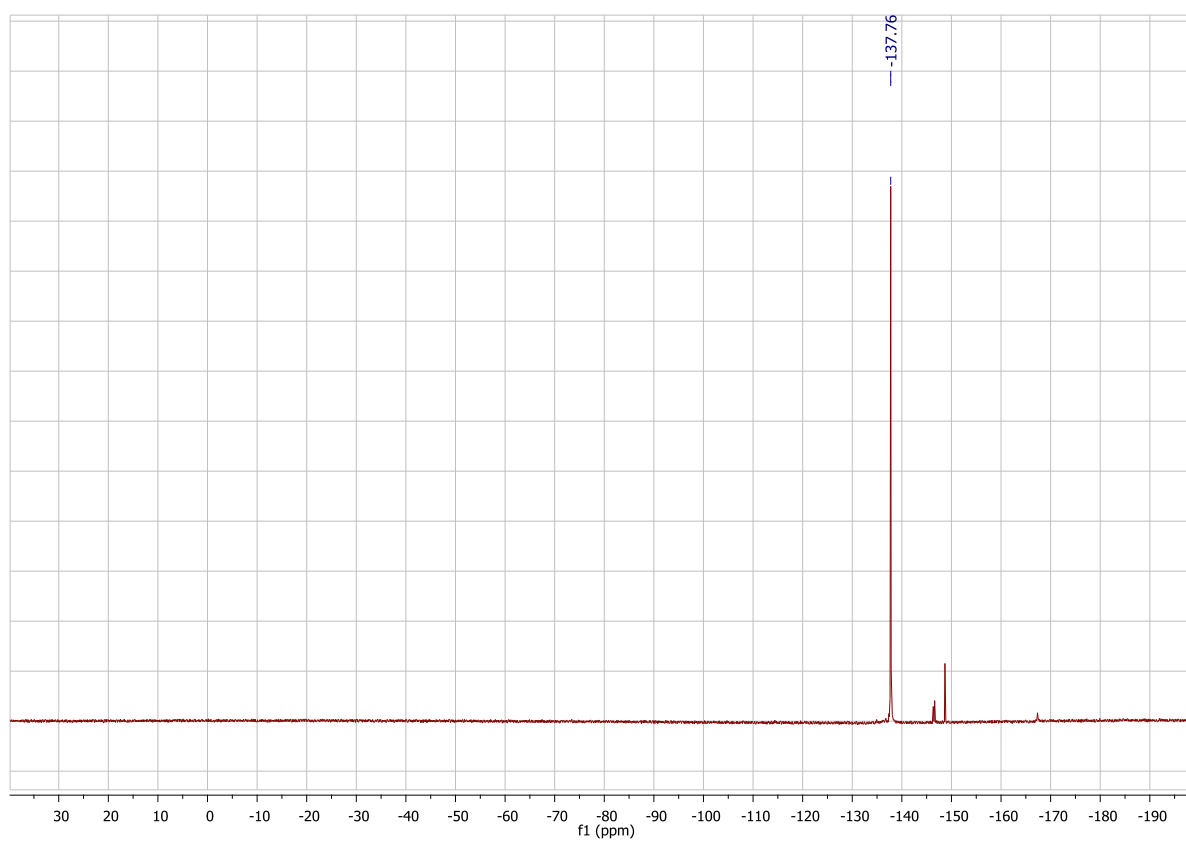


**Figure S16:**  $^{19}\text{F}\{^1\text{H}\}$  NMR spectrum (188 MHz,  $\text{DMSO}-d_6$ ) of **2d**.

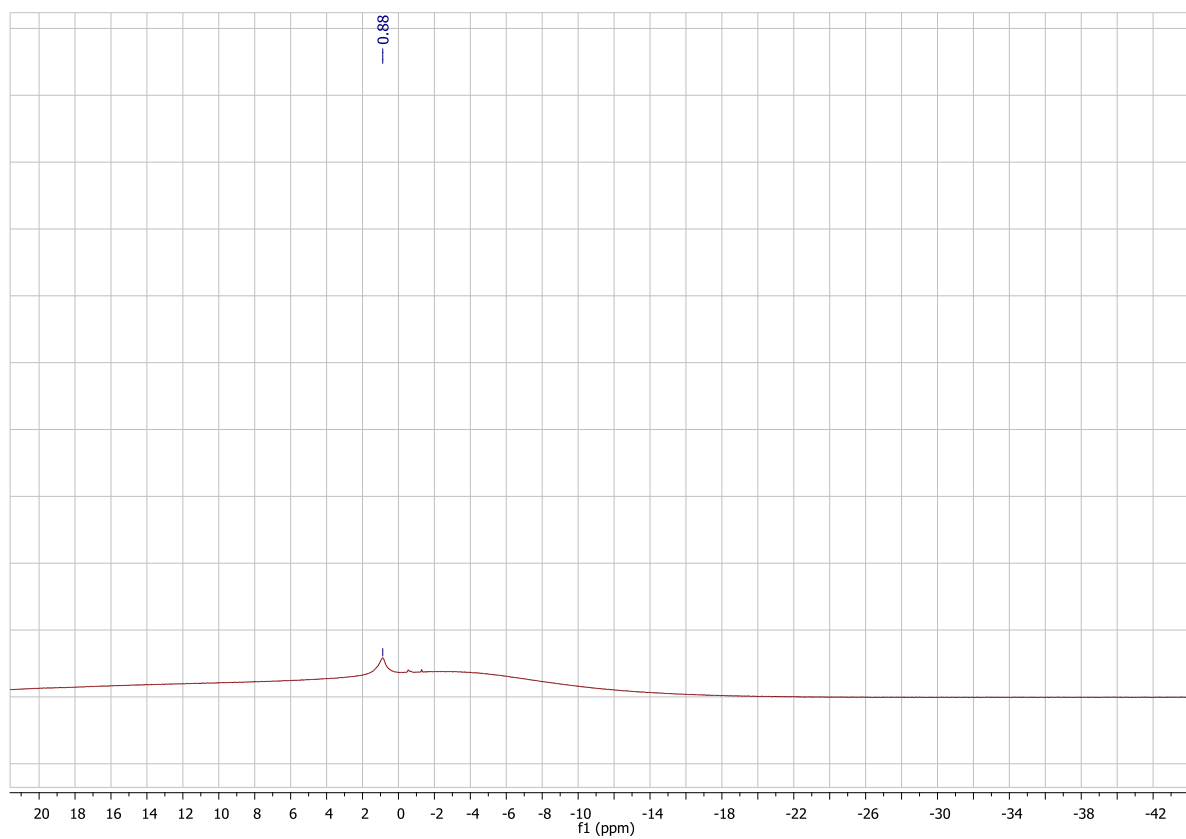


**Figure S17:**  $^{11}\text{B}\{^1\text{H}\}$  NMR spectrum (128 MHz,  $\text{DMSO}-d_6$ ) of **2d**.

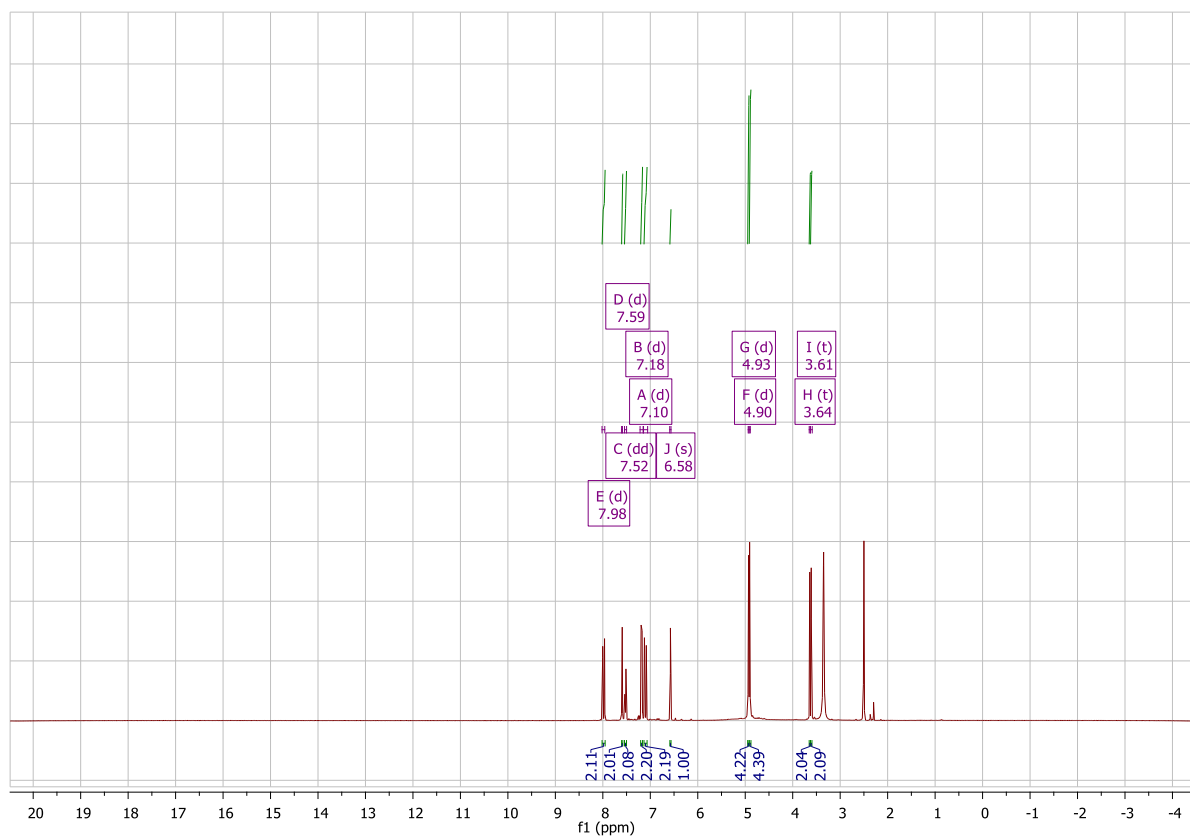


**Figure S18:** <sup>1</sup>H NMR spectrum (400 MHz, DMSO-*d*<sub>6</sub>) of **2e**.

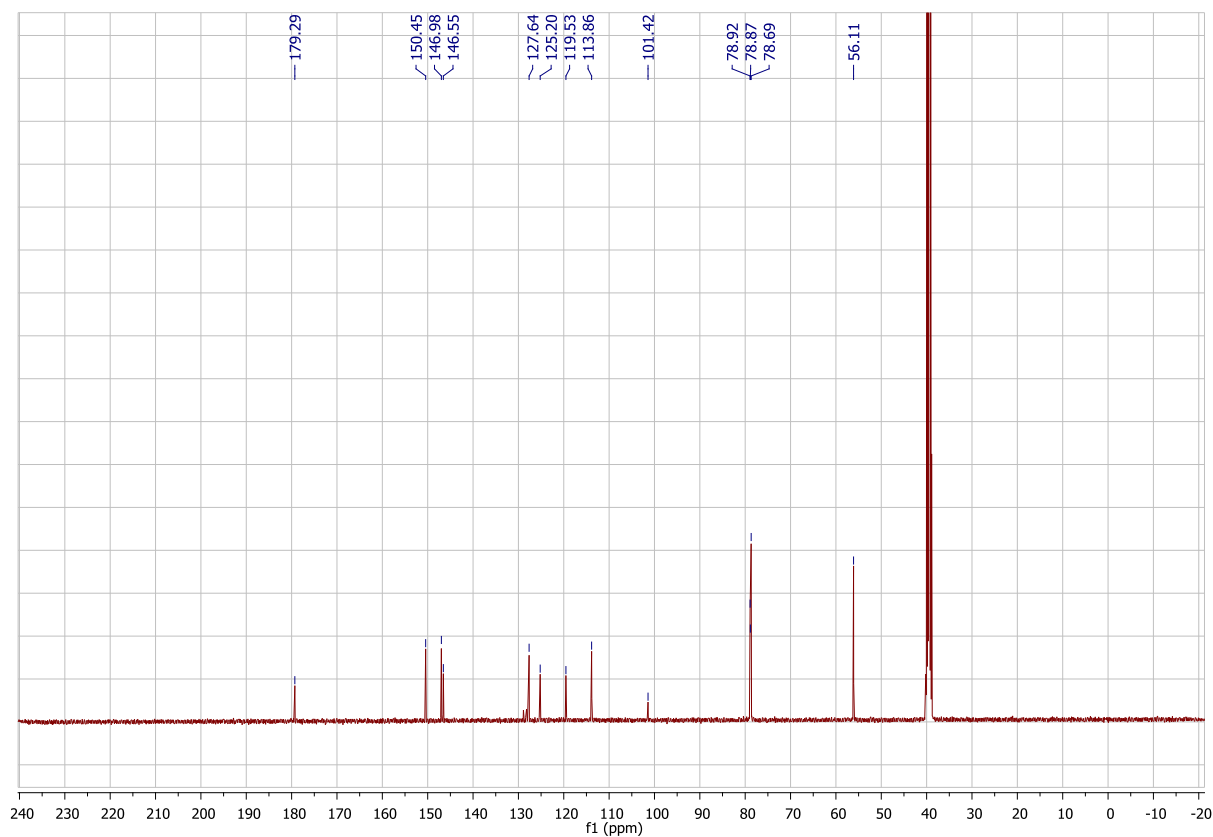


**Figure S19:** <sup>13</sup>C{<sup>1</sup>H} NMR spectrum (100 MHz, DMSO-*d*<sub>6</sub>) of **2e**.

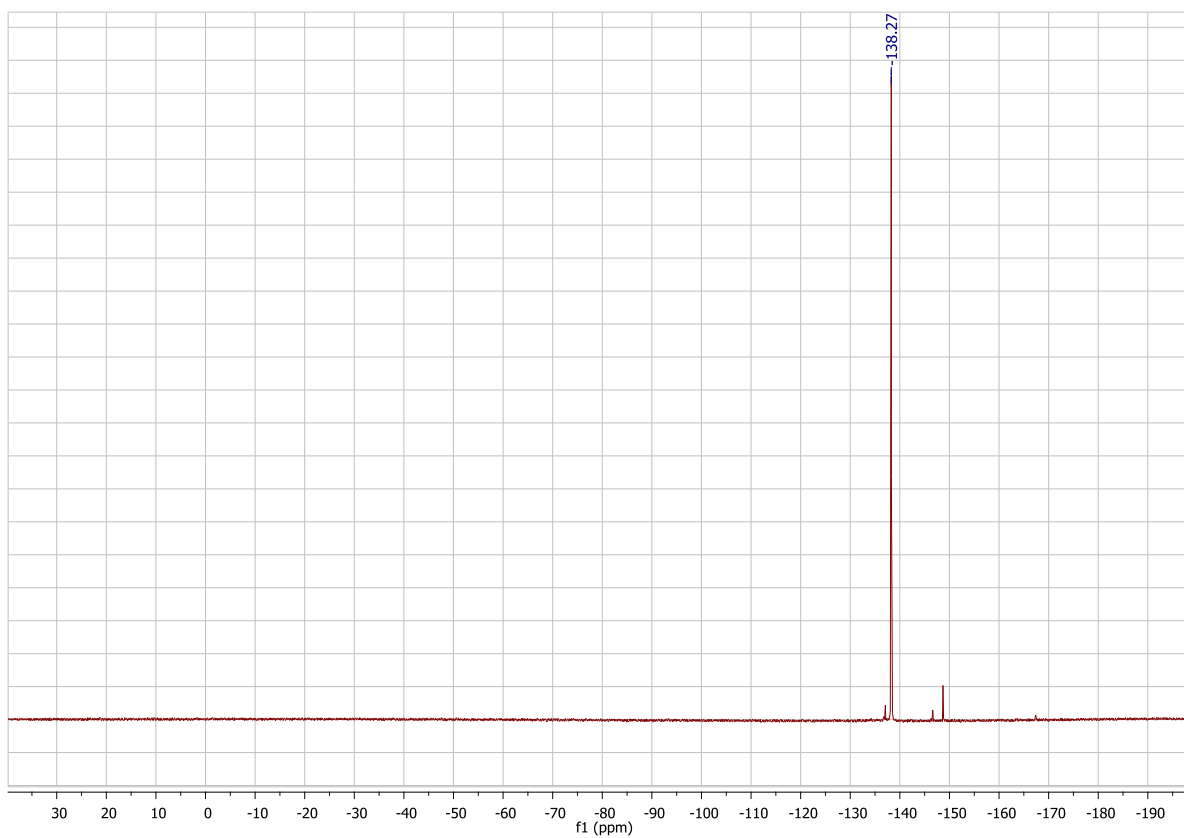


**Figure S20:**  $^{19}\text{F}\{^1\text{H}\}$  NMR spectrum (188 MHz,  $\text{DMSO}-d_6$ ) of **2e**.

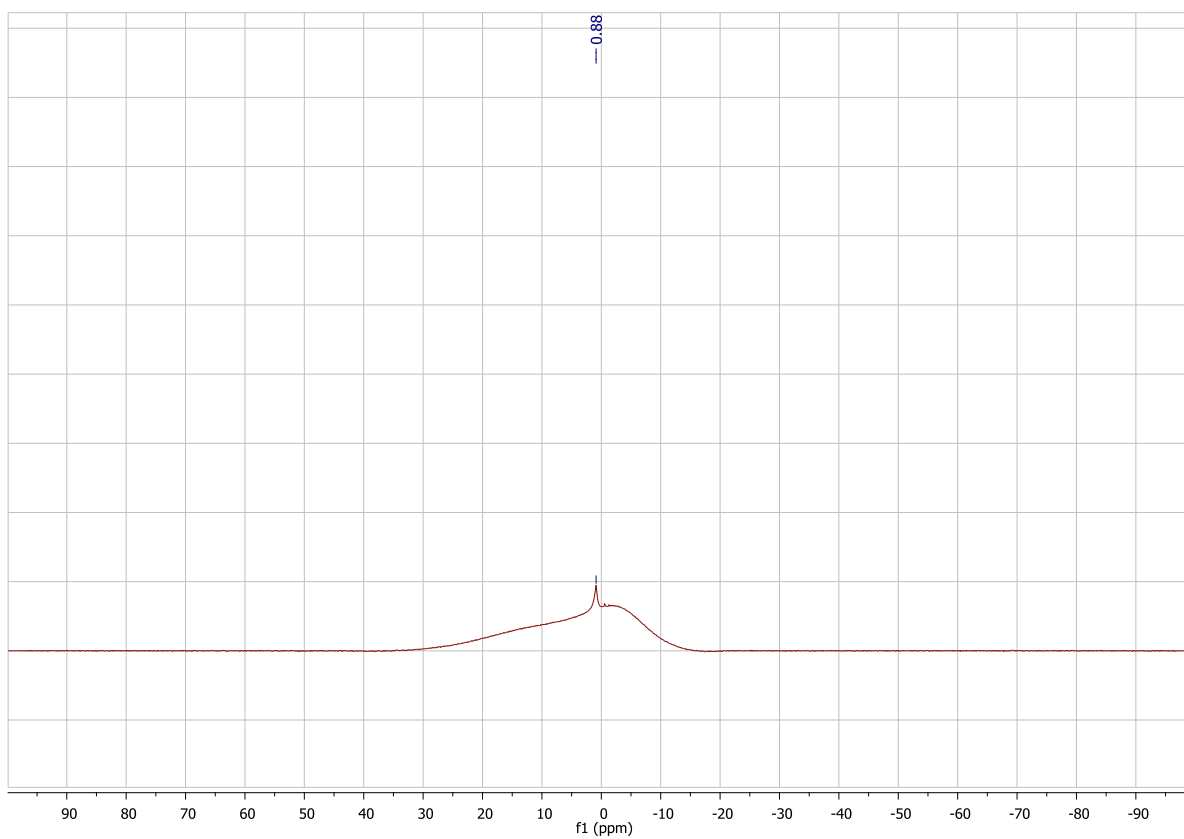


**Figure S21:**  $^{11}\text{B}\{^1\text{H}\}$  NMR spectrum (128 MHz,  $\text{DMSO}-d_6$ ) of **2e**.

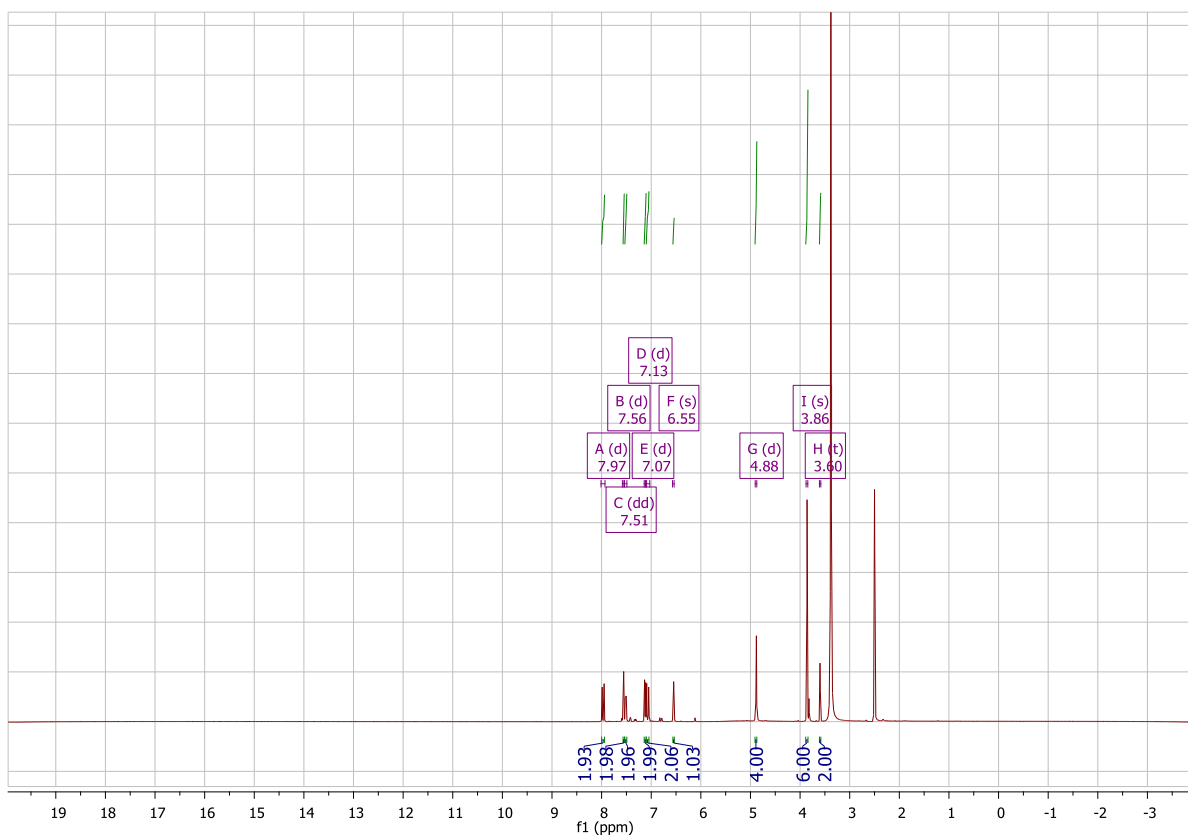


**Figure S22:** <sup>1</sup>H NMR spectrum (400 MHz, DMSO-*d*<sub>6</sub>) of **2f**.

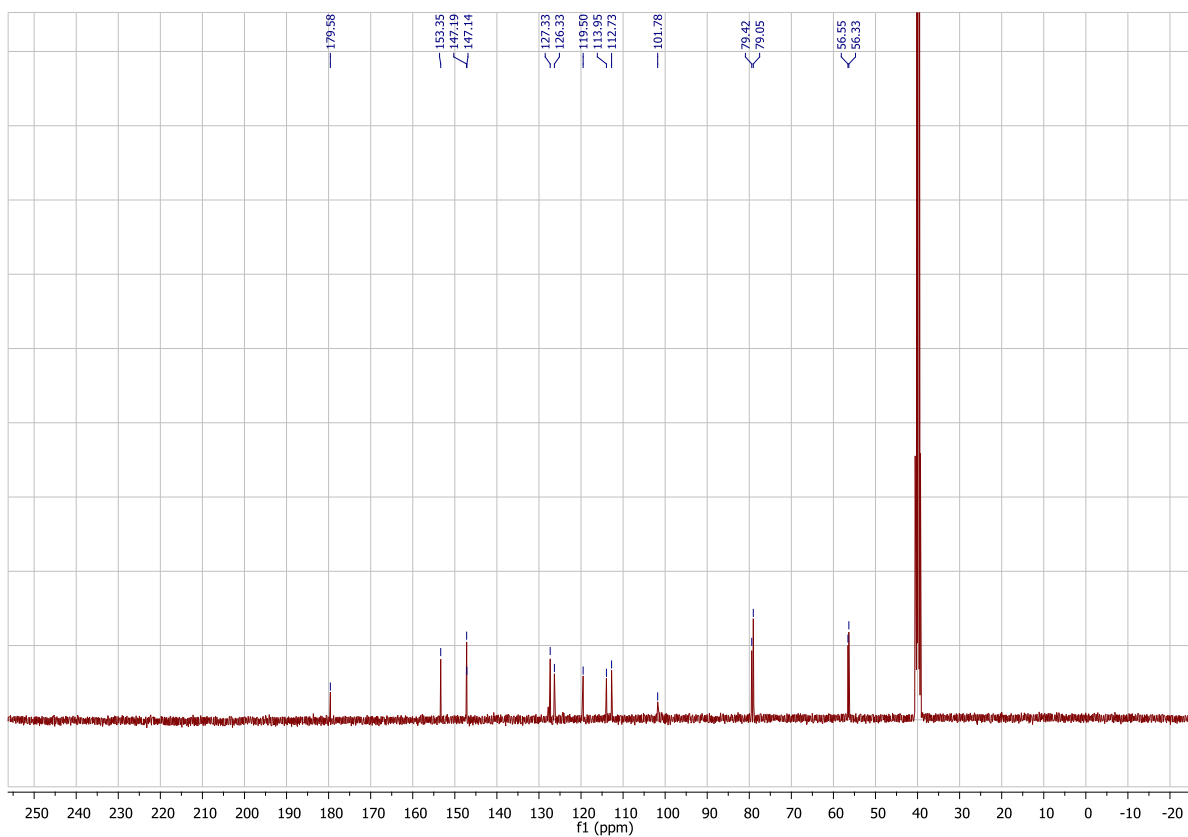


**Figure S23:** <sup>13</sup>C{<sup>1</sup>H} NMR spectrum (101 MHz, DMSO-*d*<sub>6</sub>) of **2f**.

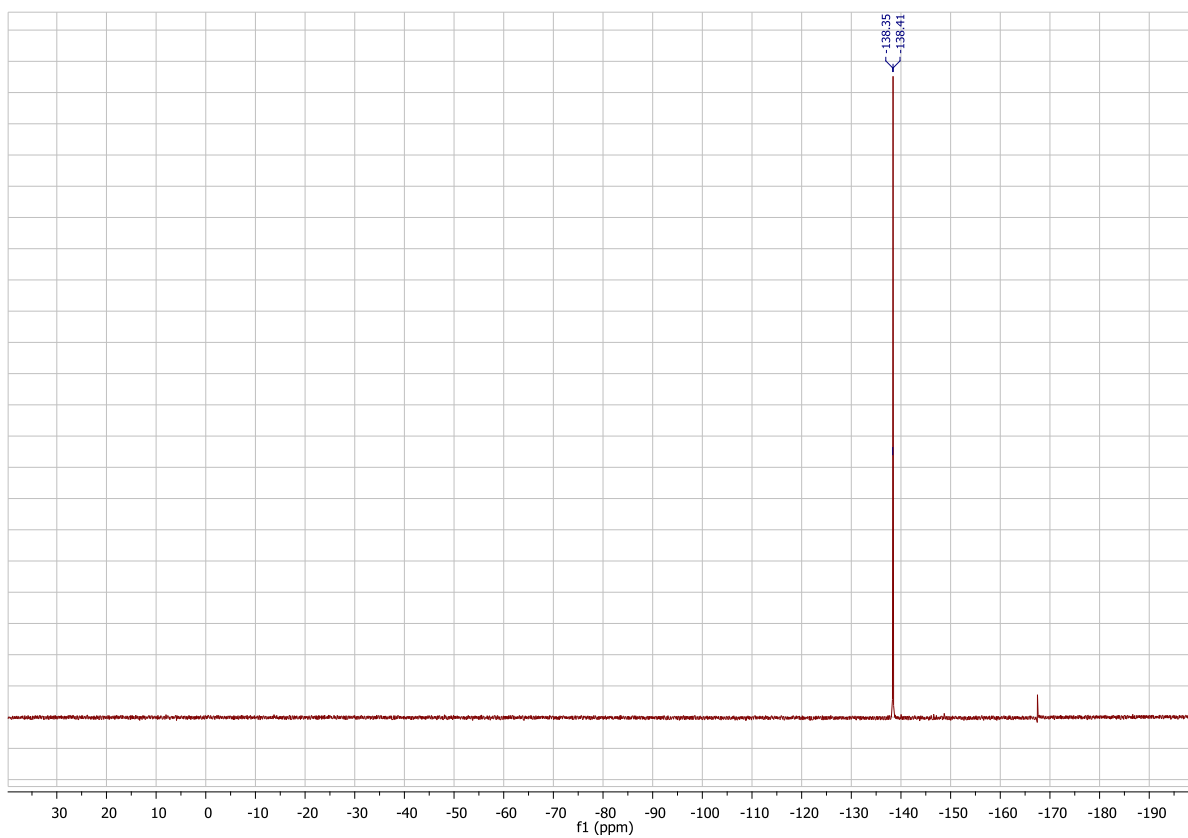


**Figure S24:**  $^{19}\text{F}\{^1\text{H}\}$  NMR spectrum (188 MHz,  $\text{DMSO}-d_6$ ) of **2f**.

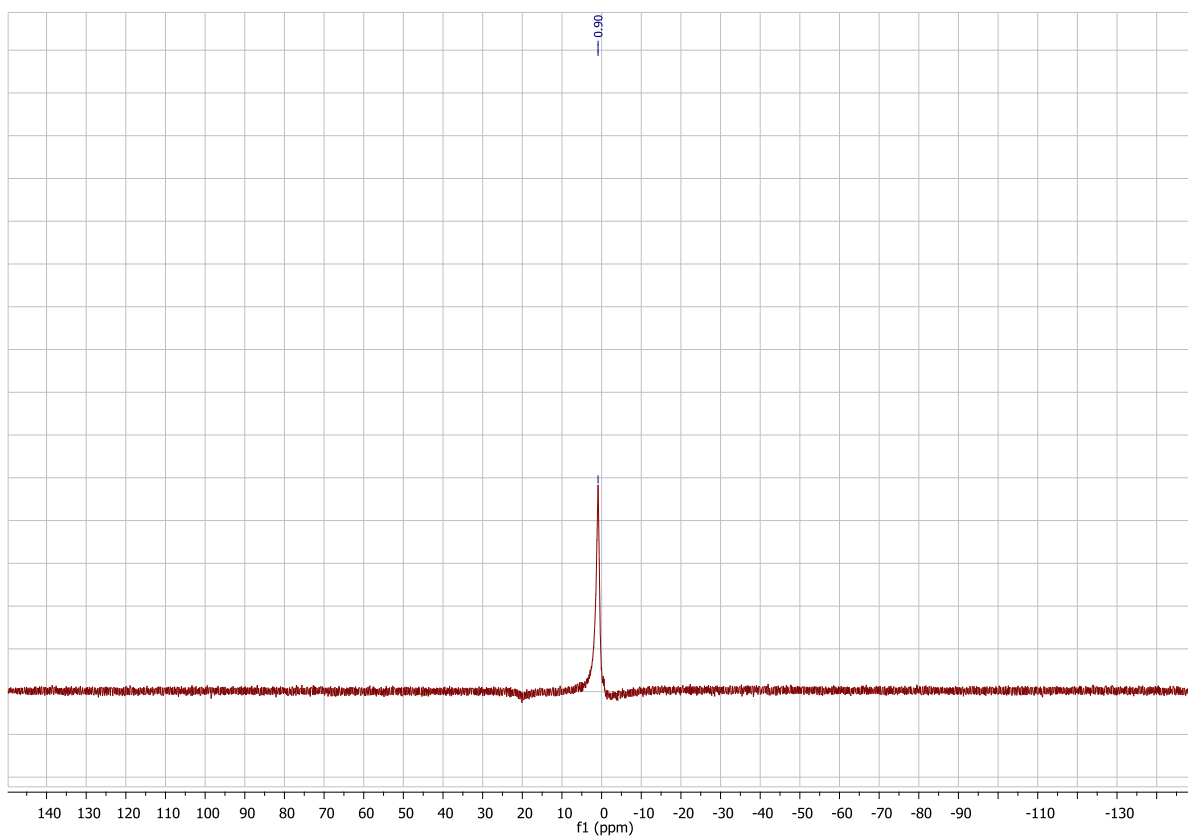


**Figure S25:**  $^{11}\text{B}\{^1\text{H}\}$  NMR spectrum (128 MHz,  $\text{DMSO}-d_6$ ) of **2f**.

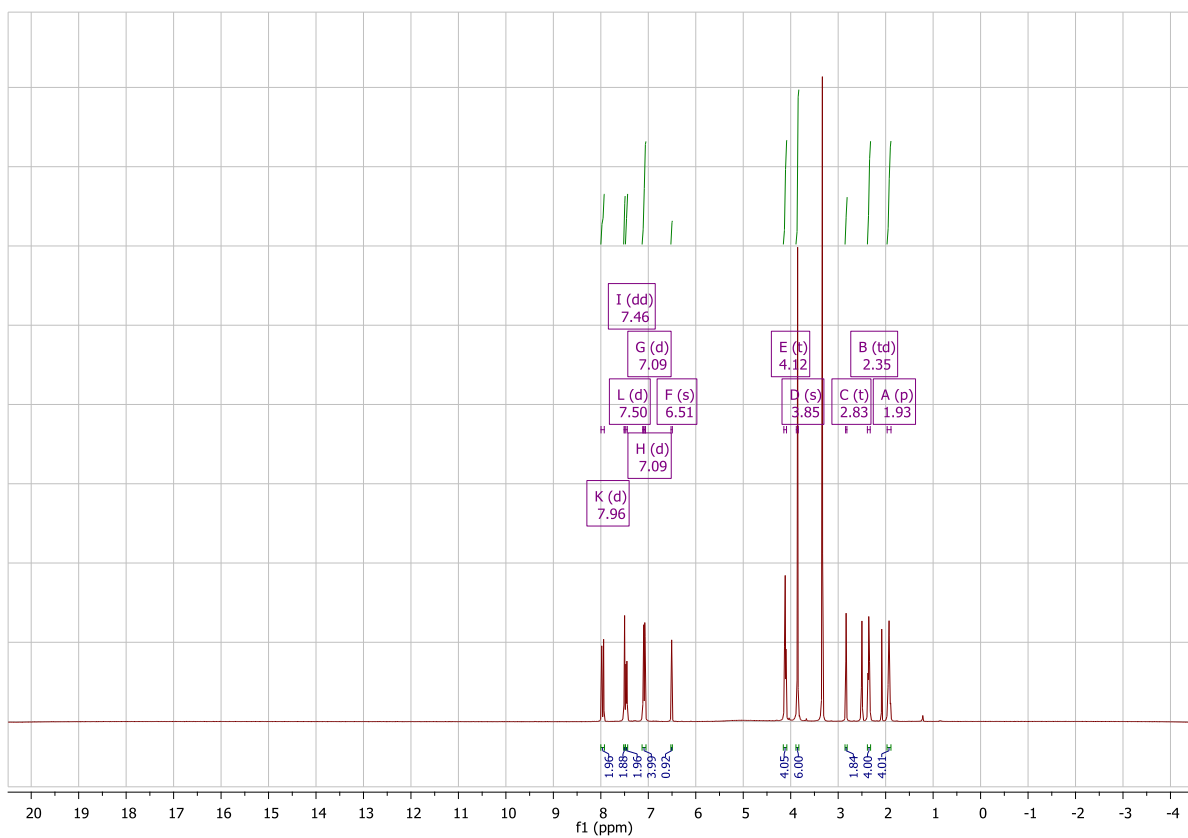


**Figure S26:** <sup>1</sup>H NMR spectrum 400 MHz, DMSO-*d*<sub>6</sub>) of **2g**.

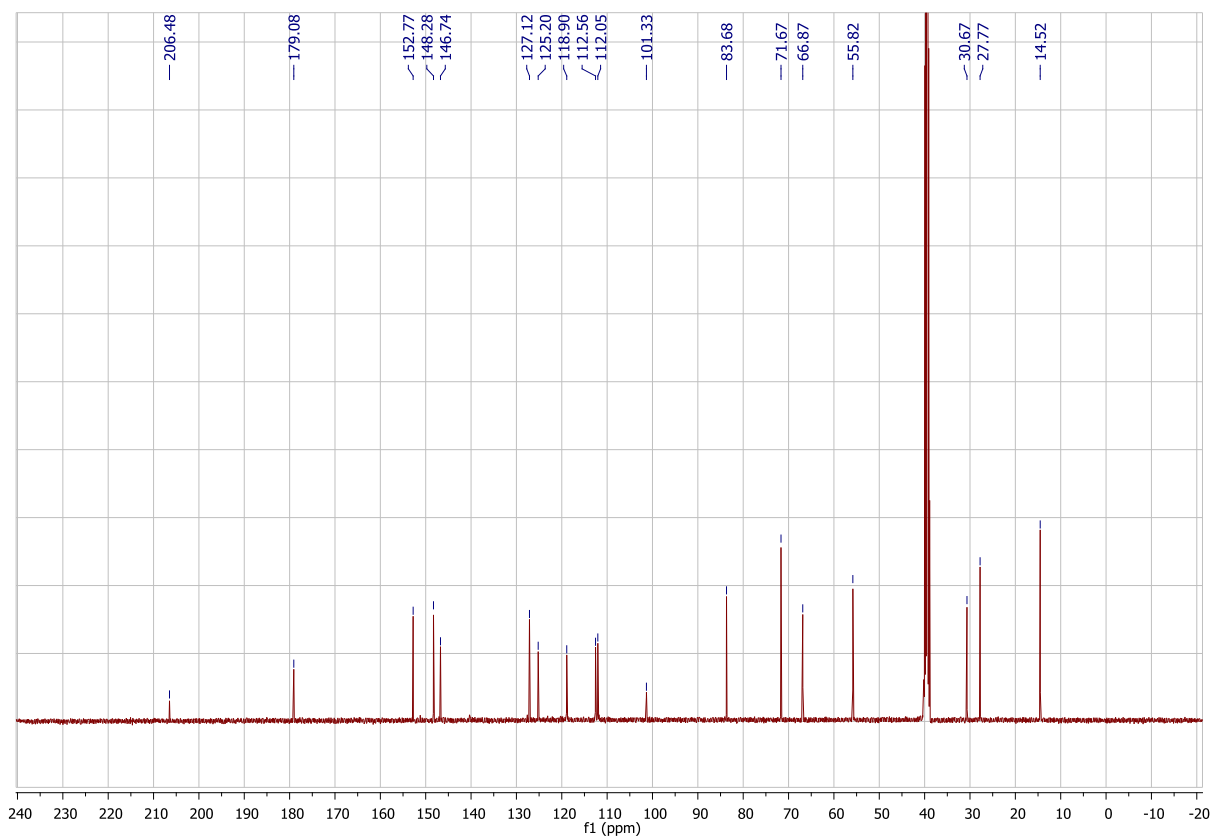


**Figure S27:** <sup>13</sup>C{<sup>1</sup>H} NMR spectrum (100 MHz, DMSO-*d*<sub>6</sub>) of **2g**.

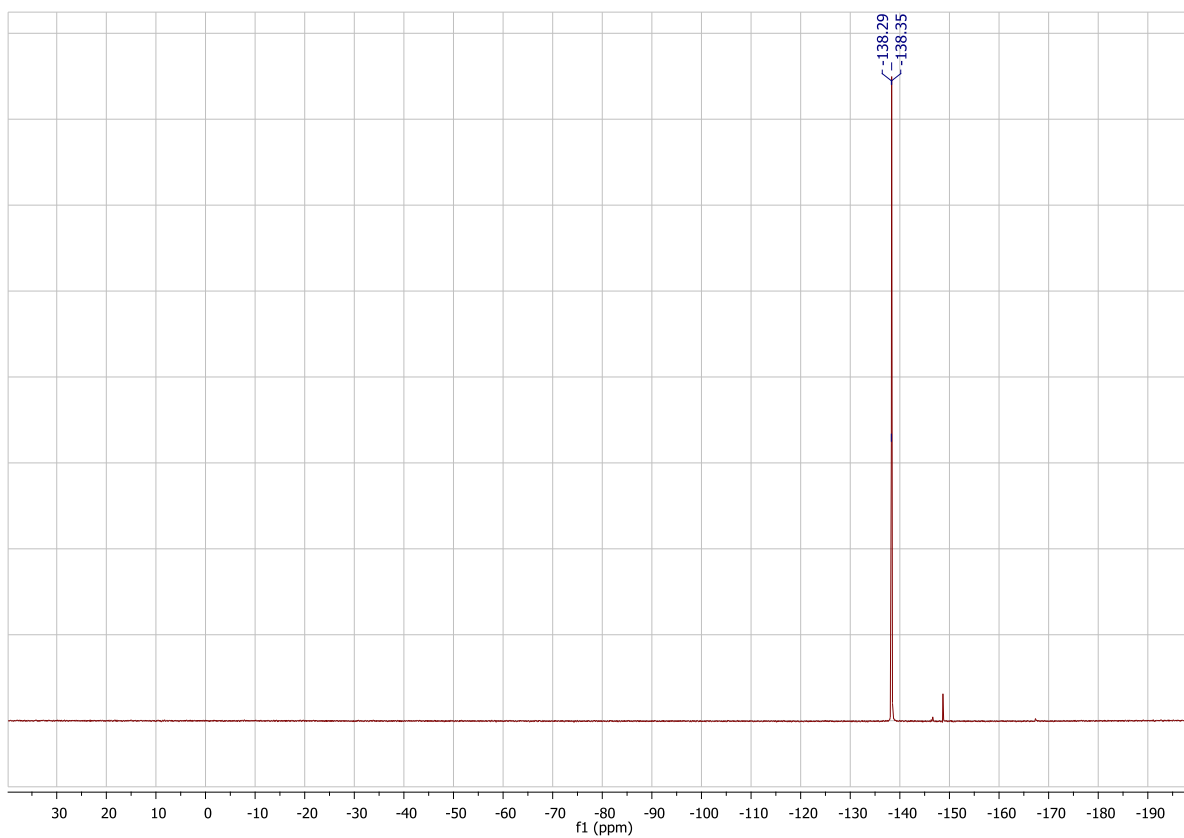


**Figure S28:**  $^{19}\text{F}\{^1\text{H}\}$  NMR spectrum (188 MHz,  $\text{DMSO}-d_6$ ) of **2g**.

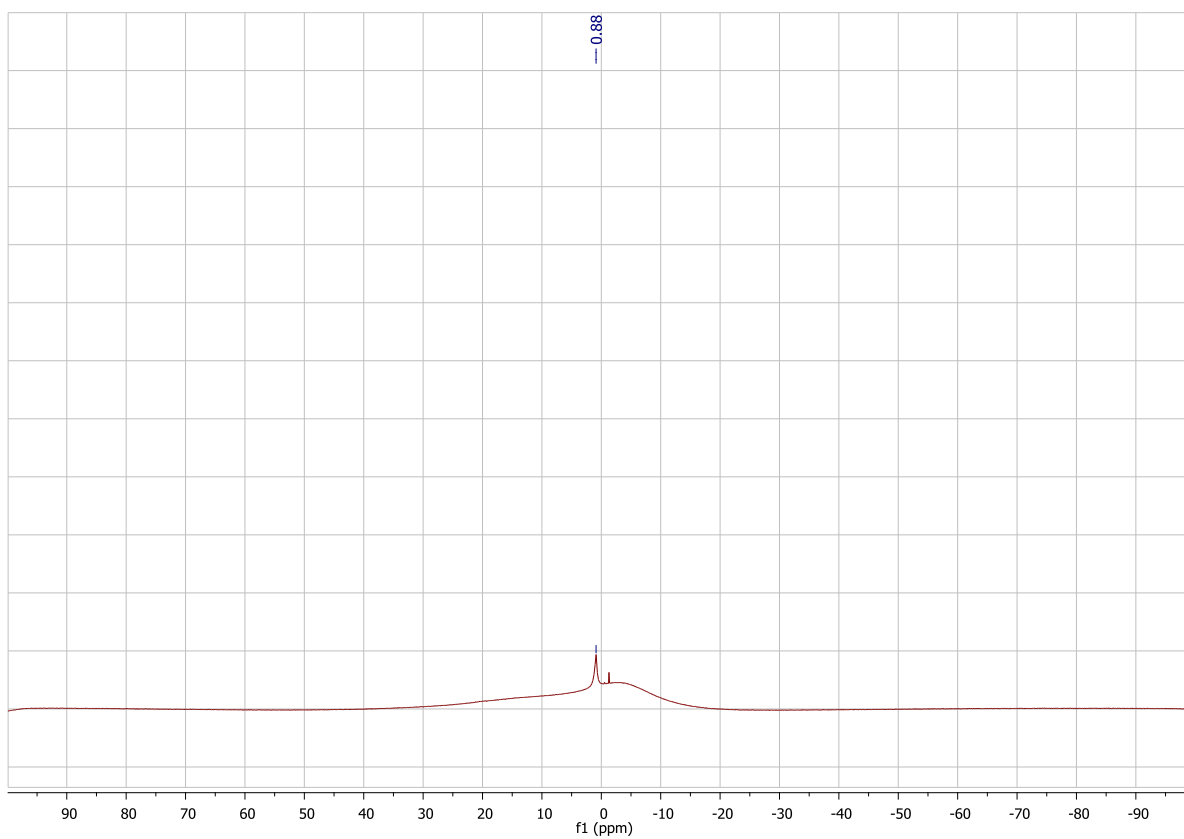


**Figure S29:**  $^{11}\text{B}\{^1\text{H}\}$  NMR spectrum (128 MHz,  $\text{DMSO}-d_6$ ) of **2g**.

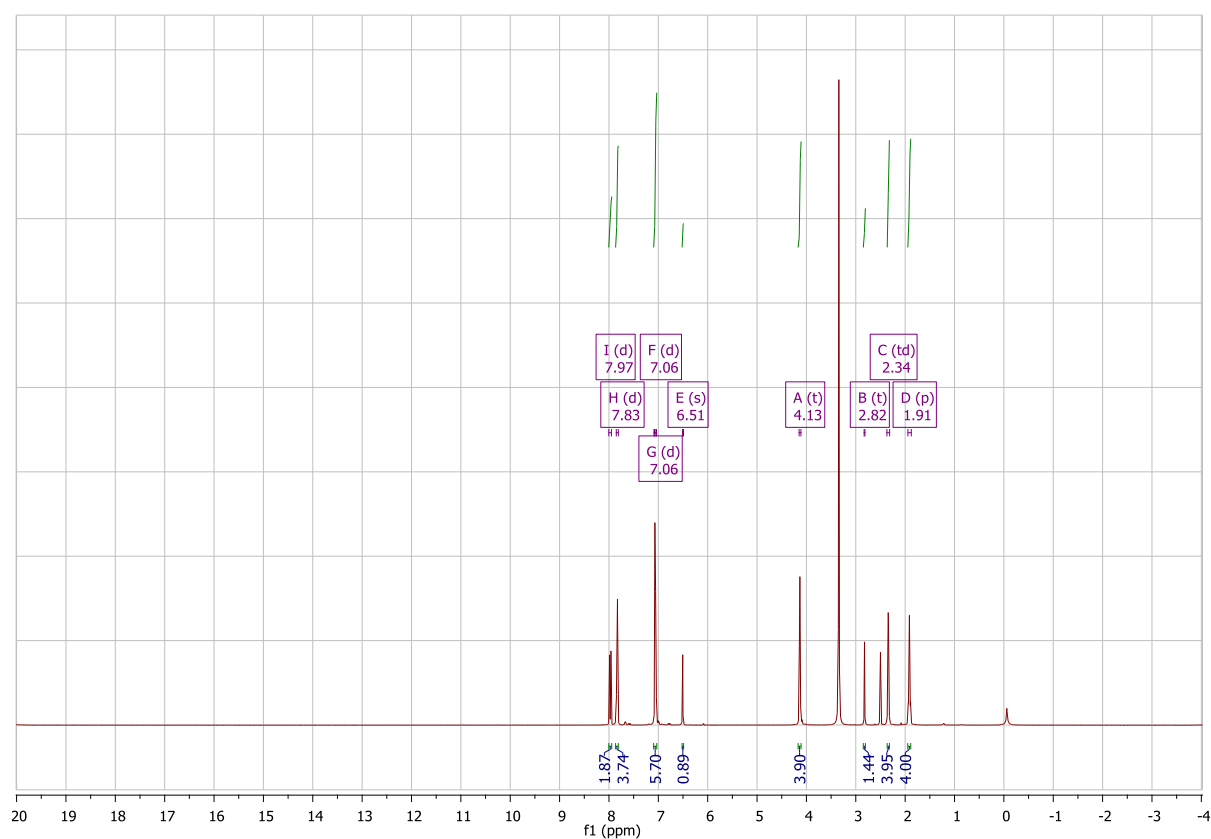


**Figure S30:** <sup>1</sup>H NMR spectrum (600 MHz, DMSO-*d*<sub>6</sub>) of **2h**.

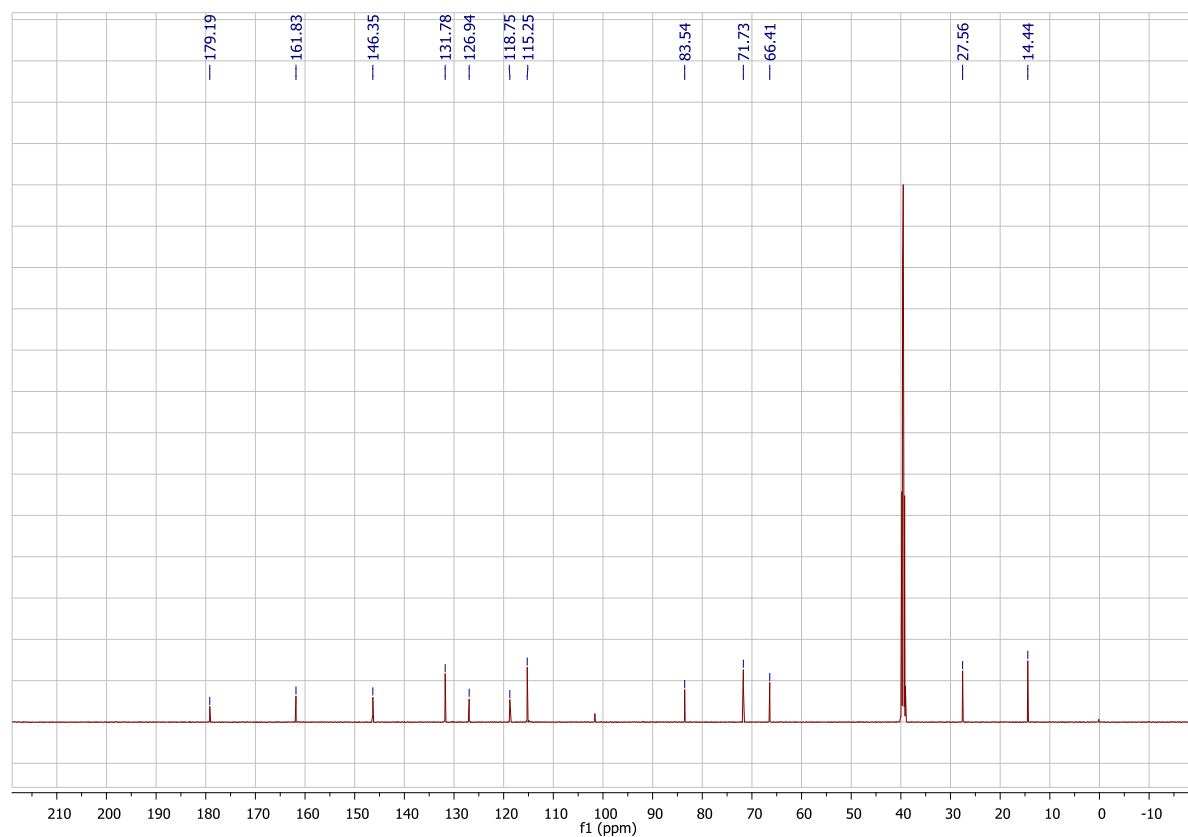


**Figure S31:** <sup>13</sup>C{<sup>1</sup>H} NMR spectrum (150 MHz, DMSO-*d*<sub>6</sub>) of **2h**.



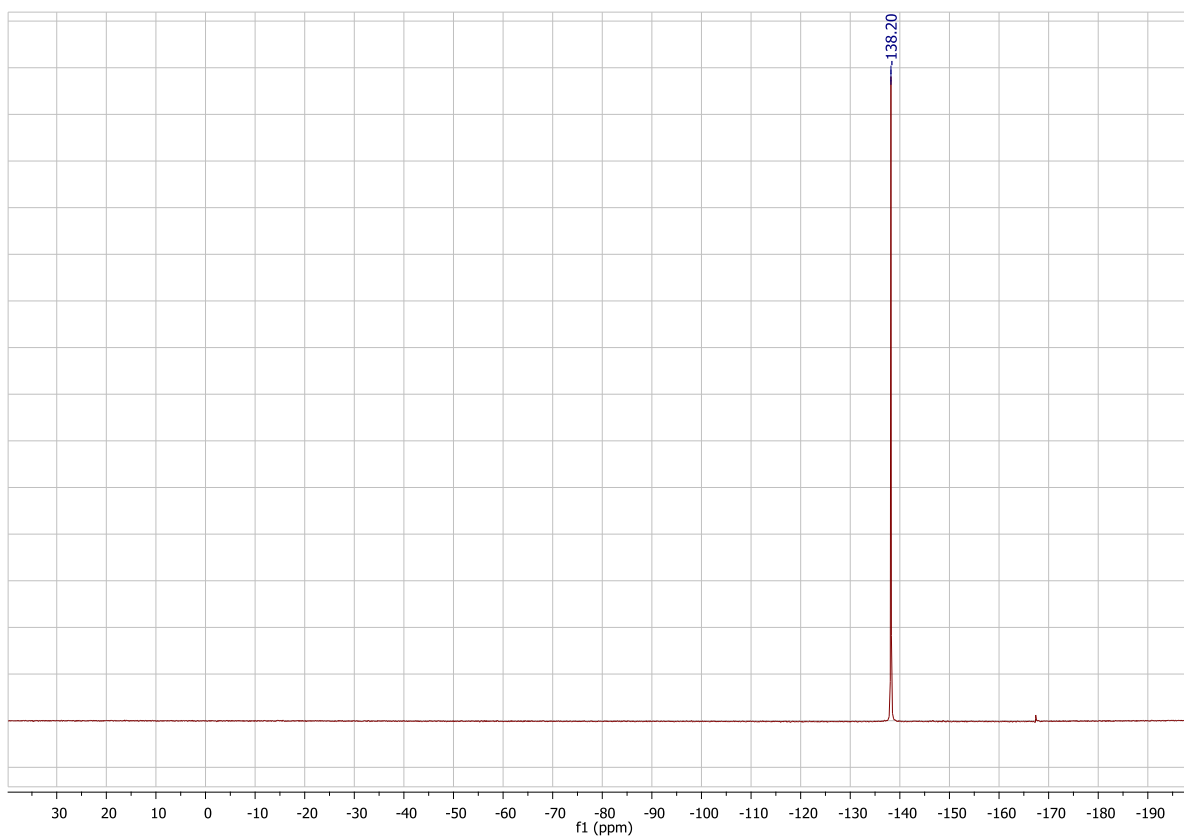


**Figure S32:**  $^{19}\text{F}\{^1\text{H}\}$  NMR spectrum (188 MHz,  $\text{DMSO}-d_6$ ) of **2h**.

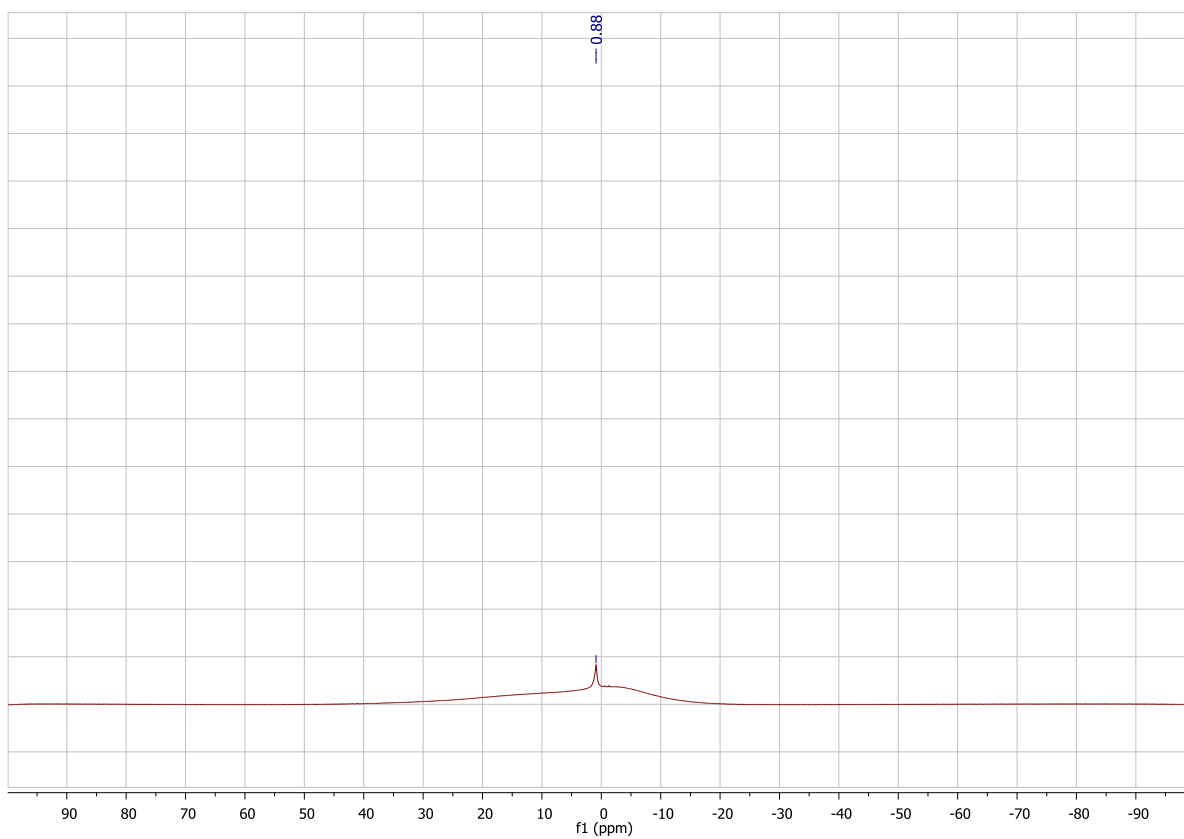


**Figure S33:**  $^{11}\text{B}\{^1\text{H}\}$  NMR spectrum (128 MHz,  $\text{DMSO}-d_6$ ) of **2h**.

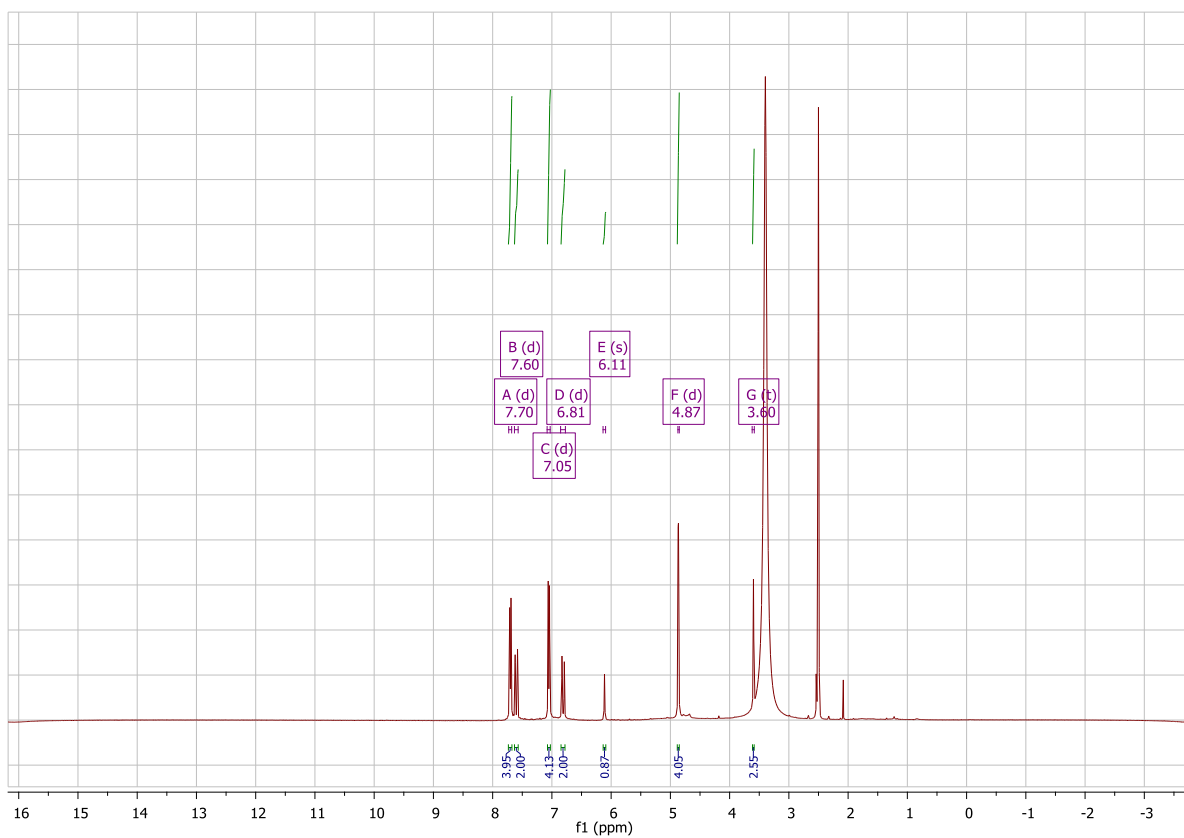


**Figure S34:** <sup>1</sup>H NMR spectrum (400 MHz, DMSO-*d*<sub>6</sub>) of **3a**.

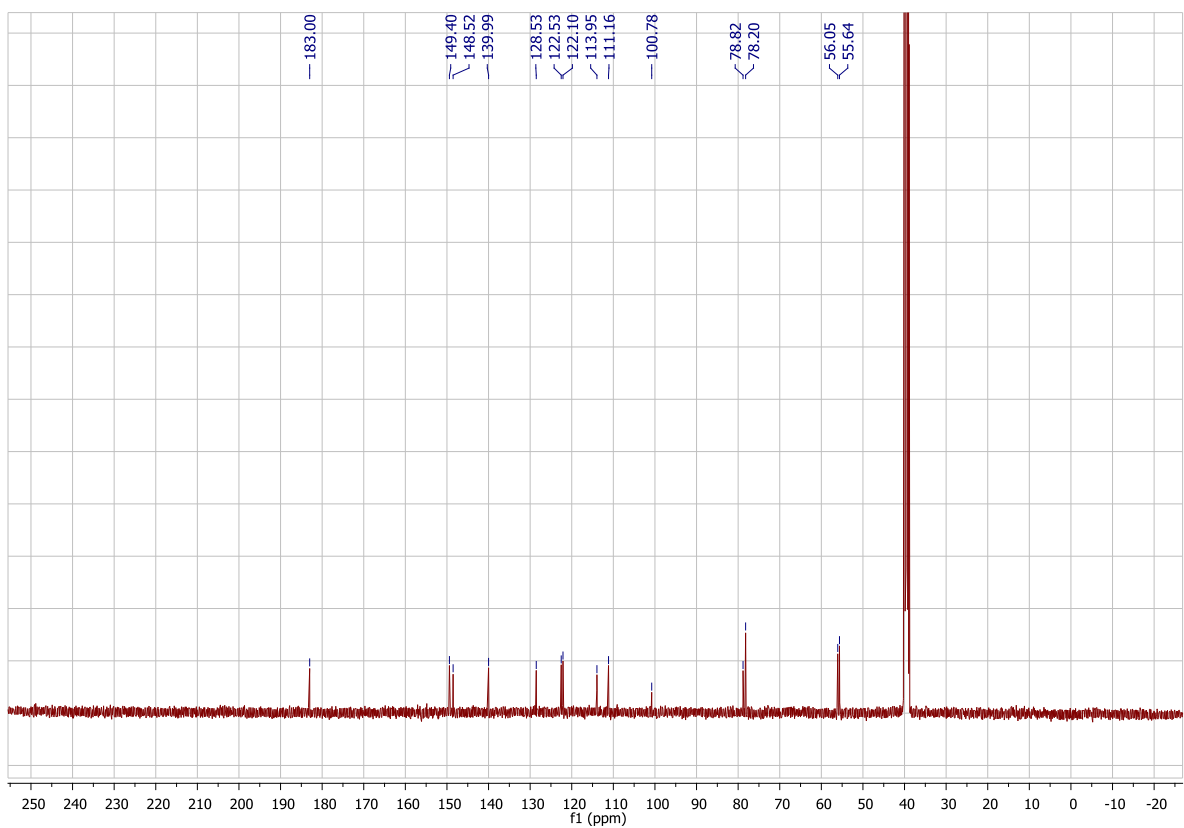


**Figure S35:** <sup>13</sup>C{<sup>1</sup>H} NMR spectrum (100 MHz, DMSO-*d*<sub>6</sub>) of **3a**.

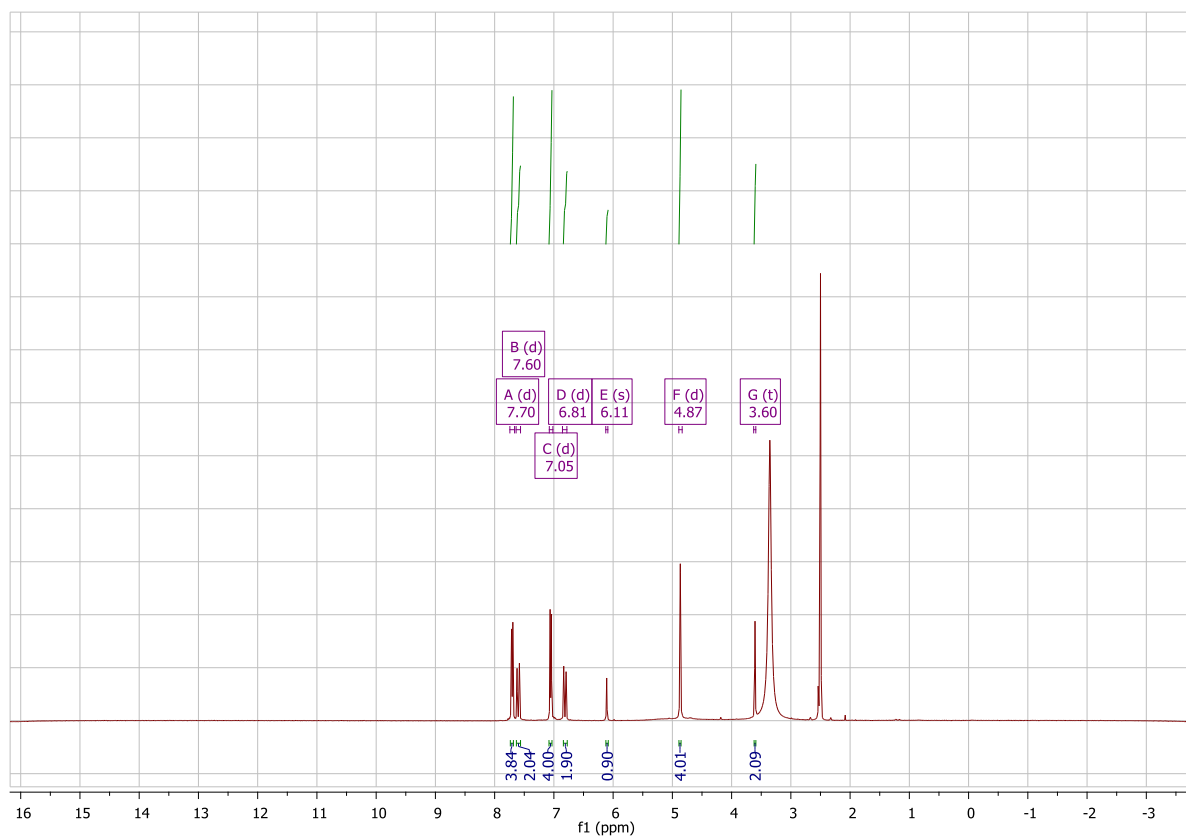


**Figure S36:** <sup>1</sup>H NMR spectrum (400 MHz, DMSO-*d*<sub>6</sub>) of **3b**.

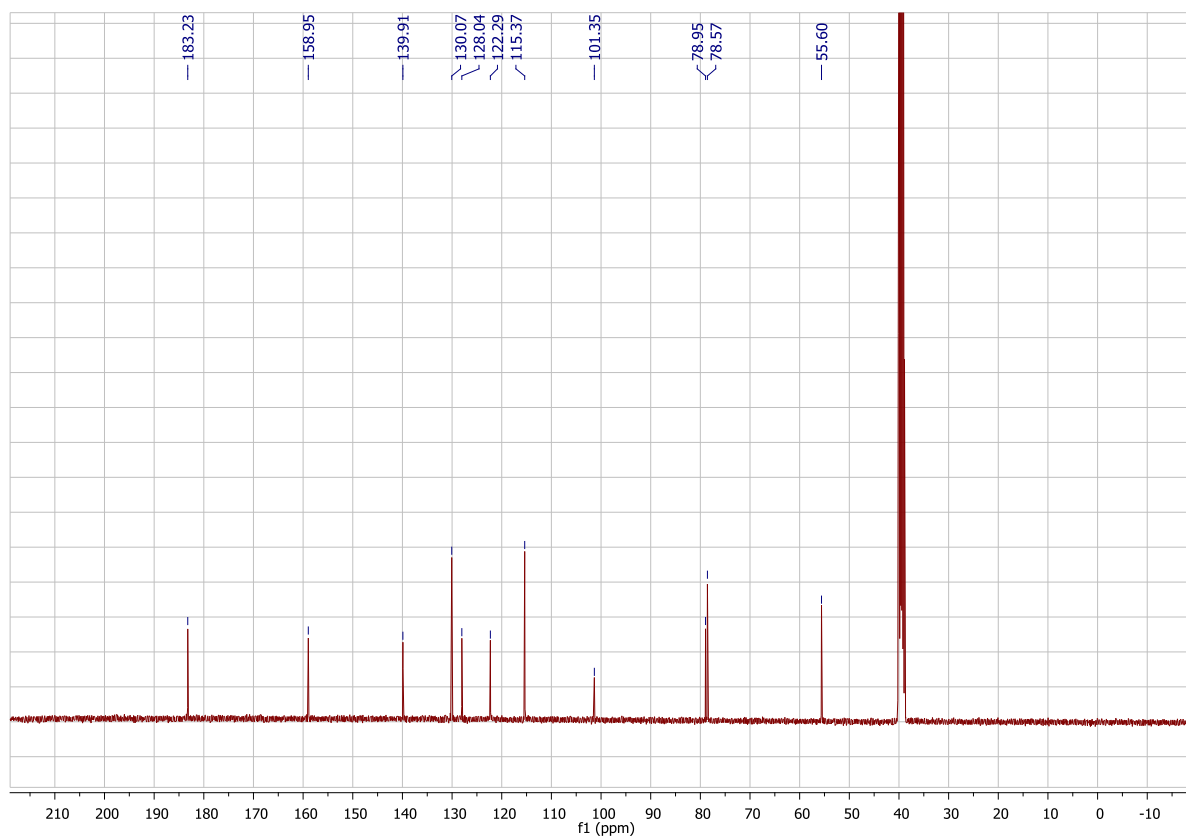


**Figure S37:** <sup>13</sup>C{<sup>1</sup>H} NMR spectrum (100 MHz, DMSO-*d*<sub>6</sub>) of **3b**.

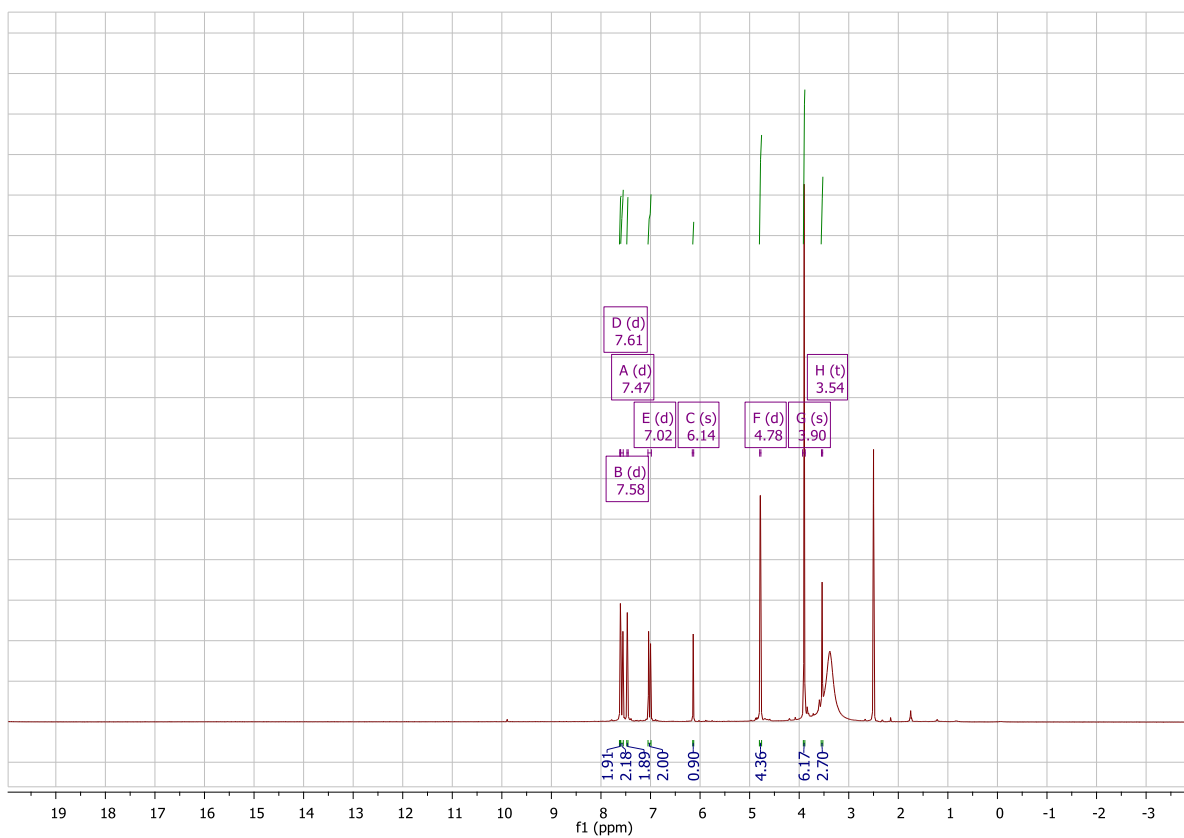


**Figure S38:** <sup>1</sup>H NMR spectrum (400 MHz, DMSO-*d*<sub>6</sub>) of **3c**.

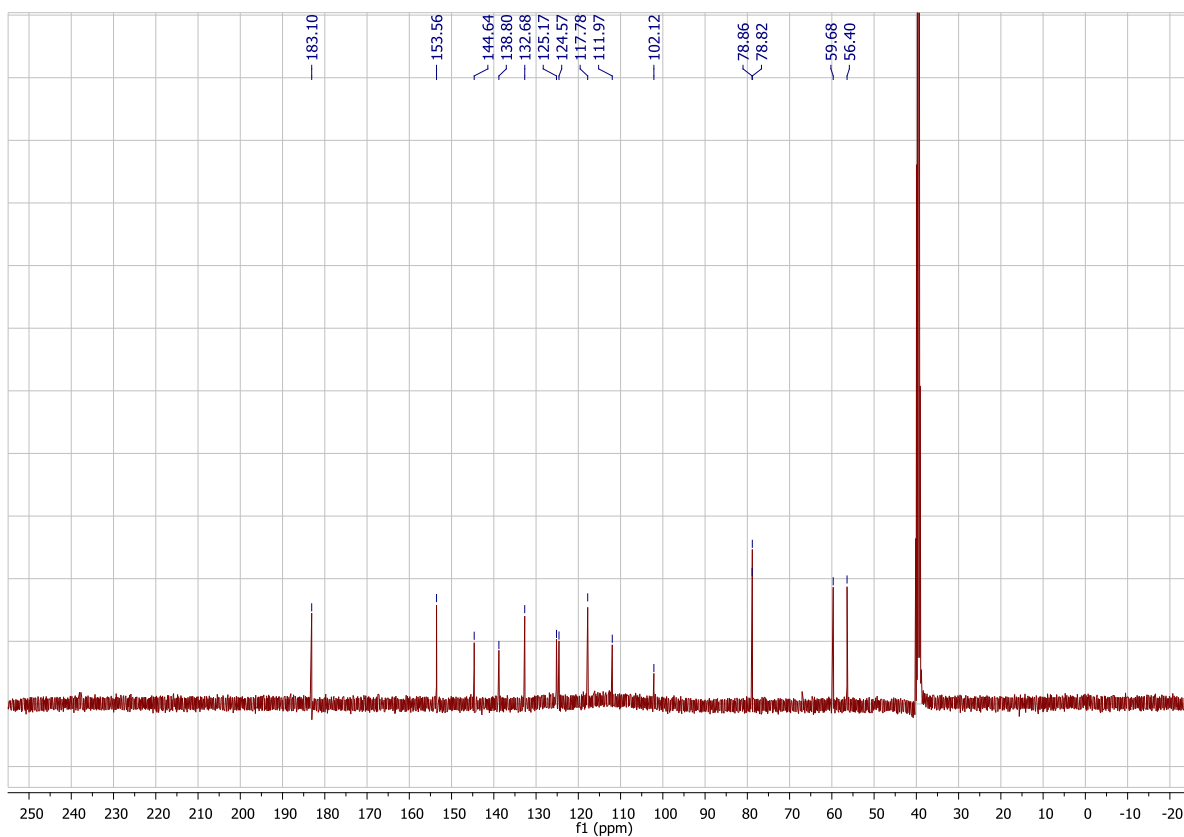


**Figure S39:** <sup>13</sup>C{<sup>1</sup>H} NMR spectrum (100 MHz, DMSO-*d*<sub>6</sub>) of **3c**.

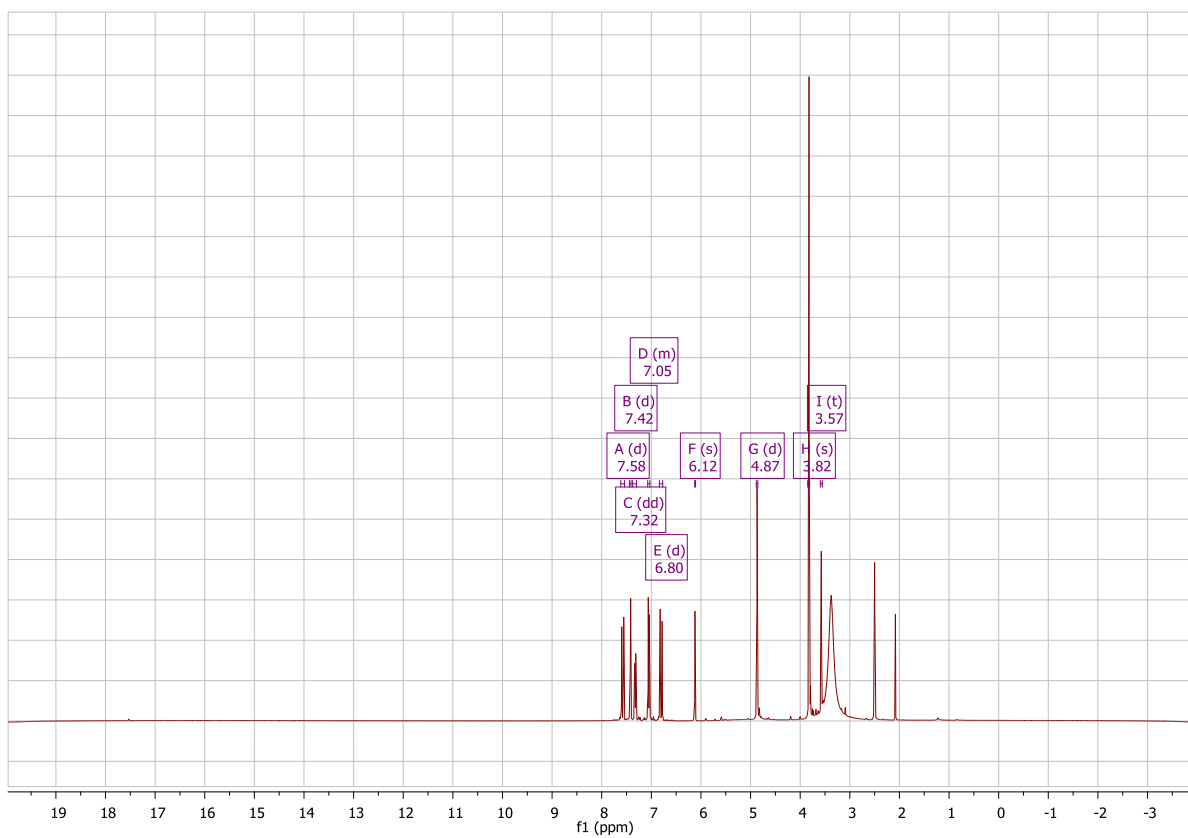


**Figure S40:** <sup>1</sup>H NMR spectrum (400 MHz, DMSO-*d*<sub>6</sub>) of **3d**.

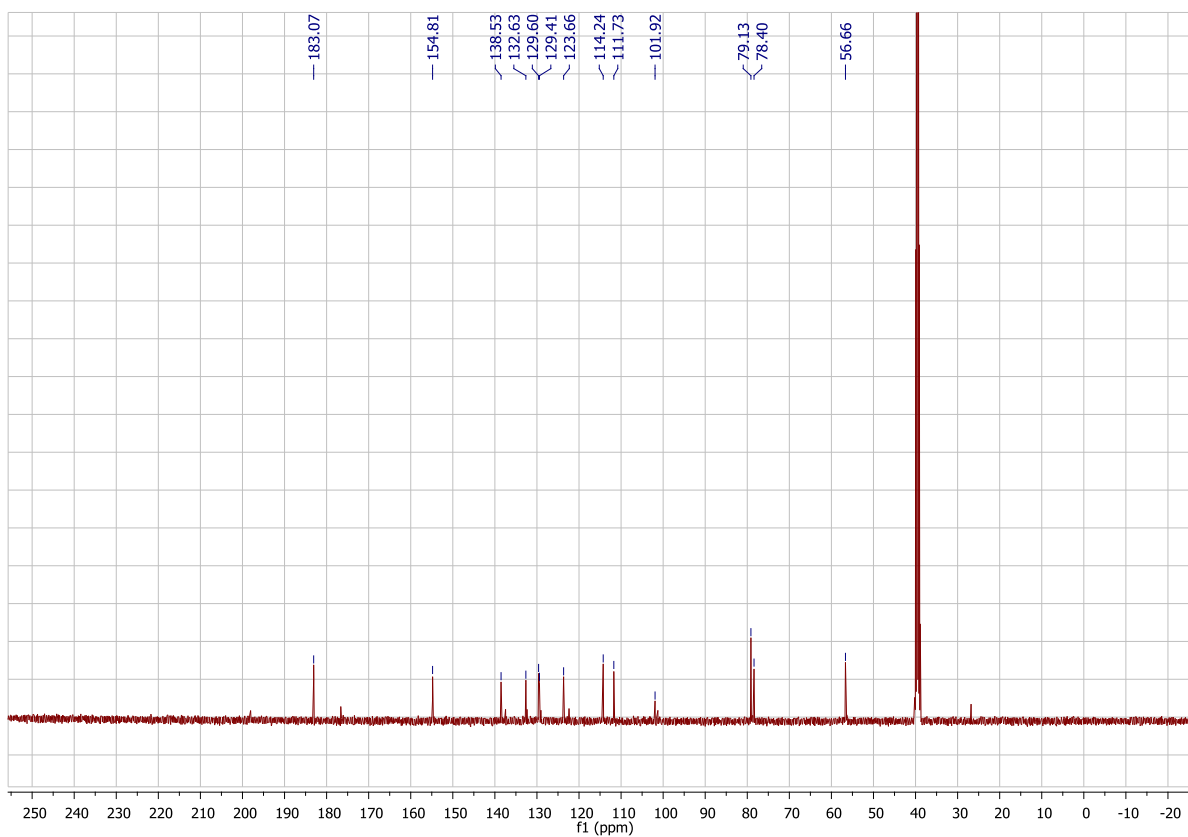


**Figure S41:** <sup>13</sup>C{<sup>1</sup>H} NMR spectrum (100 MHz, DMSO-*d*<sub>6</sub>) of **3d**.

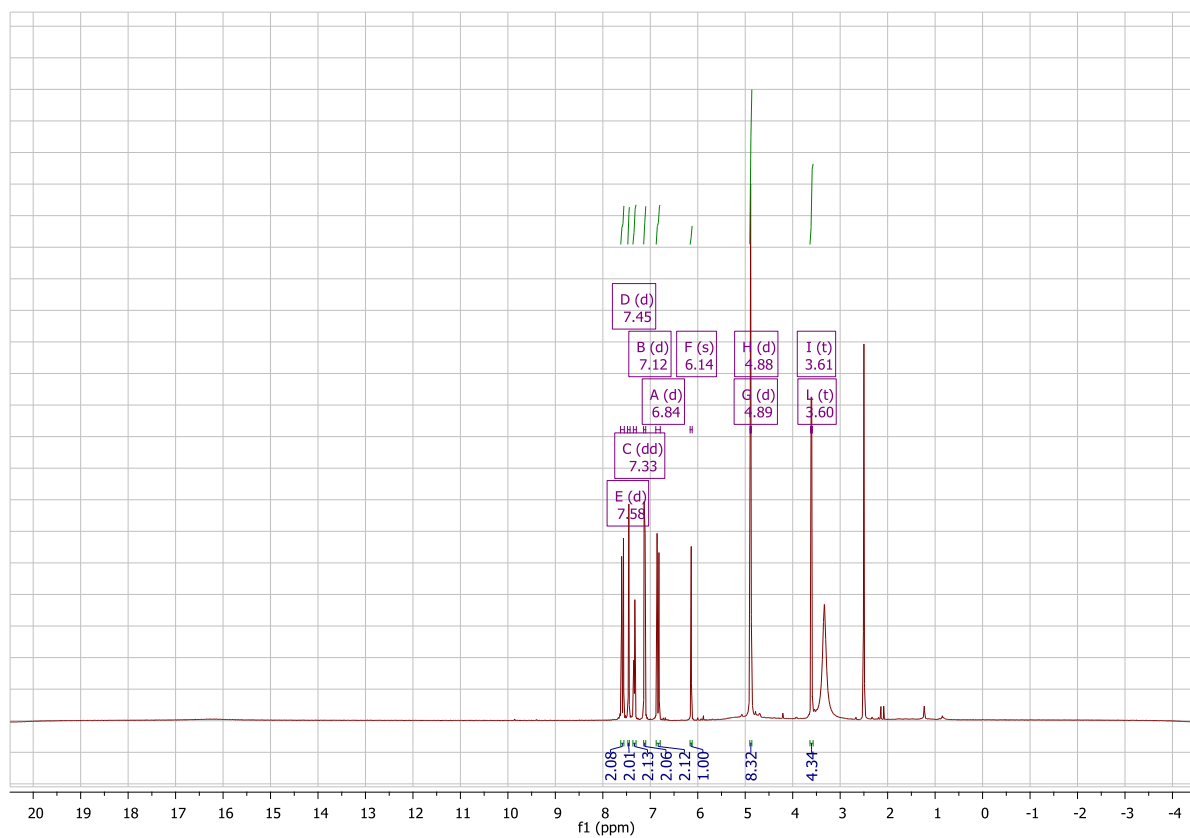


**Figure S42:** <sup>1</sup>H NMR spectrum (400 MHz, DMSO-*d*<sub>6</sub>) of **3e**.

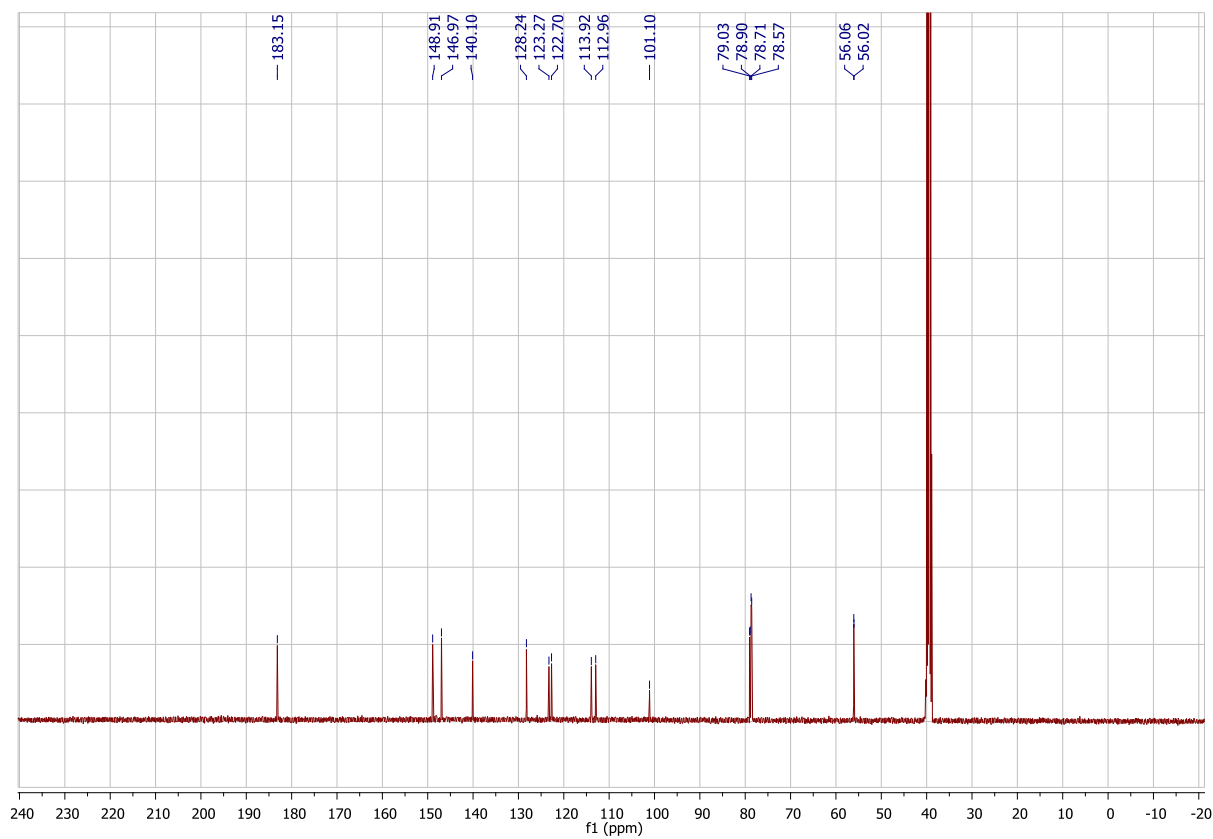


**Figure S43:** <sup>13</sup>C{<sup>1</sup>H} NMR spectrum (100 MHz, DMSO-*d*<sub>6</sub>) of **3e**.

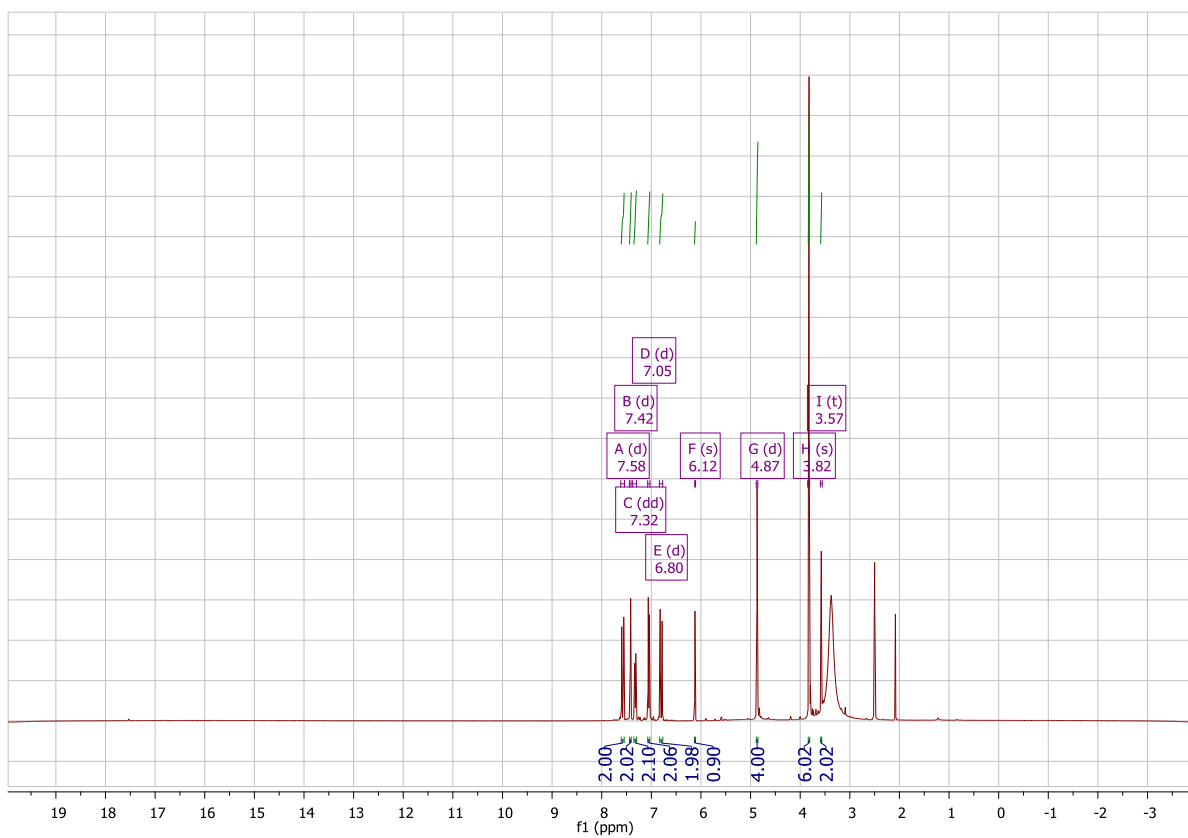


**Figure S44:** <sup>1</sup>H NMR spectrum (400 MHz, DMSO-*d*<sub>6</sub>) of **3f**.

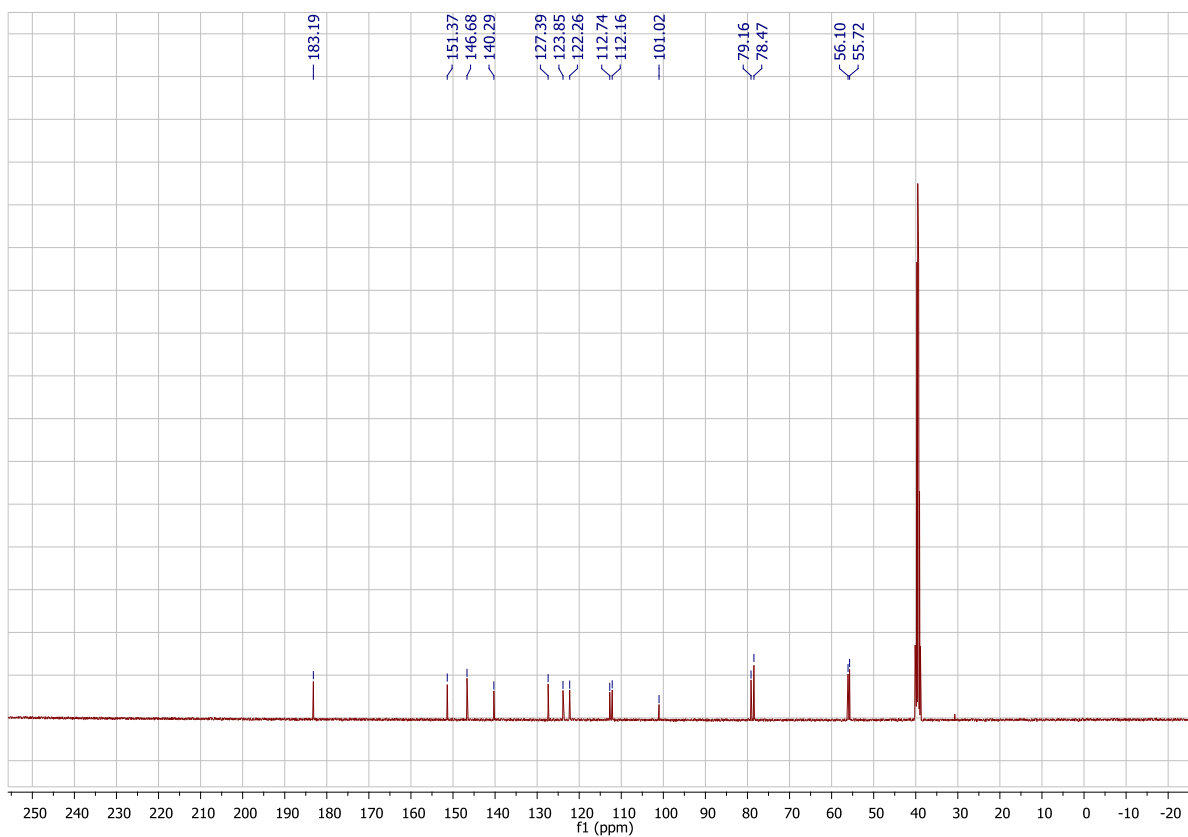


**Figure S45:** <sup>13</sup>C{<sup>1</sup>H} NMR spectrum (100 MHz, DMSO-*d*<sub>6</sub>) of **3f**.

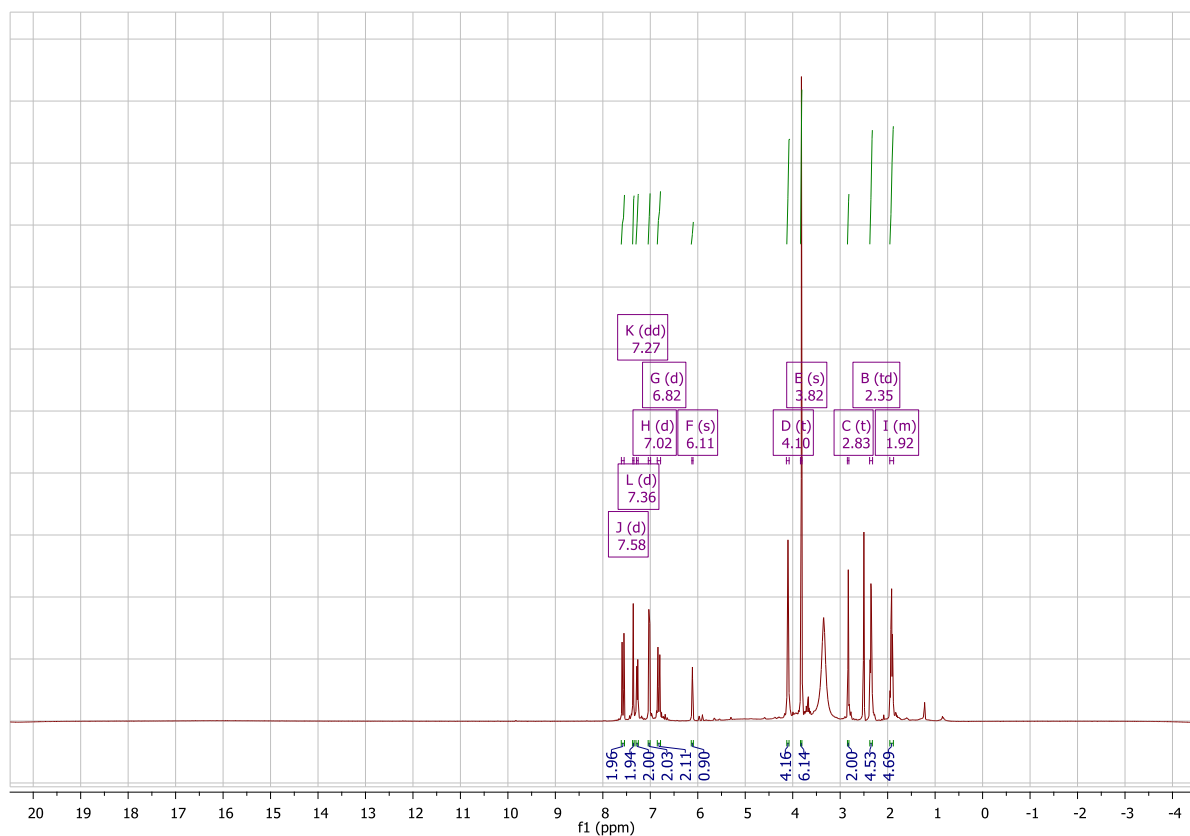


**Figure S46:** <sup>1</sup>H NMR spectrum (400 MHz, DMSO-*d*<sub>6</sub>) of **3g**.

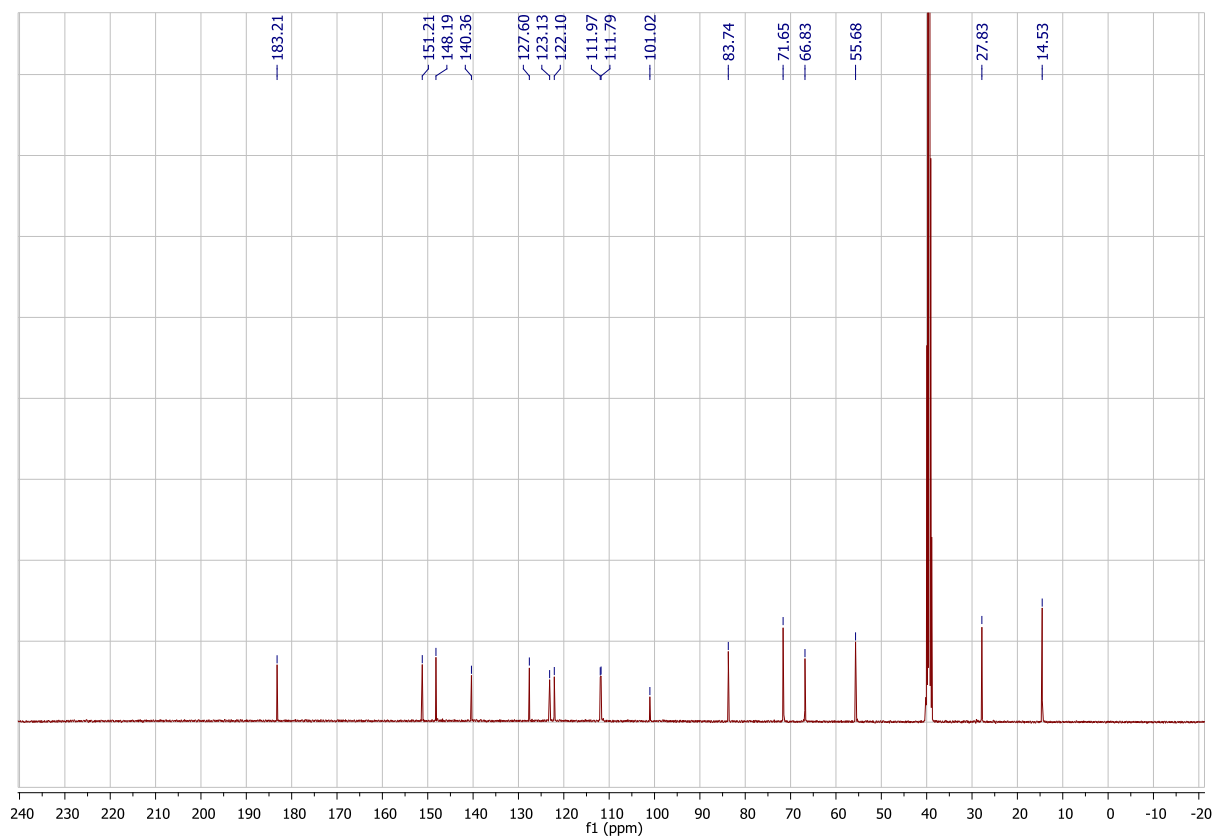


**Figure S47:** <sup>13</sup>C{<sup>1</sup>H} NMR spectrum (100 MHz, DMSO-*d*<sub>6</sub>) of **3g**.



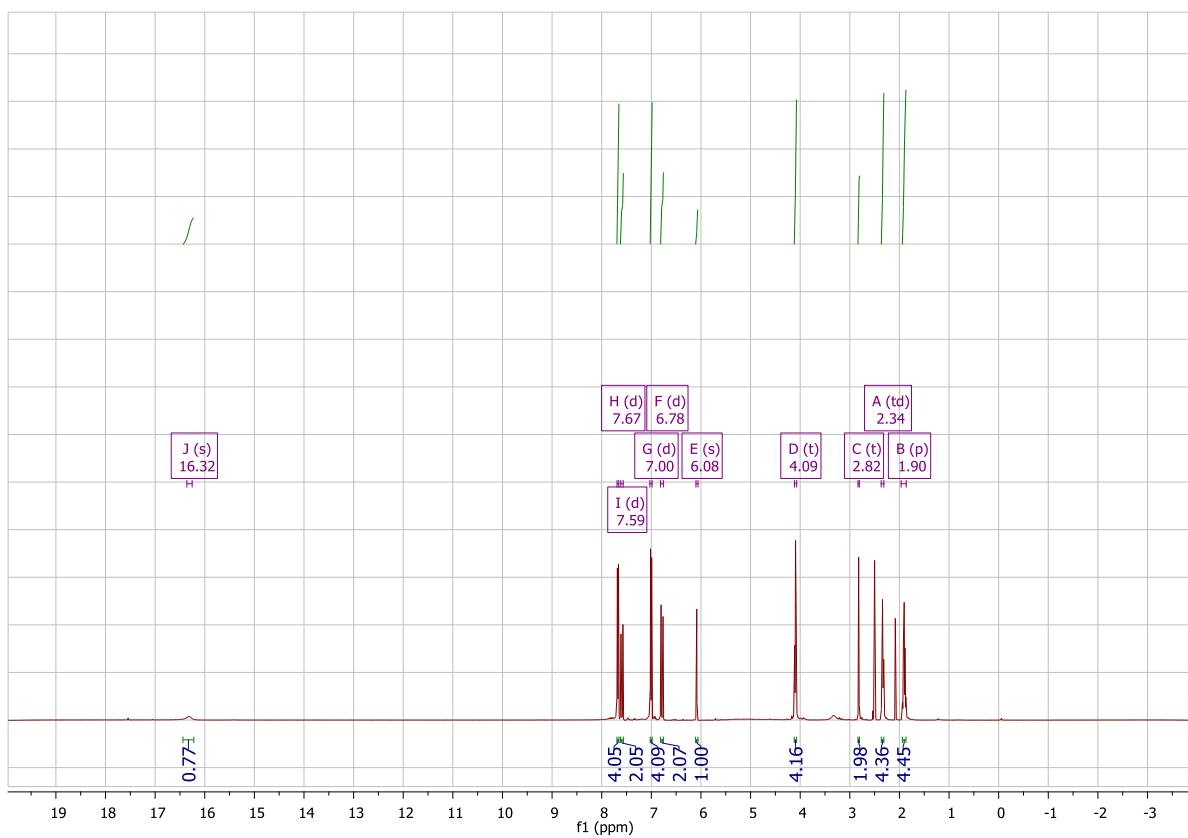


**Figure S48:** <sup>1</sup>H NMR spectrum (400 MHz, DMSO-*d*<sub>6</sub>) of **3h**.

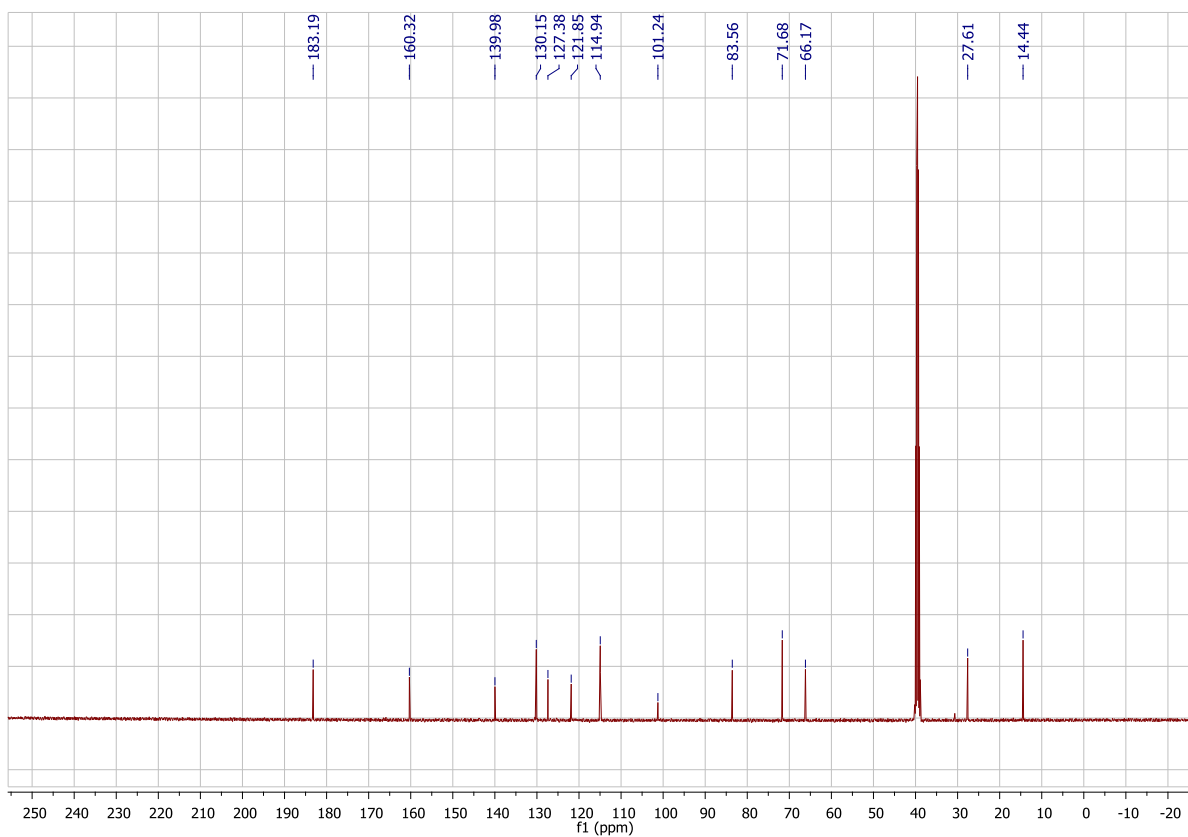


**Figure S49:** <sup>13</sup>C{<sup>1</sup>H} NMR spectrum (100 MHz, DMSO-*d*<sub>6</sub>) of **3h**.